An investigation of the relationship between coal and gas properties in the Huntly coalfield, New Zealand.

A thesis submitted in partial fulfilment

of the requirements for the Degree

of

Doctor of Philosophy

in the

University of Canterbury

by

Tennille E. Mares

University of Canterbury

2009.

Table of Contents

List of Figures

Chapter 4: Coal Petrology 98

List of Tables

Chapter 7: Gas associations 238

Abstract

The exploration for unconventional energy reserves has rapidly increased over the last five to ten years. Currently, there are a number of companies actively exploring for coalbed methane (CBM) in New Zealand. This study investigates one of these prospects, the subbituminous Huntly coalfield.

Coal core was retrieved from the two major seams in the coalfield, the Renown and the Kupakupa. Three coals types were identified (1) bright lustre, non-banded, (2) bright lustre, moderately banded and (3) bright lustre, highly banded. As the degree of banding increases, the average thickness of the vitrain bands increase, the amount of structured vitrinite macerals also increase and the vitrodetrinite content decreases. The Renown seam is predominantly composed of bright non-banded coal while in the Kupakupa seam the more banded coal types are dominant.

On average, the Renown seam has both the capacity to hold more gas and has higher gas contents than the stratigraphically lower Kupakupa seam. Additionally, gas content, on average, was found to be highest in intervals of the non-banded coal type and lowest in the highly banded coal type. Cluster analysis found that gas content is associated with hydrogen, volatile matter, calorific value and collodetrinite. As such, gas appears to be preferentially retained/produced in the matrix-dominated material. While not causally linked with gas content, gas holding capacity showed associations with the sporinite, inertodetrinite, funginite

and vitrodetrinite; of note, these macerals are highest in the non-banded coal type. Gas holding capacity is thought to be a function of coal texture.

Ash yield was found to inversely affect total gas content when ash yield is >10%. Below 10%, it is thought that inorganic elements are organically bound. The small angle scattering analysis indicated that inorganic matter was in the 12.5 Å < r < 125 Å pore size range. The influence of inorganic material was more noticeable in vitrain than matrix samples and is proposed to exist as thin inorganic coatings.

Total porosity of the Huntly coal is primarily composed of micropores with macroporosity only contributing a small proportion. In addition, the specific surface area of the coals is also largely contributed by the micropores. Methane holding capacity on a dry, ash-free basis showed positive correlations with both micro- and macroporosity. When methane holding capacity was considered on an 'as analysed' basis, correlation was only identified with macroporosity. Possibly gas holding capacity is affected by the presence of moisture blocking access to gas adsorption sites in smaller pores.

Considerable variation is present in both gas adsorption and gas desorption results between drill holes, between seams and also within individual seam intersections. Gas adsorption capacity and gas content are used to calculate % saturation for a reservoir, a key assessment parameter. It was found that multiple samples of both gas adsorption capacity and gas content are required to reduce the uncertainty around the calculated % saturation (at least three of each in the current study). Additionally, adsorption isotherm samples need to be collected as fresh as possible to minimize oxidation and moisture loss. Delaying sample analysis was found to result in an overestimation of gas adsorption capacity.

Acknowledgements

There are of course many people to thank….

- First and foremost, Tim Moore my supervisor. Tim has of course been instrumental in the successful completion of this thesis and the publications produced. Thank you for the brilliant opportunities I have had during this project, for all your support, for promoting both me and my work and for giving me the space to do my own thing. I will be eternally grateful.
- Jane Newman for teaching me organic petrology and for reviewing chapters. I have thoroughly enjoyed both working with and discussing work with you. Thank you for being so generous, thoughtful and such good company.
- Andrzej Radlinski for enabling me to conduct the small angle scattering study and for reviewing papers and chapters. Thank you for providing me with this amazing experience which was one of the most challenging and most rewarding parts of this work. I had a brilliant time working with you.
- My co-supervisor Steve Weaver for reviewing work and helping me to navigate the university system.
- The Department of Geological Sciences, University of Canterbury.
- Solid Energy NZ Ltd., Resource Development Technology LLC, and Coal Bed Methane Ltd for project support and for permission to publish.
- The New Zealand Foundation for Research, Science and Technology through its Technology New Zealand funding provided me with a stipend.

Acknowledgements

- The Royal Society of New Zealand, Education New Zealand and the Mason Trust fund for travel grants.
- Joan Esterle for suggesting I apply for this project.
- The Beverland family for putting up with me running around their property.
- The Huntly CBM team: Grant Gillard, Jaco Fourie, Sadiq Zarrouk, Tom Bowman, Greg Twombly, Steve Stepanek, Carol Butland and John Lavis. I really enjoyed working with you all.
- The drilling crew: Bruce McKeown, Phil Van Houtte, Cliff Brown, Des Oxam, Chad Brown, Shawn Fleet, Phil Martin, and Hayden. For making my time in the field so educational and entertaining…
- Jan Ilavsky, David Cookson, Thiyaga and Denis Wozniak at Argonne, and Jurgen Klepp and Stephan at ILL.
- Geological sciences administrative and technical staff, particularly Jennifer Jackson, Rob Speirs, John Southward and Pat Roberts.
- Additionally, thanks to Peter Crosdale, Ray Williams, Cath Moore, Jane Shearer, Nathan Deisman, James Pope, Chris Nelson, Richard Punt, Alfred Marerwa, Tony McWhinney, Alan Hinde, Tony Watson, Carlos Galceran, Grant Murray and Doug Phelps.
- My family and friends who have been overwhelmingly tolerant and supportive over the years. Looking forward to spending more time with you all.
- Finally to Jack, for all his support and understanding.

Chapter One

Introduction

Changing key market drivers worldwide have resulted in the exploration for, and development of, unconventional energy reserves such as coalbed methane (CBM), i.e. methane naturally occurring within coal seams. Although CBM has been extracted from high rank coals for at least the past two decades, until the success of work in the Powder River Basin, U.S.A., low rank coals containing biogenic methane gas have not been thought to contain sufficient CBM to be economically producible. Natural gas (methane – CH_4) is an important source of clean fossil-fuel energy that is experiencing growing demand in New Zealand and elsewhere. At the same time there has been a reduction in supply from existing conventional natural gas fields. This has prompted investigation for CBM potential in New Zealand (Hayton et al., 2004; Johnson, 2004; Manhire and Hayton, 2003; Moore et al., 2004; 2002; Stepanek, 2008; Twombly et al., 2004).

Unlike conventional hydrocarbon plays, coal acts as both the source and the reservoir for the gas, meaning that the coal should be either (1) sealed by an impermeable layer, (2) be under a sufficient hydrostatic pressure or (3) have low permeability to prevent the gas from migrating out of the coal. For a coal bed to contain methane, there must be capacity within the coal to store the gas, and of course the methane has to have been generated (either biogenically or thermogencially). Variability in gas content can be the result of coal rank, type and grade. For commercial amounts of gas to flow, the CBM reservoir has to have some degree of permeability. Generally there are two scales of permeability present in coal, a macroscopic system composed of regular, persistent fractures (Close, 1993) and a microscopic system consisting of pores and cavities (Gamson et al., 1996). Hence the microstructural properties of the coal play an important role in both gas storage and gas transportation.

The development of CBM plays in low rank coal deposits is still in its infancy. Worldwide there have been very few studies of the characteristics specific to low rank coals, and the studies that have considered them often use very limited datasets. The current study will contribute to filling this gap, both in the knowledge gained and in the extent of the dataset. In addition to presenting a large dataset on the coal and gas properties of a Tertiary low rank coal deposit, it is hoped that the results produced will benefit reservoir modelers as well as future explorers in terms of sampling techniques and site selection.

Looking to the future, there is also increasing concern over the environmental impact of anthropogenic greenhouse gas emissions, particularly carbon dioxide (CO_2), with targets and taxes being implemented to decrease gas release to the atmosphere. With coal, oil and natural gas currently supplying around 85% of the world's energy requirements, together

with the abundance of fossil fuels and the significant infrastructure already in place, it is likely that burning of fossil fuels will continue to be the dominant form of energy for at least 25 to 50 years (Kaldi and Cook, 2006). As such, attention has turned to the capture and storage of CO_2 in geological structures. One of the options being explored is the sequestration of CO_2 into deep, unmineable coal seams, with the additional possibility of production through enhanced coal bed methane (ECBM). This has also been examined in the Huntly coalfield (Mares and Zarrouk, 2008; Zarrouk and Moore, 2007; 2009). Although not the focus of this thesis, much of the work presented here has relevance to ECBM and CO_2 sequestration. With this in mind, some data are presented on carbon dioxide storage capacity.

1.1. Objectives

In the current study, the overall objective was to characterize coal from the Huntly coalfield, a prospective CBM play, at both the macroscopic and microscopic levels, and to identify the influences these coal properties have on gas content and gas holding capacity.

In order to accomplish this objective, the aims were as follows:

- To classify and log the distribution of macroscopic coal type in retrieved coal cores.
- To characterise the chemical composition (both organic and inorganic) of the coal and to consider the mode of occurrence of inorganic elements present in the coal.
- To investigate the organic petrology of the coal and its relationship to coal chemistry and macroscopic coal type.
- To determine gas content and gas holding capacity from the coal seams in the Huntly coalfield.

- To investigate the microstructural features of the coal such as specific surface area available for gas adsorption, total porosity, pore size distribution and pore morphology.

The thesis is composed of eight chapters, five of which present results. The first three results chapters (Chapters 3, 4, and 5) consider the coal chemistry (both organic and inorganic), the coal petrology (macroscopic and microscopic) and the coal microstructure (small angle scattering study) separately. The fourth results chapter (Chapter 6) presents the gas properties of the Huntly coalfield without consideration of coal properties, and the final results chapter (Chapter 7) considers the gas properties in relation to coal properties.

1.2. Location

The two major coal seams present in the Huntly coalfield, the Renown and Kupakupa seams (Fig. 1.1 and 1.2), are located within the Waikato Coal Measures (Edbrooke et al., 1994). The coal measures are typically 50 – 100 m thick and are dominated by claystone and siltstone lithologies (Kirk et al., 1988). The Waikato Coal Measures are thought to have formed in a fluvial-dominated environment with extensive mire complexes located in areas restricted from sediment input (Edbrooke et al., 1994; Newman et al., 1997).

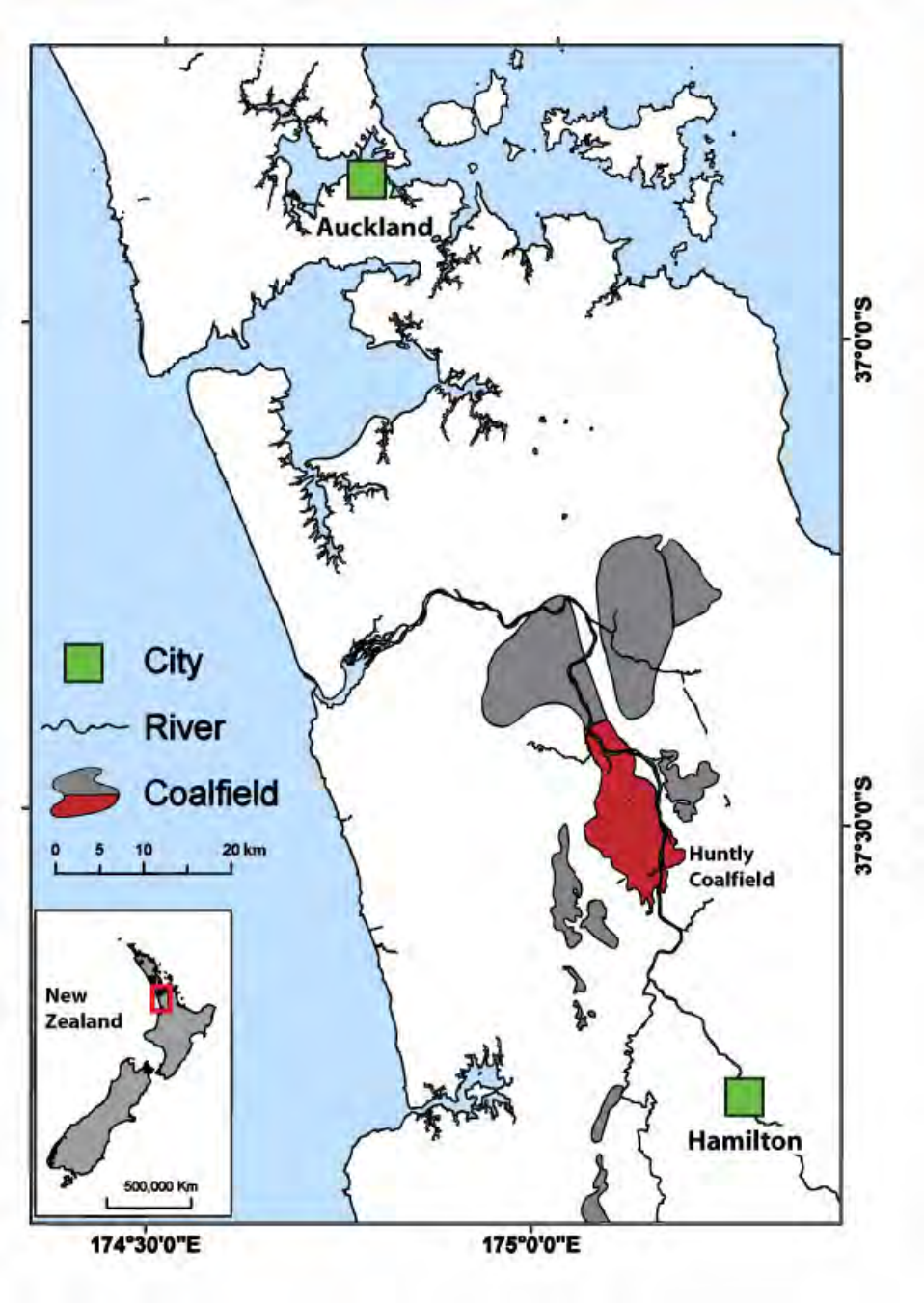

Figure 1. 1. Location of the Waikato coalfields, coloured grey, with the Huntly coalfield coloured red, North Island, New Zealand.

The Renown seam tends to be located in the upper half of the coal measures and is generally less extensive, more split and thinner (<8 m) than the Kupakupa seam (Fig. 1.3). The Kupakupa seam, found in the lower half of the coal measures, is typically 3 – 12 m in thickness, occasionally exceeding 20 m. Generally the Kupakupa is separated from the

Renown by approximately 20 m of interburden, although locally this can be only a few metres and in a few locations the seams merge (Newman et al., 1997). Lateral thickness variations, particularly in the Kupakupa, are often quite rapid (Edbrooke et al., 1994) and are interpreted to have been controlled by basement paleotopography and fluctuations in sediment supply (Hall, 2003; Hall et al., 2006). Both seams are generally low in sulphur and have low to medium ash yields (Edbrooke et al., 1994; Newman et al., 1997). In the study area of this thesis the groundwater table resides at about 20 m below surface.

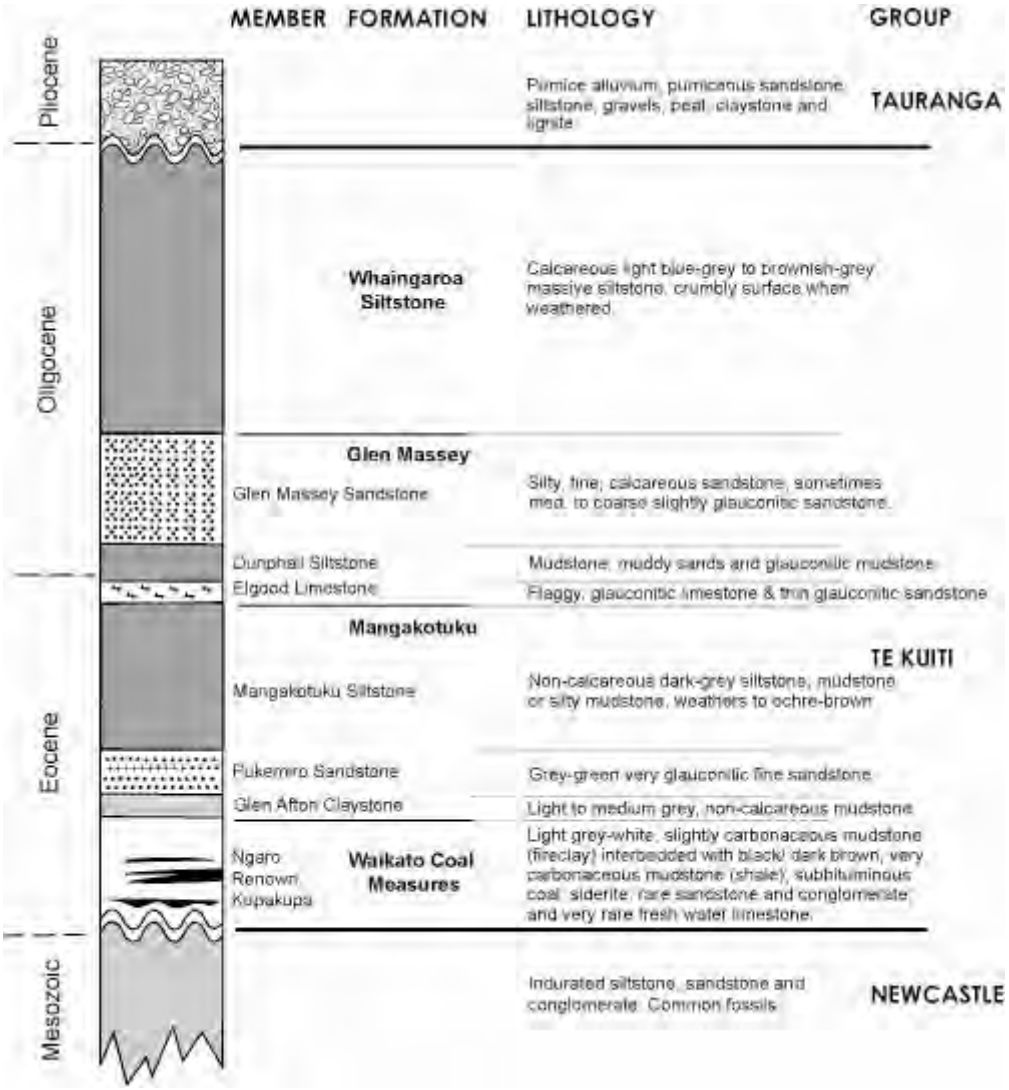

Figure 1. 2. Stratigraphic column showing typical stratigraphy of the Huntly coalfield, New Zealand (modified from (Hall et al., 2006)). The three coal seams in the Waikato Coal Measures in this area are the Ngaro, the Renown and the Kupakupa.

The depth of the coal beds ranges from essentially zero at the sub-crop, to over 850 m in the most northern parts of the coal field (Edbrooke et al., 1994). The present target depths for CBM production in the Huntly coalfield lie generally between 350 and 600 m. These depths are dictated by the depth of local underground mining (to depths of approximately 300 m) and the significant reduction in permeability below 600 m. Only normal faults exist in the coalfield and these are thought to all have occurred after deposition of the coal measures (Hall et al., 2006). Major faults (>20 m throw) occur about every 2 - 5 km and most of these trend northeast-southwest (Edbrooke et al., 1994; Hall et al., 2006). The cleat system has been determined to be sub-parallel to the strike of the normal faults (Cameron, 1995).

The coal seams in the Huntly coalfield are subbituminous C to A in rank (Edbrooke et al., 1994; Newman et al., 1997) and have reported R_o values of 0.42 – 0.52% (Edbrooke et al., 1994; Li et al., 2009; Vu, 2008; Vu et al., 2008). At this low rank, coal seam gas generation is thought to be of biogenic origin, similar to the coal seams in the Powder River Basin (Flores et al., 2008; Rice, 1993). Previous studies indicate that the gas is primarily of secondary biogenic origin generated by the reduction of CO_2 (Butland and Moore, 2008; Moore and Butland, 2005; Moore and Twombly, 2006). CBM gas has been produced from the pilot pod since late 2007 (Stepanek, 2008).

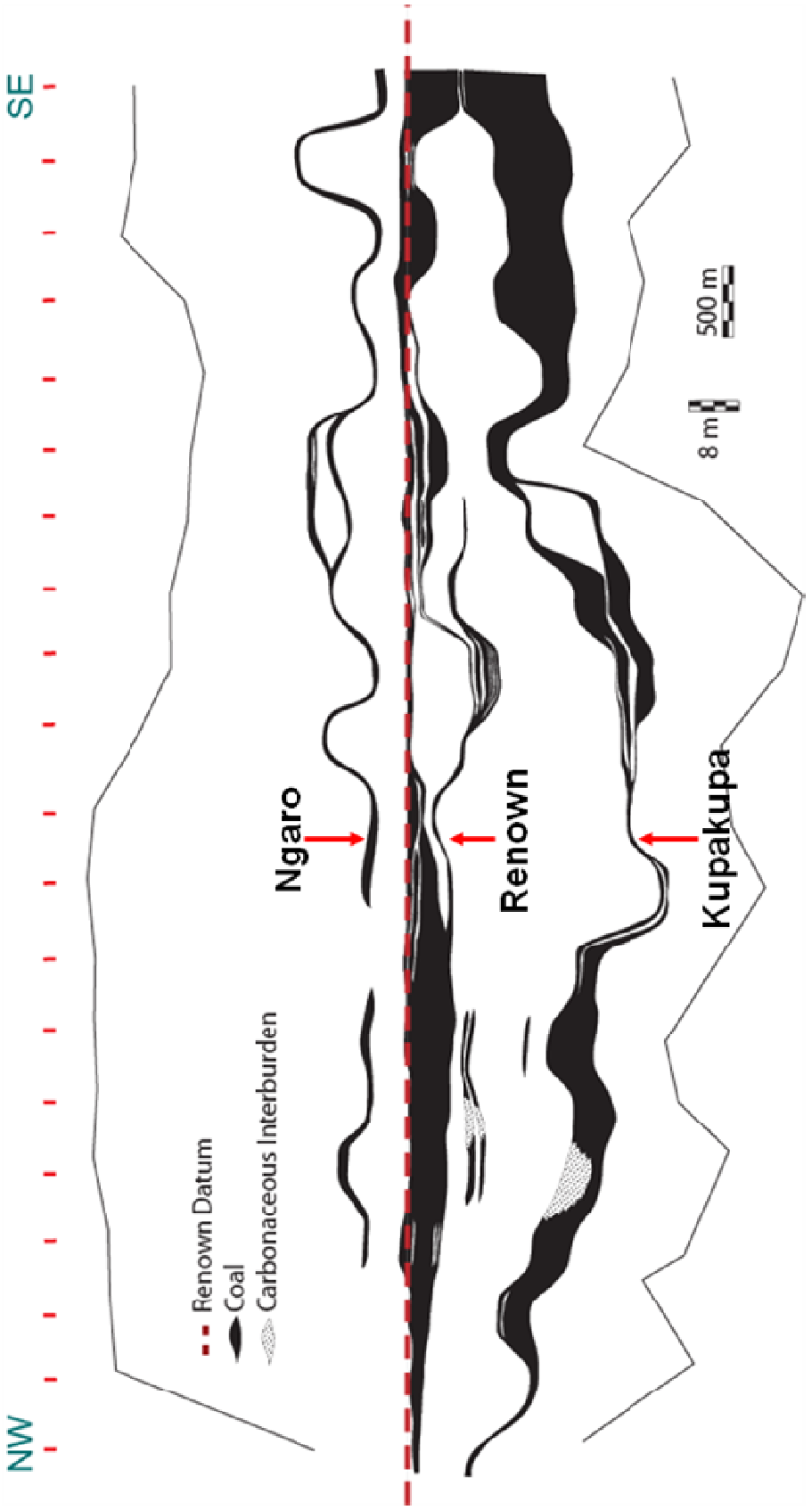

Figure 1. 3. Cross-section through the Waikato Coal Measures using the Renown seam as a datum. Faults have been removed.

Chapter Two

Methods

To determine the effect of coal properties on gas content and holding capacity, coal was collected from eight drill holes cored as part of a CBM prospect assessment (2006). One drill core was collected in 2003 (TW1; see Butland and Moore (2008), Moore and Butland (2005) and Twombly et al. (2004)), four during 2005 (Ruawaro 1, Ruawaro 2, Rotongaro 1 and Mangapiko 1) and three in 2006 (Baco 1, Mimi 1 and Jasper 1). All coal cores were collected from the northern part of the Huntly coalfield (Fig. 2.1). TW1 and the drill holes cored in 2005 targeted both the Renown and Kupakupa coal seams, while the 2006 holes cored only the Renown seam. The thin Ngaro seam was not present in all locations and, where present, was frequently used as a marker to change from rotary ('open hole') drilling to wireline[1] coring. As such, and due to its inconsistent nature, the Ngaro seam is a 'bonus' to production rather than a target and will not be addressed further in this study.

[1] Wireline core drilling is a type of core drilling where a barrel of core can be removed from the bottom of the hole without removing the entire rod string.

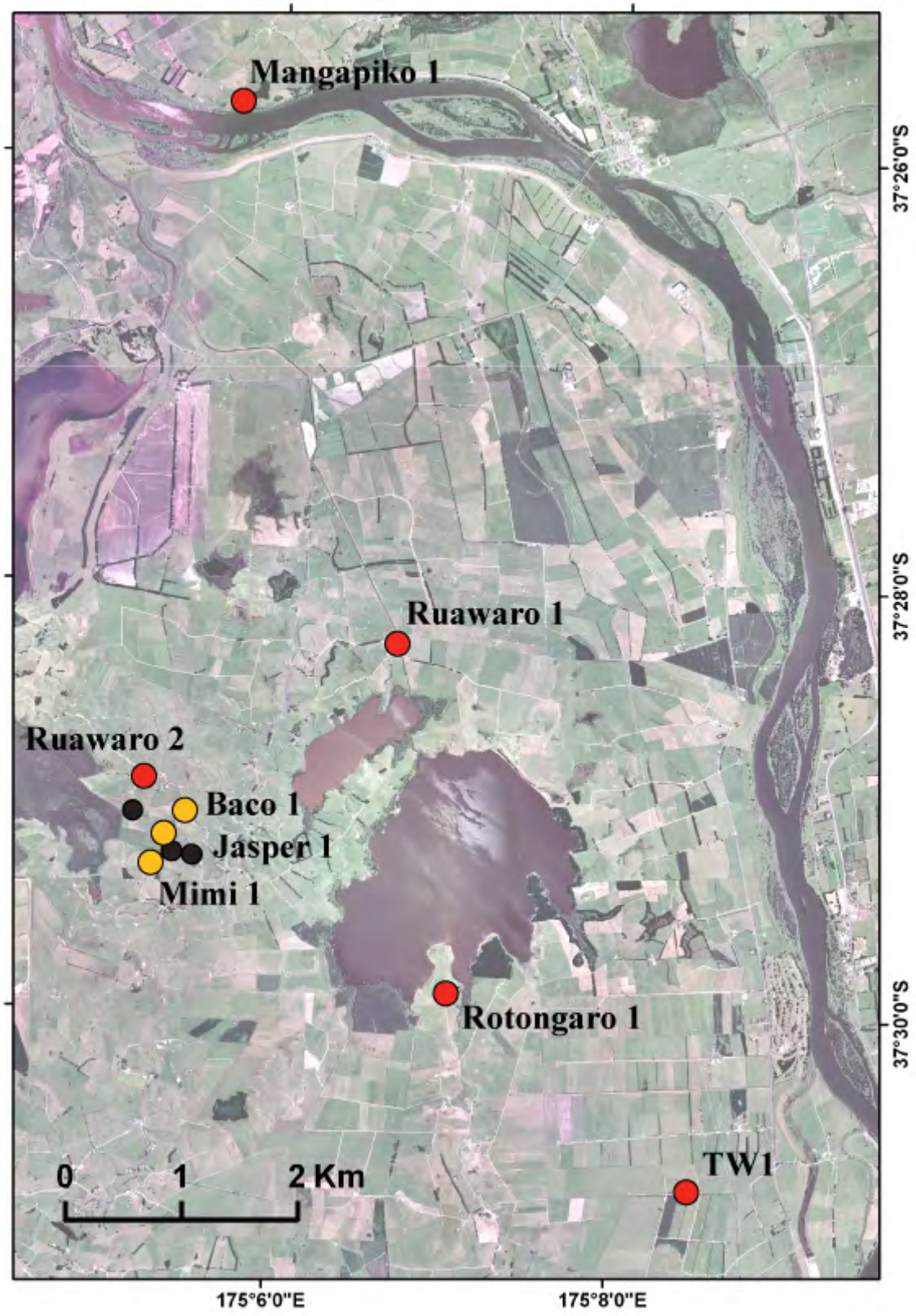

Figure 2. 1. Location of the drill holes utilised in this study. Red circles indicate drill holes cored in both the Renown and Kupakupa seams, yellow circles indicate drill holes cored in the Renown seam only and black circles indicate non-cored CBM holes drilled in this area prior to 2008.

All cores were retrieved using a wire-line coring system in order to minimize loss of gas during the time taken to bring the core to the surface. Once at the surface, the coal core was immediately taken from the core barrel (Fig. 2.2), quickly described to identify any inorganic partings and sealed within PVC gas desorption canisters (see Moore et al. (2004) for procedures).

Figure 2. 2. Opening the core barrel at the Jasper-1 site.

2.1. Gas properties

Standard procedure in assessing CBM plays is to determine how much gas a coal can hold (adsorption), quantify how much gas the coal is currently holding (desorption), and from these analyses determine how full (saturated) a reservoir is. In addition to these analyses gas composition is frequently assessed to identify the genesis of the gas (biogenic or

thermogenic) using isotopic analyses. The gas quality (percentage methane content) is also measured to establish the economic value of the gas reservoir.

2.1.1. Gas adsorption

Samples for adsorption were collected to assess the potential methane holding capacity of the target coal seams. Adsorption samples were collected both from the freshly retrieved core (i.e. pre-desorption) and after the core was desorbed for approximately 10 days (i.e. post-desorption).

Pre-desorption core samples of approximately 0.15m in length (or approximately 250g) were collected soon after the core barrel was opened and these samples were sealed in plastic film, wrapped in aluminium foil and finally placed in an air-tight plastic bag with the aim of minimizing oxidation and desiccation. For post-desorption samples representative splits of the coal were taken from the gas desorption canister material after desorption was completed. Eight methane adsorption samples were collected from both seams. Three pre-desorption samples from each seam were also analysed for carbon dioxide adsorption capacity to assess the potential for future enhanced-CBM and carbon dioxide sequestration.

Adsorption analyses were conducted according to procedures outlined by Crosdale et al. (Crosdale et al., 2008) and Moore and Crosdale (2006) at a reservoir temperature of approximately 32 °C (Moore and Crosdale (2006), see also Zarrouk and Moore (2007) for how the geothermal gradient for the area was determined). All gas adsorption analyses were conducted at the same laboratory (Energy Resources Consulting, Australia) under the same temperature (~32°C) and equilibrium moisture (~20%) conditions. For methane gas nine

pressure steps were used up to a maximum pressure of 8 MPa while for carbon dioxide seven pressure steps were used to 5 MPa. At each pressure step a fixed volume of gas was introduced and monitored to the nearest 1 kPa until there was no change in pressure for a period of at least 1 hour. Equilibrium generally took around 2 - 4 hours to obtain. Adsorption isotherms for both gases were fit to the Langmuir equation assuming a mono-layer gas adsorption mechanism (Gregg and Sing, 1982) and results have been standardized to 20°C and 1 atmosphere pressure (101.3 kPa).

2.1.2. Gas desorption

All coal and any surrounding material that had visible gas was quickly separated into approximately 0.5 m lengths and sealed in gas desorption canisters with the aim of minimizing time of coal exposure and gas loss (for canister design see Moore et al. (2004) and Barker et al. (2002)). Overall 163 canisters were collected, 85 in the Renown seam and 78 in the Kupakupa seam. The Kupakupa seam was not cored in the Baco 1, Mimi 1 and Jasper 1 drill holes.

The canisters were maintained at reservoir temperature during desorption analyses using a heated water bath (Fig.2.3), and later a controlled temperature room, with gas volume readings initially being taken every 15 minutes. The time interval between readings was increased as the desorbed volume of gas decreased (Barker et al., 2002; Moore and Butland, 2005; Moore et al., 2004). The canisters for the drill holes cored in 2005 and 2006 were generally only desorbed over a 10 day period.

Residual gas was determined using methods outlined in Moore et al. (2004) and Moore and Butland (2005), while the lost gas correction and total gas volume were calculated using the Barker et al. (2002) methodology. It is important to note that this method does not take free gas into consideration (Bodden and Ehrlich, 1998).

Figure 2. 3. Gas desorption set up- water baths, desorption canister and manometer.

2.1.3. Gas variation and saturation

To address variability in gas content, gas holding capacity and hence saturation, a complete seam profile was sampled from the Renown seam in the Jasper 1. This part of the study was designed so that all results could be considered on a canister by canister interval basis with the aim of assessing the uncertainty and variability present in standard reservoir assessment parameters and ultimately to determine the number of samples required to estimate reservoir saturation.

As gas desorption and adsorption data (post-desorption) was collected for each canister sample (as described in Sections 2.1.1 and 2.1.2), saturation was also able to be calculated for each canister interval and reported on an in-situ basis using the formula:

$$\text{Saturation} = 1-[(\text{adsorption} - \text{desorption})/\text{adsorption}] \quad (2.1)$$

Average in-situ basis, data corrected to seam average moisture and ash contents, has been used as it is thought to be the best representative of reservoir conditions. This method has also been suggested as the most accurate basis to use for estimates of gas in-place (Mavor and Nelson, 1997).

Coalbed methane plays draw gas from the whole seam and not just selected parts of the seam. Therefore, in the exploration stage, accurately assessing the behavior of the whole seam intersection is necessary. To consider what would have been the minimum number of samples needed from the 10 canisters in order to approximate the mean within 'acceptable' limits of uncertainty the mean of the ten samples for adsorption and desorption were taken as representative for the seam. Each adsorption or desorption value for a canister was assigned a random number. These numbers were then selected randomly and averaged accordingly. Thus, the first two in the sequence was averaged. Then the first three were averaged, then the first four and so on till all 10 were averaged and thus representing the 'true' mean. This procedure (i.e. randomly selecting the sample order) was repeated ten times, giving ten lines. A more statistically rigorous investigation of this question, with the aid of a statistician is presented in Mares et al. (2009).

2.1.4. Gas composition analysis

Gas composition was conducted on representative coal-seam gas samples collected from several canisters within each drill hole using Teflon bags and analysed using procedures described in Pope (2005). All analyses were conducted at CRL Energy Ltd. Laboratories. To confirm the biogenic origin of the gas, carbon stable isotopes of methane (methane $\delta^{13}C$ and δD) were also analysed; the procedures have been thoroughly described elsewhere including Lyon and Giggenback (1994) for New Zealand coal seam gases.

2.2. Coal composition

Coal composition can be broken into three major components: (1) macroscopic analysis of coal core is conducted to quantify the visual character of the coal, (2) microscopic analysis of representative samples can be used to understand the coal formational environment and to predict some coal properties and behavior during utilization, and (3) coal chemistry which is influenced by maceral composition, organically bound elements and mineral matter.

2.2.1. Macroscopic description technique

To gain an understanding of the macroscopic variation of the Huntly coal, once the coal sample was removed from the desorption canisters it was classified by coal type and also point counted for vitrain bands. In the Huntly coal basin, three primary coal types have been recognized (Ferm et al., 2000; Newman et al., 1997) and are distinguished visually, hence

qualitatively, by the degree of vitrain banding present (with a 0.5mm diameter minimum cut off for measuring vitrain). The coal types were identified as follows: (a) bright luster, non banded (BNB), (b) bright luster, moderately banded (BMB), and (c) bright luster, highly banded (BHB) (Fig. 2.4). The latter two coal types roughly correspond to the bright, vitrain banding <20% and bright, vitrain banding >20% as described in Ferm et al. (2000) and Newman et al. (1997). The names were changed as a section of coal qualitatively called and then described as bright, vitrain banding <20% (i.e. up to 20% of the surface area consisting of vitrain material) did not necessarily equate to <20% vitrain counts (i.e. could consist of many thin bands up to 30% of point counts or a few thick bands equaling only around 10% of counts).

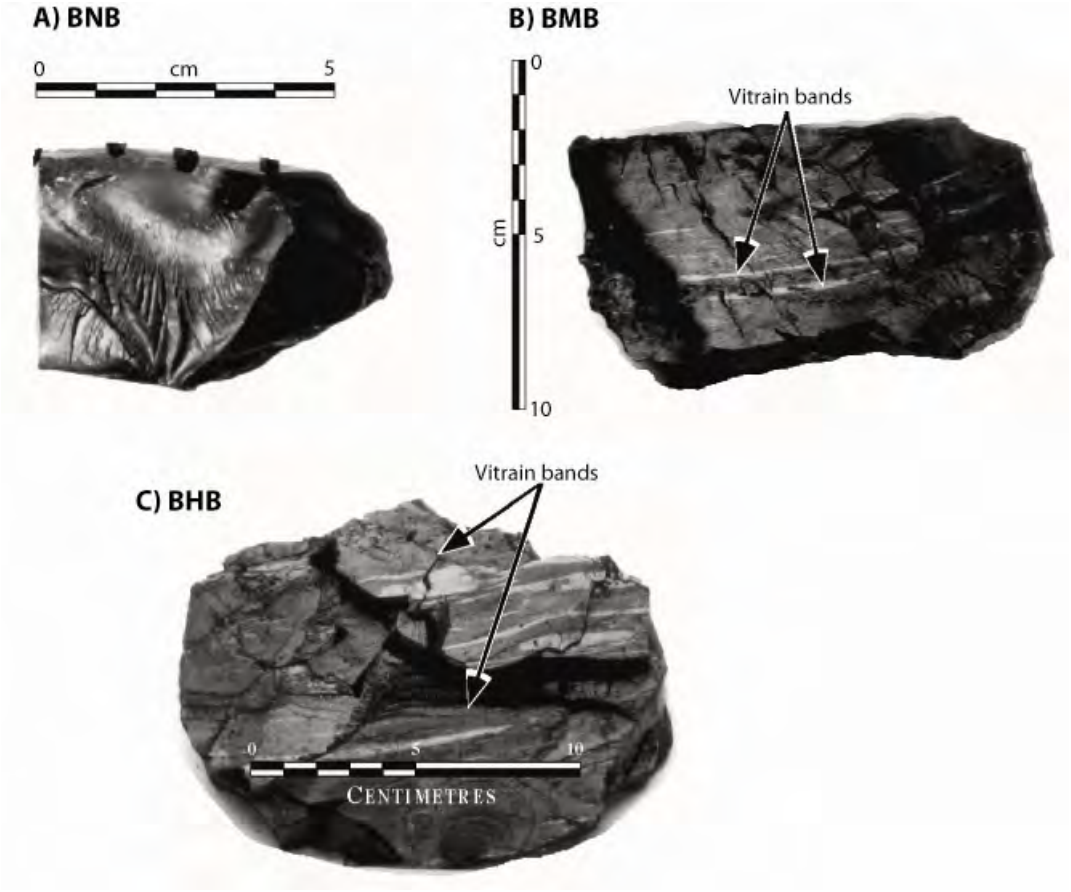

Figure 2. 4. Coal types identified in the Huntly coalfield are: (A) bright luster, non banded coal (BNB), (B) bright luster, moderately banded coal (BMB), and (C) bright luster, highly banded coal (BHB).

Within each section, coal type banding was quantified by point counting matrix versus vitrain bands on 1cm spacing, with the vitrain band thickness in the shortest dimension being recorded (Moore and Ferm, 1992; Shearer and Moore, 1994b). Vitrain band thickness data was transformed to the phi (φ) scale ($-\log_2$) as it has been shown that organic components, like other sediments, display log normality in their size distribution, making the phi scale ideal for comparing components from different coal types (Moore and Hilbert, 1992; Shearer and Moore, 1994b).

A coal type dataset was produced to determine the association of specific coal types with gas content; thus, for this analysis any canisters containing more than one coal type were removed from this analysis, reducing the data set to 100 canisters – 42 in the Renown and 58 in the Kupakupa seam. Coal types are not evenly distributed across all locations and some locations have more than double the gas content of others. As such, in order to consider the relationship between coal type and gas content, without any location specific bias, the dataset was normalized by drill hole and by seam (and also removing samples with >20% ash yield) using the formula:

$$z = (x-\mu)/\sigma \qquad (2.2)$$

Where: z is the normalized total gas content

x is total gas content on a dry ash free (daf) basis

μ is the average seam total gas content at each location

σ is the standard deviation (Moore and McCabe, 1999).

2.2.2. Coal microscopic composition

As maceral compositions from TW1 and around the Waikato coalfields have been presented previously (Butland and Moore, 2008; Edbrooke et al., 1994; Newman et al., 1997) it was decided to concentrate on the locations of most interest (i.e. those with the highest gas contents) to ascertain if there was any correlation between coal composition and gas content variability. Complete profiles of the Renown seam at Jasper 1 and Mimi 1 were completed along with Kupakupa seam profiles from Ruawaro 1 & 2. Other canister intervals were selected to complement the microstructural study (Section 2.4). Maceral groups on the sampled 0.5 m intervals were quantified by point-counting a random sample of 500 grains, 250 points on each of the two prepared pellet samples, following procedures set out in ASTM D2799 (ASTM, 2005).

As the Huntly coals are subbituminous in rank they border the region between brown and black coals and either terminology scheme, huminite or vitrinite, is acceptable for use (Sýkorová et al., 2005). Black coal terminology was utilized to be comparable with previous studies of coal from the Huntly coalfield (Butland, 2006; Butland and Moore, 2008; Edbrooke et al., 1994) following standard ICCP nomenclature (ICCP, 1998). Some modifications were made to the ICCP nomenclature (ICCP, 1998; ICCP, 2001) to try to capture features, such as porosity and structure, which might impact on gas adsorption (See Table 2.1). Modifications are as follows:

- Collotelinite was divided into four different size categories with the option of being combined later on. The ICCP vitrinite nomenclature scheme (ICCP, 1998) separates collotelinite from vitrodetrinite at 10 µm while Butland and Moore (2008) made a distinction between ‘cell filling’ telovitrinite and ‘band’ telovitrinite at 20 µm, with

'large' telovitrinite at >100 µm. To combine both of these schemes divisions are: (1) 'collotelinite A'- 10-20µm which is typically larger isolated corpocollinite bodies (see below) not captured by vitrodetrinite, (2) 'collotelinite B'- 20-50µm, typically thin bands, (3) 'collotelinite C'- bands between 50-100µm thick, and (4) 'collotelinite D'- large homogenous areas >100µm is size. Thicknesses were measured along the shortest dimension.

- The maceral corpogelinite occurs as structureless bodies of humic cell fillings either within tissue structure or isolated within the matrix. As the macroscopic work suggested that texture may influence gas properties in the Huntly coals, it was decided to capture the corpogelinite in structured tissue under the term 'corpocollinite' with the smaller isolated bodies falling into the vitrodetrinite category and the larger ones into collotelinite A.
- Because of the coal rank some degraded cell lumens, and wood tissue are more accurately described as porigelinite, a granular, porous gel that sometimes contains fine liptinite particles. Petrographically the gel appears very similar to collodetrinite, which is also an amorphous product of tissue degradation, with the distinguishing criteria being that generally porigelinite does not envelop other macerals. Edbrooke et al. (1994) dealt with this issue by referring to all porigelinite as collodetrinite regardless of location. However, in this study texture is of particular interest and thus it was decided to use the term 'porigelinite' to identify porous cell lumens in structured material with other non-structured material being described as 'collodetrinite'.

On each pellet sample for the first ten telovitrinite grains encountered showing porosity (typically collotelinite C and D) the pores were examined in UV light to determine if

the pores were filled with resin. This was done with the aim of estimating the proportion of 'open' pores. Additional telovitrinite grains showing porosity were tallied to obtain an estimate of the proportion of telovitrinite containing porosity.

Table 2. 1. Maceral classification scheme, modified from (ICCP, 1998; ICCP, 2001).

Maceral Group	Subgroup	Maceral
Vitrinite	Telovitrinite	Telinite
		Collotelinite A-D
	Detrovitrinite	Vitrodetrinite
		Collodetrinite
	Gelovitrinite	Corpocollinite
		Porigelinite
Liptinite		Cutinite
		Suberinite
		Sporinite
		Resinite
		Liptodetrinite
		Alginite
		Bituminite
Inertinite		Fusinite
		Semi-fusinite
		Funginite
		Inertodetrinite
		Macrinite
		Micrinite
Mineral Matter		Quartz
		Clay
		Mica
		Sulphide
		Carbonate
		Iron oxide

Mean vitrinite fluorescence results are thought to be linked to hydrogen and/or volatile matter content of coals and have also been suggested to reflect the activity of methanogenic and sulfate-reducing bacteria (Quick, 1994). To investigate this possibility,

mean vitrinite fluorescence was determined for each of the Jasper 1 Renown samples and the Kupakupa samples from Ruawaro 2 using methods described by Quick (1992; 1994).

2.2.3. Coal rank

Rank of the Huntly coal was assessed in two ways, by vitrinite reflectance and Suggate Rank. Mean maximum vitrinite reflectance (R_{max}) of collotelinite was determined by Newman Energy Research using method ISO 7404-5 (1994) on representative seam composites from the Renown seam (for Jasper 1 and Mangapiko 1), and from the Kupakupa seam (for Ruawaro 2 and Mangapiko 1). Vitrinite reflectance was further examined with vitrinite-inertinite reflectance and fluorescence (VIRF) analyses on three samples from the Renown seam in Jasper 1 and three from the Kupakupa seam in Ruawaro 2 (Newman et al., 2000). For VIRF analyses random reflection and fluorescence was measured on around twenty-five different grains capturing the range of vitrinite and inertinite macerals present. Suggate plots can also be used to differentiate between type and rank differences. Suggate plots were generated using methods described in Suggate (1959; 2000) and Butland (2006).

2.2.4. Coal chemical composition

Once the canisters were decommissioned from desorption, the residual gas content determined and the coal macroscopically described, the remaining coal was submitted for proximate analysis (at the CRL Energy Ltd laboratories in New Zealand). Analysis methods used were ISO 5068–2 for moisture (ISO, 2006), ISO 1171 for ash yield (ISO, 1997), ISO

562 for volatile matter (ISO, 1998), ASTM D 4239 for sulphur (ASTM, 2004a), ISO 1928 for calorific value (ISO, 1995), whilst fixed carbon, as usual, was calculated by difference.

The ash constituents were also determined for all samples using X-ray fluorescence techniques following ASTM D4326-01 (ASTM, 2004b). It is acknowledged that some minerals, particularly carbonates, can be volatilized by the combustion temperature used by this method. Some work on the Huntly coals (on drill hole TW1) has previously been conducted using a low temperature asher (Butland, 2006; Newman et al., 1997) however for this study, because of the low mineral matter content of the coal, composition of the inorganic material was not a primary focus.

Ultimate analysis was additionally conducted on the Renown seam profiles at Mimi 1 and Jasper 1, the Kupakupa profile at Ruawaro 2 and the samples used in the microstructural study. Carbon, hydrogen and nitrogen analysis were performed using AL-038 (an accredited procedure by ACIRL Ltd. Laboratories in Australia) with oxygen calculated by difference. In other locations ultimate analysis was conducted on representative seam splits only. Relative density (AS 1038.21.1.1 (SAI, 2002)) was measured for the seam profiles of Mimi 1 and Jasper 1 as well as the microstructural samples (discussed below).

2.3. Coal microstructure

Various methods have been used to investigate coal microstructure, the most common techniques being mercury injection and nitrogen adsorption. Techniques involving fluids are affected by accessibility, the connectivity of the pore network, as well as sorption phenomena

and modification of the coal microstructure depending on the sorbate used (Levine, 1993). Small angle scattering (SAS) is a relatively inexpensive, noninvasive technique requiring little material and sample preparation, with both open and closed porosity being measured. As such it is an attractive alternative to using fluid for probing pore space (Radlinski, 2006; Radlinski et al., 2004b; 2001). Scattering theory is further discussed in Chapter 5.

2.3.1. SAS Sample selection

After macroscopic description of the coal core, block samples were collected from each desorption canister interval (usually 0.5 m). From this suite, suitable samples of matrix coal (Moore and Shearer, 1999) and pure vitrain were selected for small angle scattering (SAS) analyses. These two types of samples were chosen as the coal from the Huntly coalfield, like most New Zealand coals, is mostly bright in luster (Beamish et al., 1998; Edbrooke et al., 1994; Ferm et al., 2000; Sherwood et al., 1992) and the major macroscopic difference between the identified coal types is the proportion of vitrain banding (Newman et al., 1997).

2.3.2. Samples for SAS experiments

Samples for SAS analyses were prepared at the Sedimentology Laboratory of Geoscience Australia. For each coal, samples were prepared in three ways: a solid platelet cut perpendicular to the bedding plane (called “perpendicular sample” for short), a solid platelet cut parallel to the bedding plane (called “parallel sample” for short) and a sample crushed to a grain diameter of about 0.8 mm. Platelet size (typically 20x30 mm) was designed to suit the

largest neutron beam size required and samples were cut as thin as possible; in most cases thickness was less than 1 mm, to avoid the effects of multiple scattering (Radlinski et al., 1999).

Only results from solid platelets (both parallel and perpendicular) are presented in this study. As the coals are of low rank and the platelets are brittle, the orientated blocks of coal (trimmed to create platelets) were encapsulated with a low viscosity epoxy resin and then sliced using a low-speed precision diamond saw lubricated with a minimal amount of water. Such conditions were used to avoid sample contamination, through lubricants and heating, and to keep the coal from imbibing water. Despite these precautions, the coals absorbed some moisture which caused the platelets to dry and shrink slightly during transport, resulting in cracking of some samples (Fig 2.5).

Figure 2. 5. Coal platelet prepared for SAS analysis.

Twelve sets (one perpendicular and one parallel) of orientated platelets were prepared. Five matrix sets and only one vitrain set were prepared from the Renown seam as there was a

distinct lack of suitable vitrain bands in the collected block samples. For the Kupakupa seam three matrix sets and three vitrain sets were prepared. Matrix samples were collected from three locations for the Renown seam: Ruawaro 2 (sample number 318), two samples at different depths were collected for both Jasper 1 (samples 319 and 610) and another two samples from Mimi 1 (samples 611 and 612). The vitrain sample was collected from Mangapiko 1 (sample 323). For the Kupakupa seam, matrix and vitrain samples were collected from three locations: Mangapiko 1 (matrix sample 320 and vitrain sample 326), Ruawaro 1 (matrix sample 321 and vitrain sample 327) and Ruawaro 2 (matrix sample 322 and vitrain sample 328).

Knowledge of scattering contrast for the analysed material is essential for quantitatively interpreting absolutely calibrated X-ray and neutron scattering data (Radlinski, 2006). Using the coal composition data obtained in Section 3.3.3, the X-ray coherent scattering contrast term and the neutron scattering length density term can be calculated for each sample using equations 2.3 and 2.4 respectively (Radlinski, 2006).

$$\rho_n = (N_A.d)/M \,.\, \sum_j p_j \left(\sum_i s_i.b_i\right)_j \qquad (2.3)$$

Where: N_A is Avogadro's number 6.022×10^{23}

d is density in g/cm^3

M is the pseudo-molar mass

s_i is the proportion by number of nucleus i in the compound j

p_j is the proportion by molecular number of the compound j in the mixture

b_i is the coherent scattering amplitude for nucleus i

$$\rho_{el} = I_e.\rho_e = (N_A.d)/M \,.\, N_e.I_e \qquad (2.4)$$

Where: ρ_e is the electron density (i.e. the number of electrons per unit volume)

$I_e = e^2/(mc^2) = 2.82 \times 10^{-13}$ cm is the scattering amplitude of a single electron

N_e is the number of electrons per one supra-molecule

M is the molecular weight of one supra-molecule

d is the bulk density in g/cm^3

2.3.3. SAS instruments

In this study, four separate instruments were used: SAXS (Small Angle X-ray Scattering), USAXS (Ultra-small Angle X-ray Scattering), SANS (Small Angle Neutron Scattering) and USANS (Ultra-small Angle Neutron Scattering). The instruments used in this study are based at synchrotron (X-rays) and nuclear (neutrons) facilities in the U.S.A. and France (Fig. 2.6).

Figure 2. 6. Nuclear reactor (dome) and synchrotron (circle) facilities in Grenoble, France.

The pinhole-geometry SAXS instrument at ChemMatCARS, sector 15 of the Advanced Photon Source (APS), Argonne National Laboratory (Fig. 2.7), was used to obtain information in the Q-range from 1.1 $Å^{-1}$ to 2.9 x 10^{-2} $Å^{-1}$ (Cookson et al., 2006). Data were collected from samples orientated perpendicular to bedding plane with a beam size of 0.2 x 0.1 mm on 15 x 15 grids (with 0.6 mm steps). More sparse 7 x 7 grids (with 1 mm steps) were used for samples orientated in-bedding plane, as these were expected to be more homogeneous.

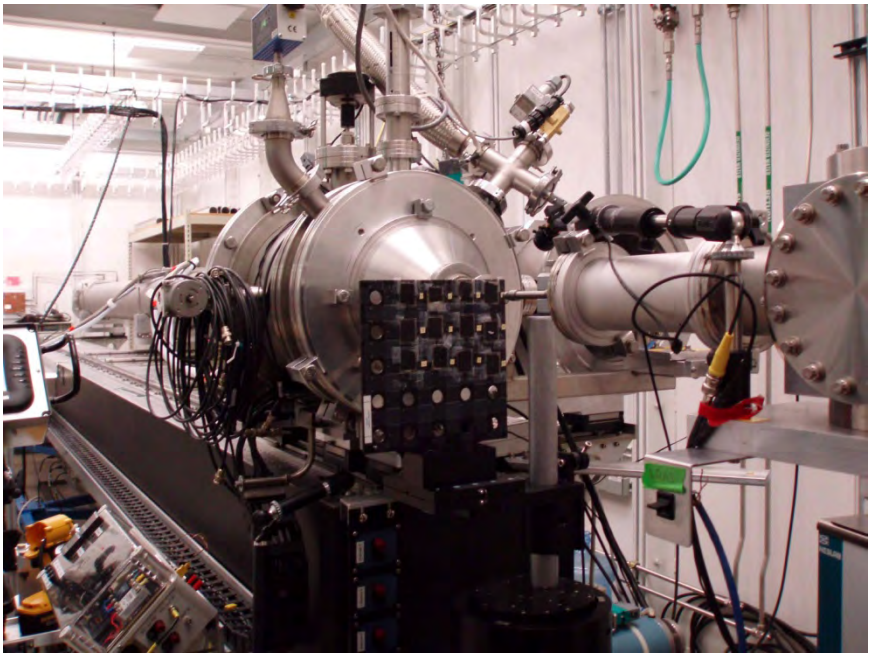

Figure 2. 7. SAXS instrument at APS with sample holder in place.

The Q-range of the SAXS data was extended into the small-Q region using the APS UNICAT USAXS instrument (Fig. 2.8) with 1-D collimated Bonse-Hart geometry (Q-range from 0.66 $Å^{-1}$ to 1.2 x 10^{-4} $Å^{-1}$; (Long et al., 2000)). As the photon flux incident on the detector of the USAXS instrument was significantly lower than for the SAXS machine, only five points were analysed per sample using the beam size of 0.6 x 0.6 mm (with 1.2 mm steps

for samples orientated perpendicular to bedding plane and 1 mm steps for samples cut parallel to bedding-plane). Points of measurements were chosen to correlate to data collected with the SAXS instrument and to avoid any large cracks.

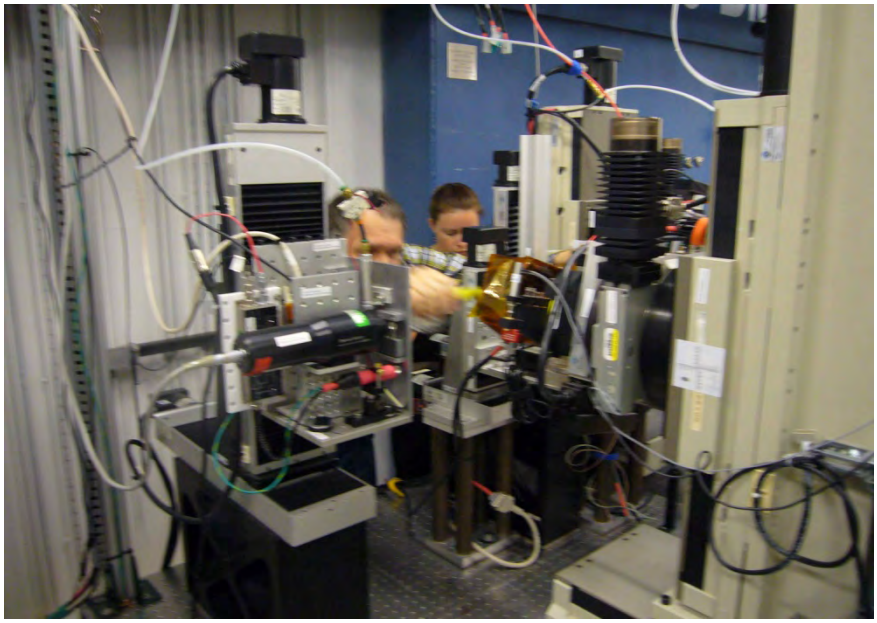

Figure 2. 8. Manipulating the crystals on the USAXS instrument, APS.

A time-of-flight instrument SAND (Fig. 2.9) at the Intense Pulsed Neutron Source (IPNS), Argonne National Laboratory was used to acquire SANS data in the Q range from 1.0 $Å^{-1}$ to 3.6 x 10^{-3} $Å^{-1}$ (Thiyagarayan et al., 1998). SANS instruments are typically characterised by large beam footprint (we used beam diameter 12.2 mm) and long acquisition times compared to SAXS instruments, hence not all orientated platelets were analysed for all samples.

Neutron scattering in the small-Q region (from 2.0 x 10^{-3} $Å^{-1}$ to 1.55 x 10^{-5} $Å^{-1}$) was measured using the Bonse-Hart geometry USANS instrument S18 (Fig. 2.10) at the Austrian Beam Line, Grenoble Research Reactor, France (Hainbuchner et al., 2000). As the technique

is only suitable for isotropic samples, only the platelets cut out in-bedding-plane (parallel samples) were analysed.

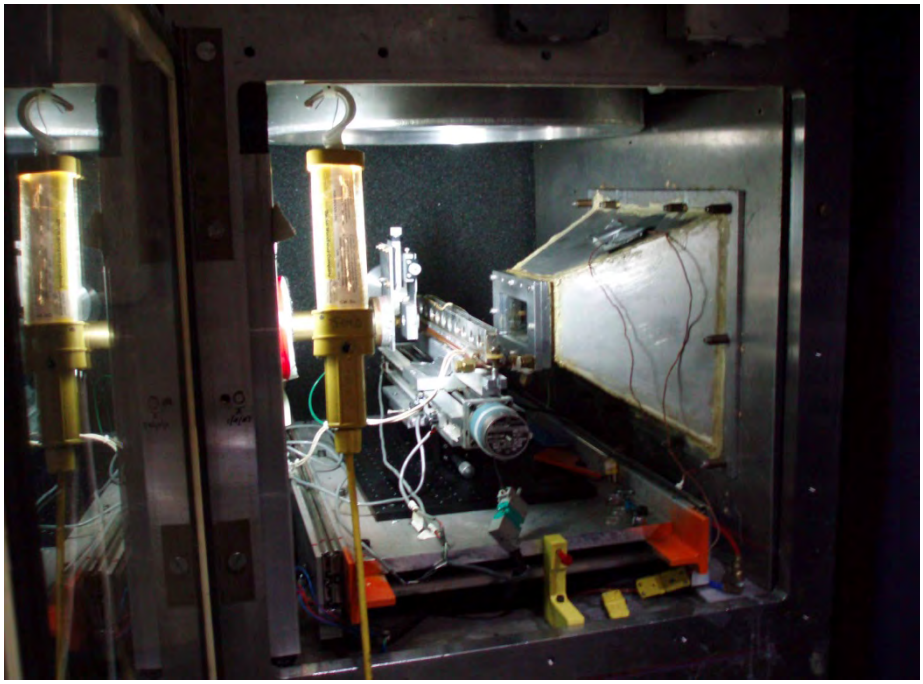

Figure 2. 9. The SANS instrument with sample holder in place, IPNS.

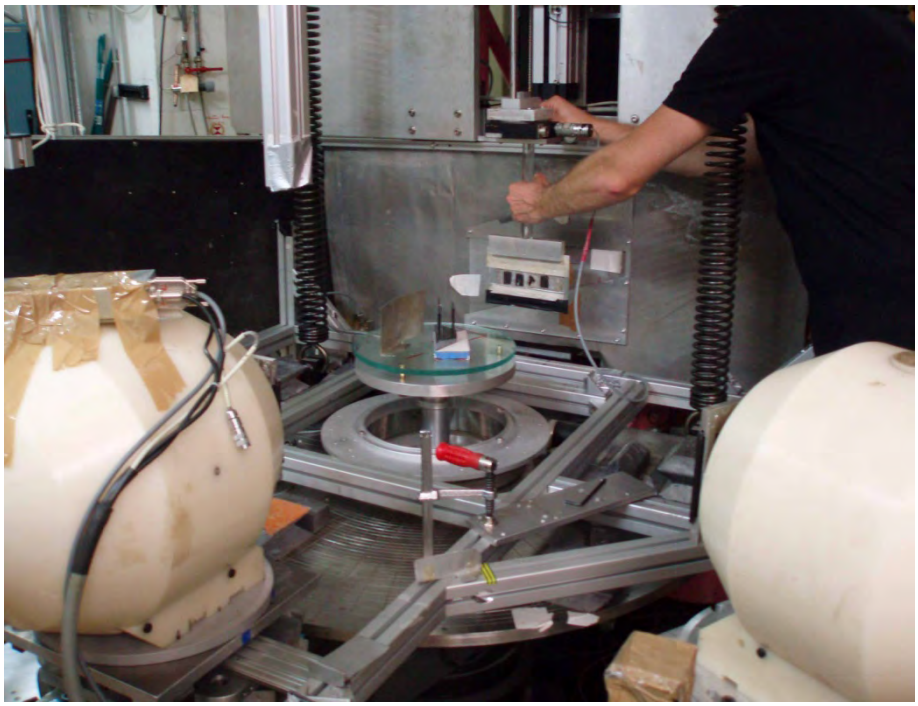

Figure 2. 10. Attaching the sample holder in the USANS instrument, Grenoble.

2.3.4. SAS data processing and analysis

Both SAXS and SANS data were acquired and processed in a way that yields the scattering intensity in absolute units of cm^{-1}, corresponding to the absolute scattering cross section. Details of the experimental and modeling procedures, as well as references to previous work, can be found in Radlinski et al. (2004b) and Radlinski (2006). USAXS data were desmeared using the IRENA software package (Long et al., 1991). Desmearing corrects for the geometry of the slit through which the beam (of electrons or neutrons) is passed before being scattered by the sample (Hinde, 2004). It is required for both USAXS and USANS measurements. The five USAXS data points per sample were then combined with the corresponding SAXS datasets. Next, the combined datasets were imported into PRINSAS software for modeling the pore size distribution (*f(r*)), specific surface area (SSA), and to calculate the total porosity (Hinde, 2004). The five scattering curves were then averaged to produce a representative scattering curve for each sample for easier presentation. Similarly, USANS data were desmeared and then combined with corresponding SANS data for each sample in PRINSAS, prior to modeling of the *f(r),* SSA and total porosity.

2.3.5. Microstructural models: fitting the shape of the scattering curves

It follows from the scattering theory and contrast considerations, based on Equations 2.3 and 2.4, that for a purely organic coal the neutron and X-ray scattering curves should be parallel to each other when plotted on a log-log scale. However, most of the X-ray scattering curves collected in this study displayed minor to considerable deviation from the shape of the associated neutron scattering curve. This indicates the presence of a third phase, likely to be inorganic matter, as scattering of X-rays is much more sensitive to the presence of the

inorganic phase in coal than the scattering of neutrons (Radlinski et al., 2004b). Therefore, X-ray scattering profiles that showed considerable deviation from the corresponding SANS/USANS profiles (the vitrain samples) were selected for further data analysis to determine the micro-geometry of regions with high concentration of inorganic material.

The following analytical procedure was used to interpret the SAXS/USAXS data. It was assumed that the scattering intensity was made up of two components: a power law scattering (characteristic of the surface fractal micro-geometry of the solid-pore interface; Radlinski (2006)) and an unknown scattering from the inorganic-rich regions. The small-Q, (linear on the log-log scale) part of the X-ray scattering curve was fit with a power law and the resulting formula was used to extrapolate the lower (large-Q) part of the scattering curve as a model for scattering in the absence of inorganic material. This predicted model curve was then subtracted from the actual measured curve to obtain the contribution from the inorganic material alone (see Fig. 2.11). This was done for the five collected scattering curves as well as the average curve produced in Section 2.3.4.

Using the resulting dataset (with new scattering intensity values) the radius of gyration can be calculated to estimate the size of the scattering object. The radius of gyration is the average squared distance of the scattering surface to the centre of the object and is routinely calculated from SAS data using the Guinier equation (Guinier et al., 1955):

$$I(Q) = I(0).\exp(-Q^2.R_g^2/3) \qquad (2.5)$$

Where: I(Q) is the scattering intensity in inverse centimeters (cm^{-1})

I(0) is the incident intensity in neutrons/X-rays per second

Q is the scattering vector in inverse angstroms ($Å^{-1}$)

R_g is the radius of gyration in angstroms (Å)

This equation is most easily solved by constructing a Guinier plot, ln I(Q) versus Q^2, where the linear part of the slope is equal to $-1/3.R_g^2$.

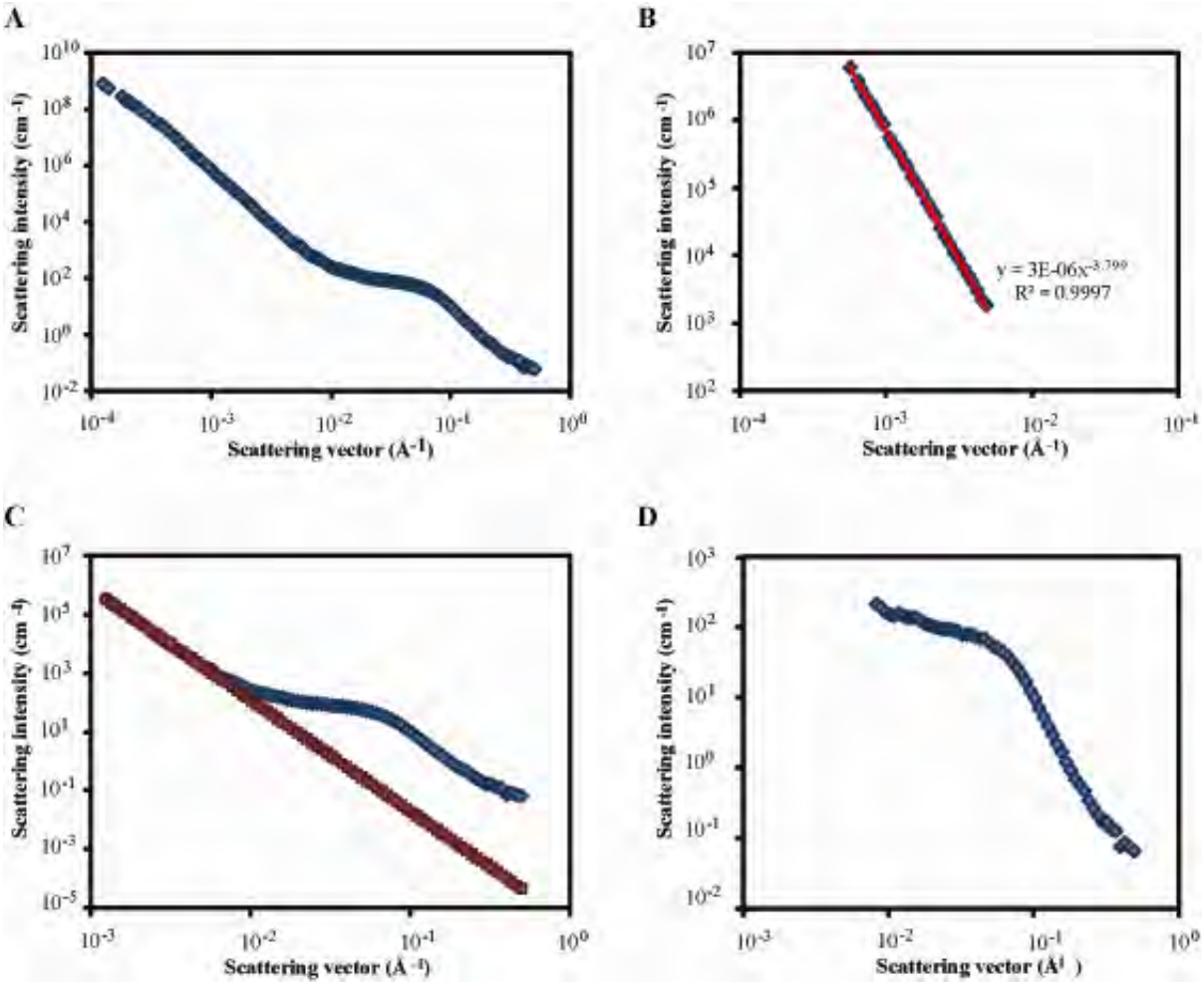

Figure 2. 11. Determining the scattering profile of the third phase. (A) The original SAXS/USAXS curve. (B) Fitting the linear, upper region of the scattering curve. (C) Plot of the original curve and the extrapolated curve. (D) The resulting scattering profile of the third phase after subtracting the extrapolated curve.

Once obtained, the R_g^2 can be used to calculate the radius of the scattering object, assuming various shapes (Equations 2.6-2.9 (Feigin and Svergun, 1987)). The field of possible (usually unknown) shapes can be narrowed down as the surface area and total volume of the scattering objects can be calculated using standard geometric equations. As very little inorganic material was observed during the microscopy study, combined with the material being concentrated in the $2\pi/Q \leq 300$ Å size range, it is possible that the material is organically bound. The shapes modeled were therefore selected with consideration of plant structure.

Sphere of radius R: $R_g^2 = 3/5.R^2$ (2.6)

Spherical shell with radii $R_1 > R_2$: $R_g^2 = 3/5.[(R_1^5 - R_2^5)/(R_1^3 - R_2^3)]$ (2.7)

For R_2 = 0.9, 0.8, 0.7, 0.6 R_1

Cylinder of radius R and height H: $R_g^2 = 1/2.R^2 + 1/12.H^2$ (2.8)

For H = 0.5, 0.8, 1, 1.2, 1.5 R

Hollow cylinder with radii $R_1 > R_2$ and height H:

$R_g^2 = (R_1^2 + R_2^2)/2 + H^2/12$ (2.9)

For R_2 = 0.9, 0.8, 0.7, 0.6 R_1

and H = 0.5, 0.8, 1, 1.2, 1.5 R_1

To ascertain the most likely shape of the scattering object the volume fraction of all the scattering objects can be compared to the ash yield of the sample. The volume fraction is determined by multiplying the number of scattering objects (per cm^3), N_i, by the volume of the individual scattering object *i*. N_i is calculated as follows:

1. Determine the Porod limit (Porod, 1951). The large-Q limit of the small-angle scattering domain is the region where atomic resolution has not been achieved, but where the observation scale is small and a well-defined interface appears to be smooth. This is the 'Porod region'. When the large-Q area of the scattering curve is plotted in a Porod plot, Q^4 x I(Q) versus Q, the large-Q intercept of the vertical axis provides a value for the Porod limit, PL (Radlinski, 2006).
2. Calculate the specific internal surface area. The Porod specific surface area (SSA) is calculated as:

$$SSA = PL/[2\pi(\rho_1-\rho_2)^2] \quad (2.10)$$

where ρ_1 and ρ_2 are the electron scattering length density of the organic coal matrix and embedded inorganic objects, respectively. Values of ρ_1 were calculated for each coal using equation 2.4, and the value of ρ_2 was assumed to be 3.75×10^{10} cm^{-1} (Radlinski, 2006)).

3. Calculate N_i. N_i is obtained by dividing the Porod SSA by the surface area of the object *i* (as determined using geometrical dimensions from equations 2.6-2.9).

Chapter Three

Coal Composition

All coals contain some inorganic components, the quantity and distribution of which gives considerable information on coal formation conditions. However these inorganic components can also limit coal utilisation and affect gas production. In general, methane has been recognized to adsorb to the organic components of coal, while increasing mineral matter content acts as a diluent to gas sorption capacity. As such, a reduction in gas content is expected for coals with higher mineral matter contents (Laxminarayana and Crosdale, 1999; 2002; Warwick et al., 2008; Yee et al., 1993). These results are consistent with previous work on New Zealand coals (Butland, 2006; Butland and Moore, 2008; Moore and Butland, 2005). Along with acting as a diluent, mineral matter in the form of secondary mineralisation in cleats and fractures can have a negative effect on methane recovery (Gamson et al., 1996).

The purpose of this chapter is to present the results for proximate analysis, ash constituents and, where available, ultimate analysis and organic petrology. These results will be compared to gas data and to other coal properties in later chapters. As referred to in the

methods section, the composition of the inorganic material is not a primary focus of this study hence mineral identification by X-ray diffraction (XRD) was not undertaken.

3.1. Inorganic matter in coal

Mineral matter present in coals can originate in the following ways: (1) as syngenetic inorganic matter that was originally incorporated into the mire flora and persists through the progression to peat and coal, (2) as syngenetic inorganic/organic complexes and minerals that were introduced by wind or water into the mire or formed in situ during the early stages of peat formation, or (3) as epigenetic minerals that form post-coalification by crystallizing in cleats and fractures in the coal from fluids moving through the system or from the alteration of original mineral matter (Taylor et al., 1998).

For coals of lower than bituminous rank, such as the Huntly coals, a significant part of the mineral matter may be contributed by inorganic elements being organically bound within the coal rather than being present as mineral phases. These organically associated elements can occur as inorganic elements dissolved in pore waters, as leachable salts, as cations held in exchangeable relationships with organic compounds or as organometallic complexes within the organic matter (Newman, 1988; Ward, 1991; 1992; 2002).

Interestingly, an artificial coalification study on peats (Bailey et al., 2000) showed that as coalification progressed, the peat expelled solutions of systematically varying compositions. Mobilisation of cations from the peat was controlled by at least three processes (1) loss of dissolved ions in original pore water expelled during compaction, (2) loss of adsorbed cations as adsorption sites are lost during modification of organic solids, and (3)

increased dissolution of inorganic phases at later steps because of increased temperatures and increased complexing by organic acids and anions. It has been suggested that organically bound elements are a major contributor for coals of lower than bituminous rank with low ash yields (Newman et al., 1997).

3.2. Proximate Analysis

3.2.1. Proximate analysis results by drill hole

Proximate analysis data for the TW1 core have been presented previously by Butland (2006) and Butland and Moore (2008). Gaps in the vertical profiles presented in Figure 3.1 are because these samples were desorbed for an extended length of time and were not further analysed. For TW1, ash yield, moisture, sulphur and volatile matter are consistent throughout the seam except where ash yield increases, and there is a concomitant decrease in moisture, volatile matter and fixed carbon; for example, the 20 cm thick high ash layer that separates the two seams at this location. It should be noted that as fixed carbon is determined by difference it has no intrinsic significance. The peak in sulphur content around 341.5 m corresponds to a region of dull lustre coal which is also high in ash yield. Full results are tabulated in Appendix 1 with seam ranges presented in Table 3.1. The Kupakupa seam on average has slightly higher moisture content and calorific value and a slightly lower ash yield than the Renown seam.

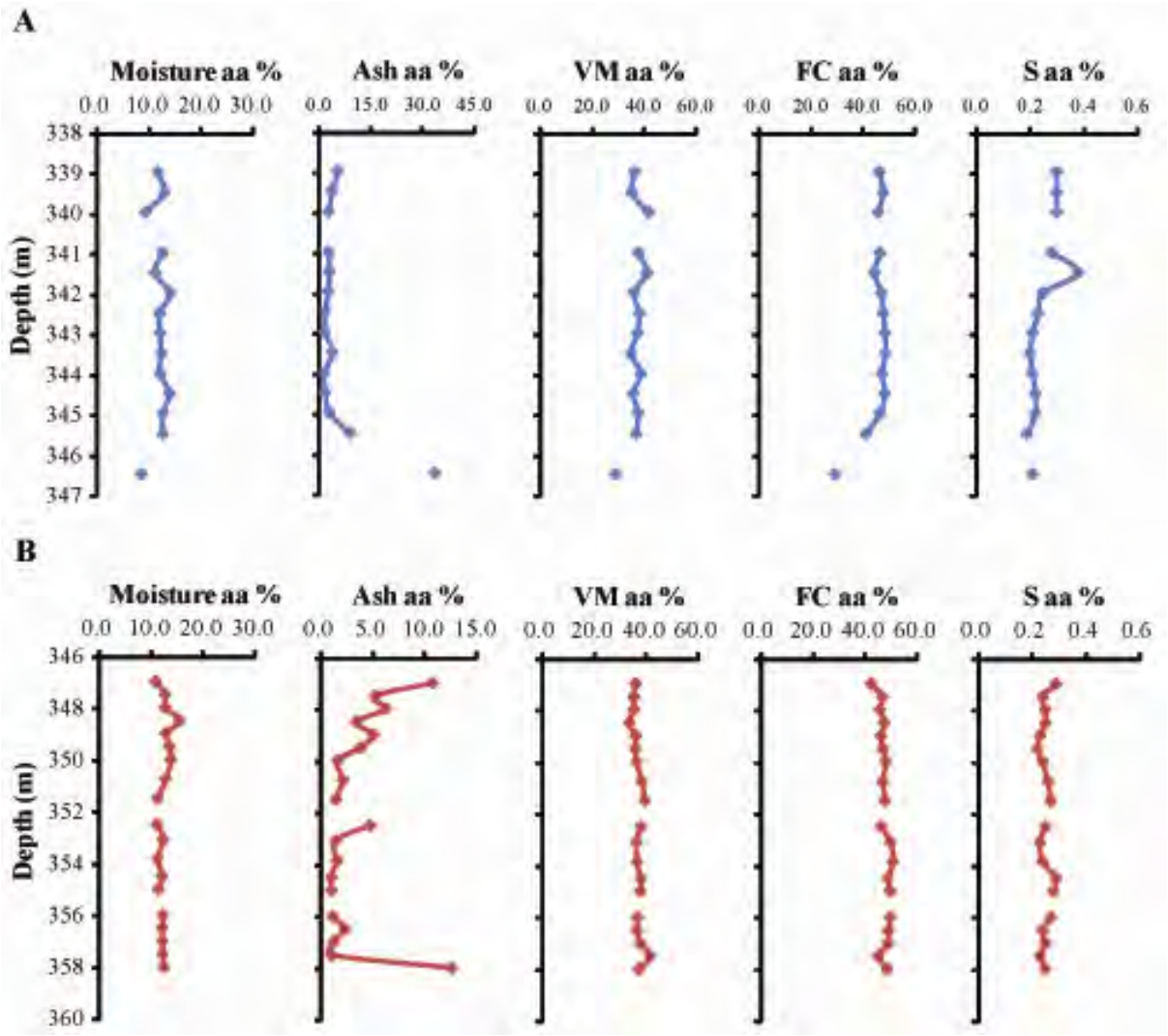

Figure 3. 1. Proximate results of samples from the (A) Renown and (B) Kupakupa seams at the TW1 location on an as analysed basis, aa. VM = volatile matter, FC = fixed carbon, S = sulphur.

Table 3. 1. Average proximate results by seam for the TW1 location on an as analysed basis.

	Renown seam				Kupakupa seam			
As analysed basis	**Min**	**Ave**	**Max**	**SD**	**Min**	**Ave**	**Max**	**SD**
Moisture %	8.4	12.0	14.0	1.6	10.9	12.4	15.5	1.1
Ash %	1.6	5.5	33.4	8.3	1.0	3.5	12.5	3.3
Volatile Matter %	29.2	37.1	42.0	3.0	33.6	37.1	41.7	1.8
Fixed Carbon %	29.0	45.5	48.8	5.1	42.4	47.6	50.7	2.0
Sulphur %	0.19	0.25	0.38	0.05	0.22	0.25	0.29	0.02
Calorific Value (MJ/kg)	16.55	24.96	28.18	2.62	23.49	25.67	27.91	1.19

Min = minimum, Ave = average, Max = maximum, SD = standard deviation

At the Ruawaro 1 location, the Renown and Kupakupa seams are separated by approximately 10 m of interburden. The Renown seam is split into three beds, as indicated by the non-sampled intervals corresponding to non-coal material in the profiles in Figure 3.2. Additionally a basal split is present for the Kupakupa seam. With the exception of two high-ash coal/ carbonaceous mudstone samples collected in the Renown seam, coal properties do not exhibit much variation. The two high-ash samples have been removed from the averages presented in Table 3.2. However, even with these two samples removed, the average ash yield for the Renown (5.1%) is still more than double that of the Kupakupa seam, which has several samples with exceptionally low (<2%) ash yields. A slight increase in both ash yield and sulphur content can be seen towards the top and base of the Kupakupa seam.

At the Ruawaro 2 location the Renown and Kupakupa seams are separated by approximately 18 m of interburden with a few thin splits identified in the Renown seam (see macroscopic logging sheets in Appendix 2) which can be noted in the ash yield profile (Figure 3.3). Between the higher ash yield peaks in the lower part of the Renown seam, moisture levels are elevated compared to those seen in the rest of the profile. Most of this interval was logged as being non-coal (Fig. 4.6). Although the other samples in the Renown seam have very low ash yields, the samples from the Kupakupa seam are even lower (Table 3.3) with seven out of the eleven samples having ash yields of <2%. As is expected there is a decrease in volatile matter and fixed carbon associated with the high ash yield sample at the base of the Renown, while the high ash yield sample at the base of the Kupakupa is also associated with a slight increase in sulphur content.

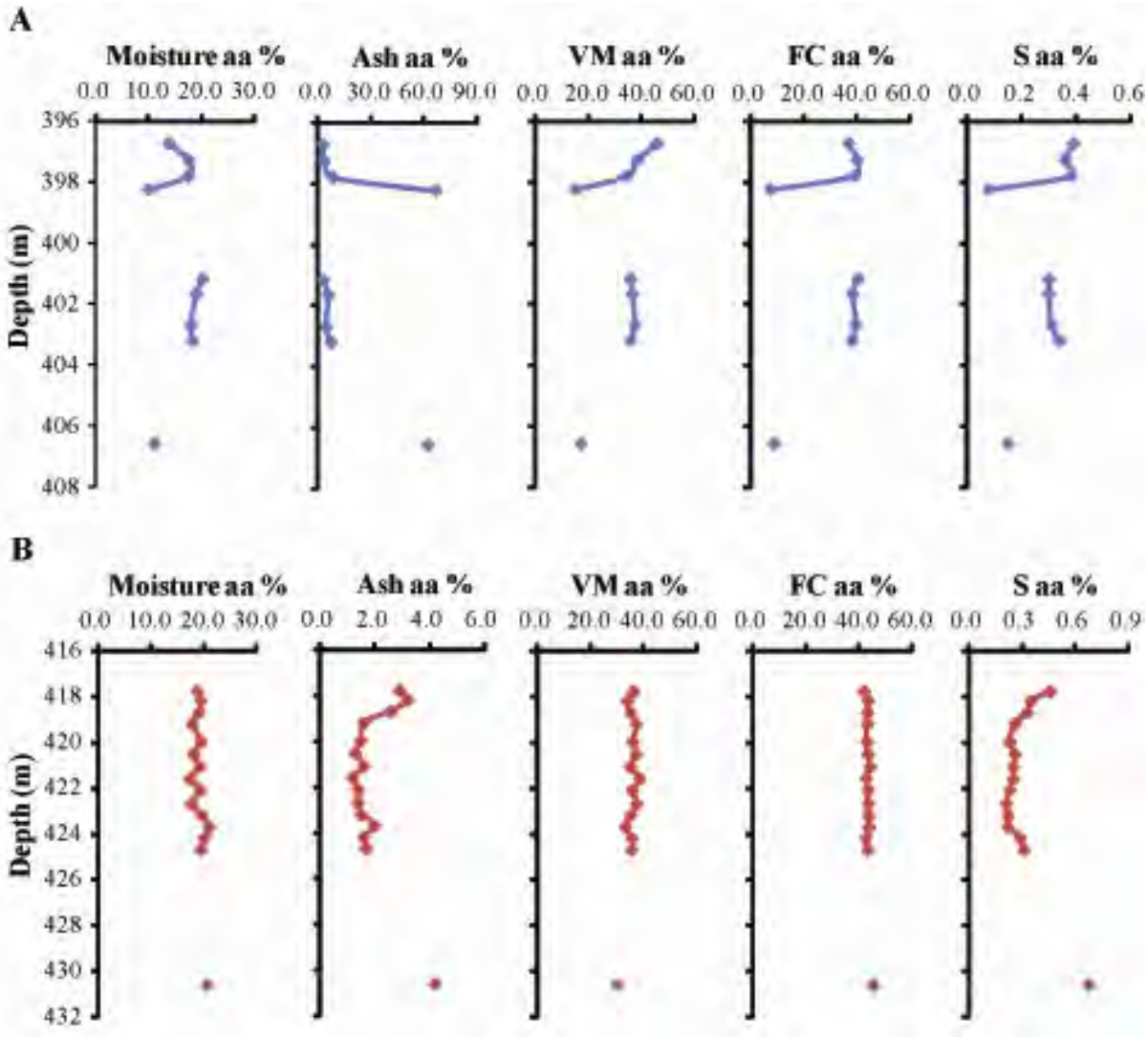

Figure 3. 2. Proximate results of samples from the (A) Renown and (B) Kupakupa seams at the Ruawaro 1 location on an as analysed basis, aa.

Table 3. 2. Average proximate results by seam for the Ruawaro 1 location on an as analysed basis.

	Renown seam				Kupakupa seam			
As analysed basis	**Min**	**Ave**	**Max**	**SD**	**Min**	**Ave**	**Max**	**SD**
Moisture %	13.9	17.8	20.2	1.9	17.3	19.1	21.0	1.1
Ash %	2.9	5.1	8.6	2.2	1.2	2.0	4.2	0.9
Volatile Matter %	34.5	37.9	46.0	3.8	29.9	35.5	38.7	2.1
Fixed Carbon %	37.2	39.2	40.7	1.2	41.9	43.4	45.4	0.8
Sulphur %	0.30	0.34	0.39	0.04	0.21	0.30	0.68	0.12
Calorific Value (MJ/kg)	22.84	23.98	27.02	1.45	23.00	24.16	25.26	0.63

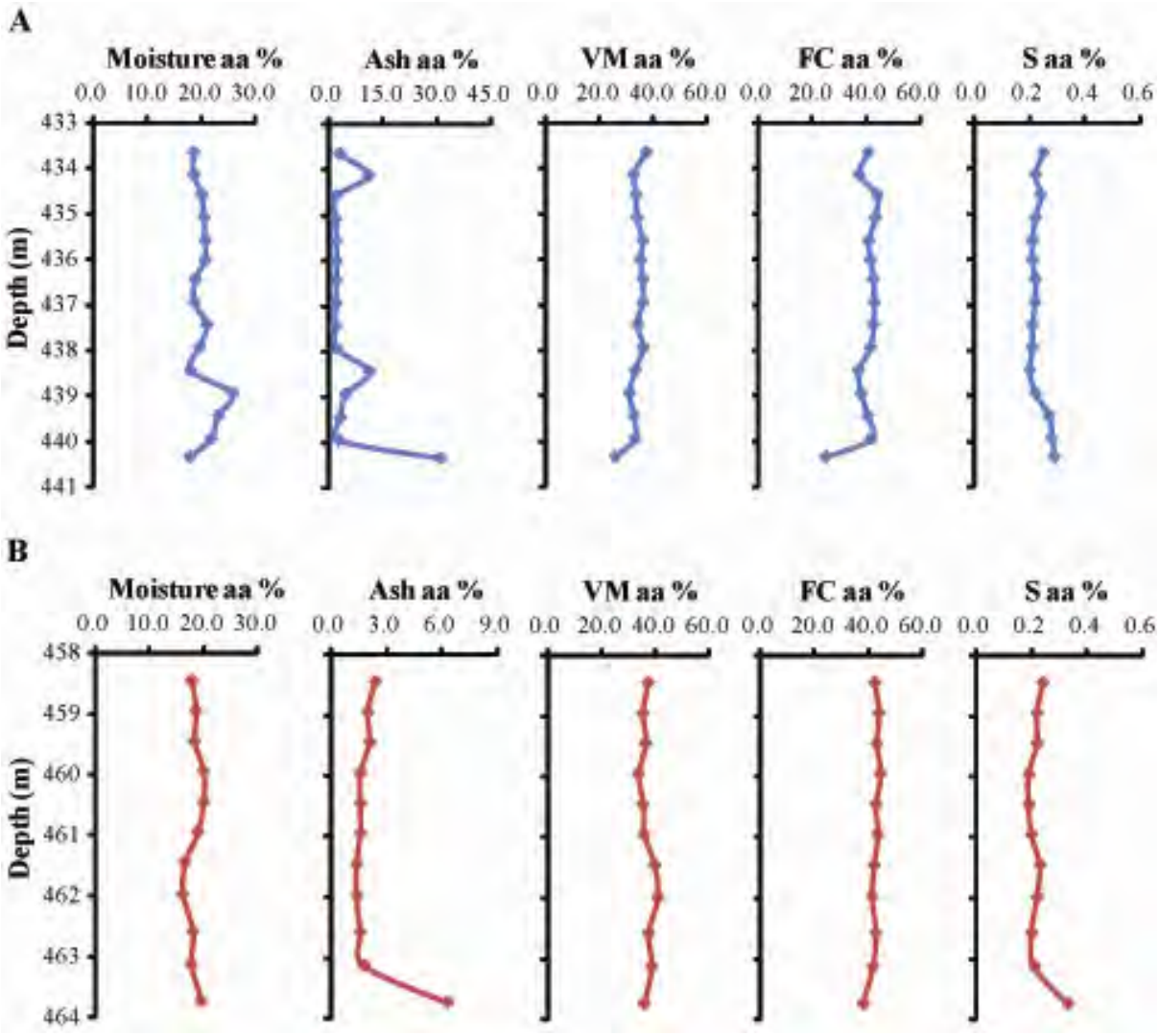

Figure 3. 3. Proximate results of samples from the (A) Renown and (B) Kupakupa seams at the Ruawaro 2 location on an as analysed basis, aa.

Table 3. 3. Average proximate results by seam for the Ruawaro 2 location on an as analysed basis.

	Renown seam				Kupakupa seam			
As analysed basis	**Min**	**Ave**	**Max**	**SD**	**Min**	**Ave**	**Max**	**SD**
Moisture %	18.0	20.4	25.8	2.1	16.2	18.4	20.1	1.3
Ash %	1.9	5.6	31.2	7.7	1.4	2.2	6.3	1.4
Volatile Matter %	25.7	33.9	37.5	2.9	33.8	37.0	41.0	2.1
Fixed Carbon %	25.1	40.1	44.1	4.7	38.1	42.4	44.5	1.7
Sulphur %	0.20	0.23	0.29	0.03	0.19	0.22	0.33	0.04
Calorific Value (MJ/kg)	15.25	22.37	23.96	2.21	23.04	24.60	26.24	0.96

The Renown seam at the Rotongaro 1 location is quite thin while the Kupakupa seam is reasonably thick. At this location the two seams are separated by around 10 m of interburden. Slight increases in sulphur content can again be seen around the top and base of the seams (Figure 3.4). At around 451 m in the upper part of the Kupakupa seam there is a peak in volatile matter, along with a decrease in moisture content and fixed carbon. Unfortunately organic petrology, which may have helped explain this curious trend in geochemical parameters, was not conducted on this sample. Once again, the lower part of the Kupakupa seam is characterised by ash yields of <2%. Average values for the seams are presented in Table 3.4.

The northern-most and deepest drill hole in this study is the Mangapiko 1 drill hole. At this location the two seams are separated by around 25 m of interburden. The top of the Renown seam is characterised by interbedded carbonaceous mudstones, high ash coal and coal (Figure 3.5). Both sulphur and moisture content increase slightly towards the base of the Renown seam. The top sample of the Kupakupa seam has slightly elevated fixed carbon and sulphur contents. While the reason for this is unclear, the sample immediately below the high sulphur sample has high moisture content. The top eight samples in the Kupakupa seam have ash yields of <2% with ash yields increasing at the base of the profile. Unfortunately, the drill core did not reach the base of the seam because of drilling problems. Based on surrounding well data, it is believed that almost the full length of the seam is represented in the Mangapiko 1 core. Average results by seam are presented in Table 3.5.

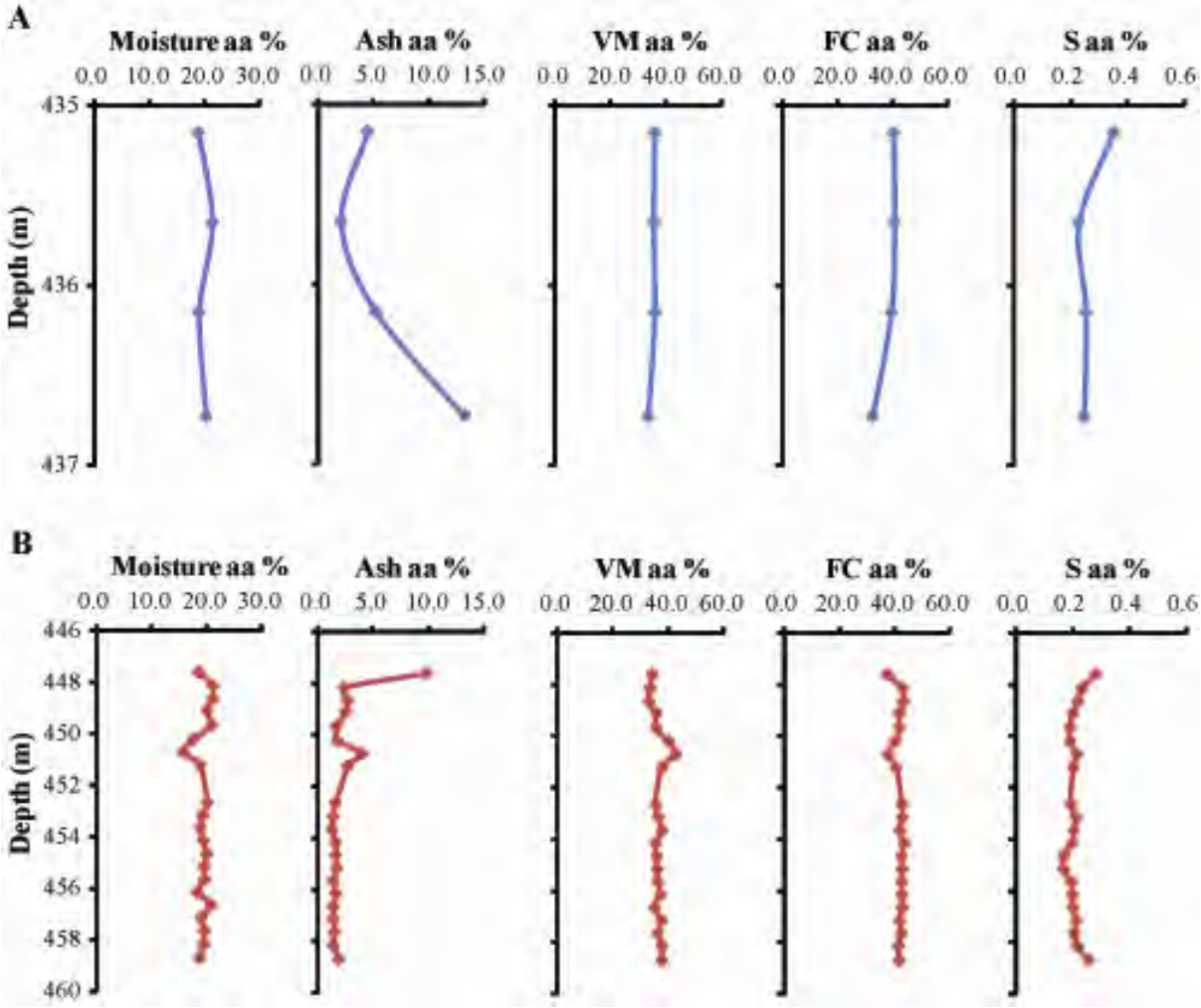

Figure 3. 4. Proximate results of samples from the (A) Renown and (B) Kupakupa seams at the Rotongaro 1 location on an as analysed basis, aa.

Table 3. 4. Average proximate results by seam for the Rotongaro 1 location on an as analysed basis.

	Renown seam				Kupakupa seam			
As analysed basis	**Min**	**Ave**	**Max**	**SD**	**Min**	**Ave**	**Max**	**SD**
Moisture %	18.9	19.9	21.4	1.2	15.7	19.3	21.1	1.3
Ash %	2.1	6.3	13.2	4.8	1.3	2.3	9.8	1.9
Volatile Matter %	33.7	35.4	36.1	1.1	33.1	36.7	42.8	2.2
Fixed Carbon %	32.8	38.5	40.9	3.8	37.4	41.7	43.4	1.6
Sulphur %	0.23	0.27	0.35	0.06	0.17	0.21	0.28	0.03
Calorific Value (MJ/kg)	20.05	22.22	23.06	1.45	21.30	23.71	25.45	0.85

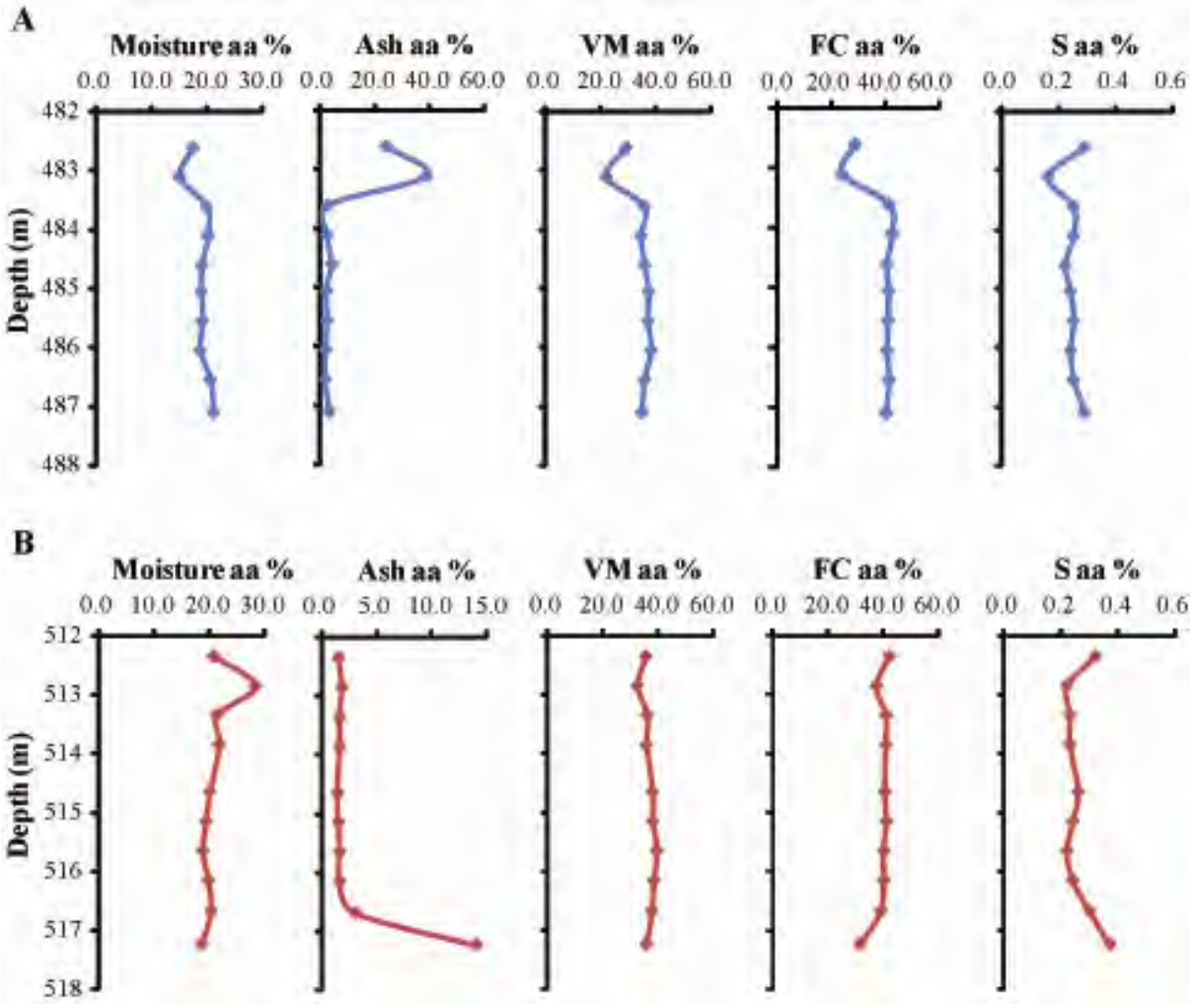

Figure 3. 5. Proximate results of samples from the (A) Renown and (B) Kupakupa seams at the Mangapiko 1 location on an as analysed basis, aa.

Table 3. 5. Average proximate results by seam for the Mangapiko 1 location on an as analysed basis.

	Renown seam				Kupakupa seam			
As analysed basis	**Min**	**Ave**	**Max**	**SD**	**Min**	**Ave**	**Max**	**SD**
Moisture %	15.1	19.1	21.2	1.7	18.7	21.0	28.4	2.8
Ash %	2.1	8.6	38.9	12.6	1.4	3.0	14.0	3.9
Volatile Matter %	21.8	33.9	38.1	4.9	32.4	36.8	39.6	2.1
Fixed Carbon %	24.2	38.4	42.7	6.3	31.5	39.3	42.0	3.0
Sulphur %	0.16	0.24	0.29	0.04	0.22	0.26	0.37	0.05
Calorific Value (MJ/kg)	13.57	21.96	24.16	3.50	20.65	23.39	24.80	1.39

The three remaining drill holes, Jasper 1, Mimi 1 and Baco 1, were drilled as part of a pilot production trial. These wells only intersected and cored the Renown seam. For these three cores the top of the Renown seam (approximately 0.5 m) is missing as the drilling procedure was to open the hole until the top of the seam and then core. As such, information about the top of the seam has not been captured.

At the Jasper 1 location the first sample collected at the top of the Renown seam is characterised by interbedded high ash coal and mudstone (Figure 3.6). Note that the two stratigraphically lower samples were taken in the carbonaceous mudstone interburden to determine what gas may be held in those rock types. Because of their very high ash yield, these three samples have been excluded from the averages presented in Table 3.6. A slight peak in moisture content can be seen for the fourth sample, with a corresponding decrease in volatile matter content. There is also a slight increase in sulphur towards the top and base of the seam. Aside from these features the proximate analysis profiles are fairly uniform.

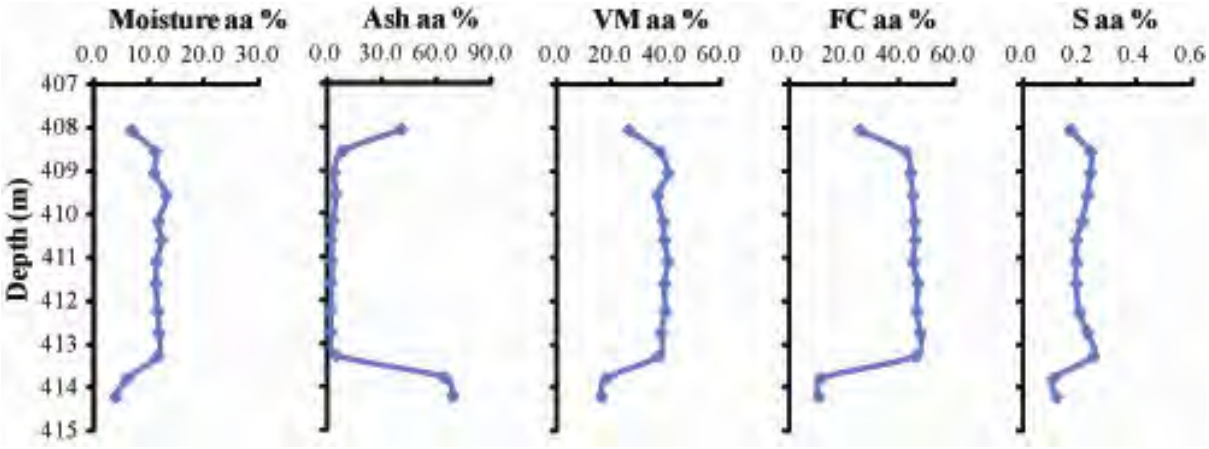

Figure 3. 6. Proximate results of samples from the Renown seam at the Jasper 1 location on an as analysed basis, aa.

Table 3. 6. Average proximate results by seam for the Jasper 1 location on an as analysed basis.

	Renown seam			
As analysed basis	**Min**	**Ave**	**Max**	**SD**
Moisture %	11.0	11.7	13.2	0.6
Ash %	2.3	4.0	9.0	2.1
Volatile Matter %	36.9	38.9	40.7	1.3
Fixed Carbon %	42.2	45.5	47.7	1.5
Sulphur %	0.19	0.22	0.25	0.02
Calorific Value (MJ/kg)	22.96	25.26	26.10	0.97

As with the Jasper 1 location, the lower most sample in the Mimi 1 drill core (Figure 3.7) is carbonaceous mudstone. Again this was deliberately collected to assess the gas content of this rock type, and has been excluded from the averages presented in Table 3.7. Of note there is a peak in volatile matter content near the top of the profile with decreased moisture contents. The lower part of the profile has lower moisture contents which could be a function of sample treatment. There is a slight increase in sulphur towards the top and base of the seam.

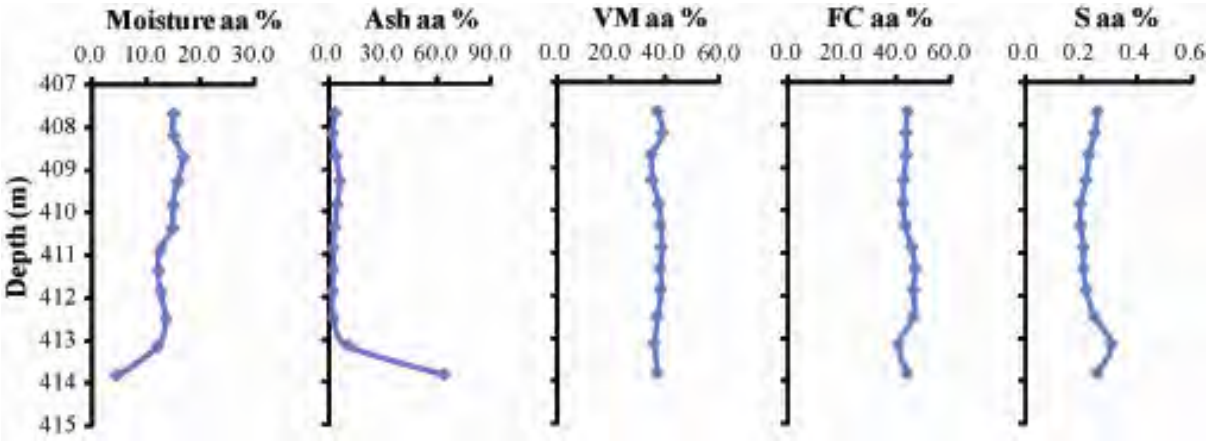

Figure 3. 7. Proximate results of samples from the Renown seam at the Mimi 1 location on an as analysed basis, aa.

Table 3. 7. Average proximate results by seam for the Mimi 1 location on an as analysed basis.

	Renown seam			
As analysed basis	**Min**	**Ave**	**Max**	**SD**
Moisture %	12.1	14.2	16.9	1.6
Ash %	2.2	4.1	10.8	2.5
Volatile Matter %	35.2	37.4	39.0	1.4
Fixed Carbon %	41.0	44.3	47.1	1.9
Sulphur %	0.20	0.23	0.31	0.03
Calorific Value (MJ/kg)	23.29	24.60	25.62	0.90

At the Baco 1 drill hole, only three metres of core was retrieved because of coring difficulties. Results for the Baco 1 location are reasonably homogeneous throughout the seam (Fig. 3.8 and Table 3.8) aside from a slight increase in ash yield and sulphur at the top of the core.

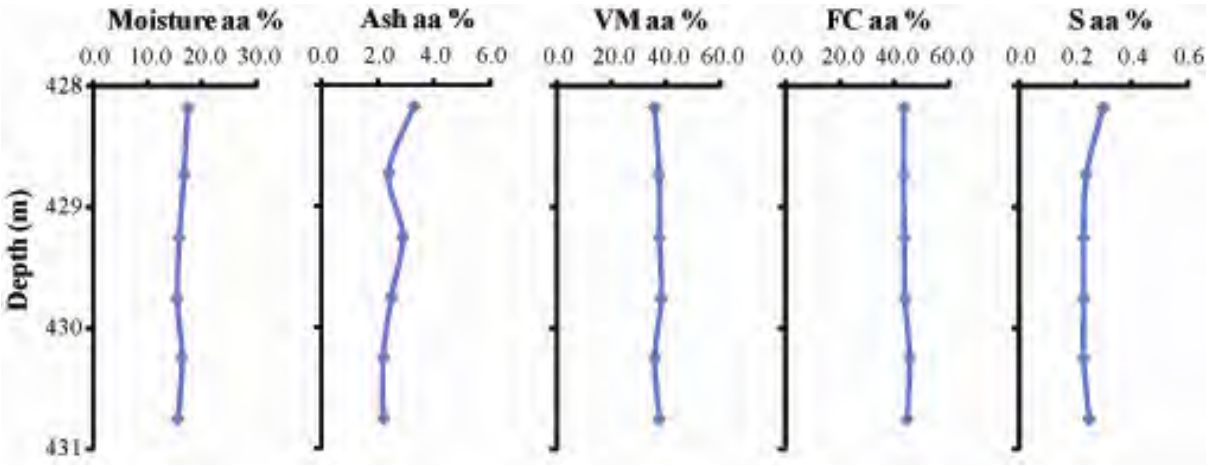

Figure 3. 8. Proximate results of samples from the Renown seam at the Baco 1 location on an as analysed basis, aa.

Table 3. 8. Average proximate results by seam for the Baco 1 location on an as analysed basis.

	Renown seam			
As analysed basis	**Min**	**Ave**	**Max**	**SD**
Moisture %	15.4	16.2	17.4	0.8
Ash %	2.2	2.6	3.3	0.4
Volatile Matter %	35.9	37.2	38.3	1.0
Fixed Carbon %	43.4	44.1	45.5	0.8
Sulphur %	0.23	0.25	0.30	0.03
Calorific Value (MJ/kg)	24.30	24.78	25.11	0.29

3.2.2. Proximate analysis results by seam

The largest source of variation present in the individual drill hole results occurs when ash yield is high. The histogram produced using the ash yields for all samples, shown in Figure 3.9A, shows a clear break between samples with ash yields <20%, (aa), and those with ash yields >20%, (aa). Overall 81% of samples have ash yields of <5%, 90% of samples have <10%, while 94% of samples have ash yields of <20%. As can be seen in Figure 3.9B, the lowest ash yields are samples from the Kupakupa seam, with 64% having ash yields of <2% and 89% of samples having ash yields of <5%. In contrast, for the Renown seam has only 7% of samples with ash yields of <2%. Samples with ash yields of <5% account for 72% of all samples.

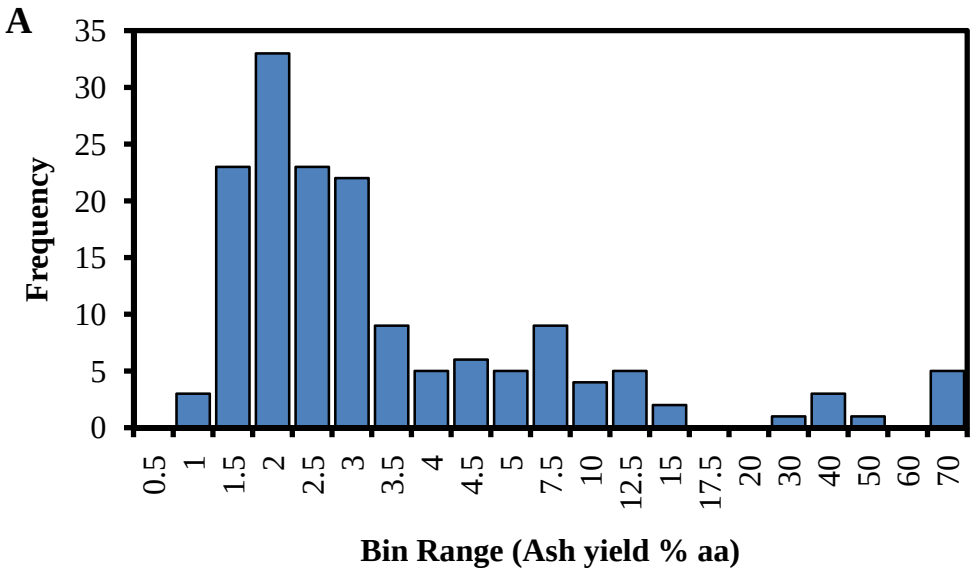

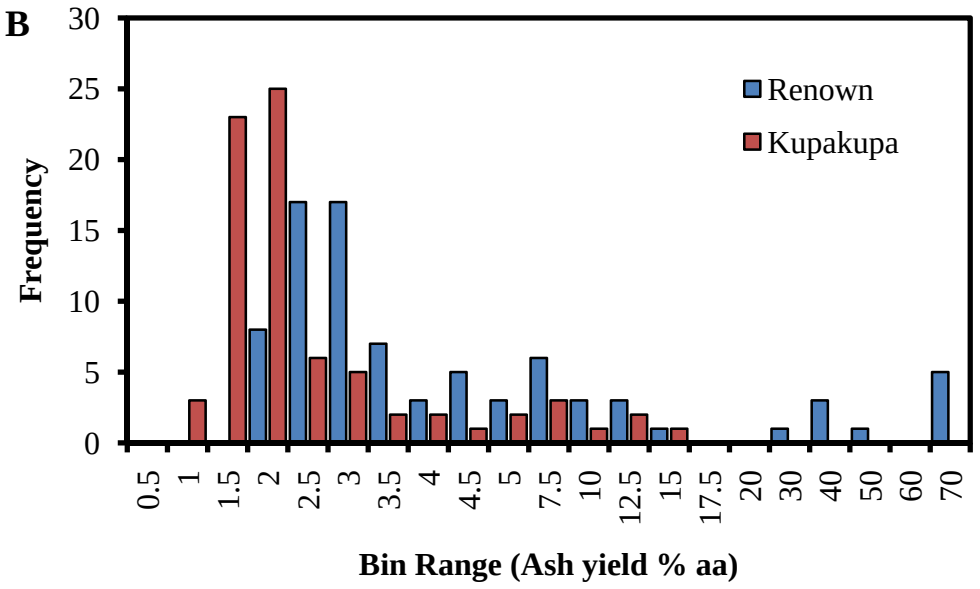

Figure 3. 9. (A) Histogram showing the distribution of coal ash yield for all samples and (B) Histogram showing the distribution of coal ash yield, for both the Renown and Kupakupa seams. All data is on an as analysed basis. Note the bin range is not linear.

Based upon these results, samples with >20% ash yield (aa) have been excluded from further analysis. Only ten samples had to be excluded. The average proximate analysis for the Renown and Kupakupa coal seams, grouped by location, is presented in Figures 3.10 A and B with overall results presented in Figure 3.10C. Greater variability can be seen in the Renown seam than in the Kupakupa seam which is consistent with results given in section 3.1.2. Of the results presented, the greatest variability exists with the percent moisture, which is also the most difficult to accurately measure because of pre-analysis sample treatment. The main concern with the moisture data is that the 2003 (TW1) and 2006 data (Jasper 1, Mimi 1 and Baco 1) are different from the 2005 data (which are all similar). Gas sampling was the priority of the sampling program and there was not a standard time between collection and proximate analysis. Additionally the Jasper 1, Mimi 1 and Baco 1 results all show significantly lower moisture contents than the Renown seam at the nearby Ruawaro 2 drill hole. Hence, differences in moisture content between seams and locations cannot be stated with confidence.

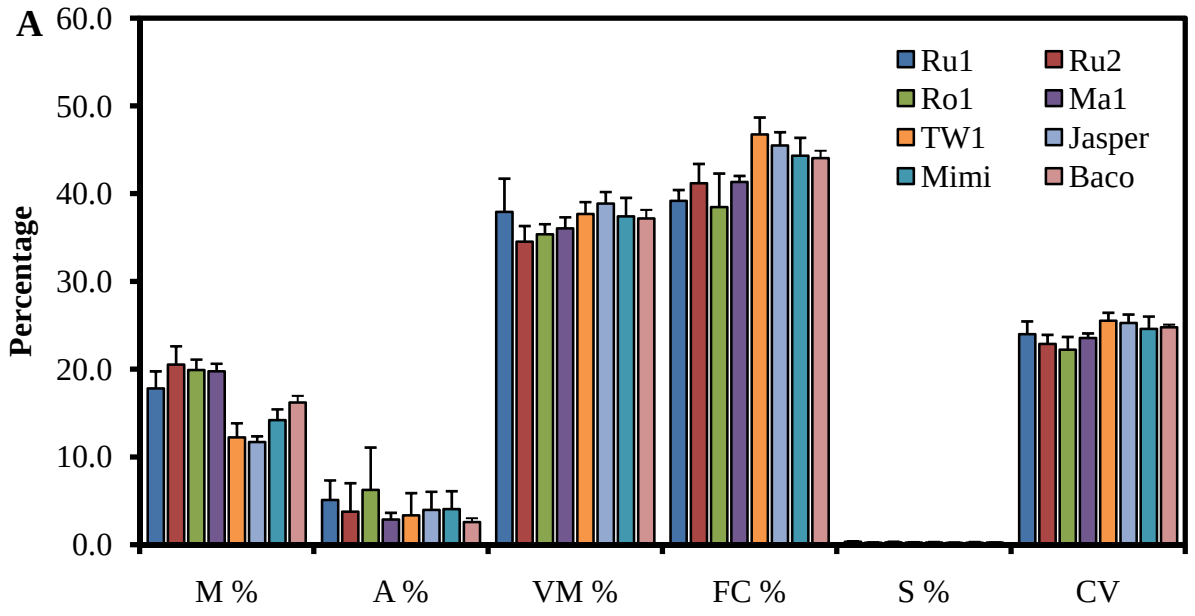
A
60.0
50.0
40.0
30.0
20.0
10.0
0.0
Percentage
Ru1
Ru2
Ro1
Ma1
TW1
Jasper
Mimi
Baco
M %
A %
VM %
FC %
S %
CV

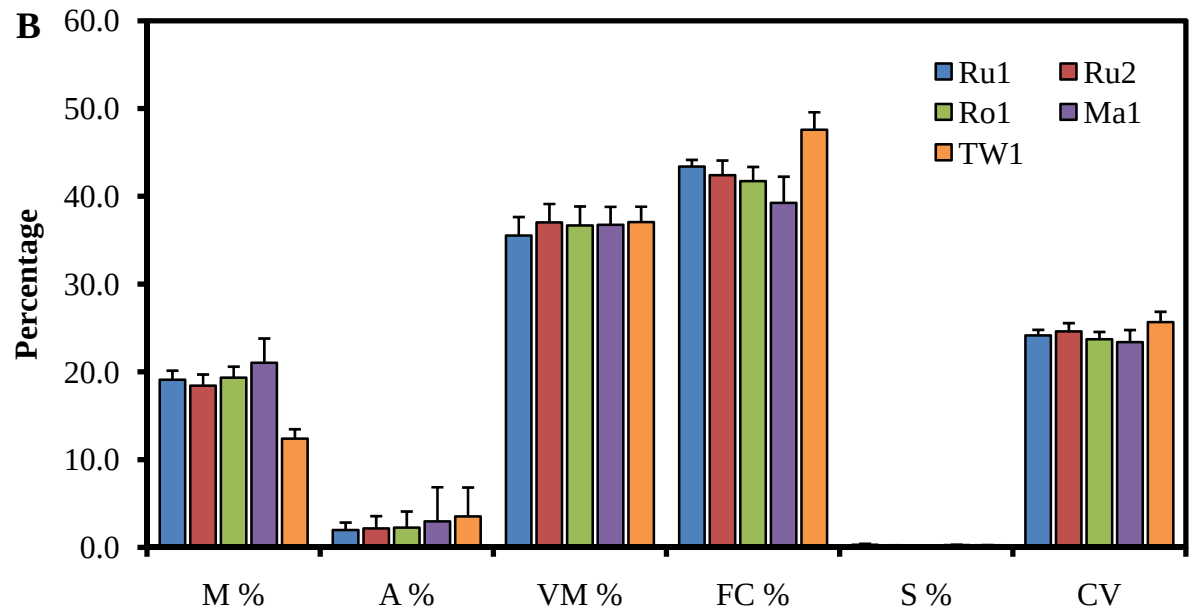
B
60.0
50.0
40.0
30.0
20.0
10.0
0.0
Percentage
Ru1
Ru2
Ro1
Ma1
TW1
M %
A %
VM %
FC %
S %
CV

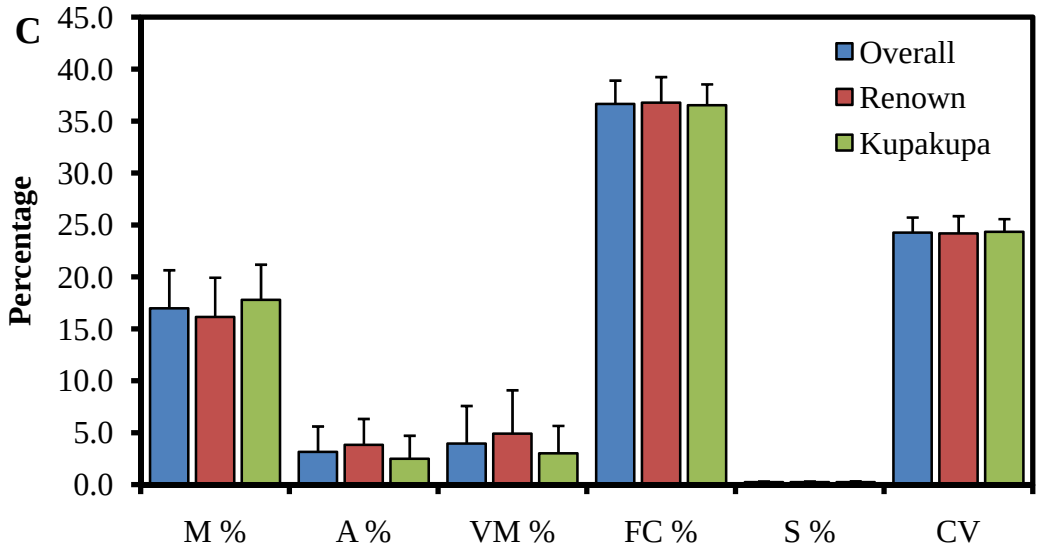

Figure 3. 10. Average proximate results by location for the (A) Renown seam, (B) the Kupakupa seam, and (C) overall and by seam on an as analysed basis. M = moisture, A = ash yield, VM = volatile matter, S = sulphur and CV = calorific value (MJ/kg).

In the overall results it can be seen that the average fixed carbon and calorific values are the same for the two seams; in contrast the Kupakupa has a lower ash yield, lower volatile matter and higher moisture content than the Renown seam. If the influence of moisture is removed (Figure 3.11), it can be seen that the Kupakupa seam still shows lower ash yield, but with fractionally higher volatile matter and fixed carbon contents.

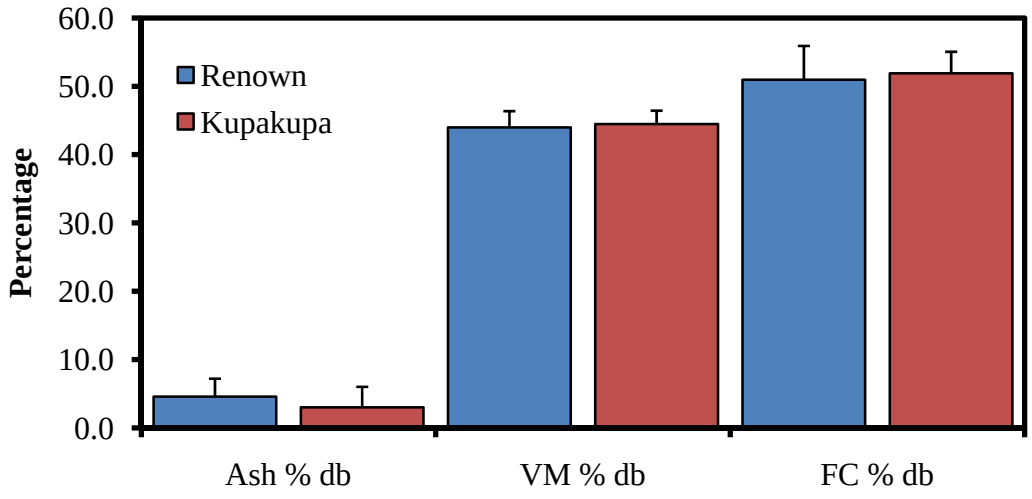

Figure 3. 11. Average proximate results overall and by seam with the influence of moisture content removed (dry basis, db).

3.3. Ash constituents

3.3.1. Ash constituent analysis results by drill hole

Ash constituent results do not add up to 100% (Appendix 1) as other, unanalysed elements may be present as well as possibly some loss on ignition occurring, as mentioned in section 2.2.4. As such, the data used for Figures 3.12 – 3.19 has been normalized. The results for TW1 (Figure 3.12) have been presented previously by Butland (2006) who reported that whole coal elemental scans of pressed coal pellets also revealed significant strontium, along with smaller amounts of zinc, nickel, copper, barium and cerium.

The silicon profile for the Renown seam in TW1 is high (~60%) in the stratigraphically upper most sample and then decreases with depth. About mid seam there is another peak in silicon, before decreasing again until reaching the base where silicon is again high. Aluminium is present throughout in concentrations of 4.0% - 31.8%. The proportion of iron is relatively stable (1.2% - 8.8%) throughout while calcium, magnesium, sodium and sulphur are higher where silicon is low (up to 74.7%, 16.6%, 9.2% and 21.1% respectively). Samples 18 and 22 have higher ash yields than their surrounding samples (4.4% and 10.3% on a dry basis, db), with low silicon and aluminium percentages. Sample 18 has high calcium and magnesium while sample 22 has a very high percentage of calcium. Titanium is highest (up to 6.9%) where there are larger proportions of silicon and aluminium.

The Kupakupa seam profile has higher silicon and aluminium contents at the top and base of the seam, similar to the Renown seam, and as expected, these vary in direct relation with the ash yield. The exception to this is sample 35 (5.3% ash yield db) which again lacks silicon and aluminium and has a very high proportion of calcium (71.0%) and magnesium

(11.0%). Sample 32 has a very high titanium percentage (~12%) for a low ash yield sample (2.4%). In the low ash yield zone in the lower half of the Kupakupa seam, combined silicon and aluminium is around or <5% with titanium very low in this region (0.06% - 0.5%). This interval of the Kupakupa is characterised by higher proportions of iron, calcium, magnesium, sodium and sulphur. The low ash intervals of coals in the Waikato have previously been noted to have high iron, calcium and sodium which can increase a coal's tendency to 'clinker' (Moore and Fergusson, 1997). Phosphorous is identifiable in the top part of the profile (which has also been noted by Newman et al. (1997)) where there are higher silicon contents. Potassium is present in small amounts throughout both seams.

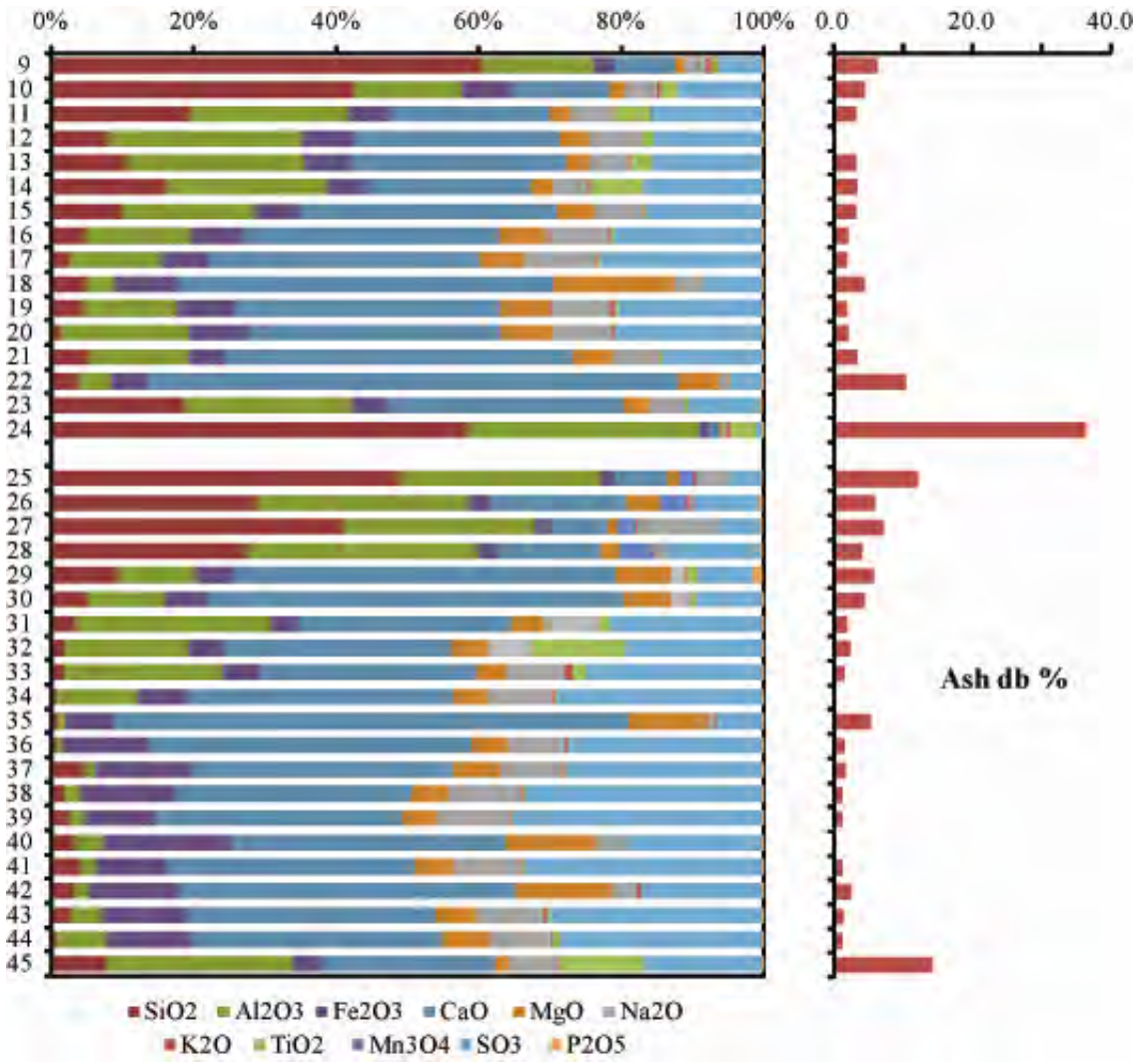

Figure 3. 12. Distribution of ash constituents for core from the TW1 drill hole.

The ash constituent distribution for the Ruawaro 1 location is presented in Figure 3.13. The Renown seam is split into several thin seams at this location and is characterised by high proportions of silicon and aluminium. Titanium is present throughout the Renown seam (0.7% - 4.0%) and interestingly there are high percentages of phosphorous in samples A8 - A12 (4.4% - 6.1%). The highest ash yield samples, A7 and A12 (74.4% and 70.0% db), have the highest percentages of potassium (1.8% and 2.0% respectively).

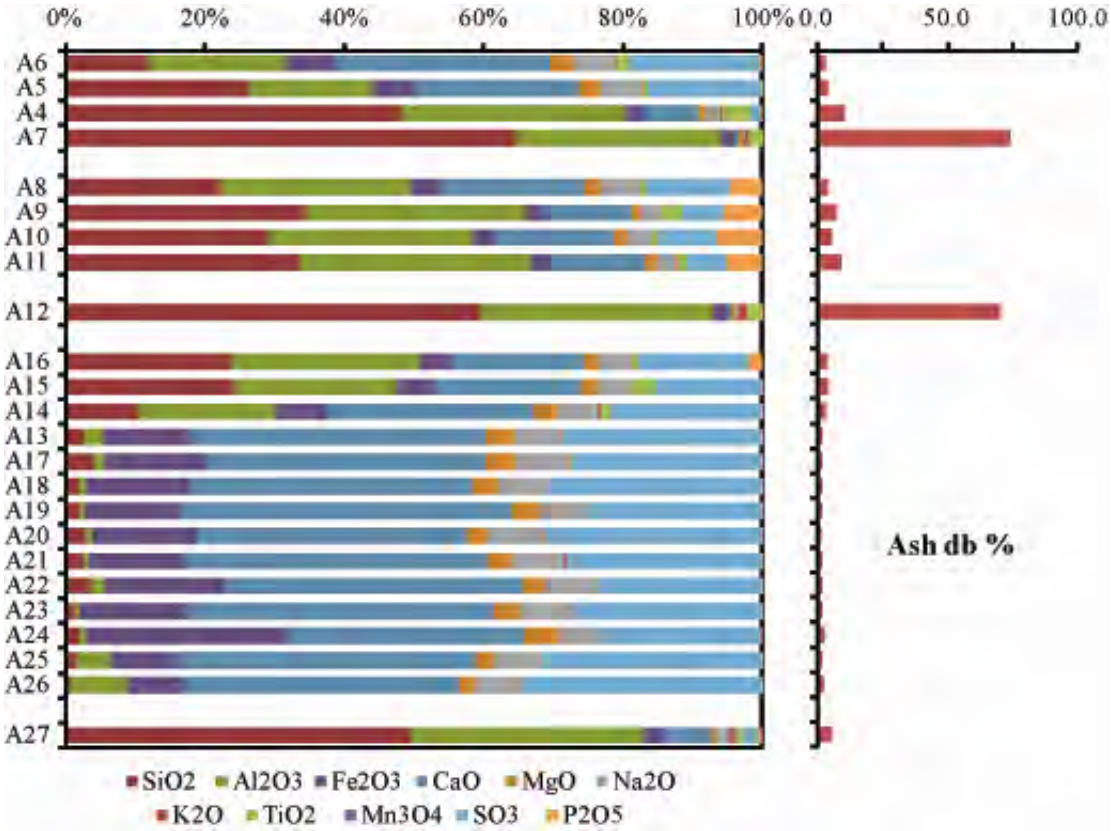

Figure 3. 13. Distribution of ash constituents for core from the Ruawaro 1 drill hole.

The Kupakupa seam has a similar profile to that seen in the TW1; that is, higher concentrations (>20%) of silicon and aluminium at the top and base of the seam and a distinct lack of silicon (< 3.2%), aluminium (<2%) and titanium (<0.2%) in the very low ash, lower part of the seam. This low ash region is characterised by higher proportions of iron, calcium,

magnesium, sodium and sulphur. The slightly higher ash sample at A24 (2.5% db) has a noticeably higher proportion of iron (26.7%). Phosphorous is again noticeable (>0.4%) in the top and bottom samples.

Ash constituent distribution at Ruawaro 2 distribution is shown in Figure 3.14. The silicon percentages are higher (>12%) at the top, middle and base of the Renown seam. Titanium is most noticeable in the lower section of the coal seam (>0.5%). The low silicon and aluminium intervals are again the samples with low ash yield, and are characterised by higher iron, calcium, magnesium, sodium and sulphur percentages. Phosphorous is noticeable in sample B2 (0.8%) while higher potassium can be seen in the lowest sample B15 (1.0%).

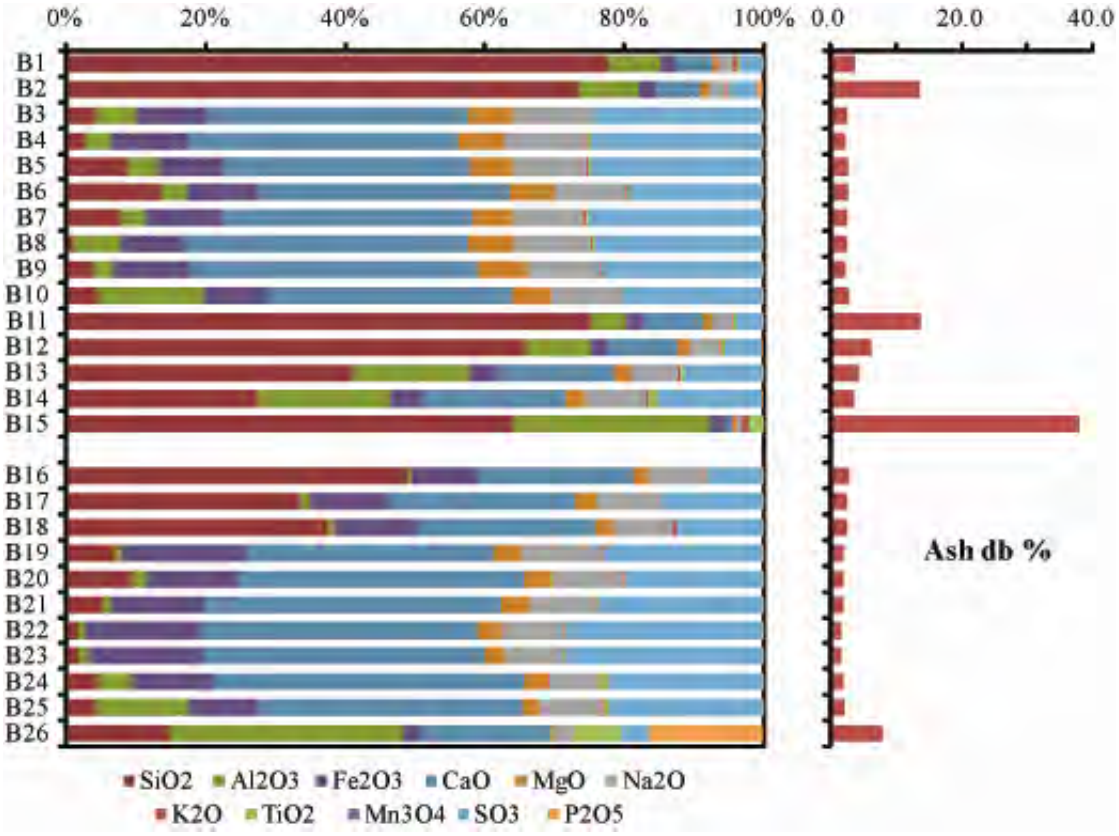

Figure 3. 14. Distribution of ash constituents for core from the Ruawaro 2 drill hole.

The Kupakupa seam at Ruawaro 2 follows a similar trend to that seen at the other locations, with silicon decreasing with depth and increasing again towards the base of the seam. Interestingly there is a distinct lack of aluminium (<2.0%) in the top half of the profile most noticeable in the top few samples with higher silicon contents. Titanium is also virtually absent (<0.12%) until the deepest three samples where aluminium percentages increase. There is a significant percentage (15%) of phosphorous in the deepest sample B26.

With the exception of sample C3, the Renown seam at the Rotongaro 1 location (Figure 3.15), shows ash constituent distribution similar to those seen for the top and base of the Renown seam at other locations. Titanium follows the pattern of aluminium, and potassium is up to 1.4% in sample C2 while phosphorous is proportionally high in C4 and C5 (1.4% and 1.7%, respectively).

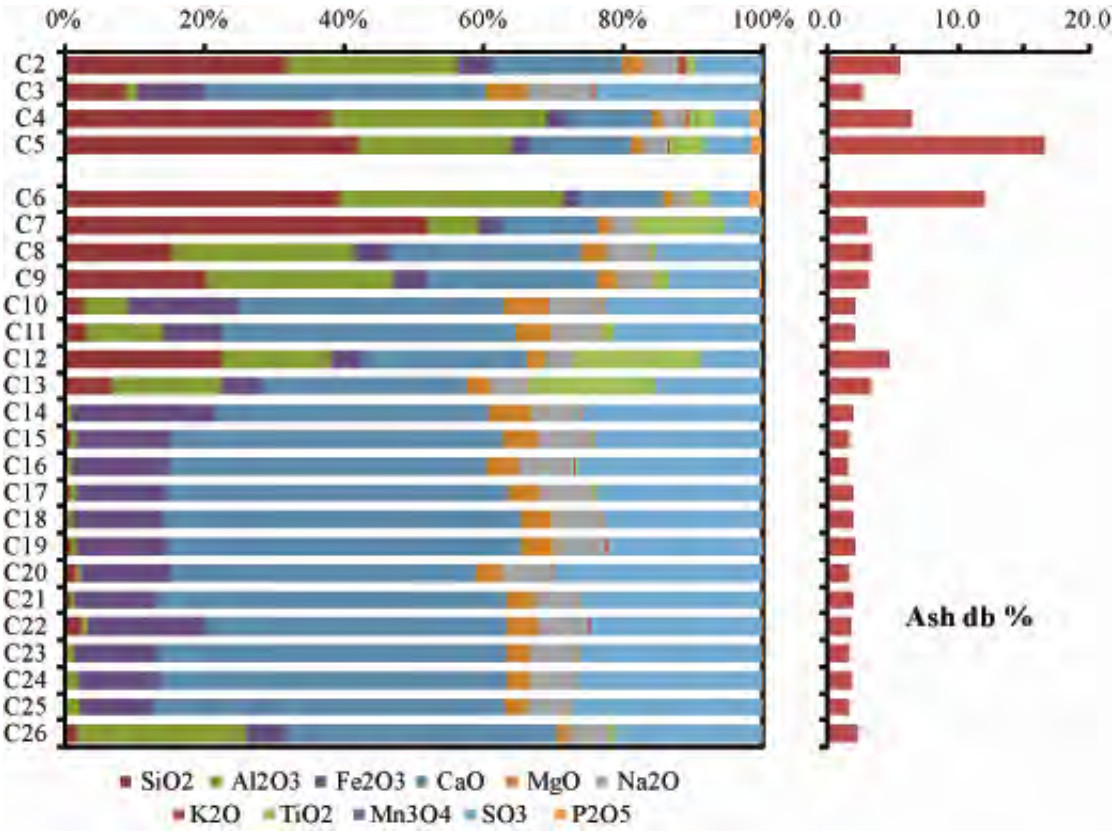

Figure 3. 15. Distribution of ash constituents for core from the Rotongaro 1 drill hole.

The upper part of the Kupakupa seam at the Rotongaro 1 location shows a decreasing contribution of silicon and aluminium with depth, with an increase again around sample C12 which also has a higher ash yield (4 % db). Samples C12 and C13 have high titanium percentages in comparison to the samples on either side (~17%), especially for low ash yield samples (<5%), while phosphorous is noticeable in the top sample C6 (1.8%). The lower part of the Kupakupa seam (C14 – C25) is remarkable for its homogeneity in ash yield (<2%) and ash composition. Silicon and titanium are virtually absent in this low ash yield region (0.06% - 2.15% and 0.08% - 0.20% respectively) with aluminium contributing only a very small amount (0.5% - 1.6%). The remaining elements in this region (which is around 6 m thick) are relatively uniform in concentration with calcium, sulphur and iron contributing the bulk of the ash yield. The deepest sample, C26, has a large concentration of aluminium (22.7%) although there is still only a minimal contribution of silicon.

Unsurprisingly at the top of the Renown seam at the Mangapiko 1 location (Figure 3.16), where there is some mudstone and high ash coal, silicon is the predominant ash constituent (≥80%). The silicon percentage can be seen to directly vary with ash yield. Interestingly the '∑' shaped distribution of silicon percentage in the Renown seam is similar to that seen in the TW1 and Ruawaro 2 cores. Phosphorous is noticeable in sample D10 (1.9%).

The Kupakupa seam, similar to the other locations, has higher concentrations of silicon, aluminium and titanium at the top and base of the seam. The centre of the seam shows relative homogeneity in the ash constituents, similar to what is seen at Rotongaro 1, albeit with slightly larger contributions of silicon and aluminium. Phosphorous increases towards the base of the Kupakupa seam (up to 2.2%).

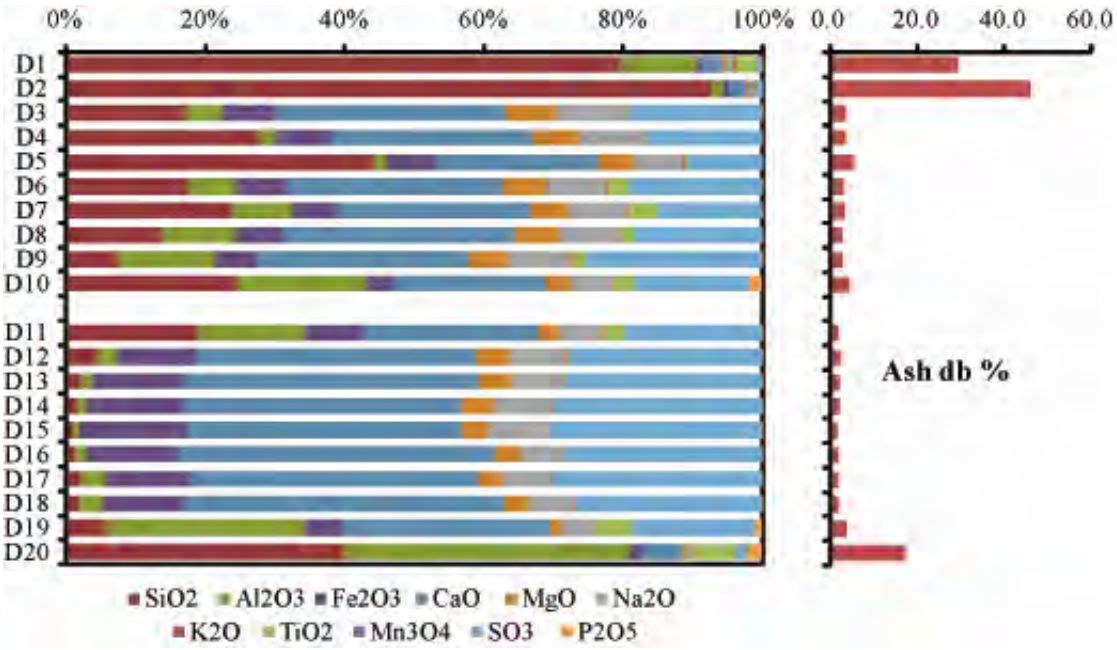

Figure 3. 16. Distribution of ash constituents for core from the Mangapiko 1 drill hole.

The distribution of ash constituents for the Jasper 1 location is presented in Figure 3.17. The Renown seam shows the same silicon pattern as seen at the locations already discussed, although there is more variability. Phosphorous is noticeable in sample J4 (1.7%), which is away from seam splits and seam edges, as well as in sample J11 (2.27%) which is the stratigraphically lowest coal sample. The composition of the carbonaceous mudstone is also presented here. The dominant constituents are silicon and aluminium, followed by titanium, iron, potassium, calcium and sodium in that order.

The Mimi 1 ash constituent profile is similar to that of Jasper 1 (Figure 3.18). Interestingly there is higher phosphorous in samples M3 and M4 (3.1% and 1.2%) at a similar depth into the profile. The phosphorous, in conjunction with the slightly higher ash yield and increase in silicon content, may hint at the possibility of a seam split nearby. The

carbonaceous mudstone sample, M12, has ash constituent proportions like those of J12 and J13.

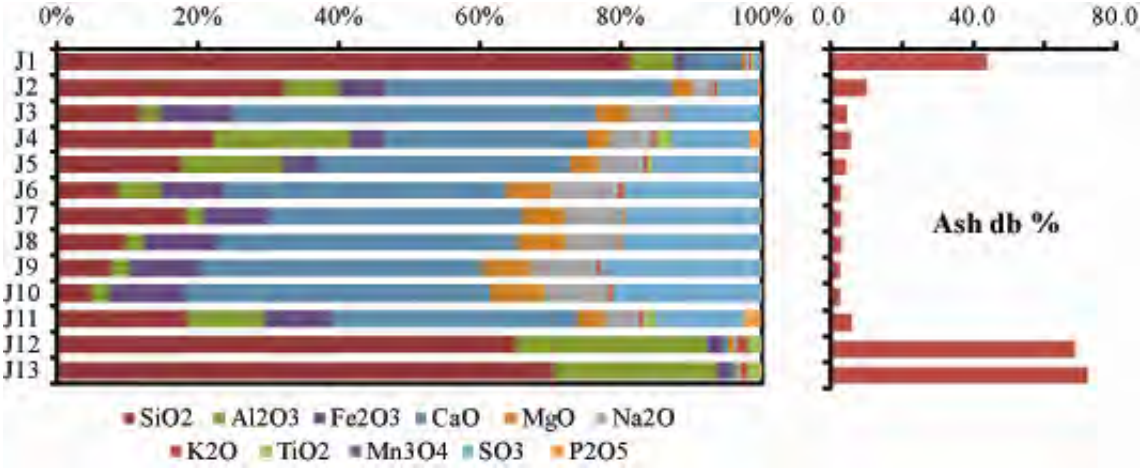

Figure 3. 17. Distribution of ash constituents for the core from the Jasper 1 drill hole.

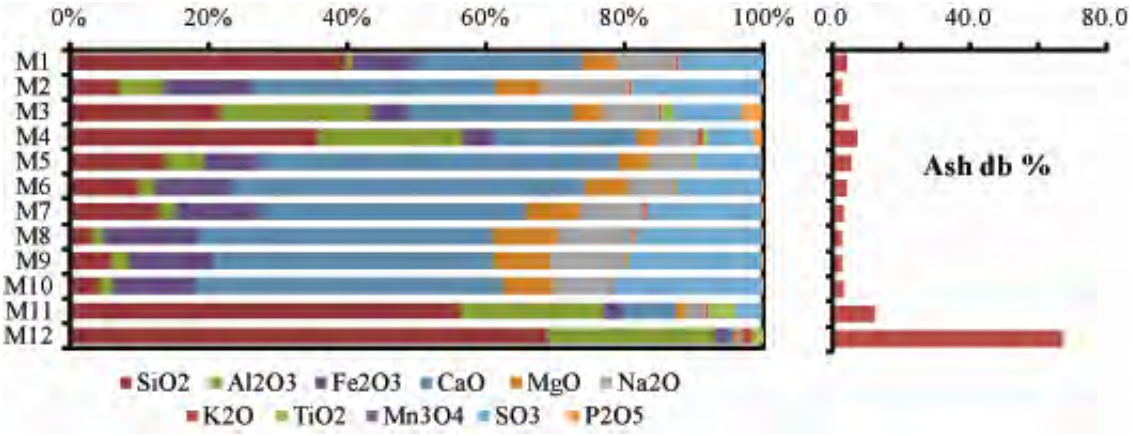

Figure 3. 18. Distribution of ash constituents for core from the Mimi 1 drill hole.

The ash constituent results for the Baco 1 location is presented in Figure 3.19. The silicon percentage roughly follows the ash yield profile and the element proportions are similar to those in the nearby Ruawaro 2 location.

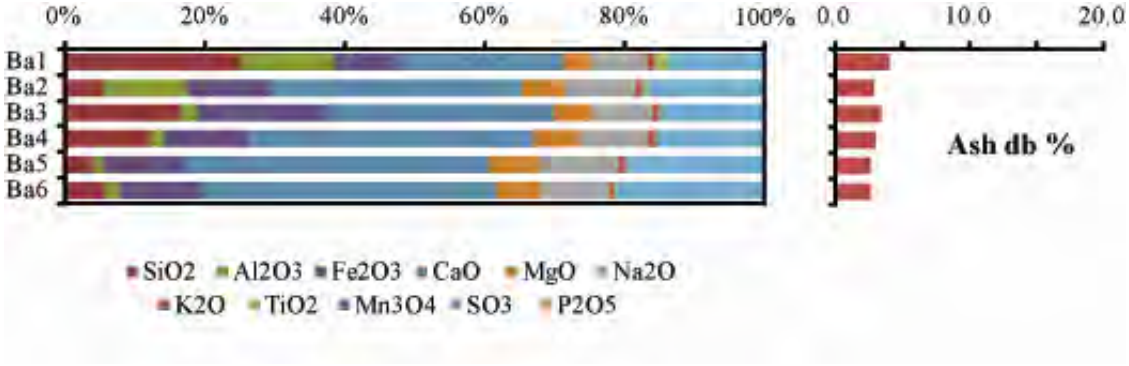

Figure 3. 19. Distribution of ash constituents for core from the Baco 1 drill hole.

3.3.2. Ash constituent analysis results by seam

As with the proximate analysis results presented in section 3.2.2, samples with >20% ash yield have been excluded from the results presented in this section. The average ash constituent results by location for the Renown and Kupakupa seams are presented in Figures 3.20A and B with overall results presented in Figure 3.20C. Again, greater variability can be seen in the Renown seam than in the Kupakupa seam possibly owing to the larger ash yields of the Renown seam samples. The Renown seam has higher silicon, aluminium, magnesium, sodium, potassium and phosphorous while the Kupakupa has higher average iron, calcium, titanium and sulphur. The largest differences in content between the seams are for silicon, calcium and sulphur. Notably, the Renown seam at the Ruawaro 1, Rotongaro 1 and TW1 locations has a 2 - 3 times greater proportion of aluminium than is present at the other locations.

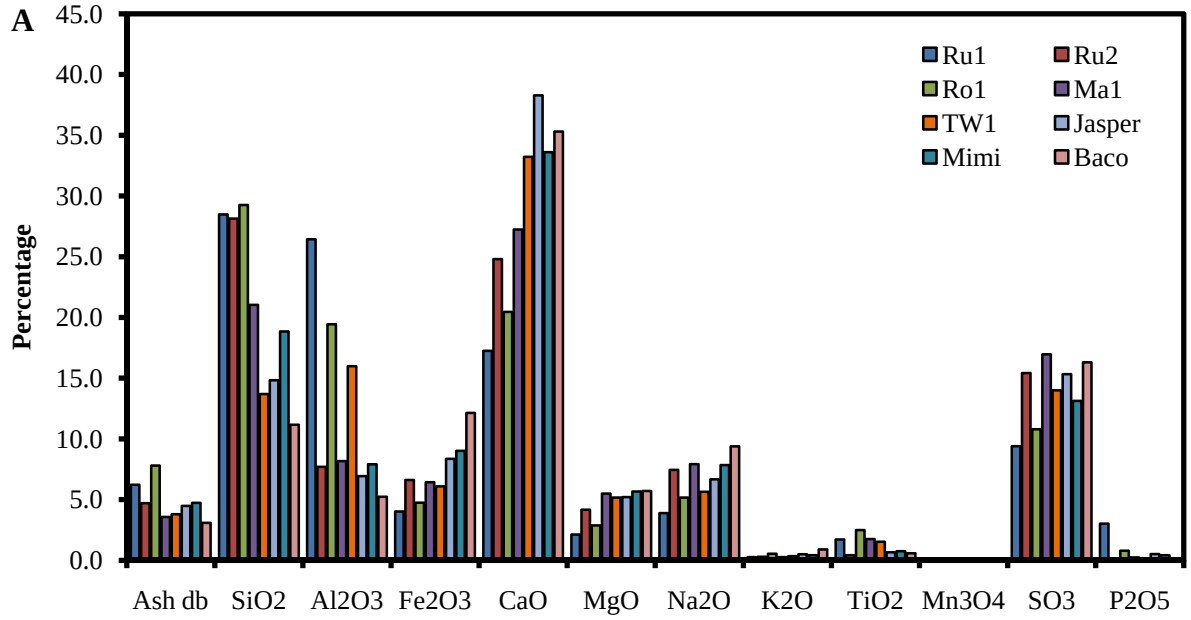
A
Percentage
45.0
40.0
35.0
30.0
25.0
20.0
15.0
10.0
5.0
0.0
Ru1
Ru2
Ro1
Ma1
TW1
Jasper
Mimi
Baco
Ash db
SiO2
Al2O3
Fe2O3
CaO
MgO
Na2O
K2O
TiO2
Mn3O4
SO3
P2O5

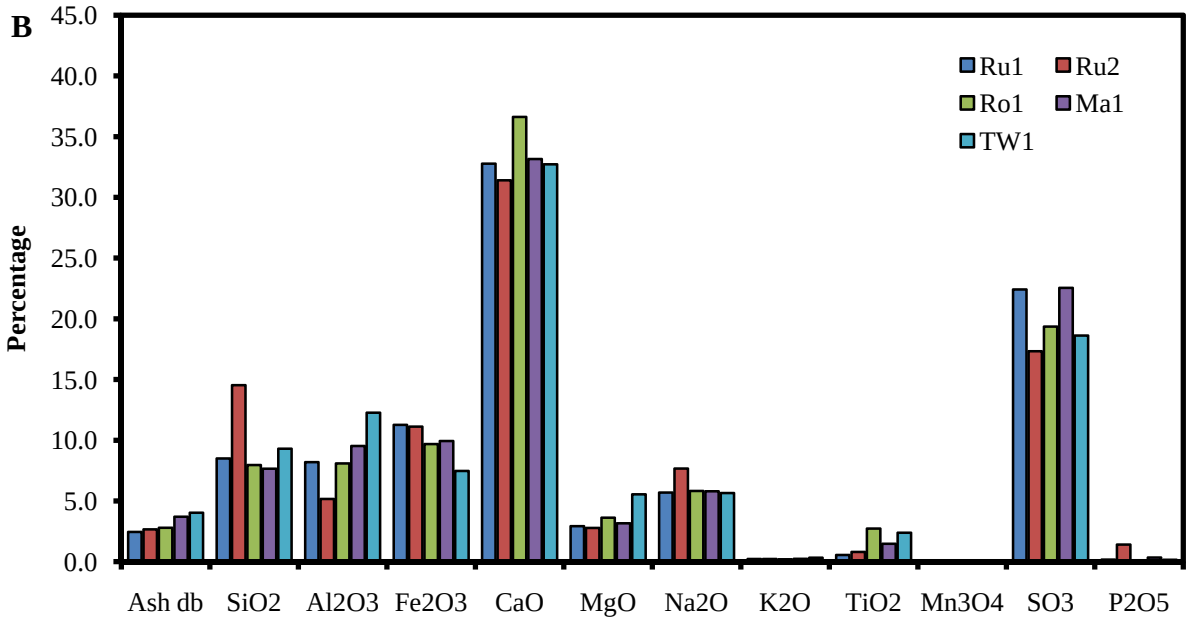
B
Percentage
45.0
40.0
35.0
30.0
25.0
20.0
15.0
10.0
5.0
0.0
Ru1
Ru2
Ro1
Ma1
TW1
Ash db
SiO2
Al2O3
Fe2O3
CaO
MgO
Na2O
K2O
TiO2
Mn3O4
SO3
P2O5

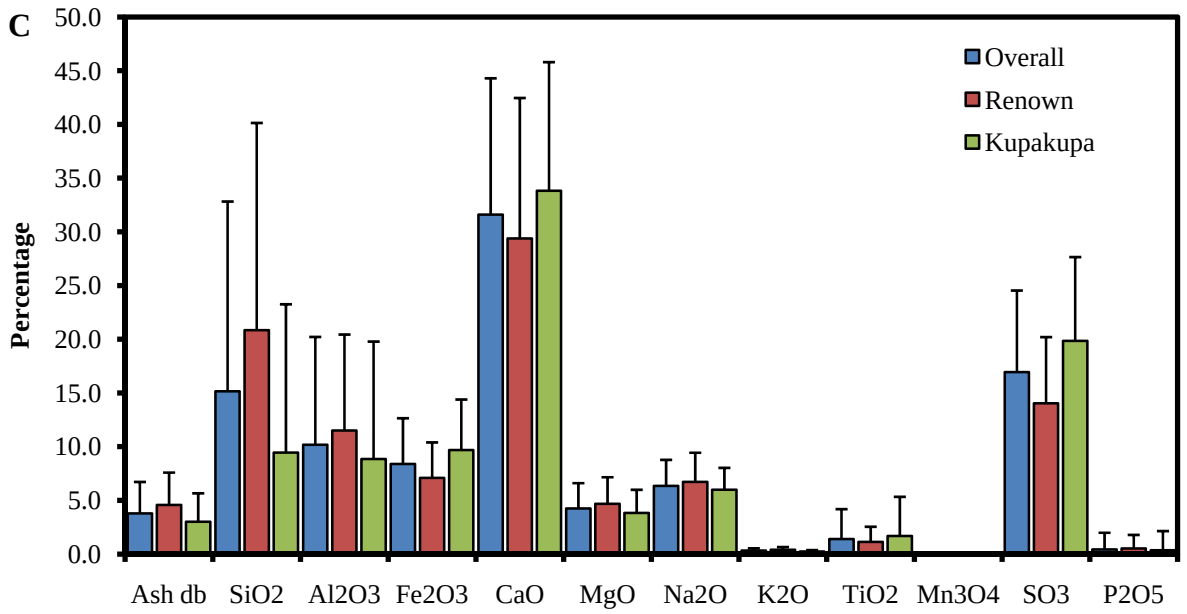

Figure 3. 20. Average ash constituents for (A) the Renown seam by location, (B) the Kupakupa seam by location and (C) overall and by seam. Ru1 = Ruawaro 1, Ru2 = Ruawaro 2, Ro1 = Rotongaro 1 and Ma1 = Mangapiko 1.

The low ash yield regions in the lower part of the Kupakupa seam were identified in section 3.2.1 as having different chemistry than the upper part of the seam; thus, it was decided to split the samples into two groups, those with <2% ash yield (as analysed, aa) and those with >2% ash yield (aa; these samples range from 2% - 14%). The average ash constituents for the two groups is presented in Figure 3.21. The two groups have clearly different signatures with the <2% group having higher iron, calcium, sodium and sulphur while the >2% group has higher silicon, aluminium, titanium and phosphorous although this group still has significant concentrations of calcium and sulphur. Both groups have the same proportion of magnesium present.

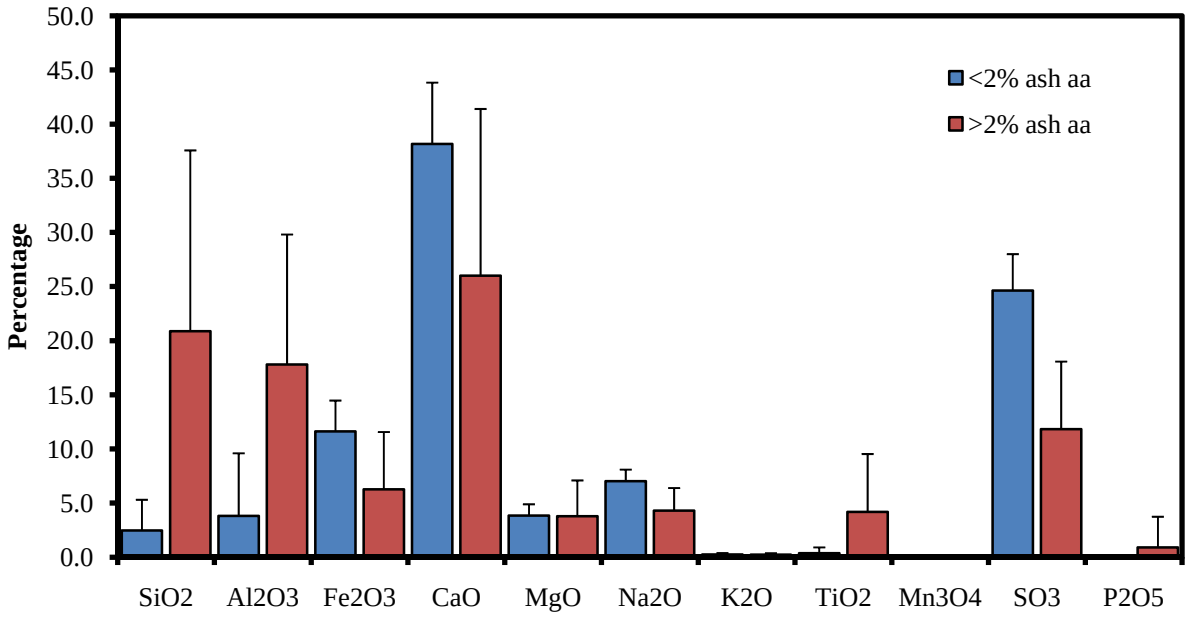

Figure 3. 21. Average ash constituents for the Kupakupa seam when ash yield is <2% aa and when ash yield is >2% aa.

3.4. Element associations

As leaching experiments and microprobe analyses were not conducted as part of this study, the inorganic and organic associations of the ash constituents were first examined by plotting results against the reciprocal of ash as done by Newman (1988) and Newman et al. (1997). Because of the differences between the seams, as identified above, this was done on a seam basis (Fig 3.22). Using this technique, organic associations will plot as a straight line, intersecting 1/ash at 0.01, while purely inorganic associations will plot with a negative slope. In addition, the relationships between the elements were examined using correlation tables and cluster analysis.

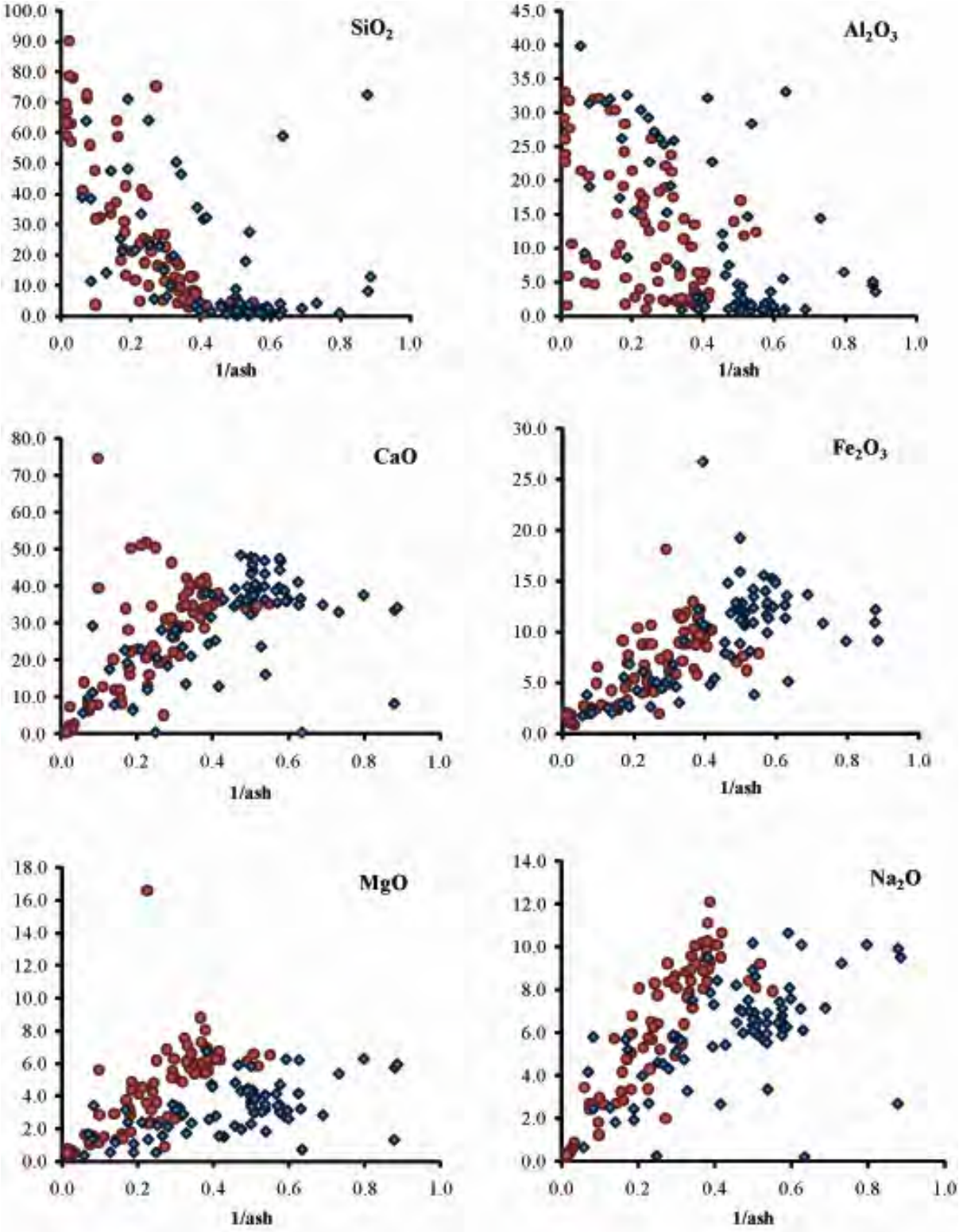
SiO2
100.0
90.0
80.0
70.0
60.0
50.0
40.0
30.0
20.0
10.0
0.0
0.0 0.2 0.4 0.6 0.8 1.0
1/ash
Al2O3
45.0
40.0
35.0
30.0
25.0
20.0
15.0
10.0
5.0
0.0
0.0 0.2 0.4 0.6 0.8 1.0
1/ash
CaO
80.0
70.0
60.0
50.0
40.0
30.0
20.0
10.0
0.0
0.0 0.2 0.4 0.6 0.8 1.0
1/ash
Fe2O3
30.0
25.0
20.0
15.0
10.0
5.0
0.0
0.0 0.2 0.4 0.6 0.8 1.0
1/ash
MgO
18.0
16.0
14.0
12.0
10.0
8.0
6.0
4.0
2.0
0.0
0.0 0.2 0.4 0.6 0.8 1.0
1/ash
Na2O
14.0
12.0
10.0
8.0
6.0
4.0
2.0
0.0
0.0 0.2 0.4 0.6 0.8 1.0
1/ash

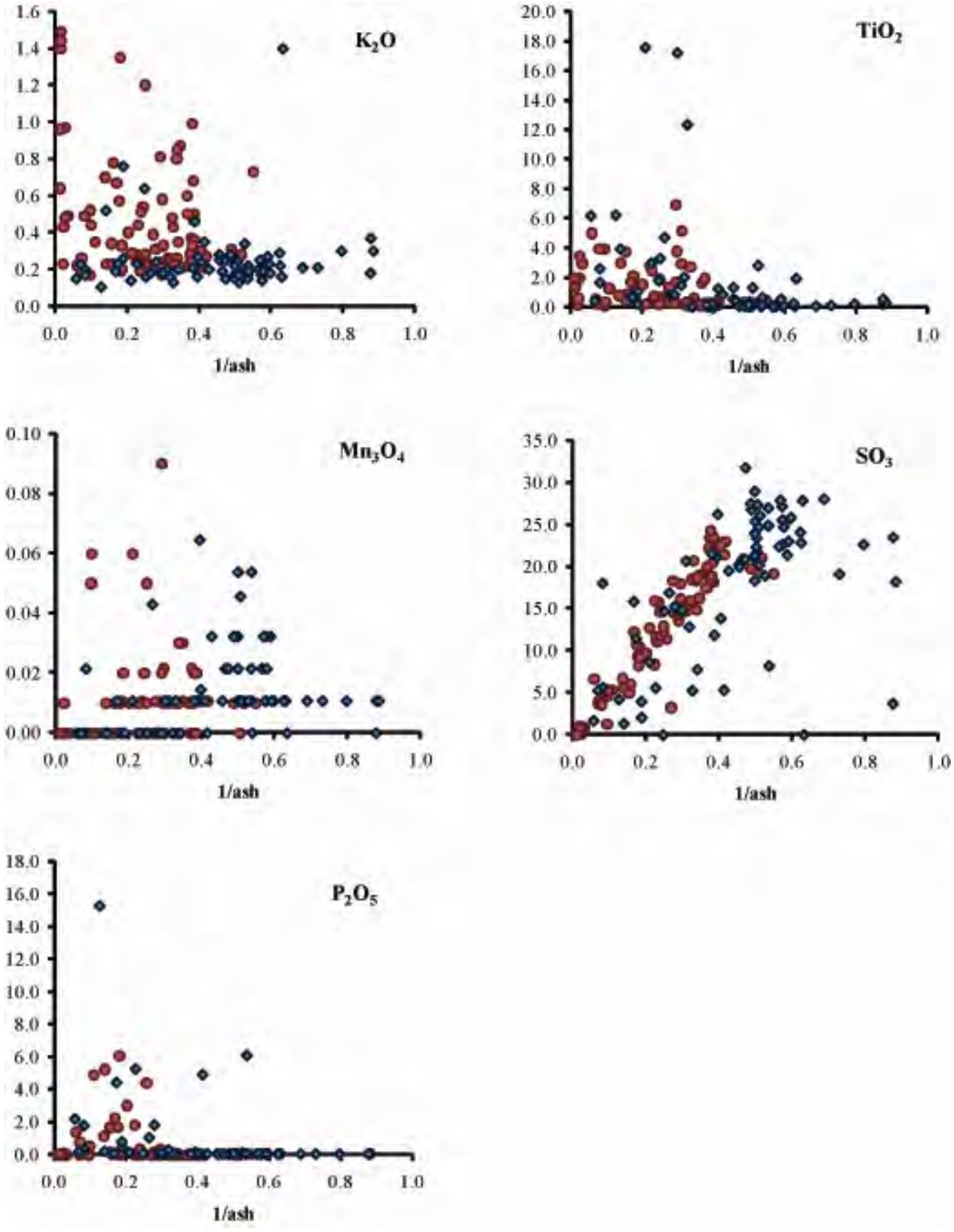

Figure 3. 22. Ash constituents by seam plotted against 1/ash yield db. Vertical axis is percentage. Red circles = Renown seam, blue diamonds = Kupakupa seam.

From Figure 3.22 it can be seen that for both seams silicon has an inorganic association, while aluminium and titanium have undefined, probably mixed association. Calcium appears to be predominately organic however some samples from the Renown form a cross-cutting line with negative slope suggesting an inorganic association. Iron, magnesium, sodium and sulphur all have predominantly organic associations. It needs to be noted that the basic ashes produced by New Zealand subbituminous coals and lignite have been reported to readily absorb sulphur oxides during ashing, even when precautions are taken. This possibility could influence the sulphur content in total ash (Gray, 1983). Possibly because of their low concentrations potassium, manganese (for which many samples were below the detection limit) and phosphorous show no clear relationships. Where associations are present, they are clearer for the Renown seam samples than for the Kupakupa seam samples.

Correlation tables were generated using the ash constituent data for both seams. One set of analyses included the high ash samples, while a second set excluded the high ash samples; the correlation tables are presented in Appendix 1. The main difference between the two sets of correlation tables is that the relationships in the Renown seam for calcium are stronger and potassium has a relationship with ash yield when all samples are included. In general, for the Renown seam, silicon and potassium are associated with inorganic material while iron, calcium, magnesium, sodium and sulphur are associated with the organic matter. Aluminium, titanium and phosphorous have no clear association but tend towards an inorganic association. Aluminium is associated with titanium while manganese is associated with iron. In the Kupakupa seam, silicon and aluminium show association with inorganic material while iron, calcium, sodium and sulphur show association with organic matter. Magnesium is associated with calcium; manganese is associated with calcium and magnesium, while phosphorous again shows a very weak association with inorganic material.

Dendrograms were produced from the results of cluster analyses using all samples by seam (Fig. 3.23). The results from the cluster analyses agree with those from the correlation tables, with separate organic (1/ash) and inorganic clusters. In both seams calcium is most closely associated with magnesium. Ambiguity exists around potassium as it is the only element to change clusters between seams. Likely potassium exists throughout but is more abundant in the high ash yield/carbonaceous mudstone samples collected in the Renown seam.

A

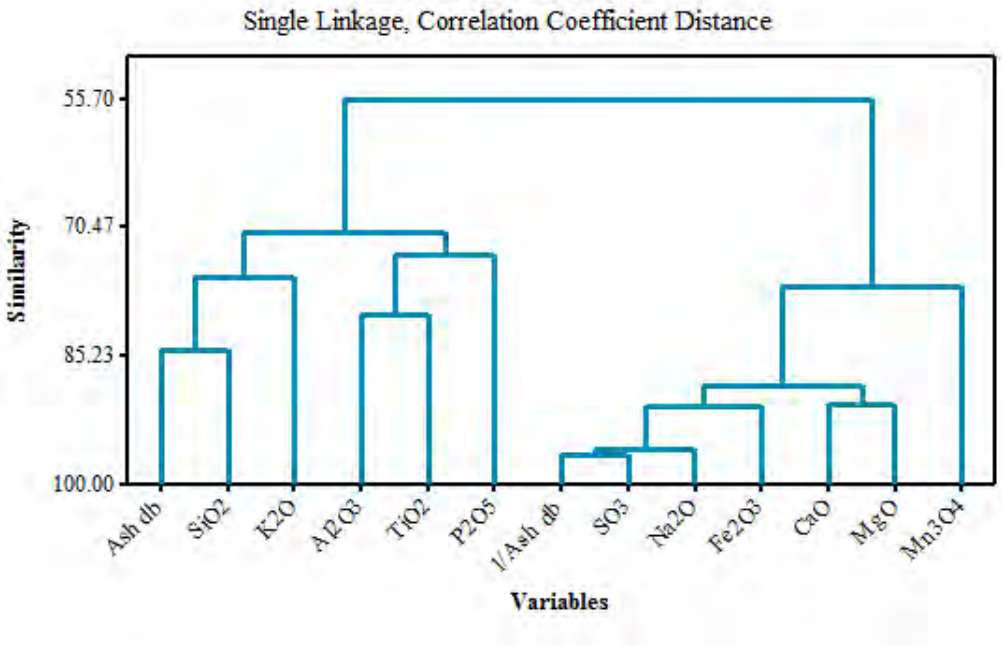

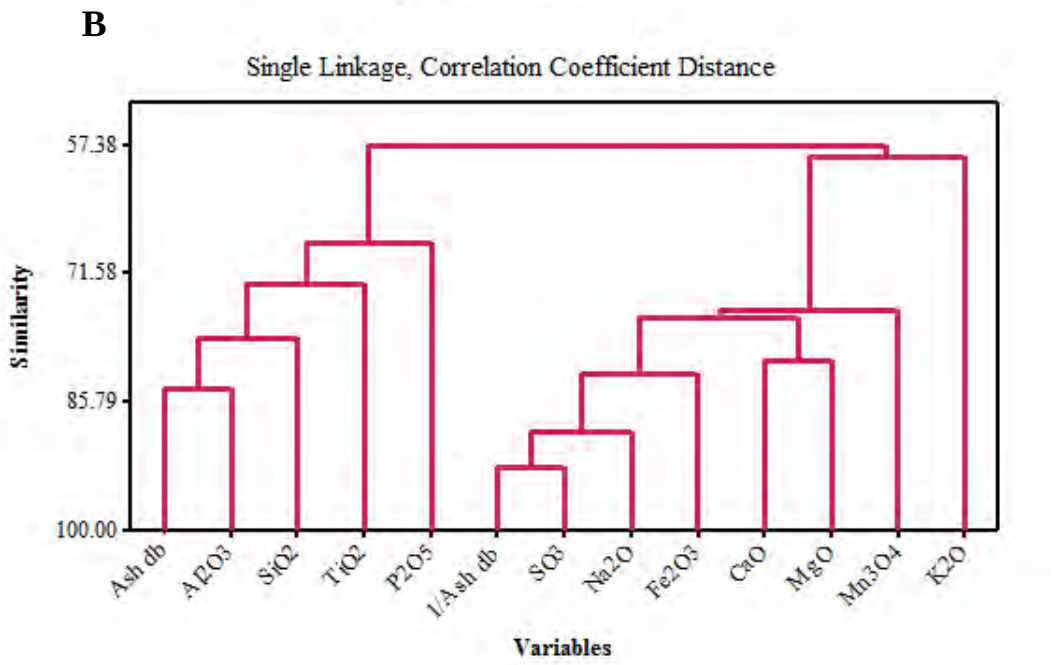

Figure 3. 23. Dendrogram of cluster analysis results of ash constituents for (A) the Renown seam and (B) the Kupakupa seam.

3.5. Visually and optically identifiable mineral matter

3.5.1. Macroscopic logging

During macroscopic logging (Appendix 2) some minor carbonate on cleat was identified at all locations, with the exception of Ruawaro 2. The Jasper 1 core (between samples J2 and J5) and the Mimi 1 core (between samples M3 and M6) have persistent carbonate on cleats and fractures (see Fig. 3.24). These intervals correspond to the samples with higher ash yields in the upper part of the Renown (Fig. 3.17 and 3.18). A small amount of clay on cleat was also noted in core from the Ruawaro 1, Rotongaro 1 and Baco 1 drill holes.

Figure 3. 24. Carbonate observed in the Mimi 1 M4 sample during macroscopic logging.

3.5.2. Organic petrology

Organic petrology investigations were conducted on samples from the Renown seam in the Jasper 1 and Mimi 1 drill holes as well as samples from the Kupakupa seam at Ruawaro 1 and Ruawaro 2 locations (Appendix 2). Counts of mineral matter, out of the 500 points counted, as well as comments on mineral matter occurrence are presented in Tables 3.9, 3.10, 3.11 and 3.12 respectively. The data are presented as raw counts rather than as weight percents or volume percents as the assumption of the Parr formula, that all sulphur is pyritic in origin, is not valid for New Zealand coals in general (Budge and MacKnight, 1976; Edbrooke et al., 1994). Forms of sulphur were analysed for the TW1 drill hole and the averages are presented in Table 3.13. A modified version of the Parr formula has been used elsewhere, however for the purpose of this study, with such low ash yield coals, presence or absence, abundant or trace is of most interest.

In general the counts presented in the tables show reasonable correlation to the ash yield profiles presented earlier in this chapter. All profiles show higher mineral matter

abundance in the top and base of the cores. The two Renown profiles, from Jasper 1 and Mimi 1, also show higher counts in the upper parts of the core, particularly for carbonate, in the areas with higher ash yield and the presence of heavier carbonate mineralisation as noted in section 3.4.1. Two samples, A18 and A21, from the Ruawaro 1 core show reasonably high carbonate counts and very low (<2% aa) ash yield. These samples possibly provide an argument for volatilisation of carbonates during proximate analyses as mentioned in section 2.2.4. The lack of aluminium in the Ruawaro 2 core, as noted in Figure 3.14, is highlighted here by clay only appearing in trace amounts if at all.

Table 3. 9. Mineral matter counts for the Jasper 1 samples. tr = trace.

	Count	Quartz	Clay	Carbonate	Fe oxide	Sulphide	Occurrence
J2	35	1	0	33	1	0	Carbonate in micro-veins/fractures
J3	10	0	0	10	tr	0	Carbonate in micro-veins/fractures as well as some carbonate crystals
J4	3	tr	tr	3	tr	tr	Few inorganic particles
J5	4	tr	tr	4	tr	tr	Carbonate in micro-veins/fractures also as carbonate crystals, mineral matter as isolated particles in matrix, quartz and clay also in a few inorganic particles
J6	2	tr	tr	2	0	0	Quartz and clay in inorganic particle
J7	3	3	0	tr	tr	tr	Carbonate in micro-veins/fractures, isolated quartz in matrix and in an inorganic particle
J8	0	tr	0	tr	0	tr	Quartz isolated in matrix
J9	0	tr	0	tr	tr	0	
J10	1	0	0	tr	0	1	
J11	6	tr	5	0	tr	1	Some interbedded coal and inorganic material

Table 3. 10. Mineral matter counts for the Mimi 1 samples. tr = trace.

	Count	Quartz	Clay	Carbonate	Fe oxide	Sulphide	Occurrence
M1	6	5	0	tr	tr	1	Some well sorted quartz with secondary growths
M2	3	0	3	tr	tr	tr	
M3	10	4	3	tr	1	2	Isolated mineral grains in matrix
M4	24	9	7	7	tr	1	Carbonate in micro-veins/fractures, iron oxide with carbonate on cleat, quartz and clay in inorganic layers, some clay and pyrite in tissue
M5	0	tr	tr	tr	tr	tr	Carbonate in micro-veins/fractures
M6	13	1	0	12	tr	tr	Carbonate in micro-veins/fractures
M7	1	tr	tr	tr	0	1	Carbonate in micro-veins/fractures, also 35 µm carbonate vein- possibly multiple pulse
M8	0	tr	0	tr	0	tr	Carbonate in micro-veins/fractures
M9	0	tr	tr	0	0	tr	Interspersed clay, possible pond?
M10	2	tr	tr	2	0	tr	Carbonate in micro-veins/fractures
M11	56	13	43	0	0	0	Carbonate in micro-veins/fractures, quartz and clay as interbedded coal and inorganic material

Quartz is frequently present as discrete grains in the coal matrix. The isolated grains are interpreted to be of detrital origin. In contrast, some quartz particles are interpreted as diagenetic based on their size, shape and occurrence in plant tissues (Fig. 3.25) (Edbrooke et al., 1994). Quartz and clay are sometimes found together in inorganic particles or laminae with clay also occasionally occurring as fine bands inter-layered with organic material. Quartz and clay in this form are interpreted as detrital mineral matter and are likely water-borne (Edbrooke et al., 1994).

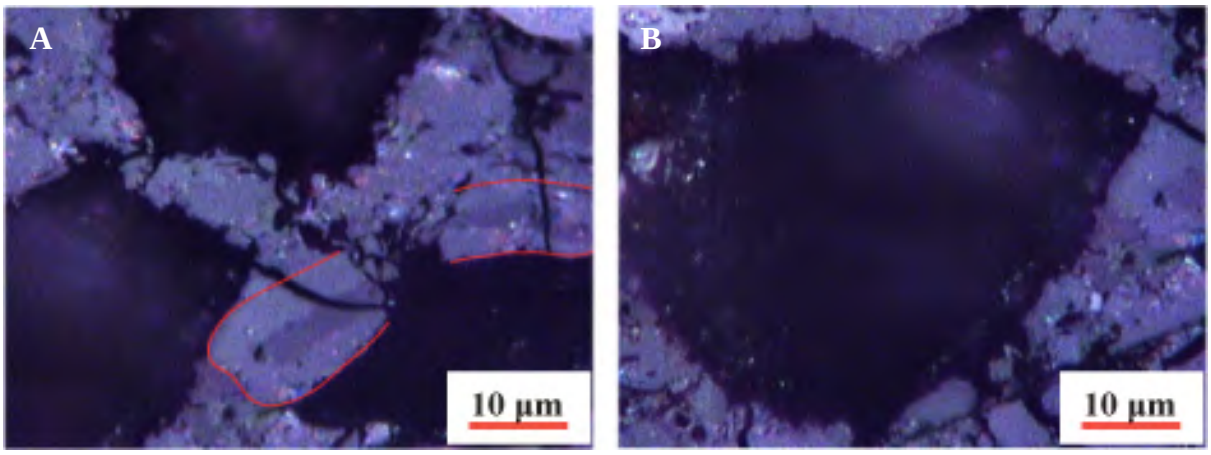

Figure 3. 25. Possible authigenic quartz from Mimi 1 sample M1. In picture (A) a broken tissue can be clearly seen, with the boundaries shaped in red, while in picture (B) fractures around the crystal can be seen.

Carbonate is generally present as fracture fillings, cutting through vitrinitic material, and also as cleat fillings (Figure 3.26). Consequently, carbonate is thought to be epigenetic (secondary) carbonate. The infilled fractures are typically orientated and sigmoidal in shape. Interval M7 (Mimi 1) contained carbonate veins in cleat up to 35 µm thick that appeared to show evidence of multiple fluid pulses, while a cluster of carbonate crystals was identified in interval J3. Where present, iron oxides tended to be associated with the carbonates, frequently inter-fingered. Where present on its own, it is possible that the iron oxide is a result of oxidation during storage of the sample, however the presence of the iron oxide inter-fingered growth with the carbonate would argue against this.

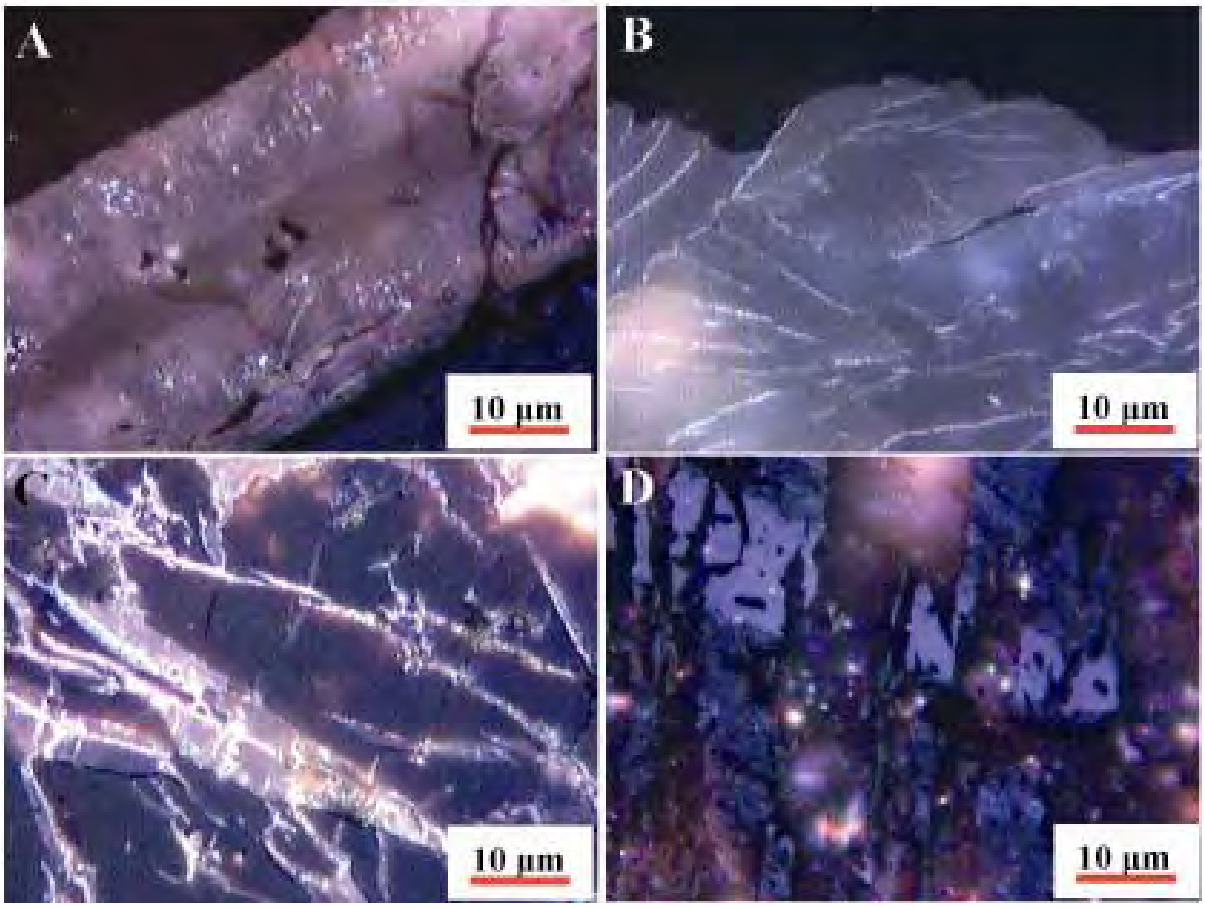

Figure 3. 26. Carbonate. (A) Thick carbonate on cleat with layers possibly suggesting multiple pulses in Mimi 1, M7. (B) Carbonate crystals in Jasper 1, J3, (C) Carbonate and iron oxide in fractures through collotelinite in Mimi 1, M2 and (D) Carbonate and iron oxide in fractures through vitrinitic matrix and an inertinite tissue in Jasper 1, J3.

Sulphides occurred rarely as small discrete grains in the matrix material and are thought to be syngenetic pyrite. Possible hydrothermal sulphides were identified in the Ruawaro 1 core in intervals A17 and A19. Hydrothermal sulphide has been seen in association with iron replacement of carbonates in other New Zealand coals (J. Newman, pers com. 2007). This possibility would also argue for formation of iron oxides in situ.

Table 3. 11. Mineral matter counts for Ruawaro 1 Kupakupa samples. * = only 250 counts, tr = trace.

	Count	Quartz	Clay	Carbonate	Fe oxide	Sulphide	Occurrence
A16	48*	31	17	0	0	0	
A15	19	4	11	1	0	3	Noticeably higher pyrite, possible pond? interbedded laminated clays
A14	3	1	2	0	0	tr	Laminated clays
A13	14	0	13	0	tr	1	Possible pond? laminated clays
crl	2	0	0	2	tr	0	Carbonate in micro-veins/fractures
A17	3	tr	0	1	2	0	Hydrothermal sulphide
A18	16	0	0	12	4	0	Carbonate and iron oxide in micro-veins/fractures
A19	0	tr	tr	tr	tr	0	Possible hydrothermal sulphide, quartz and clay in inorganic particle
A20	0	tr	tr	tr	tr	0	Quartz and clay were part of a thinly interbedded coal/inorganic particle
A21	12	1	1	8	2	0	Carbonate and iron oxide in micro-veins/fractures
A22	0	tr	0	0	tr	0	
A23	0	0	0	0	tr	0	
A24	1	tr	0	0	1	0	
A25	0	tr	0	0	0	0	
A26	8	5	3	0	tr	0	Quartz and clay were part of a thinly interbedded coal/inorganic particle or as an inorganic particle

Table 3. 12. Mineral matter counts for Ruawaro 2 Kupakupa samples. tr = trace.

	Count	Quartz	Clay	Carbonate	Fe oxide	Sulphide	Occurrence
B16	16	15	tr	0	1	tr	Quartz throughout tissue and in inorganic particle, iron oxide in micro-veins/fractures
B17	0	tr	0	0	0	tr	
B18	0	tr	tr	tr	tr	tr	
B19	0	tr	tr	0	tr	0	Iron oxide in micro-veins/fractures
B20	0	tr	0	tr	tr	tr	Carbonate and iron oxide in micro-veins/fractures
B21	0	0	0	0	0	0	
B22	0	tr	tr	0	tr	tr	Iron oxide in micro-veins/fractures
B23	0	tr	0	0	0	tr	
B24	0	tr	tr	0	0	tr	
B25	1	1	tr	0	0	tr	
B26	15	1	14	0	0	tr	

Table 3. 13. Average forms of sulphur from the TW1 drill hole on a dry basis, db.

	Minimum	Average	Maximum	SD
Sulphate Sulphur (db)	3%	5%	12%	0.02
Pyritic Sulphur (db)	3%	7%	14%	0.03
Organic Sulphur (db)	77%	91%	97%	0.04

SD = standard deviation

3.6. Ultimate Analysis

3.6.1. Ultimate analysis by drill hole

Complete ultimate analysis profiles were conducted for the Renown seam from Jasper 1, Mimi 1 and for the Kupakupa seam from the Ruawaro 2 location (Figs. 3.27, 3.28 and 3.29 respectively). However the high ash yield/carbonaceous mudstone samples (J1, J12, J13 and M12) have been excluded from the results presented here. Additionally ash yield profiles (db) for each location have been included to identify intervals where mineral matter may be diluting the organic material.

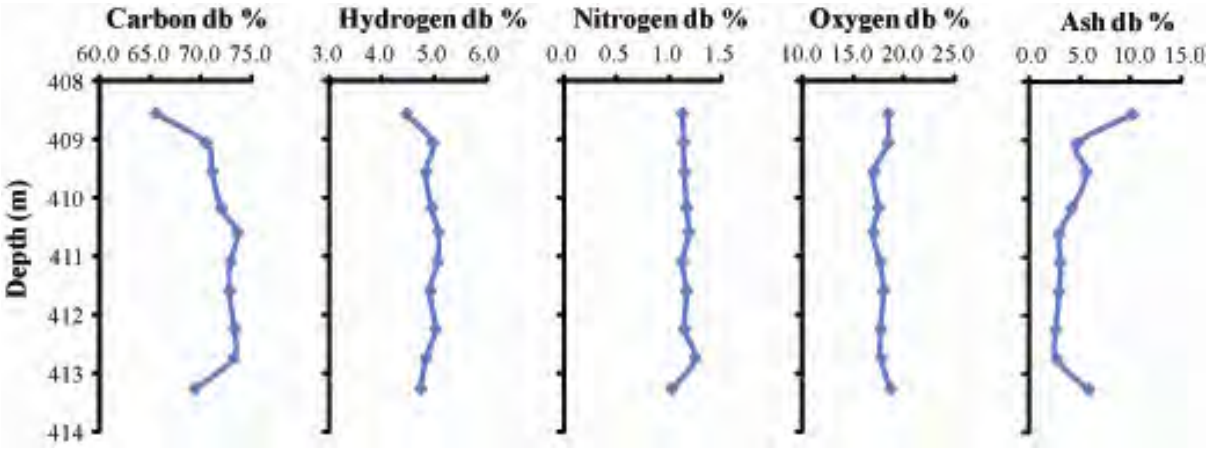

Figure 3. 27. Ultimate analysis results for Jasper 1 Renown samples J2 – J11 on a dry basis, db.

At the Jasper 1 location carbon content can be seen to be lowest at the top and base of the coal seam (where ash yield is high) and has a general trend of increasing carbon with depth, with the exception of sample J6, which has the highest carbon content. Hydrogen is quite variable, while nitrogen is relatively uniform in the top half of the seam and more variable with depth. Oxygen content is highest at the top and base of the seam and tends to be

lower in the central parts of the core. Oxygen is calculated by difference; hence it includes all the errors in the elements which have been directly measured.

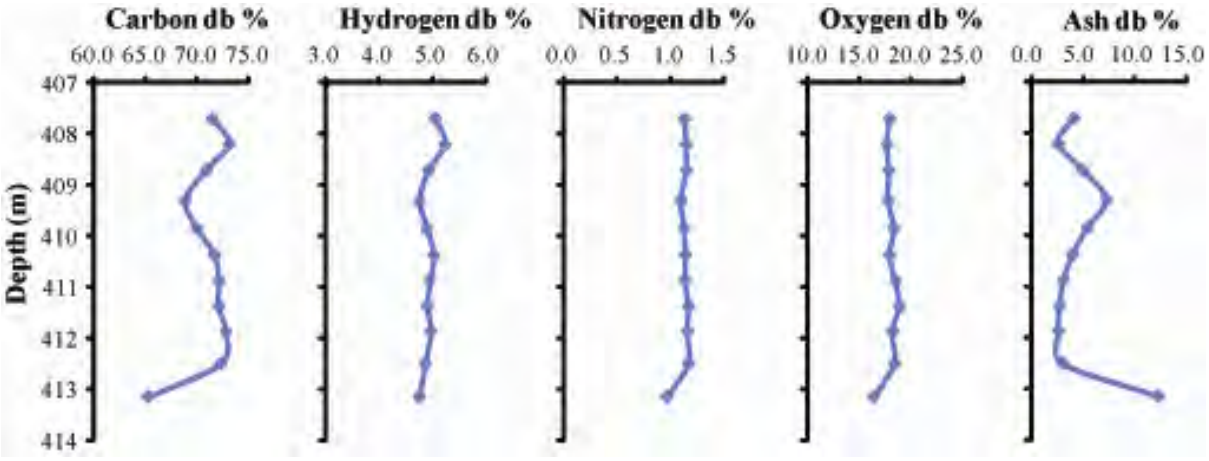

Figure 3. 28. Ultimate analysis results for Mimi 1 Renown samples M1 – M11 on a dry basis, db.

In the Mimi 1 core, carbon tends to be lowest where ash yield is higher (and where visible carbonate was present), for example in the samples M3 - M6 and M11. Hydrogen is variable with a similar profile to that in the Jasper 1 core, while nitrogen, with the exception of the deepest sample, has little variation throughout. Oxygen content at the Mimi 1 location also has little variation; however there is a decrease in the bottom sample

In contrast to the results for the two Renown cores, the Ruawaro 2 Kupakupa core results for carbon, hydrogen, nitrogen and oxygen all show much larger variation in the top part of the seam despite very low ash yields. Less variation is seen for samples from the bottom third of the seam. One source of both within and between seam variability of ultimate analyses may be that samples were analysed at different times. The Jasper 1 and Mimi 1 samples were analysed within a few weeks of being cored (November 2006). In contrast the Ruawaro 2 samples were collected in 2005 but were analysed much later.

Additionally, the samples were analysed at different times, with samples B17, B20 and B24 (Fig. 3.29) being analysed in June 2007 while the remaining samples were analysed in October 2007. To assess the possible effects of analysing samples at a later date three of the Mimi 1 samples were analysed a second time in October 2007. The difference between results in 2006 and 2007 is presented in Figure 3.30.

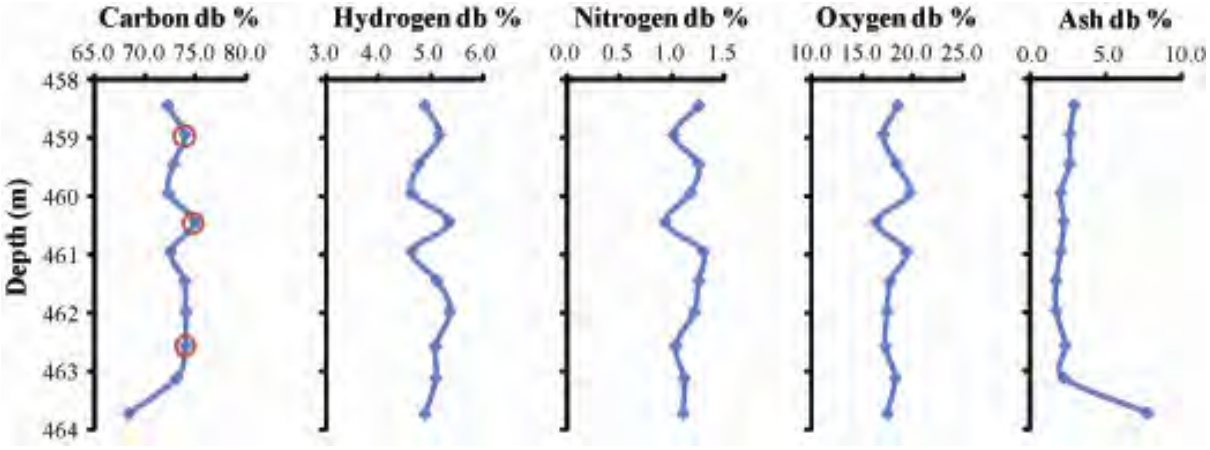

Figure 3. 29. Ultimate analysis results for Ruawaro 2 Kupakupa samples B16 – B26 on a dry basis, db. The samples marked with red circles were analysed in June 2007.

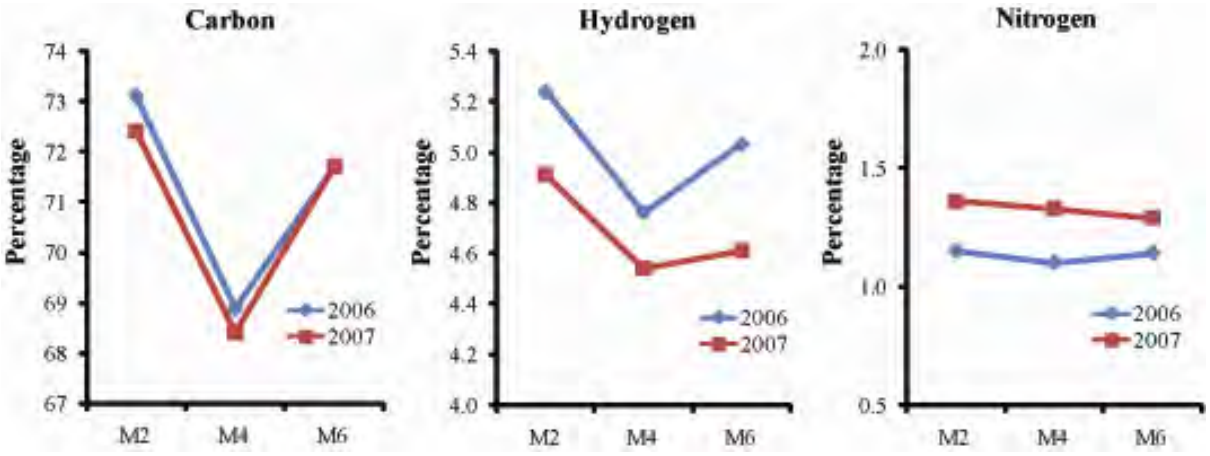

Figure 3. 30. Comparison of ultimate analysis results for Mimi 1 samples analysed in November 2006 and repeated in October 2007.

As can be seen, only one value was the same as it was analysed in 2006. In general, carbon decreased by up to 1%, hydrogen decreased by up to 8% and nitrogen increased by up to 20%. The trend of decreasing carbon and hydrogen contents with time is in agreement with previous studies (Fredericks et al., 1983; Mathews and Bustin, 1984). Laboratory reproducibility of these analyses is 0.6% for carbon, 0.2% for hydrogen and 0.08% for nitrogen (Grant Murray, pers. com. 2007). All differences, except for the carbon analyses on samples M4 and M6, are greater than these reproducibility numbers. Three of the Ruawaro 2 samples (B17, B20 and B24) were also analysed twice for ash yield (2005 and 2007) and there was an increase seen, on a dry basis, of between 6 and 18%. Fredericks et al. (1983) also reported an increase in mineral matter content with coal weathering. Waikato coals have been previously reported to be highly reactive (Shaw, 1997).

In addition to the concern about comparability of samples from the Kupakupa seam because of sampling times, in both of the Renown cores, hydrogen content followed a pattern similar to that of volatile matter (Fig. 3.31) with correlation coefficients of 0.81 for Jasper 1 and 0.87 for Mimi 1. In contrast, in the Ruawaro 2 core hydrogen shows some divergence with a correlation coefficient of 0.58. Because of these reasons, there is some concern over the reliability of the Kupakupa results and as such, they should only be used with caution.

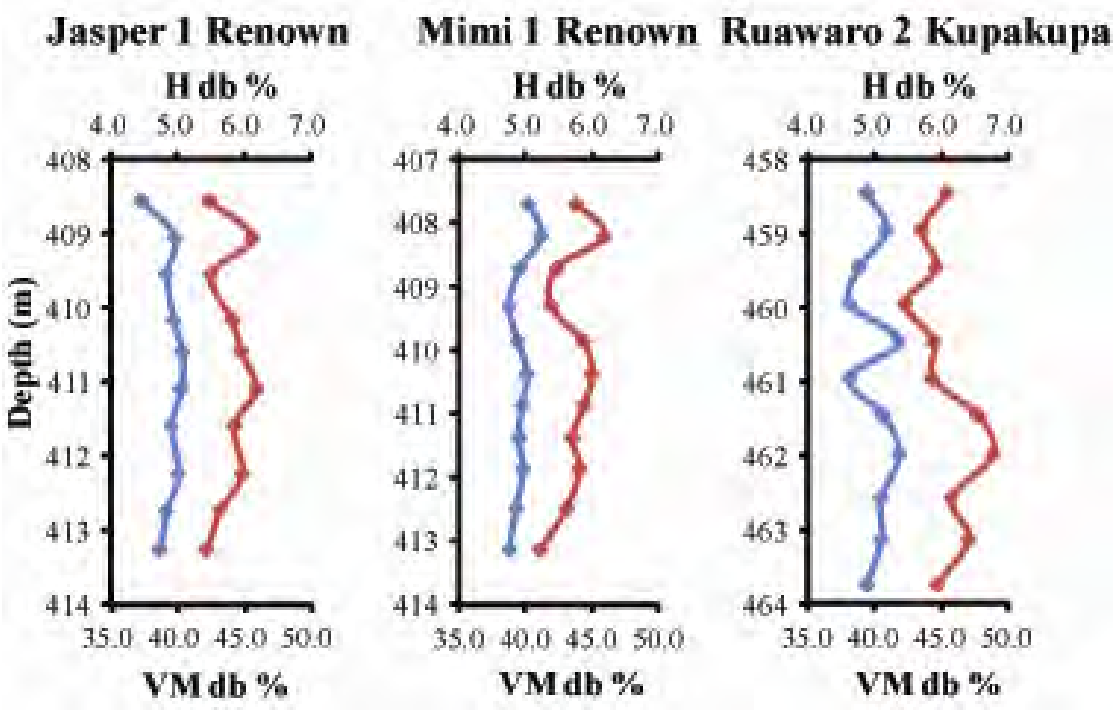

Figure 3. 31. Hydrogen content and volatile matter contents for the Jasper 1 Renown, Mimi 1 Renown and Ruawaro 2 Kupakupa cores on a dry basis, db. H = hydrogen (blue line), VM = volatile matter (red line).

3.6.2. Ultimate analysis by seam

The results of the ultimate analyses on a by seam basis show lower values of carbon, hydrogen and nitrogen for the Renown seam than for the Kupakupa seam (Table 3.14). Unfortunately, as the representative seam splits included all samples, regardless of ash yield or the presence of interbedded inorganic material, this difference between seams is strongly influenced by non-coal material. All samples, regardless of seam, that have an ash yield of <5% also have >70% carbon content.

The table also shows that the Baco 1, Mimi 1 and Jasper 1 locations (where the results exclude high ash yield samples) all have higher carbon content than the other Renown

locations. The averages for each of these three locations are not that dissimilar to the averages for the cores from the Kupakupa seam.

Table 3. 14. Ultimate analysis results by location on a dry basis, db.

Location	Seam	Carbon %	Hydrogen %	Nitrogen %	n
Ruawaro 1	Renown	62.1	4.80	1.00	1
Ruawaro 1	Kupakupa	74.2	4.98	1.16	1
Ruawaro 2	Renown	71.1	4.88	1.15	1
Ruawaro 2	Kupakupa	74.4	5.36	1.02	1
Rotongaro 1	Renown	68.7	4.90	1.07	1
Rotongaro 1	Kupakupa	73.9	5.11	1.00	1
Mangapiko 1	Renown	67.8	4.80	1.31	1
Mangapiko 1	Kupakupa	72.4	5.30	1.23	1
Baco 1	Renown	72.8	5.07	1.15	1
Jasper 1	Renown	71.4	4.89	1.15	10
Mimi 1	Renown	71.0	4.94	1.13	11

n = number of samples

3.7. Discussion

3.7.1. Low ash yield coal deposits

Amijaya and Littke (2005) suggested that the very low mineral matter content seen in Tertiary coals from Indonesia could be explained by three main processes (1) the process of doming of the peat deposits, (2) the leaching of mineral matter from previously deposited peat, or (3) the deposition of peat on surfaces where inorganic sedimentation processes are not active. They concluded that the doming of the peat with the most likely explanation. Most coal deposits with ash yields of <5% are interpreted to be formed as raised, ombrogenous mires. Because of their elevated surface level, and the flocculation of clays at the margins of the mire, ombrogenous peats are relatively shielded from inorganic influxes (Amijaya and Littke, 2005; Cohen et al., 1987; Esterle and Ferm, 1994; Staub and Cohen, 1978; Staub and

Esterle, 1994; Wust and Bustin, 2001). The primary source of moisture for such deposits is thought to be precipitation (Cohen and Stack, 1996; Moore, 1995; Staub and Esterle, 1994).

For a domed Indonesian peat with low ash yield and low sulphur content Neuzil et al. (1993) found that in general, silicon, aluminium and iron, are the abundant inorganic constituents, although magnesium, calcium, and sodium dominate in the middle horizon in the geographic interior of the peat deposits. They suggest that the domed ombrogenous peat deposits will result in low ash and sulphur coal, probably less than 10% ash yield and 1% sulphur. Plant material was found to contribute from 1-2% of inorganic material to peat. In the Miocene Yallourn brown coal seam in Victoria, Australia, Holdgate et al. (2007) identified that the thickest region (~100 m) has very low ash yields of generally less than 1.5% (db). This area was characterised by low silicon and aluminium and high iron content. They suggested that significant factors influencing this trend may have been lowered paleo-relief in the surrounding highlands, changes in Tertiary paleoclimates, increasing aridity and increased weathering.

Extremely low ash yields were identified from the Greymouth coals by Li et al (2001). Most of the studied coal plies had ash yields in the range of 0.58% to 2.5%. For comparison, although still very low, the lowest ash yield found in this study was 1.2% (aa). The highest ash yields were identified at the top and base of the seam while the lowest ash yields were located in the centre of the seam. Etching features were identified on quartz and clay minerals within the seam, as well as the remobilisation of liptinitic material into voids and the cleat networks, led to the conclusion that leaching processes, both during the peat stage and after burial, were responsible for the exceptionally low ash yields (Li et al., 2001). Dissolution features on minerals in peat have been previously identified by Ruppert et al.

(1993) and Andrejko et al. (1983). Unfortunately the current study did not go into this level of detail; however the lower part of Kupakupa seam should possibly be examined for these features.

3.7.2. Mineral matter in the Huntly coal

Butland (2006) analysed 8 samples from the TW1 core using XRD and found quartz (SiO_2) and kaolinite ($Al_2Si_2O_5(OH)_4$) to be the predominant inorganic components. The carbonates calcite ($CaCO_3$) and ankerite ($Ca(Fe,Mg,Mn)(CO_3)_2$) are also present in one of the analysed samples with calcite being the dominant phase. Three of the samples did not yield any minerals. Soong and Gluskoter (1977) also reported calcite and ankerite for run of mine Waikato coal while Gray and Daly (1981) suggested iron and calcium mineralisation to explain scatter plots. Ankerite alters to iron oxides (Nesse, 1991) possibly explaining the presence of the iron oxide identified in the petrological examination in this study. The presence of kaolinite, rather than illite suggests little to no marine influence on the coals (Taylor et al., 1998). Much of the clastic (detrital quartz and clay) material present in the Waikato coals is thought to be deposited by surface water flows (Edbrooke et al., 1994; Shearer et al., 1997). Additionally, Shearer et al. (1997) identified a tephra layer in the upper part of two out three cores analysed from the Kupakupa seam. In an analysed coal sample including tephra material the ash yield (using low-temperature ashing) was dominated by kaolinite with smaller contributions from bassanite ($CaSO_4 \cdot 1/2H_2O$) and anatase (TiO_2) (Clemens et al., 2000).

Calcite and ankerite, can be precipitated in cracks or fissures by hydrothermal waters or directly from groundwater (Nesse, 1991; Taylor et al., 1998). Support for a hydrothermal

fluid source for the carbonates is presented by Zarrouk and Moore (2007) who identified that the water chemistry indicated that the reservoir water has originated from the deep basement through sedimentary rocks (high chloride/boron ratio) with an equilibrium temperature of around 90 ºC. This argument is further strengthened by the possible hydrothermal sulphide identified and the carbonate seen on cleat. Hydrothermal sulphide has been seen previously in association with iron replacement of carbonates in New Zealand coals (J. Newman, pers com. 2007).

An alternate possibility, proposed by Ward (2002), is that the carbonate infillings were formed by the expulsion of inorganically associated calcium from the organic components of the coal during coalification. In agreement with this, Taylor et al. (1998) state that it is likely that some ankerites form as a result of cation release from carboxylate during coalification in the subbituminous range of rank. It has been suggested that the sigmoidal pattern of carbonates in coal results from brittle failure of the vitrinite, with other macerals behaving in a more ductile manner, under a post-depositional stress regime (Ward, 2002). It is thought that multiple episodes of faulting have occurred in the Waikato with the faults currently collectively accommodating low strains of ~2 – 5% across the region (Hall et al., 2006).

In addition to the minerals identified by Butland (2006), Edbrooke et al. (1994) in their study of the Waikato coalfields also report siderite ($FeCO_3$) concretions (within the coal measures) diagenetic quartz, diagenetic sulphides, and rare mica. These siderite hardpans and concretions, frequently noted during the drilling campaign, have been analysed further by Middleton and Nelson (1996) and Pearson and Nelson (2005) (see example shown in Figure 3.32), and indicate iron rich carbonate precipitation throughout the coal measures. These

concretions frequently have calcite cement where septarian cracking has occurred. Interestingly this calcite cement shows that some of the carbonate was derived from the oxidation of methanogenic carbon ascending from the coal seams (Middleton and Nelson, 1996). The calcite cement in the concretions, and the discussion above, leads to the proposal that the majority of carbonate material in the Huntly coalfield was precipitated by hydrothermal fluids.

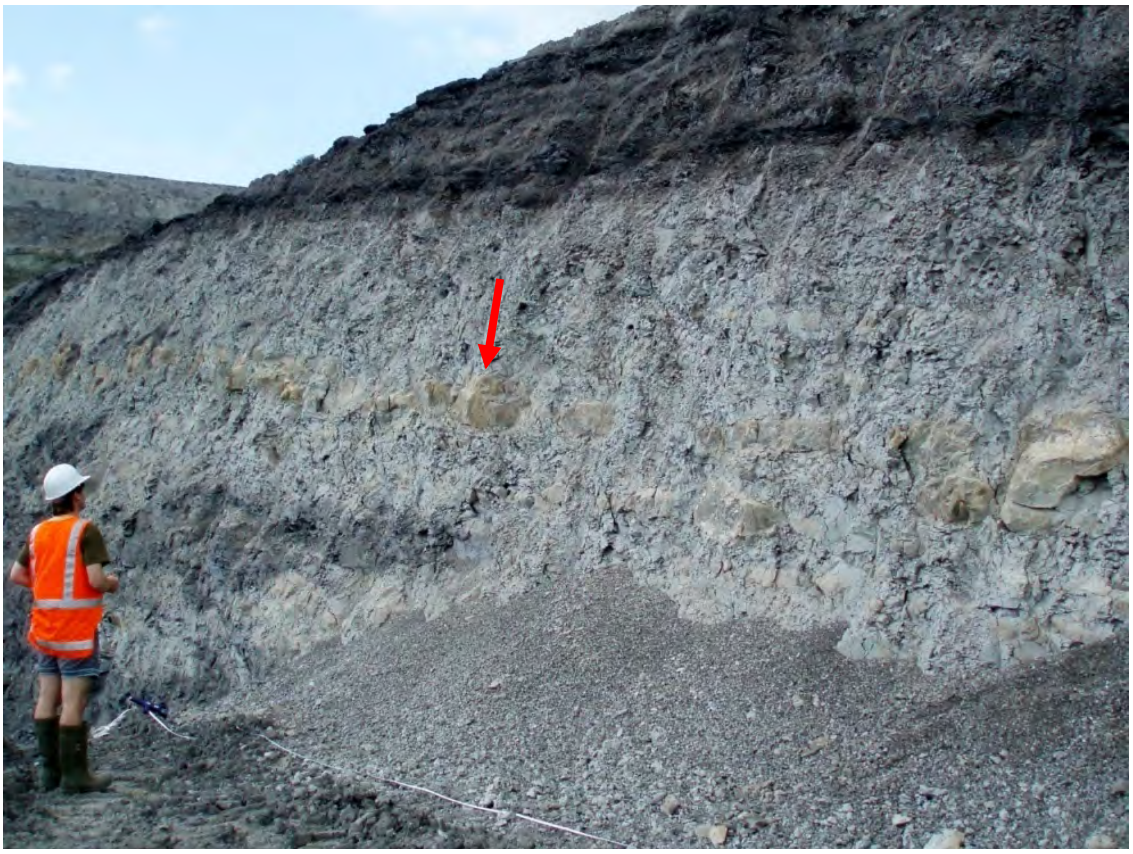

Figure 3. 32. Example of concretions in the Waikato coal measures.

Both Edbrooke et al. (1994) and Sykes and Lindqvist (1993) identified diagenetic quartz in the Waikato coalfields, with the mode of occurrence varying from sparse micro-crystals disseminated in the matrix, to intensely silicified, sub-horizontal bands of very hard, dull stone or stony coal. Edbrooke et al. (1994) did not find areas of heavy silicification in the Huntly coalfield however some diagenetic quartz was identified in several of the analysed

profiles. The diagenetic silica present in the Waikato coals is thought to represent early precipitation of quartz from silica-saturated ground waters within the peat forming environment during/or shortly after burial (Sykes and Lindqvist, 1993). Ruppert et al. (1985) interpreted quartz in the upper Freeport coal bed to be authigenic in origin. The quartz grains were postulated to have been sourced from plant-derived silica (phytoclasts). It has been highlighted by Andrejko et al. (1983) that the interiors of modern peat deposits are substantial reservoirs of amorphous silica. This silica is derived from the degradation of diatoms, sponge spicules and siliceous phytoliths associated with plant material.

While pyrite tends to be more abundant in marine influenced coals (Ward et al., 1999) it can still be abundant in lacustrine environments (Ward, 1991). Syngenetic pyrite is thought mainly to precipitate resulting from the interaction of dissolved iron with H_2S generated by the bacterial reduction of sulphate ions in the peat environment (Ward, 2002). Budge and MacKnight (1976) and Newman et al. (1997) reported that pyrite is insignificant in the low-sulphur Kupakupa coals. A distinct lack of pyrite was noted in this study and also by Butland (2006) and agrees with the forms of sulphur analyses. Low pyrite abundances may be attributed to a low dissolved sulphate concentrations of the waters in which the peat forms (Price and Casagrande, 1991), influxes of fresh water (unlikely in this case as there is low mineral matter overall) or low pH in the peat body suppressing bacterial reduction (Renton and Bird, 1991).

Unlike many coals, for which the assumption is that the majority of sulphur is pyritic in origin (Parr, 1928), sulphur in New Zealand coals is commonly present as organic sulphur (Budge and MacKnight, 1976). It has also been proposed that when total sulphur content of a coal is small, the sulphur is largely organically bound (Smith and Batts, 1974). For Waikato

coals, Edbrooke et al. (1994) suggest that for coals where sulphur, on a dry basis, is < 1%, then that sulphur is essentially organic (70 - 100%). In contrast, where sulphur is ≥ 1% there is likely a co-occurrence of both organic and pyritic sulphur with sulphate sulphur never contributing > 17% of the total sulphur. In the current study, total sulphur ranges from 0.09 – 0.86% (db) with an average of 0.29% suggesting sulphur is predominantly present as organic (Table 3.13).

3.7.3. Element associations

In this study (Figure 3.22) silicon was found to be associated with ash yield. Iron, calcium, magnesium, sodium and sulphur were found to be primarily associated to organic material, while relationships for aluminium, potassium, titanium, manganese and phosphorous were unclear (likely of mixed association). Newman et al. (1997) identified strong correlations between organic matter and calcium, magnesium, iron, sodium and boron. Using a nuclear microprobe, Vickridge et al. (1990) concluded that boron and a large proportion of calcium were likely organically bound in Waikato coals. Similar to calcium percentages presented here, Clemens et al. (1999) reported 55% calcium for a low ash yield (3.5%) coal sample from the Waikato. Moore and Fergusson (1997) also identified an inverse relationship between iron and ash yield, noting that the percentage iron is highest in the upper middle, low ash yield parts of the Kupakupa seam.

Li et al. (2007) mapped the concentration of inorganic elements in visibly clean macerals of low-rank coals using microprobe techniques and found that a majority of these elements occur as non-mineral entities, possibly even as an inherent part of the organic structure of the macerals. In agreement with this, Ward et al. (2008) found small but

consistent quantities of aluminium, calcium and sometimes iron, in clean macerals from low-rank coals which were not found in macerals from coals of higher rank. In a study analysing low rank coals from several countries (Li et al., 2009), collotelinite from the Huntly coalfield was found to include up to approximately 0.27% aluminium, 1.35% calcium, 0.11% magnesium, 0.12% iron and 0.16% titanium, with collodetrinite containing fractionally smaller quantities. As there is very little silicon (0.01%) the aluminium is not present as sub-micron clay minerals. Where organically associated elements occur they are generally more abundant in vitrinite than inertinite components (Li et al., 2009; Ward et al., 2008). It has been suggested that the primary (or inherent) inorganic material fixed in vitrinite was fixed in the original coal-forming plants (Shibaoka, 1972).

A study of non-mineral inorganics in Tertiary, low-rank coals of the Mae Moh basin, Thailand (Ward, 1991), found that much of the reported calcium, magnesium, sodium and iron concentrations were present in mobile form. In contrast, potassium and aluminium had very low mobile concentrations. Ward (1992) also found similar results for low-rank coals from South Australia. He concluded that the majority of the sodium, as well as a large proportion of sulphur, seems to be present as dissolved ions (or soluble) in pore waters, while most of the calcium, magnesium, manganese and the remaining sodium, occurs as exchangeable ions attached to carboxylate groups. Large proportions of iron and aluminium, along with the remaining calcium, magnesium and manganese appears to be present in acid-soluble organometallic complexes (Ward, 1992; 2002; Ward et al., 2005). Li (2002) reports for a leaching experiment on a Huntly coal sample that 5% - 55% of calcium, 0% - 15% of magnesium and 5% - 10% of sodium are acetate soluble (present as weakly bound exchangeable cations). To leach aluminium, potassium, titanium, phosphorous, iron and

manganese, acids were required. The organically associated portions of these elements are therefore likely to be present as acid-soluble organometallic complexes.

Potassium in the Huntly coal samples is relatively low varying from 0.09% - 1.35%. For the low rank Mae Moh coals Ward (1991) suggested that most of the potassium is probably tightly held in clay mineral structures, while for the low rank coals in South Australia, Ward (1992) found potassium up to 1% with an absence of illite. Newman et al. (1997) reported potassium values of up to 0.5% and like the current study found that potassium was neither organic nor mineral but may be a combination of both. Soong and Gluskoter (1977) reported rare illite in Waikato coals and Newman et al. (1997) identified minor illite in some high-ash, high-potassium samples.

Considerable variation in titanium values between adjacent plies in the Kupakupa seam has been noted previously (Newman et al., 1997). Titanium levels in this study (in coals with <20% ash yield) range from 0.05% - 17.57%. Of these samples, 33 (22%) had titanium levels greater than worldwide mean values (1.6% oxide in ash) (Briet and Finkelman, 1998). High titanium levels were also identified in the Waikato by Clemens et al. (2000). One analysed sample had an ash yield of 7.4% and 8.32% titanium while the other sample had an ash yield of 3% and 5.77% titanium. The first sample included what was thought to be a titanium-rich tephra layer, using the geochemical signature of tephra deposits identified for North Island peat (Shearer et al., 1997), however they were unsure as to the cause of the high titanium in the second sample. Three samples from this study stand out because of their very high titanium percentages and difference to surrounding samples. Samples 32 (~12% titanium) from TW1 and samples C12 and C13 (both ~ 17% titanium) from Rotongaro 1 are

in the upper portion of the Kupakupa seam and have ash yields <5%. The position in the seam is similar to that found for tephra layers in the Waikato by Shearer et al. (1997).

Manganese has been reported previously to be negligible in Waikato coals (Moore et al., 2005). In agreement, in the samples of this study manganese is only present in low quantities (<0.09%) and in some samples is below the limits of detection. Where present, manganese was found to have some association to iron in the Renown seam and to calcium and magnesium in the Kupakupa seam. In Tertiary Indian coals, Mukherjee et al. (1992) found manganese shows an affinity with both organic and mineral matter while, in a statistical study of 24 different coals, Wang et al. (2008) found manganese is correlated with calcium and to a lesser extent iron.

Although phosphorus is a very important biogenic element, its concentration in coal is generally very low. Phosphorus concentrations typically range from 0.001% to 0.23% in coals from the U.S.A. however, Rao and Walsh (1997) found phosphorous concentrations up to 17.03% in a subbituminous coal from Alaska. Phosphorous values reported here range from below detection to 15.3%, with 29 samples (19%) having phosphorous >0.23%. Newman et al. (1997), found phosphorous to range from 0% to 4.18% with a good association between phosphorous and ash yield for the Kupakupa seam, however XRD analysis did not reveal any minerals with phosphorous associations. As identified in this chapter, phosphorous was found to be present in proximity to seam edges or seam splits. Newman et al. (1997) suggested that phosphorous is present as either some poorly crystallised authigenic mineral, or in some organic combination with the coal. Rao and Walsh (1997) found the high phosphorous contents to be caused by the presence of crandallite-group minerals.

3.8. Conclusions

A considerable dataset has been presented for proximate analysis and ash constituent values and their distribution within the Huntly coalfield. The Renown seam shows greater variability than the Kupakupa seam and many differences have been identified between the seams suggesting that the seams should be considered as separate entities. Where available mineral matter counts from organic petrology and ultimate analysis results have also been presented. Conclusions are as follows:

- On average (excluding samples with >20% ash yield) the Renown seam has a higher ash yield (~3.8% aa) than the Kupakupa seam (~2.5% aa). In the Renown seam 72% of samples have ash yields of <5% (aa) while in the Kupakupa seam 89% of samples have ash yields of <5% and 64% have ash yields of <2% (aa). The lower half of the Kupakupa seam is characterised by compositionally homogeneous coal with <2% ash yield.
- On average ash constituents in the Renown seam have higher proportions of silicon, aluminium, magnesium, sodium, potassium and phosphorous while the Kupakupa has higher average iron, calcium, titanium and sulphur.
- The Kupakupa seam samples were divided into two groups, <2% and >2% ash yield. The two groups have clearly different signatures with the former group having higher proportions of iron, calcium, sodium and sulphur while the latter group has higher silicon, aluminium, titanium and phosphorous although this group still has significant concentrations of calcium and sulphur.
- Silicon was found to be associated with ash yield, whereas iron, calcium, magnesium, sodium and sulphur were found to be primarily associated with organic material. Relationships for aluminium, potassium, titanium, manganese and phosphorous were

unclear (likely of mixed association). When analysed using cluster analysis two distinct groups occur, an ‘inorganic associated group’ consisting of silicon, aluminium, titanium and phosphorous and an ‘organically associated group’ composed of iron, calcium, magnesium, sodium, manganese and sulphur. Potassium changes group depending on seam.

- Detrital and diagenetic quartz, detrital clay, epigenetic carbonates (likely calcite and ankerite); iron oxides and syngenetic pyrite were identified in the organic petrology study.
- There is a good relationship between hydrogen content (db) and volatile matter (db).

Chapter Four

Coal Petrology

The macroscopic texture of the Renown coal seam was assessed from eight cores, while coal of the Kupakupa seam was assessed from five cores. Each of the core intersections were macroscopically described for coal type as well as point counted for the abundance of vitrain versus matrix (Moore and Ferm, 1992; Moore and Hilbert, 1992; Shearer and Moore, 1994b). In all 1,893 macroscopic point counts were conducted on the Renown seam and 2,438 were counted on the Kupakupa seam. In addition, petrographic analysis was conducted on two profiles from each seam. The Jasper 1 and Mimi 1 cores were analysed for the Renown seam while the Ruawaro 1 and Ruawaro 2 cores were analysed for the Kupakupa seam. The results of these macroscopic and microscopic analyses are presented in this chapter, with all the raw data and complete coal logging sheets given in Appendix 2.

4.1. Coal rank

Mean maximum vitrinite reflectances for seam composites are presented in Table 4.1, with the reflectance histograms given in Appendix 2. The range of reflectance values, 0.42 – 0.45%, fits well with previously reported reflectance values of the Huntly coalfield, 0.42 – 0.52 % (Edbrooke et al., 1994; Li et al., 2009; Vu, 2008; Vu et al., 2008).

Table 4. 1. Measured vitrinite reflectance (R_{max}%) on seam composites.

Location	Seam	R_{max}%	SD
Mangapiko 1	Renown	0.43	0.044
Mangapiko 1	Kupakupa	0.42	0.048
Jasper 1	Renown	0.45	0.041
Ruawaro 2	Kupakupa	0.45	0.044

Vitrinite in some New Zealand coals are hydrogen-rich when compared with coals elsewhere (Newman, 1997b; Suggate, 1959). Reflectance suppression is thought to be primarily caused by: (1) variation in the hydrogen content of vitrinite (with higher hydrogen contents resulting in lower measured vitrinite reflectance), and (2) marine influence (Newman and Newman, 1982; Smith and Smith, 2007; Ward et al., 2007). Interestingly, Quick and Tabet (2003) found suppressed reflectance associated with higher methane yields in the Ferron coalbed gas fairway in Utah (U.S.A.). They ascribed this result to an overpressure during the early stages of coalification. It is commonly accepted that to identify reflectance suppression ideally more than one parameter should be used to determine rank (Newman, 1997b; Newman et al., 2000; Quick, 1994; Wilkins et al., 1992).

The Suggate rank scale (Suggate, 2000) plots the maturity of coals of differing coal types using two diagrams, one based on the Van Krevelen diagram, and the other with axes of

calorific value and volatile matter. The Suggate plot has an average-type line showing progressive coalification and iso-rank lines that indicate variation resulting from changing coal type. All samples, excluding those where ash yield is >10%, have been plotted using the calorific value versus volatile matter values for each seam (Fig. 4.1).

For the samples in this study, Suggate rank is generally between 6.0 and 7.0. However there are a few outliers. For example, two samples in Figure 4.1A have Suggate values < 6.0. Sample J2 from the Jasper 1 drill hole has a Suggate rank of 5.1 while sample 22 from the TW1 core has a rank of 4.3. Both of these samples have ash yields of 9%. Sample C12 from the Rotongaro drill hole plots above the New Zealand coal band in marked Figure 4.1B. This sample has been previously shown in Figure 3.4 to have a higher ash yield and a higher volatile matter content than the samples surrounding it. Previous Suggate ranks for the Huntly coalfield have been reported to vary from 5.0 to 9.2 (Butland, 2006; Edbrooke et al., 1994; Vu, 2008; Vu et al., 2008).

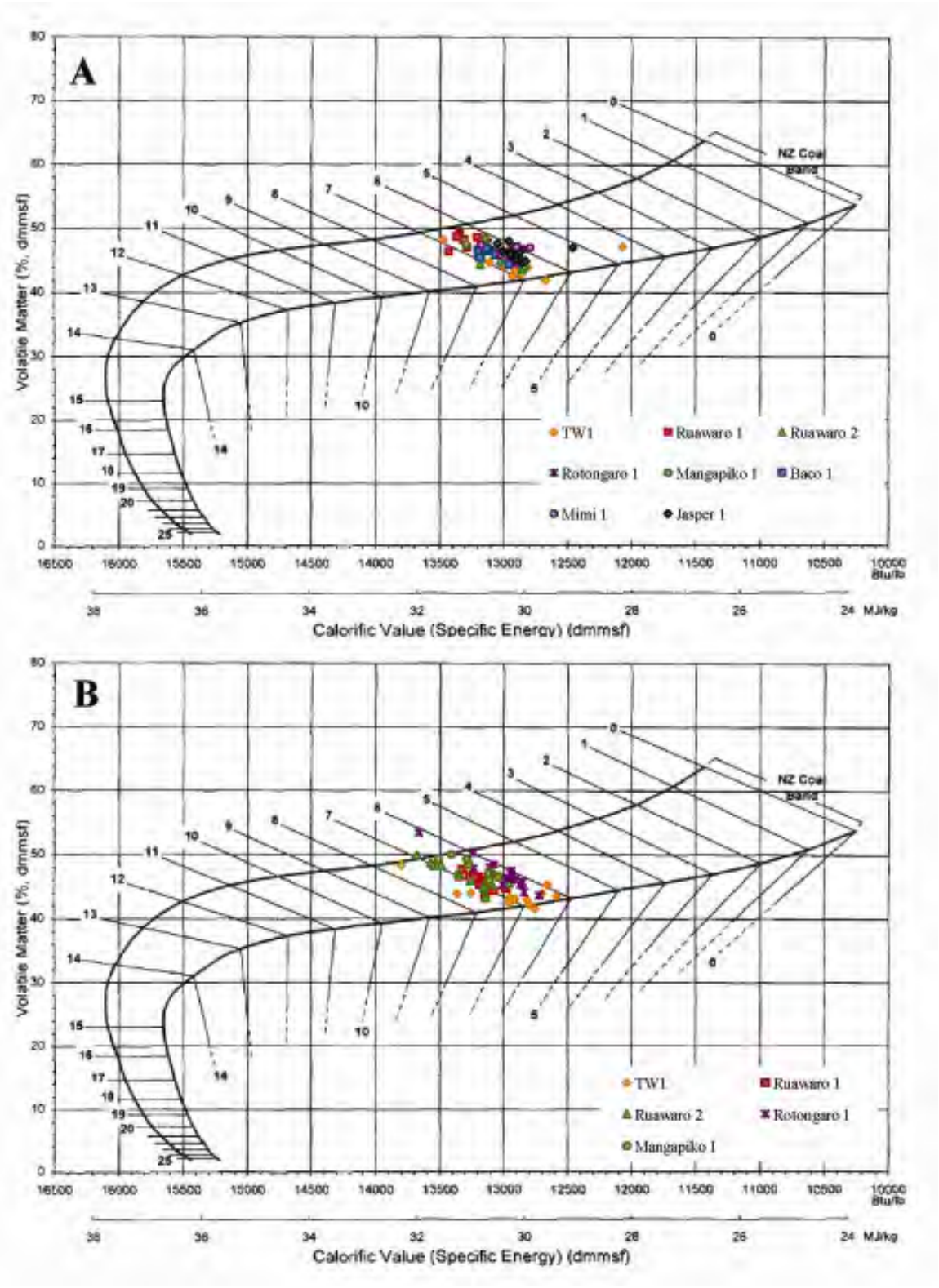

Figure 4. 1. Suggate plot for volatile matter versus calorific value on a dry, mineral matter and sulphur free basis (dmmsf – for corrected data see Appendix 2) for (A) the Renown seam and (B) the Kupakupa seam.

Greater lateral variation in Suggate rank values can be seen for each location in the Renown seam samples than for the Kupakupa samples. The Kupakupa samples plot reasonably parallel to the iso-rank lines. Data points spread parallel to iso-rank lines result from variation in the volatile matter content and calorific value related to coal type changes rather than from rank changes. The lateral variation in rank seen for the Renown seam samples is likely a result of the higher ash yield and inertinite content of the Renown seam. Confirmation of sample differences being from type changes, as opposed to rank differences, can be seen in the results of the VIRF analyses (Fig. 4.2 and Appendix 2). If there were any rank differences between the samples it would be identifiable by lateral shifts in the sample profiles (Newman, 1997b). There is no evidence for reflectance suppression in the Huntly coalfield.

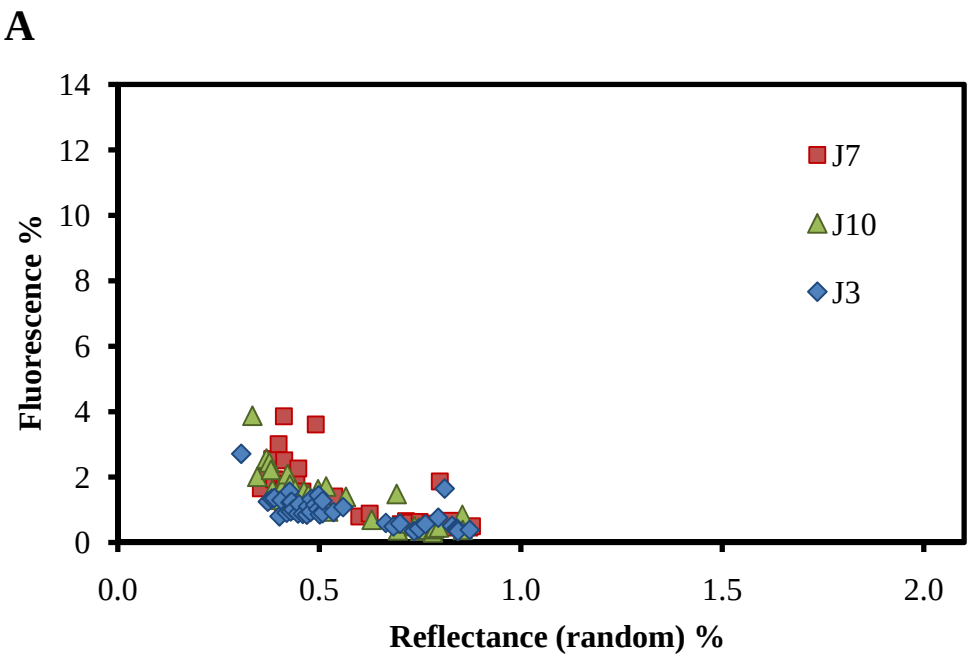

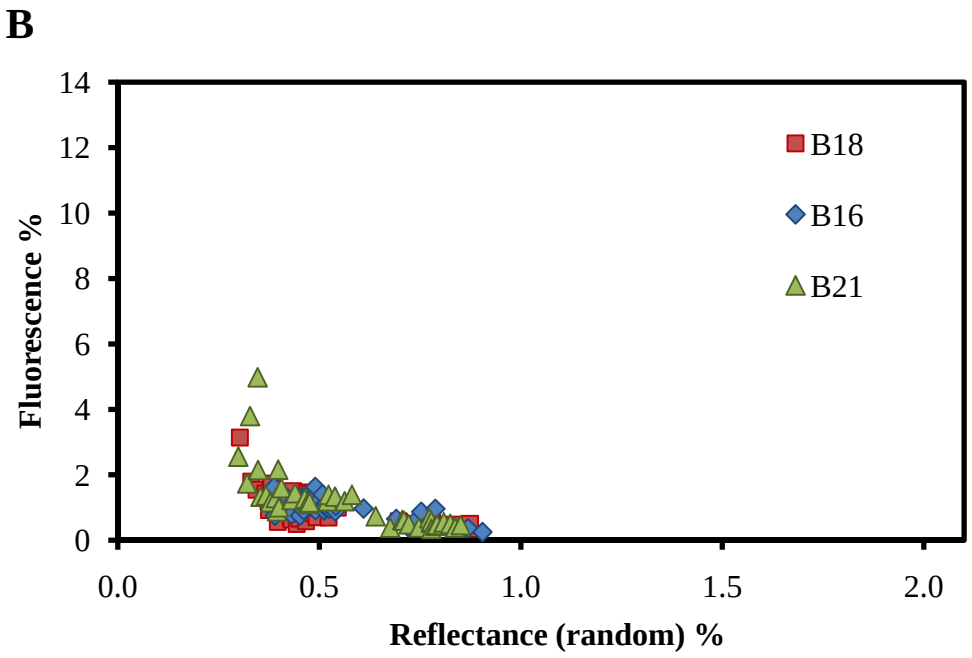

Figure 4. 2. Results for selected samples analysed using the VIRF technique. (A) Renown samples from the Jasper 1 core. (B) Kupakupa samples from the Ruawaro 2 core.

The freshness and storage history of a sample is known to have considerable influence on vitrinite fluorescence, with very high fluorescence values collected from pristine coals and much lower values obtained from stored and outcrop samples (Newman, 1997a; Quick, 1992; Quick, 1994). Newman (1995) found that fluorescence equilibrium conditions were reached within approximately one year of sampling under conventional storage conditions. As such, the difference in fluorescence between the Jasper 1 and Ruawaro 2 samples (Figure 4.3) is likely primarily a function of sample history with the Ruawaro 2 samples being collected over two years prior to VIRF analysis while the Jasper 1 samples were collected about one year prior to analysis.

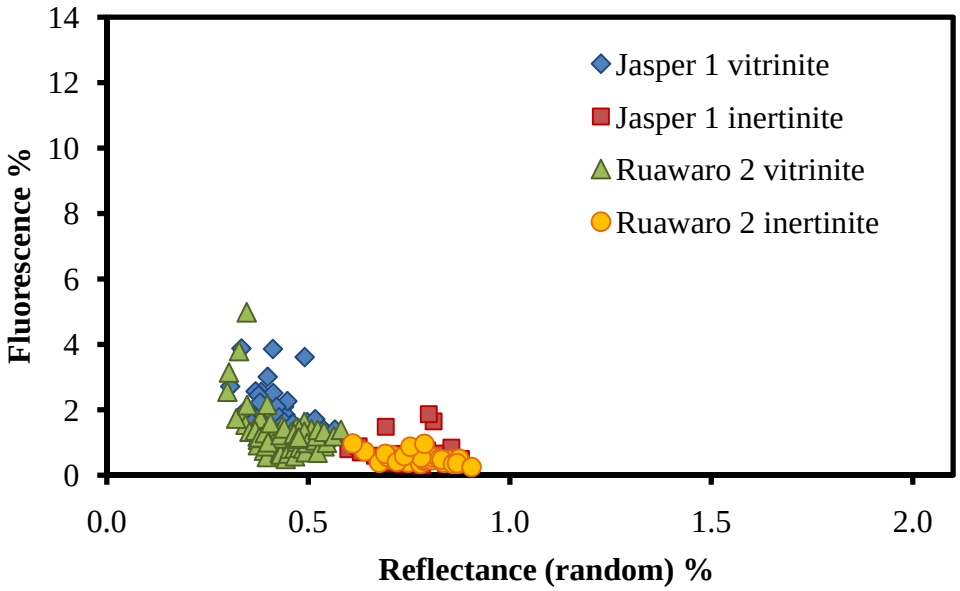

Figure 4. 3. VIRF analysis results grouped by seam.

4.2. Macroscopic texture

4.2.1. Macroscopic texture by drill hole

The distribution of coal types in the TW1 core is presented in Figure 4.4. Coal type distribution and percent vitrain information for the TW1 location was first presented by Butland (2006), however the phi size data for TW1 has not previously been presented.

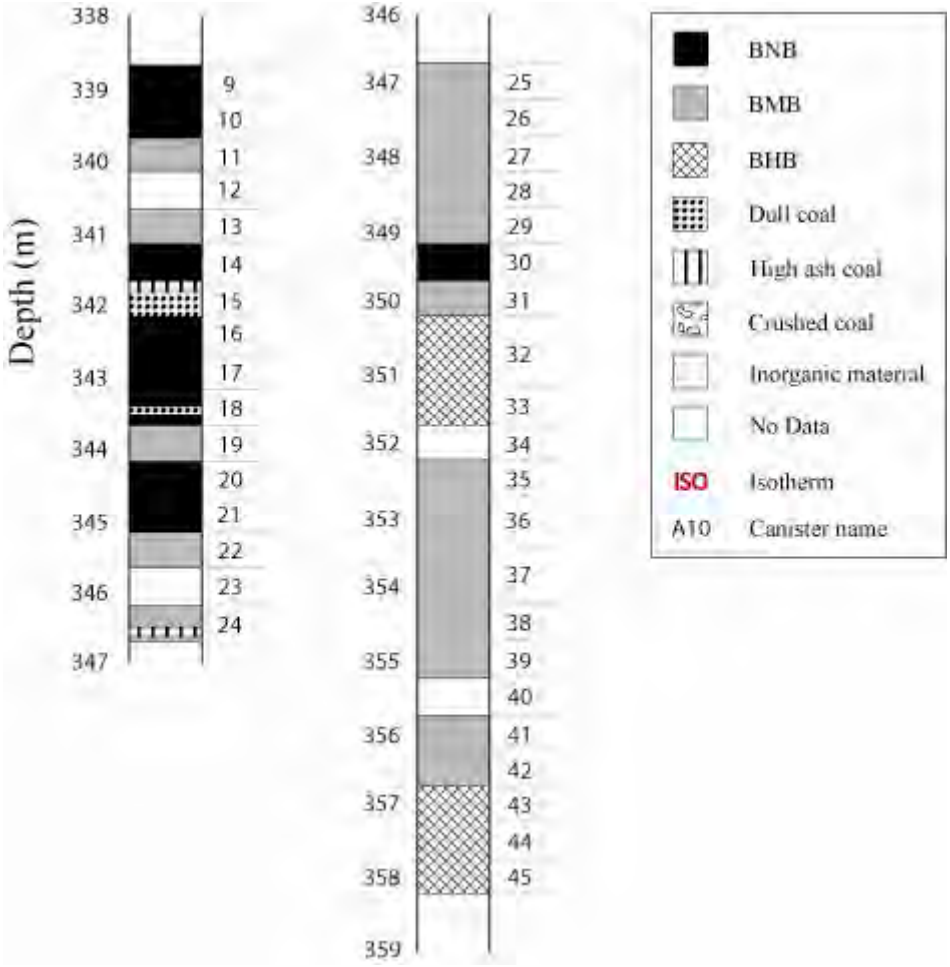

Figure 4. 4. Distribution of coal types in the TW1 core. The Renown seam is shown on the left with the Kupakupa seam shown on the right.

Much greater variation in coal type can be seen in the Renown seam at TW1 than for the Kupakupa seam. The Renown seam is dominated by the bright luster, non banded (BNB) coal type while the Kupakupa seam is relatively homogenous composed predominately of bright luster, moderately banded (BMB) coal with intervals of bright luster, highly banded (BHB) coal in the middle and at the base of the seam.

The split Renown seam at the Ruawaro 1 location, as presented in Figure 4.5, is generally moderately banded with BHB coal in the A10 and A11 samples. In contrast, the

Kupakupa seam has alternating intervals of BNB followed by banded coal. BHB coal is again present in the middle and at the base of the seam.

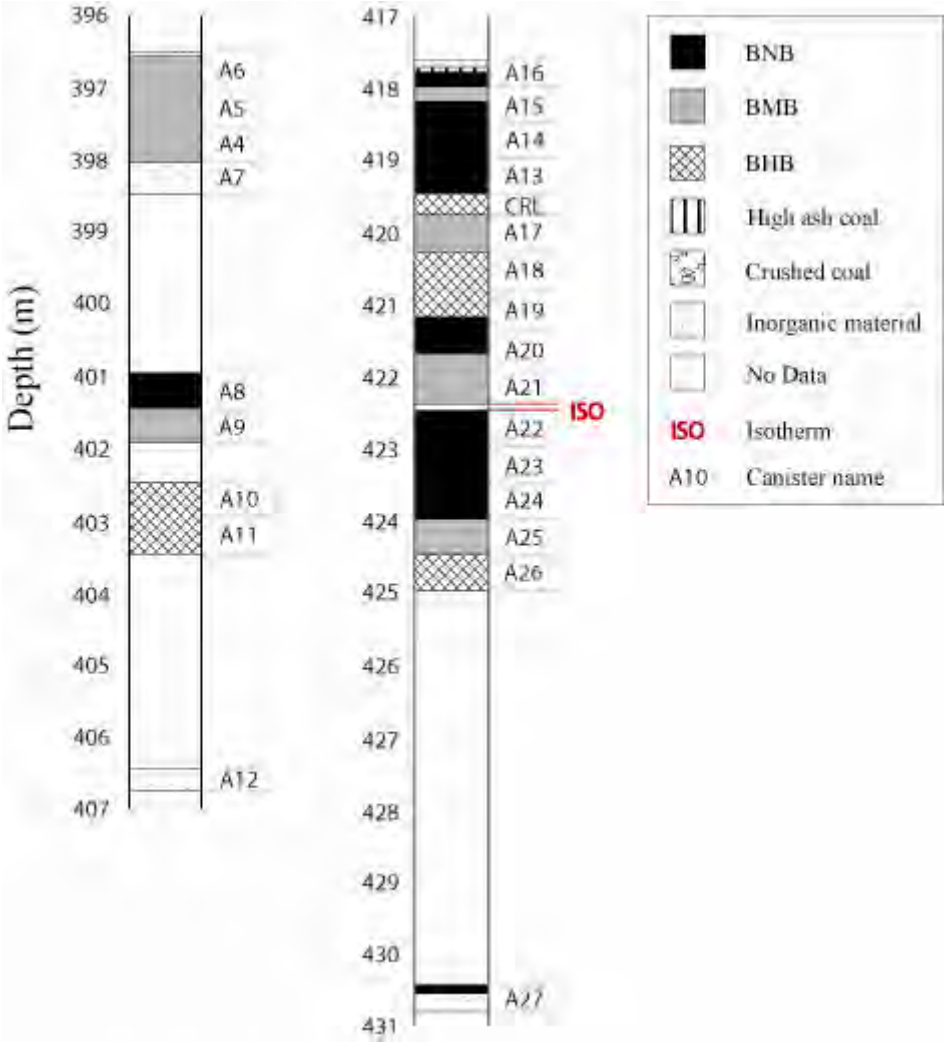

Figure 4. 5. Distribution of coal types in the Ruawaro 1 core. The Renown seam is shown on the left with the Kupakupa seam shown on the right.

The vertical coal type distribution for the Ruawaro 2 core is shown in Figure 4.6. The majority of the coal in the Renown seam in this core is BNB, while the bulk of the Kupakupa seam is non- to moderately banded. In both seams there is an interval of BHB coal occurring at the base of the seam. There were several non-coal layers, within the 0.5 m canister

intervals, identified during logging. Some of these canister intervals do not show an increase in ash yield results (Chapter 3) from the surrounding coal on either side. From this there were concerns about the methods used for some of proximate analyses. It is thought that for some of the canisters (in which both coal and lithic material was present) only the coal material was used for proximate analysis as opposed to using a representative split of the entire canister interval (as requested). Samples B11, B12 and B13 from Ruawaro 2 analyses and sample A27 from Ruawaro 1 appear to confirm this.

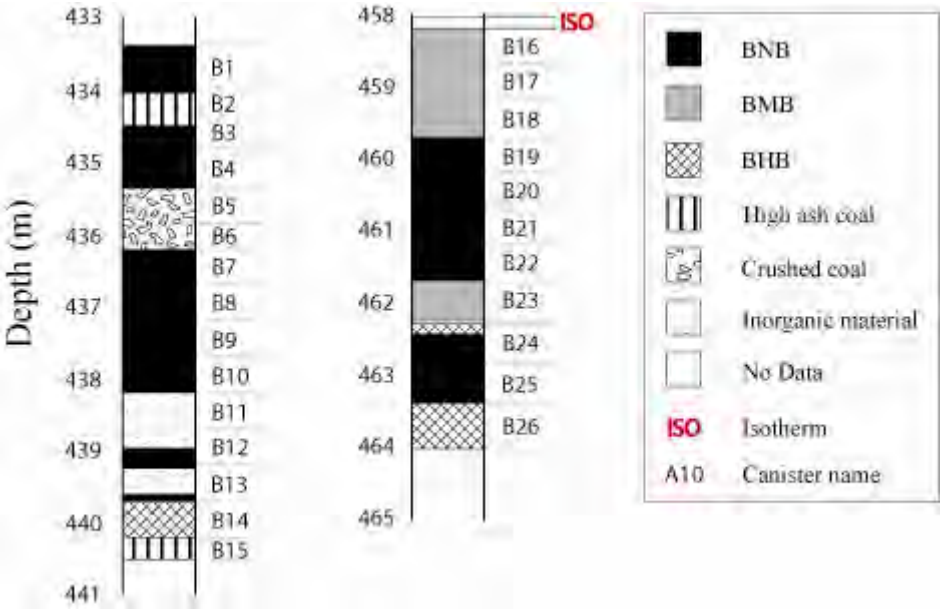

Figure 4. 6. Distribution of coal types in the Ruawaro 2 core. The Renown seam is shown on the left with the Kupakupa seam shown on the right.

The thin Renown seam cored at the Rotongaro 1 location is predominantly composed of the BNB coal type with the lower part of the seam being too crushed to identify any textural features (Figure 4.7). The almost 12 m thick Kupakupa however, is largely banded in the upper half and non-banded in the lower half of the seam. Unlike the other locations presented, the coal at the base of the Kupakupa seam in this location is not BHB.

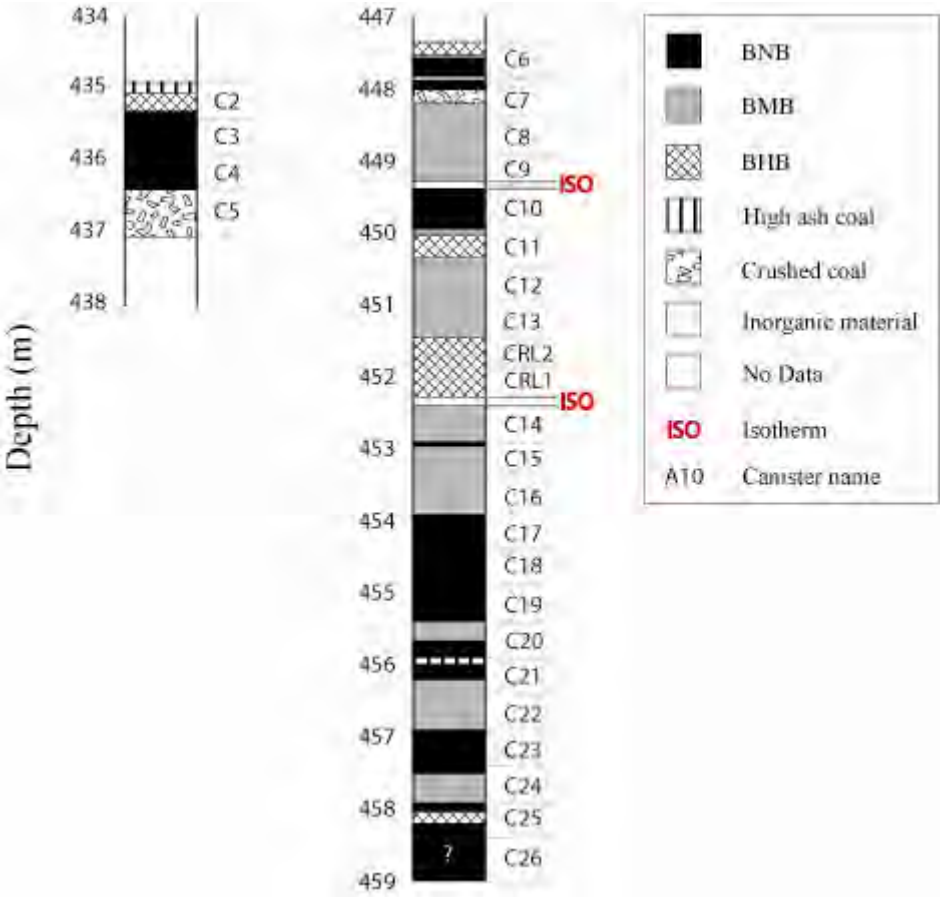

Figure 4. 7. Distribution of coal types in the Rotongaro 1 core. The Renown seam is shown on the left with the Kupakupa seam shown on the right.

In contrast to the Renown seam in most of the other locations, at the Mangapiko 1 location the Renown seam is dominated by the banded coal types with the coal at the base of the seam being BHB (Fig. 4.8). The Kupakupa seam at this location is completely composed of banded coal types, although with a greater proportion of BHB coal than seen in the Renown seam. The BHB coal type is predominantly present in the lower half of the Kupakupa seam.

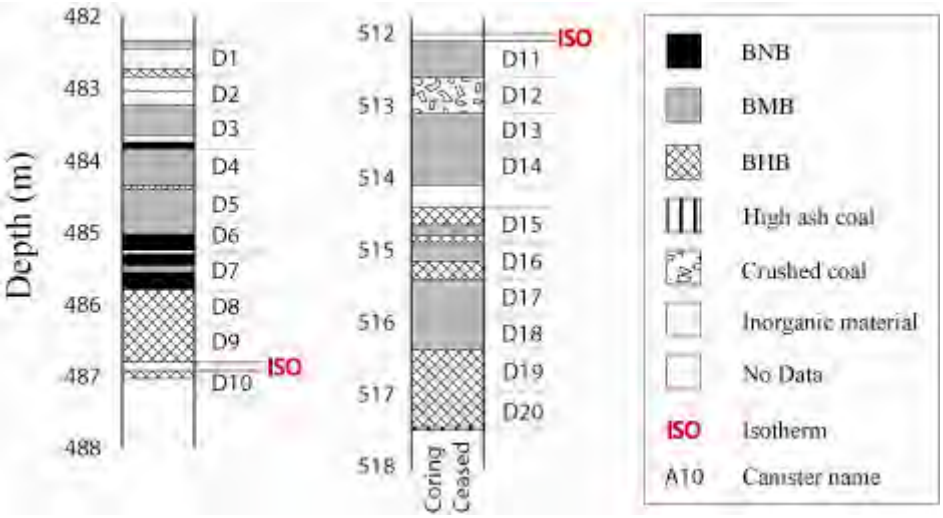

Figure 4. 8. Distribution of coal types in the Mangapiko 1 core. The Renown seam is shown on the left with the Kupakupa seam shown on the right.

The coal type profiles for the Renown seam at the Jasper 1, Mimi 1 and Baco 1 locations are all presented in Figure 4.9. Both the Jasper 1 and Mimi 1 profiles show thick intervals of BNB coal in the mid-seam areas with banded material in the upper and lower parts of the seam (sample J2 is difficult to classify because of the persistent calcite mineralization while J11 is noted as being banded). Unfortunately very little information was able to be collected from the Baco 1 location because of the highly crushed coal retrieved.

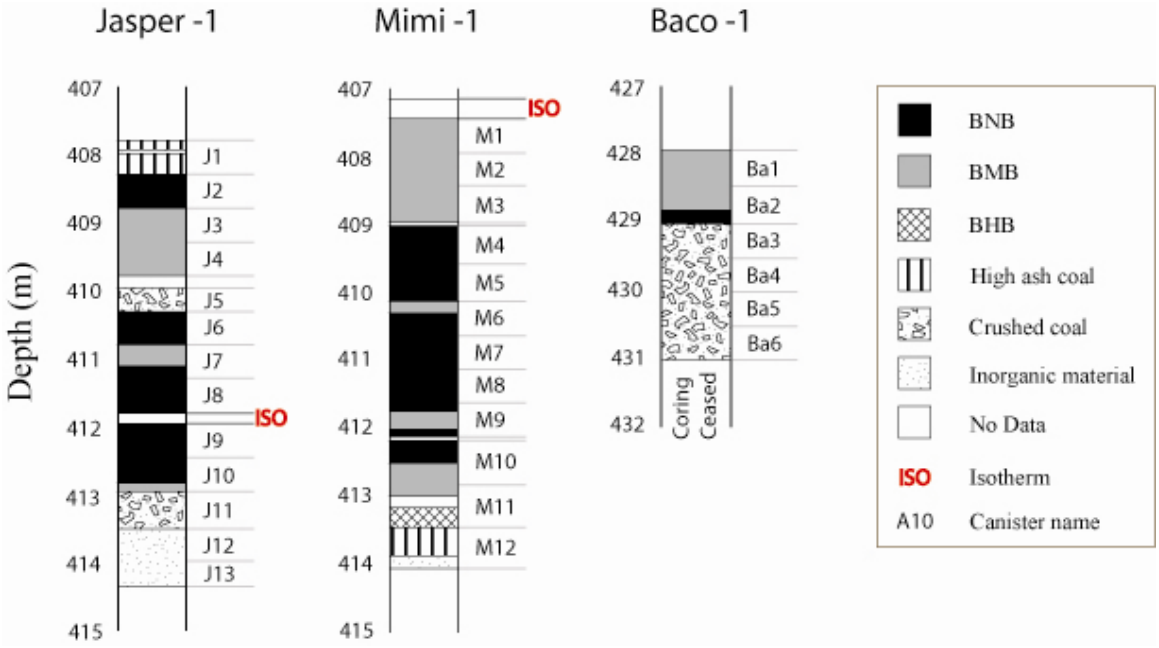

Figure 4. 9. Distribution of coal types in the Jasper 1, Mimi 1 and Baco 1 cores.

4.2.2. Macroscopic texture by seam

In the location profiles just discussed it can be seen that, with the exception of Rotongaro 1, the coal at the base of the Kupakupa seam is highly banded. This is also true of several of the Renown seam profiles. Edbrooke et al. (1994) and Newman et al. (1997) also report an increase in banded material around the seam floor and inorganic partings in the Waikato coalfields. Resin nodules of various sizes were observed in samples throughout the coal in both seams. Resin nodules are common in low rank coals (Suggate, 1959). Cleat spacings in the coal were found to vary from 1 – 4 cm.

A total of 1,077 vitrain bands were point counted and measured in this study. In the Renown seam 404 vitrain bands were counted as opposed to the Kupakupa seam cores in which 673 were counted. Thus the Kupakupa seam cores contained more vitrain, in general,

than the Renown seam (28% of all counts, as opposed to 21%). The percentage of each coal type identified at each location is presented in Table 4.2. From this data, it becomes clear that generally a high proportion of the coal in the Renown seam is composed of the BNB coal type. This is further seen from plotting the percentage of each coal type by seam (Fig. 4.10). As expected the relationship between coal type and percentage vitrain shows that the percentage vitrain increases from BNB to BHB coal, quantitatively substantiating the qualitative classification scheme (Fig. 4.11).

Table 4. 2. Percentage composition of coal types in core at each location.

	Renown			Kupakupa		
	BNB	**BMB**	**BHB**	**BNB**	**BMB**	**BHB**
TW 1	72%	28%	0%	7%	48%	45%
Ruawaro 1	18%	49%	33%	50%	26%	24%
Ruawaro 2	89%	11%	0%	47%	39%	13%
Rotongaro 1	83%	0%	17%	41%	46%	14%
Mangapiko 1	20%	46%	34%	0%	64%	36%
Jasper 1	64%	36%	0%			
Mimi 1	52%	42%	6%			

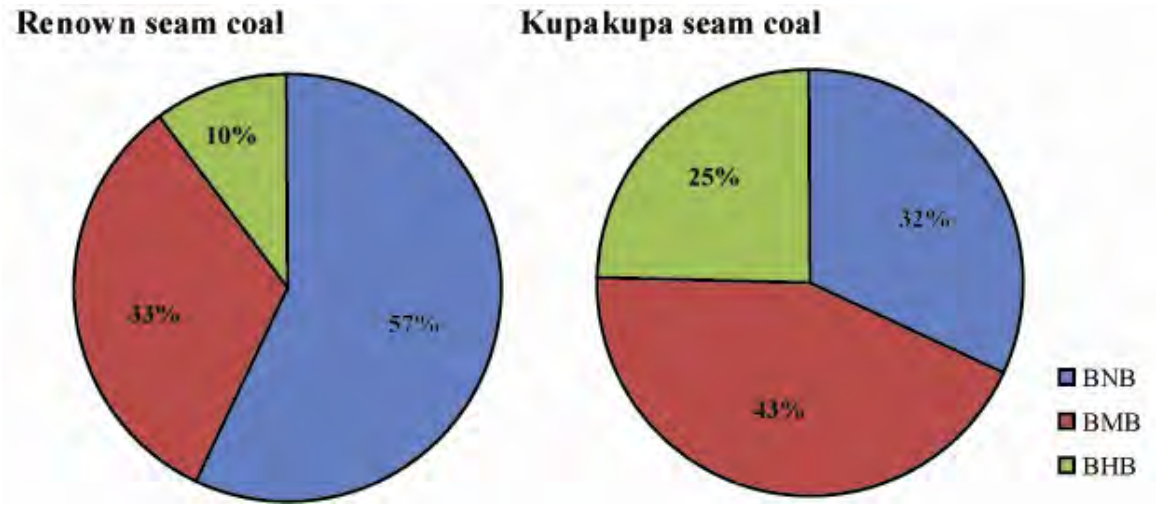

Figure 4. 10. Percentage coal type for the Renown and Kupakupa seams. BNB= bright luster, non banded coal, BMB= bright luster, moderately banded coal and BHB= bright luster, highly banded coal.

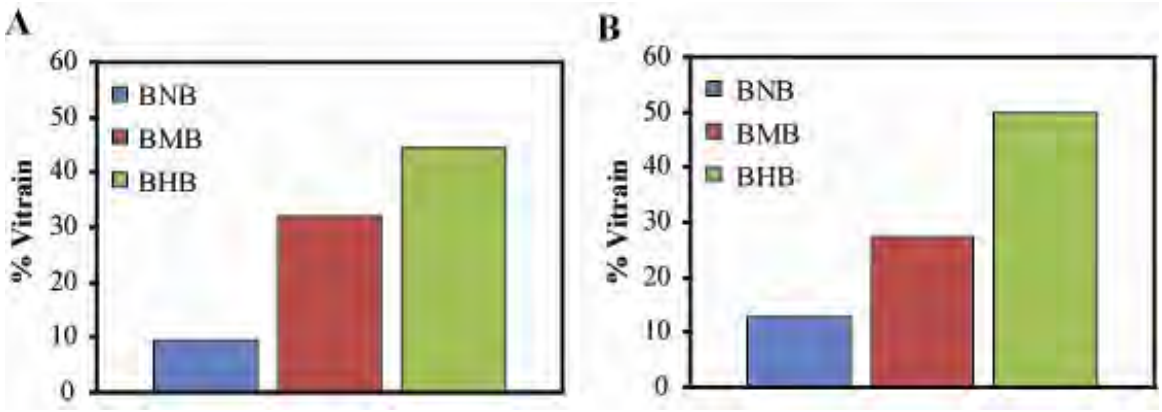

Figure 4. 11. Percentage vitrain shown versus coal type for (A) the Renown seam and (B) the Kupakupa seam. BNB= bright luster, non banded coal, BMB= bright luster, moderately banded coal and BHB= bright luster, highly banded coal.

A comparison of average phi size by coal type shows that the vitrain bands become coarser from BNB to BHB. This suggest that the more banded the coal, the thicker the bands, with the more highly banded material in the Renown seam being coarser than that in the Kupakupa seam (Fig. 4.12). The average phi sizes by location and by seam are presented in Table 4.3. It must be noted that average phi sizes are small, showing that the vitrain bands are generally thin. Of all the vitrain bands measured approximately 70% have a diameter of 1 mm or less, 90% have a diameter of 3mm or less, and 99% have a diameter of 10 mm or less.

Table 4. 3. Average phi size for each location by seam.

	Renown	Kupakupa
TW1	-0.12	-0.69
Ruawaro 1	-0.11	-0.10
Ruawaro 1	0.13	-0.21
Rotongaro 1		0.12
Mangapiko 1	-0.24	0.18
Jasper 1	0.13	
Mimi 1	0.00	
Average	-0.06	-0.11

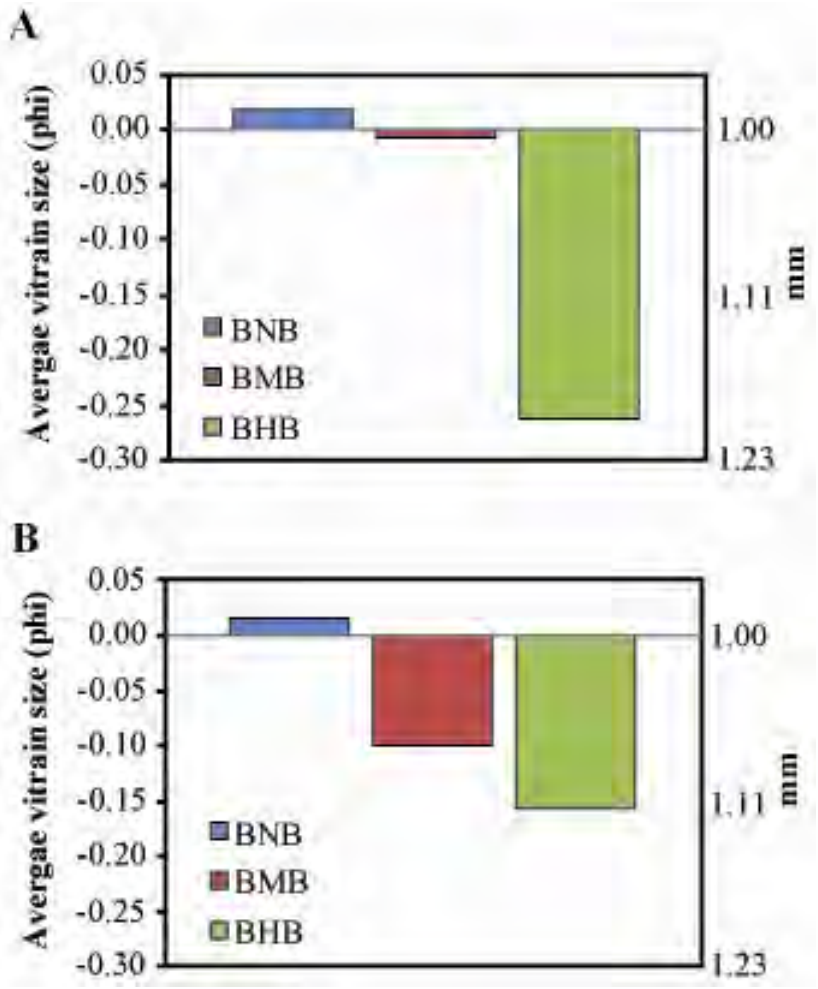

Figure 4. 12. Average vitrain band thickness (phi size) versus coal type for (A) the Renown seam and (B) the Kupakupa seam. BNB= bright luster, non banded coal, BMB= bright luster, moderately banded coal and BHB= bright luster, highly banded coal.

4.2.3. Macroscopic texture by location

Four of the drill holes (Ruawaro 2, Baco 1, Mimi 1 and Jasper 1) are located in the same area (designated the 'Beverland Road' area), while the other drill holes are distributed throughout the coalfield. If coal type results for the Renown seam are grouped by location, the Beverland Road cores are composed of 67% BNB whilst the other Renown seam sites (Ruawaro 1, Rotongaro 1 and Mangapiko 1) are composed of only 48% BNB coal types (Fig.

4.13). The average phi size is also much finer at the Beverland Road location, 0.07 φ, compared with an average of –0.17 φ at the other locations. These results identify the coal retrieved from the Beverland Road site as being compositionally different to coal retrieved from the Renown seam in drill holes located in other parts of the coalfield.

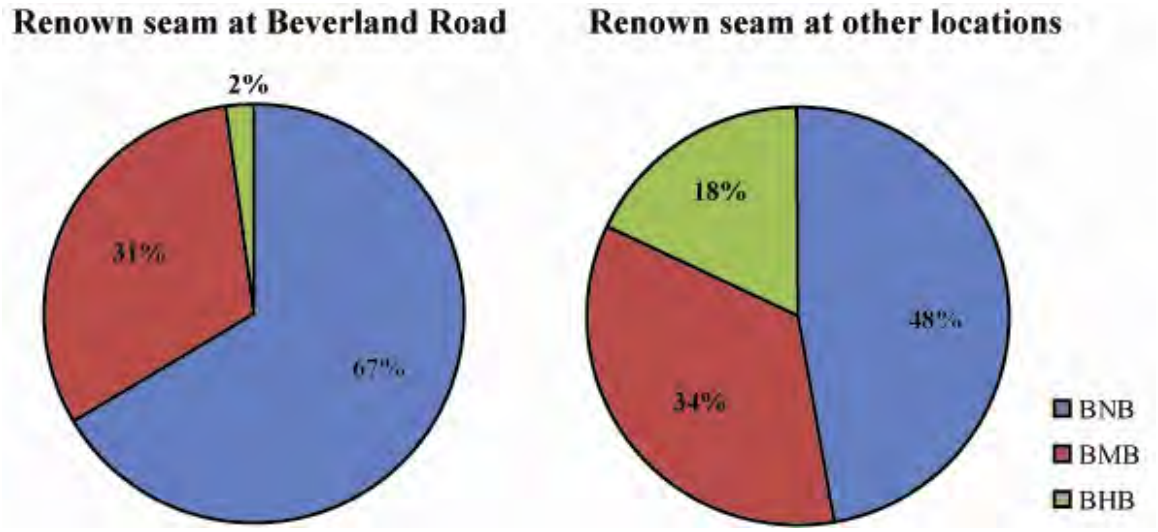

Figure 4. 13. Coal type distribution for the Renown seam at the Beverland Road site and the Renown seam of the other drill holes combined. BNB= bright luster, non banded coal, BMB= bright luster, moderately banded coal and BHB= bright luster, highly banded coal.

4.3. Organic Petrology

4.3.1. Organic petrology by drill hole

The major maceral groups identified for the samples collected from the Renown seam at the Jasper 1 location are presented in Figure 4.14 (For full table see Appendix 2). Clearly, vitrinite is the dominant component ranging from 69% (in sample J7) to 86% (J4), on a mineral matter free basis (mmf). Noticeably the vitrinite component is dominated by detrovitrinite.

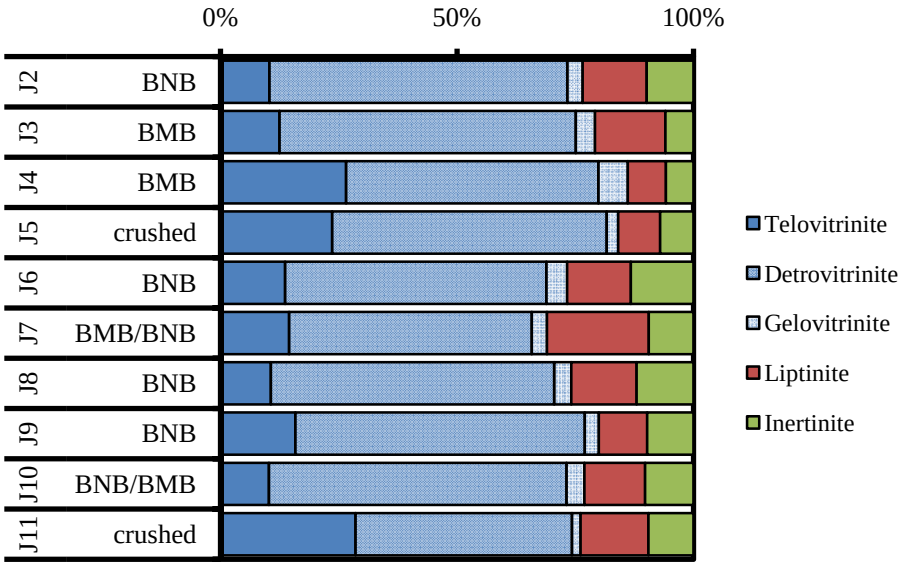

Figure 4. 14. Organic petrology results for samples for the Renown seam from Jasper 1 core.

For the samples analysed in the Jasper 1 drill hole, the most abundant maceral of the telovitrinite subgroup is collotelinite D, contributing 3% – 22% of the total composition, followed by collotelinite A contributing up to 5%. Collodetrinite and vitrodetrinite are the predominant macerals identified throughout the profile having ranges of 21% – 35% and 23% – 41% of the total composition respectively. Gelovitrinite represents only a small proportion of the total composition, with corpocollinite reaching a maximum of 3% while porigelinite is as high as 4%.

The highest liptinite content (22%) was recorded in sample J7. No other sample from this location contained more than 15% liptinite. During the petrographic analysis it was noted that sample J7 has some liptinite-rich particles that have abundant sporinites. The major contributor in the liptinite group was liptodetrinite, 6% - 15%, with resinite contributing up to 3% and sporinite up to 2%. The inertinite group is the least represented maceral group within

the samples from the Jasper 1 location, reaching a maximum of 13% in sample J6. The two most predominant macerals in the inertinite group are inertodetrinite and funginite contributing 3% - 7% and 1% - 4% respectively.

The second Renown seam profile analysed, from the Mimi 1 location (Figure 4.15), has a noticeably similar trend for maceral group percentages to that identified from the Jasper 1 location. This was not unexpected because of the close proximity of these two locations. Total vitrinite content ranged from 72% (sample M6) to 86% (sample M3). As was noted in the Jasper 1 samples, vitrinite is again primarily composed of detrovitrinite. Interestingly for both seams the samples with the highest vitrinite content (J4 and M3) also have the highest gelovitrinite content.

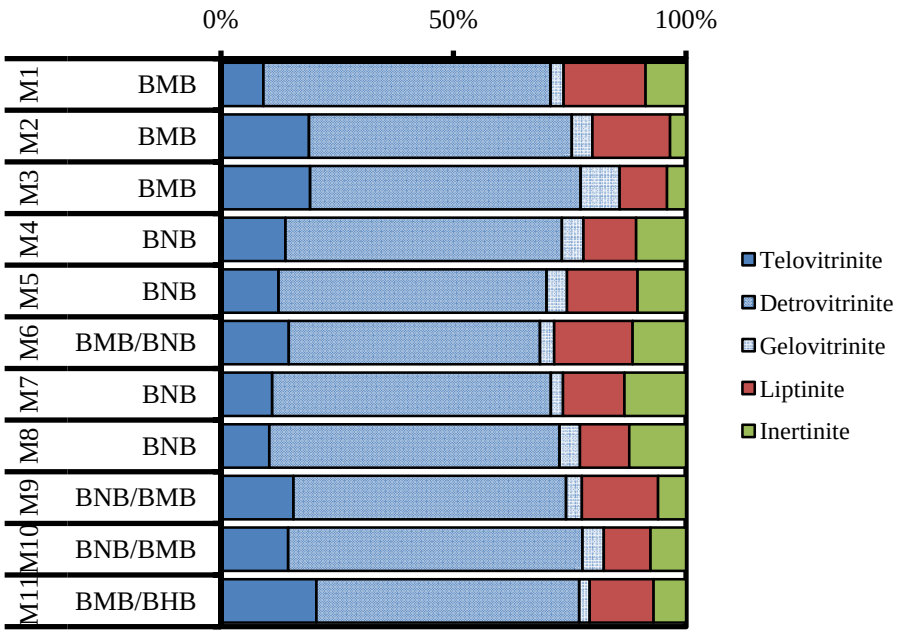

Figure 4. 15. Organic petrology results for samples for the Renown seam from Mimi 1 core.

In samples analysed from the Mimi 1 drill hole, the most abundant maceral of the telovitrinite subgroup is collotelinite D, contributing 3% – 12% of the total composition, followed by collotelinite B and collotelinite A contributing up to 6% and 5% respectively. Collodetrinite and vitrodetrinite were again the predominant macerals identified, having ranges of 17% – 35% and 22% – 45% of the total composition respectively. The gelovitrinite macerals, corpocollinite and porigelinite have concentrations of up to 4% and 6% respectively.

The highest liptinite percentage in the Mimi 1 core is 18% (sample M1). In general there is less variability in liptinite content in the Mimi 1 samples than for the Jasper 1 samples. Liptinite-rich and liptinite- inertinite-rich areas were identified mid-seam (samples M5, M6 and M7). The liptinite group was composed predominately of liptodetrinite, 6% - 13%, with suberinite, resinite and sporinite each contributing up to 3%. The inertinite content was highest in sample M7, at 13%, with inertodetrinite contributing 2% - 7% and funginite 1% - 6%.

The Kupakupa seam profile analysed from the Ruawaro 1 location (Figure 4.16) shows that the Kupakupa seam is also dominated by the vitrinite group, particularly detrovitrinite, with a larger contribution of telovitrinite macerals and noticeably less gelovitrinite macerals than the Renown seam profiles. Total vitrinite content ranged from a low of 75% (sample A13) to a high of 86% (sample A24).

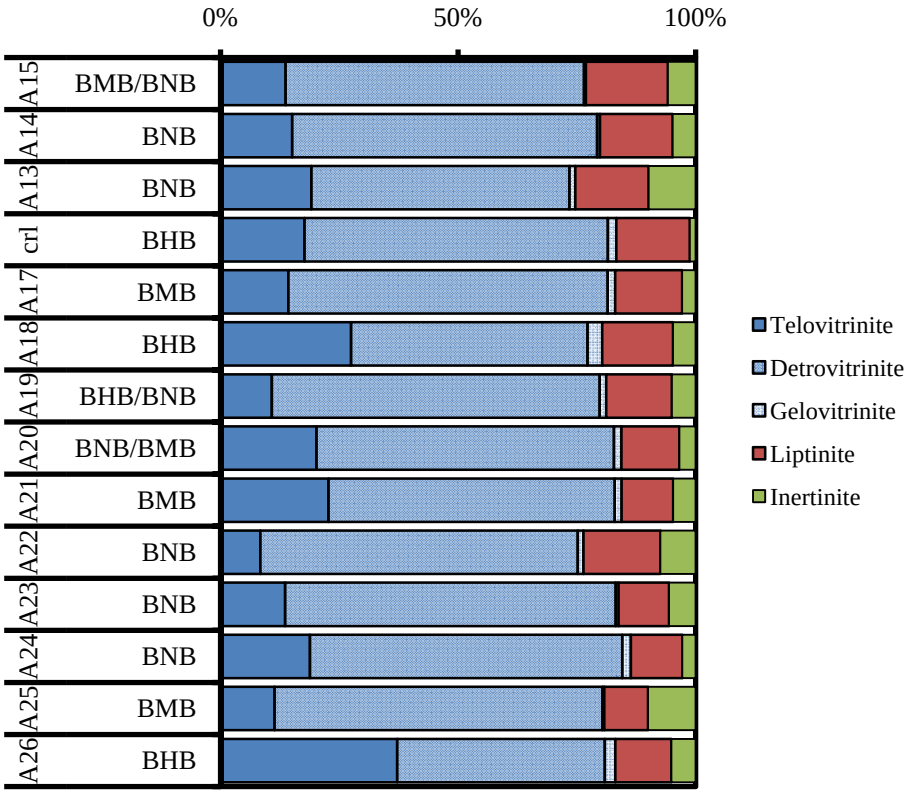

Figure 4. 16. Organic petrology results for samples for the Kupakupa seam from Ruawaro 1 core.

In the Ruawaro 1 drill hole, the dominant maceral of the telovitrinite group is again collotelinite D, contributing from 3% to 31% of the total composition, followed by collotelinite A contributing up to 7%. The sample with the highest structured vitrinite content, A26, also contains thick particles of cutinite. Collodetrinite and vitrodetrinite are still in general the predominant macerals identified, having ranges of 19% – 42% and 18% – 50% of the total composition respectively. As mentioned above, the gelovitrinite content is lower than seen for the Renown seam profiles, with corpocollinite and porigelinite only contributing up to 3% and 1% of the total composition, respectively.

The largest liptinite contribution, in the Kupakupa seam from the Ruawaro 1 drill hole, is 17% (sample A15). This sample also contains particles with laminated clays and concentrated liptinite and inertinite. These features were also noted in the two stratigraphically lower samples (A14 and A13). Overall the seam interval liptinite is predominately composed of liptodetrinite, 6% - 13%, with resinite contributing up to 3%. The inertinite content was highest in sample A25 (10%), with inertodetrinite contributing up to a maximum of 8% and funginite up to 3%.

The second Kupakupa profile was analysed from the Ruawaro 2 location (Fig. 4.17). The profile is not dissimilar to that seen for the Ruawaro 1 profile although there is a larger contribution by gelovitrinite macerals. Total vitrinite content is again very high ranging from 74% (sample B26) to 88% (sample B23).

Collotelinite D is again the dominant maceral of the telovitrinite subgroup in the Ruawaro 2 core, ranging from 5% to 19% of the total composition, with collotelinite A contributing up to 5%. Collodetrinite and vitrodetrinite are abundant with ranges of 24% – 38% and 18% – 43% respectively. The gelovitrinite macerals, corpocollinite (up to 4%) and porigelinite (up to 6%), are more common in the Ruawaro 2 profile than in the Ruawaro 1 profile.

The largest liptinite percentage in the Ruawaro 2 core is 23% (sample B26). Texturally, this sample was noted to have frequent fine liptinites mixed throughout the matrix material. The liptinite group is predominately composed of liptodetrinite (6% - 15%), with resinite contributing up to 4% and suberinite up to 3% of the total composition. The inertinite

content is highest in sample B20, at 7%, with inertodetrinite and funginite each contributing up to 4%.

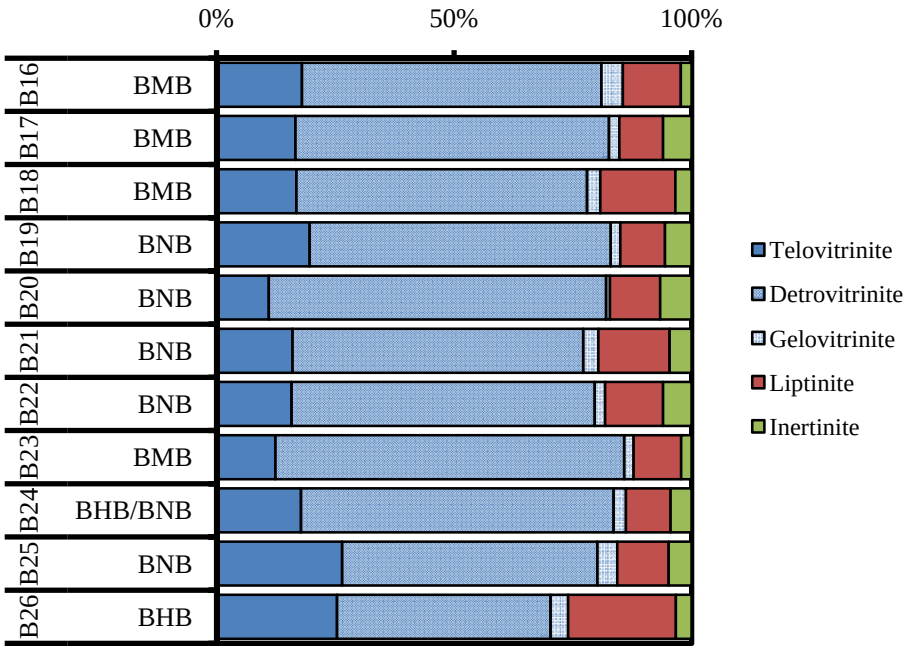

Figure 4. 17. Organic petrology results for samples for the Kupakupa seam from Ruawaro 2 core.

4.3.2. Organic petrology by seam

The average vitrinite, liptinite and inertinite contents of the Renown and Kupakupa seams, using the samples discussed above, are presented in Figure 4.18A. The difference between the seams is that the Renown seam has less vitrinite and more inertinite than the Kupakupa seam. Both seams have a similar liptinite percentage. The average percentage that each of the different textural components of vitrinite, structured vitrinite (telovitrinite and gelovitrinite), collodetrinite and vitrodetrinite, contributes to the total coal composition is presented by seam in Figure 4.18B. The Kupakupa seam has higher average percentages of all three types of vitrinite. For both seams vitrodetrinite is the dominant maceral. A more

detailed comparison of the composition of the two seams is presented in Figure 4.19. It can be seen that, on average, the Renown seam has higher proportions of telinite, gelovitrinite (corpocollinite and porigelinite), sporinite, semifusinite, funginite and inertodetrinite, while the Kupakupa seam has higher telovitrinite (most noticeably telocollinite A and D), collodetrinite, vitrodetrinite and cutinite. Figure 4.18 and 4.19 show the Kupakupa seam has both higher vitrinite content and a higher proportion of larger, more structured tissue than the Renown seam. This agrees well with the Section 4.2.2 finding a higher prevalence of banding in the Kupakupa seam rather than the Renown seam.

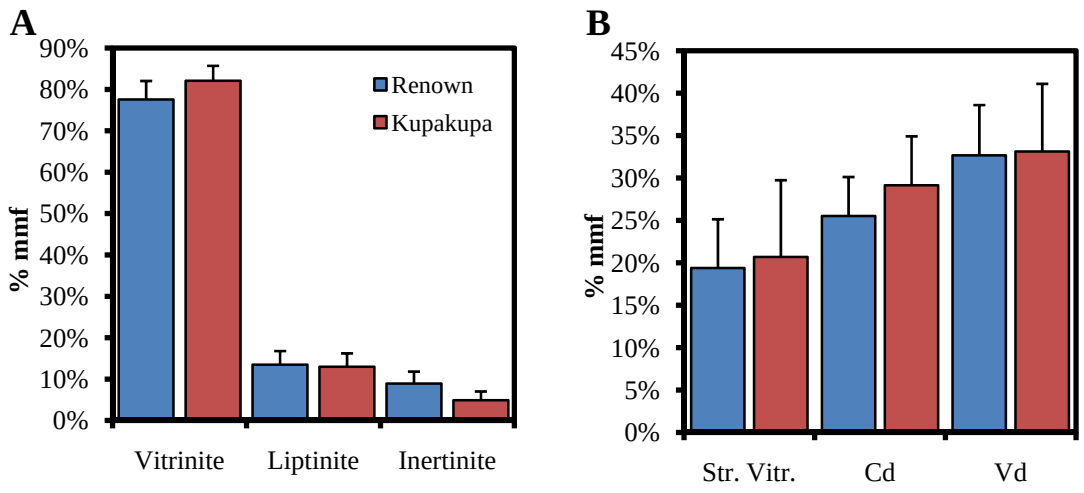

Figure 4. 18. (A) Maceral group averages by seam. (B) Average percentage of vitrinitic textural components by seam. Str. Vitr =Structured vitrinite, Cd = collodetrinite, Vd = vitrodetrinite.

The maceral group proportions reported here for samples from the Huntly coalfield are similar to those published in previous studies (Butland, 2006; Edbrooke et al., 1994). Organic petrology results presented in Figures 4.14 – 4.17 above were combined with those of two samples from Rotongaro 1 (C4 and C11), three from Mangapiko 1 (D13, D18 and D19), eight from TW1 (Butland, 2006) and six samples from profiles 9 - 14 as reported by Edbrooke et al. (1994) to create overall seam averages (Table 4.4). It can be seen that on

average the Renown seam has lower vitrinite content and almost double the inertinite content of the Kupakupa seam.

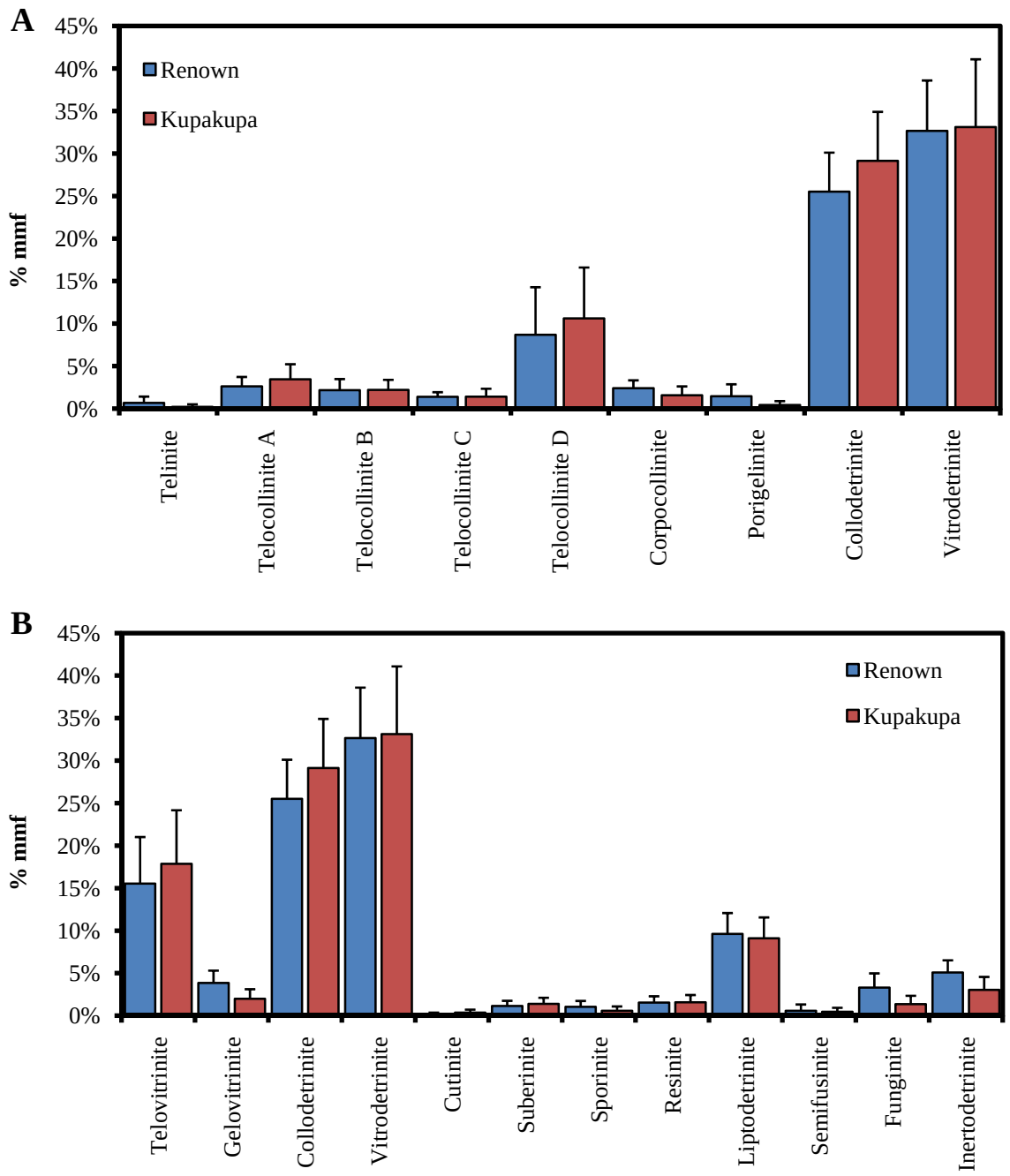

Figure 4. 19. (A) Average percentage of vitrinite macerals by seam. (B) Average percentage of vitrinite subgroups and liptinite and inertinite macerals by seam.

Table 4. 4. Maceral group seam averages (mmf) by seam including data from TW1 (Butland, 2006) and for profiles P9-P14 (Edbrooke et al., 1994).

	Seam	Minimum	Average	Maximum	SD	n
Vitrinite	Renown	69.01	79.44	88.89	5.17	29
	Kupakupa	74.02	83.85	92.93	4.25	36
Liptinite	Renown	4.12	12.00	21.53	4.15	
	Kupakupa	2.06	11.30	22.68	4.19	
Inertinite	Renown	3.42	8.52	13.25	2.10	
	Kupakupa	1.20	4.79	10.00	2.91	

4.3.3. Microscopic texture

As shown in Sections 4.3.1 and 4.3.2, the high vitrinite content of the coal samples is predominantly composed of collodetrinite and vitrodetrinite. Additionally, the dominant macerals for the liptinite and inertinite components were liptodetrinite and inertodetrinite. As such, the texture at the microscopic level is frequently mottled, fine-grained and unstructured with numerous small grains.

Two different matrix textures were observed that could not be characterized by standard petrographic classification schemes. One appeared ‘mushy’ and unconsolidated with no distinct orientation, while the other appeared more consolidated and exhibited a preferred alignment (Figure 4.20). Although this distinction is subjective, it is thought that the more unconsolidated-looking matrix is more common in BNB coal intervals, while the more consolidated-looking matrix material is more common in banded coal type intervals.

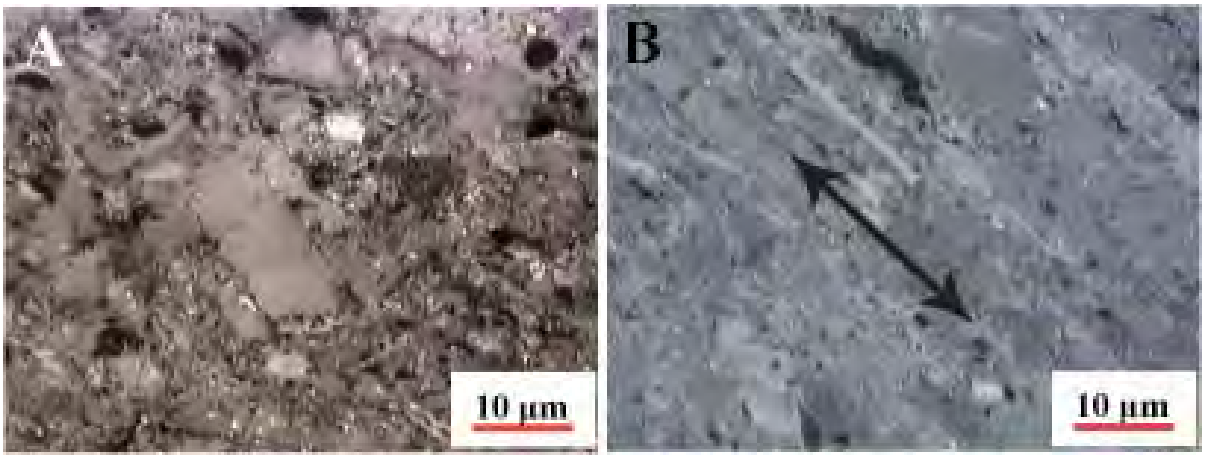

Figure 4. 20. (A) Less consolidated 'mushy' matrix material. (B) More consolidated matrix material showing preferential orientation.

Micro-deformation features (micro-faults and micro-brecciation) were also noted during petrographical examination. These features were observed in samples from all locations and were particularly noticeable in samples J9 (Jasper 1), A17, A21 (Ruawaro 1) and C4 (Rotongaro 1). The far majority of observations of micro-deformation were noted in macerals sourced from plant tissue.

4.3.4. Porosity

In the macroscopic examination of the coals from the Huntly coalfield, visible porosity in hand held specimens tended to only be in the form of cleats. Some pores were observed using microscopic methods (Figure 4.21). Larger pores, up to around 30 µm in diameter, were seen in funginite, although funginite only contributes 1% - 6% of Huntly coal, while smaller pores (generally <3 µm) were seen in structured vitrinite (telovitrinite). Of the 2871 collotelinite C and D, >50 µm in diameter, tissues point counted, 35% have visible pores. It was found that 51% of the pores checked under UV light were open while the

remaining pores had fluorescent resin infill. It is thought that finer porosity, in the sub-micron size range, exists in the matrix material, around grain boundaries, in the sometimes porous collodetrinite and, where present, in porigelinite.

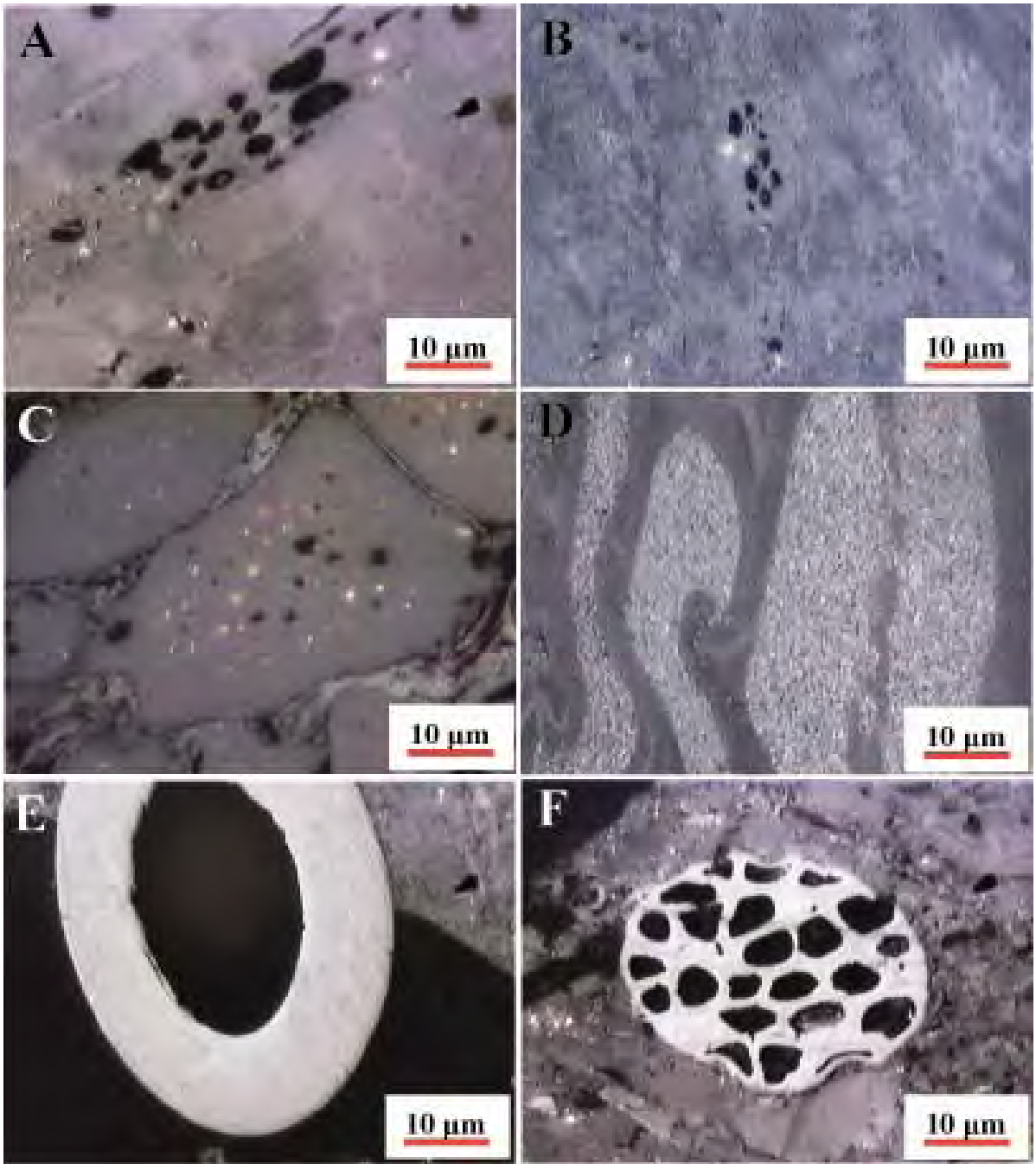

Figure 4. 21. Porosity observed in Huntly coals. (A-B) porosity in collotelinite D, (C) porosity in corpocollinite, (D) micro-porous porigelinite, (E) large pore in a unicellular funginite, and (F) porosity in funginite.

4.3.5. Hydrocarbons

Under UV light, greenish blurring and occasional bubbles were observed moving from the cracks and cleats in some samples. This phenomenon was particularly noticeable in the Jasper 1 suite of samples. Bubbles were noticed escaping in samples J4, J5, J6 (Jasper 1), M2, M6, M9 (Mimi 1), A15 (Ruawaro 1), B17, B18, B19 and B21 (Ruawaro 2). In sample B17 a particle cracked to release a bubble. It is thought that this fluorescence is mobile hydrocarbons rapidly emitted from micro-fractures and porosity. Bubbling occurs when hydrocarbons vapourise because of heating under UV illumination (J. Newman, pers com. 2007).

4.3.6. Average fluorescence intensity

The average fluorescence results for the vertical profiles from the Jasper 1 Renown seam (samples J2 – J11) and the Ruawaro 2 Kupakupa seam (samples B16 – B26) are presented in Figure 4.22. The Renown seam samples show higher variability in average fluorescence than the samples from the Kupakupa seam. Sample J7 from Jasper 1 has noticeably higher average fluorescence intensity, and sample B19 has distinctly lower average fluorescence intensity, than the remaining samples of their respective profiles. Sample J7 has the highest volatile matter content (Fig. 3.31) as well as a significantly larger proportion of liptinite material than the other samples from the Jasper 1 drill hole. In contrast, sample B19 has the lowest volatile matter content and one of the lowest liptinite percentages when compared to the other Ruawaro 2 samples.

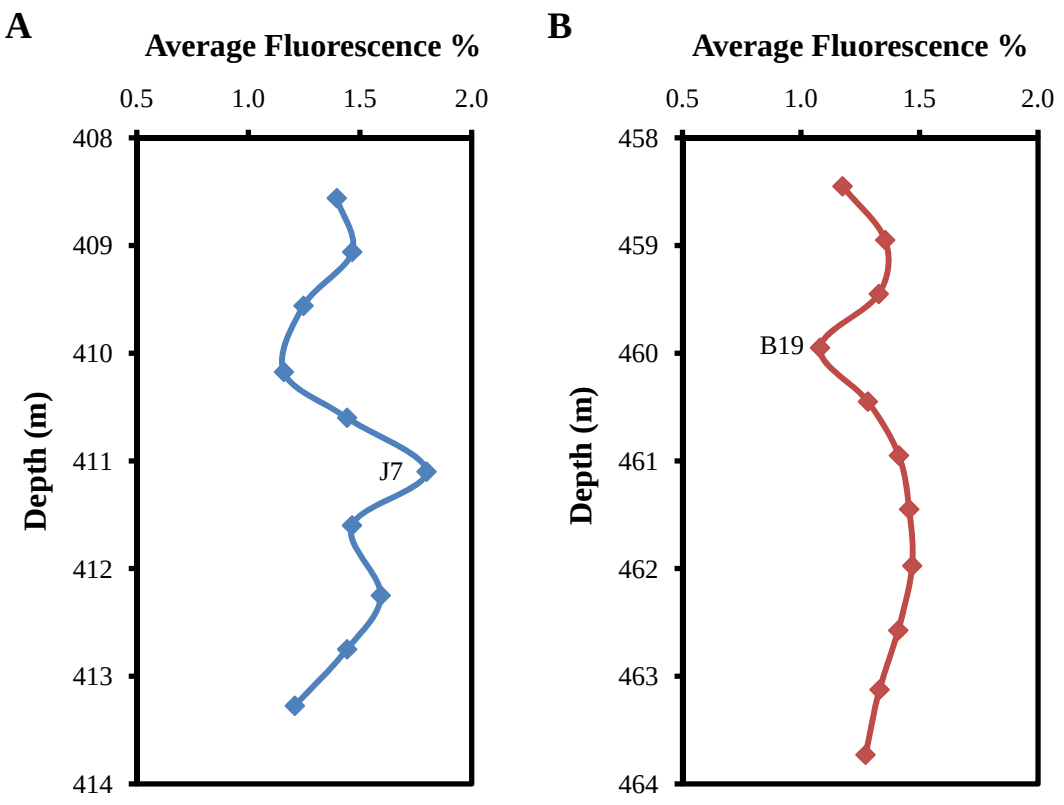

Figure 4. 22. Average fluorescence profiles for (A) Jasper 1 Renown seam, and (B) Ruawaro 2 Kupakupa seam.

The relationship of average fluorescence with other organic components was investigated using correlation tables with the correlation coefficients presented in Table 4.5. Average fluorescence has a good relationship with volatile matter content and is also somewhat associated with hydrogen content. The Renown seam shows a good association between average fluorescence and liptinite materials, however this association is not present for the Kupakupa seam. Vitrinite fluorescence is known to vary primarily with vitrinite chemistry and is hence not controlled by maceral group proportions. The correlation identified with liptinite in the Renown samples may indicate a period of sapropelic depositional conditions, i.e. the formation of a pond where liptinite macerals concentrated

and oxygen supply was deficient (hence relatively hydrogen-rich vitrinite) (J. Newman, pers com. 2008).

Table 4. 5. Correlation table comparing average fluorescence by seam with coal chemistry and composition. Only variables with correlations greater than 0.40 have been included in the table. Variables with correlations >0.50 have been highlighted in yellow.

	Jasper 1 Renown	Ruawaro 2 Kupakupa
Hydrogen db	0.42	0.46
Volatile Matter db	0.70	0.67
Telinite	0.52	-0.35
Collotelinite B	0.45	0.40
Collotelinite C	0.03	0.65
Collodetrinite A	0.61	0.17
Cutinite	-0.40	0.45
Suberinite	0.42	0.13
Sporinite	0.70	0.00
Liptodetrinite	0.61	0.20
Liptinite	0.70	0.15

4.4. Coal type properties

4.4.1. Coal chemistry and macroscopic coal type

To identify any coal properties typical of the coal types, a coal type database was generated by excluding any canister intervals not composed of a single coal type. This reduction left 106 canister intervals; 43 BNB, 48 BMB and 15 BHB, with no interval having an ash yield of >20%. Proximate results, grouped by coal type (regardless of seam), are presented in Figure 4.23. Interestingly, ash yield can be seen to increase as the degree of banding increases. Additionally the BHB coal type shows lower fixed carbon content than the other coal types.

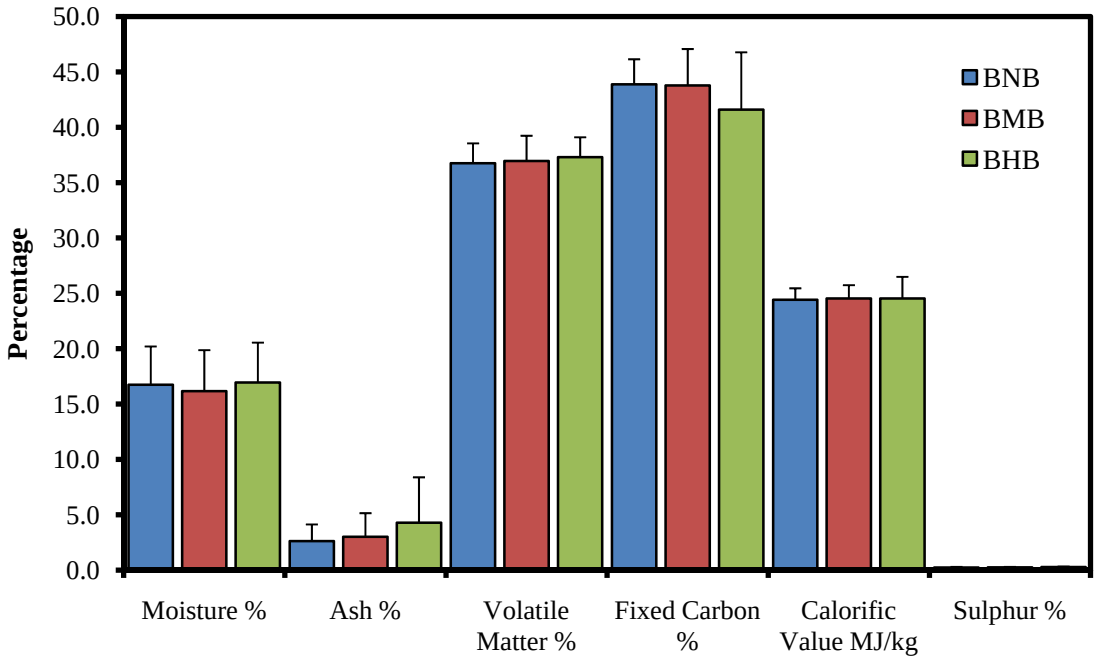

Figure 4. 23. Proximate analysis results (aa) grouped by coal type.

As the percentages of some ash constituents (e.g. silicon, aluminium and sulphur) differed significantly between the seams (see Chapter 3), it was necessary to present the ash constituents for each coal type by seam so as not to cloud trends (Figs 4.24). For both seams it can be seen that the more inorganically associated elements (silicon, aluminium, titanium and phosphorous) tend to increase as the degree of banding increases. This trend is similar to what is seen between coal type and ash yield. In contrast, the more organically associated elements (iron, calcium, magnesium, sodium and sulphur) tend to decrease as banding increases. Moore and Fergusson (1997) also found that the least banded coal types have the highest percentage of iron.

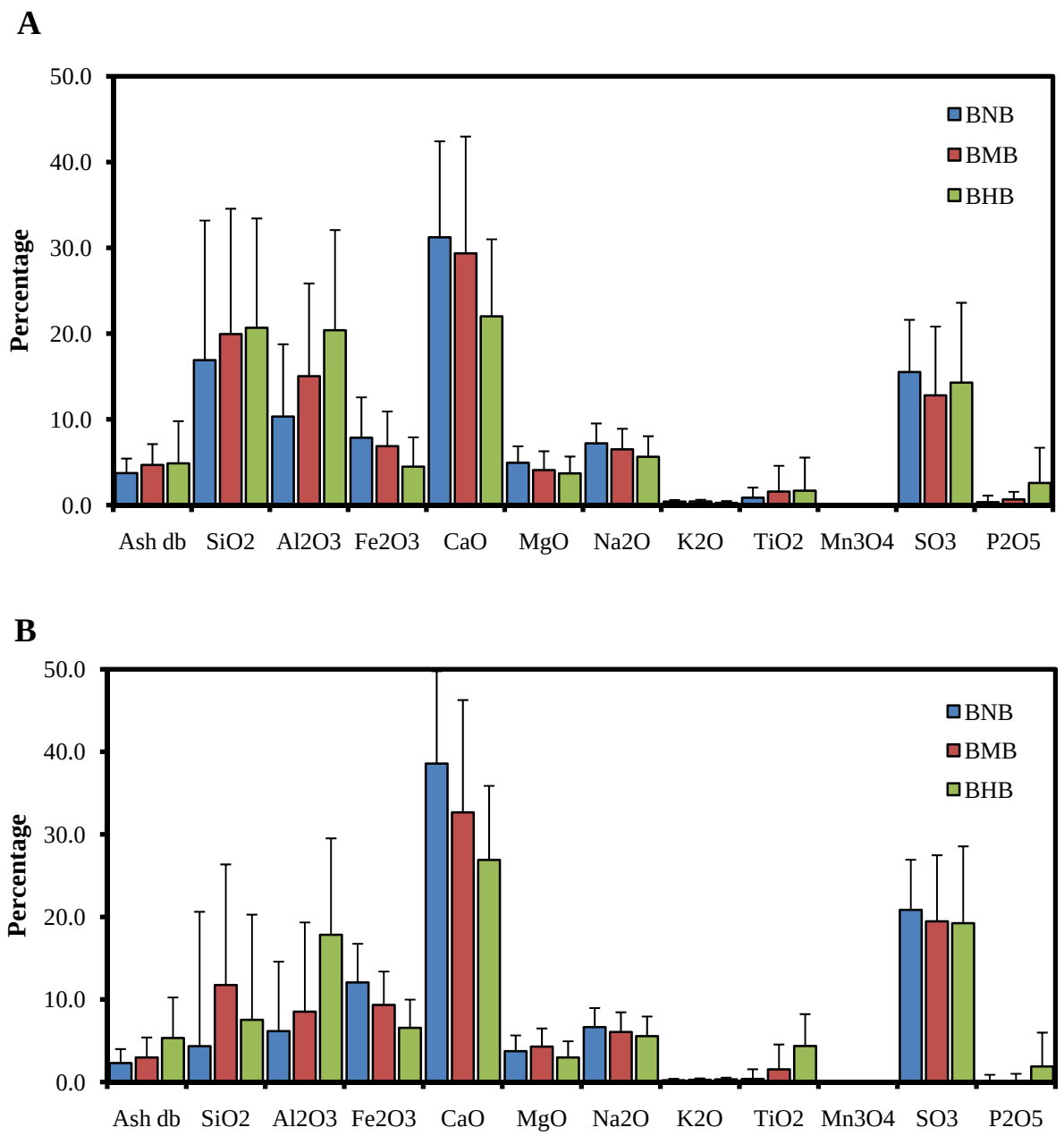

Figure 4. 24. Ash constituents grouped by coal type for (A) the Renown seam samples and (B) the Kupakupa seam samples.

To further investigate the relationships between coal type and elements, a cluster analysis was performed (Fig. 4.25). As expected percent vitrain was closely related to coal type. Interestingly the dendrogram not only shows the inorganic and organic groupings identified in Chapter 3 but also reveals that the ash yield and the predominately inorganically associated elements are related to coal type.

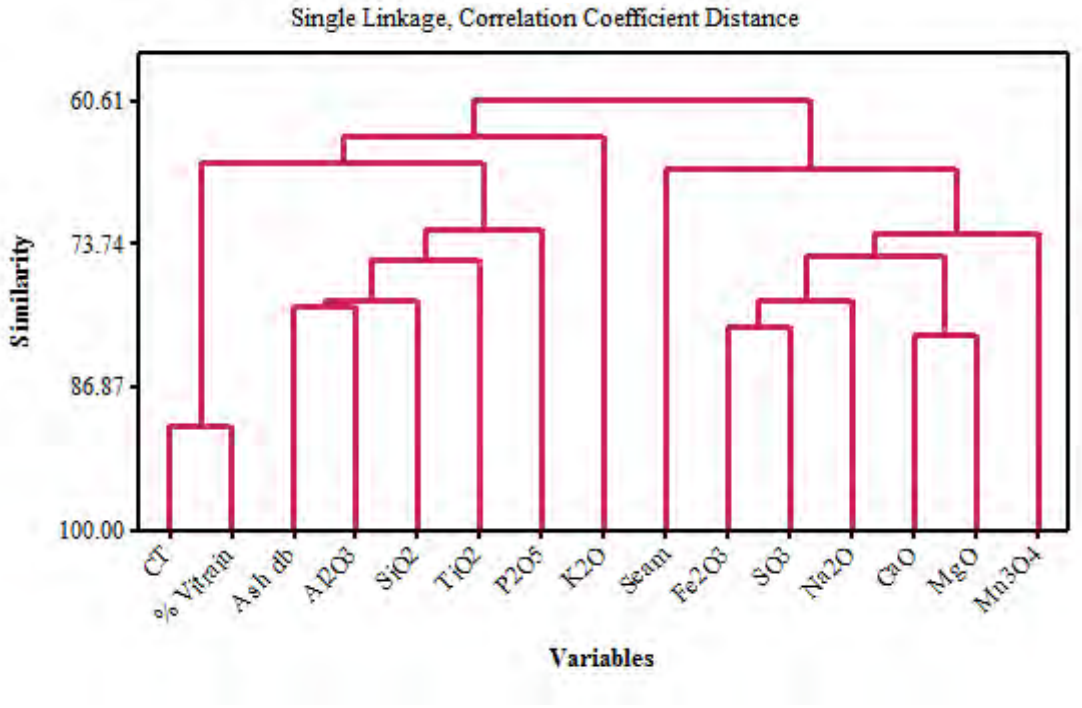

Figure 4. 25. Dendrogram presenting the cluster analysis results examining relationships between elements and coal type for data from both the Renown and Kupakupa seams.

Although there was limited data, ultimate analysis results were also evaluated for variation by coal type (Table 4.6). As there was only 1 BHB sample in the dataset, only the BNB (13 samples) and BMB (9 samples) coal types could be compared. No significant differences were identified between the coal types.

Table 4. 6. Average ultimate analysis results by coal type (db).

	BNB	BMB
Carbon %	71.93	72.22
Hydrogen %	4.91	5.03
Nitrogen %	1.15	1.16
Sulphur %	0.21	0.24
Oxygen %	18.17	17.82
n	13	9

4.4.2. Organic petrology and macroscopic coal type

The organic petrology of the samples was also compared on the basis of macroscopic coal type (Fig. 4.26A). The most noticeable difference between the coal types is the inertinite content, which decreases as macroscopic banding increases. The BHB coal type also has the highest liptinite content. As would be expected, the proportion of structured vitrinite increases and vitrodetrinite decreases as banding increases (Fig. 4.26B). A more detailed comparison of maceral differences between coal types is presented in Figure 4.27. As the degree of macroscopic banding increases, the concentration of all telovitrinite, telinite and collotelinite A-D, cutinite, suberinite, and resinite also increases. Alternately, the less banded the coal the greater the vitrodetrinite, sporinite, funginite and inertodetrinite contents. From Figures 4.26 and 4.27, it can be stated that as banding increases at the macroscopic level the proportion of structured tissue increases at the microscopic level.

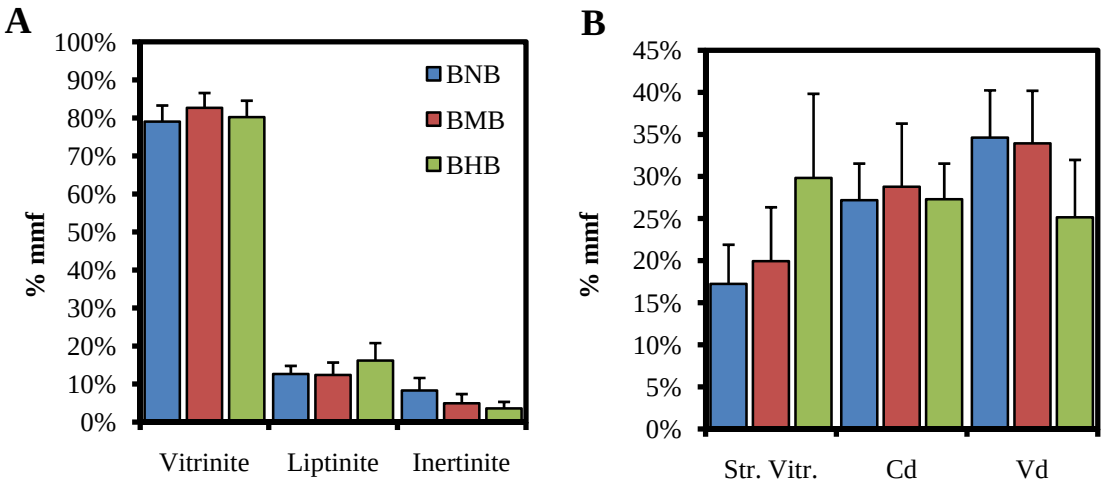

Figure 4. 26. (A) Maceral group averages by coal type. (B) Average percentage of vitrinitic textural components by coal type. BNB= bright luster, non banded coal, BMB= bright luster, moderately banded coal and BHB= bright luster, highly banded coal, Str. Vitr =Structured vitrinite, Cd = collodetrinite, Vd = vitrodetrinite.

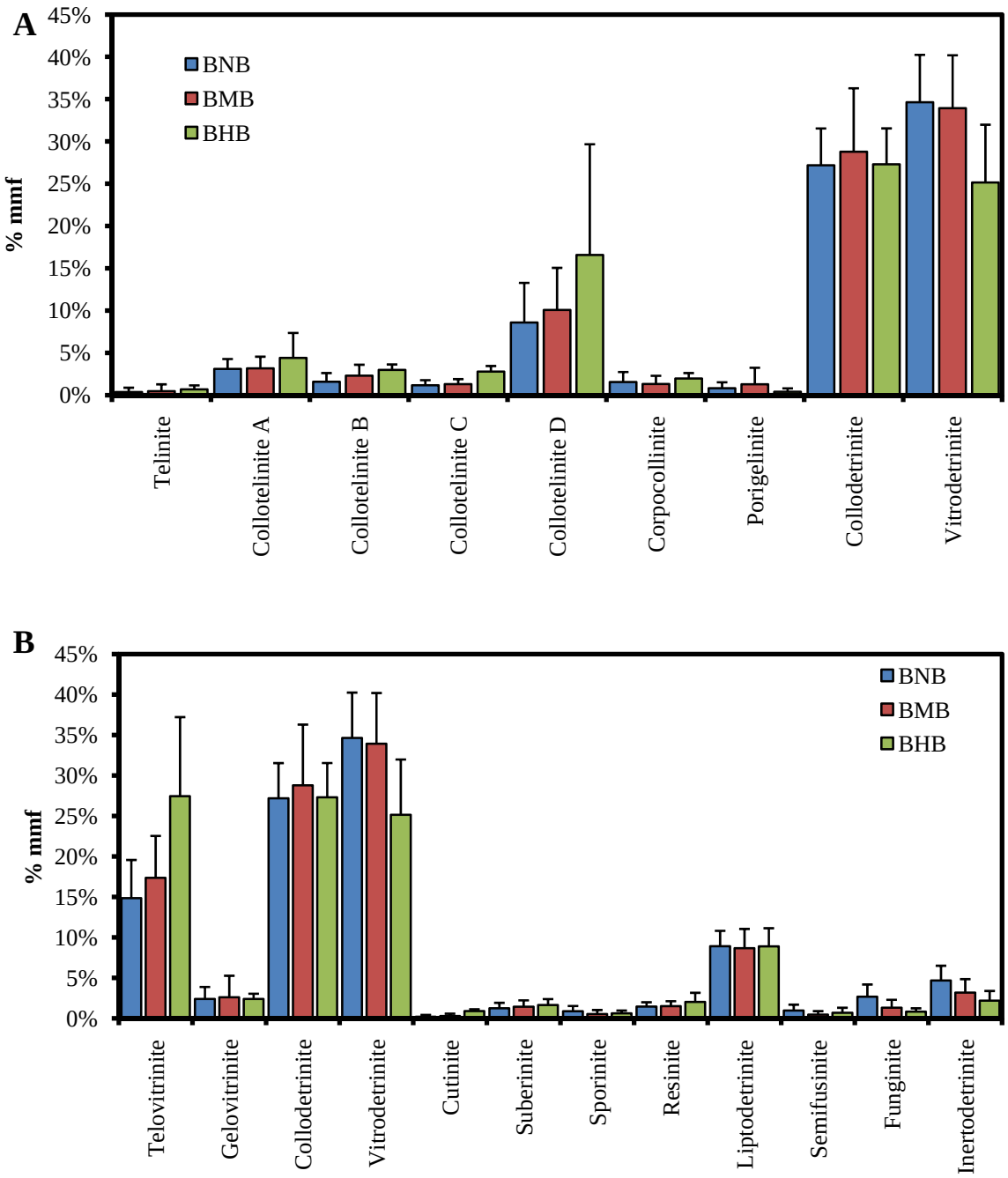

Figure 4. 27. (A) Average percentage of vitrinite macerals by coal type. (B) Average percentage of vitrinite subgroups and liptinite and inertinite macerals by coal type. BNB= bright luster, non banded coal, BMB= bright luster, moderately banded coal and BHB= bright luster, highly banded coal.

The average maceral group composition by seam for both the BNB and the BMB coal types is presented in Figure 4.28. BHB samples were only available for the Kupakupa seam and hence have not been presented here. The maceral group averages show that for the BNB

coal type the Renown seam has lower vitrinite content and roughly double the inertinite content of the Kupakupa seam. The compositional distinction between seams is not as noticeable for the moderately banded samples. This difference in composition between BNB coal from the two seams suggests the higher abundance of inertinite associated with the BNB coal type is possibly the reason for the higher inertinite content of the Renown seam.

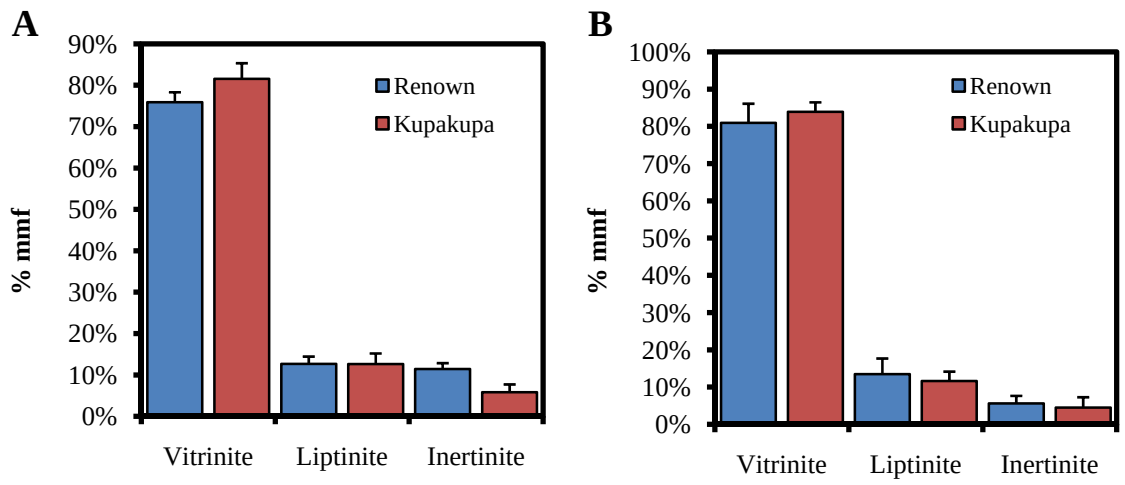

Figure 4. 28. Maceral group averages by seam. (A) Bright luster, non banded coal type (B) bright luster, moderately banded coal type.

4.4.3. Organic petrology and ash constituents

In Section 4.4.1 an association was identified between coal type and ash constituents, with the largest percentages of the predominately inorganically bound elements being linked to the most banded coal type. To see how this extends into the microscopic realm a correlation table was generated with the strongest maceral associations shown in Table 4.7.

For three of the four seam intersections, there is a good association (correlation coefficients of 0.6 - 0.9) between structured vitrinite and aluminium, titanium and to some

degree phosphorous. It must be acknowledged that the phosphorous contribution is very small and in some samples is below detection limits. In contrast silicon shows little to no relationship with structured material. This suggests that although silicon is more common when banding is present it is not intimately bound with any particular macerals. In addition this fits well with the inorganic association for silicon identified in Figure 3.22, and the more mixed association for aluminium and titanium. For both Kupakupa locations inorganic material is linked to liptinitic material, primarily liptodetrinite. The Jasper 1, Mimi 1 and Ruawaro 2 drill holes are all from the Beverland Road location from which the Ruawaro 1 drill hole is located several kilometers away.

Table 4. 7. Correlation table comparing the 'inorganically bound' ash constituents by location with coal composition. Only macerals with associations have been included in the table. Variables with correlations >0.50 have been highlighted in yellow.

		Collotelinite D	Collotelinite	Telo-vitrinite	Vitrinite	Lipto-detrinite	Liptinite
Jasper 1 Renown	**Ash db**	0.04	0.15	0.13	0.20	-0.05	-0.10
	SiO_2	0.21	0.30	0.29	0.15	-0.02	0.02
	Al_2O_3	0.80	0.82	0.81	0.70	-0.61	-0.61
	TiO_2	0.83	0.90	0.90	0.51	-0.42	-0.39
	P_2O_5	0.75	0.84	0.83	0.35	-0.28	-0.25
Mimi 1 Renown	**Ash db**	0.67	0.49	0.45	0.12	-0.14	-0.11
	SiO_2	0.41	0.25	0.22	0.02	-0.02	0.07
	Al_2O_3	0.70	0.60	0.64	0.55	-0.31	-0.41
	TiO_2	0.76	0.65	0.65	0.34	-0.17	-0.15
	P_2O_5	0.36	0.21	0.38	0.63	-0.40	-0.48
Ruawaro 1 Kupakupa	**Ash db**	-0.02	-0.16	-0.17	-0.27	0.55	0.40
	SiO_2	-0.19	-0.24	-0.25	-0.42	0.70	0.60
	Al_2O_3	0.05	-0.06	-0.07	-0.39	0.56	0.48
	TiO_2	-0.15	-0.21	-0.22	-0.44	0.69	0.60
	P_2O_5	-0.01	-0.10	-0.10	0.28	0.02	-0.10
Ruawaro 2 Kupakupa	**Ash db**	0.45	0.59	0.57	-0.78	0.75	0.85
	SiO_2	-0.02	0.02	0.01	-0.02	0.11	0.15
	Al_2O_3	0.58	0.73	0.72	-0.71	0.64	0.74
	TiO_2	0.43	0.60	0.58	-0.73	0.68	0.78
	P_2O_5	0.42	0.55	0.53	-0.79	0.74	0.84

4.5. Discussion

4.5.1. Controls on the distribution of coal types

The coal types described in this study are defined by the proportion of vitrain bands present. Vitrain band abundance in the Huntly coals range from 0% to 70%. Although Esterle et al. (1992) reported bands in the Kupakupa seam of up to 6 cm (-5.91 φ) in diameter, the maximum measured band thickness in this study was 30 mm (-4.91 φ), with only 1% vitrain bands having diameters greater than 10 mm (-3.32 φ). The average phi size increased from the bright, non-banded to the bright, highly banded coal type. In comparison, Flores et al. (2001) and Moore et al. (2001) working on the subbituminous Tertiary coals of the Fort Union Formation in the Powder River Basin, USA, found vitrain band abundances ranging from 9 - 63% and band thicknesses in excess of 160 mm (-7.3 φ). Four coal types were identified in their study ranging from attrital dominated to very coarsely laminated (the latter consisting of on average 54% vitrain bands). Similar to what is seen in the Huntly coal types, the band thickness increased from the attrital dominated to the very coarsely laminated coal types (Moore et al., 2001). In contrast, Moore et al. (2006) as part of a genetic study on the Spring Creek Main seam in the Cretaceous Greymouth coalfield, NZ, found that phi size histograms of the banded coal types revealed that although the proportion of vitrain bands may vary, the mean size of the bands remains the same. It was suggested that variability in vitrain band proportion was most likely a reflection of degradational processes and that all coal types were formed from roughly the same vegetational components.

Shearer and Moore (1994a; 1994b) conducted grain-size and botanical analysis on the predominantly non-banded, Eocene Brunner coal and the predominantly well banded, Cretaceous Morley coal located in the South Island of New Zealand. They found the attrital

material of the coals to be similar in organic composition (e.g. macerals) although the plant organs/tissues in the Morley coal tended to be larger than those in the Brunner coal. As such, the major difference between the two coals was the macroscopic texture (Shearer and Moore, 1994b). This agrees with the work of Moore and Ferm (1988) on Tertiary Indonesian coals which indicated that the coal types are differentiated by variations in the level of preservation of plant parts as there is no significant variation between their matrix compositions. Further analysis of the botanical data for the Brunner and Morley coals led Shearer and Moore (1994a) to hypothesize that in the Cretaceous/Tertiary coals of New Zealand, banding character may be dominantly controlled by the presence or absence of gymnosperms in the paleo-mire vegetation because of their resistance to decay. Vitrain bands have been recognized in the Kupakupa seam to be composed of gymnosperm wood (Moore and Swanson, 1993; Newman et al., 1997; Shearer and Moore, 1994b).

Newman et al. (1997) compared the Kupakupa seam to the underlying Taupiri seam in the Rotowaro coalfield (located about 5 km to the south-west of the Huntly coalfield; the Kupakupa seam is widespread in the Waikato coalfields whereas the Renown is not) noting that despite gymnosperm pollen being present throughout both seams, the Taupiri showed a distinct lack of vitrain banding. Generally the Taupiri seam was found to have higher funginite content. Interestingly, areas of higher funginite content in the Kupakupa seam more closely resembled the compositional characteristics of the Taupiri seam.

The organic petrology results show that the major difference between the coal types is the proportions of structured vitrinite rather than overall composition. As such, it is proposed that for the Huntly coalfield macroscopic coal type is primarily a function of tissue

preservation. Hence, it is the degree of tissue preservation controlling the presence/absence of vitrain bands (and therefore coal types) rather than the presence/absence of gymnosperms.

4.5.2. Petrological differences between seams

The major difference in macroscopic composition between the two seams is that the Renown seam is mainly comprised of bright, non-banded coal (57%) while the Kupakupa seam is dominated by banded coal types (68%). Shearer et al. (1995) found that typically only Tertiary coals contain significant proportions of non-banded coal. The maceral percentages presented in this study are not unusual for Tertiary coals (Bechtel et al., 2007; de Sousa and Vasconcelos, 1999; Diessel, 2009; Hackley et al., 2007; Shearer et al., 1995) or New Zealand coals (Crosdale, 1995; Edbrooke et al., 1994; Newman et al., 1997). In comparison to the Kupakupa seam, elevated funginite/ inertodetrinite contents were identified in the Renown seam as well as lower proportions of structured vitrinite. This higher inertinite content is associated with the bright, non-banded coal type.

From a study of the Pittsburgh coal, Renton and Bird (1991) proposed that a coal formed in a low pH (< 4.5) mire would be bright with low (predominantly organic) sulphur content and, because of the favourable conditions for preservation the of plant material, the mineral matter in the coal would be relatively low. This describes the attributes of the Kupakupa seam. Renton and Bird (1991) also propose that the degradation of plant material and peat via dissolved oxygen, in percolating groundwater or rainwater, will result in an enrichment of pre-inertinite materials but will inhibit formation of iron minerals. This would result in a coal with inertinite-rich layers with low (predominantly organic) sulphur content. In an experimental coalification of peat and buried wood Orem et al. (1996) found that highly

degraded peat produced an artificial coal similar to a Miocene lignite, in overall chemical composition and structure, while a well-preserved wood sample did not. They suggested that the extent of microbial degradation of organic matter during early and late diagenesis and before early-stage coalification likely plays an important role in determining the organic composition of the final coal.

In a Sumatran peat deposit studied by Esterle and Ferm (1990) inertinite was found to increase towards surface. It was suggested that this trend was caused by the peat being oxidized at the surface. Oxidation and degradation of surficial peat likely results from changes in the mire water table (Shearer, 1997). Dehmer (1995) recognized, for recent peat bogs, that the proportion of humotelinite was related to the depth of the water table and the frequency of dry periods. The frequency of dry periods increases aeration in the peat which in turn influences the degree of decomposition. Funginite content was found to reflect these changes in the oxygen status of the mire. This is in agreement with Moore et al. (1996) who proposed that lower-than-normal or abnormally fluctuating water tables result in the formation of fungally oxidised plant material. As the changes in the water table level can be frequent, ephemeral and sometimes extreme, oxidised macerals are not solely related to the height of the mire surface above the water table (Wust et al., 2001).

Studying a low ash Tertiary coal from Russia, containing substantially higher inertinite than the Huntly coalfield (1% - 90%), Crosdale et al. (2002) interpreted cyclic intervals of decreasing huminite and increasing inertinite as progressively drier mire conditions. Wetter conditions were identified as brighter intervals with increased huminite and sometimes also an increase in mineral matter. Crosdale et al. (2002) theorised that the brighter coal could be a result of an increased nutrient supply, associated with the clastic

inputs, and the growth of larger plants. This is a likely explanation for the association between silicon and vitrain banding in the Huntly coal seams (Fig. 4.24), as the silicon shows no relationship to the vitrinite maceral components (Table 4.7). Vitrain banding is found, in this study and in the study by Newman et al. (1997), to increase around seam boundaries and seam splits. Li et al. (2009) confirms that there is only minimal silicon within macerals reporting only 0.01% silicon in collotelinite and collodetrinite from the Huntly coalfield.

The Waikato coalfields are thought to have formed in a fluvial dominated environment with extensive mire complexes located in areas restricted from sediment input (Edbrooke et al., 1994; Newman et al., 1997). While Edbrooke et al. (1994) give a thorough overview of the mire forming conditions for the whole Waikato coalfields, they do not differentiate the seams into different units. As with this study, Edbrooke et al. (1994) found no evidence to support burning of the peat, with inertinite contents averaging 6%, primarily fungal in origin. As the two organic petrology profiles from this study are located in close proximity, it is possible that raised inertinite contents of the Renown seam is a localised phenomenon, however greater variation in all measured properties was identified for the Renown seam than the Kupakupa seam. The ‘sapropelic’ intervals identified in the organic petrology study as being liptinite rich (sometimes also including inertinite and clay) have been interpreted by Edbrooke et al. (1994) to be areas where ponds formed. They suggested that although ponds tend to be a relatively common feature of the bog plains, they were small and quickly displaced.

It may be that coal texture is predominantly controlled by the influence of depositional environment and peat chemistry at the time of formation. Although not a focus of this thesis, considering the discussion above, it is proposed that, in the northern part of the

Huntly coalfield, the stratigraphically deeper Kupakupa seam formed under wet, relatively stable climatic and groundwater conditions. The lack of partings in the Kupakupa seam suggests that flooding of the mire was infrequent and, where present, minor. This lack of clastic influence, in addition to the very low ash yield of the Kupakupa seam, supports the presence of raised ombrogenous peats in the interior part of the mire (Amijaya and Littke, 2005; Edbrooke et al., 1994; Esterle and Ferm, 1994; Wust and Bustin, 2001). In contrast, the Renown seam likely formed under drier, more degradational, less stable conditions with some areas of the mire being completely flooded (seam split present in the upper half of some the profiles) before re-establishing. Conditions were least stable in the latter half of the coal formation. Although more variable it is still thought that the coal was formed by ombrogenous mires.

4.6. Conclusions

In this chapter petrological properties of the Huntly coalfield are reported on both the macroscopic and microscopic levels. Conclusions are as follows:

- Maximum vitrinite reflectance values for the analysed seam splits vary from 0.42% to 0.45%. Suggate rank is generally between 6.0 and 7.0.
- Average fluorescence intensity profiles show a good association to volatile matter content (db) and a weak association to hydrogen content (db).
- Macroscopically, the Kupakupa seam cores contain more vitrain bands than the Renown seam (28% of all counts, as opposed to 21%). The Kupakupa seam also has more structured tissue than the Renown seam at the microscopic level.

- Vitrinite content ranges from 69% - 88%, liptinite from 8% – 23% and inertinite from 1% - 13%. The vitrinite component is dominated by collodetrinite and vitrodetrinite, the liptinite component by liptodetrinite and the inertinite component is primarily composed of inertodetrinite and funginite.
- There are three coal types recognized in the coalfield: (1) bright non-banded, (2) bright, moderately banded, and (3) bright, highly banded. A greater percentage of the bright, non-banded coal type was described in the Renown seam while the Kupakupa seam is dominated by the banded coal types.
- On average the Renown seam has less vitrinite and almost double the inertinite content of the Kupakupa seam. This greater inertinite content is contributed predominantly by the non-banded coal type. It is proposed that the Renown seam formed in drier, less stable climatic and groundwater conditions than the Kupakupa seam.
- The Beverland Road cores from the Renown seam have a much greater proportion of the bright, non-banded coal type, as well as a smaller average phi size for the vitrain bands, when compared with the Renown seam cores from the other locations.
- The average phi size increases from the bright, non-banded to the bright highly banded coal types although, in general, vitrain bands are thin with only 1% of bands having a diameter >10 mm.
- As the degree of banding increases, the amount of structured vitrinite increases and the amount of vitrodetrinite decreases. Hence, as banding increases at the macroscopic level the proportion of structured tissue increases at the microscopic level.
- As the degree of banding increases, the ash yield also increases. When considering the relationship between ash constituents and coal type it can be seen that silicon, aluminium, titanium and phosphorous increase as banding increases, while in contrast iron, calcium, magnesium, sodium and sulphur decrease. Aluminium, titanium and to some degree

phosphorous, have some association with telovitrinite (structured vitrinite macerals) however silicon does not. This suggests that while there is frequently an increase in silicon when coal is more banded, it is not intimately associated with the plant material.

Chapter Five

Coal Microstructure

Generally coals are known to be extremely heterogeneous microporous materials with very high surface areas (Berkowitz, 1979). The pore network serves as a path by which gases and fluids enter and move through the coal. In addition, gas adsorption upon the internal surface area of coal is considered to be the most important mechanism for gas retention. As such, knowledge of surface area, pore size distribution and porosity is beneficial. Most small angle scattering (SAS) studies on coal to date have either compared rank effects on the pore space geometry (pore size distribution and surface area) and porosity of single coal samples originating from different coalfields or of different rank (Prinz et al., 2004; Radlinski et al., 2004b; Radlinski and Radlinska, 1999). Other studies were focused on the effect of solvents on the pore structure (Foster and Jensen, 1990; Hall et al., 1998; Hall et al., 2000; Melnichenko et al., 2009; Radlinski et al., 2009; Winans et al., 2006; Winans and Thiyagarajan, 1988). This chapter presents microstructural information, gathered using SAS

techniques, about multiple coal samples of similar rank (Chapter 4) from the Huntly coalfield.

5.1. Permeability and porosity in coal

In situ, most low rank coal deposits are water saturated and require reduction of hydraulic pressure for gas desorption to occur (Gray, 2003; Twombly et al., 2004). In accordance to Darcy's Law, the gas then diffuses through the matrix via micropores until it can flow through micro- and macrostructures towards the low pressure area created by a production well (Gamson et al., 1996; McElhiney et al., 1993). Generally there are two scales of permeability present in coal, a macroscopic system composed of regular, persistent fractures and a microscopic system consisting of pores, cavities and the remains of original plant material. The degree to which these two systems connect and combine governs the flow rate and the quantity of gas that can be obtained.

5.1.1. Macroscopic transport system

Cleats are the natural fracture system found in coal. Cleats are thought to be formed by interdependent processes such as desiccation, lithification, coalification and tectonic stress (Close, 1993). As cleats provide the principal permeability pathway for the flow of gas and water throughout the coal, an understanding of their orientation, spacing, size, aperture width, connectivity and mineralization would greatly enhance the strength of gas field predictive models (Clarkson and Bustin, 1997; Close, 1993; Faraj et al., 1996; Laubach et al., 1998; Law, 1993). The cleat system generally occurs as an orthogonal set of fractures that is

essentially perpendicular to bedding planes. The primary set, known as the face cleat, is the more dominant and continuous set while the secondary set, the butt cleat, is the more discontinuous set tending to terminate at intersections with the longer face cleats (Close, 1993; Laubach et al., 1998; Law, 1993; Pattison et al., 1996). Face and butt cleats extend parallel to the maximum and minimum in situ stress directions respectively and hence can identify principal stress directions at the time of cleat formation (Li et al., 2004; Pashin et al., 1999). Because of the lateral continuity, and directionality, of face cleats permeability can be anisotropic. Previous studies have noted that permeability may be enhanced from three to ten times in one direction because of this anisotropy (Close, 1993; Laubach et al., 1998; Law, 1993; Pashin et al., 1999). Permeability anisotropy can be used when planning well placement in a CBM play.

Uniformity of cleat orientations over wide areas containing relatively flat-laying, undeformed rocks is common (Close, 1993; Laubach et al., 1998). However, face and butt cleats are also known to strike essentially perpendicular and parallel to structures such as fold axes and faults (Close, 1993). So even though a regional scale orientation pattern may exist, caution must be exercised as abrupt variations, particularly at the local scale around deformation features, can impede or channelize flow through the cleat system (Laubach et al., 1998; Pattison et al., 1996). The coals of the Waikato possess a defined cleat system (St George, 1997) that is approximately parallel to regional bedding strike, with the exception of areas in the vicinity of faults, where cleat frequency increases and orientation is highly variable. They are thought to be tectonic in origin and the principal permeability direction is considered to run NE-SW (Cameron, 1995; Moon and Roy, 2004).

Cleat spacings in subbituminous coals have been reported as 0.01 - >12.7 cm in the Powder River Basin, USA (Flores, 2004), 0.5 cm in Yima, China (Su et al., 2001) and 0.29 - 0.5 cm in Kushiro, Japan (Li et al., 2004). Coal in the present study has a cleat spacing of 1 - 4 cm (Chapter 5). Cleat size can be affected by changes in ash yield, bed thickness and lithotype (Close, 1993; Gamson et al., 1993; Su et al., 2001). Collecting meaningful data on the width of cleat apertures is very difficult to achieve under natural or replicated natural conditions. Sample collection may involve drilling or blasting and the de-stressing effects associated with overburden (open-cut) or coal removal (underground) can produce fracture systems that can either be misinterpreted as the natural fracture system or effectively overprint the pre-existing network (Pattison et al, 1996). However, data on non-stressed coals as a function of lithotype may still be useful (Close, 1993; Harpalani and Chen, 1995; Laubach et al., 1998). Measurements of aperture width, obtained using SEM and optical microscopy, include 0.004-0.006 mm (Karacan and Okandan, 2000), 0.001 - 8 mm (Su et al., 2001), 0.01 - 0.3 mm (Close, 1993) and 0.1 - 2 mm (Gamson et al., 1996), while estimates of aperture width under in situ confining pressure vary from 0.1 to 100 nm (Harpalani and Chen, 1995).

A key component of cleat permeability is connectivity. The cleats must join to allow flow of gas and water and must also be open in situ, not held closed by effective stress (Close, 1993; Gamson et al., 1993). Secondary mineralization in the form of authigenic minerals such as calcite, quartz and clays, or organic material, such as mobilized resin, may be present in cleat apertures. Mineralization of cleats hinders the flow of gas and water and has been found to negatively influence the producibility of gas from coal (Close, 1993; Faraj et al., 1996; Laubach et al., 1998; Pashin et al., 1999). Law (1993) suggests that high rank

coals commonly have mineral filled cleats and hence their effective permeability may be less than low rank coals with wider cleat spacing.

5.1.2. Microscopic transport system

The microstructural features with an influence on permeability include pores, microfractures, microcavities and phyteral porosity (formed by the remnants of original plant material) (Clarkson and Bustin, 1997; Gamson et al., 1996). It has been shown that the size, continuity, connectivity and secondary mineral infill of these microfeatures have a significant contribution to overall permeability (Gamson et al., 1996). The nature of the pores, their size, abundance and surface area, is greatly influenced by rank and maceral composition (Crosdale et al., 1998; Lamberson and Bustin, 1993; Levine, 1993), while the other microstructures have been found to be controlled mostly by coal type (Clarkson and Bustin, 1997; Gamson et al., 1996).

Current classifications of pore sizes are (van Krevelen, 1993):

1. micropores: diameter <2 nm,
2. mesopores: diameters of 2-50 nm, and
3. macropores: diameters >50 nm

The distribution of pore size has been shown to vary with rank (Gan et al., 1972). Porosity in lignite (<75% C) has been found to be dominated by macroporosity, high volatile bituminous B and C coals by macro- and mesopores, while higher rank coals are composed of mainly micropores (Gan et al, 1972). From the data of Gan et al. (1972), Harris and Yust (1976) concluded that a relationship exists between vitrinite content and microporosity. Their

study on high volatile bituminous coals observed that the porosity in the liptinite and inertinite fractions falls mainly in the mesopore range. Unsworth et al. (1989) found that both vitrinite and inertinite contained significant proportions across all pore sizes (micro-, meso- and macropores); however, they agreed that inertinite contained more macroporosity and less microporosity than vitrinite equivalents.

Minimal work has been conducted on pore morphology. Although considerable variability exists it has been proposed that the heterogeneity of pore surfaces decreases with increasing rank (Laxminarayana and Crosdale, 1999; Radlinski and Radlinska, 1999). Gan et al. (1972) reported surface areas to be large in lignite (225-359 m^2/g), lower in the high volatile bituminous coal range (96-228 m^2/g) then increasing again in the higher ranks (197-426 m^2/g). Surface area has been found to increase with increasing vitrinite content, reflecting differences in the pore size distribution in vitrinite as compared to other macerals (Lamberson and Bustin, 1993).

Microfractures have been found to be common in bright coal lithotypes, typically forming a dense orthogonal network of fractures between the cleats. These in turn were found to be linked by smaller, less continuous, conchoidal fractures and striae (Gamson et al., 1996; 1993). Microstructure in dull lithotypes is dominated by phyteral porosity and microcavities (Clarkson and Bustin, 1997; Gamson et al., 1996; 1993). Phyteral pores, associated with wood fibres, are cylindrical features that tend to occur in sheet like layers parallel to bedding. Microcavities are generally smaller than the other microstructures and vary in shape from small angular pores in between maceral fragments to complex, contorted pores between fibrous clay particles (Gamson et al., 1993). Detailed scanning electron microscopy imaging of phyteral porosity in a Turkish coal showed that the pores were connected to each other

with microfractures less than 1 μm in aperture. This feature is promising in terms of gas transport and storage by increasing the accessibility of storage regions (Karacan and Okandan, 2001).

It was suggested by Gamson et al. (1996) that microstructures play a rate-limiting role between diffusion at the micropore level and flow at the cleat level as evidenced by the various microstructures and the different sorption behaviour of bright and dull coals. Differences in diffusivity of coals have important implications for gas drainage. Considering this, higher permeability may not necessarily offer higher gas flow rates if diffusivity is low, and low rank coals that possess low gas contents, because of low storage capacity, may offer better gas flow rates than some higher rank coals.

5.2. Small angle scattering theory

In many branches of science, small angle scattering (SAS) of neutrons and X-rays is widely used as a diffraction method for studying the structure of matter on all scales, from elementary particles to macro-objects (Fig. 5.1) (Feigin and Svergun, 1987). Small angle neutron (SANS) and small angle X-ray scattering (SAXS) have been used for decades to study the geometry of supra-molecular objects in both the suspended or solid phase (Radlinski, 2006) with is application to rocks being considerably enhanced by the discovery of the fractality of rock microstructure by Bale and Schmidt (1984). In the last decade small angle scattering techniques have been integrated into main stream petroleum, coal and engineering geology (Prinz et al., 2004; Radlinski et al., 2000; 1996; 2009; Radlinski and Hinde, 2001; 2002; Radlinski et al., 2004a; 2004b; 2001; 1999; Winans et al., 2006).

The scattering of neutrons and X-rays by a material is the result of scattering contrast between the various components within the chosen media (Radlinski and Hinde, 2002). Rocks are somewhat transparent to neutrons and also X-rays to a lesser extent. The physical property responsible for neutron scattering is the coherent scattering amplitude (nuclear potential), while for X-rays it is the electron density (electric charge) (Radlinski, 2006). As such, neutron scattering probes the fluctuations of the nuclear scattering cross section, while X-ray scattering probes the fluctuations in electronic density (Radlinski and Hinde, 2001; 2002). Values for scattering length densities (calculated from formulas 2.3 and 2.4) for various components are presented in Figure 5.2 (Radlinski, 2006). Scattering contrast is the square of the difference between the scattering length densities of the components being anlaysed.

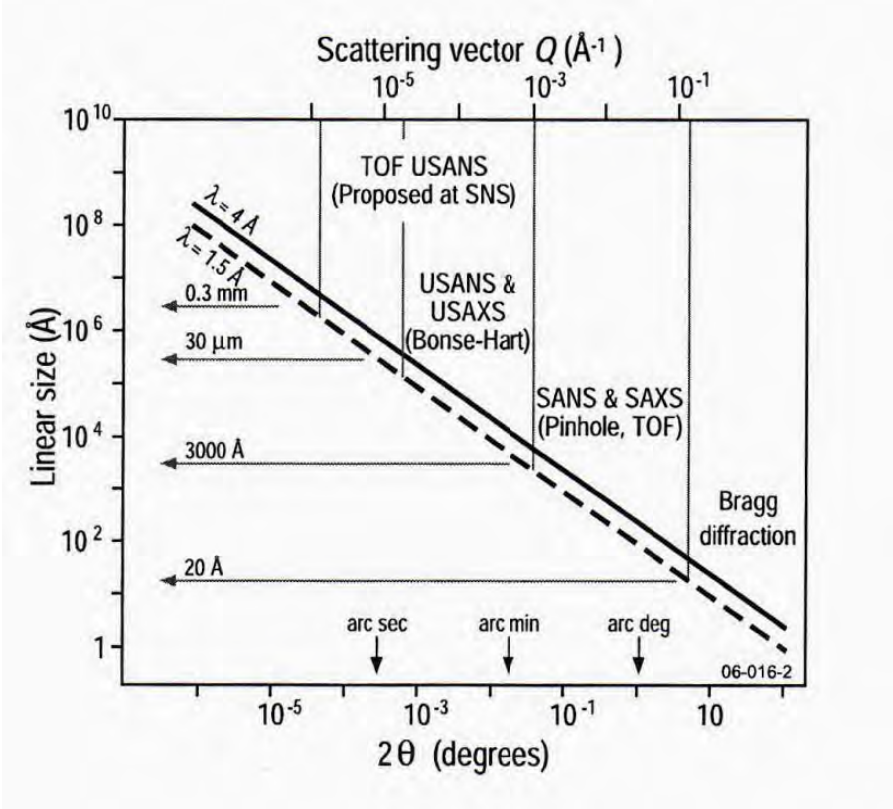

Figure 5. 1. Linear scale size range accessible with Bragg diffraction, small angle neutron (SANS) and small angle X-ray scattering (SAXS) techniques, ultra SANS and SAXS (USANS and USAXS) and the proposed time of flight (TOF) USANS at the SNS Oak Ridge facility. Scattering vectors (Q) are calculated for a wavelength (λ) of 4 Angstrom (Å). Figure from Radlinski (2006).

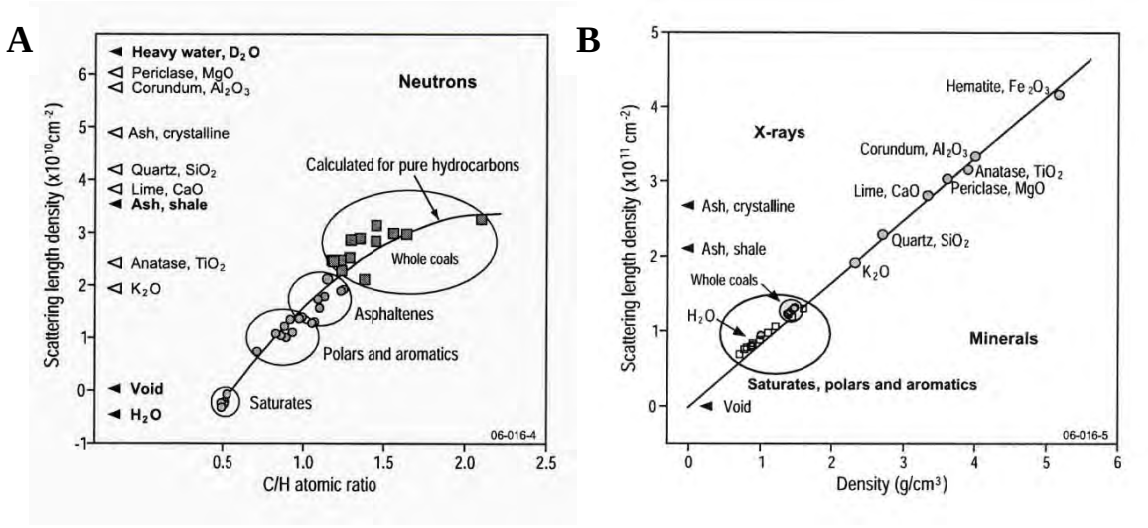

Figure 5. 2. (A) Neutron scattering length density and (B) X-ray scattering length for coals, hydrocarbons and common minerals. Figure from Radlinski (2006).

Coals are chemically heterogeneous materials at every scale level. However, the scattering contrast between the coal matrix and the pore (void) space is considerably larger than the contrast variations within the coal matrix itself (Radlinski et al., 2004b). The scattering length densities, shown in Figure 5.2A, indicate that there is little contrast between the solid organic and inorganic components of rock. As such, neutron scattering sees sedimentary rocks as a two-phase system, rock material and pore space, irrespective of the organic/inorganic composition (Radlinski, 2006). For X-rays (Fig. 5.2B), the matrix-void contrast for organic material is about 25% of that for inorganic material. Hence, if the rock is composed purely of organic material or inorganic material the system remains two-phase and the information obtained using X-ray scattering will be the same as that for neutron scattering. However where there are contributions of both organic and inorganic matter in the rock, the system will be three-phase for X-ray scattering and the data obtained will differ from that obtained by neutron scattering (Radlinski, 2006; Radlinski et al., 1996).

The principle of a SAS experiment is illustrated in Figure 5.3 (Radlinski, 2006). A flux of monochromatic neutrons or X-ray photons propagated in the direction of their wave vector ($\mathbf{k_0}$) is elastically scattered inside the sample of uniform thickness. The magnitude of $\mathbf{k_0}$ is λ^{-1}, where λ is the radiation wavelength. In the experiment the intensity dI scattered in the direction $\mathbf{k}$ is measured, where by convention $\mathbf{k} - \mathbf{k_0} = \mathbf{s}$ and the quantity $Q = 2\pi|\mathbf{s}|$ is called the scattering vector, where $|\mathbf{s}|$ is the magnitude of $\mathbf{s}$. The magnitude of $\mathbf{s}$ is $2\sin\theta/\lambda$. The scattering vector is thus related to radiation wavelength λ and the scattering angle 2θ by $Q = (4\pi/\lambda)\sin\theta$ (Radlinski, 2006; Radlinski and Radlinska, 1999). The incident flux of the scattering radiation (particles) is denoted by Φ_0, i.e. $\Phi_0 = I_0/A$, where I_0 is the incident intensity and A is the bean cross sectional area at the sample position.

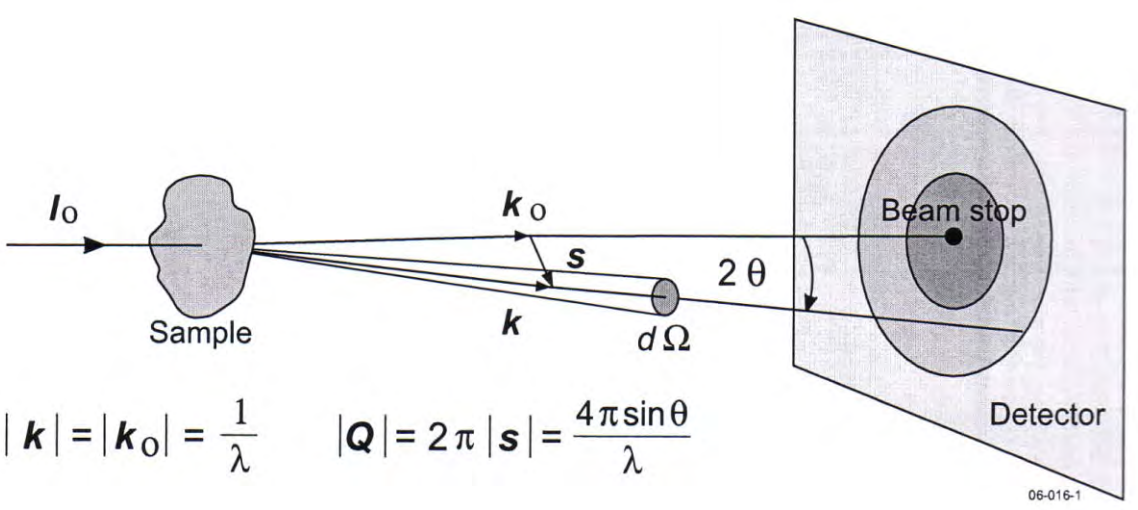

Figure 5. 3. The principle of a small angle scattering experiment. Figure from Radlinski (2006).

5.3. Sample characteristics

The coal for the twelve samples analysed in this study was collected from seventeen different gas desorption canisters at different depths within the basin. Both the chemical and petrographic properties of these samples are summarized in Tables 5.1 and 5.2. As previously discussed in Chapter 3, the coals from the Huntly coalfield typically have low ash yields, with the samples used for SAS analysis ranging from 2.9 - 5.4% in the Renown seam, on a dry basis (db) (although one interval had a higher ash yield of 12.9%). The samples from the Kupakupa seam generally have ash yields of less than 4.6% (db), with one sample having an ash yield of 25.4%.

For the remaining proximate and ultimate analyses, results were found to be similar for both seams, with carbon content on a dry ash free basis (daf) ranging from 74.0 - 76.89%, hydrogen from 5.07 - 6.03% (daf), nitrogen from 0.91 - 1.23% (daf) and sulphur from 0.22 - 0.59% (daf). Relative density generally ranged from 1.32 to 1.36 g/cc with the exception of the two higher ash yield intervals which had densities of 1.41 g/cc (B1) and 1.50 g/cc (D20). For the samples analysed with optical microscopy, the maximum mineral matter estimate point counted was 0.4%.

Table 5. 1. Drill holes and properties of samples used for small angle scattering analyses.

	Drill hole	Seam	Canister	Mid point m	Samples	Relative density g/cc	Ash % db	Sulphur % daf	Carbon % daf	Hydrogen % daf	Nitrogen % daf	Oxygen % daf	X-ray SLD	Neutron SLD
Matrix	Ruawaro 2	Renown	B1	433.49	318 x	1.41	12.90	0.36	74.63	5.27	1.08	18.71	9.10E+10	2.49E+10
	Ruawaro 2	Renown	B10	437.79	318 p	1.36	2.70	0.28	75.44	5.12	1.16	17.99	8.78E+10	2.46E+10
	Jasper 1	Renown	J6	410.60	319 x, p	1.35	2.96	0.22	75.85	5.24	1.23	17.47	8.71E+10	2.42E+10
	Jasper 1	Renown	J8	411.60	610 x, p	1.35	2.93	0.22	75.00	5.07	1.21	18.51	8.71E+10	2.46E+10
	Mimi 1	Renown	M5	409.86	611 x, p	1.36	5.41	0.25	74.00	5.18	1.19	19.37	8.78E+10	2.42E+10
	Mimi 1	Renown	M7	410.88	612 x, p	1.35	3.09	0.25	74.40	5.12	1.18	19.06	8.71E+10	2.43E+10
	Mangapiko 1	Kupakupa	D13	513.35	320 p	1.35	2.20	0.29	75.05	5.12	1.18	18.40	8.71E+10	2.44E+10
	Mangapiko 1	Kupakupa	D18	516.15	320 x	1.33	2.20	0.32	75.66	5.41	1.06	17.59	8.58E+10	2.32E+10
	Ruawaro 1	Kupakupa	A19	420.91	321 x, p	1.32	1.70	0.31	75.89	5.18	1.10	17.50	8.52E+10	2.38E+10
	Ruawaro 2	Kupakupa	B20	460.30	322 p	1.33	2.20	0.26	76.58	5.48	0.96	16.77	8.58E+10	2.30E+10
	Ruawaro 2	Kupakupa	B24	462.41	322 x	1.34	2.30	0.25	75.74	5.21	1.06	17.71	8.65E+10	2.40E+10
Vitrain	Mangapiko 1	Renown	D8	486.05	323 x	1.33	2.60	0.31	75.24	5.38	1.21	17.86	8.58E+10	2.32E+10
	Mangapiko 1	Renown	D9	486.55	323 p	1.33	2.80	0.32	75.18	5.32	1.18	18.00	8.58E+10	2.34E+10
	Mangapiko 1	Kupakupa	D19	516.68	326 x	1.34	4.60	0.41	75.49	5.48	1.01	17.61	8.65E+10	2.30E+10
	Mangapiko 1	Kupakupa	D20	517.23	326 p	1.50	25.40	0.59	71.83	6.03	0.91	20.64	9.68E+10	2.31E+10
	Ruawaro 1	Kupakupa	A13	419.05	327 x, p	1.32	2.20	0.35	76.90	5.43	1.06	16.26	8.52E+10	2.31E+10
	Ruawaro 2	Kupakupa	B17	458.80	328 x, p	1.34	2.60	0.26	75.84	5.31	1.05	17.55	8.65E+10	2.37E+10

x = perpendicular sample, p = parallel sample, db = dry basis, daf = dry ash free basis, SLD = scattering length density

Table 5. 2. Petrography of some matrix samples used for small angle scattering analyses.

Drill hole	Seam	Samples	Vitrinite mmf	Liptinite mmf	Inertinite mmf	Telovitrinite	Collodetrinite	Corpogelinite	Vitrodetrinite
Jasper 1	Renown	319 x, p	73.00%	13.40%	13.20%	13.60%	24.40%	4.40%	30.60%
Jasper 1	Renown	610 x, p	74.15%	13.83%	12.02%	10.62%	22.85%	3.61%	37.07%
Mimi 1	Renown	611 x, p	74.40%	15.20%	10.40%	12.40%	25.40%	4.40%	32.20%
Mimi 1	Renown	612 x, p	73.40%	13.20%	13.20%	11.00%	27.00%	2.60%	32.80%
Mangapiko 1	Kupakupa	320 p	87.20%	8.40%	4.40%	11.00%	33.80%	3.60%	38.80%
Mangapiko 1	Kupakupa	320 x	85.40%	11.80%	2.60%	15.00%	36.20%	4.60%	29.60%
Ruawaro 1	Kupakupa	321 x, p	81.20%	13.80%	5.00%	10.80%	19.00%	1.40%	50.00%
Ruawaro 2	Kupakupa	322 p	82.80%	10.60%	6.60%	11.00%	27.80%	0.80%	43.20%
Ruawaro 2	Kupakupa	322 x	86.20%	9.40%	4.40%	17.80%	35.00%	2.60%	30.80%

Samples	Cutinite	Suberinite	Sporinite	Resinite	Liptodetrinite	Semifusinite	Funginite	Inertodetrinite	Mineral Matter
319 x, p	0.00%	1.80%	0.40%	1.20%	10.00%	2.60%	4.20%	6.40%	0.40%
610 x, p	0.20%	0.60%	2.40%	1.20%	9.42%	1.40%	3.21%	7.41%	Trace
611 x, p	0.00%	2.20%	1.80%	1.00%	10.20%	1.60%	3.60%	5.20%	Trace
612 x, p	0.20%	1.20%	2.00%	1.20%	8.60%	1.40%	5.80%	6.00%	0.20%
320 p	0.20%	2.60%	0.40%	0.40%	4.80%	0.40%	2.20%	1.80%	Trace
320 x	0.40%	2.60%	0.00%	2.40%	6.40%	0.20%	2.00%	0.40%	0.20%
321 x, p	0.40%	1.00%	0.20%	0.80%	11.40%	0.40%	1.20%	3.00%	Trace
322 p	0.00%	1.20%	0.20%	1.00%	8.20%	0.20%	2.80%	3.60%	Trace
322 x	0.20%	2.00%	0.20%	0.80%	6.20%	0.40%	2.00%	2.00%	Trace

x = perpendicular sample, p = parallel sample

5.4. Small angle scattering results

5.4.1. Anisotropy of the coal matrix

It is well established that mechanical properties of coal are dependent upon orientation relative to the bedding plane. It has also been recognised that coal swells as a result of gas sorption (Goodman et al., 2006; Larsen, 2004; St. George and Barakat, 2001). Cody et al. (1988) studied anisotropy using solvent induced swelling on a suite of coals ranging in rank from lignite to high volatile A bituminous coal. In all of the coals, the swelling was greater in the direction perpendicular to the bedding plane rather than the parallel. It was also observed that the anisotropy of swelling increased with rank. Cody et al. (1988) suggested that swelling anisotropy may be caused by gravity influence on particle settling during the formation of organic sediments, followed by lithostatic pressure acting during the coalification process. In a more recent study using carbon dioxide and methane, Zarębska and Ceglarska-Stefańska (2008) also reported anisotropic swelling and observed that the expansion of coal samples as a result of carbon dioxide sorption was about twice that of methane sorption.

5.4.2. Anisotropy observed in SAS measurements

Anisotropy of the pore shape reflects the primary direction of pressure at the time of coalification. Pore shape is hence reduced in the direction perpendicular to the bedding plane compared to the direction parallel to the bedding plane.

As discussed previously ((Radlinski et al., 2004b) see Figure 5.4), the pinhole geometry SAS techniques (usually SANS and SAXS) only perceive pore dimensions in the direction perpendicular to the incident beam of neutrons or X-ray photons. Consequently, the 2D SANS and SAXS patterns acquired for samples cut in-bedding-plane (parallel samples) are isotropic (circular) and correspond to the collective scattering power of the larger (in-bedding-plane) dimension of squash-shaped pores. These patterns are usually azimuthally averaged to produce one-dimensional scattering curves.

In contrast, the SANS and SAXS patterns are typically anisotropic (ellipsoidal) for samples cut perpendicular to bedding plane (perpendicular samples). Scattering intensity in the vicinity of the short axis of the ellipsoid corresponds to the collective scattering power of the larger (in-bedding-plane) dimension of the squash-shaped pores (similar to parallel samples) whereas the intensity adjacent to the long axis reflects the collective scattering power of the shorter (perpendicular to bedding plane) direction of the pores.

Consequently, the 2D scattering patterns of perpendicular samples are processed by taking two sector averages, along the long and short axis. These 1D scattering curves contain information about the collective scattering power along both the small and large dimension of the squash-shaped pores, the former theoretically coinciding with the 1D scattering curves for parallel samples.

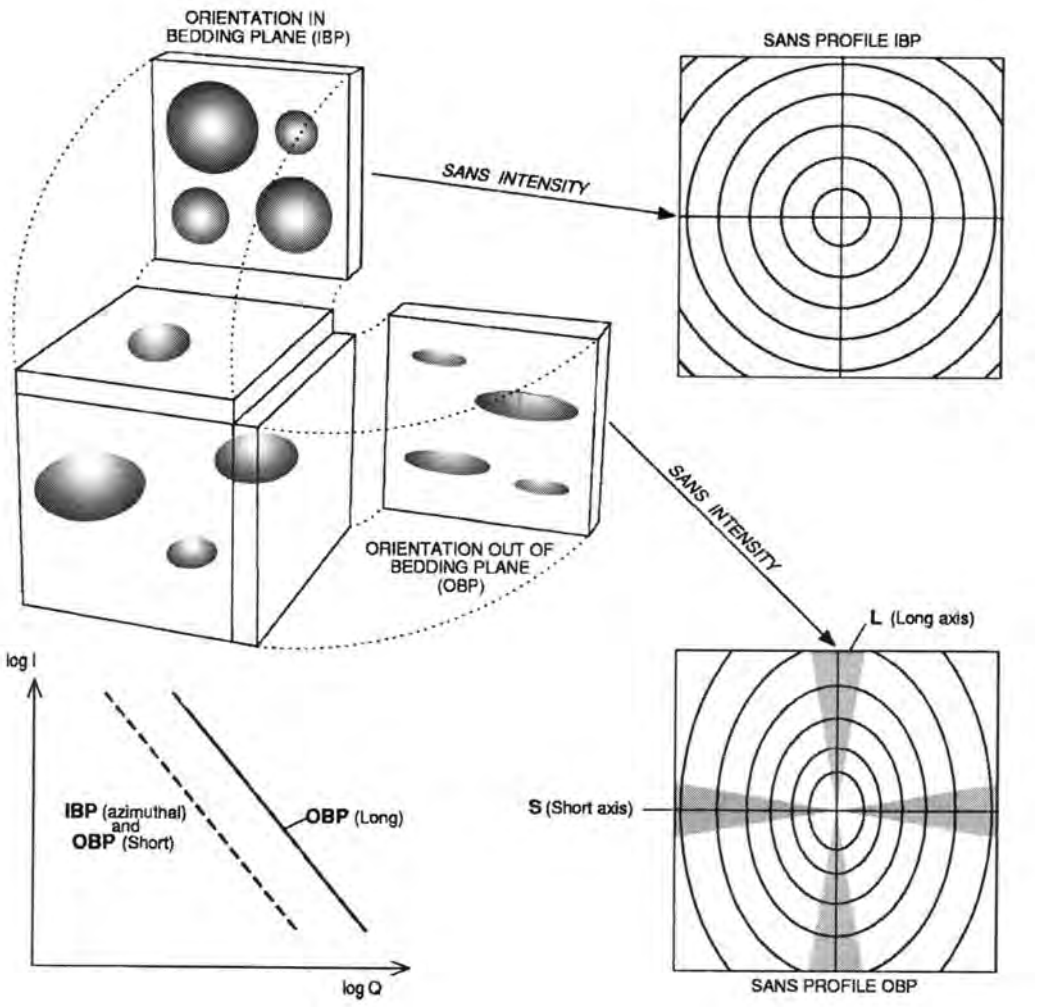

Figure 5. 4. From upper left corner, clockwise: (1) Schematic graphical representation of the shape of pores as present in coal slices cut out in-the bedding plane (IBP) and perpendicular to the bedding plane (out-of-bedding plane, OBP). During the SANS experiment, the neutron beam is incident on a sample perpendicular to the large face, and a planar 2D detector comprising a large number of elements (pixels) is placed at some distance behind the sample. (2) Schematic SANS intensity profile observed with a 2D detector for an IBP oriented coal sample. The concentric circles are iso-intensity lines, with intensity increasing towards the center of the detector. The scattering pattern has an axial symmetry, which reflects the fact that pores are statistically identical in any in-plane direction (i.e., isotropic). One-dimensional SANS curves are obtained from such isotropic scattering patterns by taking an azimuthal average over the entire detector area. The scattering vector, Q, is proportional to the distance between a detector element (pixel) and the detector center. (3) Schematic SANS intensity profile observed with a 2D detector for an OBP-oriented coal sample. The iso-intensity lines are now ellipsoidal, reflecting the fact that statistically the pores are larger in the in-bedding plane directions than in the perpendicular-to-the-bedding direction. Shaded sectors indicate those sections of the detector over which the signal has been averaged to produce the in-bedding plane (along the short axis of the ellipsoid) and out-of-bedding (along the long axis of the ellipsoid) one-dimensional SANS curves. The sectors are selected to be narrow enough (typically no more than 20 degrees of arc) to well approximate iso-intensity lines with circular arcs. (4) One-dimensional SANS data averaged as described in (2) and (3) and plotted on a log–log scale, where Q is the scattering vector (proportional to the scattering angle), and I is the scattering intensity. The azimuthal average for the in-bedding plane sample (IBP) and the sector average for the perpendicular-to-bedding sample along the short axis of the 2D SANS ellipsoid (OBP short) are expected to fully coincide, as they both represent scattering on the in-bedding plane elements of the pore space. The sector average for the perpendicular-to-bedding sample along the long axis of the SANS ellipsoid (OBP long) corresponds to scattering on the gravitationally squashed, perpendicular to the bedding plane, elements

of the pore space, and for anisotropic coals it is distinctly different from the other two averages. Caption and figure from Radlinski et al. (2004b).

However, in reality these two scattering curves do not always coincide completely, most likely because the vertical heterogeneity of coal on scales comparable to the SANS beam size (about 15mm). Additionally, the 1D SANS/SAXS curve for a parallel sample is usually less noisy than its "short axis" counterpart from the perpendicular sample (owing to much better counting statistics). As such it is used preferentially as the representation of the scattering power along the larger dimension of pores. Therefore, it is good practice to use both perpendicular and parallel samples for SAS work on coal.

A third argument in favour of using parallel samples is purely practical. Pinhole geometry SANS and SAXS instruments can only provide data about pore sizes in the range 2 nm to about 300 nm (Radlinski, 2006). Microstructural information in the important pore size region 300 nm to about 20 μm can only be obtained using double-crystal-diffraction (Bonse-Hart) geometry instruments (USANS in particular), which provide convoluted 1D scattering data not suitable for analysis of anisotropic scattering objects (Bonse and Hart, 1965). Therefore, even though SAS experiments on perpendicular samples provide inherently richer microstructural information, the SANS-USANS and SAXS-USAXS pairs of data, needed to cover as wide as possible range of pore sizes, are only meaningful for parallel samples.

An example (data shown is from sample 610) of the anisotropy identified in the Huntly coals is illustrated in Figure 5.5 where sector averages taken along the long and short axes of the 2D scattering intensity pattern (scattering surface) are presented for SANS data from a perpendicular sample. The anisotropy seen in the coals analysed is generally less than 2:1, where the numbers refer to the ratio of scattering intensity along the short and long axis

at a fixed scattering angle (Q-value). Given that the variation of SAS intensity over the combined SANS and USANS Q-range is typically 13 orders of magnitude, the effect of anisotropy can be considered small, and even neglected in some cases.

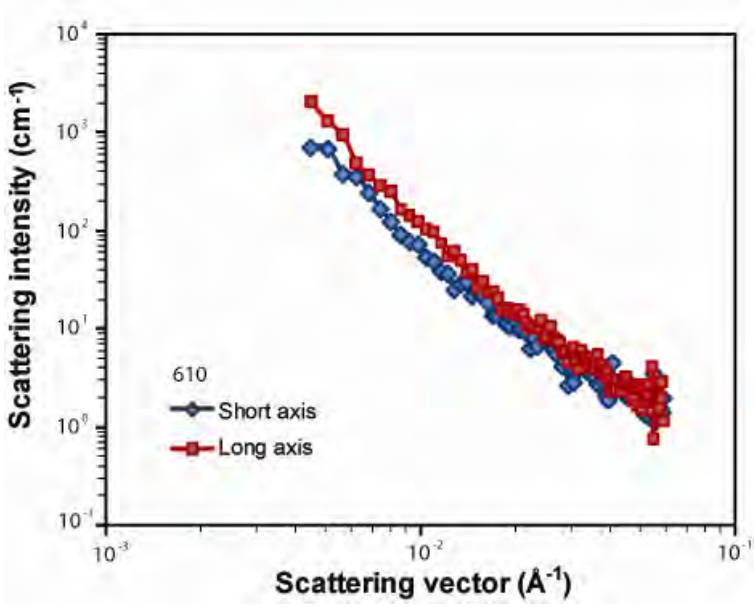

Figure 5. 5. An example of sample anisotropy identified in the Huntly coals. Sector averages taken along the long and short axes of the 2D scattering intensity pattern (scattering surface) are presented for SANS data from a perpendicular sample (610).

5.4.3. Scattering curves

Combined SAXS and USAXS data acquired from both perpendicular and parallel samples are shown for matrix samples in Figures 5.6A and B and for vitrain samples in 5.6C and D. Because of experimental time constraints, the corresponding SANS data were not collected for both orientations for all samples. Therefore, assuming negligibly small anisotropy, SANS curves acquired for perpendicular samples 319, 611, 612, 321 and 326 were combined with USANS data for corresponding parallel samples. SANS and USANS

data were not obtained for the vitrain sample 328. Note that there is no overlap of SANS and USANS data points, which creates an additional small uncertainty when connecting the two curves. In principle this problem could be eliminated at the cost of substantially longer USANS acquisition time, which was not available during this experiment. The combined SANS and USANS scattering curves are presented in Figure 5.7A and B for matrix and vitrain samples respectively.

In general, both the SAXS/USAXS and SANS/USANS data have good signal-to-noise characteristics for $Q < 0.2$ $Å^{-1}$, which slowly deteriorate for larger scattering angles, up until $Q > 0.5$ $Å^{-1}$ where the data becomes exceedingly noisy. It can be seen that the vitrain samples have a noticeably different shape, particularly for the perpendicular samples, to the coal matrix samples with a more pronounced hump in the $Q > 0.001$ $Å^{-1}$ region. Of note, this hump is not seen in the SANS/USANS curves.

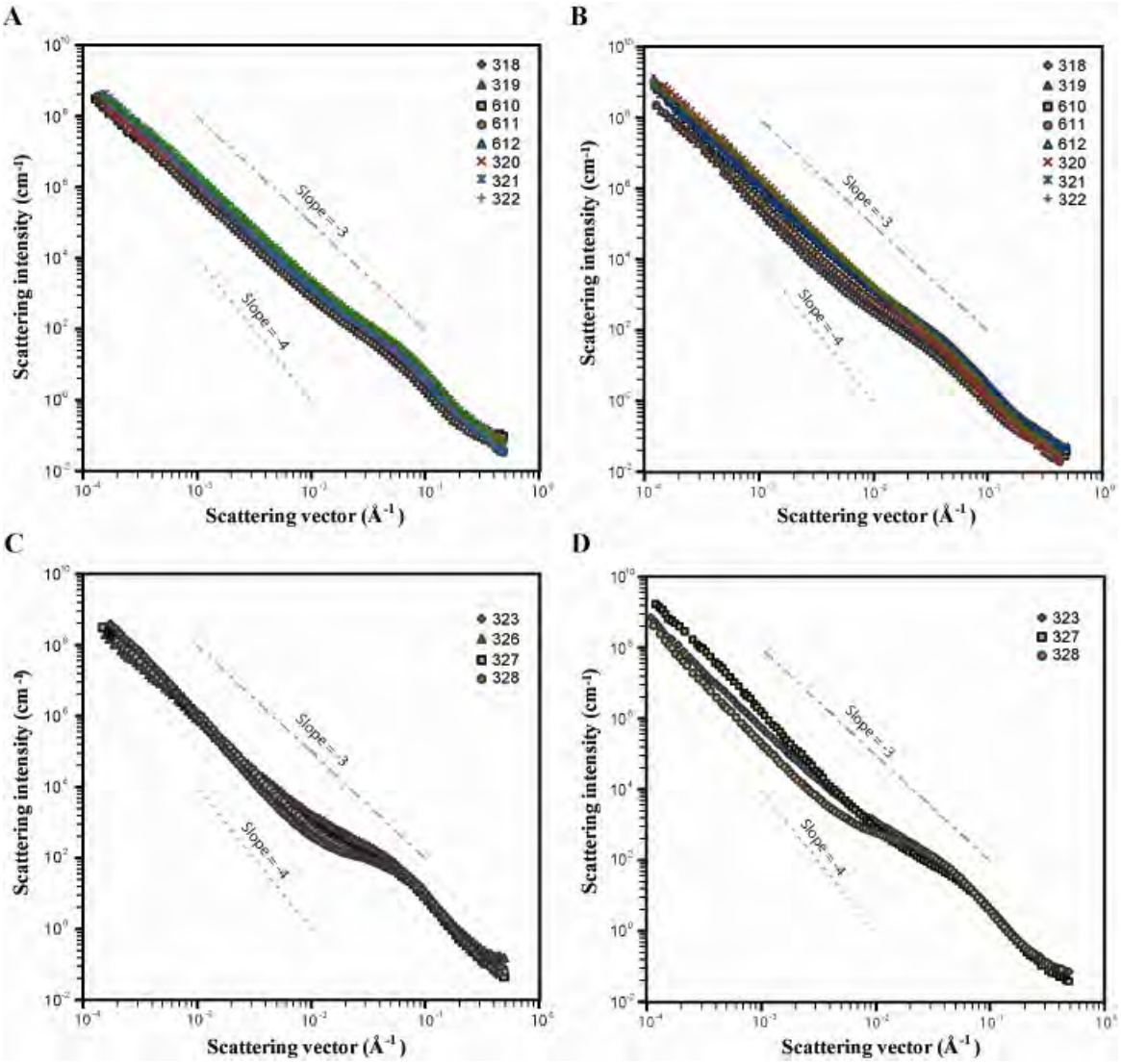

Figure 5. 6. (A) Scattering curves for coal matrix samples orientated perpendicular to bedding plane measured using SAXS/USAXS. (B) Scattering curves for coal matrix samples orientated parallel to bedding plane measured using SAXS/USAXS. (C) Scattering curves for vitrain samples orientated perpendicular to bedding plane measured using SAXS/USAXS, and (D) Scattering curves for vitrain samples orientated parallel to bedding plane measured using SAXS/USAXS.

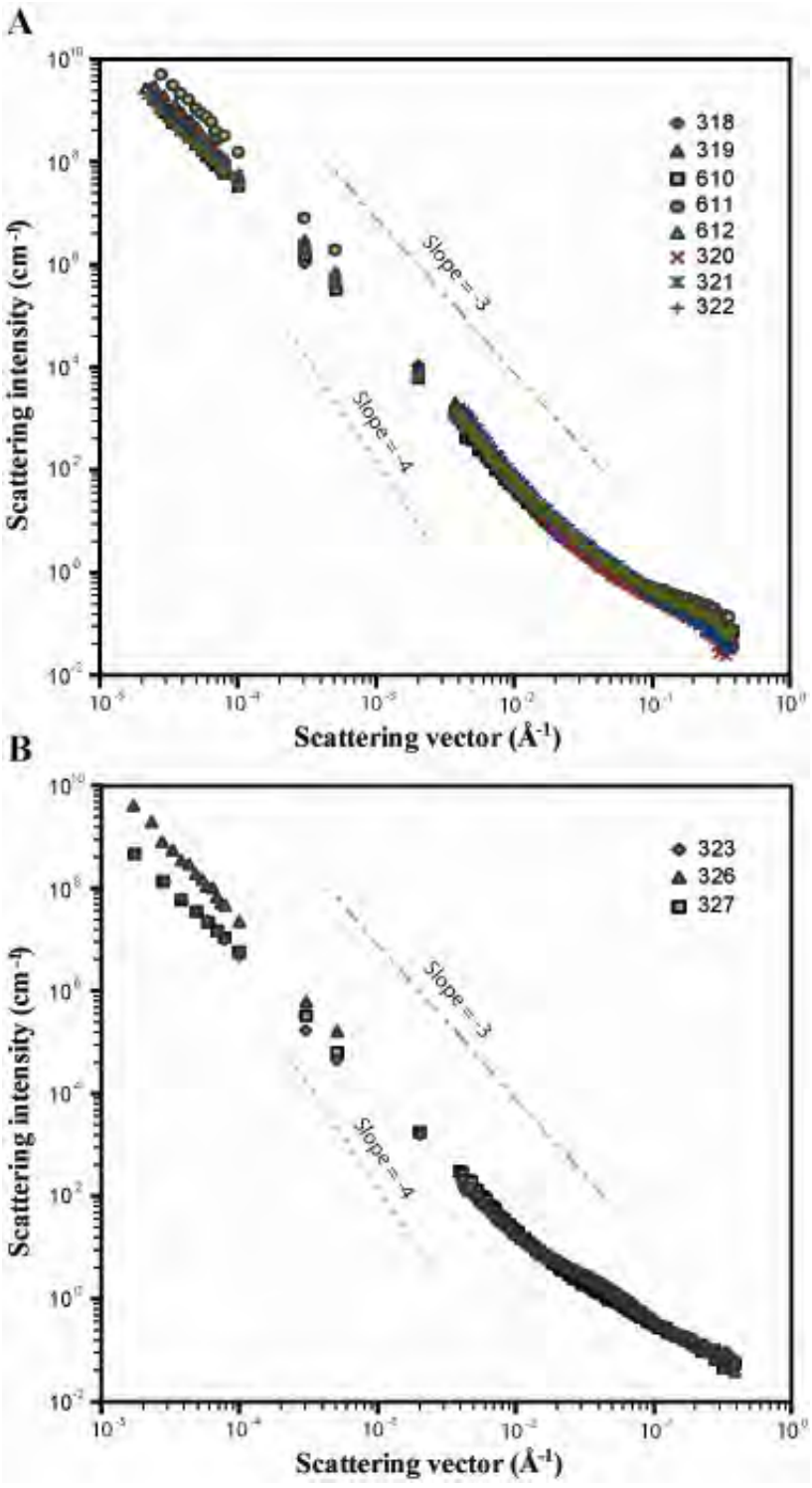

Figure 5. 7. (A) Scattering curves for coal matrix samples measured using SANS/USANS, and (B) Scattering curves for vitrain samples measured using SANS/USANS.

5.4.4. Location of mineral matter in the pore space

For coals with low mineral matter content (low ash yield), SAXS and SANS techniques provide equivalent microstructural information. When mineral matter is present in a quantity more than about 1 wt%, it can be identified by differences between the X-ray and neutron scattering curves. These differences follow from detailed contrast considerations (Radlinski, 2006; Radlinski et al., 2004b).

For both matrix and vitrain samples the X-ray scattering curves for both orientations have very similar shape and intensity (Fig. 5.6). However, when compared to the neutron scattering curves collected from the same samples (Fig. 5.8), there are shape differences (particularly accentuated in the Q-range 0.02 $Å^{-1}$ < Q < 0.2 $Å^{-1}$ on the right-hand side of the figure) in perpendicular samples, and possibly (to a lesser extent) in the parallel samples. The combination of a strong SAXS and weak SANS signature, when considering the scattering length density data for the organic and inorganic components of coal (Radlinski and Hinde, 2001), strongly suggests that the scattering contrast in the micropore region is not caused by scattering difference between the coal matrix and voids, bitumen, or water. Matrix–void scattering would result in strong SAXS/USAXS and SANS signatures, matrix–bitumen scattering a weak SAXS/USAXS and SANS/USANS signature and matrix–water scattering a weak SAXS/USAXS and a strong SANS/USANS signature (Radlinski et al., 2004b). The current scenario of a strong SAXS/USAXS and a weak SANS/USANS signature is scattering between the coal matrix and inorganic matter in the micropores. Inorganic matter in the micropore region was also identified by Radlinski et al. (2004b). Note that on the log-log scale the vertical shift of a SAXS/USAXS curve in relation to the SANS/USANS curve for the same sample corresponds to multiplication of the scattering intensity for each Q-value by

a constant, which simply reflects different scattering mechanisms for both types of radiation (X-rays and neutrons).

For a broad distribution of pore sizes (fractal scattering objects), a relationship $r = 2.5/Q$ generally holds (where r is the radius of pores contributing most to the scattering intensity; Radlinski et al. (2000)) which leads to the estimated size ranges for pores contaminated with inorganic matter: 12.5 Å < r < 125 Å (10 Å = 1 nm). Above this 'contaminated' region (Q-values > 0.2 $Å^{-1}$), on the left-hand side of the figure, the scattering intensity for all samples can be represented on a log-log scale by a straight line with a slope, *S*. In the present case S is close to -3, indicating a very rough fractal pore-matrix interface (Radlinski et al., 1996; Wong and Bray, 1988). For surface fractals (including coals), there is a relationship between the slope of the power law scattering and fractal dimension, D_s: $S=6-D_s$.

As to be expected at this rank, there is no evidence for the development of polyaromatic sheets, which would be detected in SAXS as a broad scattering peak centered around Q = 0.3 $Å^{-1}$.

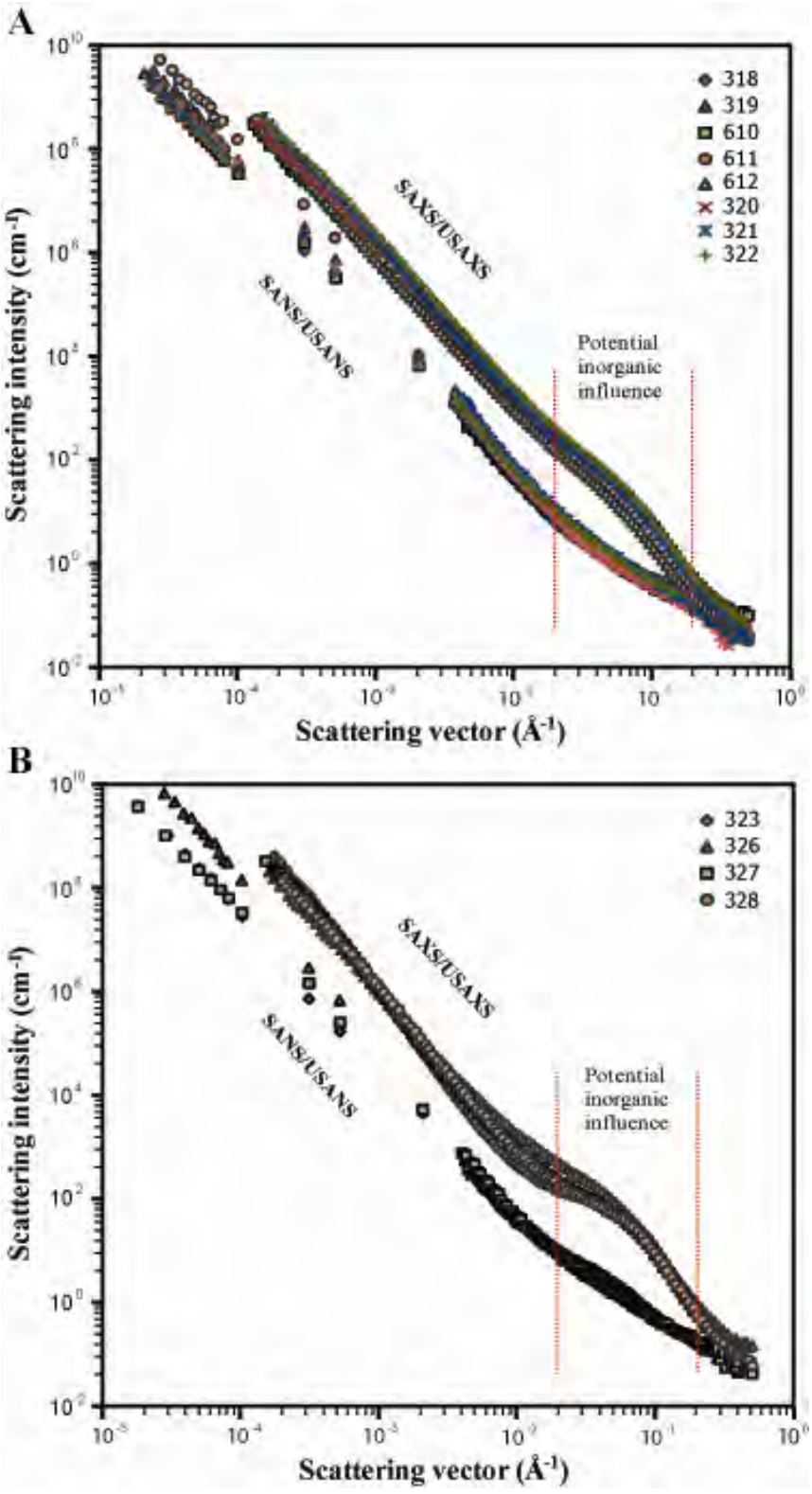

Figure 5. 8. (A) Comparison of SAXS/USAXS scattering curves for coal matrix samples orientated perpendicular to bedding plane and SANS/USANS scattering curves, highlighting the region influenced by inorganic material, and (B) Comparison of SAXS/USAXS scattering curves for vitrain samples orientated perpendicular to bedding plane and SANS/USANS scattering curves, highlighting the region influenced by inorganic material

5.5. Pore size distribution

5.5.1. Polydisperse Spherical Pore Model.

The pore size distribution is the fraction of pores of a diameter within a narrow band centered on a pore size, *r*, within the total population of pores, represented as the function of *r* (Radlinski et al., 2004b). The pore size distribution, $f(r)$, was computed for each dataset using the Polydisperse Spherical Pore Model (PDSP) embedded in the PRINSAS software (Hinde, 2004; Radlinski et al., 2004a; 2001) and the results are expressed as histograms. The scattering length densities (SLD) used for these computations (calculated from elemental composition and matrix density of coals using formulas 2.3 and 2.4 (Radlinski, 2006)) are listed in Table 5.1.

The PDSP model is based on a two-phase approximation, which assumes that coal is composed of a solid matrix of a uniform scattering length density and a pore space characterized by another single value of SLD. This approximation is strictly valid for both SAXS/USAXS and SANS/USANS for mineral-matter-free coals, and only for SANS/USANS for any coal (Radlinski, 2006). The PDSP model starts to break down for SAXS and USAXS when there is significant amount (more than several weight %) of mineral matter present within a sample.

5.5.2. Pore size distributions for Huntly samples.

Pore size distributions were obtained for SANS/USANS data in the pore size range of 1 nm to 10 μm (10-100,000 Å) and for SAXS/USAXS data between 1 nm and 2 μm (Figs.

5.9A - D). Note that SAXS/USAXS data not only cover a smaller Q-range than SANS/USANS (because of the smaller size of the largest observable pore, resulting from a larger minimum Q-value for USAXS instruments), but also are potentially subject to a distortion caused by the presence of a third phase (inorganic matter) in addition to the coal matrix (phase 1) and pore space (phase 2). The plot for parallel samples is very similar to that for perpendicular samples and hence is not shown. The pore size distributions for both matrix and vitrain samples appear to be very similar. Greater variation is seen in the SAXS/USAXS data than for the SANS/USANS data which, in agreement with the observations above, is more noticeable for the vitrain samples than for the matrix samples. The largest variation is for sample 323 which can be seen to have the most defined hump (Fig. 5.6C). Slight anisotropy is noticeable in SAXS/USAXS data for parallel and perpendicular samples, as shown for one sample (610) in Figure 5.10.

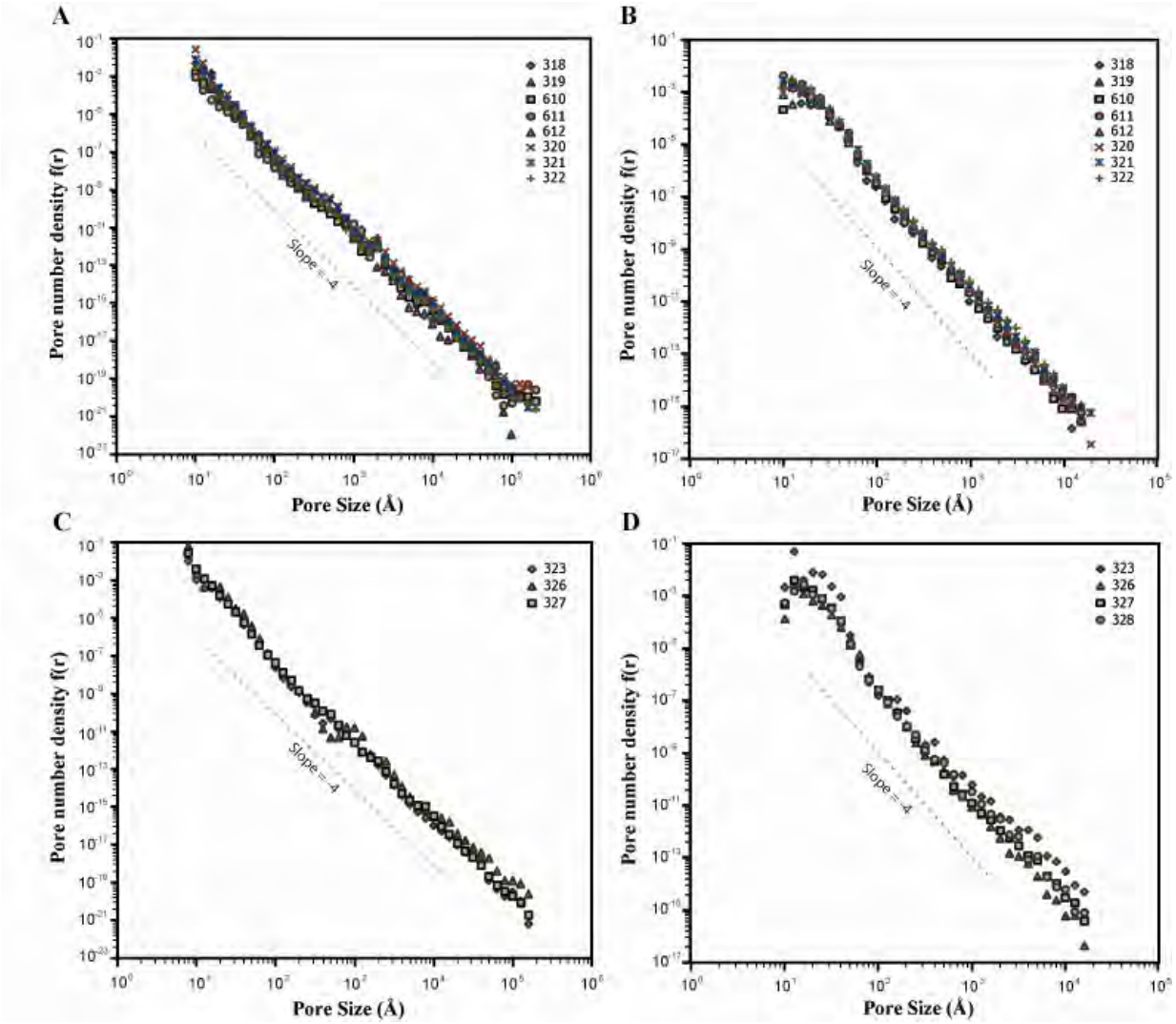

Figure 5. 9. (A) Pore size distribution calculated from SANS/USANS data for coal matrix samples. (B) Pore size distribution calculated for coal matrix samples orientated perpendicular to bedding plane from SAXS/USAXS data. (C) Pore size distribution calculated from SANS/USANS data for vitrain samples, and (D) Pore size distribution calculated for vitrain samples orientated perpendicular to bedding plane from SAXS/USAXS data.

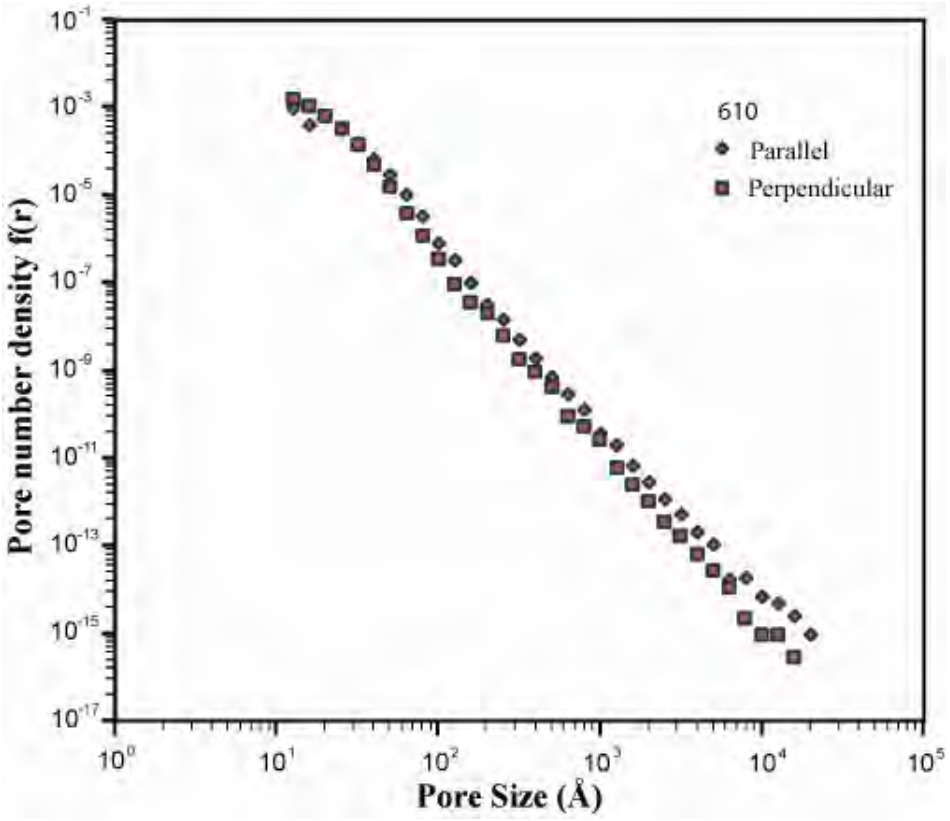

Figure 5. 10. A comparison of pore size distributions calculated from sample 610 using SAXS/USAXS data, from both the parallel and the perpendicular orientated samples, showing slight anisotropy.

The pore size distributions of the Huntly coals follows the power law $f(r) = Ar^{-B}$, where the exponent B is close to 4. This is to be expected, as scattering on fractal objects is equivalent to scattering on a power law distribution of spherical scattering objects (Schmidt, 1982; Schmidt, 1989) and the following relationship holds: $B = 7\text{-}S$, where S is the absolute value of the slope of the scattering intensity, I(Q), versus Q curve (close to 3 for all coals analysed here). The power law equation was fitted for each sample for $r > 25$ Å, as data for $r < 25$ Å are exceedingly noisy. Numerical values of parameters A and B are listed in Table 5.3.

Table 5. 3. Values of parameters A and B obtained by fitting the power law model $f(r) = Ar^{-B}$ to the data presented in Figure 5.9.

Sample		Analysis Type	A	B	R^2
Renown	318	SANS/USANS	13.91	4.11	0.996
		SAXS/USAXS perpendicular	110.74	4.25	0.994
		SAXS/USAXS parallel	126.04	4.11	0.997
	319	SANS/USANS	15.55	4.25	0.987
		SAXS/USAXS perpendicular	111.32	4.17	0.996
		SAXS/USAXS parallel	123.35	4.06	0.997
	610	SANS/USANS	9.94	4.13	0.996
		SAXS/USAXS perpendicular	208.44	4.32	0.998
		SAXS/USAXS parallel	134.59	4.09	0.996
	611	SANS/USANS	1.03	3.88	0.974
		SAXS/USAXS perpendicular	120.76	4.16	0.995
		SAXS/USAXS parallel	236.54	4.16	0.997
	612	SANS/USANS	9.81	4.11	0.994
		SAXS/USAXS perpendicular	94.79	4.12	0.997
		SAXS/USAXS parallel	296.04	4.10	0.993
Kupakupa	320	SANS/USANS	23.59	4.07	0.998
		SAXS/USAXS perpendicular	278.75	4.31	0.999
		SAXS/USAXS parallel	101.09	3.87	0.999
	321	SANS/USANS	36.64	4.19	0.999
		SAXS/USAXS perpendicular	122.57	4.11	0.997
		SAXS/USAXS parallel	119.71	4.14	0.997
	322	SANS/USANS	15.78	4.19	0.998
		SAXS/USAXS perpendicular	163.37	4.12	0.997
		SAXS/USAXS parallel	155.23	4.01	0.999
Vitrain	323	SANS/USANS	10.82	4.21	0.996
		SAXS/USAXS perpendicular	98.71	3.99	0.968
		SAXS/USAXS parallel	238.17	4.40	0.994
	326	SANS/USANS	4.35	3.97	0.988
		SAXS/USAXS perpendicular	304.18	4.45	0.994
	327	SANS/USANS	13.94	4.20	0.998
		SAXS/USAXS perpendicular	90.01	4.18	0.988
		SAXS/USAXS parallel	45.24	3.94	0.989
	328	SAXS/USAXS perpendicular	76.79	4.12	0.989
		SAXS/USAXS parallel	127.84	4.37	0.988

R^2 = correlation coefficient

5.6. Specific surface area

The distinction must be made between the total pore volume and the size of corresponding pore surface area. A large total pore volume need not necessarily imply that the pore surface area is also large, as pore surface area is determined by the pore size distribution and pore morphology (van Krevelen, 1993). Coal provided one of the first examples of fractal surface microstructure (Bale and Schmidt, 1984) and the SAXS and SANS study by Radlinski and Radlinska (1999) found by using fractal analysis that the pore-coal interface is rough in lower rank coals throughout the entire pore size range. The degree of roughness was found to decrease with increasing rank, with the pore-matrix interface becoming smooth (throughout the length scale range) for anthracites. As illustrated in Figure 5.9, the pore size distribution covers multiple length scales and, consequently, the specific internal surface area, SSA, depends on the size of the measuring probe.

5.6.1. Specific surface area by probe size

The SSA of the coal samples, presented in Figure 5.11 for SAXS and 5.12 for SANS, was calculated from the pore size distributions as a function of probe size *R* (Radlinski et al., 2004b). Although both the matrix and the vitrain samples had reasonably similar pore size distributions, some differences can be seen in the calculated SSA. SSA of the coal matrix material, obtained from SAXS/USAXS data for perpendicular samples, indicates that the three samples from the Kupakupa seam (320, 321 and 322) have greater SSA for probe sizes >100 Å (Fig. 5.11A). However, such an effect is only seen for 320 and 322 for the parallel samples. In addition, SSA values for parallel samples 611 and 612 (both from the Renown

seam in the Mimi 1 drill hole) are significantly smaller than those for the other samples across all probe sizes (Fig. 5.11B). For the vitrain samples, the SSA of the three perpendicular samples (Fig. 5.11C) are reasonably similar. In contrast to this, considerable variation is seen for the parallel samples when probe size > 100 Å (Fig. 5.11D).

For larger probe sizes, it is noted that the SANS/USANS value of SSA for samples 611 and 326 appears to be larger than average for probe sizes >1000 Å, despite rather noisy data (Fig. 5.12). This possibly results from joining the data of a parallel and a perpendicular sample. The variation seen between samples most likely reflect small variations in pore shape deformation for various coals, which is yet another aspect of the heterogeneity of coal and a good demonstration of the benefits of analysing large number of samples.

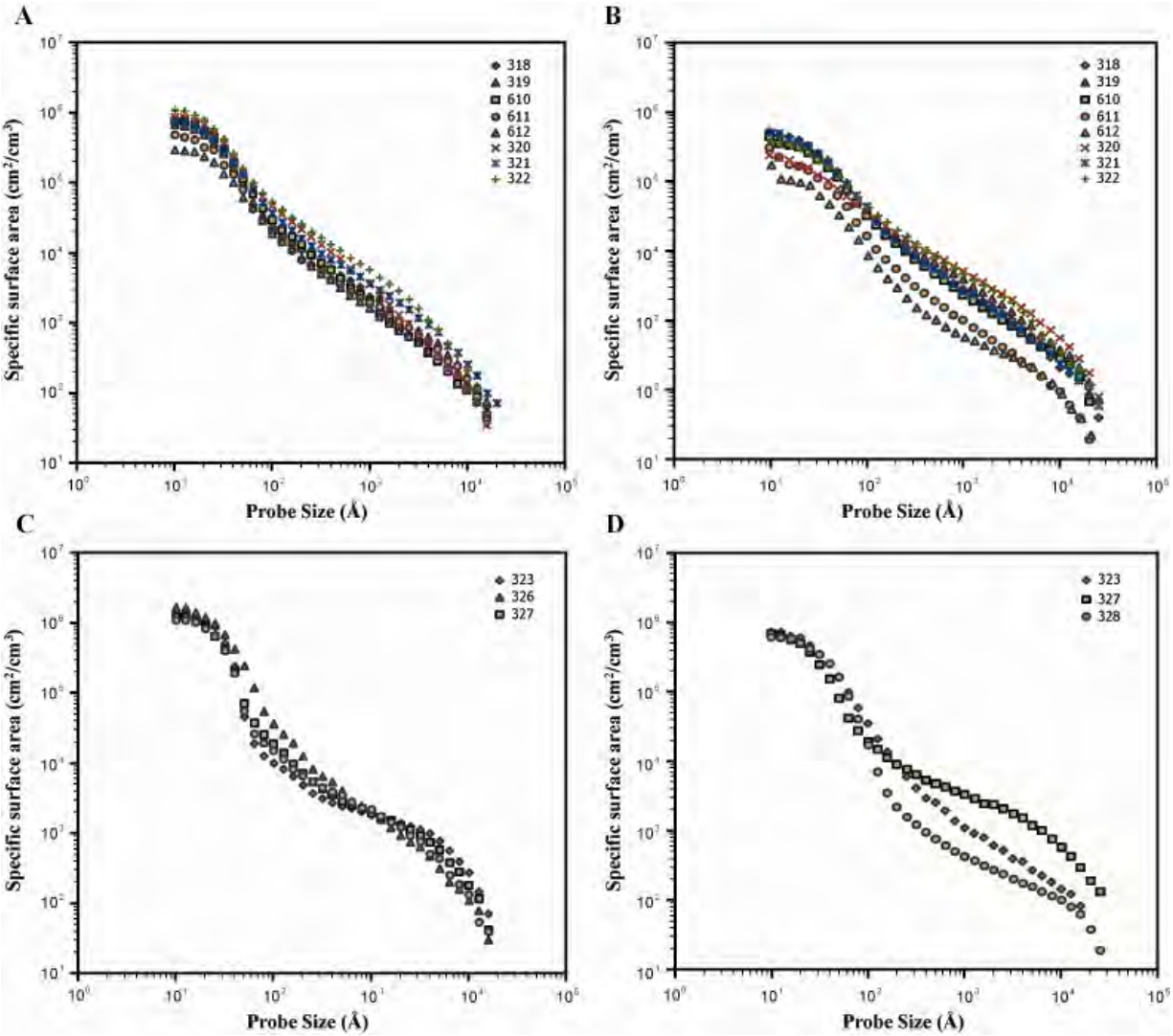

Figure 5. 11. (A) Specific surface area versus probe size calculated for perpendicular orientated coal matrix samples using SAXS/USAXS data. (B) Specific surface area versus probe size calculated for parallel orientated coal matrix samples using SAXS/USAXS data. (C) Specific surface area versus probe size calculated for perpendicular orientated vitrain samples using SAXS/USAXS data. (D) Specific surface area versus probe size calculated for parallel orientated vitrain samples using SAXS/USAXS data.

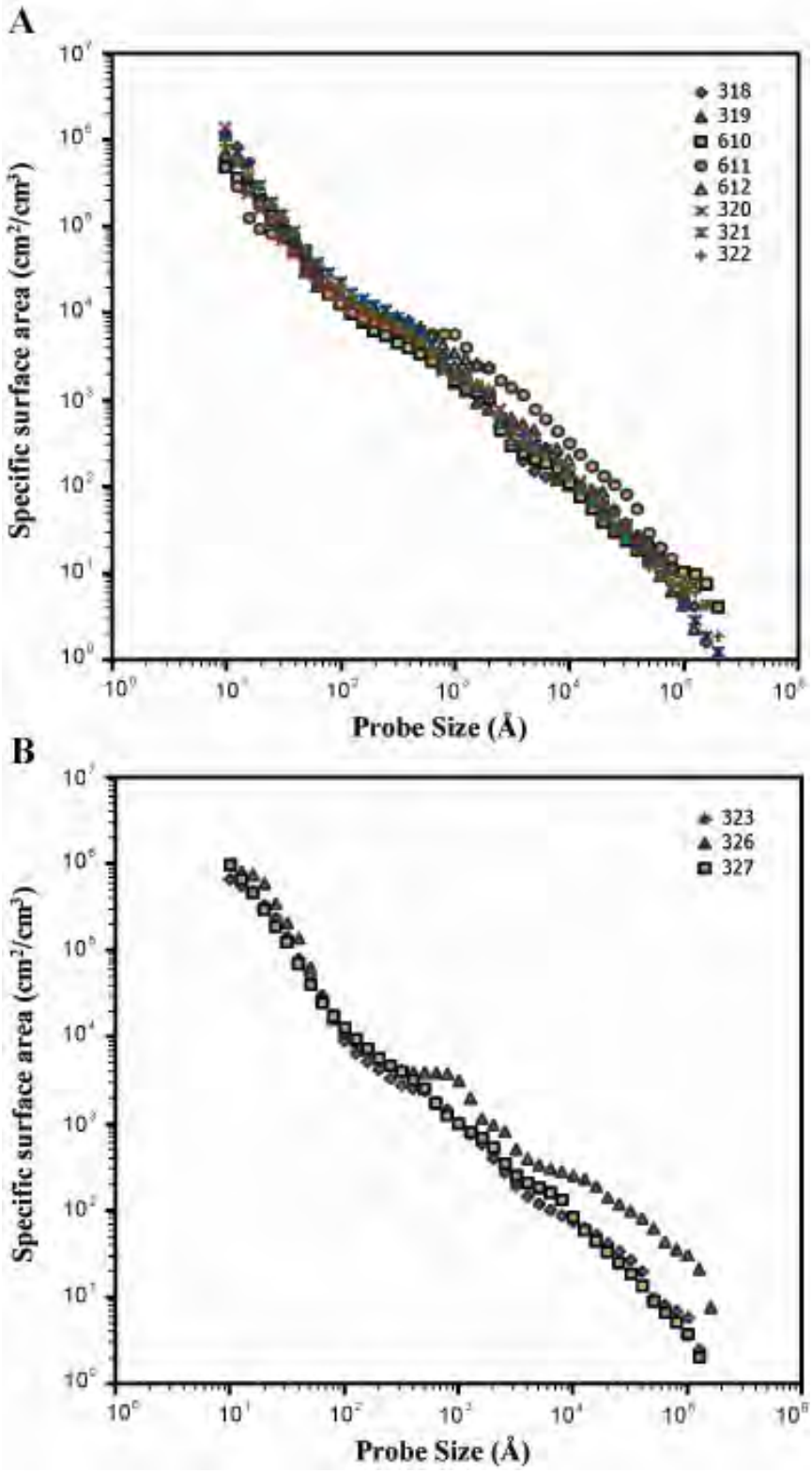

Figure 5. 12. (A) Specific surface area versus probe size calculated for coal matrix samples using SANS/USANS data, and (B) Specific surface area versus probe size calculated for vitrain samples using SANS/USANS data.

5.6.2. Specific surface area at probe size 4 Å.

For practical applications, the most important information is the SSA at probe size 4 Å, corresponding roughly to the molecular size of CBM gases (kinetic diameters for nitrogen, methane and carbon dioxide molecules are 3.3 Å, 3.8 Å and 3.64 Å respectively; (Cui et al., 2004b)). In order to estimate the SSA of the Huntly coals for a probe size of 4 Å, the SSA data in the region 20 Å < R < 100 Å was extrapolated. This is a more reliable procedure than relying on the 'noisy' results calculated directly for the smallest probe sizes (Table 5.4). As the extrapolation procedure is only based on eight experimental points, it is recognised that the uncertainty is significant, generally of the order of +/- 50% of the quoted value (Radlinski et al., 2004b; Radlinski et al., 2001).

Table 5. 4. Specific surface areas (m^2/cm^3) at a probe size of 4 Å extrapolated from small angle scattering data.

	Sample	SANS/USANS	SAXS/USAXS perpendicular	SAXS/USAXS parallel
Renown	318	426	2006	662
	319	255	1317	431
	610	271	1397	409
	611	210	762	271
	612	125	325	121
Kupakupa	320	133	905	99
	321	412	885	435
	322	405	1725	186
Vitrain	323	1705	36302	1668
	326	2878	8124	
	327	596	6772	1988
	328		9716	2263

Radlinski et al. (2004b) compared SSA obtained from extrapolating SANS data to R = 4 Å to the direct SSA measurements using the nitrogen adsorption method, and found that

both sets of data displayed a similar pattern versus rank with the SAS SSA systematically yielding somewhat higher values (See Fig 5.13). The results presented in this study for SANS/USANS data, ranging from SSA = 1.25 x 10^6 cm^{-1} (cm^2/cm^3) to 2.88 x 10^7 cm^{-1}, fit well with the long-established trend of SSA increasing with decreasing rank for coals with vitrinite reflectance less than 1.0%. Gan (1972) reported surface areas for lignite to be 225-359 m^2/g, while Radlinski et al (2004b) reported surface areas of 5.7 m^2/cm^3 and 34 m^2/cm^3 for coals with vitrinite reflectance of 0.55% and 0.59% respectively.

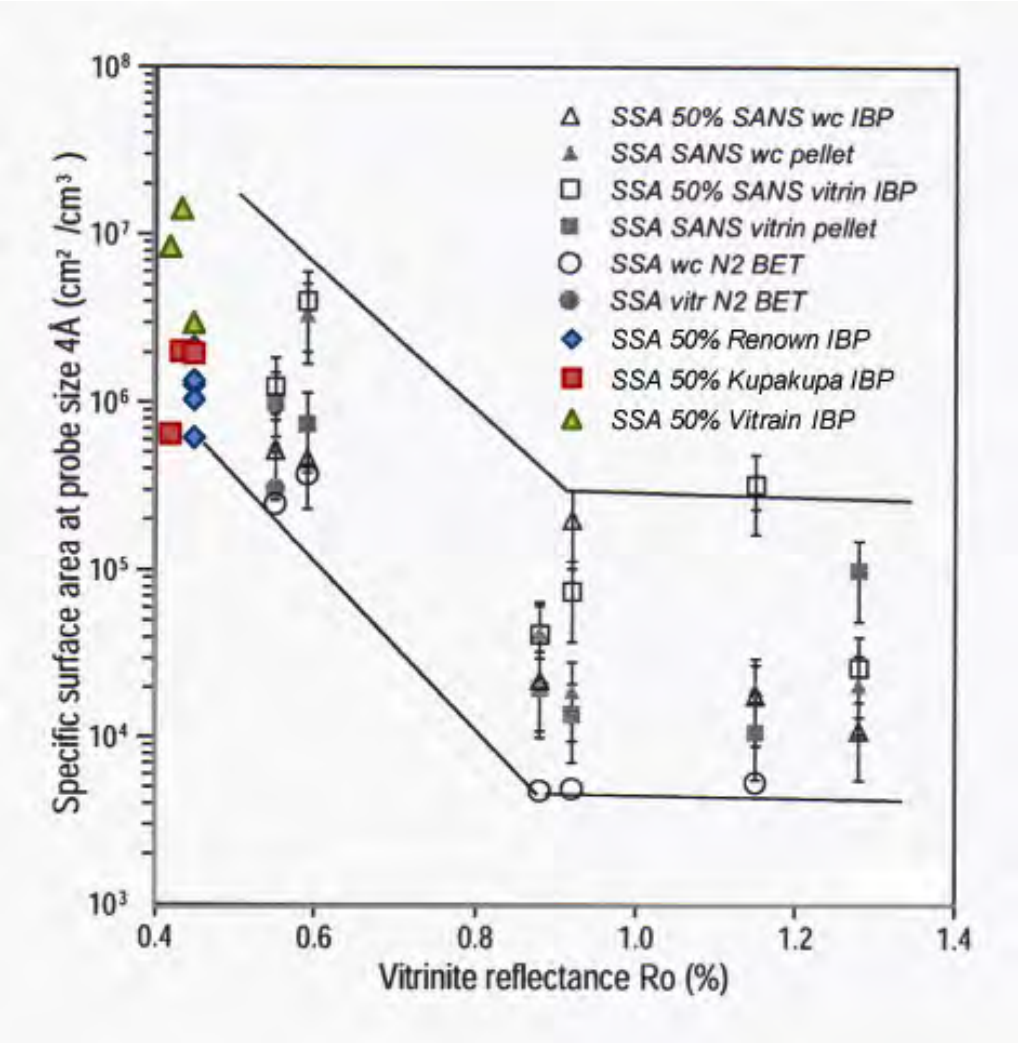

Figure 5. 13. Comparison between specific surface area (cm^2/cm^3) for coals of different ranks and the Huntly samples extrapolated to probe diameter 4 Å from SANS and nitrogen adsorption techniques (N_2 BET). The original graph is from Radlinski et al. (2004b). wc = whole coal, IBP = in bedding plane or parallel sample. As Radlinski et al. (2004b) used 50% of the value for platelets to compare to crushed pellet samples the Huntly samples presented here were also divided by two however the full value also fits the trend lines.

Figure 5.14 compares the results of the extrapolation of SSA data to the probe size of 4 Å for both SANS/USANS and SAXS/USAXS analyses. As expected, the X-ray and neutron results for parallel samples are close to each other. The extrapolated SSA values for corresponding perpendicular samples are systematically higher than those for parallel samples. This probably results from a combination of the influence of inorganic material and pore anisotropy on sample scattering. It is clearly noticeable, regardless of analysis type and sample orientation, that all of the vitrain samples have a larger SSA at a probe size of 4 Å than any of the matrix samples.

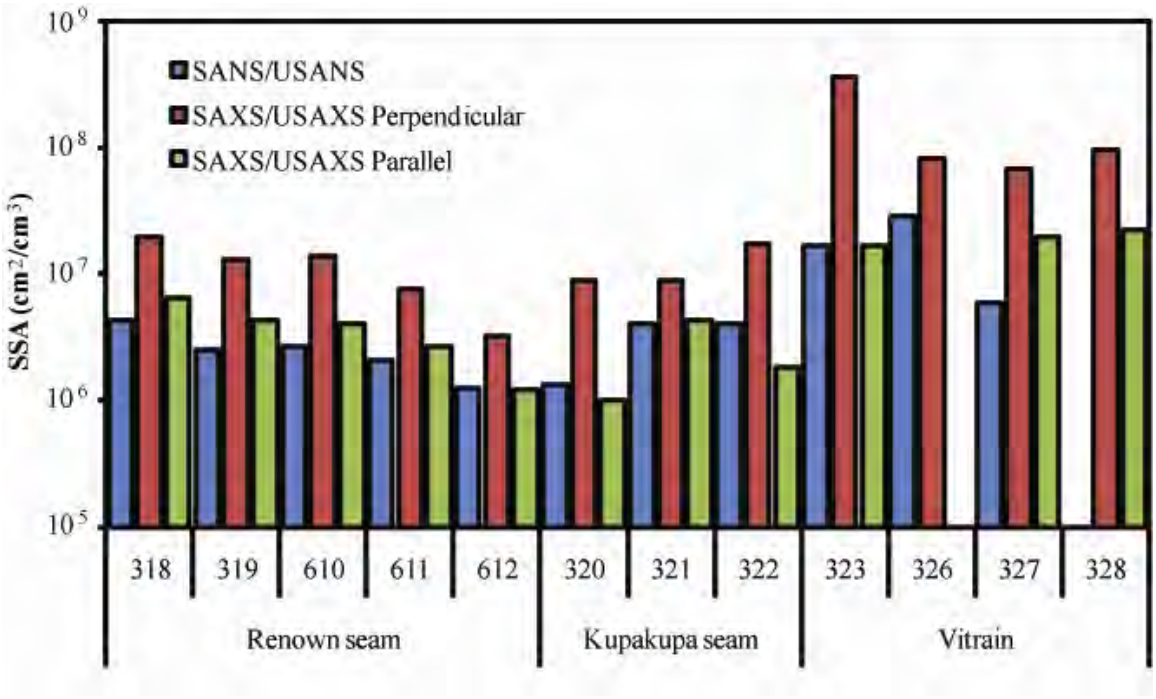

Figure 5. 14. Specific surface area (cm^2/cm^3) for coal samples extrapolated to probe diameter 4 Å from SANS/USANS and SAXS/USAXS data for both perpendicular and parallel to bedding plane orientated samples.

5.6.3. Specific surface area anisotropy.

The anisotropy of SSA for probe sizes of 4 Å, 20 Å, 500 Å and 1000 Å, as quantified by the SAXS/USAXS dataset (by plotting perpendicular SSA values versus parallel SSA values), is illustrated in Figure 5.15. It can be seen that the degree of anisotropy increases with the decreasing probe size (increasing value of SSA), thus indicating that the smaller pores are affected most by the effects of gravity and lithostatic stress. Interestingly, although having a similar SSA for the larger probe sizes, the vitrain samples have a slightly larger SSA at R = 20 Å (2 nm) and a noticeably larger SSA for R = 4 Å.

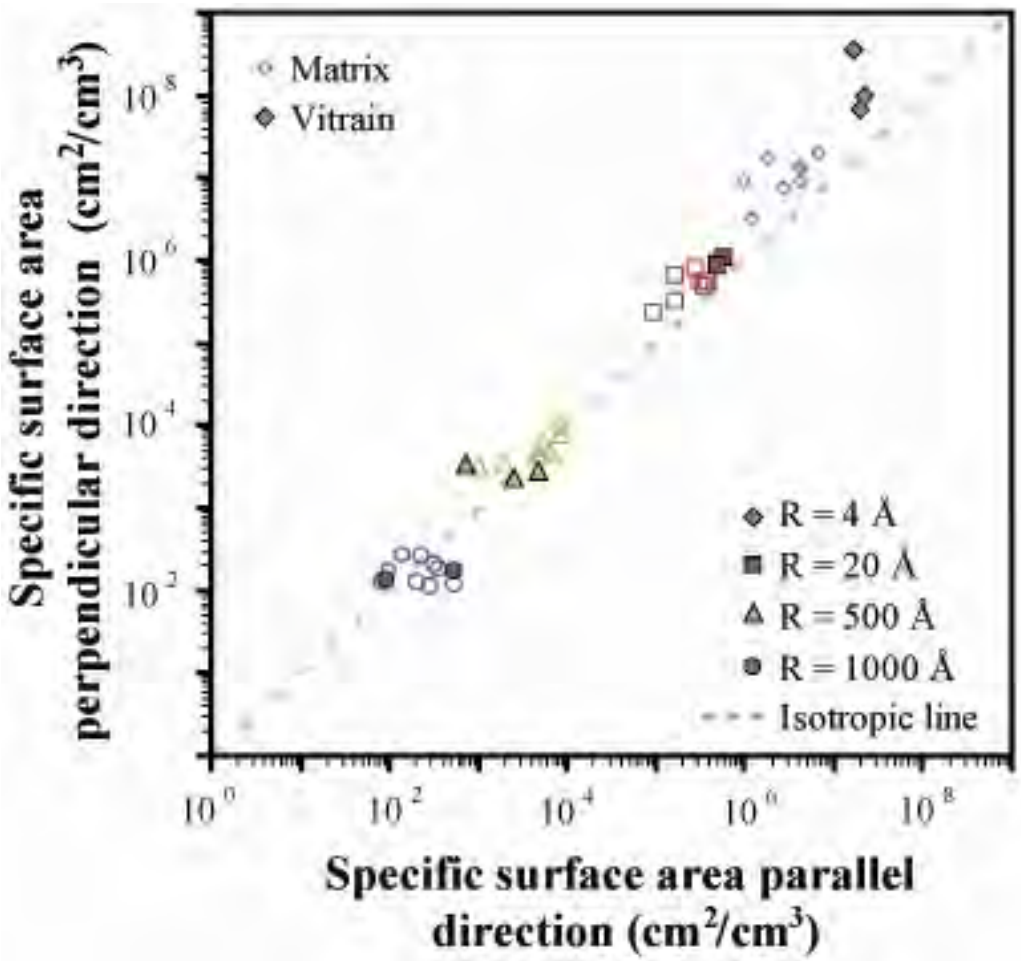

Figure 5. 15. The anisotropy of specific surface area (SSA) calculations for probe sizes of 4 Å, 20 Å, 500 Å and 1000 Å as quantified by the SAXS/USAXS dataset (by plotting perpendicular SSA versus parallel SSA).

5.7. Total porosity

The total porosity of each sample can be readily determined by summing the volumes of all pores in the pore size distribution. The pore size distributions obtained from PRINSAS analysis of SANS/USANS datasets were utilized for this purpose, as they extend over a larger size range than SAXS/USAXS datasets. The distributions were trimmed to the range 10 Å – 100,000 Å (1 nm – 10 μm) as data become noisy outside these limits. To determine the proportion of the porosity contributed by each pore class, as defined in section 5.1.2, sub-total porosity was recalculated for size ranges 20 Å - 100,000 Å and 500 Å - 100,000 Å, and the values were subtracted from the total porosity.

Total porosity of the dry coal samples analysed was found to vary from 16% to 25%. The total porosity for each sample is shown in Figure 5.16; it is interesting to note that for all samples, micropores contribute around 45 to 60% of the total porosity. Gan et al. (1972) reported porosity < 12 Å in size to contribute 12.3% - 40.9% of the total porosity for lignite, 29.9% - 66.7% for high volatile bituminous coals, 61.9% - 73.0% for medium to low volatile bituminous and 75% for anthracite. The average total porosities for matrix and vitrain samples are presented in Figure 5.17. It can be seen that on average the vitrain samples have a larger total porosity than the matrix samples. In addition, the vitrain samples have a larger proportion of mesopores than the matrix samples in spite of having a similar proportion of micropores in the 10 Å – 20 Å size range.

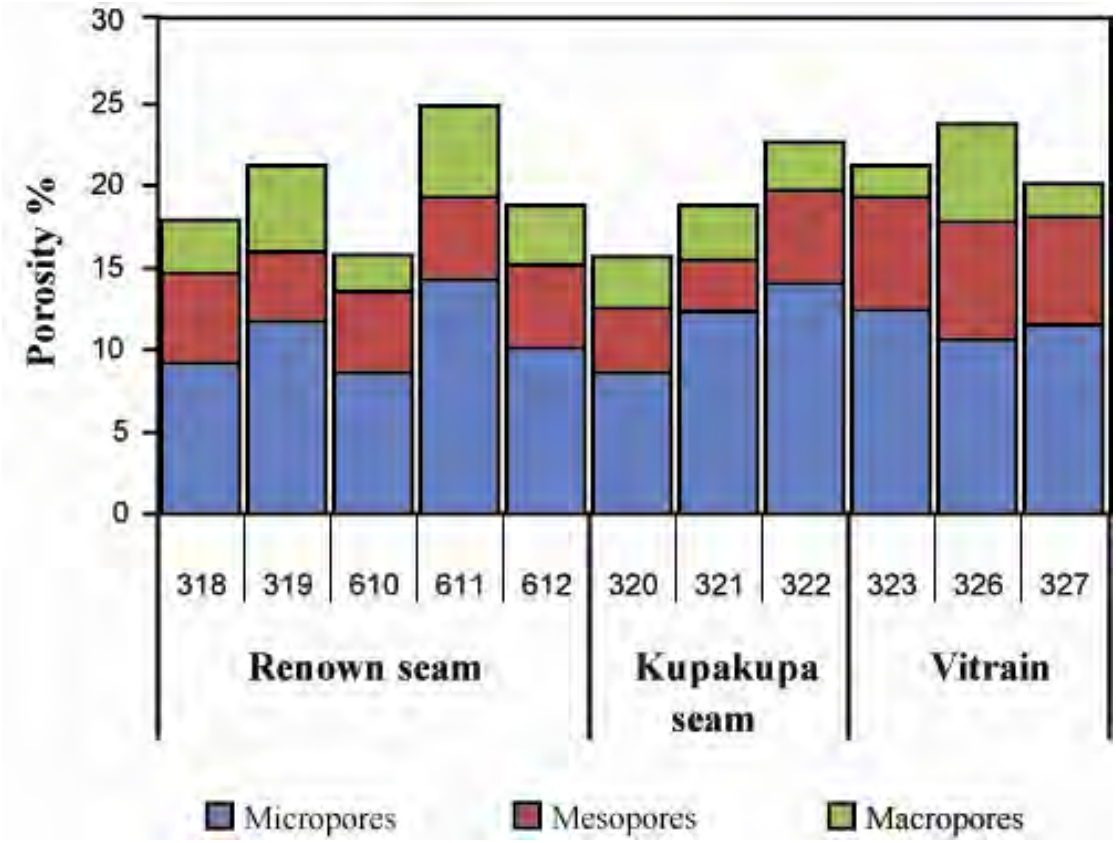

Figure 5. 16. Porosity of coal samples calculated from SANS/USANS data for the range 10 – 100,000 Å (1 nm – 10 µm).

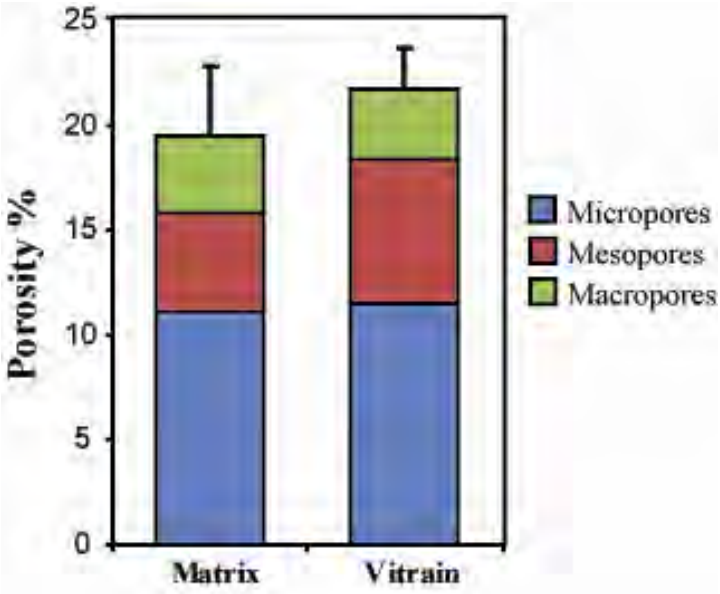

Figure 5. 17. Average porosity by seam calculated from SANS/USANS data for the range 10 – 100,000 Å (1 nm – 10 µm).

The proportion of SSA contributed by each of the pore size classes is shown in Figure 5.18. Clearly, the micropores contribute the greatest amount of SSA with the macropores contributing an almost negligible fraction.

Figure 5.19 presents the total porosity results for the Huntly coal samples superimposed on coal porosity trend curves from Berkowitz (1979), supplemented with data from King and Wilkins (1944), Gan et al. (1972), Radlinski et al. (2004b) and Day et al. (2008a). The data from this study fits reasonably well with the previously cited trend, possibly even being a little lower than might be expected for coals of this rank, although more microporosity is likely to exist below the 10 Å SAS experimental cut-off.

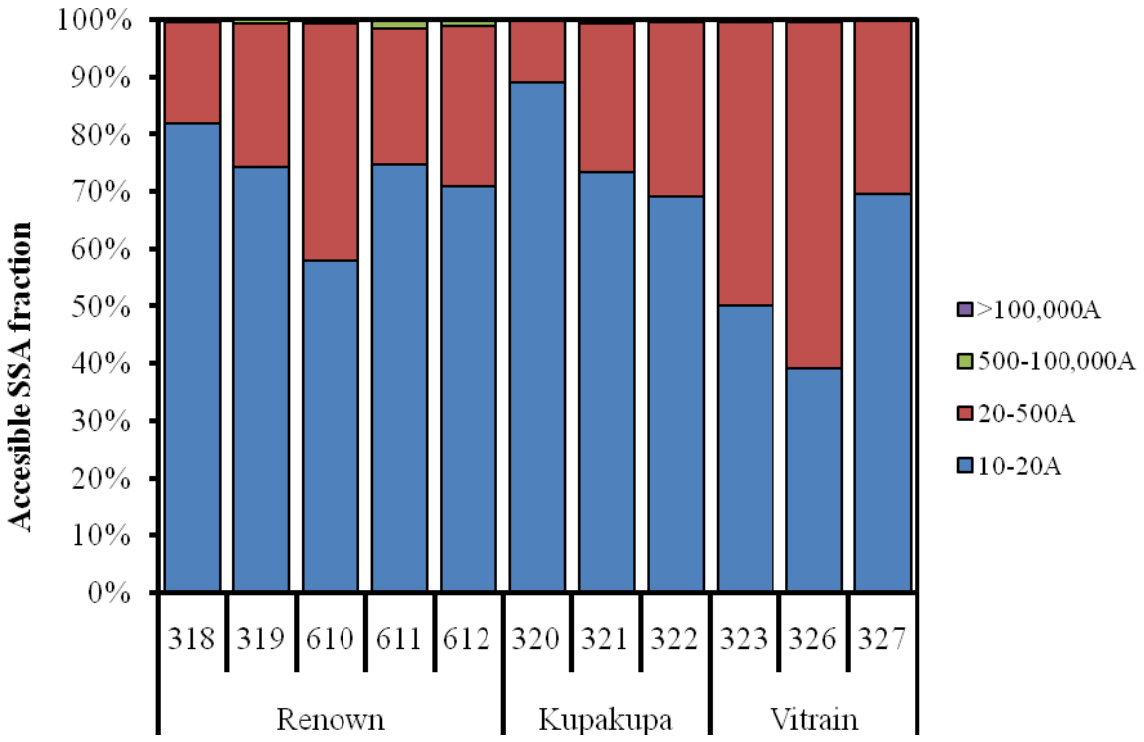

Figure 5. 18. Proportion of specific surface area (SSA) contributed by the different pore size classes. Each size class represent the fraction of the SSA accessible for objects (molecules) larger than the lower limit but smaller than the upper limit of the probe size, R.

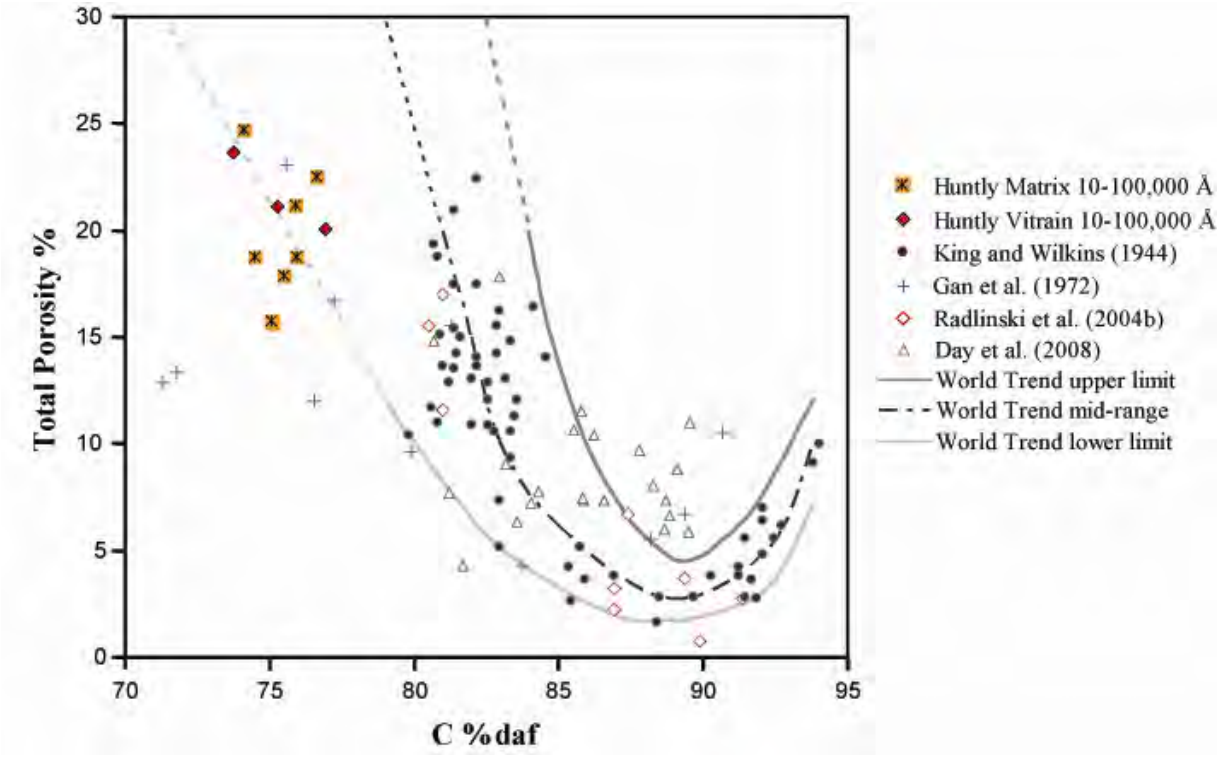

Figure 5. 19. Porosity of coal samples from this study, calculated from SANS/USANS data and plotted with respect to carbon % dry ash free (daf), compared to porosities reported in other published studies. World trend lines have been extended, marked with dashed lines.

5.8. Correlation between coal microstructure and composition

Acknowledging that there was a limited number of samples analysed for this study, correlation tables were used to look for statistical associations between measured properties. Table 5.5 lists correlation coefficients between coal microstructure of matrix samples and coal composition, using the most abundant macerals, for the eight SAS samples.

Table 5. 5. Correlation table comparing coal microstructure with coal composition. Correlation coefficients greater than 0.5 have been highlighted in yellow.

	SSA at 4 Å	Micro-porosity	Meso-porosity	Meso- and macro-porosity	Macro-porosity	Total porosity
Vitrinite	0.18	-0.09	-0.31	-0.56	-0.45	-0.30
Liptinite	0.14	0.34	0.01	0.41	0.47	0.40
Inertinite	-0.37	-0.10	0.40	0.55	0.38	0.17
Telovitrinite	-0.07	0.42	-0.06	0.73	0.90	0.60
Collodetrinite	-0.60	-0.28	0.29	0.10	-0.08	-0.15
Vitrodetrinite	0.72	0.13	-0.40	-0.72	-0.58	-0.22
Liptodetrinite	-0.71	-0.52	-0.46	0.02	0.33	-0.35
Inertodetrinite	-0.39	-0.39	0.05	0.21	0.22	-0.17
Funginite	-0.67	-0.19	0.39	0.56	0.39	0.11

As reported earlier, in the macroscopic study of the Huntly coals no porosity is apparent in hand held specimens. Vitrinite content of the samples ranges from 73% to 87%, most of which is composed of collodetrinite and vitrodetrinite, which together contribute between 54% and 73% of the total coal composition. As such, the texture at the microscopic level is frequently mottled; fine-grained and unstructured with numerous small grains (hence many grain boundaries).

As discussed in Chapter 4, some larger pores were observed, with diameters up to around 30 μm in funginite (which contributes 1.2% - 5.8% of coal composition for the samples used here), while smaller pores (generally <3 μm) were seen in structured vitrinite (telovitrinite). The correlation coefficients listed in Table 5.5 confirm these observations, with telovitrinite showing a strong association with macroporosity and some association with porosity and combined meso- and macroporosity. Funginite also shows a weak association with combined meso- and macroporosity, while vitrodetrinite (defined as vitrinite particles <10 μm in diameter; (ICCP, 1998)) has a good correlation with SSA values at 4 Å.

5.9. Shape fitting scattering curves

In section 5.4.4 inorganic material was identified in the pore size region 12.5 Å < r < 125 Å. Interestingly the inorganic material is present in the same size range for both the coal matrix and the vitrain samples, although in larger quantities in the vitrain samples. As seen in Table 5.2 the matrix material contains some structured vitrinite material while the vitrain samples were cut from thick vitrain bands and should therefore be predominantly structured vitrinite material. When considered in conjunction the associations identified in section 4.4.3 and with Li et al. (2009), this inorganic material is likely to contain aluminium and titanium, as well as calcium, iron and magnesium.

Although X-ray scattering from inorganic material was observed for all samples only the perpendicular vitrain samples and one parallel vitrain sample (328) showed sufficient deviation from the neutron scattering curves to warrant shape fitting analysis. The calculated volume fraction (the number of scattering objects (per cm^3) multiplied by the calculated volume of each individual scattering object; see section 2.3.5) for each shape was compared to the ash yield to determine the most likely shape. The results for the 323 perpendicular average scattering curves are presented in Figure 5.20 with the results for the other samples in Appendix 3.

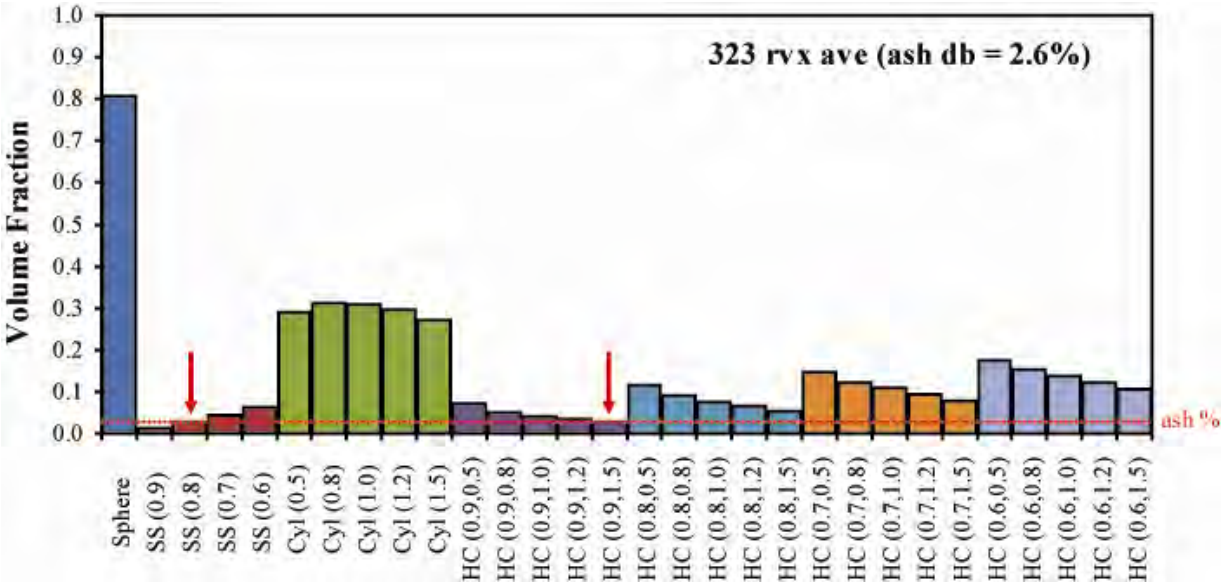

Figure 5. 20. Calculated volume fraction for each shape for the sample 323 average scattering curve compared to ash yield. SS = spherical shell, Cyl = cylinder, HC = hollow cylinder

Figure 5.20 shows two most likely solutions for the shape of the inorganic material in sample 323, a spherical shell with the internal radius (R2) equal to 0.8 times the external radius (R1) or a hollow cylinder with and internal radius equal to 0.9 times R1 and a height equal to 1.5 times R1. For almost all other trialed shapes the calculated volume fraction that the number of objects would contribute exceeds the available material (ash yield). These two shapes were identified for all samples except the perpendicular sample 326 for which the hollow cylinder had a height equal to 1.2 times R1. These results suggest that the inorganic material present in the samples exists as an inorganic coating within the micropores rather than filling them. As the coatings are mainly present in the structured tissues, it is possible they are remnant of the original plant material. The average external radius, thickness and height for shapes from the analysed samples are presented in Table 5.6.

Table 5. 6. Average shape fitting solutions for the analysed samples.

	Shape	R2	H	R1 (Å)	T (Å)	H (Å)
323 x	Spherical Shell	0.8 x R1		31.20	6.24	
	Hollow Cylinder	0.9 x R1	1.5 x R1	27.14	2.71	40.71
326 x	Spherical Shell	0.8 x R1		40.63	8.13	
	Hollow Cylinder	0.9 x R1	1.2 x R1	36.49	3.65	29.49
327 x	Spherical Shell	0.8 x R1		34.01	6.80	
	Hollow Cylinder	0.9 x R1	1.5 x R1	29.58	2.96	44.38
328 x	Spherical Shell	0.8 x R1		32.77	6.55	
	Hollow Cylinder	0.9 x R1	1.5 x R1	27.60	2.85	42.76
328 p	Spherical Shell	0.8 x R1		67.44	13.49	
	Hollow Cylinder	0.9 x R1	1.5 x R1	58.66	5.87	87.99

x = perpendicular, p = parallel, R1 = external radius, R2 = internal radius
H = height, T = thickness (R1 - R2)

For each identified shape the average external radius, thickness and height were calculated and are presented in Table 5.7. Most noticeably the values for the parallel samples are around twice the values calculated for the perpendicular samples suggesting anisotropy (as highlighted previously) of roughly 2:1. Sketches of the average shapes and a possible spherical shell showing anisotropy are presented in Figure 5.21.

Table 5. 7. Average external radius, thickness and height for calculated shapes.

Shape		Minimum	Average	Maximum	SD	n
Spherical Shell x	**R1 (Å)**	29.35	34.65	43.20	4.12	24
R2 = 0.8 x R1	**T (Å)**	5.87	6.93	8.64	0.82	
Spherical Shell p	**R1 (Å)**	63.79	67.44	72.59	3.25	6
R2 = 0.8 x R1	**T (Å)**	12.76	13.49	14.52	0.65	
Hollow Cylinder x	**R1 (Å)**	32.75	36.49	38.80	2.36	6
R2 = 0.9 x R1	**T (Å)**	3.27	3.65	3.88	0.24	
H = 1.2 x R1	**H (Å)**	39.29	43.78	46.55	2.83	
Hollow Cylinder x	**R1 (Å)**	25.53	28.41	32.67	1.78	18
R2 = 0.9 x R1	**T (Å)**	2.55	2.84	3.27	0.18	
H = 1.5 x R1	**H (Å)**	38.29	42.62	49.00	2.67	
Hollow Cylinder p	**R1 (Å)**	55.48	58.66	63.14	2.82	6
R2 = 0.9 x R1	**T (Å)**	5.55	5.87	6.31	0.28	
H = 1.5 x R1	**H (Å)**	83.23	87.99	94.71	4.24	

x = perpendicular, p = parallel, R1 = external radius, R2 = internal radius
H = height, T = thickness (R1 - R2), SD = standard deviation, n = number of data points

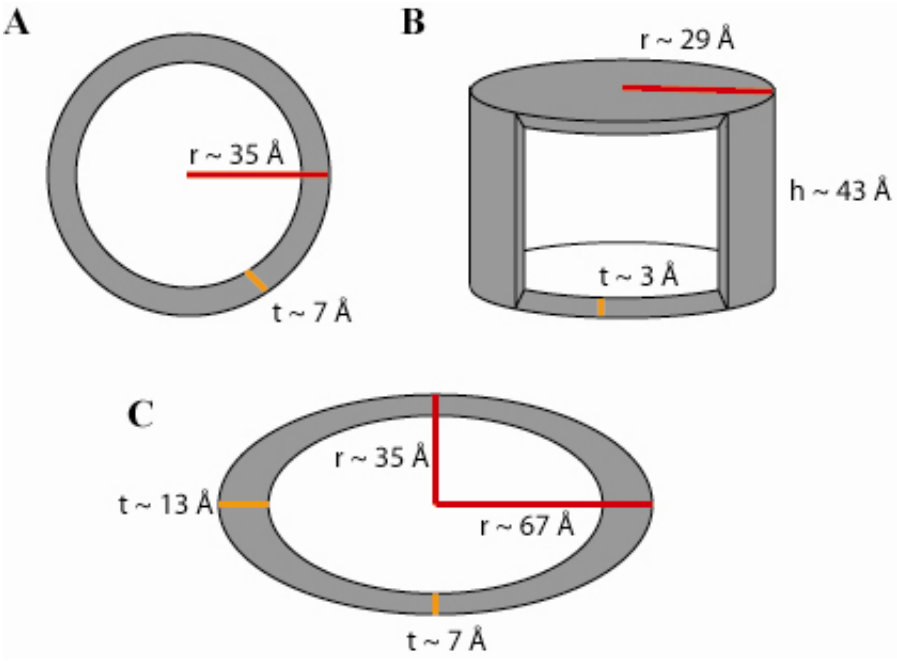

Figure 5. 21. Possible shapes calculated for the inorganic material, r = radius, t = thickness and h = height. (A) Spherical shell with R2 = 0.8 x R1 calculated from perpendicular samples. (B) Hollow cylinder with R2 = 0.9 x R1 and H = 1.5 R1 calculated from perpendicular samples, and (C) Possible spherical shell with R2 = 0.8 x R1 showing anisotropy calculated from perpendicular and parallel samples.

5.10. Discussion

5.10.1. Porosity

In a fundamental coal porosity study, Gan et al. (1972) found that the pore volume distribution is dependent on coal rank and suggested that in lower rank coals (C<75% daf) porosity is primarily because of the presence of macropores. Even though their pore size classification is different from that adopted here (micropores: 4 Å -12 Å, mesopores: 12 Å - 300 Å and macropores: 300 Å - 29600 Å), their lower rank coals still had significant porosity contribution from micropores according to their definition. In contrast, Gurdal and Yalcin (2001) found that micropore volume decreases with increasing maturity up to a value of 1.0%

vitrinite reflectance and then increases with further increase in coal rank. The work of Gurdal and Yalcin (2001), along with data presented here, agree well with the results of SANS studies using contrast matching (Hall et al., 2000), which reported the presence of microporosity in low rank coals (the Wyodak seam in Wyoming and some lignite in North Dakota) while for higher rank coals (the Pocahontas, Upper Freeport and Pittsburgh No. 8 coals from the Appalachian coal fields) very low to essentially zero levels of microporosity were identified (Hall et al., 1998; Hall et al., 2000).

The relatively low contribution of macropores to total porosity (9% to 25%) and the high contribution of micropores, 44% – 60% may possibly be caused by coal composition and texture. It has been reported that bright or banded coals (high vitrinite, low ash) have greater micropore volume than dull coals (high inertinite, high ash) of the same rank (Clarkson and Bustin, 1996; 1999; Crosdale et al., 1998; Lamberson and Bustin, 1993) and that vitrinite has a greater micropore capacity than other macerals (Unsworth et al., 1989). New Zealand coals are typically high in vitrinite (Beamish et al., 1998; Butland and Moore, 2008; Newman et al., 1997). The importance of a link between microporosity and bright coals lies in the observation of Clarkson and Bustin (1999) for the Gates Formation coals. Their study suggested that micropore volume exerts primary control upon high pressure adsorption of CH_4 and CO_2 gases.

5.10.2. Variability within seam

For the Mimi 1 and Jasper 1 Renown seam two samples were collected from each core, roughly 1 m apart, with the aim to assess variability within the seam. The Jasper 1 samples, 319 and 610, had similar extrapolated SSA values at 4 Å (Fig. 5.14). However,

considerably different porosities (21% and 16%, respectively, Fig. 5.16) were calculated for these two samples, suggesting that the internal surface for sample 610 was rougher. Also, in relative terms, sample 610 had a larger proportion of mesoporosity and a smaller proportion of macroporosity than sample 319.

For the Mimi 1 samples (611 and 612) it was determined that sample 611 had both SSA and porosity values larger than sample 612. Considering that such significant variability occurred within a single seam accessed from a single drill hole, it was deemed that no reliable comparison between seams could be conducted using these data alone. The variations were not greater than the differences identified between ranks elsewhere (Radlinski et al., 2004b). As differences were observed between these 'matrix' samples and pure vitrain samples, it is likely that variations between seams and coal types are related to the differing proportions of these components. As shown and discussed within this chapter, the results presented in this study are consistent with expectations for coals of low rank.

5.10.3. Differences between matrix and vitrain samples

In comparison to the matrix samples, all of the vitrain samples had larger SSA at 4 Å. However, for two of the three vitrain samples in Figure 5.18, the vitrain samples had a significantly lower proportion of accessible SSA in the micropore size range than the matrix samples. When comparing the average porosities for matrix samples to vitrain samples (Fig. 5.16), it can be seen that the vitrain samples have greater total porosity. This additional porosity is contributed by mesopores (matrix has 4.7% porosity contributed by mesopores while vitrain has 6.8%) as both groups have the same contribution by micropores (~11%) and similar contributions by macropores (3.6% for matrix samples and 3.3% for vitrain samples).

It must be noted that the samples with the lowest amount of macroporosity are the vitrain samples 323 and 327. The vitrain samples also have a more noticeable influence by inorganic material.

Matrix samples have an association between telovitrinite and macroporosity as well as combined meso- and macroporosity, a weak association between funginite and combined meso- and macroporosity and a good correlation between vitrodetrinite and SSA at 4 Å. As the vitrain samples are composed of predominantly structured material, the increased telovitrinite content is likely the cause of the increased mesoporosity.

5.10.4. Inorganic material

In Chapter 4 a positive association between ash yield and the proportion of vitrain bands was identified. In addition, associations between aluminium, titanium and phosphorous with telovitrinite were found. That the inorganic material is prevalent in the structured tissue has been confirmed in this chapter. Microprobe analysis of 'clean' macerals has found small but consistent contributions of elements such as aluminium, calcium, iron, magnesium and titanium present as non-mineral entities in low rank coals (Li et al., 2007; Li et al., 2009; Ward et al., 2008). These studies only have resolution to approximately 5 – 10 µm. Studies using scanning transmission X-ray microscopy on spores and bacterial biomineralisation report resolutions of 25 – 50 nm (Benzerara et al., 2008; Bernard et al., 2009; Chan et al., 2009) but have the benefit of determining chemistry. The inorganic material identified in this study is in the size range 12.5 Å < r < 125 Å (~1 - 12 nm). As such the mode of occurrence has not previously been identified. In agreement with Li et al. (2007; 2009) and Ward et al. (2008) the inorganic material is not thought to exist as mineral entities. It is instead present as

inorganic coatings in micropores. As the inorganic material was present in both matrix and vitrain, but to a larger extent in the vitrain samples, it is thought that the source of the inorganic material is from the original plant material as opposed to post depositional processes.

In modern plants, macronutrients (phosphorous, potassium, nitrogen, sulphur, calcium and magnesium) can contribute around 0.5% - 3% of a plant's dry weight while micronutrients (iron, sodium, chlorine, copper, manganese, cobalt, zinc, molybdenum, and boron) contribute up to a few parts per million of the dry weight (Stern, 1982). It is well known that plants uptake and retain elements from the atmosphere and their substrate is a well recognized process and forms the basis of many environmental monitoring studies (Chang et al., 2009; Chiarenzelli et al., 2001; de Caritat et al., 2001; Divan Junior et al., 2009; Dongarrá et al., 2003; Dunn and Hoffman, 1986; Kubin and Lippo, 1996; Reimann et al., 2007; Wickman and Jacks, 1993). The cells of modern plants typically range from 10 – 100 µm in diameter with the sizes of intracellular bodies being: nuclei 2 – 15 µm, mitochondria 1 - 3 x 0.5 µm, chloroplasts 2 - 10 µm, ribosomes 20 nm and microtubules 15 – 25 nm in diameter. Bacterial cells are generally around 0.5 µm in diameter (Stern, 1982). Phytoliths (inorganic minerals formed inside plants) have been reported to range from 0.5 µm to several centimeters in size (Hart, 1988; Wust and Bustin, 2003).

The most common minerals in the Huntly coal are reported to be quartz and kaolinite (Butland, 2006). While clay crystals typically have grain sizes of < 2 µm, the dimensions of the unit cell for kaolinite are a = 5.15 Å and b = 8.95 Å with a thickness of 7.15 Å. For comparison, the effective ionic radii of cations commonly contained in clays (potassium, calcium, sodium, magnesium, iron, aluminium and silicon) range from 0.4 – 1.78 Å

(Meunier, 2005). The coatings identified in this study have radii ranging from 25.5 – 72.6 Å with thicknesses ranging from 2.6 – 14.5 Å. Radlinski et al. (2004b) suggested that the inorganic material in the micropores was likely to be clay. However considering the work of Li et al. (2009), who found very little silicon in coal macerals, this may not be the case.

5.11. Conclusions

The microstructure of low-rank coals from the Huntly coalfield, New Zealand, was investigated with X-rays and neutrons using the non-invasive SAXS, USAXS, SANS and USANS techniques. Pore size distributions and internal specific surface area (SSA) were able to be measured with SAXS/USAXS for the linear scale range from 1 nm and 2 μm and with SANS/USANS for the linear scale range from 1 nm and 10 μm. Findings are as follows:

- SSA of the samples ranged from 1.25 x 10^6 cm^{-1} to 2.88 x 10^7 cm^{-1}, in accordance with the previously established trend of SSA increasing with decreasing rank for coals with vitrinite reflectance less than 1.0%. The vitrain samples had higher SSA than the matrix samples.
- Pore geometry anisotropy in the samples was generally less than 2:1. The degree of anisotropy increases with the decreasing pore size (increasing value of SSA), thus indicating that the smaller pores are affected most by the effects of gravity settling of particles and lithostatic stress.
- Total porosity of analysed dry samples varies from 16% to 25%. The contribution of microporosity to total porosity was 45% to 60%, in spite of the lower limit for micropore size set at 10 Å (1 nm). Macroporosity contributed 9% to 25% of total

porosity. On average the vitrain samples have larger total porosities than the matrix samples, with the extra porosity predominantly contributed by mesopores.

- Micropores were found to contribute the majority of the available specific surface area, with macropores contributing only a negligible amount.
- The Huntly coal samples are vitrinite-rich with the predominant macerals generally being vitrodetrinite, collodetrinite and telovitrinite, in that order. Some porosity was seen at the microscopic level and correlations were identified between telovitrinite content and macroporosity and vitrodetrinite content and SSA.
- X-ray scattering data indicates that the inorganic matter present in coal samples studied here is confined in the same size range of 12.5 Å < r < 125 Å (10 Å = 1 nm). Inorganic material had a larger effect on X-ray scattering in the vitrain samples than for matrix samples, suggesting that the inorganic matter is contained predominantly in the more structured vitrinite material.
- The identified inorganic material was calculated to exist as inorganic coatings (shells) in the micropores of either spherical or cylindrical shape. For perpendicular samples the radius was found to vary from 25.5 – 43.2 Å, the thickness from 2.6 – 8.6 Å and for the cylinders, the height was found to range from 38.3 – 49.0 Å. Where analysed, shapes calculated from parallel samples had dimensions approximately double those seen for perpendicular samples again highlighting the roughly 2:1 anisotropy in pore geometry.
- Variations between samples from within the same seam and drill hole were too great to allow comparison between seams with such limited number of samples, clearly highlighting the heterogeneity of low-rank coals. The results presented fit well with rank trends reported in other studies.

Chapter Six

Gas Properties

When assessing the commercial viability of a coalbed methane prospect, gas content (desorbed gas) and gas holding capacity (adsorbed gas) are two of the key geological parameters measured. These two measures are used to give an estimate of the % gas saturation of the reservoir. Typically gas saturation has been assessed by collecting one adsorption isotherm sample and assuming it is representative of the whole seam reservoir conditions.

This chapter presents gas adsorption and desorption data for the Huntly coalfield irrespective of coal properties. Gas results will be compared to coal properties in Chapter 7.

6.1. Gas in coal

6.1.1. Origin of gas in coal

In a general sense, coal seam gas is generated in coals by two different processes, biogenic and thermogenic. Biogenic gas is derived from either the fermentation of organic matter or reduction of CO_2 by microorganisms and is predominately CH_4 in composition. Alternately, thermogenic gas generation occurs at higher temperatures and pressures (i.e. with increasing coalification) as a result of devolatilization of the coal, with the most common byproducts being CH_4, CO_2 and water (Rice, 1993). Although gases of mixed origin occur (Butland, 2006; Flores et al., 2008; Rice et al., 2008), coals possessing a vitrinite reflectance ($\%R_o$) of less than 0.6% primarily generate methane biogenically, whereas thermogenic methane generation predominates in coals with $\%R_o$ greater than 0.6% (Clayton, 1998; Flores, 1998; Rice, 1993). As reported in Chapter 4 and elsewhere (Edbrooke et al., 1994; Li et al., 2009; Newman et al., 1997; Twombly et al., 2004) the Waikato coals have been found to have $\%R_o$ of 0.34 - 0.53%. As such, the method of coal seam gas generation should be biogenic.

As previously stated, biogenic gas can be generated via two different pathways, CO_2 reduction and methyl-type fermentation (Rice, 1993; Smith and Pallasser, 1996) and roughly follow these reactions:

Microbial reduction of CO_2: $CO_2 + 4H_2 \rightarrow CH_4 + 2H_2O$ (6.1)

Acetate fermentation: $CH_3OOH \rightarrow CH_4 + CO_2$ (6.2)

It has been suggested that the depth of burial and the age of the organic rich material are regulating factors on the method of generation with fresh, near surface sediments generating gas via both pathways and deeper sediments mainly via CO_2 reduction (Rice, 1993). The dominant pathway can be identified by isotopic analyses (Smith and Pallasser, 1996) and the gas produced in the Waikato has been shown to be created by CO_2 reduction (Butland and Moore, 2008; Moore and Butland, 2005).

Additionally, there are two different stages of biogenic gas generation. In early stage generation the gas is formed early in the burial history of low rank coal and is infrequently preserved if there was rapid deposition. Late stage, or secondary biogenic gas, is a result of bacteria being introduced to the coal, after burial and coalification, via active groundwater systems. This accessibility may also suggests that reasonable permeability could exist within the seam (Rice, 1993; Scott et al., 1994). Carbon isotope data and the high CH_4 contents, averaging >90%, present in the Waikato indicate that the gas is primarily of secondary biogenic origin (Butland and Moore, 2008; Moore and Butland, 2005).

6.1.2. Storage of gas in coal

Gas is stored by the coal in four basic ways: (1) as limited free gas within the micropores and cleats (fractures); (2) as dissolved gas in water; (3) as adsorbed gas held by molecular attraction on coal particles, micropore, and cleat surfaces; and (4) as absorbed gas within the molecular structure (Yee et al., 1993). The theoretical maximum amount of gas a coal can hold is estimated through adsorption analysis, while the amount of gas actually held within the coal is measured by desorption (Diamond and Schatzel, 1998). Percent gas saturation is the difference between maximum holding capacity and the actual measured gas

'charge'. Thus if a coal at a given temperature and pressure can hold 5 m^3/t of methane, but only 2.5 m^3/t was measured, the gas saturation would be 50%. In a study of subbituminous coals in the Powder River Basin, Stricker and Flores (2002) found them to frequently be undersaturated. Twombly et al (2004) and Butland and Moore (2008) also found this to be true for coal of similar rank in the Waikato.

The ability of a coal to store gas is a function of pressure, temperature, mineral matter, moisture, rank, petrographic composition as well as gas composition (Montgomery, 1999; Yee et al., 1993). It has generally been accepted that gas sorption capacity increases with increasing pressure, which in turn is partially related to increasing depth as well as changes in temperature and rank. Increases in temperature result in more 'free' gas rather than gas in the sorbed state (Yee et al., 1993). Some studies have shown that gas adsorbs to the organic components of coal, with mineral matter acting as a diluent, resulting in gas contents decreasing with increasing inorganic material (Butland and Moore, 2008; Laxminarayana and Crosdale, 2002; Warwick et al., 2008). Coals with less than 10% ash yield still exhibit significant variation in gas volume which is apparently unrelated to the proportion of inorganic material. When ash yield is low it is more likely that the majority of elements are organically bound within the coal rather than being present as mineral matter (Li et al., 2007; 2009; Newman et al., 1997).

Inherent moisture is greatest in low rank coals (Ward and Barnsley, 1984). Laboratory experiments have demonstrated that the CH_4 sorption capacity of low to medium rank coals is strongly suppressed when the coals are initially saturated with moisture, as compared with the CH_4 capacity of the same coal on a dry basis (Crosdale et al., 2008; Levine, 1992). It is thought that moisture influences gas holding capacity by either competing with gases for

adsorption sites or blocking access to some of the micropores (Bustin and Clarkson, 1998; Day et al., 2008c; McElhiney et al., 1993). The equilibrium moisture content has been found to be a critical moisture value above which there is no further reduction in methane adsorption (Yee et al, 1993; Levy et al, 1997).

Two different trends have been recognized between gas sorption and rank. One trend is U-shaped with a minimum at high volatile bituminous A rank. This minimum is believed to be created by the collapse of macroporosity because of physical compaction. Porosity increases again at higher ranks, resulting from the creation of secondary porosity by devolatilization of part of the coal structure. In the other trend, CH_4 sorption increases with rank (Levine, 1993; Yee et al., 1993). When interpreting changes of anything related to rank, caution should be exercised as many properties change along with rank.

Vitrinite rich coals have been generally been found to have greater CH_4 adsorption capacity than inertinite rich coals of the same rank (Crosdale and Beamish, 1993; Crosdale et al., 1998; Lamberson and Bustin, 1993; Warwick et al., 2000). It has been reported that bright or banded coals (high vitrinite, low ash) have greater micropore volume than dull coals (high inertinite, high ash) of the same rank (Clarkson and Bustin, 1996; 1999; Crosdale et al., 1998; Lamberson and Bustin, 1993) and that vitrinite has a greater micropore capacity than other macerals (Unsworth et al., 1989).

Coal seam gas generally is composed of a mixture of CH_4, CO_2, N_2 and heavier hydrocarbons (Clarkson and Bustin, 2000). The gases do not sorb independently and can be competing for sorption sites. CO_2 is sorbed preferentially over CH_4 which is in turn greater than N_2 (Yee et al., 1993).

6.2. Gas adsorption capacity of the Huntly coal

6.2.1. Pre- and post-desorption isotherms

Adsorption isotherms are presented for all samples in Figure 6.1 and are colour coded depending on the time between collection and analysis (Table 6.1, for complete isotherm data see Appendix 4). There is strong evidence that the samples collected post-desorption yield consistently larger gas adsorption capacities than the samples collected and analysed immediately (fresh samples with no desorption).

At the reservoir pressure of approximately 4 MPa, the average adsorption isotherm for fresh samples have a holding capacity of 3.4 m^3/t while the average isotherm for post-desorption samples is 4.1 m^3/t, almost 20% larger. This result is much greater than the experimental error value of ± 7% for within laboratory repeatability based on an Australian inter laboratory study (Crosdale et al., 2005).

The differences between the fresh and post-desorption isotherms is likely a result of sample oxidation and sample moisture loss. This clearly highlights the need for the collection of fresh gas adsorption isotherm samples to get a realistic gas adsorption capacity. Using a larger value for gas adsorption capacity in the calculation of percent gas saturation (equation 2.1) results in a lower saturation. The significance of this is that low gas saturation can decrease the attractiveness of a prospective gas play. A full discussion on ideal isotherm sampling conditions for the Huntly coalfield and a comparison of the significance of pre- and post-desorption sampling is presented in Moore and Crosdale (2006) and Crosdale et al. (2008).

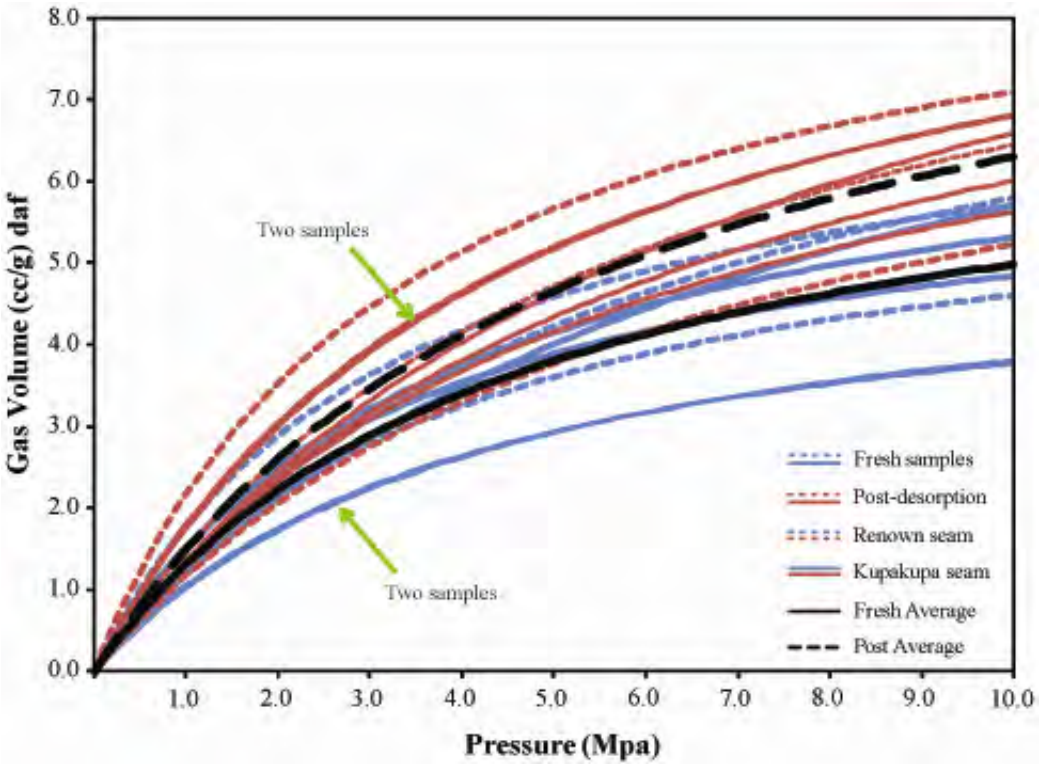

Figure 6. 1. Methane adsorption isotherms from the Huntly Coalfield showing samples taken pre-desorption (fresh) and post-desorption isotherms.

Table 6. 1. Adsorption isotherm data for all samples collected from the Huntly coalfield.

Drill hole	Sample	Collection time	Mid-point (m)	Seam	Langmuir Pressure (MPa) daf	Langmuir Volume (m^3/t) daf	Adsorption capacity at 4 MPa (m^3/t) daf
Mimi 1	Mimi 1	Field	407.34	Renown	3.25	7.57	4.18
Jasper 1	Jasper 1	Field	411.93	Renown	5.90	9.22	3.73
Mangapiko 1	Ma1 A	Field	486.85	Renown	3.84	6.37	3.25
Ruawaro 1	Ru1 A	Field	422.40	Kupakupa	4.30	5.46	2.63
Ruawaro 2	Ru2 A	Field	458.12	Kupakupa	3.92	7.42	3.75
Rotongaro 1	Ro1 A	Field	449.34	Kupakupa	3.26	6.43	3.54
Rotongaro 1	Ro1 B	Field	452.34	Kupakupa	3.99	5.28	2.64
Mangapiko 1	Ma1 B	Field	512.04	Kupakupa	7.41	9.96	3.49
				Average	**4.48**	**7.21**	**3.40**
Jasper 1	M4	Post	409.31	Renown	6.32	8.53	3.31
Mimi 1	J10	Post	412.75	Renown	5.77	10.17	4.16
Ruawaro 2	Ru2 -B10	Post	438.14	Renown	4.41	9.80	4.66
Rotongaro 1	Ro1 -C4	Post	436.09	Renown	4.65	9.99	4.62
Mangapiko 1	Ma1 -D3	Post	483.70	Renown	3.40	9.52	5.15
Ruawaro 2	Ru2 -B22	Post	461.54	Kupakupa	6.23	9.77	3.82
Rotongaro 1	Ro1 -C11	Post	450.11	Kupakupa	5.43	8.68	3.68
Mangapiko 1	Ma1 -D20	Post	517.39	Kupakupa	7.34	11.46	4.04
				Average	**5.44**	**9.74**	**4.13**

6.2.2. Fresh adsorption isotherms

Adsorption isotherms for the fresh samples (Table 6.1) are presented in Figure 6.2. Considerable variation exists with a range in holding capacity at 4 MPa from 2.63 m^3/t to 4.18m^3/t, a difference of almost 40% (expressed on a dry ash free [daf] basis). As presented above, the average holding capacity from these results is 3.4 m^3/t (at 4 MPa) with a standard deviation (sd) of 0.54 m^3/t. The two samples collected from Rotongaro 1 are of particular note as despite being only 3 m apart they have almost 1 m^3/t difference in gas holding capacity.

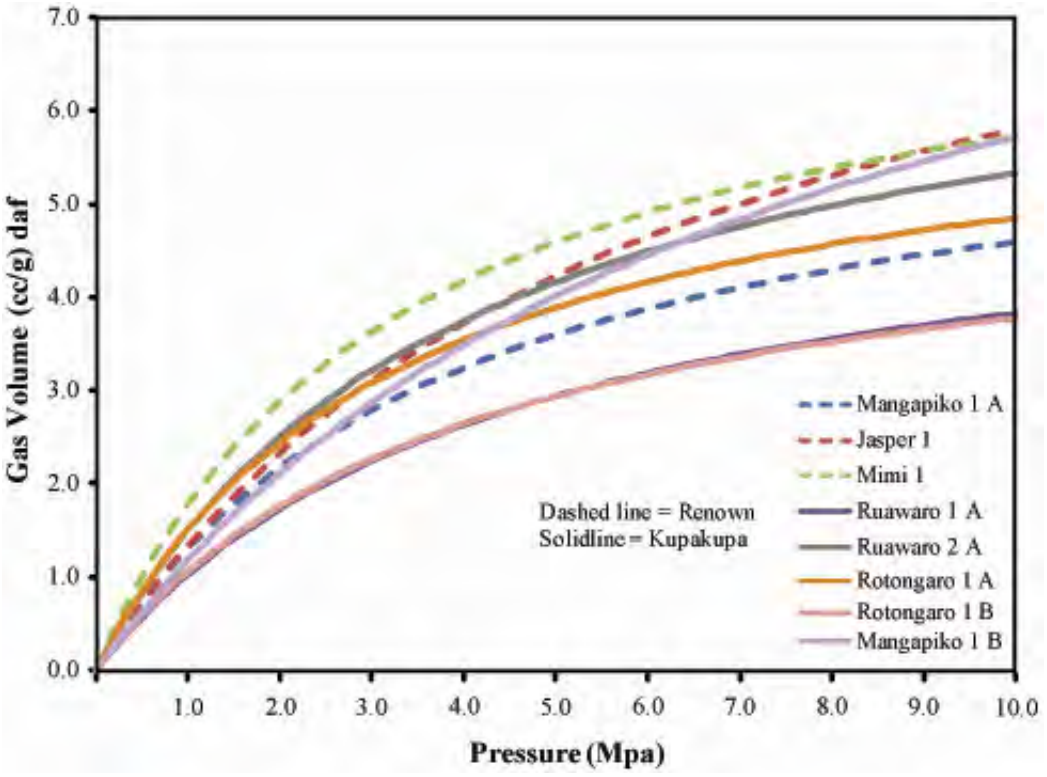

Figure 6. 2. Fresh adsorption isotherms from the Huntly coalfield.

Acknowledging that there are only a limited number of samples available, the adsorption isotherms were colour coded by seam and seam average isotherms were created

(Fig. 6.3). Considerable variation is present with the Renown seam ranging from 3.25 m^3/t to 4.18 m^3/t and the Kupakupa seam from 2.63 m^3/t to 3.75 m^3/t. Comparison of the average adsorption curves for each seam indicated that the Renown seam has a greater average methane adsorptive capacity at 4 MPa (3.72 m^3/t) than the Kupakupa seam (3.21 m^3/t). This is an approximate 15% difference. Note that the Renown coal seam is stratigraphically higher than the Kupakupa seam.

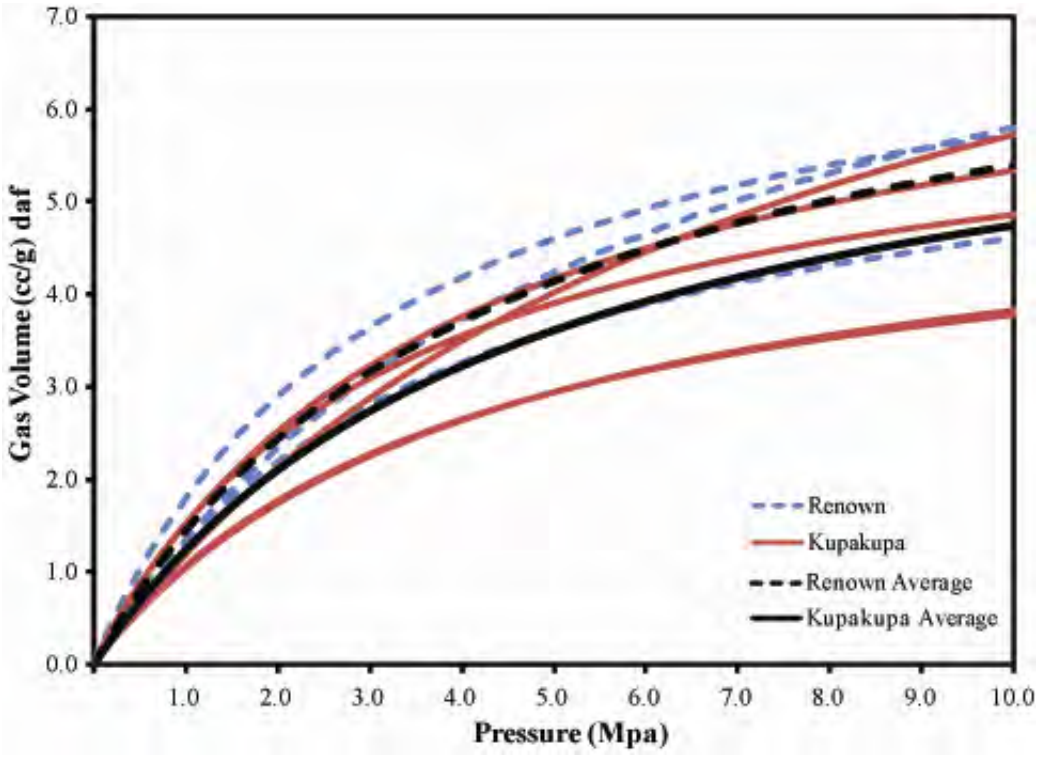

Figure 6. 3. Fresh adsorption isotherms colour coded by seam with the Renown and Kupakupa seam averages shown in black.

6.2.3. Adsorption of methane and carbon dioxide

Samples with analyses for both methane and carbon dioxide isotherms are presented in Table 6.2 and Figure 6.4. Adsorption isotherms for both methane and carbon dioxide

showed considerable variation with methane holding capacity at the reservoir pressure (approximately 4 MPa) ranging from 2.63 to 4.18 m^3/t (daf) and carbon dioxide holding capacities ranging from 22.00 to 23.72 m^3/t (daf). Relative to the volume of gas adsorbed, greater variation was seen for methane than carbon dioxide at 4 MPa. In contrast to the relationship found between the Renown seam and methane holding capacity, the Kupakupa seam has a higher average carbon dioxide holding capacity than the Renown, 23.21 m^3/t versus 22.77 m^3/t.

Table 6. 2. Gas adsorption capacities at reservoir pressure 4MPa.

Drill hole	Seam	Mid-point (m)	CH_4 adsorption at 4 MPa (m^3/t) daf	CO_2 adsorption at 4 MPa (m^3/t) daf	CO_2/CH_4 Ratio daf
Mimi 1	Renown	407.34	4.18	23.72	5.68
Jasper 1	Renown	411.93	3.73	22.59	6.06
Mangapiko 1	Renown	422.40	3.25	22.00	6.77
Mangapiko 1	Kupakupa	458.12	3.49	23.50	6.73
Ruawaro 1	Kupakupa	486.85	2.63	22.55	8.57
Ruawaro 2	Kupakupa	512.04	3.75	23.56	6.29

The samples with the greatest methane holding capacity do not necessarily have the highest holding capacity for carbon dioxide. Instead, relative to volume adsorbed, greater variation was seen for methane than carbon dioxide at 4 MPa. Thus, ratios of the coals holding capacity for carbon dioxide versus that for methane range from 5.7 to 8.6, with the average being 6.7:1 (daf). That is, the coal can theoretically hold 6.7 times more carbon dioxide than methane, making the coal seams of the Huntly coalfield an attractive prospect for potential ECBM and CO_2 sequestration (Mares and Zarrouk, 2008; Zarrouk and Moore, 2007; 2009).

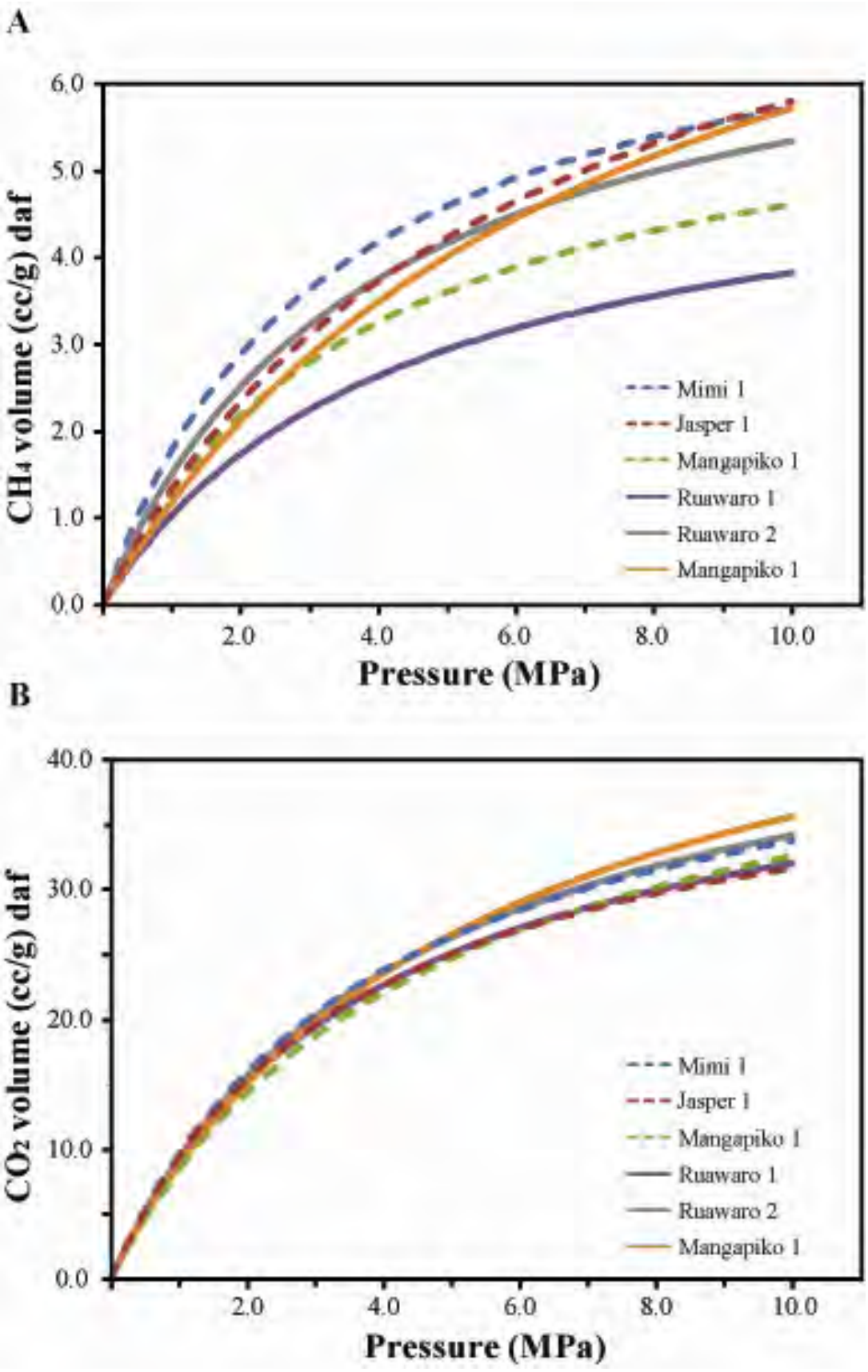

Figure 6. 4. (A) Methane and (B) carbon dioxide adsorption isotherms. Dashed lines are Renown seam samples while solid lines are the Kupakupa samples.

Published results where both vitrinite reflectance and CO_2:CH_4 ratios have been reported (Busch et al., 2003; Mastalerz et al., 2004; Rodrigues and Lemos de Sousa, 2002; Saghafi et al., 2007), including data from this study, have been plotted in Figure 6.5. This does not mean that all of the methane can be removed and replaced with carbon dioxide in situ, or that the carbon dioxide can be sequestered at maximum capacity (Bromhal et al., 2005).

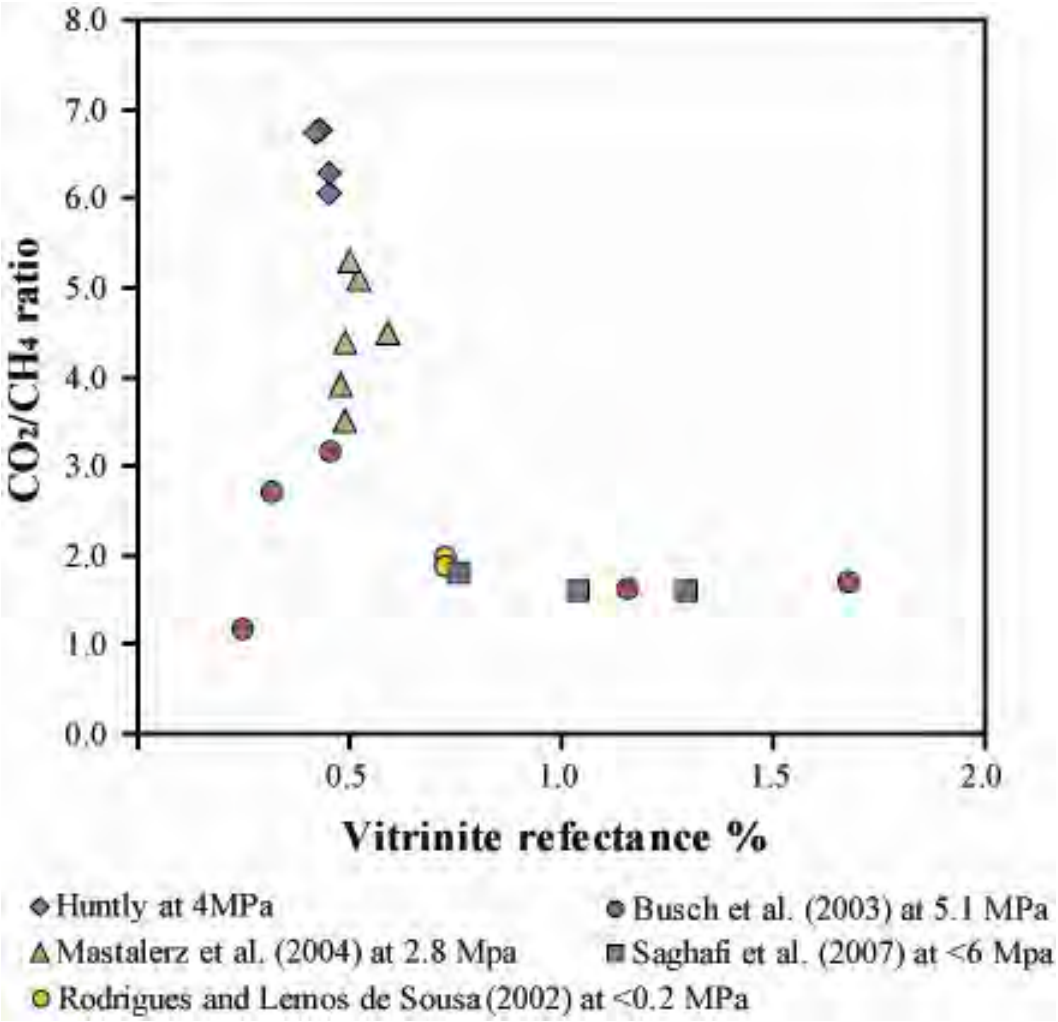

Figure 6. 5. Ratio of carbon dioxide to methane adsorption versus rank. The Huntly data and that from Saghafi et al. (2007) are reported as R_{max}, while all other data reported for random vitrinite reflectance.

6.3. Total gas content of the Huntly coal

6.3.1. Total gas content by drill hole

Gas data for the TW1 drill hole has been presented previously by Twombly et al. (2004), Butland (2006) and Butland and Moore (2008). The two seams in this location are separated by only a 20 cm high ash layer and a gradual increase in total gas content has been identified with increasing depth (Fig. 6.6).

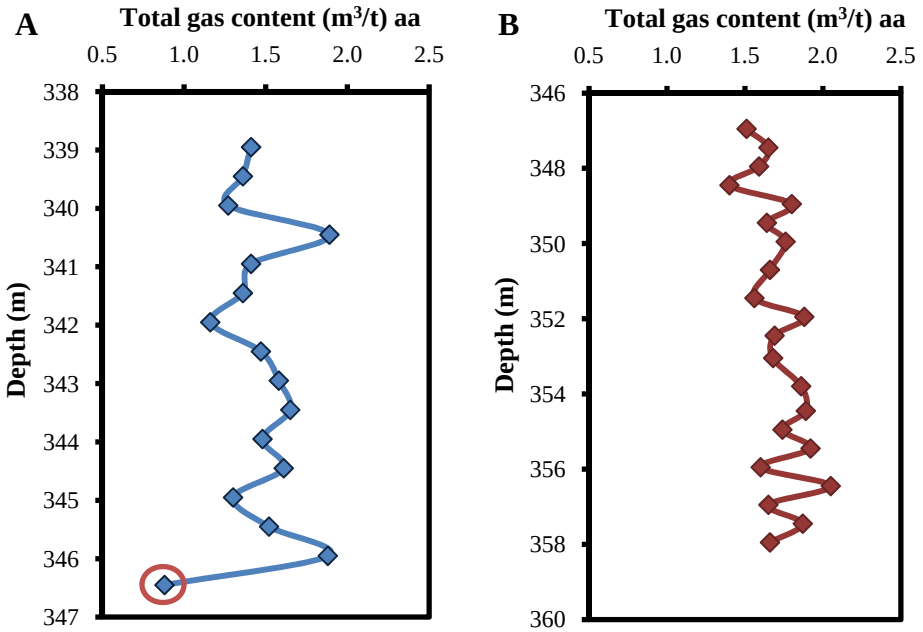

Figure 6. 6. Vertical profiles of total gas content (aa) for the TW1 drill hole. (A) Renown seam (B) Kupakupa seam. Data points circled yielded >20% ash.

For the Renown seam, 16 coal intervals were retrieved from the TW1 drill hole for desorption analysis, with total gas contents ranging from 1.16 m^3/t to 1.89 m^3/t as analysed (aa; excluding 1 interval where ash yield was >20%, the cut off defined in Chapter 4). An

additional 21 canisters of coal were collected from the Kupakupa seam with gas contents ranging from 1.4 m^3/t to 2.05 m^3/t aa. The full gas content dataset is given in Appendix 4.

At the Ruawaro 1 location, the Renown seam is split into multiple beds and the total gas content is highly variable for the 7 intervals collected. The gas volume ranges from 0.70 m^3/t to 1.26 m^3/t (aa; excluding 2 intervals where ash yield was >20%). Total gas content is much less variable in the Kupakupa seam (15 canisters) where total gas content ranged from 0.94 m^3/t to 1.37 m^3/t (aa) (Fig. 6.7).

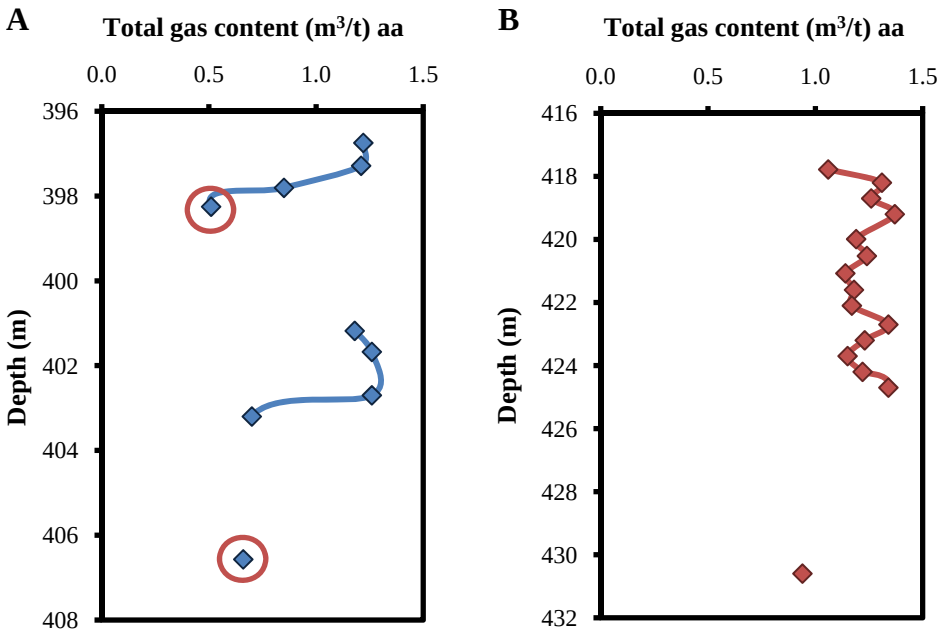

Figure 6. 7. Vertical profiles of total gas content (aa) for the Ruawaro 1 drill hole. (A) Renown seam (B) Kupakupa seam. Data points circled yielded >20% ash.

Similar to the Ruawaro 1 location, the Renown seam in Ruawaro 2 drill hole shows much greater heterogeneity in its total gas content profile than that seen in the Kupakupa seam (Fig. 6.8). Fifteen canisters were collected from the Renown seam with a total gas content range of 1.11 m^3/t to 3.22 m^3/t (aa; excluding 1 interval with ash yield >20%), while

the 11 canister collected from the Kupakupa seam had a range from 1.85 m^3/t to 2.55 m^3/t (aa).

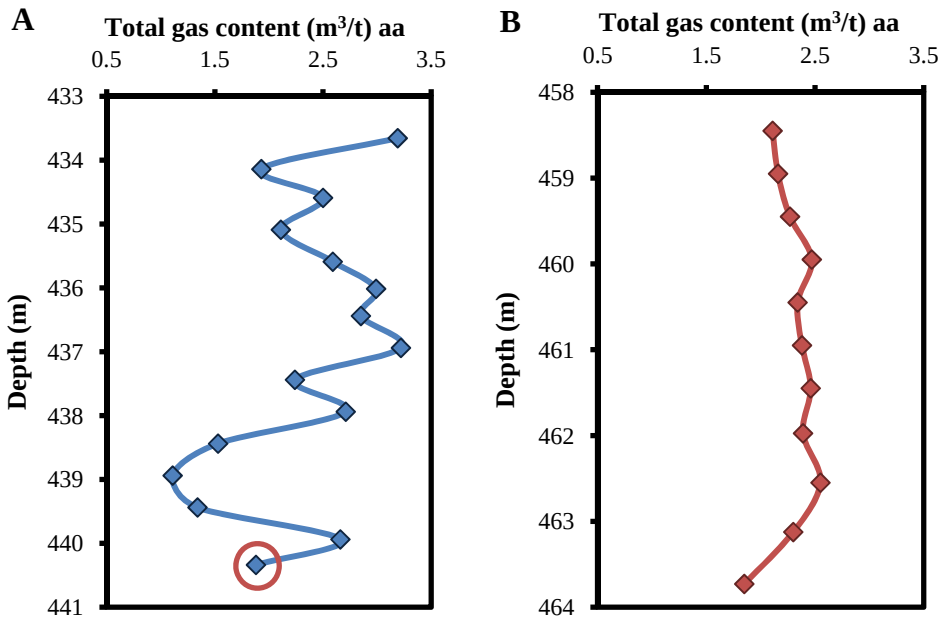

Figure 6. 8. Vertical profiles of total gas content (aa) for the Ruawaro 2 drill hole. (A) Renown seam (B) Kupakupa seam. Data points circled yielded >20% ash.

As stated in Chapter 3, the Renown seam at Rotongaro 1 location is very thin (~2 m) while the Kupakupa seam is reasonably thick (~12 m). In contrast to the thick Kupakupa seam identified in TW1, total gas content decreases with increasing depth (Fig. 6.9), while the Renown seam has gas contents equivalent to the upper part of the Kupakupa. Although of similar depth to the Ruawaro 1 and 2 drill holes, total gas contents are significantly lower with a range of 0.63 m^3/t to 0.69 m^3/t (aa) for the Renown seam (4 canisters) and 0.39 m^3/t to 0.71 m^3/t (aa) for the Kupakupa seam (21 canisters).

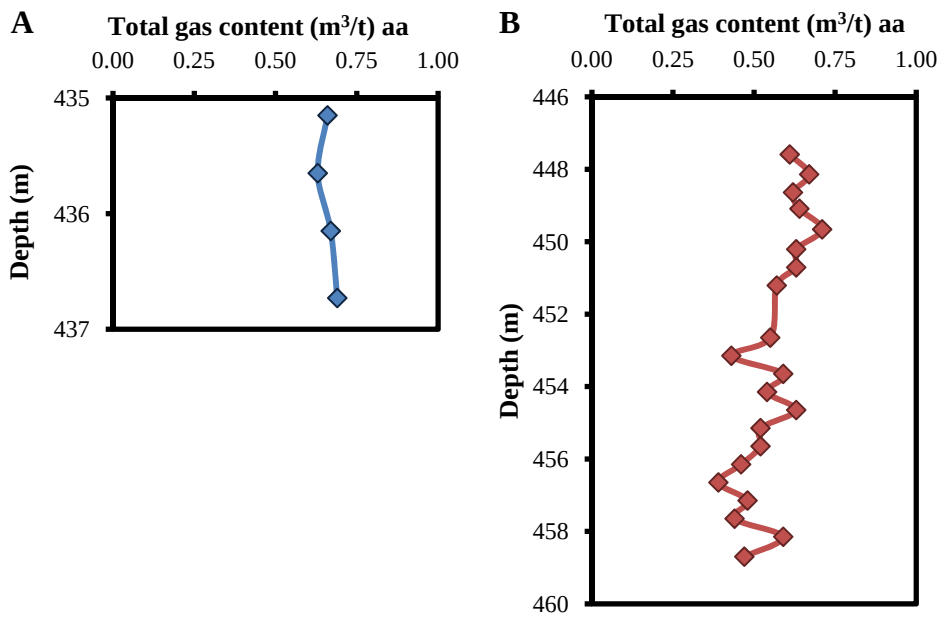

Figure 6. 9. Vertical profiles of total gas content (aa) for the Rotongaro 1 drill hole. (A) Renown seam, (B) Kupakupa seam.

As with Rotongaro 1, the Mangapiko 1 drill hole, yielded relatively low total gas contents (Fig. 6.10). The Renown seam had a range in gas contents from 0.77 m^3/t to 1.12 m^3/t (aa) while the Kupakupa ranged from 0.36 m^3/t to 0.55 m^3/t (aa). Ten canisters were collected from each seam, however two intervals in the Renown were excluded from the ranges as ash yield >20%.

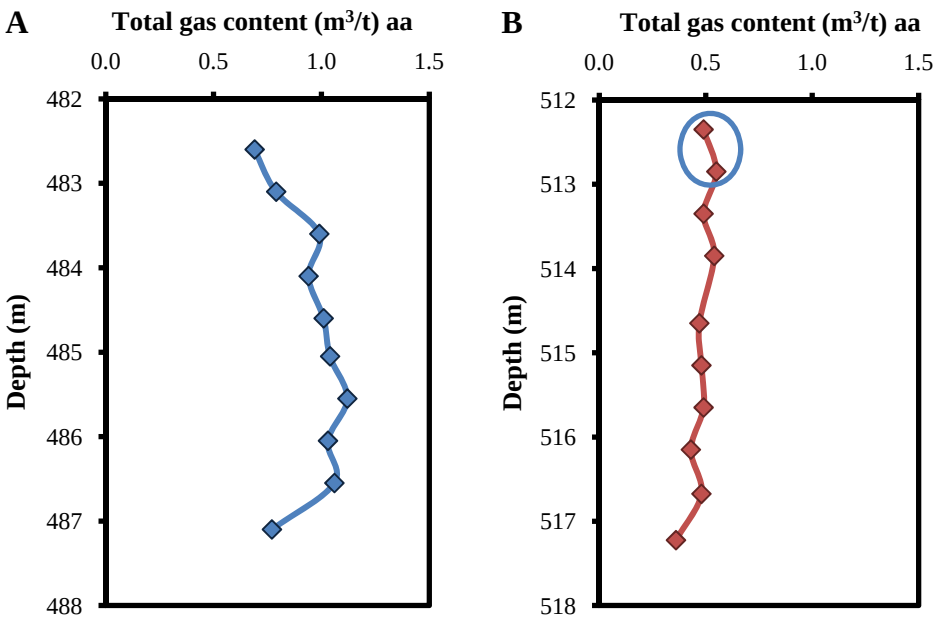

Figure 6. 10. Vertical profiles of total gas content (aa) for the Mangapiko 1 drill hole. (A) Renown seam (B) Kupakupa seam. Data points circled yielded >20% ash.

The remaining three drill holes, drilled as part of a five well pilot production test, cored the Renown seam only and targeted the area identified in the exploration drilling that showed the highest gas contents. As such, Jasper 1, Mimi 1 and Baco 1 drill holes are very close to the Ruawaro 2 drill hole (Fig. 2.1). For these three cores the top of the Renown seam (approximately 0.5 m) was tagged prior to changing to a wireline core barrel, hence, the top of the seam was not sampled.

The vertical profile of total gas content for Jasper 1 is presented in Figure 6.11. Excluding sample J1, which has an ash yeild of 41%, total gas content for the coal samples (10 intervals) ranges from 2.27 m^3/t to 2.91 m^3/t (aa). The two deepest samples, J12 and J13, were collected from the interburden and contained 0.86 and 0.71 m^3/t (aa) of gas respectively.

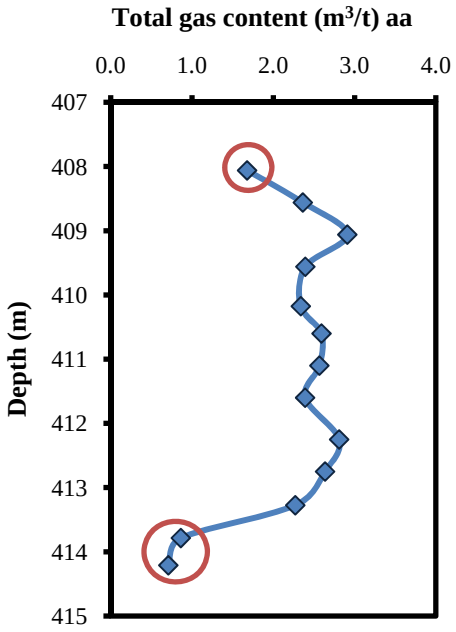

Figure 6. 11. Vertical profile of total gas content (aa) for the Jasper 1 drill hole. Data points circled yielded >20% ash.

On average, the Mimi 1 location, had the highest gas contents with a range from 2.78 m^3/t to 3.16 m^3/t (aa) for the 11 canisters (Fig. 6.12). The canister of interburden, collected below the Renown seam (sample M12), yielded 0.87 m^3/t (aa). The series of peaks in gas content in the Mimi 1 drill hole appear to be stratigraphically similar, yet less pronounced, than those recognizable in the Jasper 1 core. Spatially, these two cores are less than 400 m apart.

Only 3 m of core was retrieved from the Baco 1 drill hole because of coring difficulties and hole collapse. Total gas contents for the 6 retrieved canisters ranged from 2.23 m^3/t to 3.00 m^3/t (aa; Fig. 6.13).

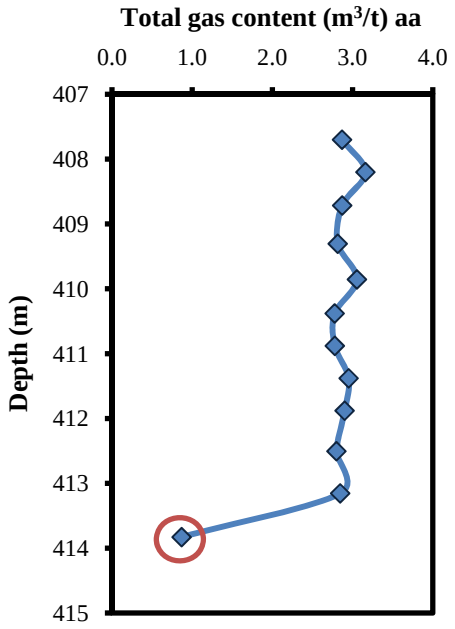

Figure 6. 12. Vertical profile of total gas content (aa) for the Mimi 1 drill hole. Data points circled yielded >20% ash.

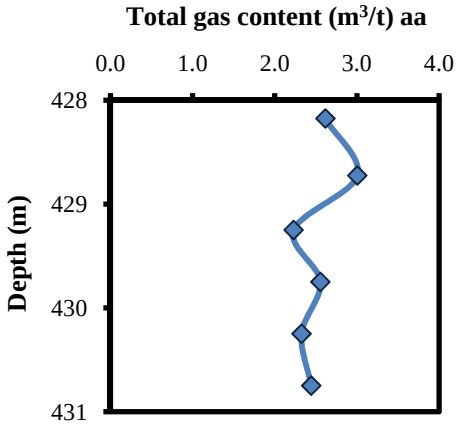

Figure 6. 13. Vertical profile of total gas content (aa) for the Baco 1 drill hole.

6.3.2. Total gas content by seam

Considerable within and between seam variation was seen for all drill holes as well as significant differences in gas volume between drill holes. In all locations, with the exception of Rotongaro 1 where the Renown seam is very thin, the Renown seam showed greater heterogeneity in gas content than the Kupakupa seam.

To investigate the differences by seam the average gas content, for the five drill holes where both seams have been cored, are presented (daf) in Figure 6.14 and Table 6.3. Averages exclude any material with >20% ash yield.

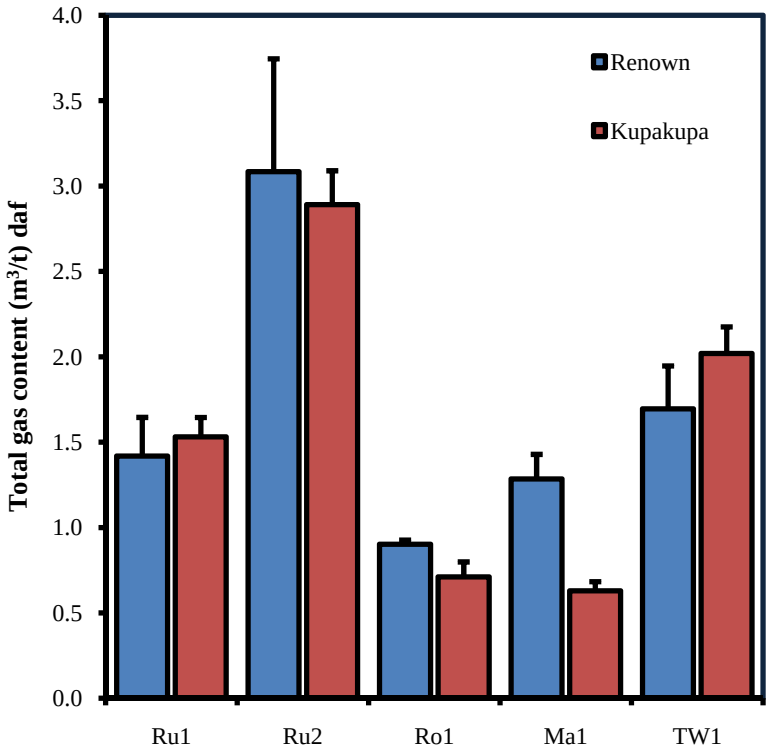

Figure 6. 14. Average total gas content (daf) by drill hole, where both seams have been cored. Coal samples with ash yield <20% have been excluded from the averages. Ru1 = Ruawaro 1, Ru2 = Ruawaro 2, Ro1 = Rotongaro 1 and Ma1 = Mangapiko 1.

Table 6. 3. Average gas contents by seam (daf) where both seams have been cored. Coal samples with ash yield <20% have been excluded from the averages.

Drill hole	Seam	Minimum (m^3/t)	Average (m^3/t)	Maximum (m^3/t)	SD	n
Ruawaro 1	Renown	0.94	1.42	1.66	0.27	7
	Kupakupa	1.25	1.53	1.70	0.13	15
Ruawaro 2	Renown	1.60	3.08	4.07	0.79	14
	Kupakupa	2.50	2.89	3.18	0.21	11
Rotongaro 1	Renown	0.82	0.90	1.04	0.09	4
	Kupakupa	0.50	0.71	0.92	0.12	21
Mangapiko 1	Renown	1.02	1.28	1.43	0.12	8
	Kupakupa	0.53	0.63	0.79	0.07	10
TW1	Renown	1.39	1.69	1.97	0.18	13
	Kupakupa	1.70	2.02	2.42	0.17	19
Average	Renown	0.82	1.94	4.07	0.92	46
	Kupakupa	0.50	1.51	3.18	0.93	76

SD = standard deviation; n = number of samples.

Overall, the Renown seam has a greater average total gas content than the Kupakupa seam by approximately 25% (Fig. 6.15). In contrast to this trend, the Kupakupa seam in the TW1 and Ruawaro 1 holes has a slightly higher total gas content than the Renown (Fig. 6.14).

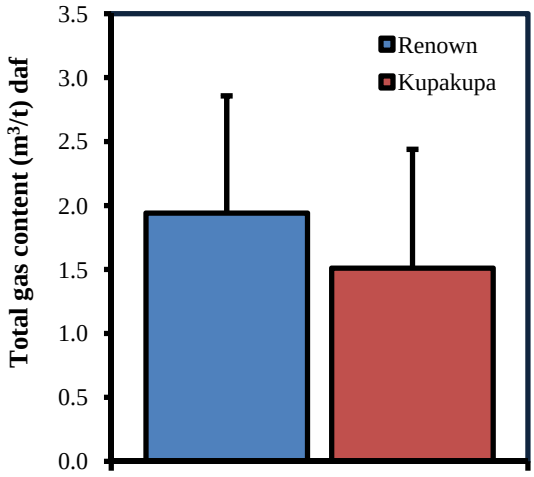

Figure 6. 15. Average total gas content (daf) by seam for drill holes where both seams have been cored (see Figure 6.14). Coal samples with ash yield <20% have been excluded from the averages.

6.3.3. Gas desorption by location

As alluded to above, four of the drill holes: Ruawaro 2, Baco 1, Jasper 1 and Mimi 1 are all located in the same area collectively known as 'Beverland Road'. To highlight the difference between the total gas contents of these cores to those of the other drill holes the average total gas content (daf; no sample >20% ash yield) has been plotted for all wells in Figure 6.16. Overall the Beverland Road cores have over double the average gas content than the average of the other cores combined (Table 6.4 and Fig 6.17).

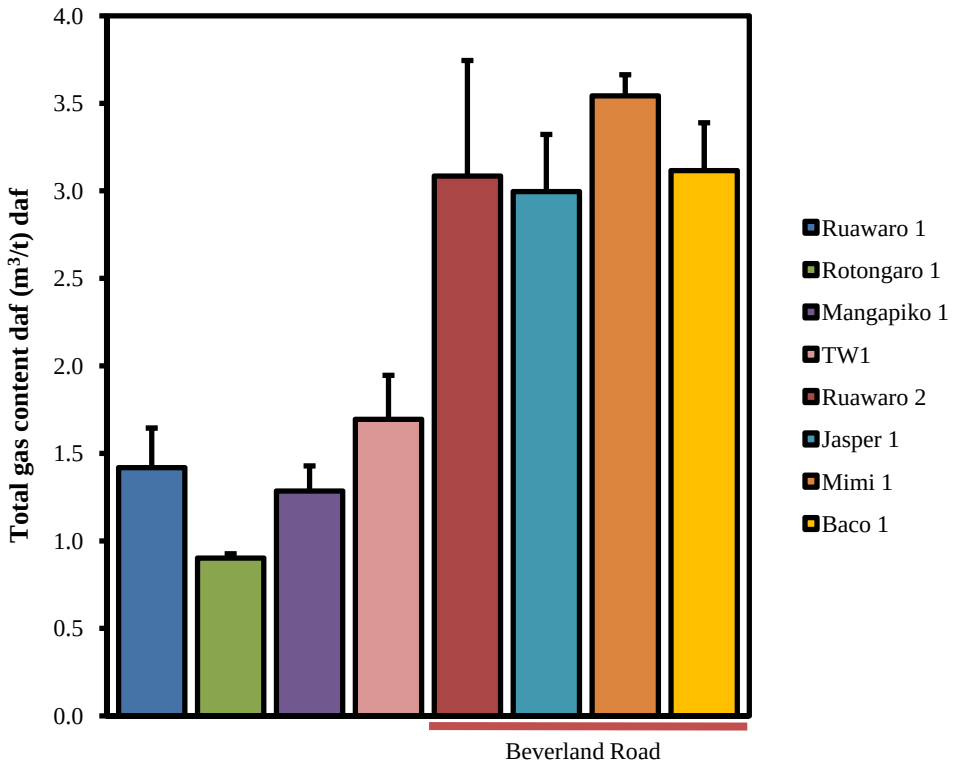

Figure 6. 16. Average total gas content (daf) for the Renown seam for all drill holes. The average gas contents at the Beverland Road site are clearly greater than for coal collected from other locations.

Table 6. 4. Average gas contents (daf) of the Renown seam from all locations. Samples with ash yield >20% have been excluded.

Drill hole	Minimum (m^3/t)	Average (m^3/t)	Maximum (m^3/t)	SD	n
Ruawaro 2	1.60	3.08	4.07	0.79	14
Baco 1	2.74	3.12	3.71	0.35	6
Jasper 1	2.73	3.02	3.43	0.22	10
Mimi 1	3.28	3.54	3.82	0.18	11
Ruawaro 1	0.94	1.42	1.66	0.27	7
Rotongaro 1	0.82	0.90	1.04	0.09	4
Mangapiko 1	1.02	1.28	1.43	0.12	8
TW1	1.39	1.69	1.97	0.18	13
Beverland Road	1.60	3.19	4.07	0.54	41
Other Renown	0.82	1.43	1.97	0.32	32

SD= Standard deviation; n = number of samples.

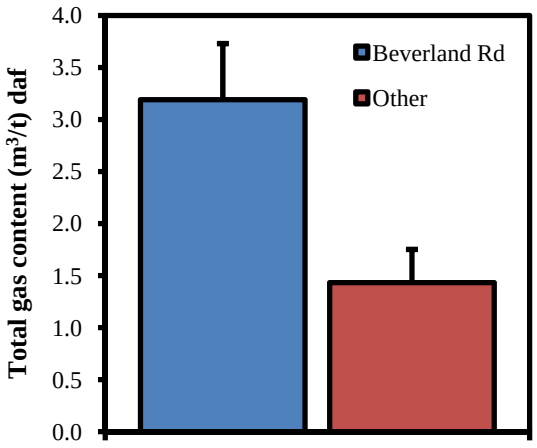

Figure 6. 17. Average total gas content (daf) for coal from the Beverland Road location versus results combined from other locations.

6.4. Variability in gas adsorption, desorption and saturation

As shown above, there is considerable variation in gas properties both within and between seam intervals. Sample retrieval in the field usually results in the collection of numerous desorption samples and very few adsorption samples. Reported numbers of adsorption: desorption samples include 47:615 (Stricker and Flores, 2002), 75:615 (Stricker et al., 2006), 4:90 (Butland and Moore, 2008), 8:163 (Mares and Moore, 2008), and 14:76 (Warwick et al., 2008). This raises the question: are the relatively low proportions of adsorption to desorption samples sufficient to characterize a core or a seam?

A frequently used method for assessing the commercial viability of coalbed methane (CBM) prospects is to calculate gas-in-place (GIP). GIP requires knowing or estimating the maximum holding capacity of a coal (i.e. from the adsorption isotherm) for any particular depth/pressure as well as the level of saturation. As such, reservoir saturation is a key parameter when assessing the economic viability of a CBM play. As saturation is calculated using results from adsorption and desorption analyses, unsurprisingly saturation has been reported to show significant variation. Stricker and Flores (2002) found saturation to vary from 23% to 66% while Butland and Moore (2008) found down hole variation in saturation values of greater than 40%. Knowledge of the saturation in a reservoir is important for economic assessment of gas deposits as the level of saturation dictates the down hole pressure required for gas desorption, which highly influences gas recoverability (see also Bustin and Bustin (2008)).

To further examine variability in gas adsorption, desorption, and gas saturation the Renown seam in the Jasper 1 drill hole was selected for closer analysis. The average moisture

content for the Jasper 1 core was the lowest reported for the Renown seam. As such, it was decided to use the average moisture (16.2%) and ash yield (3.8%) for Renown seam (Figure 3.10) to correct gas desorption and adsorption data to average in situ basis.

6.4.1. Variability in gas adsorption capacity

The adsorption samples presented in this part of the study are all post-desorption analyses. Hence, it needs to be stated that the gas holding capacities are likely to be greater than the actual gas holding capacity of the reservoir. However, as the aim of this section is to study in seam variability, it is the relative differences between samples that are important.

The methane adsorption isotherm curves (Fig. 6.18) clearly show the variability in maximum holding capacity for the Jasper 1 samples. Three of the curves, J6, J8 and J11, have a different curvature to the other isotherms, despite all material having been collected from within a 5 m interval. At 4 MPa, the J6 and J8 samples are the two most extreme samples, in spite of their close proximity and very similar coal properties.

Methane gas adsorption capacity was found to vary substantially from 2.20 m^3/t to 3.66 m^3/t (a 40% difference), at a pressure of 4 MPa on average in situ basis, with an average of 3.16 m^3/t and a standard deviation of 0.40 m^3/t (Table 6.5). As the adsorption capacity for J6 is actually 0.63 m^3/t less than the next smallest sample and approximately 1 m^3/t less than the samples either side (see Figure 6.19A), there was some concern about its validity. The experimental procedures for the adsorption analysis for J6 were reviewed and showed no abnormalities. Other than the macroscopic log noting that the interval had a “fairly solid looking matrix” no other unusual properties were identified. If J6 is excluded, the gas

adsorption capacity varies from 2.83 m^3/t to 3.66 m^3/t (23% difference) at 4 MPa, with an average of 3.27 m^3/t and a standard deviation of 0.23 m^3/t. Whether J6's adsorption value is real or erroneous, it does illustrate the risk of using only a few samples to estimate the properties of a whole seam.

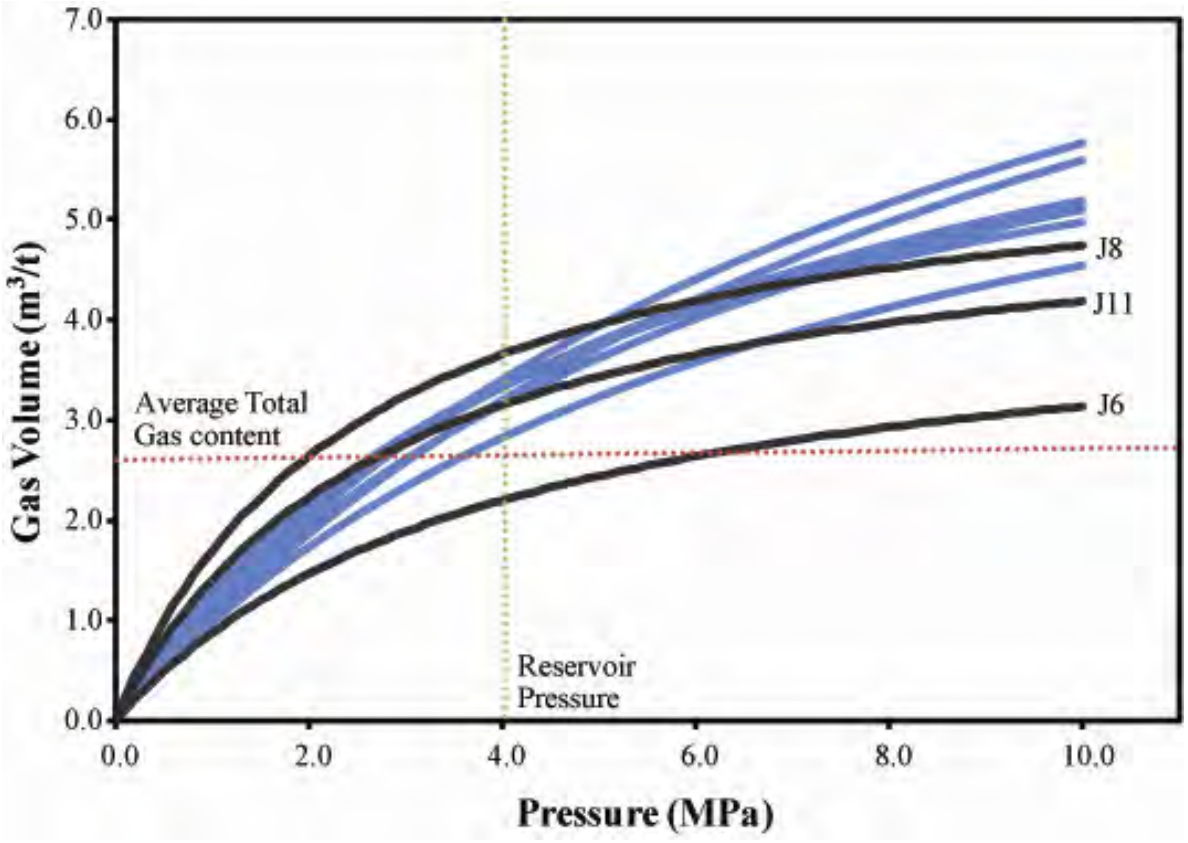

Figure 6. 18. Adsorption isotherms for the ten Jasper 1 samples. The three highlighted samples J6, J8 and J11 show different curvature. Average total gas content (red) and reservoir pressure (green) for the seam are marked.

Table 6. 5. Total gas content, gas adsorption capacity and saturation by canister on average in situ basis.

Canister	Total gas content (m^3/t)	Adsorption capacity at 4 MPa (m^3/t)	Saturation (%)
J2	2.61	3.40	76.68
J3	3.01	3.16	95.20
J4	2.59	2.83	91.47
J5	2.48	3.20	77.63
J6	2.65	2.20	120.25
J7	2.58	3.33	77.54
J8	2.42	3.66	66.26
J9	2.85	3.36	84.93
J10	2.72	3.34	81.59
J11	2.44	3.15	77.52
Minimum	2.42	2.20	66.26
Average	2.64	3.16	84.91
Maximum	3.01	3.66	120.25
SD	0.19	0.40	14.85

SD= Standard deviation

6.4.2. Variability in total gas content

Total gas content (on an average in situ basis) in the Jasper 1 drill hole was found to vary from 2.42 m^3/t to 3.01 m^3/t (a 20% difference), with an average of 2.64 m^3/t and a standard deviation of 0.19 m^3/t (see Table 6.5 and Fig. 6.19A). A total variation of 0.59 m^3/t, or about 22%, of the average total measured gas content is significant over the seam interval, particularly when there is no correlation with depth as evidenced from Figure 6.19A. There is a distinct lack of relationship between gas content and gas holding capacity. This can be explained as the gas adsorption capacity is a physical property of the coal whilst total gas content, in this case, is formed from secondary biogenic processes (i.e. post-coalification) and is hence not dependent on the coal structure.

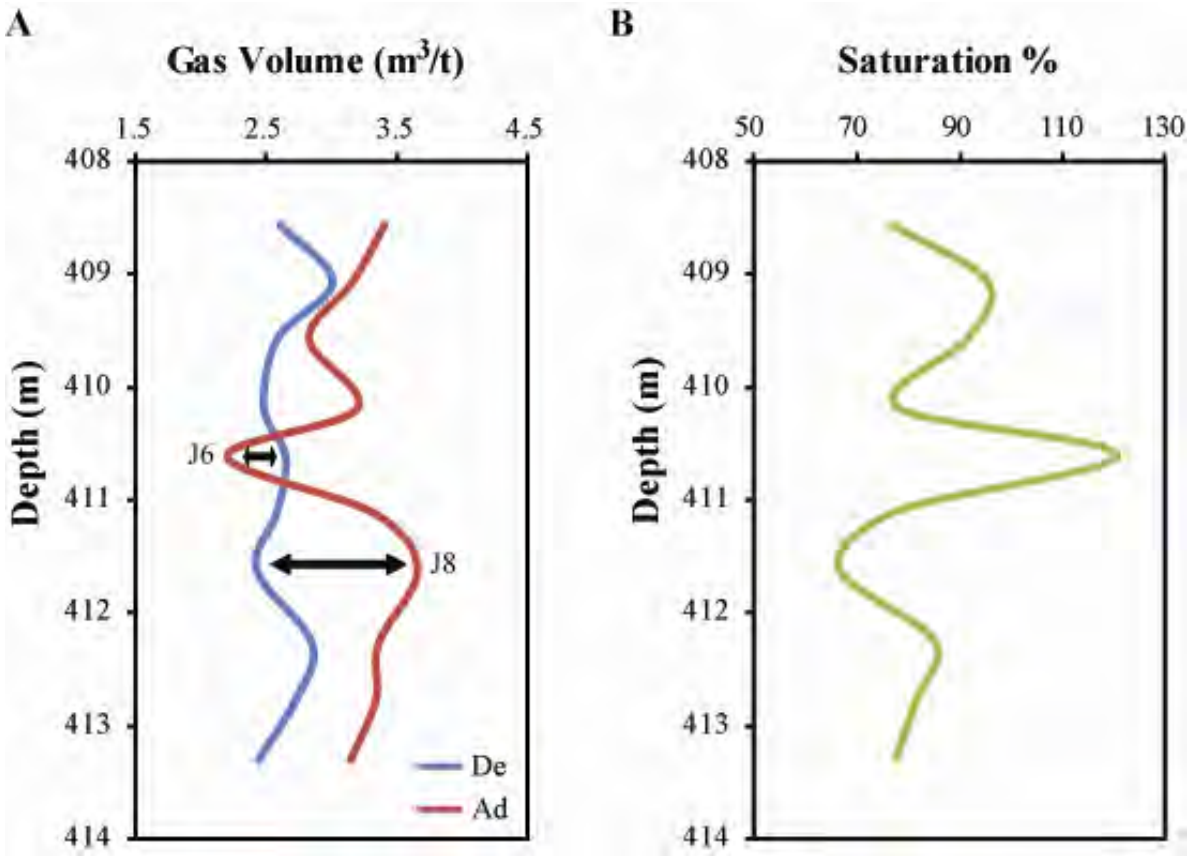

Figure 6. 19. (A) Vertical profiles of total gas content (De= desorption) and gas adsorption capacity (Ad= adsorption) showing no relationship between the two. The samples J6 and J8 are marked. (B) Saturation profile of Jasper 1.

6.4.3. Variability in gas saturation

If the sample J6 is included, the percent gas saturation varies from 66.3% to 120.3% (45% difference) with an average of 84.9% and a standard deviation of 14.9 (Table 6.5). If J6 is excluded, saturation still shows considerable variation with a range from 66.3% to 95.2% (30% difference) and an average of 81.0% (sd = 8.6). The vertical profile displayed in Figure 6.19B shows that if only one sample was collected for adsorption and desorption analyses from either the J6 or J8 regions very different estimates on reservoir content, potential gas retrieval and commercial viability would be obtained.

6.4.4. How many samples?

Sections 6.4.1 and 6.4.3 report values and averages for gas adsorption and gas saturation including and excluding J6. This section of the study excludes J6. The inclusion of J6 had the effect of further increasing the uncertainty around gas adsorption and gas saturation and increasing the number of samples required for the average to be within one standard deviation of the overall mean.

Ten averaging runs for gas adsorption isotherms for the Jasper 1 drill hole (see section 2.1.3 for procedure) are plotted in Figure 6.20 along with the mean of the nine samples and lines indicating ± one standard deviation (± 7.0%). For the Jasper 1 well, 7 out of 10 of the averaging runs were within one standard deviation of the mean when averaging only two randomly selected samples. Thus for whole seam estimates if one standard deviation is an acceptable level of uncertainty, only three or more samples for adsorption would have been required.

The same procedure was applied to the total gas content results (i.e. desorption). The overall mean value for total gas content with one standard deviation (± 7.0%) uncertainty is shown in Figure 6.21. This time 9 out of 10 of the averaging runs were within one standard deviation of the mean when averaging only two randomly selected samples and all runs are within one standard deviation when 3 samples are averaged.

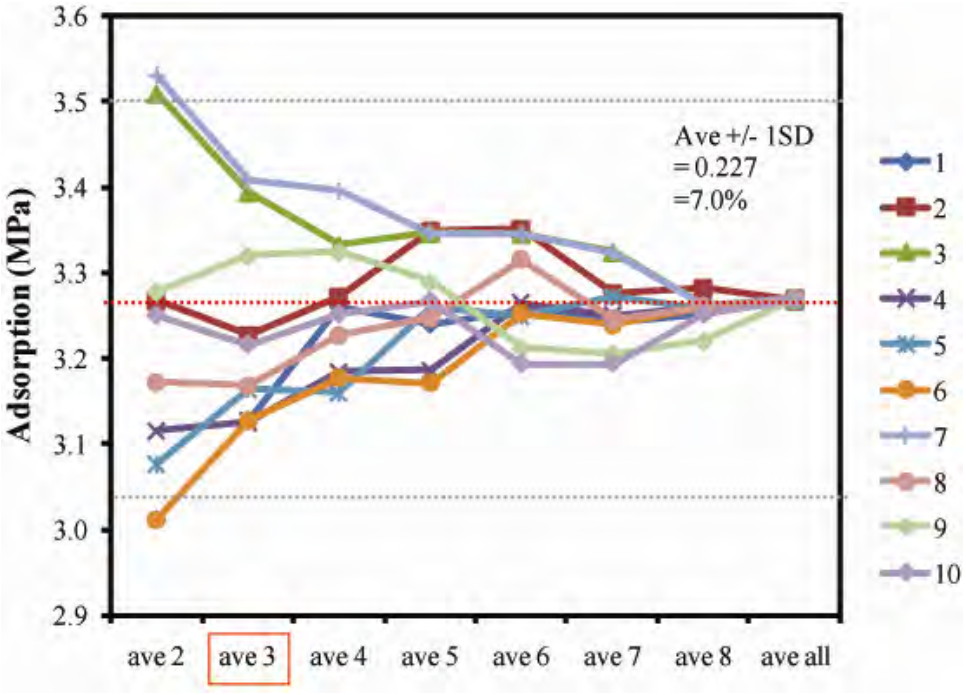

Figure 6. 20. Results of assessment of how many gas adsorption capacity samples are required to be within one standard deviation of the overall mean.

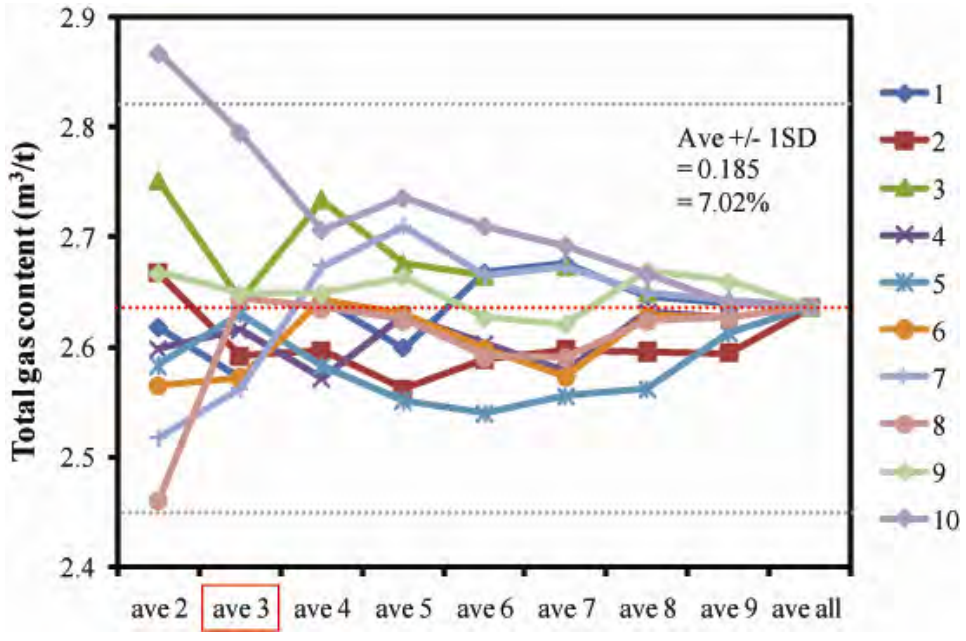

Figure 6. 21. Results of assessment of how many gas desorption samples are required to be within one standard deviation of the overall mean.

For calculated percent saturation, at least three saturation calculations are again required to be within one standard deviation (± 10.7%) of the mean (Fig. 6.22). So in all analyses at least three samples would have been required to be within ± 10% of the mean. An additional benefit of collecting at least three samples is that anomalous or unusual results can be more easily identified and treated with caution.

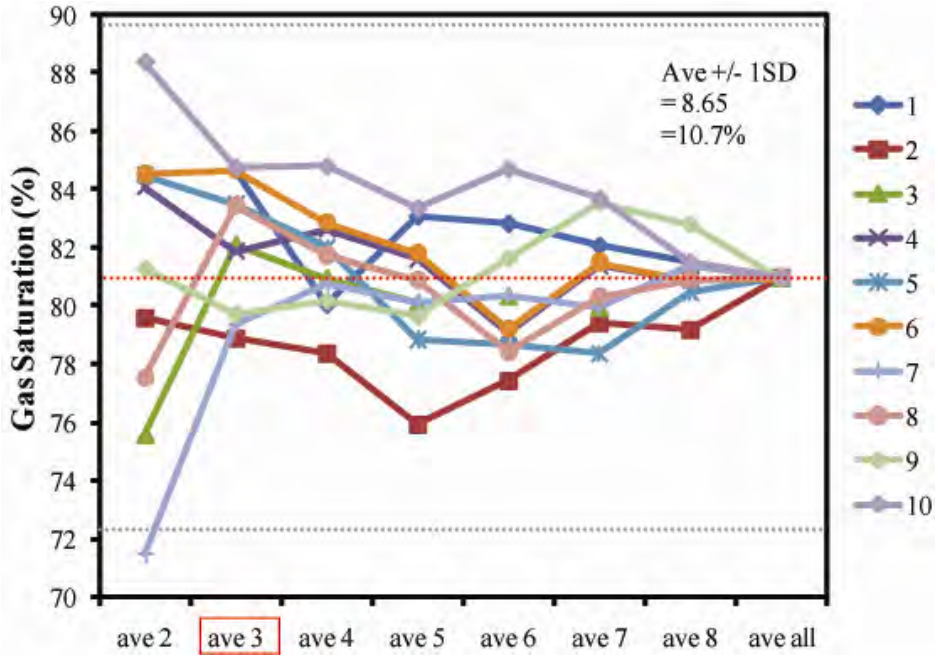

Figure 6. 22. Results of assessment of how many gas saturation analyses are required to be within one standard deviation of the overall mean.

6.5. Gas quality and isotopic composition

Where analysed, gas from the wells was always greater than 90% methane in composition and generally composed of <2% carbon dioxide. The average gas composition from 41 measurements (reported with oxygen, nitrogen and air free corrections) is given in Table 6.6.

Methane $\delta^{13}C$ and δD isotope data from eight collected gas samples (Table 6.7) ranged from about –66 to –68‰ and –201 to –225‰ respectively. When these values were plotted in Figure 6.23, the results indicate a secondary biogenic origin for the methane gas present in the Huntly coalfield. All values fall within the CO_2 reduction compositional field of Whiticar et al. (1986).

Table 6. 6. Mean gas composition (from 41 measurements) from the Renown and Kupakupa coal seams.

Gas	basis	Mean	SD
CH_4	%	98.43	1.77
CO_2	%	1.52	1.77
C_2H_4	ppm	0	0
C_2H_6	ppm	338.72	280.38
H_2	ppm	154.9	403.96
O_2	%	0	0
N_2	%	0	0

SD = standard deviation

Table 6. 7. Gas isotope data from the Huntly Coalfield.

Drill hole	∂D per mil	∂^{13}C per mil
Ruawaro 1	−216.0	−65.70
Rotongaro 1	−204.0	−67.60
Mangapiko 1	−210.6	−65.77
Mangapiko 1	−206.5	−65.50
Mangapiko 1	−209.7	−65.88
Mangapiko 1	−205.4	−65.71
TW1	−225.0	−67.50

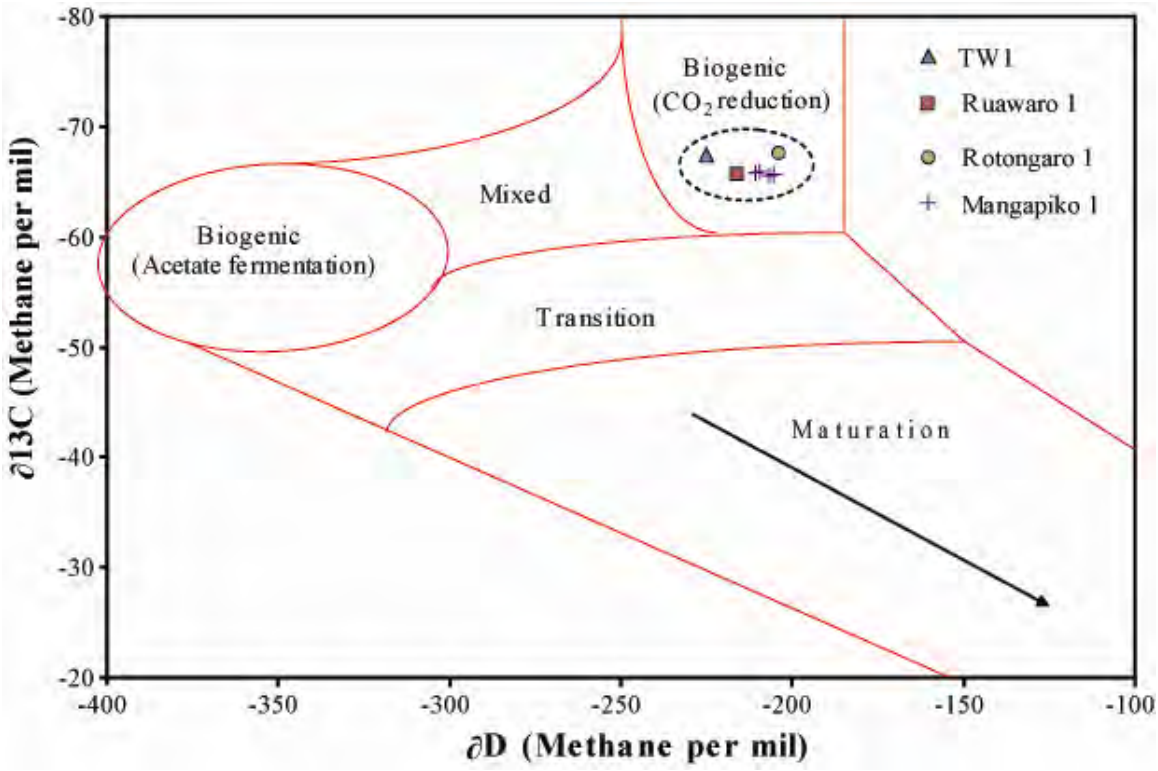

Figure 6. 23. Gas isotopes from the Huntly coalfield showing the secondary biogenic origin of the gas.

6.6. Discussion

6.6.1. Within seam variation in methane adsorption and gas desorption

Within seams, total gas content was found to vary by between 20% and 45% (difference between maximum and minimum total gas content) while, for the Renown seam intersection in the Jasper 1 drill hole, methane adsorption capacity varies by 40%. As stated previously, considerable variation has been reported to exist within seams for total gas content (Butland and Moore, 2008; Flores et al., 2001; Moore et al., 2001; 2008; Stricker et al., 2006). However, very few studies have examined adsorption variation in such detail. Stricker et al. (2006) analysed six, two-foot gas adsorption samples within a ~40 m interval

of the Big George coal in the Powder River Basin, U.S.A, however this only represent around 9% of the coal core. They still found considerable variation and some relationship to depth with the lower part of the seam having a maximum holding capacity of 207 - 279 ft^3/t at 571 - 918 psia and the upper part 171 - 230 ft^3/t at 529 - 911 psia.

To facilitate the generation of secondary biogenic gas there must exist reasonable permeability to allow the introduction of the microorganisms into the coal via groundwater recharge (Rice, 1993; Scott et al., 1994). Methanogenic consortia are composed of anaerobic archaea and bacteria which convert organic substrates (including hydrogen, CO_2, acetate and formate; see equations 6.1 and 6.2) into methane (Budwill, 2003). Bustin and Downey (2002) proposed that possibly many low rank coals contain little to no gas because the groundwater conditions are unsuitable for biogenic gas production or because of the presence of an inhibitor to the microorganism consortia necessary for biogenic gas production. Warwick et al. (2008) found that in the Wilcox coal beds the coal gases are primarily generated where formation water is saline while shallow (< 150 m) areas containing freshwater have little or no biogenic gas.

Researchers have identified and/or sequenced methanogens collected from both coal (Klein et al., 2008; Li et al., 2008) and coal formation waters (Green et al., 2008; Klein et al., 2008; McIntosh et al., 2008; Shimizu et al., 2007; Strapoc et al., 2008b; Thielemann et al., 2004) while Ulrich and Bower (2008) confirmed current, in situ active methanogenesis in the Powder River Basin, U.S.A. Experiments culturing both indigenous and foreign methanogenic consortia have successfully produced CH_4 under laboratory conditions, both with and without nutrient enhancement (Budwill et al., 2005; Chou et al., 2008; Green et al., 2008; Harris et al., 2008; Ulrich and Bower, 2008). Rate limiting factors of methanogenesis

were found to be temperature, pH, pressure and available surface area (Budwill et al., 2005; Green et al., 2008; Harris et al., 2008). It has also been suggested that methane production may be rate limited (Jones et al., 2008). Methanogens have been reported to be around 0.2 – 6.0 μm in diameter (Gilcrease and Shurr, 2007; Strapoc et al., 2008b), which is larger than many coal pores. Thus, it has been proposed that microbial access may be limited to cleat surfaces (Gilcrease and Shurr, 2007; Scott, 1999). As such, accessibility may be a significant control on the in-seam variability identified in gas content (Strapoc et al., 2007; 2008a).

The variation in total gas content can be at least partially explained in terms of controls on methanogenesis. However, the difference in methane holding capacity is a physical property (i.e. differences in porosity and available surface area) created during the coalification process and thus is unrelated to gas generation. Within seam variation was seen for both fresh (the two Rotongaro 1 Kupakupa samples) and post-desorption samples (Jasper 1), hence the variation in adsorption isotherms cannot simply be ascribed to sample oxidation.

6.6.2. Between seam variation in methane adsorption and gas desorption

It has generally been accepted that gas sorption capacity increases with increasing pressure, which in turn is partially related to increasing depth as well as changes in temperature and rank (Yee et al., 1993). There is 10 – 25 m of interburden between the Renown and Kupakupa seams in the drill holes with only a minimal difference in reservoir temperature over this interval (Zarrouk and Moore, 2007). Chapter 4 did not reveal any major rank differences between the seams. Yet, in drill holes where both seams are represented, the stratigraphically higher Renown seam has a greater average methane adsorption capacity by

approximately 15% and an approximately 20% higher average total desorbed gas content (1.96m^3/t) than the underlying Kupakupa seam (1.51m^3/t). Thus, not only does the Renown seam have the capacity to hold more gas, it also contains/retains more gas. The greater total gas content can possibly be explained by: (1) vertical migration of gas from the Kupakupa to the Renown seam, in spite of the siltstone/claystone interburden, (2) the presence of a better seal above the Renown seam in comparison to the Kupakupa seam, or (3) differences in rate or quantity of biogenic gas generation.

6.6.3. Sampling to minimize uncertainty in gas adsorption, desorption and saturation

In the uncertainty part of the study (section 6.4), the total variance of the Jasper 1 sample set was considered to be the sum of experimental or measurement error and the error that occurs from incomplete sampling of the natural variation in physical properties within a coal seam. Any single sample taken from a coal seam will incorporate both sources of uncertainty if sampling is being used to assess a representative mean physical property value for a seam.

Estimating the first source of error, experimental or measurement error, in either adsorption or desorption analyses is complicated. Firstly, there are very few studies which quantify repeatability in adsorption tests because of concerns of the effect that repeated tests may have on the same sample. Crosdale et al. (2005) indicate within laboratory repeatability (experimental error) to be ± 7% based on an Australian inter-laboratory study, however this is likely to also include the second source of error as sample heterogeneity was cited as an contributor to the variances seen in the study results. For a full discussion of potential sources of error see Mavor (2004).

Estimating experimental error for measured gas (desorption) is even more difficult as once a canister has been desorbed, it cannot be desorbed again, thus precluding any type of quantification. It is recognized that desorption values can be the greatest source of error in saturation calculations because of lost gas and oxidation, particularly in low-rank coals (Hayton, 2003; Mavor and Nelson, 1997). Nelson et al. (2000) have suggested that underestimation errors of 15% or greater are possible when efforts are not made to minimize the effects of oxidation and desiccation. If robust experimental error data was available for gas adsorption and desorption, the impact of this error on the accuracy calculations of the average seam saturation could be assessed in isolation of seam variability.

Estimating the second source of error in gas data, the additional error that occurs when sampling at discrete points within heterogeneous coal seams, is now discussed. As a coalbed methane play draws gas from the whole seam, and not just selected parts of the seam, assessing the behavior of the whole seam intersection in the exploration stage is necessary. Traditionally, either the whole seam is sampled numerous times (as is often the case for desorption analyses) or only a limited number of samples are taken across the whole seam (as seen for most adsorption tests). The first method may ‘over sample’ (i.e. needlessly take more samples than needed to estimate a seam’s average value) and the latter method may give an abnormally high or abnormally low value that is not representative for the whole seam.

The within seam variation of gas properties in the Jasper 1 well is substantial. Considering Figure 6.19, neither a single adsorption nor desorption analyses reflects the average property of the whole seam. As such, the extent of sampling required to fully capture natural variations, such that the maximum possible accuracy for an average seam saturation estimate is achieved, needs to be determined on a seam by seam basis. It is important to note

that the number of samples required to reduce the variance of the mean to an acceptable level will depend on both the innate heterogeneity (variability) of a particular seam, and the level of uncertainty (e.g. as described in terms of variance or standard deviation) deemed acceptable. While this study found that at least three adsorption and desorption analyses would be required to obtain an average within 10% of the overall group mean, a more statistically rigorous analyses by Mares et al. (2009) found that at least five samples would be required. Unfortunately, it is impossible to know within seam variability prior to initial exploration sampling.

What are 'acceptable' limits of uncertainty? This depends on the level of accuracy that is required by the individual, the bank, the investor or the available budget. There is no right answer for this. In a preliminary study, explorers may be comfortable with an uncertainty of ± 20%, for example. With more investment however, banks or investors may demand lower levels of uncertainty (thus ensuring less risk). Nevertheless it should be stressed that others, for whatever reason, may be more or less tolerant in their uncertainty. However, the minimum level of uncertainty to be sought is clearly limited by the measurement errors, as is consistent with the principle of consistent crudeness (Elms, 1992), whereby no greater accuracy should be sought than the most imprecise component.

6.6.4. Potential for enhanced coal bed methane (ECBM) and CO_2 sequestration

It has been long recognised that coal can absorb greater volumes of CO_2 than CH_4, and the volumetric ratio of 2:1 has been widely reported for sub-critical CO_2 partial pressures (Cui et al., 2004; Gentzis, 2000; Krooss et al., 2002; Rodrigues and de Sousa, 2002). With the growing interest in low rank coal deposits for both CBM production and CO_2 sequestration,

evidence has emerged that this ratio can vary greatly in lignite and subbituminous coals. Several studies suggest ratios for low rank coals of 10:1 (Bustin, 2002; Stanton et al., 2001a; Stanton et al., 2001b); Burress (2003) found ratios in subbituminous coals ranging from 7.4 to 10:1 and a ratio for lignite of 13.3:1, while Gluskoter et al. (2002) report that low-rank coals can hold 6 to 18 times more CO_2 than CH_4. These results clearly demonstrate that low-rank coals, particularly subbituminous coal, have good potential for CO_2 sequestration. However, this does not mean that all of the CH_4 can be removed and replaced with CO_2 in situ or that the CO_2 can be sequestered at maximum capacity (Bromhal et al., 2005). For instance, in an ECBM laboratory experiment Mazumder and Wolf (2008) found that for dry coals the sweep efficiency of CO_2 on CH_4 ranges from 60% to 90% of the CH_4 initially in place. It must also be noted that some of the injected CO_2 will dissolve into the immobile reservoir water under the high injection pressures. This is an exothermic (heat of solution) process that releases heat into the coal in the proximity of the well bore.

While the replacement of CH_4 by CO_2 may sound simple, this is not the case. As coal actually adsorbs the solvents into its molecular structure (Yee et al., 1993) adsorption and desorption of adsorptive gases, such as CO_2 and CH_4, cause volumetric changes in the coal matrix (Harpalani and Chen, 1992; 1995; Harpalani and Schraufnagel, 1990; Harpalani et al., 2006). During the production phase of a CBM project depressurization of the reservoir and desorption of gas leads to the coal matrix shrinking, resulting in opening of the cleats and hence an increase in permeability (Harpalani and Chen, 1992; 1995; Harpalani and Schraufnagel, 1990). This has been confirmed by field projects such as the Fruitland Formation in the San Juan Basin where absolute permeability increased with continued production (Mavor and Vaughn, 1998). Swelling of coal because of the sorption of gases and liquids is a well reported phenomenon (Bustin et al., 2008; Cody et al., 1988; Day et al.,

2008b; Harpalani et al., 2006; Karacan and Mitchell, 2003; Kelemen et al., 2006; Levine, 1996; Mazumder and Wolf, 2008; Mitra and Harpalani, 2007; Pone et al., 2008; Zarebska and Ceglarska-Stefanska, 2008). Unfortunately, swelling of coal in a confined pressure environment results in closure of the cleats and a decrease in permeability. Siriwardane et al. (2008) found that while the permeability of fractured coal samples did not change with time when exposed to an inert gas (argon), exposure to CO_2 resulted in a permeability reduction of up to 70% of the original size for larger fractures and up to 90% for smaller fractures. Permeability of the smaller fractures was found to be similar to the matrix permeability leading to hypothesis that these fractures would be completely closed in situ.

The cost incurred for the separation of CO_2 from flue gases currently makes CO_2-ECBM uneconomic (Sander and Allison, 2008). As such, the injection of untreated flue gases is also being investigated by many researchers (Deng et al., 2006; Jessen et al., 2007; Law et al., 2003; Mares and Zarrouk, 2008; Mazumder et al., 2006; Zarrouk and Moore, 2009). The injection of flue gases both enhances CBM production and sequesters some CO_2, but has the side effect of early breakthrough of nitrogen (N_2), which is the major component of flue gas. Field research trials into the effectiveness of ECBM are underway, or are in the planning stages, in many countries including Australia, Canada, Japan, China, Poland and the USA (Connell, 2008; Damen et al., 2005; Hamelinck et al., 2002; Mavor et al., 2004; Ohga et al., 2005; Reeves et al., 2004; Shi and Durucan, 2005; Wong et al., 2006)

6.7. Conclusions

For both gas adsorption and gas desorption analyses considerable variation was identified at all levels, within drill holes, within seams and between seams. Additional conclusions about gas properties are as follows:

- Adsorption samples collected post-desorption yield consistently larger gas adsorption capacities than the samples collected and analysed immediately (fresh samples with no desorption). As such, to get a realistic assessment of gas adsorption capacity, samples for gas adsorption isotherms need to be collected fresh in the field.
- The methane adsorption capacity for fresh samples range from 2.63 m^3/t to 4.18 m^3/t (daf). On average, the Renown seam has a greater average methane adsorptive capacity at 4 MPa (3.72 m^3/t) than the Kupakupa seam (3.21 m^3/t).
- Carbon dioxide holding capacities of fresh samples range from 22.00 to 23.72 m^3/t (daf). The Kupakupa seam has a higher average carbon dioxide content (23.21 m^3/t) than the Renown seam (22.77 m^3/t). The ratio of the holding capacity of carbon dioxide to methane is 6.7:1.
- Total gas content varies from 0.53 m^3/t to 4.07 m^3/t in the Renown seam and 0.50 m^3/t to 3.18 m^3/t in the Kupakupa seam (daf; no sample with >20% ash yield). For the locations where both seams have been sampled, the Renown seam has a higher average total gas content (1.94 m^3/t) than the Kupakupa seam (1.51 m^3/t).
- The four drill holes located in the Beverland Road area (Ruawaro 2, Jasper 1, Mimi 1 and Baco 1) had considerably higher total gas contents than the other drill holes (TW1, Ruawaro 1, Rotongaro 1 and Mangapiko 1). Considering only the Renown seam, the

Beverland Road cores have an average total gas content of 3.19 m^3/t while the remaining locations have an average of only 1.43 m^3/t (daf; no sample with >20% ash yield).

- Where analysed, gas from the wells was always greater than 90% methane in composition. Gas isotope results indicate a secondary biogenic origin for the methane gas present in the Huntly coalfield created by CO_2 reduction.
- An examination of gas adsorption, gas desorption and calculated saturation for the Jasper 1 well found considerable variability existed within the ~5 m interval. Methane gas adsorption capacity varies from 2.20 m^3/t to 3.66 m^3/t, at a pressure of 4 MPa on average in situ basis, total gas content varies from 2.42 m^3/t to 3.01 m^3/t, while the percent gas saturation varies from 66.3% to 120.3%. For gas adsorption, gas desorption and calculated saturation it was found that at least three samples would have been required to be within one standard deviation (~10%) of the group mean.
- Determination of how many samples are required to make a realistic assessment of average reservoir properties requires a consideration of: (i) the level of accuracy desired, (ii) the limit of accuracy possible, which is governed by the magnitude of experimental error, and (iii) the innate variability of the seam.

Chapter Seven

Gas Associations

Previous studies have shown there can be considerable variability in gas volume, both within a seam and between stratigraphically different coal seams in the same location (Butland and Moore, 2008; Flores, 2004; Flores et al., 2001; Moore et al., 2001; Stricker et al., 2006). The same type of variability was seen in the Huntly coal samples studied here. Variability in gas content can be the result of rank, type and grade. Some studies have shown that gas content decreases with increasing moisture (Hackley et al., 2007) and with increasing inorganic material (Butland and Moore, 2008; Laxminarayana and Crosdale, 2002; Warwick et al., 2008). In other studies, some of the variation has been associated with the degree of vitrain banding (Butland and Moore, 2008; Flores et al., 2001; Moore et al., 2001; Stricker et al., 2006), although the relationships are still poorly defined and certainly not universal (Butland and Moore, 2008).

7.1. Gas content and coal composition

7.1.1. Proximate analysis and gas content

In this section, the proximate results from Chapter 3 are compared with gas content. Proximate analysis data from all locations (< 20% ash yield, aa) were combined and a correlation table generated. The results relating to gas content are presented in Table 7.1.

Table 7. 1. Correlation table comparing proximate analysis data with gas content (aa). Variables with correlations >0.50 have been highlighted in yellow. Overall = 149 samples, Renown = 73 samples and Kupakupa = 76 samples.

		Lost gas (m^3/t)	Measured gas (m^3/t)	Residual gas (m^3/t)	Total gas (m^3/t)
Overall	**Depth (m)**	0.10	-0.24	-0.37	-0.30
	Moisture (%) aa	0.03	-0.35	-0.42	-0.43
	Ash (%) aa	0.03	0.04	-0.11	0.01
	Volatile matter (%) aa	-0.04	0.12	0.22	0.16
	Fixed carbon (%) aa	-0.04	0.28	0.44	0.37
	Calorific value (MJ/kg)	-0.09	0.23	0.44	0.32
	Sulphur (%) aa	-0.07	-0.14	-0.15	-0.17
Renown seam	**Depth (m)**	0.20	0.04	-0.19	0.01
	Moisture (%) aa	0.03	-0.24	-0.25	-0.28
	Ash (%) aa	-0.07	-0.16	-0.19	-0.21
	Volatile matter (%) aa	0.00	0.15	0.19	0.18
	Fixed carbon (%) aa	0.02	0.31	0.30	0.36
	Calorific value (MJ/kg)	-0.02	0.22	0.27	0.26
	Sulphur (%) aa	-0.14	-0.38	-0.31	-0.44
Kupakupa seam	**Depth (m)**	0.21	-0.43	-0.54	-0.51
	Moisture (%) aa	0.33	-0.39	-0.65	-0.52
	Ash (%) aa	-0.07	-0.01	0.03	0.00
	Volatile matter (%) aa	-0.26	0.03	0.28	0.11
	Fixed carbon (%) aa	-0.17	0.42	0.55	0.51
	Calorific value (MJ/kg)	-0.26	0.43	0.60	0.54
	Sulphur (%) aa	-0.01	0.02	-0.06	0.00

Only a few weak associations were identified by the correlation coefficients (Table 7.1). The only direct associations identified are in the Kupakupa seam with fixed carbon and calorific value associated with both residual and total gas content. Indirect associations were also identified in the Kupakupa seam with both depth and moisture associated with residual and total gas content.

As stated previously, studies have found total gas content to be inversely related to moisture content and ash yield. Hence, total gas content is plotted against moisture (aa; no samples with ash yield >20%) in Figure 7.1 and ash yield (db; all data) in Figure 7.2.

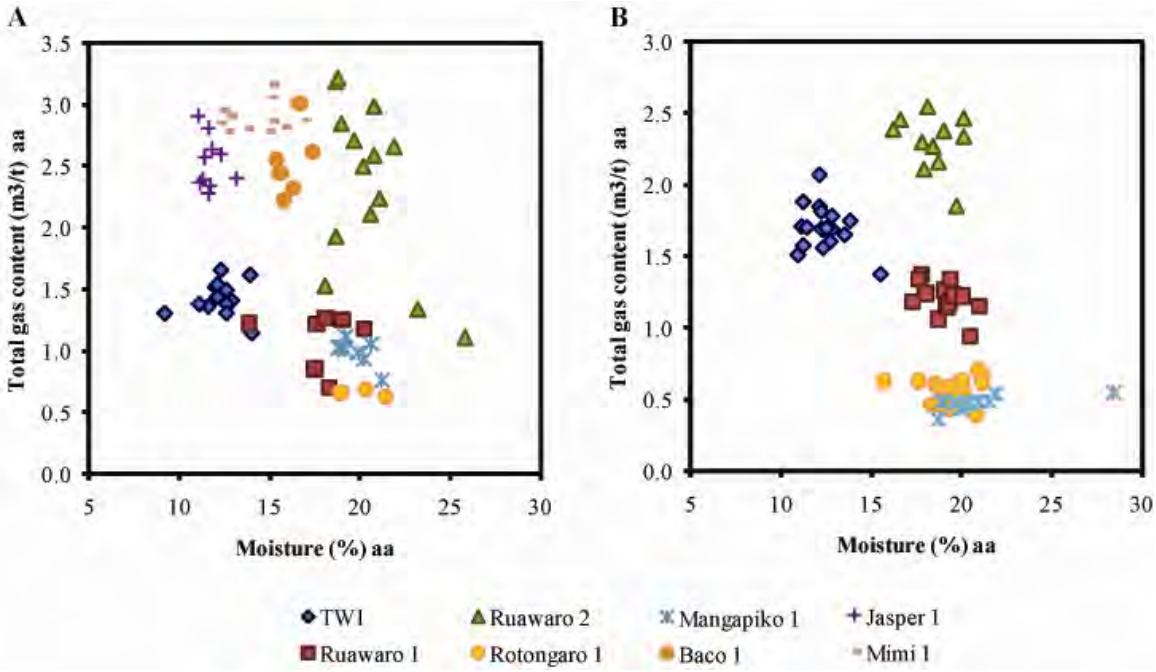

Figure 7. 1. Moisture content (aa) versus total gas content (aa) by location for (A) the Renown seam and (B) the Kupakupa seam. Samples with ash yield >20% have been excluded.

No clear associations were identified between total gas and moisture contents. Ash yields were generally very low with the majority (90%, Section 3.2.2) of samples yielding

<10%. It can be seen that when all of the available data are included (Fig. 7.2A), there is an indirect association with total gas content, whereas when ash yield is <10% (Fig.7.2B) no association can be identified.

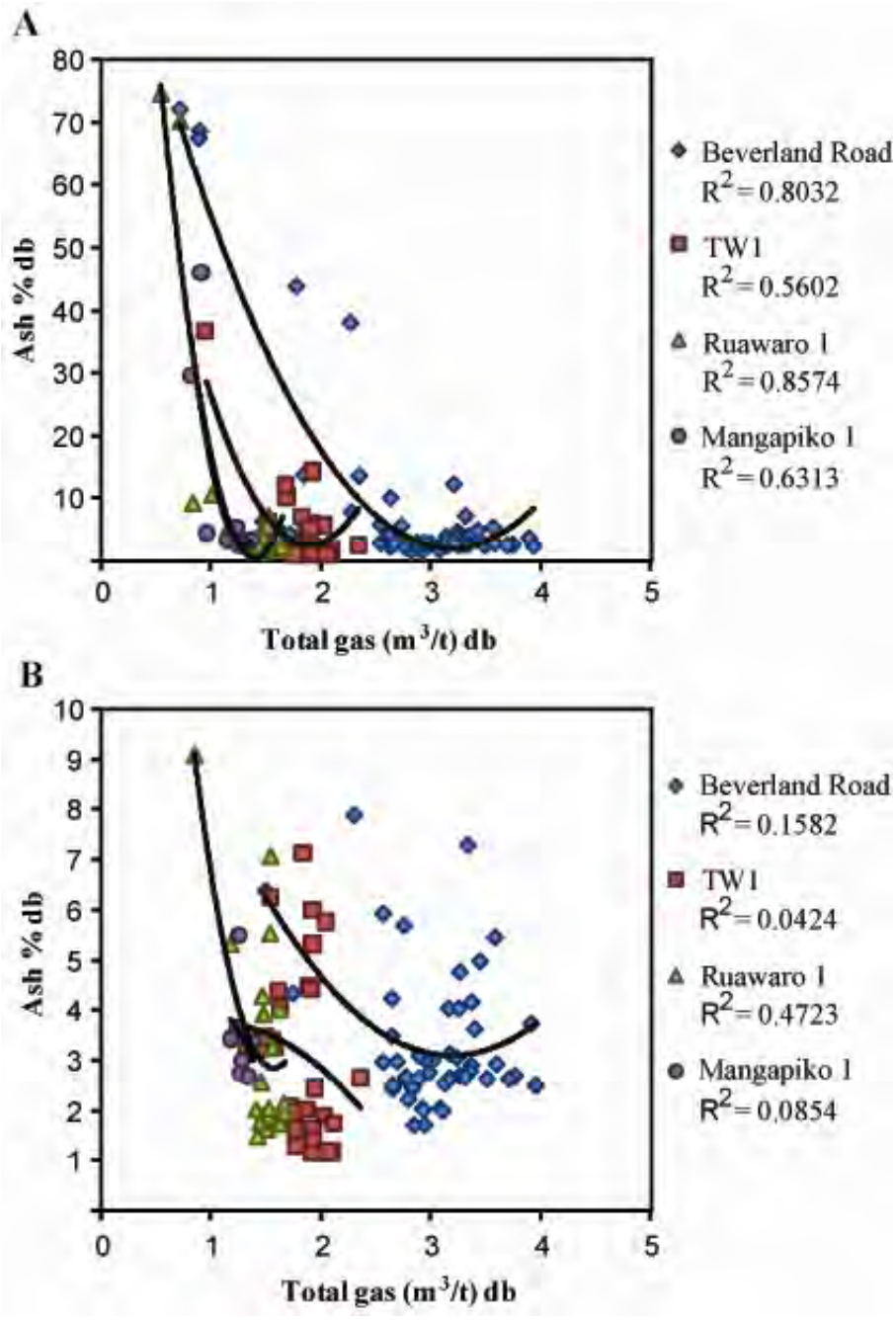

Figure 7. 2. Total gas content (db) versus percentage ash (db) for (A) all data and (B) samples with ash yields <10%. The Beverland Road sites were grouped together because of their proximity and similar gas content. Data for Rotongaro 1 were not presented as only one value had >10% ash db, while for Mangapiko 1 only the Renown was plotted as the Kupakupa seam had significantly less gas and again only one value >10% ash db.

7.1.2. Ultimate analysis and gas content

Ultimate analysis data are available for three seam intersections, for the Renown seam at the Jasper 1 and Mimi 1 locations and for the Kupakupa seam at the Ruawaro 2 location. Hydrogen in the Renown seam has some association with volatile matter and average fluorescence (see Section 4.3.6). Volatile matter and average fluorescence were therefore included in the correlation table between the ultimate analysis results and total gas content (Table 7.2).

Table 7. 2. Correlation table comparing ultimate analysis data (db) with total gas content (db). Volatile matter and average fluorescence have been included because of their association with hydrogen identified in Section 5.3.6. Variables with correlations >0.50 have been highlighted in yellow.

	Jasper 1 Renown Total gas (m^3/t)	Mimi 1 Renown Total gas (m^3/t)	Ruawaro 2 Kupakupa Total gas (m^3/t)
Carbon (%) db	0.41	0.21	0.69
Hydrogen (%) db	0.54	0.54	0.02
Nitrogen (%) db	0.37	0.23	-0.01
Sulphur (%) db	-0.15	-0.09	-0.75
Oxygen (%) db	-0.10	0.02	0.20
Volatile matter (%) db	0.66	0.44	0.02
Average Fluorescence (%)	0.56		0.16

For the Renown seam intersections, total gas content has some association with hydrogen content, volatile matter and average fluorescence (Fig. 7.3A & B). Increasing gas content with increasing hydrogen content has also been identified by Hemza et al. (2009) in coals from the Czech Republic. Noting the concerns about the ultimate analysis results for the Ruawaro 2 Kupakupa seam data (Section 3.6.1), total gas content in the Kupakupa seam does not show association with hydrogen content, volatile matter or average fluorescence (Fig. 7.3C). Instead in the Kupakupa seam total gas content shows an association with carbon content.

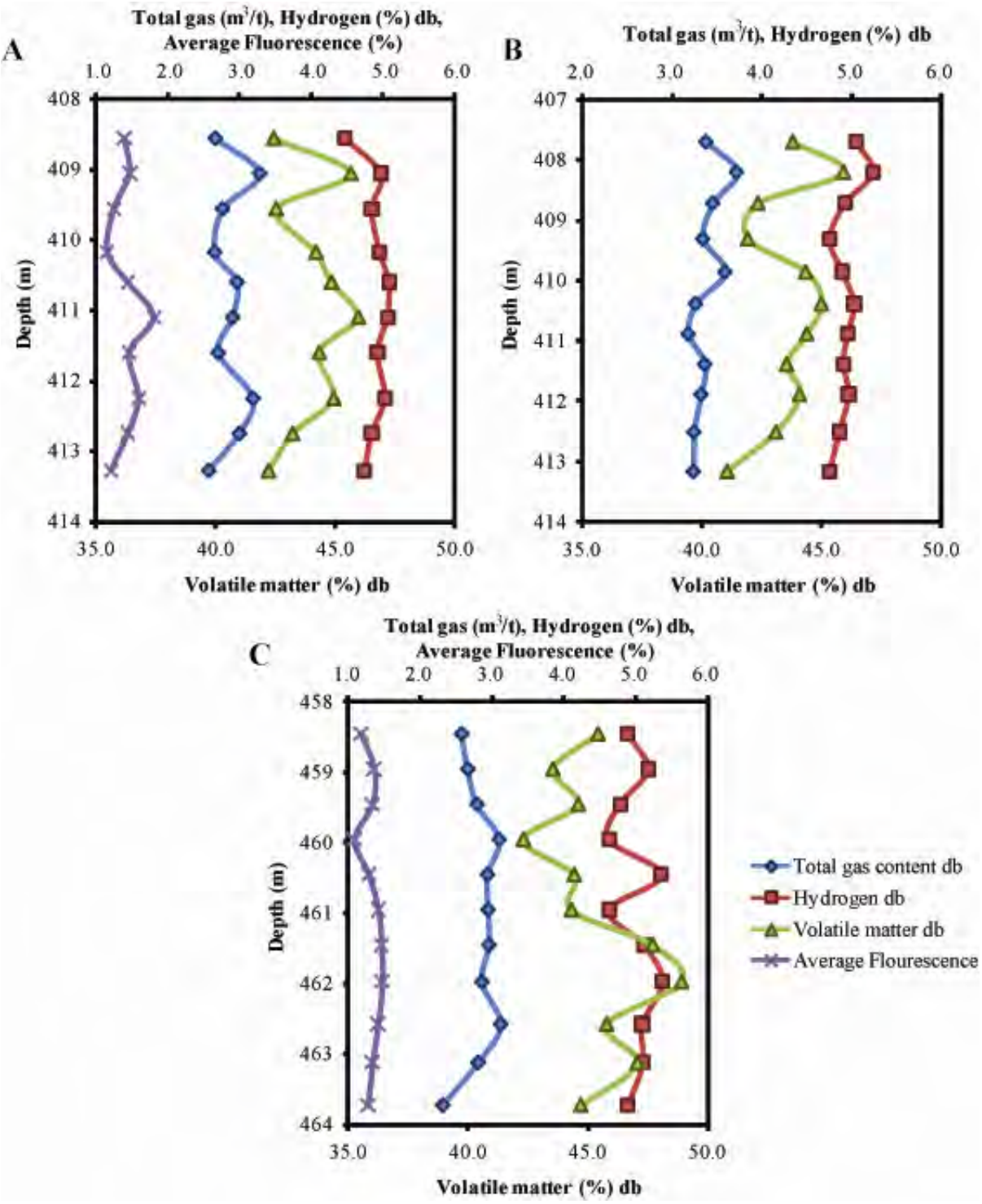

Figure 7. 3. The association of hydrogen content (db), volatile matter (db) and average fluorescence with total gas content (db) at the (A) Jasper 1 location and (B) Mimi 1 location. A distinct lack of association between these variables can be seen for the Kupakupa seam at the Ruawaro 2 location (C).

7.2. Gas content and coal petrology

7.2.1. Percentage vitrain and gas content

Some previous studies have identified an association between the degree of vitrain banding and total gas content (Butland and Moore, 2008; Flores et al., 2001; Moore et al., 2001; Stricker et al., 2006). To examine this possibility, percentage vitrain is plotted against total gas content (aa) for each location in Figure 7.4. The plotted results show that, for the current study, there does not appear to be an association between the amount of vitrain banding and total gas content.

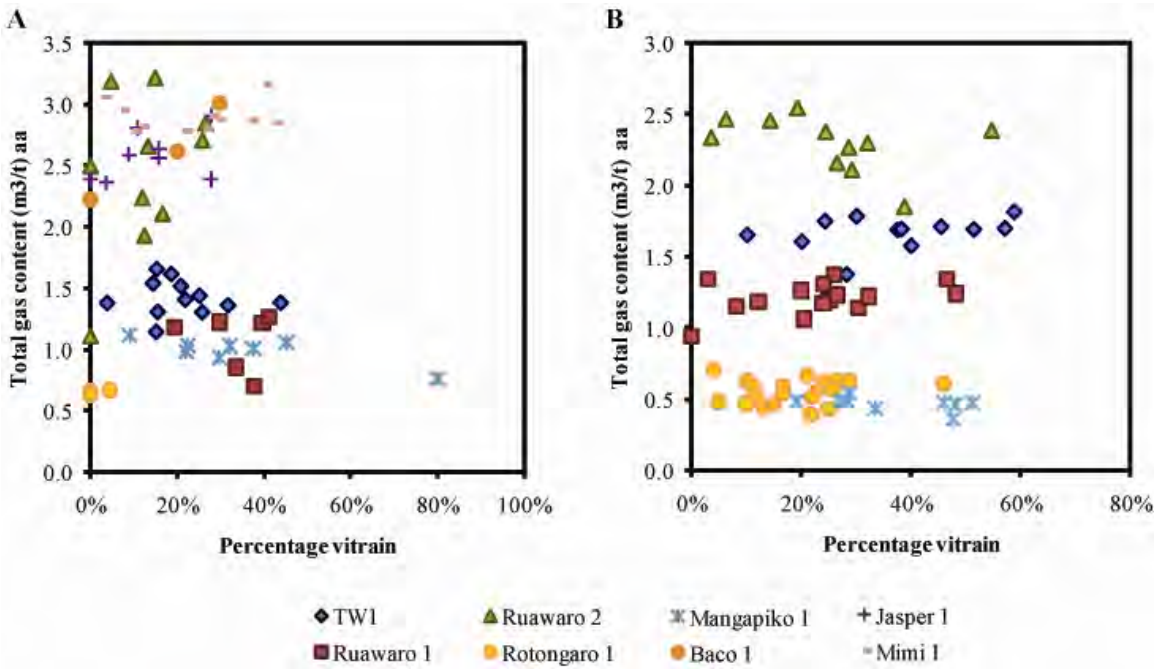

Figure 7. 4. Percentage vitrain plotted against total gas content for (A) the Renown seam and (B) the Kupakupa seam.

7.2.2. Average phi size and gas content

For each location, the average total gas content by seam is plotted against the average phi size by seam (Fig. 7.5). Interestingly, for the Renown seam an *indirect* association between total gas content and average phi size can be recognized, i.e. decreasing gas content with increasing vitrain band thickness, while for the Kupakupa seam there appears to be a *direct* association. Total gas content plotted against average phi size for the combined dataset is not presented as it was found that the volume of data collected from the Kupakupa seam swamped that of the Renown seam. It should be remembered that phi size data only take into account vitrain bands (20% - 30% of all point counts). In the BNB coal types, vitrain bands are only a minor component and thus might not be a good proxy for coal texture to compare with gas content.

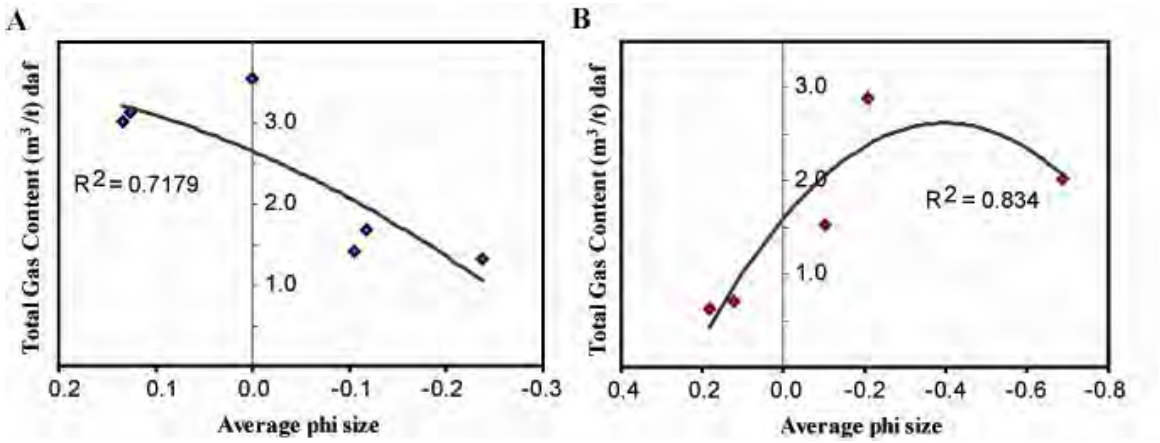

Figure 7. 5. Average vitrain band thickness (phi size) versus average total gas content (daf), by drill hole for (A) the Renown seam and (B) the Kupakupa seam. R^2= coefficient of determination.

7.2.3. Coal type and gas content

To assess the influence of coal type on total gas content the z-scores (equation 2.2) in the normalized dataset were averaged by coal type (Fig. 7.6). Average normalized total gas content appears to decrease from the BNB to the BHB coal type, however there is considerable variation. An analysis of variance (ANOVA) test was conducted on the coal type data set to look for statistical differences but when the three coal types were considered together, variation within groups was greater than any variation between the groups. However, when just the two extremes are compared, i.e. BNB and BHB, (the coal types are, after all, a continuum, separated qualitatively) then a difference is apparent between the two groups (Table 7.3). It must be recognized that the BHB dataset contains only 14 samples and hence ideally more data would be required to further support this observation. Further breakdown of the dataset by seams was not possible because of an insufficient number of samples.

Table 7. 3. Analysis of variance (ANOVA) results conducted on the normalized coal type dataset comparing the extremes, the bright luster, non banded coal (BNB), and the bright luster, highly banded coal (BHB). The null hypothesis (H_o) is that the mean (μ) of the BNB coal type is the same as the mean of the BHB coal type. The alpha level (α) is the significance level related to the probability of rejecting a true hypothesis.

Source	Degrees of freedom	Sum of Squares	Mean Square	F Ratio	Probability > F Ratio
Coal type	1	3.2879	3.2879	4.6303	0.0361
Error	52	36.9239	0.71007		
Total	53	40.2118			
ANOVA	*$\alpha = 0.05$*	*H_o: μ BNB = μ BHB*			

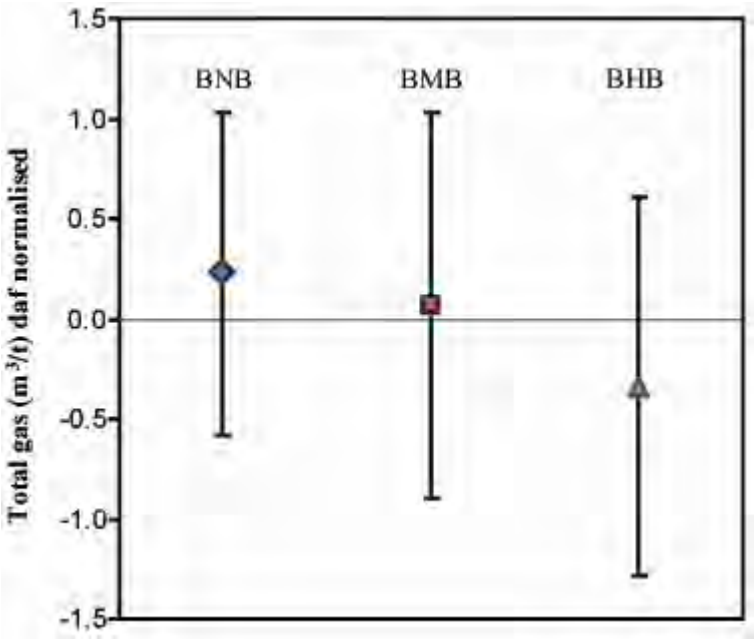

Figure 7. 6. Average normalized total gas displayed by coal type on a dry ash free (daf) basis +/- 1 standard deviation (SD) (normalization procedure explained in text). BNB= bright luster, non banded coal, BMB= bright luster, moderately banded coal and BHB= bright luster, highly banded coal.

7.2.4. Organic petrology and gas content

Organic petrology was conducted on two cores from each seam. The Jasper 1 and Mimi 1 locations were analysed for the Renown seam, while the Ruawaro 1 and Ruawaro 2 locations were analysed for the Kupakupa seam. The correlation coefficients for the comparison of gas content to organic petrology by seam are presented in Table 7.4. Very few associations are present between gas content and the organic components. In the Renown seam a direct association is present between suberinite and measured and total gas content. However, as suberinite is only present in amounts up to 2%, it is unlikely to have significant influence on gas content, and thus is only a casual association rather than causal. In the Kupakupa seam, residual and total gas content have a direct association with corpocollinite and the gelovitrinite sub-group, while lost gas content has an association with funginite content. Indirect associations in the Kupakupa seam can be seen for both lost and measured

gas content with cutinite. Additionally, all gas components have an indirect association with semifusinite. Again these organic components are minor contributors to the total coal composition in the Kupakupa seam with corpocollinite and the gelovitrinite sub-group only contributing up to 5%, funginite only up to 4%, cutinite up to 1% and semifusinite up to 2%.

Table 7. 4. Correlation table comparing organic petrology data (mmf) with gas content (aa) by seam. Variables with correlations >0.50 have been highlighted in yellow.

	Renown Seam				Kupakupa seam			
	Lost gas (m^3/t)	Measured gas (m^3/t)	Residual gas (m^3/t)	Total gas (m^3/t)	Lost gas (m^3/t)	Measured gas (m^3/t)	Residual gas (m^3/t)	Total gas (m^3/t)
Vitrinite	0.39	0.10	-0.29	-0.01	-0.01	0.22	0.35	0.29
Liptinite	-0.23	0.13	0.16	0.21	-0.14	-0.16	-0.26	-0.22
Inertinite	-0.35	-0.31	0.28	-0.24	0.23	-0.15	-0.23	-0.17
Telinite	0.08	0.24	-0.04	0.26	-0.21	-0.13	-0.21	-0.19
Collotelinite	0.00	-0.12	-0.35	-0.40	-0.12	-0.08	0.02	-0.05
Telovitrinite	0.01	-0.09	-0.35	-0.36	-0.13	-0.08	0.01	-0.06
Corpocollinite	0.25	0.48	-0.27	0.42	-0.08	0.29	0.75	0.50
Porigelinite	0.18	-0.06	0.01	-0.02	-0.03	0.19	0.08	0.15
Gelovitrinite	0.34	0.25	-0.17	0.25	-0.09	0.35	0.73	0.53
Collodetrinite	-0.07	0.00	0.21	0.13	0.41	0.46	0.15	0.38
Vitrodetrinite	0.26	0.10	-0.01	0.17	-0.22	-0.18	-0.10	-0.17
Detrovitrinite	0.27	0.13	0.19	0.36	0.11	0.20	0.01	0.14
Cutinite	0.22	0.05	-0.20	-0.03	-0.63	-0.50	-0.29	-0.49
Suberinite	0.11	0.53	-0.01	0.63	0.14	0.06	0.43	0.24
Sporinite	-0.32	0.12	0.11	0.14	0.06	-0.24	-0.38	-0.31
Resinite	-0.01	0.07	-0.27	-0.12	-0.18	-0.17	0.01	-0.12
Liptodetrinite	-0.26	-0.02	0.29	0.12	-0.05	-0.30	-0.20	-0.28
Semifusinite	-0.26	-0.46	0.45	-0.26	-0.54	-0.60	-0.65	-0.70
Funginite	-0.23	0.02	0.08	0.03	0.74	0.48	0.20	0.45
Inertodetrinite	-0.35	-0.42	0.27	-0.38	0.00	-0.26	-0.29	-0.29

7.3. Gas properties in detail

The Jasper 1 location was sampled for gas adsorption and gas desorption on a canister by canister basis and is the only core for which coal properties can be directly compared with gas adsorption capacity. As such, the Jasper 1 location is subjected to closer scrutiny in this

section. For comparison, the Kupakupa seam core from the Ruawaro 2 location is also presented in greater detail.

7.3.1. Renown seam- Jasper 1

Gas content and gas adsorption capacity (aa) are compared to all available coal properties, the results of which are summarized in Table 7.5. The adsorption capacity at reservoir capacity (~4 MPa) for sample J6 was identified in Section 6.4.1 as being significantly lower than the surrounding coal material. Lost, measured and residual gas contents are plotted in Figure 7.7A. There is a significant difference in the lost gas content in samples J2 – J5 compared to samples J6 – J11. The higher lost gas contents in the upper part of the core indicate higher gas desorption rates than for the lower part of the seam. This change in desorption rate suggests a permeability change in sample J6. It was therefore decided to also compare coal properties with adsorption capacity excluding the J6 sample.

Table 7. 5. Correlation table comparing proximate analysis (aa), ultimate analysis (db), organic petrology and data (mmf) with gas content (aa) and adsorption capacity (aa; both including and excluding sample J6) for the Renown seam at the Jasper 1 location. Variables with correlations >0.50 have been highlighted in yellow.

	Lost gas (m^3/t)	Measured gas (m^3/t)	Residual gas (m^3/t)	Total gas (m^3/t)	Adsorption Capacity @ 4 MPa	Adsorption Capacity @ 4 MPa No J6
Moisture	0.06	0.17	-0.40	-0.23	-0.64	-0.66
Ash yield	0.70	-0.48	-0.43	-0.43	-0.04	-0.36
Volatile matter	-0.37	0.33	0.71	0.67	0.24	0.53
Fixed Carbon	-0.66	0.29	0.14	0.11	0.12	0.28
Calorific value	-0.72	0.53	0.50	0.51	0.15	0.42
Sulphur	0.42	0.03	-0.31	-0.14	-0.06	-0.65
Carbon	-0.63	0.42	0.38	0.38	-0.06	0.30
Hydrogen	-0.53	0.54	0.45	0.52	-0.17	0.20
Nitrogen	-0.09	-0.02	0.46	0.34	0.01	0.34
Oxygen	0.04	-0.07	-0.01	-0.04	0.50	0.19
Vitrinite	0.67	0.22	-0.41	-0.08	-0.18	-0.68
Liptinite	-0.53	-0.04	0.37	0.16	0.27	0.46
Inertinite	-0.56	-0.38	0.28	-0.09	-0.04	0.78
Telinite	-0.13	0.46	0.37	0.50	-0.02	-0.14
Collotelinite	0.29	0.05	-0.78	-0.54	-0.34	-0.72
Telovitrinite	0.28	0.10	-0.75	-0.50	-0.35	-0.74
Corpocollinite	-0.55	0.12	0.11	0.02	-0.18	0.39
Porigelinite	0.43	0.28	-0.08	0.18	-0.27	-0.59
Gelovitrinite	0.03	0.38	0.00	0.20	-0.41	-0.36
Collodetrinite	0.20	0.37	0.56	0.69	0.09	0.01
Vitrodetrinite	0.10	-0.30	0.13	-0.02	0.29	0.40
Detrovitrinite	0.24	-0.01	0.53	0.49	0.34	0.38
Cutinite	0.78	-0.24	-0.49	-0.34	0.05	-0.29
Suberinite	-0.53	0.02	0.47	0.27	-0.36	0.35
Sporinite	-0.68	0.10	0.37	0.20	0.71	0.87
Resinite	-0.13	-0.22	-0.27	-0.36	0.08	0.01
Liptodetrinite	-0.45	0.00	0.45	0.27	0.21	0.37
Semifusinite	-0.12	-0.29	0.25	0.03	-0.36	0.48
Funginite	-0.42	-0.45	0.31	-0.07	-0.12	0.58
Inertodetrinite	-0.68	-0.22	0.16	-0.14	0.21	0.69
SiO_2	0.70	-0.52	-0.57	-0.57	0.00	-0.37
Al_2O_3	0.64	-0.16	-0.83	-0.62	-0.44	-0.77
Fe_2O_3	-0.80	0.39	0.70	0.58	0.29	0.56
CaO	-0.16	0.27	0.71	0.68	0.24	0.42
MgO	-0.78	0.26	0.68	0.51	0.23	0.67
Na_2O	-0.67	0.33	0.54	0.46	-0.10	0.36
K_2O	-0.10	-0.22	-0.25	-0.34	-0.81	-0.59
TiO_2	0.27	0.11	-0.82	-0.55	-0.37	-0.80
Mn_3O_4	0.45	-0.03	0.19	0.24	-0.04	-0.17
SO_3	-0.75	0.35	0.55	0.45	0.15	0.50
P_2O_5	0.23	-0.01	-0.79	-0.60	-0.31	-0.73

Lost gas content shows a positive association to ash yield, vitrinite, cutinite, silicon and aluminium. Lost gas is compared with ash yield and vitrinite in Figures 7.7 B and C respectively. The upper part of the core (J2 – J5) shows a similar trend between lost gas content and the higher ash yields (>3%) while, with the exception of the increase in the sample at the base of the seam, there appears to be minimal similarity between the trends in the lower part of the core. In contrast, the lower part of the core shows a very similar trend to vitrinite content while the upper part does not. In an investigation of the effect of coal type on gas sorption, Crosdale et al. (1998) found that, in general, bright, vitrinite-rich coals had the slowest desorption rates, while dull and mineral-rich coals had faster desorption rates. In agreement, Radlinski et al. (2009) identified that faster sorption kinetics for CO_2 were correlated with areas of higher mineral matter. Possibly in the current study when ash yield is >3% it has some influence on the gas desorption rate, while when ash yields is <3% gas desorption rate is more influenced by the vitrinite content.

Measured gas content shows very few associations. There is a direct association with calorific value and hydrogen content and a weak indirect association with silicon content. Residual gas content shows a direct association with volatile matter, calorific value, collodetrinite, the detrovitrinite sub-group and the 'organically associated' elements iron, calcium, magnesium, sodium and sulphur. Associations with residual gas contents are mostly indirect, for example with collotelinite, the telovitrinite sub-group and the elements identified as being 'inorganically associated'- silicon, aluminium, titanium and phosphorous. The associations between residual gas content and coal properties suggest that less gas is retained in the coal when there are higher contents of structured vitrinite and inorganic matter present.

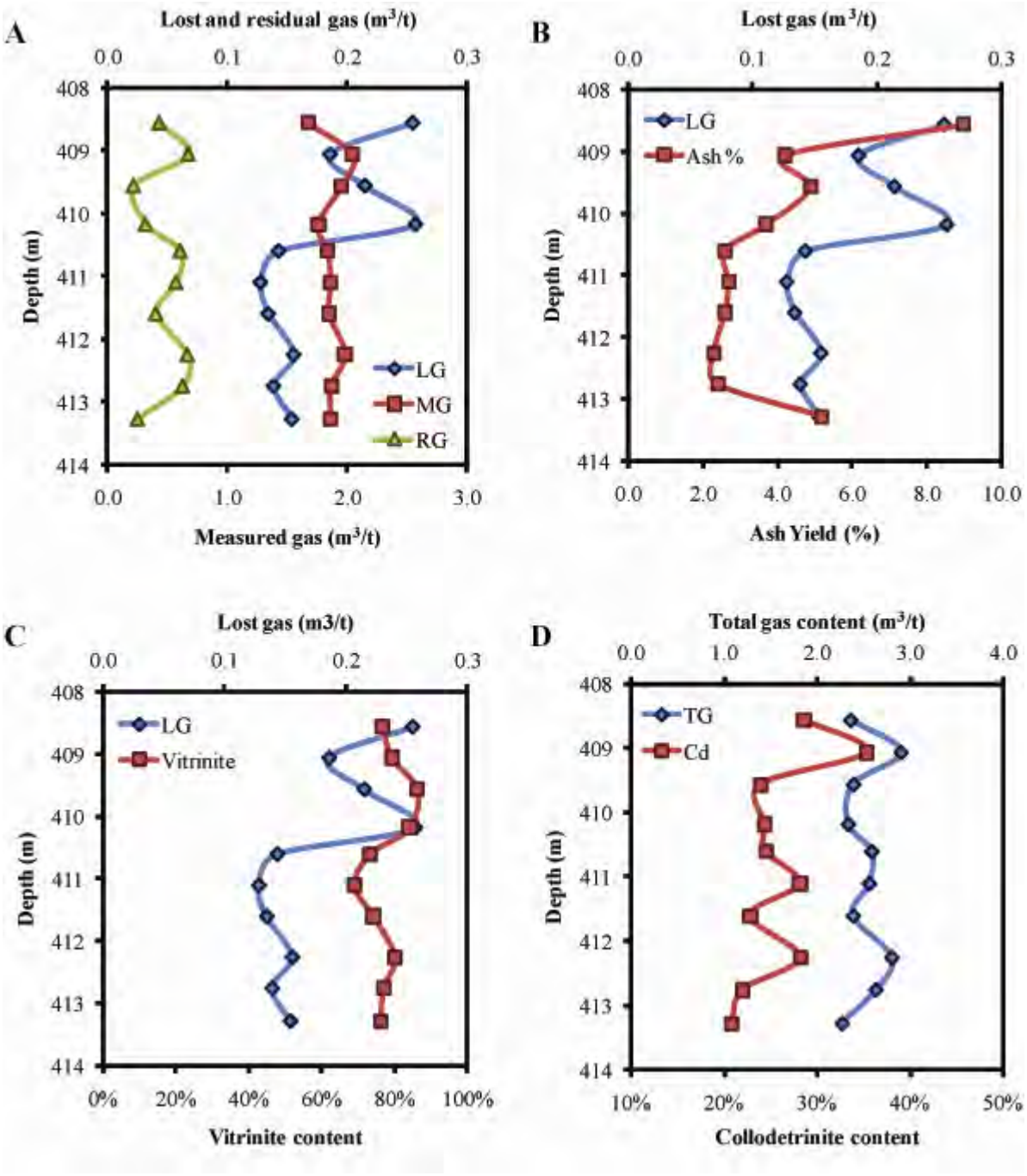

Figure 7. 7. All figures present data from the Renown seam at the Jasper 1 location (A) Lost, measured and residual gas content (aa). (B) Lost gas content (aa) and ash yield (aa). (C) Lost gas (aa) and vitrinite content (mmf). (D) Total gas content (aa) and collodetrinite content (mmf). LG = lost gas content, MG = measured gas content, RG = residual gas content, TG = total gas content, Cd = collodetrinite.

Similar to measured and residual gas contents, total gas content shows a positive association with volatile matter, calorific value and hydrogen content. Calorific value in the Jasper 1 core has a correlation coefficient of 0.91 with hydrogen content and 0.68 with

volatile matter. Hydrogen has been previously shown to be correlated with volatile matter (Section 3.6.1). In addition total gas content shows a direct association with telinite, collodetrinite (see Fig. 7.7D) and the 'organically bound' elements iron, calcium and magnesium. Likely the association with organically bound elements exists as these elements are primarily related to the matrix material (Section 4.4.1). As seen for residual gas content, total gas content shows an indirect association with collotelinite, the telovitrinite sub-group and the 'inorganically bound' elements silicon, aluminum, titanium and phosphorous. The lost gas content shows a very similar trend to the total gas content profile (Fig. 7.7). Possibly the gas is being preferentially retained in the matrix material in situ. The results presented in this section agree with the relationship identified in Figure 7.6.

Very few associations can be seen with adsorption capacity when all samples are included. Adsorption capacity has a direct association with oxygen content and sporinite and an indirect association with moisture content and potassium. When sample J6 is excluded the association with oxygen disappears. Unfortunately as sample J6 has one of the lowest oxygen contents, potential oxidation does not explain the difference in adsorption capacity. When J6 is excluded, adsorption capacity shows a direct association with volatile matter, sporinite, funginite, inertodetrinite and the inertinite group. Adsorption capacity is compared with sporinite and inertinite in Figure 7.8. With the exception of sample J6, which has the highest inertinite content, trends appear to be very similar particularly for the lower part of the core (J7 – J11). Sporinite contributes only up to 2% of the total coal composition while funginite, inertodetrinite and the inertinite group contribute up to 4%, 7% and 13% respectively. Possibly as the components are minor contributors to the overall composition, when considered together they may indicate that the environmental conditions in which the peat formed may exert influence upon the resultant coal structure and subsequent adsorption

capacity. Adsorption capacity (excluding J6) shows an indirect association with moisture, sulphur, collotelinite, the telovitrinite sub-group, the vitrinite group, porigelinite, aluminium, potassium, titanium and phosphorous. Interestingly these macerals and elements can be grouped into structured tissues and the elements thought to be bound within structured tissue (Sections 4.4.1 and 4.4.3).

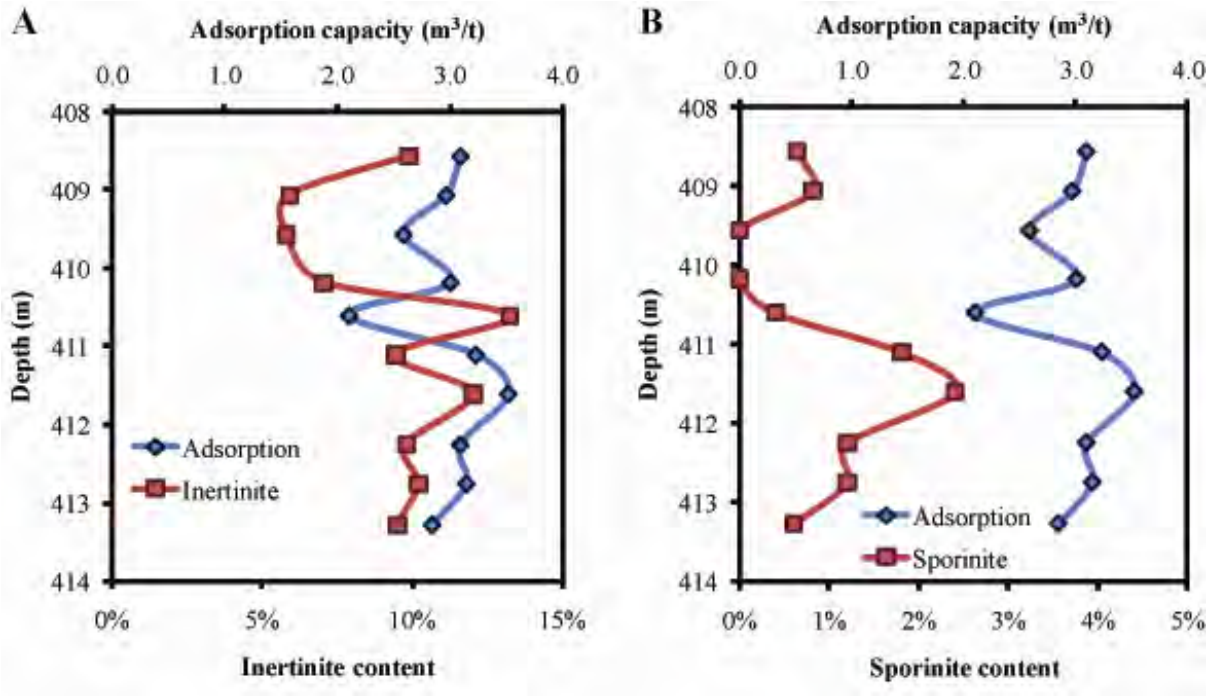

Figure 7. 8. (A) Adsorption capacity (aa) and inertinite content (mmf), and (B) adsorption capacity (aa) and sporinite content (mmf) in the Jasper 1 Renown seam core.

To further define the associations of gas content and adsorption capacity with coal properties, cluster analysis (including sample J6) was conducted and the results are presented as a dendrogram, which groups variables by similarity (Fig. 7.9).

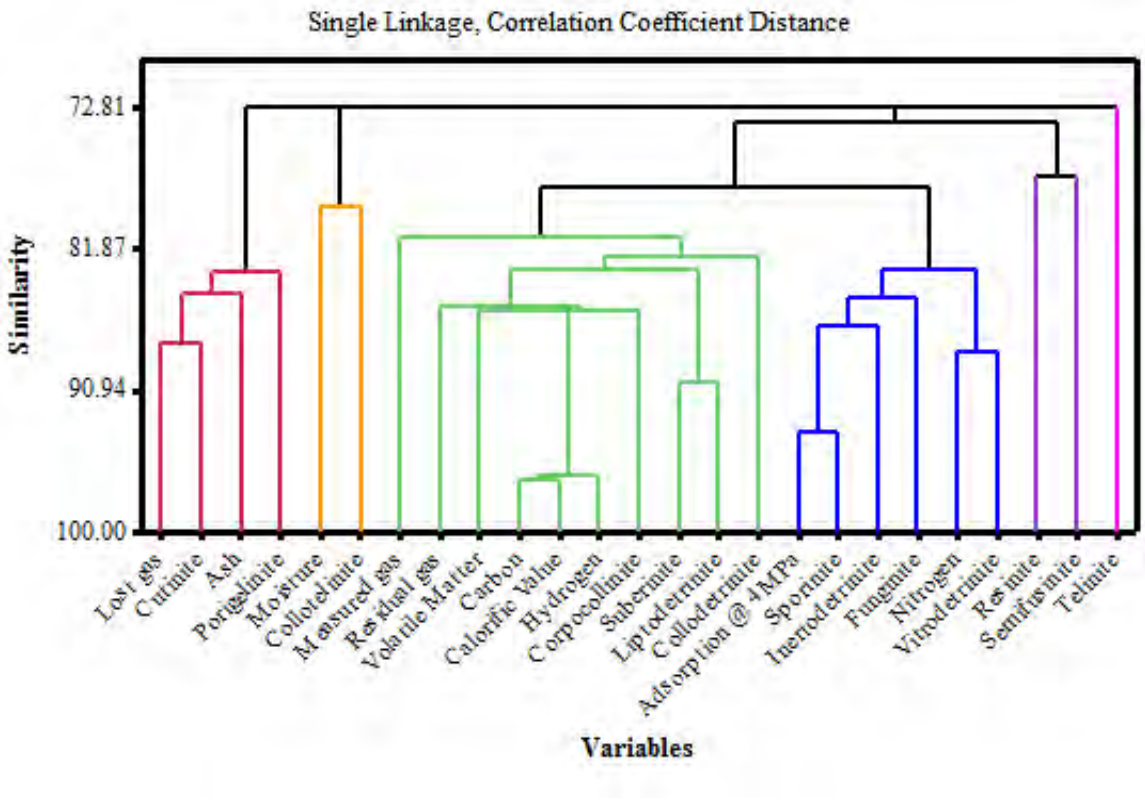

Figure 7. 9. Dendrogram presenting the results of cluster analysis of data from the Renown seam at the Jasper 1 location.

In the first (red) cluster, lost gas content is grouped with ash yield, cutinite and porigelinite while the in the orange cluster collotelinite is grouped with moisture. These two clusters and telinite are somewhat separate from the three remaining clusters. Measured and residual gas contents fall into the green cluster which includes volatile matter, hydrogen and calorific value as well as corpocollinite, suberinite, liptodetrinite and collodetrinite. The variables in the green cluster agree well with the correlation table results (Table 7.5). The blue cluster shows the variables most similar to adsorption capacity, as explained below. The blue cluster includes the macerals sporinite, inertodetrinite, funginite and vitrodetrinite. This cluster of macerals is the same as the group identified in Section 4.4.2 as being highest in the non-banded coal type, suggesting texture (and thus probably influences from the original

depositional environment) is the predominant control on adsorption capacity. Finally in the purple cluster, resinite is grouped with semifusinite.

7.3.2. Kupakupa seam- Ruawaro 2

Gas content is compared with coal properties for the Ruawaro 2 Kupakupa seam in Table 7.6. Lost, measured and residual gas content profiles are presented in Figure 7.10A. Sample B20 shows the highest lost gas content and one of the lowest residual gas contents suggesting this sample has a high gas desorption rate and poor gas retention. The reason for this is unclear. The B20 sample is BNB coal with the highest inertinite content, one of the highest detrovitrinite contents and the lowest telovitrinite and gelovitrinite contents of all the samples in this seam intersection.

Lost gas content shows a weak direct association with carbon content, collodetrinite, the detrovitrinite sub-group, funginite, the inertinite group, calcium, magnesium and manganese. Unlike the Jasper 1 Renown seam intersection, only one sample has an ash yield of >3%. The inertinite group contributes up to 7% of the coal composition in this seam intersection with funginite contributing up to 4%. The strongest direct correlation for lost gas is with funginite (Fig. 7.10B) however the similarity between the trends is weak. Lost gas content shows an indirect association with total sulphur, corpocollinite, the gelovitrinite sub-group, liptodetrinite and the liptinite group.

Table 7. 6. Correlation table comparing proximate analysis (aa), ultimate analysis (db), organic petrology and data (mmf) with gas content (aa) for the Kupakupa seam at the Ruawaro 2 location. Variables with correlations >0.50 have been highlighted in yellow.

	Lost gas (m^3/t)	Measured gas (m^3/t)	Residual gas (m^3/t)	Total gas (m^3/t)
Moisture	0.25	0.32	-0.59	-0.27
Ash yield	-0.41	-0.12	-0.62	-0.85
Volatile matter	-0.14	-0.11	0.34	0.22
Fixed Carbon	0.33	-0.01	0.54	0.64
Calorific value	-0.02	-0.16	0.64	0.51
Sulphur	-0.54	-0.27	-0.43	-0.84
Carbon (db)	0.52	0.23	0.38	0.73
Hydrogen (db)	0.37	0.23	-0.19	0.10
Nitrogen (db)	-0.58	-0.45	0.59	0.07
Vitrinite	0.39	-0.16	0.63	0.61
Liptinite	-0.56	-0.08	-0.47	-0.70
Inertinite	0.51	0.60	-0.31	0.36
Telinite	0.25	0.07	0.02	0.15
Collotelinite	-0.37	-0.17	-0.20	-0.46
Telovitrinite	-0.36	-0.17	-0.20	-0.45
Corpocollinite	-0.67	-0.80	0.32	-0.57
Porigelinite	-0.22	0.19	-0.01	0.12
Gelovitrinite	-0.76	-0.67	0.30	-0.49
Collodetrinite	0.54	0.34	0.11	0.56
Vitrodetrinite	0.18	-0.10	0.32	0.29
Detrovitrinite	0.51	0.12	0.38	0.63
Cutinite	-0.38	0.12	-0.38	-0.37
Suberinite	-0.30	-0.49	0.37	-0.14
Sporinite	-0.10	0.29	-0.58	-0.37
Resinite	-0.31	-0.11	-0.42	-0.62
Liptodetrinite	-0.56	-0.01	-0.48	-0.65
Semifusinite	0.34	0.31	-0.01	0.36
Funginite	0.65	0.44	-0.10	0.47
Inertodetrinite	-0.03	0.42	-0.44	-0.07
SiO_2	-0.47	-0.80	0.30	-0.55
Al_2O_3	-0.27	0.11	-0.69	-0.69
Fe_2O_3	0.48	0.26	0.45	0.83
CaO	0.56	0.62	0.16	0.88
MgO	0.53	0.38	0.29	0.78
Na_2O	0.38	0.09	0.46	0.67
K_2O	0.03	-0.12	0.22	0.13
TiO_2	-0.23	0.11	-0.68	-0.67
Mn_3O_4	0.51	0.52	0.18	0.79
SO_3	0.46	0.50	0.28	0.87
P_2O_5	-0.30	0.06	-0.70	-0.75

Similar to the Jasper 1 location, measured gas in the Ruawaro 2 Kupakupa core showed very few associations. Measured gas showed a direct association with inertinite content (Fig. 7.10C), calcium, magnesium and sulphur and an indirect association with corpocollinite, the gelovitrinite sub-group and silicon.

Residual gas content shows a direct association with fixed carbon, calorific value, nitrogen and vitrinite content (Fig. 7.10D) and an indirect association with moisture content, sporinite, ash yield, aluminium, titanium and phosphorous. Like the Jasper 1 location, total gas content shows similar associations to residual gas content. Total gas content shows direct associations with fixed carbon, calorific value, carbon, collodetrinite, the detrovitrinite sub-group (Fig. 7.10E), the vitrinite group and the 'organically associated' elements iron, calcium, magnesium, sodium, manganese and sulphur. Calorific value in the Ruawaro 2 core has a correlation coefficient of 0.88 to volatile matter and only 0.41 to hydrogen content. As discussed previously there is concern with regards to the integrity of the hydrogen data for the Ruawaro 2 Kupakupa core. The combination of direct associations for total gas content is actually not that different to what is seen in the Renown seam for the Jasper 1 core. Total gas content shows indirect associations with corpocollinite, resinite, liptodetrinite, the liptinite group, ash yield and the 'inorganically bound' elements silicon, aluminium, titanium and phosphorous. The combination of liptinite and ash yield agrees with the associations identified for the Kupakupa seam in Table 4.7.

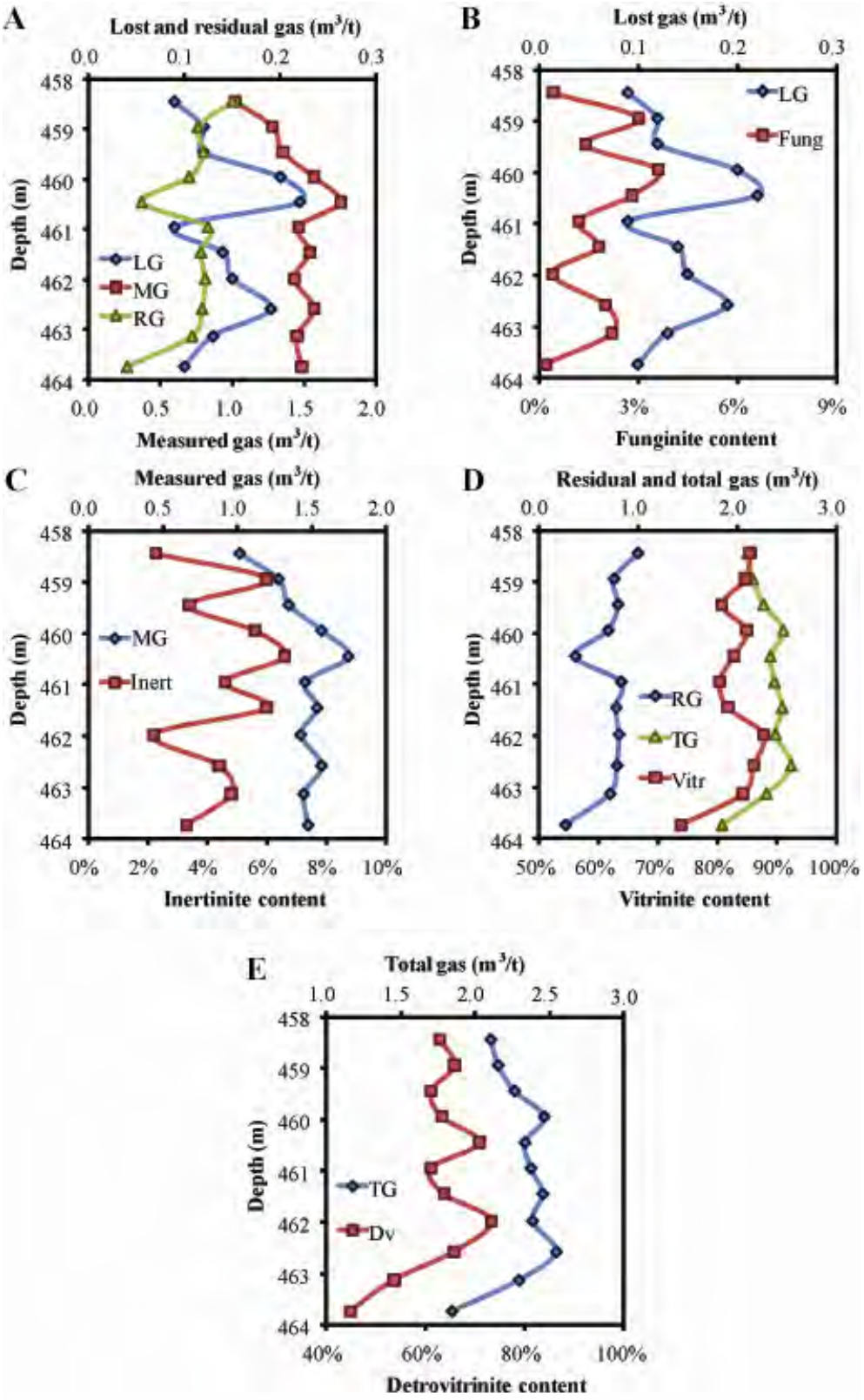

Figure 7. 10. All figures present data from the Kupakupa seam at the Ruawaro 2 location (A) Lost, measured and residual gas content (aa). (B) Lost gas content (aa) and funginite content (mmf). (C) Measured gas content (aa) and inertinite content (mmf). (D) Residual and total gas contents (aa) and vitrinite content (mmf). (E) Total gas content (aa) and detrovitrinite content (mmf). LG = lost gas content, MG = measured gas content, RG = residual gas content, TG = total gas content, Fung = funginite, Inert = inertinite, Vitr = vitrinite, Dv = detrovitrinite.

Gas content and coal property data from the Ruawaro 2 Kupakupa core was subjected to cluster analysis with the results presented as a dendrogram grouping variables by similarity in Figure 7.11. Two major clusters can be identified. The first cluster (red) includes gas content (lost, measured and residual), hydrogen, volatile matter and calorific value as well as the macerals collodetrinite, vitrodetrinite and funginite. Collodetrinite and vitrodetrinite are the predominant macerals in all samples (Section 4.3.1). The second major cluster includes ash yield, the liptinite macerals and macerals associated with structured tissue- collotelinite, porigelinite, corpocollinite and telinite. The clustering of variables in this way suggests that gas content is more associated with hydrogen and the coal matrix material than with structured tissue. This possibility is also consistent with the relationship seen in Figure 7.6.

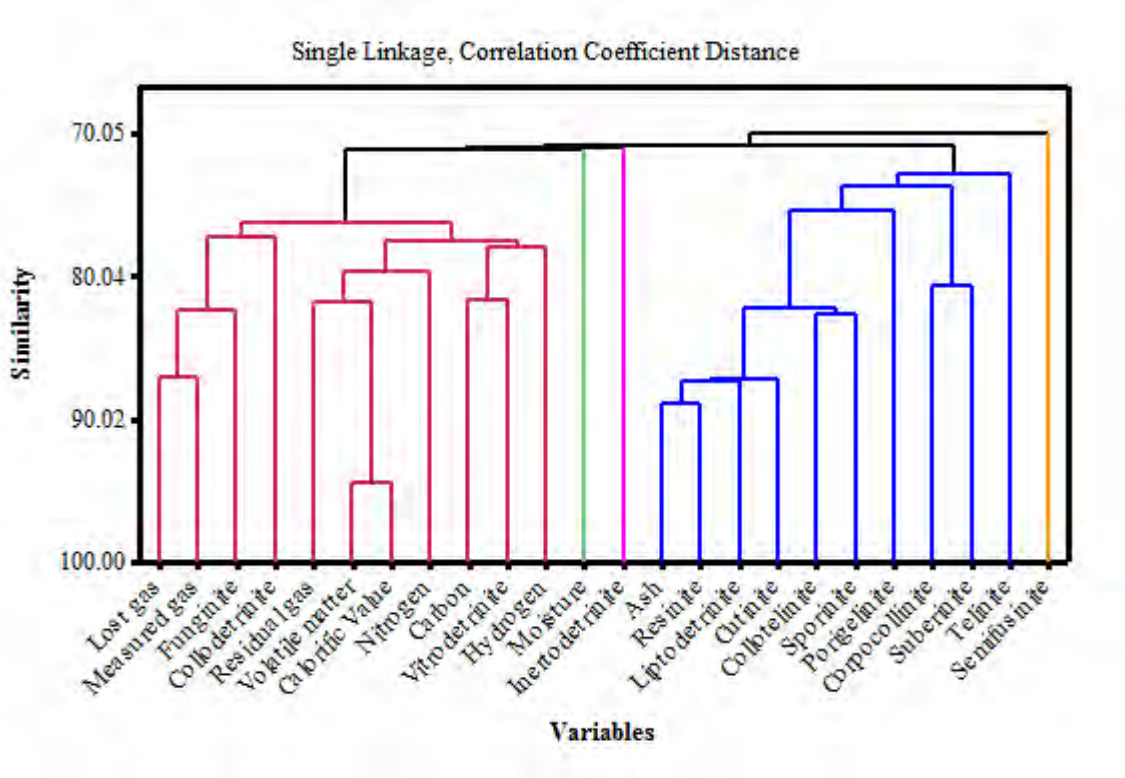

Figure 7. 11. Dendrogram presenting the results of cluster analysis of data from the Kupakupa seam at the Ruawaro 2 location.

7.4. Gas properties and microstructure

Acknowledging that there are a limited number of samples analysed in this study, correlation tables were used to look for statistical associations between coal microstructure and gas properties. Table 7.7 lists correlation coefficients between pairs of gas desorption and adsorption parameters and various microstructural parameters of matrix samples. The table uses the average seam gas content (no ash yield >20%) for each location, and isothermal adsorption data obtained for five coals (as there are no counterpart SAS data for the Mangapiko 1 Renown coal sample). These gas properties are compared to microstructural quantifiers of the corresponding matrix SAS samples (where the properties of the two samples for Mimi 1 and Jasper 1 were averaged).

Total gas content shows a direct association with all porosity sizes (regardless of reported basis) and is more strongly associated with the larger pore sizes (Table 7.7). No association is present between SSA and total gas content. When methane and carbon dioxide holding capacities are compared on a dry ash-free (daf) basis, direct associations can be seen with both microporosity and total porosity, with methane holding capacity also linked to macroporosity. In contrast, when using “as analysed” values, holding capacities for carbon dioxide are indirectly associated with SSA, microporosity, mesoporosity and total porosity, whereas holding capacity for methane continues to be directly associated with macroporosity and mesoporosity. Because the Huntly coals have very low inorganic matter content, the difference between “as analysed” holding capacities and the adsorption capacities recalculated to dry ash-free basis must predominantly be caused by moisture. From the results in Table 7.7 it appears that micropores are particularly affected.

Table 7. 7. Correlation table comparing gas adsorption capacities with coal microstructure.

	Total gas content		Adsorption capacity at 4 MPa			
	aa	daf	CH_4 aa	CH_4 daf	CO_2 aa	CO_2 daf
SSA at 4 Å	0.09	0.11	-0.73	0.27	-0.64	0.45
Microporosity	0.52	0.55	-0.2	0.59	-0.77	0.86
Mesoporosity	0.70	0.71	0.64	0.22	-0.74	0.2
Macroporosity	0.66	0.64	0.62	0.74	0.14	0.32
Meso + Macroporosity	0.89	0.89	0.83	0.57	-0.49	0.33
Total Porosity	0.79	0.81	0.22	0.7	-0.79	0.79

7.5. Discussion

7.5.1. Ash yield and gas content

It has been previously recognized that the coal seams of the Waikato coalfields have very low ash yields of generally <10% (Edbrooke et al., 1994). This was confirmed in this study (Chapter 3) for the Huntly coalfield, with the majority of samples yielding <5% ash. However, ash yield does vary considerably in the samples studied (from 1 to 69%) and as ash yield increases, gas volume decreases. This indirect relationship is to be expected as methane has been recognized to adsorb to the organic components of coal, while increasing mineral matter content acts as a diluent to gas sorption capacity resulting in a reduction in gas content (Laxminarayana and Crosdale, 1999; 2002; Warwick et al., 2008; Yee et al., 1993). These results are consistent with previous work on New Zealand coals (Butland, 2006; Butland and Moore, 2008; Moore and Butland, 2005; Newman et al., 1997). However, when ash yield is less than 10%, variation in gas content seems to be unrelated to ash yield. As discussed in previous chapters when ash yield is low it is more likely that the majority of elements are organically bound within the coal rather than being present as mineral matter. Considering

the low ash yields of the Huntly coals it is reasonable to assume that when ash yields are less than 10% inorganic material has a minimal control on the total gas content.

7.5.2. Macroscopic texture and gas content

The ANOVA analysis of the normalized data set for the Huntly coalfield suggests that the higher methane contents are associated with the least banded (bright, non-banded) coal type. This is further supported by: (1) the greater percentage of the bright, non-banded coal type and a higher average gas content in the Renown seam than the Kupakupa seam, and (2) the greater percentage of the bright, non-banded coal type and a high average gas content in the Renown seam at the Beverland Road site, which has significantly more gas, than the Renown seam at the other locations. This is in contrast to the Powder River Basin studies where the highest gas contents were associated with the highest proportions of vitrain bands in low (<5%) inertinite coal (Moore et al., 2001). Additionally, Stricker et al. (2006) suggested that there was greater gas storage capacity in the more woody parts of the coal. It was proposed that the woodier parts maintain structure and potentially greater porosity. That there is greater porosity available in the structured material (vitrain) than matrix in the Huntly coalfield is confirmed in Chapter 5. In the Jasper 1 Renown seam core, telovitrinite is identified as being indirectly related to residual and total gas content suggesting that gas may move out of the structured tissue because of the porosity and is preferentially retained in the matrix material (Figs. 7.9).

When considering average phi size versus total gas content by seam, the indirect association recognized for the Renown seam suggests that gas content is highest in the finer/least banded coal type. It can also be seen for the Beverland Road drill hole samples that

the average phi size for vitrain is finer than the average of the other sites where the Renown seam was analysed. However the Kupakupa seam exhibits the opposite association between band thickness and gas content. That is, greater gas content is associated with the coarser banded material. Like the Kupakupa seam, it was recognized in the Powder River Basin that there was some correlation between higher gas contents and increased vitrain band thickness (Flores et al., 2001), suggesting that variability of methane gas content in those coals are influenced by textural changes (Moore et al., 2001). Possibly in the Huntly coalfield, the differing environmental conditions between the seams at the time of formation (as suggested in Chapter 4) resulted in different vitrain band characteristics, as certainly the Renown seam is less banded than the Kupakupa seam. It is also possible that the thin nature of the bands present in the Huntly coalfield, particularly those associated with the finer banded coal types, may be too limited in extent and frequency to provide significant gas storage. Alternately, the open porosity that can exist within the bands could have been substantially degraded, compacted or infilled with resins (Chapter 4 found half of the pores contained fluorescent infillings). It is interesting to note that voids (i.e. porosity) can be seen macroscopically in the Powder River Basin coals (Stanton et al., 1989; Warwick and Stanton, 1988) while in the Huntly coal seams, voids can only be seen microscopically.

Previous studies that have considered the relationship of coal type to methane storage capacity have generally compared bright or vitrinite-rich coals to dull or inertinite-rich coals. Vitrinite-rich coals have been generally been found to have greater methane adsorption capacity than inertinite-rich coals for coals of the same rank (Crosdale and Beamish, 1993; Crosdale et al., 1998; Lamberson and Bustin, 1993). In contrast, Hackley et al. (2007) found no relationship between coal type (though the study was based only on maceral composition with no macroscopic analysis) and gas storage. It is difficult to compare these studies to the

Huntly coalfield as all the coal types presented here, and New Zealand coals in general, are predominately vitrinite-rich (>80%) in composition and hence are all bright coals (Beamish et al., 1998; Edbrooke et al., 1994; Sherwood et al., 1992).

7.5.3. Microstructure and gas content

It is thought that moisture influences gas holding capacity in coal by either competing with gases for adsorption sites or blocking access to some of the micropores (Bustin and Clarkson, 1998; Day et al., 2008c; McElhiney et al., 1993; Prinz and Littke, 2005). Moisture content has previously been found to be critical in evaluating the storage capacity of the Huntly coals (Crosdale et al., 2008).

Coals are considered to be hydrocarbon wet, and water molecules are thought to attach to polar sites on the pore wall (Day et al., 2008c). However, a comparison of neutron scattering and X-ray scattering data (Section 5.4.4) provides pore-size-specific information about the location of inorganic matter in Huntly coals: it is concentrated in pores within the size range 12.5-125 Å. Therefore, as water adsorption sites seem to be located preferentially in pores of certain sizes, moisture tends to condense in these water-wet regions thus blocking access to micropores for gases. The phenomenon could potentially be greater in the vitrain material than the matrix material.

It has been suggested that although pores <100 nm in diameter are favourable for gas adsorption, they are not favourable for coal permeability (Liu et al., 2009; Yao et al., 2008). Considering the possibility of water blocked micropores and potentially limited connectivity with mesopores (2 – 50 nm in diameter) it is likely that smaller pores do not contribute to

porosity and permeability tested in the field. For coals from the Czech Republic, Hemza et al. (2009) suggests that while macropores are important for total gas content, the micropores do not markedly contribute to the gas content of the coal seams. It was found that regardless of the volume of micropores, the amount of gas contained in the coal could be correlated with other parameters and processes that are determined by the geological history of the given coal bed (Hemza et al., 2009).

7.5.4. Controls on gas properties in the Huntly coalfield

Strapoc et al. (2008a) suggested that gas content is controlled by the amount of gas generated, adsorbed and preserved by the coal. The question raised by the current data set is whether the gas content differences in relation to macroscopic texture are because the non-banded coal type successfully retains more gas, as it has a greater storage capacity, or whether its composition contributes to biogenesis. For the Renown seam at the Jasper 1 location it appears both of these are possibly true while for the Kupakupa seam at Ruawaro 2 it may be a little more complicated.

It appears that hydrogen content is having some control on gas content, possibly acting as a food source for the methanogenic consortia. Budwill and Muehlenbachs (2007) found in growth experiments of methanogenic cultures, using deuterated water and coal as the carbon substrate, that only two of the hydrogen molecules in the produced methane were sourced from the water (via the CO_2 reduction pathway). This suggests that the other two hydrogen molecules are synthesised from the coal. Previous studies had suggested that most of the hydrogen was sourced from the formation water (Budwill, 2003; Gorody, 1999).

Figure 7.6 shows greater gas content in the bright non-banded coal than in the more banded coal types while, in Figures 7.9 and 7.11, gas content is clustered separately from telovitrinite. Together these figures suggest that the non-banded (matrix-dominated) coal type retains more gas. This is possibly because the vitrain bands act as: (1) gas conduits, (2) that their porosity is clogged by moisture or resins or (3) that there is lower hydrogen content in telovitrinite material. It has previously been reported that hydrogen content is higher in collodetrinite than other vitrinite macerals in Waikato coals (Shaw, 1997). Alternately, as the vitrain samples used for the microstructural study were collected from larger vitrain bands (>3 mm in diameter) their structure integrity (and higher porosity contents) may be better maintained than thinner vitrain bands more typical of the Huntly coal field.

In Chapter 4 it is suggested that the Renown seam formed in a more variable, geochemically degradational (to organic components) environment than the Kupakupa seam. This environment resulted in the coal being higher in matrix constituents and inertinite content. In Chapter 6 the Renown seam (which has a greater proportion of non-banded material) is shown to have a greater adsorption capacity than the Kupakupa seam. In addition, Figure 7.9 shows that adsorption capacity is associated with vitrodetrinite, sporinite, funginite and inertodetrinite. The percentage of these macerals is shown (in Chapter 4) to decrease as the degree of banding increases. It is therefore proposed that gas adsorption capacity is a function of coal texture, which is ultimately controlled by the original plant types and the environment of deposition. This agrees with work by Crosdale et al. (1998) who suggested that coal rank and type are not the critical factors controlling gas adsorption capacity, but rather it is the influence they exert over pore structure development that is important.

7.6. Conclusions

In this chapter coal compositional, petrological and microstructural information presented in Chapters 4, 5 and 6 have been compared to the gas data presented in Chapter 7. Conclusions are as follows:

- There is an indirect association between ash yield and gas content when ash yield is >10%, however there is no relationship when ash yield is <10%.
- When the dataset was normalized to remove any location specific bias, an association between coal type and gas content was recognized with the higher gas contents linked to the bright, non-banded coal type and the lower gas contents with the bright, highly banded coal type. An ANOVA test of the two extremes (bright, non-banded and bright, highly banded) showed a statistical difference between the two end member coal types. This is in contrast to previous studies on low rank coals in the Powder River Basin (Flores et al., 2001; Moore et al., 2001).
- An indirect association was identified between average phi size and average gas content in the Renown seam; this relationship is supported at the macroscopic level, where the highest gas contents are associated with the least banded coal types. However, the Kupakupa seam appears to show a direct association. This difference might be explained by textural or porosity differences of the vitrain bands between the two seams.
- For both seams, cluster analysis identified that total gas content variability is associated with hydrogen content, volatile matter and calorific value as well as collodetrinite and some other macerals which form the coal matrix. The structured vitrinite maceral collotelinite is not correlated to gas properties for either seam.

- Cluster analysis of the Jasper 1 Renown seam core shows that gas adsorption capacity at reservoir pressure is correlated with vitrodetrinite, sporinite, funginite and inertodetrinite contents. These macerals were identified to increase as banding decreased, i.e. they are highest in the non-banded coal type (Chapter 5).
- Holding capacities for methane and carbon dioxide on a dry, ash-free basis were found to be correlated with microporosity. However, for "as analysed" gas holding capacities, there was no correlation between methane and microporosity data, whereas the carbon dioxide data were negatively correlated with both SSA and microporosity. This is thought to be caused by moisture which is likely concentrated in the pore size range 12.5-125 Å. Both dry ash-free and "as analysed" methane holding capacity showed positive correlation with macroporosity, suggesting that gas holding capacity is affected by the presence of moisture blocking access to gas adsorption sites in smaller pores.
- It is proposed that hydrogen content (which may be a food source for methanogens) could be a control on gas content. Additionally, it appears that gas is preferentially stored (or more successfully retained) in the matrix material of the coal. Adsorption capacity appears to be controlled by coal texture which is a function of the environment of deposition.

Chapter Eight

Conclusions

This study has presented and interpreted a dataset generated by analyses of ~84 m of coal core collected from the subbituminous Huntly coalfield in the North Island of New Zealand. Results include data from proximate analysis, ultimate analysis, ash constituents, macroscopic logging, organic petrology, gas desorption, gas adsorption, gas isotopes and gas composition, most of which were conducted on 0.5 m coal intervals. In addition, a microstructural study was conducted on selected matrix and vitrain samples using small angle scattering techniques. These data have allowed a few conclusions to be made about the gas coal properties of Kupakupa and Renown seams in the Huntly coal field. In addition, observations regarding sample collection for gas properties have been made.

8.1. Sample collection and data integrity

The results on sample collection and data integrity with regards to adsorption isotherms should be of particular interest to industry and explorers of CBM in low rank coalfields. It was found that adsorption samples should be collected as fresh as possible from the field and not left for collection until after gas desorption analysis. Delaying sample retrieval yielded substantially larger holding capacities which in turn can (negatively) effect saturation calculations, a key field assessment parameter. This change in holding capacity with time is likely a result of sample moisture loss and oxidation. For further detail on this subject readers should look to Crosdale et al. (2008).

Additionally, considerable variation in both gas adsorption and gas desorption properties can be seen within a seam intersection within a single drill hole. This vertical variation is also echoed by lateral variation of gas properties within a single seam. For the Jasper 1 Renown seam core, gas adsorption capacity was found to vary from 2.20 m^3/t to 3.66 m^3/t and total gas content from 2.42 m^3/t to 3.01 m^3/t. These adsorption and desorption results led to calculated saturation varying from 66% to 120%. As a CBM well draws from the whole seam interval a seam average is more desirable than single data points and clearly, from these results, more than one sample should be collected. The current study found that at least three gas adsorption and gas desorption samples, as well as three gas saturation calculations, would be required to be within one standard deviation (~10%) of the overall group mean. A more statistically rigorous version of this work (Mares et al., 2009) found that at least five samples for each analyses should be collected for the calculated saturation to be within the same level of uncertainty.

8.2. Inorganic constituents in the Huntly coalfield

Ash yield was shown to adversely affect gas content when >10%. Most of the samples in the dataset (90%) had ash yields of less than 10% hence; ash yield is not the dominant control on gas content in the Huntly coalfield. On average the Renown seam has a higher ash yield than the Kupakupa seam. In addition, ash yield increased along with the degree of vitrain banding. Detrital and diagenetic quartz, detrital clay, epigenetic carbonates (likely calcite and ankerite), iron oxides and syngenetic pyrite were identified in the organic petrology study. However, mineral matter counts (using optical microscopy) were very low and it is thought that the majority of the ash yield for the Huntly coal is contributed by organically associated elements.

From ash constituent analysis, silicon was thought to be associated with ash yield, while iron, calcium, magnesium, sodium and sulphur were primarily associated with organic material. Aluminium, potassium, titanium, manganese and phosphorous showed unclear relationships and hence likely have mixed associations. Cluster analysis placed the ash constituents into two groups, an ‘inorganically associated’ group which included silicon, aluminium, titanium and phosphorous and an ‘organically associated’ group which included iron, calcium, magnesium, sodium, manganese and sulphur. The ‘inorganically associated’ elements were present in greater proportions in the Renown seam as well as the highly banded coal type. Aluminium, titanium and phosphorous showed some association to structured tissue while silicon did not. This association suggests that while silicon is frequently present in more banded coal it is not intimately associated with the plant material.

Microstructural analysis on matrix and vitrain samples from the Huntly coalfield found that there is inorganic matter located in the 12.5 Å < *r* < 125 Å pore size range. The inorganic matter had greater influence on X-ray scattering curves in the vitrain samples than the matrix samples suggesting that inorganic material is present in the more structured tissues. The inorganic material is thought to be present as inorganic coatings, shaped as either spherical shells or hollow cylinders. A previous study where inorganic material was identified in this size range suggested that the inorganic material maybe clay (Radlinski et al., 2004b). However, the almost complete absence of silicon identified by Li et al. (2009) in coal macerals from the Huntly coalfield and the lack of association identified between silicon and structured tissue suggests otherwise. It is thought that the inorganic material was held in the original plant material rather than being precipitated post deposition.

8.3. Coal type distribution in the Huntly coalfield

Three coal types were identified in the Huntly coalfield, defined by the proportion of vitrain bands present, (1) bright lustre, non-banded, (2) bright lustre, moderately banded and (3) bright lustre, highly banded. The average phi size (diameter of the shortest dimension) of the vitrain bands increases as the proportion of banding increases, however in general the bands are thin. The bright non-banded coal type was predominant in the Renown seam while the more banded coal types were dominant in the Kupakupa seam. As the degree of banding increases, the amount of structured vitrinite macerals increases and the amount of vitrodetrinite decreases.

Similar to the difference in coal type distribution between the seams, overall the Kupakupa seam has more vitrain bands and more structured vitrinite than the Renown seam.

In contrast, the Renown seam has almost double the inertinite component of the Kupakupa seam, which is predominantly within the non-banded coal type. Inertodetrinite and funginite are the most common inertinite components. It is thought that the presence or absence of vitrain bands is controlled by the degree of tissue preservation rather than mire flora.

8.4. Coal microstructure

The total porosity of coal samples from the Huntly coalfield was found to vary from 16% to 25%. Microporosity contributed 45% - 60% of the total porosity while macroporosity contributed 9% - 25%. Specific surface area ranges from 1.25 x 10^6 cm^{-1} to 2.88 x 10^7 cm^{-1} and is predominantly contributed by the micropores. On average the vitrain samples have larger total porosities than the matrix samples, with a greater amount of mesopores. In addition, the vitrain samples had higher specific surface areas than the matrix samples.

For both methane and carbon dioxide gases, storage capacity (daf) was found to be correlated with microporosity. However, for “as analysed” gas holding capacities, there was no correlation between methane and microporosity data, while the carbon dioxide data was negatively correlated with both SSA and microporosity. In both bases, methane holding capacity showed positive correlation with macroporosity. It is thought that gas holding capacity is affected by the presence of moisture blocking access to gas adsorption sites in smaller pores.

8.5. Controls on gas properties

Although there existed considerable variation, on average the Renown seam was found to have higher total gas content and a higher adsorption capacity than the stratigraphically lower Kupakupa seam. Gas content was found to be highest in the non-banded coal types and lowest in the highly banded coal type. In addition to being the predominant coal type in the Renown seam, the bright non-banded coal type represents the largest proportion of the coal present in the Renown seam at the Beverland Road site. The Beverland Road site has significantly higher gas contents than the other locations.

Hydrogen content was found to have a good correlation with volatile matter and calorific value. These parameters were correlated to gas content in the Renown seam and to a much lesser degree in the Kupakupa seam. When a cluster analysis was conducted in both seams, measured gas content was clustered with hydrogen, volatile matter, calorific value and collodetrinite with the telovitrinite macerals clustered separately. Considered with the coal type association, gas appears to be preferentially retained in the matrix-dominated material. As vitrain bands were found to have greater porosity and surface area than matrix material, possibly the vitrain bands act as conduits or alternately contain more moisture. It is therefore thought that gas content in the Huntly coalfield is controlled by (1) accessibility- the microbes need to be introduced post coalification, (2) food source- the microbes require a food source to generate gas, and (3) preservation- there needs to be storage capacity available to hold the gas and a seal to prevent gas migration. These three factors appear to be influenced by coal type.

Gas holding capacity was found to be unrelated to gas content. This is because gas formation in the Huntly coalfield is generated by a secondary biogenic process, post coalification, while gas holding capacity is a physical property of the coal. A series of adsorption analyses, representing a full seam intersection, was conducted on the Jasper 1 Renown seam. Gas holding capacity has a similar vertical trend to sporinite and inertinite content, which only contribute up to 2% and 13% of the total coal composition respectively. Cluster analysis grouped adsorption capacity with sporinite, inertodetrinite, funginite and vitrodetrinite contents. These macerals are highest in the non-banded coal type and are hence indicative of coal texture which is in turn controlled by the original peat vegetation and the environment of coal deposition.

References

Amijaya, H. and Littke, R., 2005. Microfacies and depositional environment of Tertiary Tanjung Enim low rank coal, South Sumatra Basin, Indonesia. International Journal of Coal Geology, 61: 197-221.

Andrejko, M.J., Raymond, R.J. and Cohen, A.D., 1983. Biogenic silica in peats: possible source for chertification in lignites. In: R.J. Raymond and M.J. Andrejko (Editors), Proceedings of workshop on minerals in peat: its occurrence, form and distribution, pp. 25-37.

ASTM, American Society for Testing and Materials, 2004a. D4239 Standard test method for sulphur in the analysis sample of coal and coke using high temperature tube furnace combustion methods., Annual Book of ASTM Standards: Section 5, petroleum products, lubricants and fossil fuels.

ASTM, American Society for Testing and Materials, 2004b. D4326 Standard test method for major and minor elements in coal and coke ash by X-ray fluorescence., Annual Book of ASTM Standards: Section 5, petroleum products, lubricants and fossil fuels.

ASTM, American Society for Testing and Materials, 2005. D2799-05a Standard test method for microscopical determination of the maceral composition of coal, Annual Book of ASTM Standards: Section 5, petroleum products, lubricants and fossil fuels, vol 05.06 (Gaseous fuels; coal and coke).

Bailey, A.M., Cohen, A.D., Orem, W.H. and Blackson, J.H., 2000. Mobilization of major inorganic ions during experimental diagenesis of characterized peats. Chemical Geology, 166(3-4): 287-300.

Bale, H.D. and Schmidt, P.W., 1984. Small-angle X-ray-scattering investigation of submicroscopic porosity with fractal properties. Physical Review Letters, 53(6): 596-599.

Barker, C.E., Dallegge, T.A. and Clark, A.C., 2002. USGS coal desorption equipment and a spreadsheet for analysis of lost and total gas from canister desorption measurements. Open File Report 02-496.

Beamish, B.B., Laxminarayana, C. and Crosdale, P.J., 1998. Contrasts in methane sorption properties between New Zealand and Australian coals. In: E.Y. Baafi, K. Cram, G.A. Gibson and P. Hanna (Editors), Proceedings of the 1st Australasian Coal Operators Conference COAL98, University of Wollongong, pp. 561-565.

Bechtel, A. Hámor-Vidó, M., Sachsenhofer, R.F., Reischenbacher, D., Gratzer, R. and Püttmann, W., 2007. The middle Eocene Márkushegy subbituminous coal (Hungary):

Paleoenvironmental implications from petrographical and geochemical studies. International Journal of Coal Geology, 72(1): 33-52.

Benzerara, K., Morin, G., Yoon, T. H., Miot, J., Tyliszczak, T., Casiot, C., Bruneel, O., Farges, F. and Brown Jr, G. E., 2008. Nanoscale study of As biomineralization in an acid mine drainage system. Geochimica Et Cosmochimica Acta, 72(16): 3949-3963.

Berkowitz, M., 1979. An introduction to coal technology. Academic Press, New York.

Bernard, S., Benzerara, K., Beyssac, O., Brown Jr, G. E., Stamm, L. G. and Duringer, P., 2009. Ultrastructural and chemical study of modern and fossil sporoderms by Scanning Transmission X-ray Microscopy (STXM). Review of Palaeobotany and Palynology, 156(1-2): 248-261.

Bodden, W.R. and Ehrlich, R., 1998. Permeability of coals and characteristics of desorption tests: Implications for coalbed methane production. International Journal of Coal Geology, 35(1-4): 333-347.

Bonse, U. and Hart, M., 1965. Small-angle scattering by spherical particles of polystyrene and polyvinyltoulene. Applied Physics Letters, 7: 238-240.

Briet, G.N. and Finkelman, R., 1998. Characterisation of coal and coal combustion products from a coal-burning power plant. USGS open file report 98-342.

Bromhal, G.S., Neal Sams, W., Jikich, S., Ertekin, T. and Smith, D.H., 2005. Simulation of CO_2 sequestration in coal beds: The effects of sorption isotherms. Chemical Geology: Geochemical Aspects of CO2 sequestering, 217(3-4): 201-211.

Budge, C.F. and MacKnight, F.J., 1976. Forms of sulphur in New Zealand coals. New Zealand Journal of Science, 19: 237-241.

Budwill, K., 2003. Microbial methanogenesis and its role in enhancing coalbed methane recovery. Canadian Society of Exploration Geophysicists Recorder (November): 41-46.

Budwill, K., Bustin, M., Muehlenbachs, K. and Gunter, W. D., 2005. Characterization of a subsurface coal bed methanogenic culture and its role in coalbed methane recovery and CO_2 utilization, Greenhouse Gas Control Technologies 7. Elsevier Science Ltd, Oxford, pp. 2213-2216.

Budwill, K. and Muehlenbachs, K., 2007. Source of hydrogen from biogenic methane production from coal as revealed by stable isotope analysis of coal enrichment cultures, 2007 GSA Denver Annual Meeting (28–31 October 2007).

Burruss, R.C., 2003. CO_2 adsorption in coals as a function of rank and composition: a new task in USGS research on geologic sequestration of CO2, Coal-Seq II., Washington.

Busch, A., Gensterblum, Y. and Krooss, B.M., 2003. Methane and CO_2 sorption and desorption measurements on dry Argonne premium coals: pure components and mixtures. International Journal of Coal Geology, 55: 205-224.

Bustin, A.M.M. and Bustin, R.M., 2008. Coal reservoir saturation: Impact of temperature and pressure. AAPG Bulletin, 92(1): 77-86.

Bustin, R.M., 2002. Research activities on CO_2, H_2S, and SO_2 sequestration at UBC, Coal-Seq I., Houston.

Bustin, R.M. and Clarkson, C.R., 1998. Geological controls on coalbed methane reservoir capacity and gas content. International Journal of Coal Geology, 38(1-2): 3-26.

Bustin, R.M., Cui, X. and Chikatamarla, L., 2008. Impacts of volumetric strain on CO_2 sequestration in coals and enhanced CH_4 recovery. AAPG Bulletin, 92(1): 15-29.

Bustin, R.M. and Downey, R., 2002. Gas in place analyses, field results, comparisons and suggestions, Third Rocky Mountain Association of Geologists Coalbed Methane Symposium, Denver, Colorado, 3 pp.

Butland, C.I., 2006. Coal seam gas associations in the Huntly, Ohai and Greymouth regions, New Zealand. MSc Thesis, University of Canterbury, Christchurch, 163 pp.

Butland, C.I. and Moore, T.A., 2008. Secondary biogenic coal seam gas reservoirs in New Zealand: A preliminary assessment of gas contents. International Journal of Coal Geology, 76(1-2): 151-165.

Cameron, M.J., 1995. Cleat Structure, Waikato Coal Region. Master of Science Thesis, University of Auckland, Auckland, 101 pp.

Chan, C.S., Fakra, S.C., Edwards, D.C., Emerson, D. and Banfield, J.F., 2009. Iron oxyhydroxide mineralization on microbial extracellular polysaccharides. Geochimica Et Cosmochimica Acta, 73(13): 3807-3818.

Chang, J.-S., Yoon, I.-H. and Kim, K.-W., 2009. Heavy metal and arsenic accumulating fern species as potential ecological indicators in As-contaminated abandoned mines. Ecological Indicators, 9(6): 1275-1279.

Chiarenzelli, J., Aspler, L., Dunn, C., Cousens, B., Ozarko, D. and Powis, K.,2001. Multi-element and rare earth element composition of lichens, mosses, and vascular plants from the Central Barrenlands, Nunavut, Canada. Applied Geochemistry, 16(2): 245-270.

Chou, H.-H., Huang, J.-S., Chen, W.-G. and Ohara, R., 2008. Competitive reaction kinetics of sulfate-reducing bacteria and methanogenic bacteria in anaerobic filters. Bioresource Technology, In Press, Corrected Proof.

Clarkson, C.R. and Bustin, R.M., 1996. Variation in micropore capacity and size distribution with composition in bituminous coal of the Western Canadian Sedimentary Basin: Implications for coalbed methane potential. Fuel, 75(13): 1483-1498.

Clarkson, C.R. and Bustin, R.M., 1997. Variation in permeability with lithotype and maceral composition of Cretaceous coals of the Canadian Cordillera. International Journal of Coal Geology, 33(2): 135-151.

Clarkson, C.R. and Bustin, R.M., 1999. The effect of pore structure and gas pressure upon the transport properties of coal: a laboratory and modeling study. 1. Isotherms and pore volume distributions. Fuel, 78(11): 1333-1344.

Clarkson, C.R. and Bustin, R.M., 2000. Binary gas adsorption/desorption isotherms: effect of moisture and coal composition upon carbon dioxide selectivity over methane. International Journal of Coal Geology, 42(4): 241-271.

Clayton, J.L., 1998. Geochemistry of coalbed gas- A review. International Journal of Coal Geology, 35(1-4): 159-173.

Clemens, A.H., Damiano, L.F., Gong, D. and Matheson, T.W., 1999. Partitioning behaviour of some toxic volatile elements during stoker and fluidised bed combustion of alkaline sub-bituminous coal. Fuel, 78(12): 1379-1385.

Clemens, A.H., Deely, J.M., Gong, D., Moore, T.A. and Shearer, J.C., 2000. Partitioning behaviour of some toxic trace elements during coal combustion- the influence of events occurring during the deposition stage. Fuel, 79(14): 1781-1784.

Close, J.C., 1993. Natural Fractures in Coal. In: B.E. Law and D.D. Rice (Editors), Hydrocarbons from coal. American Association of Petroleum Geologists, Tulsa, Oklahoma, pp. 119-132.

Cody, G.D., Larsen, J.W. and Siskin, M., 1988. Anisotropic solvent swelling of coals. Energy & Fuels, 2: 340-344.

Cohen, A.D., Spackman, W. and Raymond, R.J., 1987. Interpreting the characteristics of coal seams from chemical, physical and petrographic studies of peat deposits. In: A.C. Scott (Editor), Coal and coal-bearing strata: recent advances. Geological Society of America Special Publication 32, pp. 107-125.

Cohen, A.D. and Stack, E.M., 1996. Some observations regarding the potential effects of doming in tropical peat deposits on the composition of coal seams. International Journal of Coal Geology, 29: 39-65.

Connell, L.D., 2008. CO2 sequestration in coal project activity in Australia, The Sixth International Forum on Geologic Sequestration of CO_2 in Deep, Unmineable Coalseams (Coal-Seq VI), Houston, TX.

Cookson, D., Kirby, N., Knott, R., Lee, M. and Schultz, D., 2006. Strategies for data collection and calibration with a pinhole-geometry SAXS instrument on a synchrotron beamline. Journal of Synchrotron Radiation, 13: 440-444.

Crosdale, P.J., 1995. Lithotype Sequences in the Early Miocene Maryville Coal Measures, New-Zealand. International Journal of Coal Geology, 28(1): 37-50.

Crosdale, P.J. and Beamish, B.B., 1993. Maceral effects on methane sorption by coal. In: J.W. Beeston (Editor), New developments in coal geology: A symposium. Coal Geology Group (GSA) Inc, Brisbane, pp. 95-98.

Crosdale, P.J., Beamish, B.B. and Valix, M., 1998. Coalbed methane sorption related to coal composition. International Journal of Coal Geology, 35(1-4): 147-158.

Crosdale, P.J., Moore, T.A. and Mares, T.E., 2008. Influence of moisture content and temperature on methane adsorption isotherm analysis for coals from a low-rank, biogenically-sourced gas reservoir. International Journal of Coal Geology, 76(1-2): 166-174.

Crosdale, P.J., Saghafi, A., Williams, R. and Yurakov, E., 2005. Inter-laboratory comparative CH_4 isotherm measurement on Australian coals. In: J.W. Beeston (Editor), Bowen Basin Symposium 2005- The future for coal- Fuel for thought. Geological Society of Australia Inc. Coal Geology Group and the Bowen Basin Geologists Group, Yeppoon, pp. 273-277.

Crosdale, P.J., Sorokin, A.P., Woolfe, K.J. and Macdonald, D.I.M., 2002. Inertinite-rich Tertiary coals from the Zeya-Bureya Basin, Far Eastern Russia. International Journal of Coal Geology, 51(4): 215-235.

Cui, X., Bustin, R.M. and Dipple, G., 2004. Selective transport of CO_2, CH_4 and N_2 in coals: insights from modeling of experimental gas adsorption data. Fuel, 83: 293-303.

Damen, K., Faaij, A., van Bergen, F., Gale, J. and Lysen, E., 2005. Identification of early opportunities for CO2 sequestration--worldwide screening for CO_2-EOR and CO_2-ECBM projects. Energy, 30(10): 1931-1952.

Day, S., Duffy, G., Sakurovs, R. and Weir, S., 2008a. Effect of coal properties on CO_2 sorption capacity under supercritical conditions. International Journal of Greenhouse Gas Control, 2(3): 342-352.

Day, S., Fry, R. and Sakurovs, R., 2008b. Swelling of Australian coals in supercritical CO_2. International Journal of Coal Geology, 74(1): 41-52.

Day, S., Sakurovs, R. and Weir, S., 2008c. Supercritical gas sorption on moist coals. International Journal of Coal Geology, 74(3-4): 203-214.

de Caritat, P., Reimann, C., Bogatyrev, I., Chekushin, V., Finne, T.E., Halleraker, J.H., Kashulina, G., Niskavaara, H., Pavlov, V. and Äyräs, M., 2001. Regional distribution of Al, B, Ba, Ca, K, La, Mg, Mn, Na, P, Rb, Si, Sr, Th, U and Y in terrestrial moss within a 188,000 km2 area of the central Barents region: influence of geology, seaspray and human activity. Applied Geochemistry, 16(2): 137-159.

de Sousa e Vasconcelos, L., 1999. The petrographic composition of world coals. Statistical results obtained from a literature survey with reference to coal type (maceral composition). International Journal of Coal Geology, 40(1): 27-58.

Dehmer, J., 1995. Petrological and organic geochemical investigation of recent peats with known environments of deposition. International Journal of Coal Geology, 28: 111-138.

Deng, X., Wong, S., Faltinson, J. and Gunter, W.D., 2006. Economics of enhanced coalbed methane (ECBM) production using different CO_2 injection sources: pure CO_2 versus coal combustion flue gas versus acid gas streams, 8th International Conference on Greenhouse Gas Control Technologies, Trondheim, Norway, 6 pp.

Diamond, W.P. and Schatzel, S.J., 1998. Measuring the gas content of coal: A review. International Journal of Coal Geology, 35(1-4): 311-331.

Diessel, C.F.K., 2009. The stratigraphic distribution of inertinite. International Journal of Coal Geology, doi:10.1016/j.coal.2009.04.004.

Divan Jr, A. M., Oliveira, P.L., Perry, C.T., Atz, V.L., Azzarini-Rostirola, L.N. and Raya-Rodriguez, M.T., 2009. Using wild plant species as indicators for the accumulation of emissions from a thermal power plant, Candiota, South Brazil. Ecological Indicators, 9(6): 1156-1162.

Dongarrá, G., Varrica, D. and Sabatino, G., 2003. Occurrence of platinum, palladium and gold in pine needles of Pinus pinea L. from the city of Palermo (Italy). Applied Geochemistry, 18(1): 109-116.

Dunn, C.E. and Hoffman, E., 1986. Multi-element study of vegetation from a zone of rare-earth rich allanite and apatite in northern Saskatchewan, Canada. Applied Geochemistry, 1(3): 375-381.

Edbrooke, S.W., Sykes, R. and Pocknall, D.T., 1994. Geology of the Waikato Coal Measures, Waikato Coal Region, New Zealand, Monograph 6. Institute of Geological and Nuclear Sciences Limited, Lower Hutt, New Zealand.

Elms, D.G. (Editor), 1992. Consistent crudeness in system construction. Optimisation and artificial intelligence in Civil Engineering, 1. Kluwer Academic Publishers, 71-85 pp.

Esterle, J.S. and Ferm, J.C., 1990. On the use of modern tropical domed peats as analogues for petrographic variation in Carboniferous coal beds. International Journal of Coal Geology, 16: 131-136.

Esterle, J.S. and Ferm, J.C., 1994. Spatial Variability in Modern Tropical Peat Deposits from Sarawak, Malaysia and Sumatra, Indonesia- Analogs for Coal. International Journal of Coal Geology, 26(1-2): 1-41.

Esterle, J.S., Moore, T.A. and Shearer, J.C., 1992. Comparison of macroscopic and microscopic size analyses of organic components in both coal and peat, 26th Newcastle Symposium: Advances in the study of the Sydney Basin, Newcastle, Australia, pp. 10-12.

Faraj, B.S.M., Fielding, C.R. and Mackinnon, I.D.R., 1996. Cleat mineralization of Upper Permian Baralaba/Rangal Coal Measures, Bowen Basin, Australia. In: R. Gayer and I. Harris (Editors), Coalbed Methane and Coal Geology. Geological Society Special Publications. The Geological Society, London, pp. 151-164.

Feigin, L.A. and Svergun, D.I., 1987. Structure analysis by small-angle X-ray and neutron scattering. Plenum Press.

Ferm, J.C., Moore, T.A., Lindsay, P. and Campbell, R.N., 2000. A guide to cored rocks and coal in the Waikato coalfield, CRL Energy Ltd, Lower Hutt.

Flores, R.M., 1998. Coalbed methane: From hazard to resource. International Journal of Coal Geology, 35(1-4): 3-26.

Flores, R.M., 2004. Coalbed methane in the Powder River Basin, Wyoming and Montana: an assessment of the Tertiary-Upper Cretaceous coalbed methane Total Petroleum System. In: U.P.R.B.P.A. Team (Editor), Total Petroleum System and assessment of coalbed gas in the Powder River Basin province, Wyoming and Montana. USGS.

Flores, R.M., Moore, T.A., Stanton, R.W. and Stricker, G.D., 2001. Textural controls on coalbed methane content in the subbituminous coal of the Powder River Basin, GSA Annual Meeting, Boston.

Flores, R.M., Rice, C.A., Stricker, G.D., Warden, A. and Ellis, M.S., 2008. Methanogenic pathways of coal-bed gas in the Powder River Basin, United States: The geologic factor. International Journal of Coal Geology, 76(1-2): 52-75.

Foster, M.D. and Jensen, K.F., 1990. Small angle X-ray scattering investigations of pore structure changes during coal gasification. Fuel, 69: 88-96.

Fredericks, P.M., Warbrooke, P. and Wilson, M.A., 1983. Chemical changes during natural oxidation of a high volatile bituminous coal. Organic Geochemistry, 5(3): 89-97.

Gamson, P., Beamish, B.B. and Johnson, D., 1996. Coal microstructure and secondary mineralization: their effect on methane recovery. In: R. Gayer and I. Harris (Editors), Coalbed Methane and Coal Geology. Geological Society Special Publications. The Geological Society, London, pp. 165-180.

Gamson, P.D., Beamish, B.B. and Johnson, D.P., 1993. Coal Microstructure and Micropermeability and Their Effects on Natural-Gas Recovery. Fuel, 72(1): 87-99.

Gan, H., Nandi, S.P. and Walker, J., P. L., 1972. Nature of the porosity in American coals. Fuel, 51(4): 272-277.

Gentzis, T., 2000. Subsurface sequestration of carbon dioxide- an overview from an Alberta (Canada) perspective. International Journal of Coal Geology, 43: 287-305.

Gilcrease, P.C. and Shurr, W., 2007. Making microbial methane work: The potential for new biogenic gas. World Oil, 228(11).

Gluskoter, H.J., Stanton, R.W., Flores, R.M. and Warwick, P.D., 2002. Adsorption of carbon dioxide and methane in low-rank coals and the potential for sequestration of carbon dioxide. AAPG Bulletin, 86(13 (Supplement)).

Goodman, A.L., Favors, R.N. and Larsen, J.W., 2006. Argonne coal structure rearrangement caused by sorption of CO_2. Energy & Fuels, 20(6): 2537-2543.

Gorody, A.W. (Editor), 1999. The origin of natural gas in the Tertiary coal seams on the eastern margin of the Powder River Basin. Coalbed methane and the Tertiary geology of the Powder River Basin in Wyoming and Montana. Wyoming Geological Association Fiftieth Field Conference Guidebook, 89-101 pp.

Gray, I., 2003. Coal seams determined. World Coal (September): 51-53.

Gray, V.R., 1983. Coal analysis in New Zealand. Report number 97. New Zealand Energy Research and Development Committee.

Gray, V.R. and Daly, T.A., 1981. Chemical properties and composition of Waikato coals. New Zealand Journal of Science, 24(179-202).

Green, M.S., Flanegan, K.C. and Gilcrease, P.C., 2008. Characterization of a methanogenic consortium enriched from a coalbed methane well in the Powder River Basin, U.S.A. International Journal of Coal Geology, 76(1-2): 34-45.

Gregg, S.J. and Sing, K.S., 1982. Adsorption, surface area and porosity. Academic Press, London, 303 pp.

Guinier, A., Fournet, G., Walker, C.B. and Yudowitch, K.L., 1955. Small-angle scattering of X-rays. John Wiley and Sons.

Gurdal, G. and Yalcin, M.N., 2001. Pore volume and surface area of the Carboniferous coals from the Zonguldak basin (NW Turkey) and their variations with rank and maceral composition. International Journal of Coal Geology, 48(1-2): 133-144.

Hackley, P.C., Warwick, P.D. and Breland, J., F. Clayton, 2007. Organic petrology and coalbed gas content, Wilcox Group (Paleocene-Eocene), northern Louisiana. International Journal of Coal Geology, 71(1): 54-71.

Hainbuchner, M., Villa, M., Kroupa, G., Bruckner, G., Baron, M., Amenitsch, H., Seidl, E. and Rauch, H., 2000. The new high resolution ultra small-angle neutron scattering instrument at the High flux reactor in Grenoble. Journal of Applied Crystallography, 33: 851-854.

Hall, P.J., Antxustegi, M. and Ruiz, W., 1998. Contrast-matching small-angle neutron scattering evidence for the absence of a connected pore system in Pittsburgh No. 8 coal. Fuel, 77(14): 1663-1665.

Hall, P.J., Brown, S.D. and Calo, J.M., 2000. The pore structure of the Argonne coals as interpreted from contrast matching small angle neutron scattering. Fuel, 79(11): 1327-1332.

Hall, S.L., 2003. Controls on deposition of coal and clastic sediment in the Waikato Coal Measures, MSc Thesis. University of Canterbury, Christchurch, 135 pp.

Hall, S.L., Nicol, A., Moore, T.A. and Bassett, K.N., 2006. Timing of normal faulting in the Waikato Coal Measures, New Zealand, and its implications for coal-seam geometry. New Zealand Journal of Geology and Geophysics, 49: 101-113.

Hamelinck, C. N., Faaij, A. P. C., Turkenburg, W. C., van Bergen, F., Pagnier, H. J. M., Barzandji, O. H. M., Wolf, K. H. A. A. and Ruijg, G. J., 2002. CO_2 enhanced coalbed methane production in the Netherlands. Energy, 27(7): 647-674.

Harpalani, S. and Chen, G., 1992. Effect of gas production on porosity and permeability of coal, Coalbed Methane Symposium, Townsville, Australia, pp. 67-78.

Harpalani, S. and Chen, G.L., 1995. Estimation of Changes in Fracture Porosity of Coal with Gas Emission. Fuel, 74(10): 1491-1498.

Harpalani, S. and Schraufnagel, R.A., 1990. Shrinkage of coal matrix with release of gas and its impact on permeability of coal. Fuel, 69(5): 551-556.

Harpalani, S., Singh, K. and Zutshi, A., 2006. CO_2/N_2 Flow Behavior of Deep Coal-Gas Reservoirs, Golden Rocks 2006, The 41st U.S. Symposium on Rock Mechanics (USRMS), Golden, CO, 9 pp.

Harris, L.A. and Yust, C.S., 1976. Transmission electron microscope observations of porosity in coal. Fuel, 55(3): 233-236.

Harris, S.H., Smith, R.L. and Barker, C.E., 2008. Microbial and chemical factors influencing methane production in laboratory incubations of low-rank subsurface coals. International Journal of Coal Geology, 76(1-2): 46-51.

Hart, D., 1988. The Plant Opal Content in the Vegetation and Sediment of a Swamp at Oxford Falls, New South Wales, Australia. Australian Journal of Botany, 36(2): 159-170.

Hayton, S., 2003. Technical Note: Oxidation of coal in desorption canisters. PR 2948, Crown Minerals.

Hayton, S., Manhire, D.A., Pope, S. and Nelson, C., 2004. Coal seam gas exploration technologies in New Zealand, 2004 New Zealand Petroleum Conference Proceedings.

Hemza, P., Sivek, M. and Jirásek, J., 2009. Factors influencing the methane content of coal beds of the Czech part of the Upper Silesian Coal Basin, Czech Republic. International Journal of Coal Geology, doi:10.1016/j.coal.2009.04.003.

Hinde, A.L., 2004. PRINSAS - a Windows-based computer program for the processing and interpretation of small-angle scattering data tailored to the analysis of sedimentary rocks. Journal of Applied Crystallography, 37: 1020-1024.

Holdgate, G.R., Cartwright, I., Blackburn, D.T., Wallace, M.W., Gallagher, S.J., Wagstaff, B.E. and Chung, L., 2007. The Middle Miocene Yallourn coal seam — The last coal in Australia. International Journal of Coal Geology, 70: 95-115.

ICCP, 1998. The new vitrinite classification (ICCP System 1994). Fuel, 77(5): 349-358.

ICCP, 2001. The new inertinite classification (ICCP System 1994). Fuel, 80: 459-471.

ISO, International Organization for Standardization, 1994. ISO 7404-5 Methods for the petrographic analysis of bituminous coal and anthracite -- Part 5: Method of determining microscopically the reflectance of vitrinite, International Organisation for Standardisation, Geneva, Switzerland, 11pp.

ISO, International Organization for Standardization, 1995. ISO 1928 Solid mineral fuels- Determination of gross calorific value by the bomb calorimetric method, and calculation of net calorific value. www.iso.org.

ISO, International Organization for Standardization, 1997. ISO 1171 Solid Mineral Fuels - Determination of ash, www.iso.org.

ISO, International Organization for Standardization, 1998. ISO 562 Hard coal and coke- Determination of volatile matter. www.iso.org.

ISO, International Organization for Standardization, 2006. ISO 5068-2 Brown coals and lignites- Determination of moisture content- Part 2: Indirect gravimetric method for moisture in the analysis sample. www.iso.org.

Jessen, K., Lin, W. and Kovscek, A., 2007. Multicomponent sorption modeling in ECBM displacement calculations, SPE Annual Technical Conference and Exhibition, Anaheim, California, pp. 10 pp.

Johnson, K.C., 2004. The New Zealand coal seam gas scene, 2004 New Zealand Petroleum Conference Proceedings.

Jones, E.J. P., Voytek, M.A., Warwick, P.D., Corum, M.D., Cohn, A., Bunnell, J.E., Clark, A.C. and Orem, W.H., 2008. Bioassay for estimating the biogenic methane-generating potential of coal samples. International Journal of Coal Geology, 76(1-2): 138-150.

Kaldi, J.G. and Cook, P.J., 2006. Geosequestration of CO2: A key strategy for the sustainability of energy industries, 2006 New Zealand Petroleum Conference. Crown Minerals, Auckland, 8 pp.

Karacan, C.O. and Mitchell, G.D., 2003. Behavior and effect of different coal microlithotypes during gas transport for carbon dioxide sequestration into coal seams. International Journal of Coal Geology, 53(4): 201-217.

Karacan, C.O. and Okandan, E., 2000. Fracture/cleat analysis of coals from Zonguldak Basin (northwestern Turkey) relative to the potential of coalbed methane production. International Journal of Coal Geology, 44(2): 109-125.

Karacan, C.O. and Okandan, E., 2001. Adsorption and gas transport in coal microstructure: investigation and evaluation by quantitative X-ray CT imaging. Fuel, 80(4): 509-520.

Kelemen, S.R., Kwiatek, L.M. and Lee, A.G.K., 2006. Swelling and sorption response of selected Argonne Premium coals to CO_2, CH_4 and N_2, International Coalbed Methane Symposium, Tuscaloosa, Alabama, 15 pp.

King, J.G. and Wilkins, E.T., 1944. The internal structure of coal, Proceedings of the Conference on Ultrafine Structures of Coals and Cokes, 1943. The British Coal Utilization Research Association, London, pp. 45-56.

Kirk, P.A., Sherwood, A.M. and Edbrooke, S.W., 1988. Waikato Coal Region: a summary of geology and resources. New Zealand Geological Survey record 34.

Klein, D.A., Flores, R.M., Venot, C.N., Gabbert, K., Schmidt, R.A., Stricker, G.D., Pruden, A. and Mandernack, K., 2008. Molecular sequences derived from Paleocene Fort Union Formation coals vs. associated produced waters: Implications for CBM regeneration. International Journal of Coal Geology, 76(1-2): 3-13.

Krooss, B. M., Van Bergen, F., Gensterblum, Y., Siemons, N., Pagnier, H.J.M. and David, P., 2002. High-pressure methane and carbon dioxide adsorption on dry and moisture-equilibrated Pennsylvanian coals. International Journal of Coal Geology, 51: 69-92.

Kubin, E. and Lippo, H., 1996. Atmospheric heavy metal deposition in Finland from 1985 to 1990. Applied Geochemistry, 11(1-2): 155-161.

Lamberson, M.N. and Bustin, R.M., 1993. Coalbed Methane Characteristics of Gates Formation Coals, Northeastern British-Columbia - Effect of Maceral Composition. AAPG Bulletin-American Association of Petroleum Geologists, 77(12): 2062-2076.

Larsen, J.W., 2004. The effects of dissolved CO_2 on coal structure and properties. International Journal of Coal Geology, 57: 63-70.

Laubach, S.E., Marrett, R.A., Olson, J.E. and Scott, A.R., 1998. Characteristics and origins of coal cleat: A review. International Journal of Coal Geology, 35(1-4): 175-207.

Law, B.E., 1993. The relationship between coal rank and cleat spacing: implications for the prediction of permeability in coal, Proceedings of the 1993 International Coalbed Methane Symposium, Birmingham, Alabama, pp. 435-441.

Law, D.H.-S., van der Meer, B. and Gunter, W.D., 2003. Comparison of numerical simulators for greenhouse gas storage in coal beds, Part II: flue gas injection. In: J. Gale and Y. Kaya (Editors), Greenhouse Gas Control Technologies, pp. 563-568.

Laxminarayana, C. and Crosdale, P.J., 1999. Role of coal type and rank on methane sorption characteristics of Bowen Basin, Australia coals. International Journal of Coal Geology, 40(4): 309-325.

Laxminarayana, C. and Crosdale, P.J., 2002. Controls on methane sorption capacity of Indian coals. AAPG Bulletin, 86(2): 201-212.

Levine, J.R., 1992. Oversimplifications can lead to faulty coalbed gas reservoir analysis. Oil and Gas Journal(Nov 23): 63-69.

Levine, J.R., 1993. Coalification: The evolution of coal as source rock and reservoir rock for oil and gas. In: B.E. Law and D.D. Rice (Editors), Hydrocarbons from coal. American Association of Petroleum Geologists, Tulsa, Oklahoma, pp. 39-77.

Levine, J.R., 1996. Model study of the influence of matrix shrinkage on absolute permeability of coal bed reservoirs. In: R. Gayer and I. Harris (Editors), Coalbed Methane and Coal Geology. Geological Society Special Publications. The Geological Society, London, pp. 197-212.

Li, D., Hendry, P. and Faiz, M., 2008. A survey of the microbial populations in some Australian coalbed methane reservoirs. International Journal of Coal Geology, 76(1-2): 14-24.

Li, H.Y., Shimada, S. and Zhang, M., 2004. Anisotropy of gas permeability associated with cleat pattern in a coal seam of the Kushiro coalfield in Japan. Environmental Geology, 47(1): 45-50.

Li, Z., 2002. Mineralogy and trace elements of the Cretaceous Greymouth coals and their combustion products, University of Canterbury, Christchurch, Volume 1, 161 pp.

Li, Z., Moore, T.A. and Weaver, S.D., 2001. Leaching of inorganics in the Cretaceous Greymouth coal beds, South Island, New Zealand. International Journal of Coal Geology, 47(3-4): 235-253.

Li, Z.S., Ward, C.R. and Gurba, L.W., 2007. Occurrence of non-mineral inorganic elements in low-rank coal macerals as shown by electron microprobe element mapping techniques. International Journal of Coal Geology, 70(1-3): 137-149.

Li, Z.S., Ward, C.R. and Gurba, L.W., 2009. Occurrence of Non-mineral Inorganic Elements in Macerals of Low-rank Coals. International Journal of Coal Geology, doi: 10.1016/j.coal.2009.02.004.

Liu, D., Yao, Y., Tang, D., Tang, S., Che, Y. and Huang, W., 2009. Coal reservoir characteristics and coalbed methane resource assessment in Huainan and Huaibei coalfields, Southern North China. International Journal of Coal Geology, doi:10.1016/j.coal.2009.05.001.

Long, G.G., Allen, A.J., Ilavsky, J., Jeminan, P.R. and Zschack, P., 2000. The Ultra-Small-Angle X-ray Scattering Instrument on UNICAT at the APS. In: P. Pianetta, J. Arthur and S. Brennan (Editors), SRI99: Eleventh U.S. National Synchrotron Radiation Instrumentation Conference, AIP Conference Proceedings CP521, Stanford Linear Accelerator Center, Stanford, CA, pp. 183-187.

Long, G.G., Jemian, P.R., Weertman, J.R., Black, D.R., Burdette, H.E. and Spal, R., 1991. High Resolution Small-Angle X-ray Scattering Camera for Anomalous Scattering. Journal of Applied Crystallography, 24: 30-37.

Lyon, G.L. and Giggenback, W.F., 1994. The isotopic and chemical composition of natural gases from the South Island, New Zealand, 1994 New Zealand Petroleum Conference. Ministry of Commerce, pp. 361–369.

Manhire, D.A. and Hayton, S., 2003. Coal Seam Gas in New Zealand: Perspective from New Zealand's most active CSG explorers, AusIMM New Zealand Branch 36th Annual Conference, Opportunities for the New Zealand Mining and Minerals Industry, Greymouth.

Mares, T.E. and Moore, T.A., 2008. The influence of macroscopic texture on biogenically-derived coalbed methane, Huntly coalfield, New Zealand. International Journal of Coal Geology, 76(1-2): 175-185.

Mares, T.E., Moore, T.A. and Moore, C.R., 2009. Uncertainty of gas saturation estimates in a subbituminous coal seam. International Journal of Coal Geology, 77(3-4): 320-327.

Mares, T.E. and Zarrouk, S., 2008. Opportunities for underground geological storage of CO_2 in New Zealand - Report CCS-08/3a - Waikato coal resource, reservoir modelling. GNS Science Consultancy Report 2009/21, University of Auckland.

Mastalerz, M., Gluskoter, H. and Rupp, J., 2004. Carbon dioxide and methane sorption in high volatile bituminous coals from Indiana, USA. International Journal of Coal Geology, 60(1): 43-55.

Mathews, W.H. and Bustin, R.M., 1984. Changes associated with natural in situ weathering of a coking coal from southeastern British Columbia. Fuel, 63(4): 548-550.

Mavor, M., 2004. Uncertainty in Sorption Isotherm Measurements, International Coalbed Methane Symposium, Tuscaloosa, Alabama.

Mavor, M., Gunter, W.D. and Robinson, J., 2004. Alberta multiwell micro-pilot testing for CBM properties, enhanced methane recovery and CO_2 storage potential, SPE Annual Technical Conference and Exhibition, Houston, Texas, 15 pp.

Mavor, M. and Nelson, C., 1997. Coalbed reservoir Gas-In-Place analysis. GRI-97/0263. Gas Research Institute, Chicago, Illinois, U.S.A.

Mavor, M.J. and Vaughn, J.E., 1998. Increasing coal natural fracture permeability in the San Juan Basin Fruitland Formation, AAPG Annual Convention, Salt Lake City, Utah, U.S.A.

Mazumder, S., van Hemert, P., Busch, A., Wolf, K.-H.A.A. and Tejera-Cuesta, P., 2006. Flue gas and pure CO2 sorption properties of coal: A comparative study. International Journal of Coal Geology, 67(4): 267-279.

Mazumder, S. and Wolf, K.-H.A.A., 2008. Differential swelling and permeability change of coal in response to CO_2 injection for ECBM. International Journal of Coal Geology, 74: 123-138.

McElhiney, J.E., Paul, G.W., Young, G.B.C. and McCartney, J.A., 1993. Reservoir engineering aspects of coalbed methane. In: B.E. Law and D.D. Rice (Editors), Hydrocarbons from coal. American Association of Petroleum Geologists, Tulsa, Oklahoma, pp. 361-372.

McIntosh, J., Martini, A., Petsch, S., Huang, R. and Nüsslein, K., 2008. Biogeochemistry of the Forest City Basin coalbed methane play. International Journal of Coal Geology, 76(1-2): 111-118.

Melnichenko, Y.B., Radlinski, A.P., Mastalerz, M., Cheng, G. and Rupp, J., 2009. Characterization of the CO_2 fluid adsorption in coal as a function of pressure using neutron scattering techniques (SANS and USANS). International Journal of Coal Geology, 77(1-2): 69-79.

Meunier, A., 2005. Clays. Springer-Verlag Heidelberg, 472 pp.

Middleton, H.A. and Nelson, C.S., 1996. Origin and timing of siderite and calcite concretions in late Palaeogene non- to marginal-marine facies of the Te Kuiti Group, New Zealand. Sedimentary Geology, 103(1-2): 93-115.

Mitra, A. and Harpalani, S., 2007. Modeling incremental swelling of coal matrix with CO_2 injection in coalbed methane reservoirs, SPE Eastern Regional Meeting, Lexington, Kentucky, U.S.A., 8 pp.

Montgomery, S.L., 1999. Powder River Basin, Wyoming: An Expanding Coalbed Methane (CBM) Play. AAPG Bulletin,, 83(8): 1207 - 1222.

Moon, V. and Roy, T., 2004. Geological controls on rock mass classification of coal from Huntly East Mine, New Zealand. Engineering Geology, 75(2): 201-213.

Moore, D.S. and McCabe, G.P., 1999. Introduction to the practice of statistics. W.H. Freeman and Company, 825 pp.

Moore, P.D., 1995. Biological processes controlling the development of modern peat-forming ecosystems. International Journal of Coal Geology, 28: 99-110.

Moore, T.A. and Butland, C.I., 2005. Coal seam gas in New Zealand as a model for Indonesia. In: S. Prihatmoko, S. Digdowirogo, C. Nas, T. van Leewen and H. Widjajanto (Editors), IAGI Special Issues 2005: Indonesian Mineral and Coal Discoveries. Indonesian Association of Geologists, Indonesia, pp. 192-200.

Moore, T.A. and Crosdale, P.J., 2006. The effect of moisture and temperature on adsorption isotherms of a low-rank coal: Implications for reservoir modelling, 2006 International Coalbed Methane Symposium, Tuscaloosa, Alabama.

Moore, T.A. and Fergusson, D.A., 1997. Coal and combustion in the Waikato: predicting ash clinkering potential for in-ground resources, Seventh New Zealand Coal Conference. Coal Research Association of New Zealand Inc., Wellington, New Zealand, pp. 66-89.

Moore, T.A. and Ferm, J.C., 1988. A modification of procedures for petrographic analysis of Tertiary Indonesian coals. Journal of Southeast Asian Earth Sciences, 2(3/4): 175-183.

Moore, T.A. and Ferm, J.C., 1992. Composition and grain-size of an Eocene coal bed in south eastern Kalimantan, Indonesia. International Journal of Coal Geology, 21(1–30).

Moore, T.A., Flores, R.M., Stanton, R.W. and Stricker, G.D., 2001. The role of macroscopic texture in determining coal bed methane variability in the Anderson-Wyodak coal seam, Powder River Basin, Wyoming. In: C.R. Robinson (Editor), Eighteenth Annual Meeting of The Society for Organic Petrology, Houston, Texas, pp. 85-88.

Moore, T.A., Gillard, G.R., Boyd, R., Flores, R.M., Stricker, G.D. and Galceran, C.M., 2004. A mighty wind: determining the methane content of New Zealand coal seams. In: T.A. Moore et al. (Editors), Abstracts of the 21th Annual Meeting of the Society for Organic Petrology, Sydney, New South Wales, Australia, pp. 114-116.

Moore, T.A. and Hilbert, R.E., 1992. Petrographic and anatomical characteristics of plant material from two peat deposits of Holocene and Miocene age, Kalimantan, Indonesia. Review of Palaeobotany and Palynology, 72: 199-227.

Moore, T.A., Li, Z.S. and Moore, N.A., 2006. Controls on the formation of an anomalously thick Cretaceous-age coal mire. In: S.F. Greb and W.A. DiMichele (Editors), Wetlands through time: Geological Society of America Special Paper 399, pp. 269-290.

Moore, T.A., Li, Z.S., Nelson, C.M., Finkelman, R.B. and Boyd, R., 2005. Concentration of trace elements in coal beds. In: T.A. Moore, A. Black, J.A. Centeno, J.S. Harding and D.A. Trumm (Editors), Metal contaminants in New Zealand. Resolutionz Press, Christchurch, pp. 81-113.

Moore, T.A., Manhire, D.A. and Flores, R.M., 2002. Coalbed methane opportunities in New Zealand: Similarities with the Powder River Basin coalbed methane paradigm, AusIMM Conference, Auckland, New Zealand.

Moore, T.A., Mares, T.E. and Butland, C.I., 2008. Gas saturation: controls and uncertainty in biogenically-derived coalbed methane, examples from New Zealand coal fields, 33rd International Geological Congress, Oslo, Norway.

Moore, T.A. and Shearer, J.C., 1999. Coal: Types and characteristics. In: C.P. Marshall and R.W. Fairbridge (Editors), The Encyclopedia of Geochemistry. Kluwer Academic Publishers, Dordrecht, pp. 87-90.

Moore, T.A., Shearer, J.C. and Miller, S.L., 1996. Fungal origin of oxidised plant material in the Palangkaraya peat deposit, Kalimantan Tengah, Indonesia: Implications for 'inertinite' formation in coal. International Journal of Coal Geology, 30(1-2): 1-23.

Moore, T.A. and Swanson, K.M., 1993. Application of Etching and SEM in the Identification of Fossil Plant-Tissues in Coal. Organic Geochemistry, 20(6): 769-777.

Moore, T.A. and Twombly, G., 2006. Cracking the CSG code with the three Rs: reasoned, rigorous and responsive development, 2006 New Zealand Petroleum Conference. Crown Minerals, Auckland.

Mukherjee, K.N., Dutta, N.R., Chandra, D. and Singh, M.P., 1992. Geochemistry of trace elements of Tertiary coals of India. International Journal of Coal Geology, 20: 99-113.

Nelson, C.R., Hill, D.G. and Pratt, T.J., 2000. Properties of Paleocene Fort Union Formation Canyon Seam Coal at the Triton Federal coalbed methane well, Campbell County, Wyoming, SPE/CERI Gas Technology Symposium, Calgary, Alberta Canada, 3-5 April 2000.

Nesse, W.D., 1991. Introduction to optical mineralogy. Second Edition. Oxford University Press, Inc., New York, 335 pp.

Neuzil, S.G., Supardi, Cecil, C.B., Kane, J.S. and Soedjono, K., 1993. Inorganic geochemistry of domed peat in Indonesia and its implication for the origin of mineral matter in coal. In: J.C. Cobb and C.B. Cecil (Editors), Modern and ancient coal-forming environments. Geological Society of America, Boulder, Colorado, pp. 23-44.

Newman, J., 1995. Relationships between Quantitative Vitrinite Fluorescence and the Chemistry and Industrial properties of West Coast coals, 6th New Zealand Coal Conference, Wellington, New Zealand, pp. 16-22.

Newman, J., 1997a. New approaches to detection and correction of suppressed vitrinite reflectance. APPEA Journal, 37: 524-535.

Newman, J., 1997b. VRFTM: combined vitrinite reflectance and fluorescence, Seventh New Zealand Coal Conference. Coal Research Association of New Zealand Inc., Wellington, New Zealand, pp. 490-498.

Newman, J., Eckersley, K.M., Francis, D.A. and Moore, N.A., 2000. Application of vitrinite-inertinite reflectance and fluorescence to maturity assessment in the East Coast and Canterbury Basin of New Zealand, New Zealand Petroleum Conference, Christchurch, New Zealand, 32 pp.

Newman, J. and Newman, N.A., 1982. Reflectance anomalies in Pike River coals: evidence of variability in vitrinite type, with implications for maturation studies and "Suggate rank". New Zealand Journal of Geology and Geophysics, 23: 233-243.

Newman, N.A., 1988. Mineral matter in coals of the west coast, South Island, New Zealand, PhD Thesis. University of Canterbury, Christrchurch, 293 pp.

Newman, N.A., Moore, T.A. and Esterle, J.S., 1997. Geochemistry and petrography of the Taupiri and Kupakupa coal seams, Waikato Coal Measures (Eocene), New Zealand. International Journal of Coal Geology, 33(2): 103-133.

Ohga, K., Fujioka, M. and Yamaguchi, S., 2005. Pilot test of CO_2 sequestration and ECBM in Japan, RECOPOL workshop: Reduction of CO_2 emission by means of CO_2 storage in coal seams in the Silesian Basin of Poland, Szczyrk, Poland.

Orem, W.H., Neuzil, S.G., Lerch, H.E. and Cecil, C.B., 1996. Experimental early-stage coalification of a peat sample and a peatified wood sample from Indonesia. Organic Geochemistry, 24(2): 111-125.

Parr, S.W., 1928. The classification of coal. University of Illinois Bulletin, 180: 62 pp.

Pashin, J.C., Carroll, R.E., Hatch, J.R. and Goldhaber, M.B., 1999. Mechanical and thermal control of cleating and shearing in coal: examples from the Alabama coalbed methane fields, USA. In: M. Mastalerz, M. Glikson and S.D. Golding (Editors), Coalbed methane: scientific, environmental and economic evaluation. Kluwer Academic Publishers, Dordrecht, pp. 305-327.

Pattison, C.I., Fielding, C.R., McWatters, R.H. and Hamilton, L.H., 1996. Nature and origin of fractures in Permian coals from the Bowen Basin, Queensland, Australia. In: R. Gayer and I. Harris (Editors), Coalbed Methane and Coal Geology. Geological Society Special Publications. The Geological Society, London, pp. 133-150.

Pearson, M.J. and Nelson, C.S., 2005. Organic geochemistry and stable isotope composition of New Zealand carbonate concretions and calcite fracture fills. New Zealand Journal of Geology and Geophysics, 48: 395-414.

Pone, J.D.N., Hile, M., Halleck, P.M. and Mathews, J.P., 2008. Three-dimensional carbon dioxide-induced strain distribution within a confined bituminous coal. International Journal of Coal Geology, doi:10.1016/j.coal.2008.08.003.

Pope, J., 2005. CSG Analyses from specialized gas sample canisters. Report 05–41110, CRL Energy Ltd., Christchurch: 8 pp.

Porod, G., 1951. Die Rontgenkleinwinkelstreuung von dichtgepackten kolloiden System I. Teil Kolloid Z, 124: 83-114.

Price, F.T. and Casagrande, D.J., 1991. Sulfur distribution and isotopic composition in peats from the Okefenokee Swamp, Georgia and the Everglades, Florida. International Journal of Coal Geology, 17(1): 1-20.

Prinz, D. and Littke, R., 2005. Development of the micro- and ultramicroporous structure of coals with rank as deduced from the accessibility to water. Fuel, 84(12-13): 1645-1652.

Prinz, D., Pyckhout-Hintzen, W. and Littke, R., 2004. Development of the meso- and macroporous structure of coals with rank as analysed with small angle neutron scattering and adsorption experiments. Fuel, 83(4-5): 547-556.

Quick, J.C., 1992. Fundamental characterisation of New Zealand bituminous coal for prediction of carbonization behaviour- with special emphasis on fluorometric analysis, PhD Thesis. University of Canterbury, Christchurch, New Zealand, 286 pp.

Quick, J.C., 1994. Iso-rank variation of vitrinite reflectance and fluorescence intensity. In: P.K. Mukhopadhyay and W.G. Dow (Editors), Vitrinite reflectance as a maturity parameter: applications and limitations. American Chemical Society Symposium Series 570, pp. 64-75.

Quick, J.C. and Tabet, D.E., 2003. Suppressed vitrinite reflectance in the Ferron coalbed gas fairway, central Utah: possible influence of overpressure. International Journal of Coal Geology, 56(1-2): 49-67.

Radlinski, A.P., 2006. Small angle neutron scattering and the microstructure of rocks. In: H.-R. Wenk (Editor), Neutron scattering in earth sciences. Reviews in Mineralogy and geochemistry. The Mineralogical Society of America, pp. 363-397.

Radlinski, A.P., Boreham, C.J., Lindner, P., Randl, O.G., Wignall, G.D. and Hope, J.M., 2000. Small angle neutron scattering signature of oil generation in artificially and naturally matured hydrocarbon source rocks. Organic Geochemistry, 31: 1-14.

Radlinski, A.P., Boreham, C.J., Wignall, G.D. and Lin, J.S., 1996. Microstructural evolution of source rocks during hydrocarbon generation: A small-angle scattering study. Physical Review B, 53: 14152-14160.

Radlinski, A.P., Busbridge, T.L., Gray, E.M.A., Blach, T.P. and Cookson, D.J., 2009. Small angle X-ray scattering mapping and kinetics study of sub-critical CO_2 sorption by two Australian coals. International Journal of Coal Geology, 77(1-2): 80-89.

Radlinski, A.P. and Hinde, A.L., 2001. Applications of small angle neutron scattering and small angle X-ray scattering to petroleum geology, Proceedings of the ESRF/ILL Joint Workshop on Environmental Studies Using Neutron and Synchrotron Facilities, Grenoble, France, pp. 11.

Radlinski, A.P. and Hinde, A.L., 2002. Small angle neutron scattering and petroleum geology. Neutron News, 13(2): 10-14.

Radlinski, A. P., Ioannidis, M. A., Hinde, A. L., Hainbuchner, M., Baron, M., Rauch, H. and Kline, S. R., 2004a. Angstrom-to-millimeter characterization of sedimentary rock microstructure. Journal of Colloid and Interface Science, 274(2): 607-612.

Radlinski, A. P., Mastalerz, M., Hinde, A. L., Hainbuchner, A., Rauch, H., Baron, M., Lin, J. S., Fan, L. and Thiyagarajan, P., 2004b. Application of SAXS and SANS in evaluation of porosity, pore size distribution and surface area of coal. International Journal of Coal Geology, 59(3-4): 245-271.

Radlinski, A. P., Mastalerz, M., Hinde, A. L., Hainbuchner, M., Rauch, H., Baron, M., Lin, J. S., Fan, L. and Thiyagarajan, P., 2001. Non-invasive measurements of pore size distribution in coal pellets using x-ray and neutron techniques, International Coalbed Methane Symposium, Tuscaloosa, Alabama.

Radlinski, A.P. and Radlinska, E.Z., 1999. The microstructure of pore space in coals of different rank. In: M. Mastalerz, M. Glikson and S.D. Golding (Editors), Coalbed methane: scientific, environmental and economic evaluation. Kluwer Academic Publishers, Dordrecht, pp. 329-365.

Radlinski, A. P., Radlinska, E. Z., Agamalian, M., Wignall, G. D., Lindner, P. and Randl, O. G., 1999. Fractal geometry of rocks. Physical Review Letters, 82(15): 3078-3081.

Rao, P.D. and Walsh, D.E., 1997. Nature and distribution of phosphorus minerals in Cook Inlet coals, Alaska. International Journal of Coal Geology, 33(1): 19-42.

Reeves, S.R., Oudinot, A.Y. and Erickson, D., 2004. The Tiffany Unit N_2 - ECBM Pilot: A Reservoir Modeling Study, Advanced Resources International.

Reimann, C., Arnoldussen, A., Finne, T.E., Koller, F., Nordgulen. O. and Englmaier., 2007. Element contents in mountain birch leaves, bark and wood under different anthropogenic and geogenic conditions. Applied Geochemistry, 22: 1549-1566.

Renton, J.J. and Bird, D.S., 1991. Association of coal macerals, sulphur species and the iron disulphide minerals in three columns of the Pittsburgh coal. International Journal of Coal Geology, 17(1): 21-50.

Rice, C.A., Flores, R.M., Stricker, G.D. and Ellis, M.S., 2008. Chemical and stable isotopic evidence for water/rock interaction and biogenic origin of coalbed methane, Fort Union Formation, Powder River Basin, Wyoming and Montana U.S.A. International Journal of Coal Geology, 76(1-2): 76-85.

Rice, D.D., 1993. Composition and origins of coalbed gas. In: B.E. Law and D.D. Rice (Editors), Hydrocarbons from coal. American Association of Petroleum Geologists, Tulsa, Oklahoma, pp. 159-184.

Rodrigues, C.F. and de Sousa, M.J.L., 2002. The measurement of coal porosity with different gases. International Journal of Coal Geology, 48(3-4): 245-251.

Ruppert, L.F., Cecil, C.B., Stanton, R. and Christian, R.P., 1985. Authigenic quartz in the Upper Freeport coal bed, west-central Pennsylvania. Journal of Sedimentary Petrology, 55(3): 334-339.

Ruppert, L.F., Neuzil, S.G., Cecil, C.B. and Kane, J.S., 1993. Inorganic constituents from samples of a domed and lacustrine peat, Sumatra, Indonesia. In: J.C. Cobb and C.B. Cecil (Editors), Modern and ancient coal-forming environments. Geological Society of America, Boulder, Colorado.

Saghafi, A., Faiz, M. and Roberts, D., 2007. CO_2 storage and gas diffusivity properties of coals from Sydney Basin, Australia. International Journal of Coal Geology, 70: 240-254.

SAI, Standards Australia International, 2002. AS 1038.21.1.1-2002: Coal and coke - Analysis and testing - Higher rank coal and coke - Relative density - Analysis sample/density bottle method. In: S.A.I. Ltd (Editor), 5pp.

Sander, R. and Allison, W.G., 2008. The effect of gas prices and carbon credits on field development for CO_2 storage in low rank coals, Asia Pacific Coalbed Methane Symposium, Brisbane, Australia, 14 pp.

Schmidt, P.W., 1982. Interpretation of small-angle scattering curves proportional to a negative power of the scattering vector. Journal of Applied Crystallography, 15: 567-569.

Schmidt, P.W., 1989. Use of scattering to determine the fractal dimension. In: D. Avnir (Editor), The fractal approach to heterogeneous chemistry. John Wiley and Sons, New York, pp. 67-79.

Scott, A.C. (Editor), 1999. Improving coal gas recovery with microbially enhanced coalbed methane. Coalbed methane: Scientific, Environmental and Economic Evaluation. Kluwer, Dordrecht, 89-110 pp.

Scott, A.R., Kaiser, W.R. and Ayers, J.W.B., 1994. Thermogenic and Secondary Biogenic Gases, San Juan Basin, Colorado and New Mexico--Implications for Coalbed Gas Producibility. AAPG Bulletin,, 78(8): 1186 - 1209.

Shaw, K., 1997. Reactivity of Waikato coals. M.Sc. Thesis. University of Auckland, Auckland, 78 pp.

Shearer, J.C., 1997. Natural and anthropogenic influences on peat development in Waikato/Hauraki Plains restiad bogs. Journal of the Royal Society of New Zealand, 27(3): 295-313.

Shearer, J.C. and Moore, T.A., 1994a. Botanical Control on Banding Character in two New Zealand Coal Beds. Palaeogeography Palaeoclimatology Palaeoecology, 110(1-2): 11-27.

Shearer, J.C. and Moore, T.A., 1994b. Grain-Size and Botanical Analysis of 2 Coal Beds from the South Island of New-Zealand. Review of Palaeobotany and Palynology, 80(1-2): 85-114.

Shearer, J.C., Moore, T.A. and Demchuk, T.D., 1995. Delineation of the distinctive nature of Tertiary coal beds. International Journal of Coal Geology, 28(2-4): 71-98.

Shearer, J.C., Moore, T.A., Vickridge, I.C. and Deely, J.M., 1997. Tephra as a control on trace element distribution in Waikato coals, Seventh New Zealand Coal Conference. Coal Research Association of New Zealand Inc., Wellington, New Zealand, pp. 505-520.

Sherwood, A.M., Lindqvist, J.K., Newman, J. and Sykes, R., 1992. Cretaceous coals in New Zealand. In: P.J. McCabe and J.T. Parrish (Editors), Controls on the Distribution and Quality of Cretaceous Coals. Geological Society of America, Boulder, Colorado, pp. 325–346.

Shi, J.-Q. and Durucan, S., 2005. A numerical simulation study of the Allison Unit CO2-ECBM pilot: The impact of matrix shrinkage and swelling on ECBM production and CO_2 injectivity. Greenhouse Gas Control Technologies 7. In: E.S. Rubin et al. (Editors). Elsevier Science Ltd, Oxford, pp. 431-439.

Shibaoka, M., 1972. Silica/alumina ratios of the ashes from some Australian coals. Fuel, 51: 278-283.

Shimizu, S., Akiyama, M., Naganuma, T., Fujioka, M. , Nako, M. and Ishijima, Y., 2007. Molecular characterization of microbial communities in deep coal seam groundwater of northern Japan. Geobiology, 5(4): 423-433.

Siriwardane, H., Haljasmaa, I., McLendon, R., Irdi, G., Soong, Y. and Bromhal, G.S., 2009. Influence of carbon dioxide on coal permeability determined by pressure transient methods. International Journal of Coal Geology, 77(1-2): 109-118.

Smith, J.R. and Smith, J.W., 2007. A relationship between the carbon and hydrogen content of coals and their vitrinite reflectance. International Journal of Coal Geology, 70: 79-86.

Smith, J.W. and Batts, B.D., 1974. The distribution and isotopic composition of sulfur in coal. Geochimica et Cosmochimica Acta, 38(1): 121-133.

Smith, J.W. and Pallasser, R.J., 1996. Microbial origin of Australian coalbed methane. AAPG Bulletin-American Association of Petroleum Geologists, 80(6): 891-897.

Soong, R. and Gluskoter, H.J., 1977. Mineral matter in some New Zealand coals Part I. Low temperature ash and mineralogical composition of such coals. New Zealand Journal of Science, 20: 273-277.

St George, J.D., 1997. Structural effects on the strength of New Zealand coal. International Journal of Rock Mechanics and Mining Sciences & Geomechanics Abstracts, 34(3-4): 666.

St. George, J.D. and Barakat, M.A., 2001. The change in effective stress associated with shrinkage from gas desorption in coal. International Journal of Coal Geology, 45(2-3): 105-113.

Stanton, R., Flores, R.M., Warwick, P.D., Gluskoter, H. and Stricker, G.D., 2001a. Coalbed sequestration of carbon dioxide. In: US.Department of Energy (Editor), National Energy Technology Laboratory, First National Conference on Carbon Sequestration, Washington, DC, 12 pp.

Stanton, R.W., Flores, R.M., Warwick, P.D. and Gluskoter, H.J., 2001b. Sequestration of carbon dioxide in low rank coals. In: C.R. Robinson (Editor), Eighteenth Annual Meeting of The Society for Organic Petrology, Houston, Texas, pp. 111.

Stanton, R.W., Moore, T.A., Warwick, P.D., Crowley, S.S. and Flores, R.M., 1989. Styles of organic facies development in Powder River Coals. In: R.M. Flores, P.D. Warwick and T.A. Moore (Editors), Tertiary and Cretaceous Coals in the Rocky Mountain Region, 28th International Geological Congress Field Trip Guidebook T132. Washington D.C., American Geophysical Union, pp. 19–27.

Staub, J.R. and Cohen, A.D., 1978. Kaolinite-enrichment beneath coals: a modern analog, Snuggedy Swamp, South Carolina. Journal of Sedimentary Petrology, 48: 203-210.

Staub, J.R. and Esterle, J.S., 1994. Peat-accumulating depositional systems of Sarawak, East Malaysia. Sedimentary Geology, 89: 91-106.

Stepanek, S., 2008. Coal seam methane at Huntly, New Zealand Petroleum Conference. Ministry of Economic Development, Wellington, New Zealand, Auckland, unpaginated.

Stern, K.R., 1982. Introductory plant biology. Second edition. Wm. C. Brown Company Publishers, Dubuque, Iowa, 493 pp.

Strapoc, D., Mastalerz, M., Eble, C. and Schimmelmann, A., 2007. Characterization of the origin of coalbed gases in southeastern Illinois Basin by compound-specific carbon and hydrogen stable isotope ratios. Organic Geochemistry, 38(2): 267-287.

Strapoc, D., Mastalerz, M., Schimmelmann, A., Drobniak, A. and Hedges, S., 2008a. Variability of geochemical properties in a microbially dominated coalbed gas system from the eastern margin of the Illinois Basin, USA. International Journal of Coal Geology, 76(1-2): 98-110.

Strapoc, D., Picardal, F.W., Turich, C., Schaperdoth, I., Macalady, J.L., Lipp, J.S., Lin, Y.-S., Ertefai, T.F., Schubotz, F., Hinrichs, K.-U., Mastalerz, M. and Schimmelmann, A., 2008b. Methane-Producing Microbial Community in a Coal Bed of the Illinois Basin. Applied Environmental Microbiology, 74(8): 2424-2432.

Stricker, G.D. and Flores, R.M., 2002. Coalbed methane content in the Powder River Basin, Wyoming: Saturation by coal rank and depth, 2002 Pittsburgh Coal Conference.

Stricker, G.D., Flores, R.M., McGarry, D.E., Stillwell, D.P., Hoppe, D.J., Stillwell, C.R., Ochs, A.L., Ellis, M.S., Osvald, K.S., Taylor. S.L., Thorvaldson, M.C., Trippi, M.H., Grose, S.D., Crockett, F.J. and Shariff, A.J., 2006. Gas desorption and adsorption isotherm studies of coals in the Powder River Basin, Wyoming and adjacent basins in Wyoming and North Dakota. U.S. Geological Survey Open-File Report 2006-1174.

Su, X., Feng, Y., Chen, J. and Pan, J., 2001. The characteristics and origins of cleat in coal from Western North China. International Journal of Coal Geology, 47(1): 51-62.

Suggate, R.P., 1959. New Zealand coals: their geological setting and its influence on their properties. New Zealand Department of Scientific and Industrial Research Bulletin, 134: 113p.

Suggate, R.P., 2000. The Rank(S-r) scale: its basis and its applicability as a maturity index for all coals. New Zealand Journal of Geology and Geophysics, 43(4): 521-553.

Sykes, R. and Lindqvist, J.K., 1993. Diagenetic quartz and amorphous silica in New Zealand coals. Organic Geochemistry, 20(6): 855-866.

Sýkorová, I. et al., 2005. Classification of huminite - ICCP System 1994. International Journal of Coal Geology, 62(1-2): 85-106.

Taylor, G.H. et al., 1998. Organic Petrology. Gebruder Borntraeger, Berlin, 704 pp.

Thielemann, T., Cramer, B. and Schippers, A., 2004. Coalbed methane in the Ruhr Basin, Germany: a renewable energy resource? Organic Geochemistry, 35(11-12): 1537-1549.

Thiyagarayan, P., Urban, V., Littrell. K., Ku, C., Wozniak, D.G., Belch, H., Vitt. R., Toeller, J., Leach, D., Haumann, J.R., Ostrowski, G.E., Donley, L.I., Hammonds, J., Carpenter, J.M. and Crawford, R.K., 1998. The performance of the small-angle diffractometer, SAND at IPNS, 14th Meeting of the International Collaboration on Advanced Neutron Sources, Starved Rock Lodge, Utica, Illinois.

Twombly, G., Stepanek, S.H. and Moore, T.A., 2004. Coalbed methane potential in the Waikato Coalfield of New Zealand: A comparison with developed basins in the United States, 2004 New Zealand Petroleum Conference Proceedings.

Ulrich, G. and Bower, S., 2008. Active methanogenesis and acetate utilization in Powder River Basin coals, United States. International Journal of Coal Geology, 76(1-2): 25-33.

Unsworth, J.F., Fowler, C.S. and Jones, L.F., 1989. Moisture in coal: 2. Maceral effects on pore structure. Fuel, 68(1): 18-26.

van Krevelen, D.W., 1993. Coal: Typology-Physics-Chemistry-Constitution. Elevier, Amsterdam.

Vickridge, I.C., Sparks, R.J. and Bibby, D.M., 1990. Nuclear Microprobe Studies of Boron and Calcium Distributions in Waikato Coals, New-Zealand. Fuel, 69(5): 660-662.

Vu, T.A.T., 2008. Origin and maturation of organic matter in New Zealand coals. PhD Thesis, Ernst-Moritz-Amdt University of Greifswald, Greifswald, 268 pp.

Vu, T.A.T., Horsfield, B. and Sykes, R., 2008. Influence of in-situ bitumen on the generation of gas and oil in New Zealand coals. Organic Geochemistry, 39(11): 1606-1619.

Wang, J., Yamada, O., Zhang, Z.-G., Suzuki, Y. and Sakanishi, K., 2008. Statistical analysis of concentrations of trace elements in a wide diversity of coals and its implications for understanding elemental modes of occurrence. Fuel, 87(10-11): 2211-2222.

Ward, C.R., 1991. Mineral Matter in Low-Rank Coals and Associated Strata of the Mae Moh Basin, Northern Thailand. International Journal of Coal Geology, 17(1): 69-93.

Ward, C.R., 1992. Mineral Matter in Triassic and Tertiary Low-Rank Coals from South-Australia. International Journal of Coal Geology, 20(3-4): 185-208.

Ward, C.R., 2002. Analysis and significance of mineral matter in coal seams. International Journal of Coal Geology, 50(1-4): 135-168.

Ward, C.R. and Barnsley, G.B., 1984. Introduction. In: C.R. Ward (Editor), Coal Geology and Coal Technology. Blackwell Scientific Publications, Melbourne, pp. 1-39.

Ward, C.R., Li, Z. and Gurba, L.W., 2007. Variations in elemental composition of macerals with vitrinite reflectance and organic sulphur in the Greta Coal Measures, New South Wales, Australia. International Journal of Coal Geology, 69(3): 205-219.

Ward, C.R., Li, Z. and Gurba, L.W., 2008. Comparison of elemental composition of macerals determined by electron microprobe to whole-coal ultimate analysis data. International Journal of Coal Geology, 75(3): 157-165.

Ward, C.R., Li, Z.S. and French, D., 2005. Geological sources of metals in coal and coal products. In: T.A. Moore, A. Black, J.A. Centeno, J.S. Harding and D.A. Trumm (Editors), Metal contaminants in New Zealand. Resolutionz Press, Christchurch, pp. 49-79.

Ward, C.R., Spears, D.A., Booth, C.A., Staton, I. and Gurba, L.W., 1999. Mineral matter and trace elements in coals of the Gunnedah Basin, New South Wales, Australia. International Journal of Coal Geology, 40(4): 281-308.

Warwick, P.D., Barker, C.E., SanFilipo, J.R. and Biewick, L.R.H., 2000. Preliminary Evaluation of the Coalbed Methane: Resources of the Gulf Coastal Plain. U.S. Geological Survey Open-File Report 00-143.

Warwick, P.D., Breland Jr, F.C. and Hackley, P.C., 2008. Biogenic origin of coalbed gas in the northern Gulf of Mexico Coastal Plain, U.S.A. International Journal of Coal Geology, 76(1-2): 119-137.

Warwick, P.D. and Stanton, R.W., 1988. Depositional models for two Tertiary coal-bearing sequences in the Powder River Basin, Wyoming, USA. Journal of the Geological Society, London, 145: 613-620.

Whiticar, M.J., Faber, E. and Schoell, M., 1986. Biogenic methane formation in marine and freshwater environments: CO_2 reduction vs. acetate fermentation– Isotope evidence. Geochimica et Cosmochimica Acta, 50: 693–709.

Wickman, T. and Jacks, G., 1993. Base cation nutrition for pine stands on lithic soils near Stockholm, Sweden. Applied Geochemistry, 8(Supplement 2): 199-202.

Wilkins, R.W.T., Wilmshurst, J.R., Russell, N.J., Hladky, G., Ellacott, M.V. and Buckingham, C., 1992. Fluorescence alteration and the suppression of vitrinite reflectance. Organic Geochemistry, 18(5): 629-640.

Winans, R.E., Clemans, T. and Seifert, S., 2006. Developing a new method for direct observation of the effects of CO_2 Injection into coal seams, 23rd International Pittsburgh Coal Conference.

Winans, R.E. and Thiyagarajan, P., 1988. Characterization of a solvent-swollen coal by small-angle neutron scattering. Energy & Fuels, 2: 356-358.

Wong, P.Z. and Bray, A.J., 1988. Porod scattering from fractal surfaces. Physical Review Letters, 60: 1344.

Wong, S., Law, D.H.-S., Deng, X., Robinson, J.M., Kadatz, B., Gunter, W. D., Jianping, Y., Sanli, F.and Zhiqiang, F., 2006. Enhanced coalbed methane- micro-pilot test at South Qinshui, Shanxi, China, 8th International Conference on Greenhouse Gas Control Technologies, Trondheim, Norway, 6 pp.

Wust, R.A.J. and Bustin, R.M., 2001. Low-ash peat deposits from a dendritic, intermontane basin in the tropics: a new model for good quality coals. International Journal of Coal Geology, 46(2-4): 179-206.

Wust, R.A.J. and Bustin, R.M., 2003. Opaline and Al-Si phytoliths from a tropical mire system of West Malaysia: abundance, habit, elemental composition, preservation and significance. Chemical Geology, 200(3-4): 267-292.

Wust, R.A.J., Hawke, M.I. and Bustin, R.M., 2001. Comparing maceral ratios from tropical peatlands with assumptions from coal studies: do classic coal petrographic interpretation methods have to be discarded? International Journal of Coal Geology, 48(1-2): 115-132.

Yao, Y., Liu, D., Tang, D., Tang, S. and Huang, W., 2008. Fractal characterization of adsorption-pores of coals from North China: An investigation on CH_4 adsorption capacity of coals. International Journal of Coal Geology, 73(1): 27-42.

Yee, D., Seidle, J.P. and Hanson, W.B., 1993. Gas sorption on coal and measurement of gas content. In: B.E. Law and D.D. Rice (Editors), Hydrocarbons from coal. American Association of Petroleum Geologists, Tulsa, Oklahoma, pp. 203-218.

Zarebska, K. and Ceglarska-Stefanska, G., 2008. The change in effective stress associated with swelling during carbon dioxide sequestration on natural gas recovery. International Journal of Coal Geology, 74(3-4): 167-258.

Zarrouk, S.J. and Moore, T.A., 2007. Preliminary assessment of the geothermal signature and ECBM potential of the Huntly coalbed methane field, New Zealand. Proceedings of the 29th New Zealand Geothermal Workshop., Auckland.

Zarrouk, S.J. and Moore, T.A., 2009. Preliminary reservoir model of enhanced coalbed methane (ECBM) in a subbituminous coal seam, Huntly Coalfield, New Zealand. International Journal of Coal Geology, 77(1-2): 153-161.

Appendix 1: Coal composition data

1.1. Proximate analysis data

Well	Canister	From	To	Thick	Seam	As Analysed					
						Moisture %	Ash %	VM %	FC %	CV (MJ/kg)	Sulphur %
TW1	9	338.70	339.20	0.50	Renown	11.6	5.5	36.5	46.4	24.98	0.30
TW1	10	339.20	339.70	0.50	Renown	12.9	3.8	35.4	47.9	25.02	0.30
TW1	11	339.70	340.20	0.50	Renown	9.2	2.9	42.0	45.9	26.90	0.30
TW1	12	340.20	340.70	0.50	Renown						
TW1	13	340.70	341.20	0.50	Renown	12.6	2.8	37.8	46.7	25.37	0.28
TW1	14	341.20	341.70	0.50	Renown	11.1	3.0	41.3	44.5	26.91	0.38
TW1	15	341.70	342.20	0.50	Renown	14.0	2.7	36.2	47.1	25.03	0.25
TW1	16	342.20	342.70	0.50	Renown	12.0	1.8	38.3	47.9	26.34	0.23
TW1	17	342.70	343.20	0.50	Renown	12.1	1.7	37.6	48.6	25.74	0.21
TW1	18	343.20	343.70	0.50	Renown	12.3	3.9	35.0	48.8	24.68	0.20
TW1	19	343.70	344.20	0.50	Renown	12.1	1.6	38.9	47.4	25.94	0.21
TW1	20	344.20	344.70	0.50	Renown	13.9	1.7	35.9	48.5	25.30	0.22
TW1	21	344.70	345.20	0.50	Renown	12.6	3.0	37.8	46.6	25.48	0.22
TW1	22	345.20	345.70	0.50	Renown	12.6	9.0	37.1	41.3	21.82	0.19
TW1	23	345.70	346.20	0.50	Renown						
TW1	24	346.20	346.70	0.50	Renown	8.4	33.4	29.2	29.0	16.55	0.21
TW1	25	346.70	347.20	0.50	Kupakupa	10.9	10.7	36.0	42.4	23.49	0.29
TW1	26	347.20	347.70	0.50	Kupakupa	12.7	5.2	35.4	46.7	24.54	0.24
TW1	27	347.70	348.20	0.50	Kupakupa	12.7	6.2	35.4	45.7	24.66	0.25
TW1	28	348.20	348.70	0.50	Kupakupa	15.5	3.4	33.6	47.5	23.99	0.25
TW1	29	348.70	349.20	0.50	Kupakupa	12.8	5.0	36.1	46.1	24.17	0.23
TW1	30	349.20	349.70	0.50	Kupakupa	13.5	3.8	35.9	46.8	24.13	0.22
TW1	31	349.70	350.20	0.50	Kupakupa	13.8	1.6	36.5	48.0	25.48	0.24
TW1	32	350.20	351.20	1.00	Kupakupa	12.8	2.1	38.4	46.8	25.97	0.26
TW1	33	351.20	351.70	0.50	Kupakupa	11.2	1.4	39.7	47.7	26.75	0.27
TW1	34	351.70	352.20	0.50	Kupakupa						
TW1	35	352.20	352.70	0.50	Kupakupa	11.1	4.7	38.1	46.1	24.68	0.25
TW1	36	352.70	353.39	0.69	Kupakupa	12.3	1.4	36.5	49.7	26.00	0.23
TW1	37	353.39	354.20	0.81	Kupakupa	11.2	1.5	36.6	50.7	25.99	0.24
TW1	38	354.20	354.70	0.50	Kupakupa	12.1	1.0	38.0	48.9	26.81	0.29
TW1	39	354.70	355.20	0.50	Kupakupa	11.4	1.0	37.9	49.7	26.80	0.28
TW1	40	355.20	355.70	0.50	Kupakupa						
TW1	41	355.70	356.20	0.50	Kupakupa	12.3	1.1	36.7	49.7	26.12	0.27
TW1	42	356.20	356.70	0.50	Kupakupa	12.1	2.3	36.6	49.0	25.49	0.24
TW1	43	356.70	357.20	0.50	Kupakupa	12.2	1.2	37.8	48.9	26.94	0.25
TW1	44	357.20	357.70	0.50	Kupakupa	12.2	1.0	41.7	45.1	27.91	0.23
TW1	45	357.70	358.20	0.50	Kupakupa	12.5	12.5	37.4	48.5	26.55	0.25

Appendix 1: Coal composition data

Well	Canister	From	To	Thick	Seam	As Analysed					
						Moisture %	Ash %	VM %	FC %	CV (MJ/kg)	Sulphur %
Ruawaro 1	A3	387.40	387.90	0.50	Ngaro	21.6	2.5	32.6	43.3	22.71	0.28
Ruawaro 1	A2	387.90	388.28	0.38	Ngaro	19.8	3.1	36.1	41.0	23.96	0.27
Ruawaro 1	A6	396.48	397.01	0.53	Renown	13.9	2.9	46.0	37.2	27.02	0.39
Ruawaro 1	A5	397.01	397.56	0.55	Renown	17.6	3.5	38.6	40.3	24.45	0.36
Ruawaro 1	A4	397.56	398.05	0.49	Renown	17.5	8.6	34.5	39.4	22.87	0.38
Ruawaro 1	A7	398.05	398.45	0.40	Renown	10.1	66.9	15.3	7.7	4.77	0.08
Ruawaro 1	A8	400.91	401.45	0.54	Renown	20.2	3.1	36.0	40.7	23.68	0.30
Ruawaro 1	A9	401.45	401.90	0.45	Renown	19.0	5.7	36.7	38.6	23.31	0.30
Ruawaro 1	A10	402.45	402.95	0.50	Renown	18.1	4.5	37.6	39.8	23.71	0.31
Ruawaro 1	A11	402.95	403.45	0.50	Renown	18.3	7.4	36.0	38.3	22.84	0.34
Ruawaro 1	A12	406.41	406.73	0.32	Renown	11.2	62.2	17.3	9.3	5.37	0.15
Ruawaro 1	A16	417.61	417.95	0.34	Kupakupa	18.7	2.9	36.5	41.9	24.10	0.46
Ruawaro 1	A15	417.95	418.45	0.50	Kupakupa	19.4	3.2	33.9	43.5	23.57	0.35
Ruawaro 1	A14	418.45	418.95	0.50	Kupakupa	19.1	2.6	35.1	43.2	23.60	0.33
Ruawaro 1	A13	418.95	419.45	0.50	Kupakupa	17.8	1.6	37.4	43.2	24.72	0.26
Ruawaro 1	A17	419.73	420.25	0.52	Kupakupa	19.4	1.5	36.1	43.0	24.15	0.23
Ruawaro 1	A18	420.25	420.80	0.55	Kupakupa	18.0	1.3	37.3	43.4	24.82	0.26
Ruawaro 1	A19	420.80	421.35	0.55	Kupakupa	19.2	1.6	35.0	44.2	24.08	0.25
Ruawaro 1	A20	421.35	421.85	0.50	Kupakupa	17.3	1.2	38.7	42.8	25.26	0.25
Ruawaro 1	A21	421.85	422.35	0.50	Kupakupa	19.3	1.4	35.8	43.5	24.33	0.23
Ruawaro 1	A22	422.45	422.95	0.50	Kupakupa	17.6	1.4	37.6	43.4	25.16	0.21
Ruawaro 1	A23	422.95	423.45	0.50	Kupakupa	19.6	1.5	35.2	43.7	23.82	0.22
Ruawaro 1	A24	423.45	423.95	0.50	Kupakupa	21.0	2.0	33.2	43.8	23.53	0.22
Ruawaro 1	A25	423.95	424.45	0.50	Kupakupa	20.1	1.6	35.7	42.6	23.93	0.29
Ruawaro 1	A26	424.45	424.95	0.50	Kupakupa	19.4	1.7	35.6	43.3	24.30	0.31
Ruawaro 1	A27	430.40	430.80	0.40	Kupakupa	20.5	4.2	29.9	45.4	23.00	0.68
Ruawaro 2	B1	433.38	433.93	0.55	Renown	18.7	3.0	37.5	40.8	23.96	0.25
Ruawaro 2	B2	433.94	434.34	0.40	Renown	18.7	11.1	32.8	37.4	21.33	0.22
Ruawaro 2	B3	434.34	434.84	0.50	Renown	20.2	2.0	33.7	44.1	23.28	0.24
Ruawaro 2	B4	434.84	435.34	0.50	Renown	20.6	1.9	34.0	43.5	23.16	0.22
Ruawaro 2	B5	435.34	435.84	0.50	Renown	20.8	2.1	36.1	41.0	23.24	0.21
Ruawaro 2	B6	435.84	436.19	0.35	Renown	20.8	2.1	35.4	41.7	23.29	0.21
Ruawaro 2	B7	436.19	436.69	0.50	Renown	19.0	2.1	36.2	42.7	23.69	0.22
Ruawaro 2	B8	436.69	437.19	0.50	Renown	18.8	2.0	36.2	43.0	23.90	0.22
Ruawaro 2	B9	437.19	437.69	0.50	Renown	21.1	1.9	34.2	42.8	23.09	0.21
Ruawaro 2	B10	437.69	438.19	0.50	Renown	19.7	2.3	36.4	41.6	23.86	0.21
Ruawaro 2	B11	438.19	438.69	0.50	Renown	18.1	11.3	33.4	37.2	21.46	0.20
Ruawaro 2	B12	438.69	439.19	0.50	Renown	25.8	4.7	31.3	38.2	20.76	0.22
Ruawaro 2	B13	439.19	439.69	0.50	Renown	23.2	3.3	32.9	40.6	22.24	0.27
Ruawaro 2	B14	439.69	440.19	0.50	Renown	21.9	2.8	33.3	42.0	23.08	0.28
Ruawaro 2	B15	440.19	440.49	0.30	Renown	18.0	31.2	25.7	25.1	15.25	0.29

Appendix 1: Coal composition data

Well	Canister	From	To	Thick	Seam	As Analysed					
						Moisture %	Ash %	VM %	FC %	CV (MJ/kg)	Sulphur %
Ruawaro 2	B16	458.20	458.70	0.50	Kupakupa	17.9	2.4	37.3	42.4	24.73	0.24
Ruawaro 2	B17	458.70	459.20	0.50	Kupakupa	18.7	2.0	35.4	43.9	24.25	0.22
Ruawaro 2	B18	459.20	459.70	0.50	Kupakupa	18.4	2.1	36.4	43.1	24.50	0.22
Ruawaro 2	B19	459.70	460.20	0.50	Kupakupa	20.1	1.6	33.8	44.5	23.93	0.19
Ruawaro 2	B20	460.20	460.70	0.50	Kupakupa	20.1	1.6	35.5	42.8	23.59	0.19
Ruawaro 2	B21	460.70	461.20	0.50	Kupakupa	19.0	1.6	35.9	43.5	24.18	0.20
Ruawaro 2	B22	461.20	461.70	0.50	Kupakupa	16.6	1.4	39.8	42.2	25.90	0.23
Ruawaro 2	B23	461.70	462.25	0.55	Kupakupa	16.2	1.4	41.0	41.4	26.24	0.22
Ruawaro 2	B24	462.30	462.85	0.55	Kupakupa	18.1	1.6	37.5	42.8	24.93	0.20
Ruawaro 2	B25	462.85	463.40	0.55	Kupakupa	17.8	1.8	38.7	41.7	25.34	0.21
Ruawaro 2	B26	463.43	464.03	0.60	Kupakupa	19.7	6.3	35.9	38.1	23.04	0.33
Rotongaro 1	C1	428.39	428.89	0.55	Ngaro	21.2	27.5	25.0	26.3	15.57	0.35
Rotongaro 1	C2	434.90	435.40	0.50	Renown	18.9	4.5	36.1	40.5	22.91	0.35
Rotongaro 1	C3	435.40	435.90	0.50	Renown	21.4	2.1	35.6	40.9	22.86	0.23
Rotongaro 1	C4	435.90	436.40	0.50	Renown	19.0	5.2	36.1	39.7	23.06	0.26
Rotongaro 1	C5	436.40	437.06	0.66	Renown	20.3	13.2	33.7	32.8	20.05	0.25
Rotongaro 1	C6	447.34	447.84	0.50	Kupakupa	18.5	9.8	34.3	37.4	21.30	0.28
Rotongaro 1	C7	447.89	448.39	0.50	Kupakupa	21.1	2.4	33.6	42.9	22.80	0.23
Rotongaro 1	C8	448.39	448.89	0.50	Kupakupa	21.1	2.7	33.1	43.1	22.50	0.22
Rotongaro 1	C9	448.89	449.29	0.40	Kupakupa	20.0	2.5	35.8	41.7	23.34	0.20
Rotongaro 1	C10	449.36	449.96	0.60	Kupakupa	20.9	1.7	35.7	41.7	23.28	0.19
Rotongaro 1	C11	449.96	450.46	0.50	Kupakupa	17.6	1.8	40.4	40.2	24.81	0.19
Rotongaro 1	C12	450.46	450.96	0.50	Kupakupa	15.7	4.0	42.8	37.5	25.45	0.22
Rotongaro 1	C13	450.96	451.46	0.50	Kupakupa	18.8	2.7	37.9	40.6	23.84	0.20
Rotongaro 1	C14	452.40	452.90	0.50	Kupakupa	20.1	1.6	35.6	42.7	23.40	0.19
Rotongaro 1	C15	452.90	453.40	0.50	Kupakupa	19.3	1.4	36.5	42.8	23.94	0.21
Rotongaro 1	C16	453.40	453.90	0.50	Kupakupa	18.8	1.3	38.0	41.9	24.35	0.21
Rotongaro 1	C17	453.90	454.40	0.50	Kupakupa	19.4	1.6	35.6	43.4	23.64	0.20
Rotongaro 1	C18	454.40	454.90	0.50	Kupakupa	20.0	1.6	36.0	42.4	23.55	0.17
Rotongaro 1	C19	454.90	455.40	0.50	Kupakupa	19.5	1.7	36.1	42.7	23.66	0.17
Rotongaro 1	C20	455.40	455.90	0.50	Kupakupa	19.6	1.4	36.4	42.6	23.81	0.20
Rotongaro 1	C21	455.90	456.40	0.50	Kupakupa	18.3	1.6	37.4	42.7	24.10	0.20
Rotongaro 1	C22	456.40	456.90	0.50	Kupakupa	20.8	1.4	35.1	42.7	23.53	0.20
Rotongaro 1	C23	456.90	457.40	0.50	Kupakupa	19.0	1.4	37.8	41.8	24.24	0.21
Rotongaro 1	C24	457.40	457.90	0.50	Kupakupa	19.6	1.5	36.4	42.5	23.76	0.21
Rotongaro 1	C25	457.90	458.40	0.50	Kupakupa	19.4	1.4	37.9	41.3	24.15	0.22
Rotongaro 1	C26	458.40	459.00	0.60	Kupakupa	18.7	1.9	37.8	41.6	24.42	0.26

Appendix 1: Coal composition data

Well	Canister	From	To	Thick	Seam	As Analysed					
						Moisture %	Ash %	VM %	FC %	CV (MJ/kg)	Sulphur %
Mangapiko 1	D1	482.35	482.85	0.50	Renown	17.5	24.4	29.1	29.0	17.72	0.29
Mangapiko 1	D2	482.85	483.35	0.50	Renown	15.1	38.9	21.8	24.2	13.57	0.16
Mangapiko 1	D3	483.35	483.85	0.50	Renown	19.9	2.9	35.6	41.6	23.30	0.25
Mangapiko 1	D4	483.85	484.35	0.50	Renown	20.2	2.7	34.4	42.7	23.02	0.25
Mangapiko 1	D5	484.35	484.85	0.50	Renown	19.1	4.4	35.7	40.8	23.29	0.22
Mangapiko 1	D6	484.85	485.25	0.40	Renown	19.0	2.4	37.2	41.4	24.06	0.24
Mangapiko 1	D7	485.30	485.80	0.50	Renown	19.2	2.7	36.9	41.2	24.15	0.25
Mangapiko 1	D8	485.80	486.30	0.50	Renown	18.8	2.2	38.1	40.9	24.16	0.24
Mangapiko 1	D9	486.30	486.80	0.50	Renown	20.6	2.1	35.7	41.6	23.52	0.25
Mangapiko 1	D10	486.90	487.30	0.40	Renown	21.2	3.5	34.8	40.5	22.84	0.29
Mangapiko 1	D11	512.10	512.60	0.50	Kupakupa	20.9	1.5	35.6	42.0	23.64	0.32
Mangapiko 1	D12	512.60	513.10	0.50	Kupakupa	28.4	1.8	32.4	37.4	21.15	0.22
Mangapiko 1	D13	513.10	513.60	0.50	Kupakupa	21.5	1.6	36.1	40.8	23.42	0.23
Mangapiko 1	D14	513.60	514.10	0.50	Kupakupa	21.9	1.6	35.8	40.7	23.33	0.23
Mangapiko 1	D15	514.40	514.90	0.50	Kupakupa	20.2	1.4	38.0	40.4	24.21	0.26
Mangapiko 1	D16	514.90	515.40	0.50	Kupakupa	19.5	1.5	38.1	40.9	24.39	0.24
Mangapiko 1	D17	515.40	515.90	0.50	Kupakupa	18.9	1.6	39.6	39.9	24.80	0.22
Mangapiko 1	D18	515.90	516.40	0.50	Kupakupa	19.9	1.6	38.5	40.0	24.25	0.24
Mangapiko 1	D19	516.40	516.95	0.55	Kupakupa	20.4	3.0	37.7	38.9	24.02	0.30
Mangapiko 1	D20	516.95	517.50	0.55	Kupakupa	18.7	14.0	35.8	31.5	20.65	0.37
Baco 1	Ba1	427.90	428.45	0.55	Renown	17.4	3.3	35.9	43.4	24.30	0.30
Baco 1	Ba2	428.45	429.00	0.55	Renown	16.7	2.4	37.5	43.4	24.86	0.24
Baco 1	Ba3	429.00	429.50	0.50	Renown	15.8	2.9	37.7	43.6	24.80	0.23
Baco 1	Ba4	429.50	430.00	0.50	Renown	15.4	2.5	38.3	43.8	25.11	0.23
Baco 1	Ba5	430.00	430.50	0.50	Renown	16.3	2.2	36.0	45.5	24.60	0.23
Baco 1	Ba6	430.50	431.00	0.50	Renown	15.6	2.2	37.6	44.6	25.01	0.25
Jasper 1	J1	407.81	408.31	0.50	Renown	6.8	40.9	26.5	25.8	15.06	0.17
Jasper 1	J2	408.31	408.81	0.50	Renown	11.1	9.0	37.7	42.2	22.96	0.24
Jasper 1	J3	408.81	409.31	0.50	Renown	11.0	4.2	40.6	44.2	25.53	0.24
Jasper 1	J4	409.31	409.81	0.50	Renown	13.2	4.9	36.9	45.0	24.52	0.23
Jasper 1	J5	410.00	410.35	0.35	Renown	11.7	3.7	39.0	45.6	25.32	0.21
Jasper 1	J6	410.35	410.85	0.50	Renown	12.3	2.6	39.3	45.8	25.65	0.19
Jasper 1	J7	410.85	411.35	0.50	Renown	11.4	2.7	40.7	45.2	26.10	0.19
Jasper 1	J8	411.35	411.85	0.50	Renown	11.3	2.6	39.3	46.8	25.96	0.19
Jasper 1	J9	412.00	412.50	0.50	Renown	11.6	2.3	39.7	46.4	26.10	0.20
Jasper 1	J10	412.50	413.00	0.50	Renown	11.8	2.4	38.1	47.7	25.68	0.23
Jasper 1	J11	413.00	413.55	0.55	Renown	11.6	5.2	37.3	45.9	24.76	0.25
Jasper 1	J12	413.55	414.02	0.47	Renown	6.1	64.4	18.0	11.5	6.65	0.11
Jasper 1	J13	414.02	414.40	0.38	Renown	3.9	69.2	16.2	10.7	5.85	0.12

Appendix 1: Coal composition data

Well	Canister	From	To	Thick	Seam	As Analysed					
						Moisture %	Ash %	VM %	FC %	CV (MJ/kg)	Sulphur %
Mimi 1	M1	407.45	407.95	0.50	Renown	15.1	3.5	37.2	44.2	24.64	0.26
Mimi 1	M2	407.95	408.45	0.50	Renown	15.1	2.2	39.0	43.7	25.37	0.25
Mimi 1	M3	408.45	408.98	0.53	Renown	16.9	4.1	35.2	43.8	23.66	0.23
Mimi 1	M4	409.03	409.58	0.55	Renown	15.8	6.1	35.3	42.8	23.29	0.22
Mimi 1	M5	409.58	410.13	0.55	Renown	15.0	4.6	37.7	42.7	23.88	0.20
Mimi 1	M6	410.13	410.63	0.50	Renown	14.9	3.4	38.3	43.4	24.51	0.20
Mimi 1	M7	410.63	411.13	0.50	Renown	12.6	2.7	38.8	45.9	25.49	0.21
Mimi 1	M8	411.13	411.63	0.50	Renown	12.3	2.4	38.2	47.1	25.57	0.21
Mimi 1	M9	411.63	412.13	0.50	Renown	12.7	2.3	38.5	46.5	25.62	0.22
Mimi 1	M10	412.18	412.83	0.65	Renown	13.7	2.6	37.2	46.5	25.10	0.25
Mimi 1	M11	412.83	413.48	0.65	Renown	12.1	10.8	36.1	41.0	23.45	0.31
Mimi 1	M12	413.58	414.08	0.50	Renown	4.6	64.3	17.8	13.3	7.20	0.14

VM = Volatile matter, FC = Fixed carbon, CV = Calorific value.

1.2. Ash constituents

				XRF											
Well	**Can**	**Seam**	**Mid-point**	**SiO2**	**Al2O3**	**Fe2O3**	**CaO**	**MgO**	**Na2O**	**K2O**	**TiO2**	**Mn3O4**	**SO3**	**P2O5**	**Total**
TW1	9	R	338.95	58.70	15.07	2.90	8.23	1.43	2.85	0.78	0.90	0.01	6.05	0.05	96.97
TW1	10	R	339.45	41.23	14.75	6.74	13.24	2.31	4.30	0.44	2.45	0.01	11.64	0.04	97.15
TW1	11	R	339.95	18.82	21.25	5.80	21.37	2.84	5.56	0.26	5.17	0.01	15.08	0.05	96.21
TW1	12	R	340.45	7.61	25.86	7.12	27.31	3.86	6.81	0.25	1.55	0.01	14.65	0.06	95.09
TW1	13	R	340.95	10.23	23.75	6.03	29.22	2.94	5.46	0.22	2.93	0.01	14.80	0.09	95.68
TW1	14	R	341.45	15.36	22.08	4.94	22.39	2.63	4.93	0.58	6.91	0.01	16.23	0.07	96.13
TW1	15	R	341.95	9.51	17.47	5.89	34.45	4.89	6.39	0.25	0.24	0.01	15.56	0.07	94.73
TW1	16	R	342.45	4.71	13.89	7.05	33.89	6.13	8.41	0.31	0.35	0.01	19.80	0.04	94.59
TW1	17	R	342.95	2.39	11.83	6.22	34.91	5.86	9.19	0.28	0.30	0.01	21.14	0.03	92.16
TW1	18	R	343.45	4.78	3.98	8.76	51.90	16.58	3.37	0.24	0.31	0.01	8.40	0.01	98.34
TW1	19	R	343.95	4.28	12.34	7.88	35.25	6.52	7.92	0.73	0.47	0.01	19.20	0.06	94.66
TW1	20	R	344.45	1.03	17.04	7.64	33.22	6.58	8.08	0.21	0.28	<0.01	19.29	0.03	93.40
TW1	21	R	344.95	5.20	13.22	4.94	46.54	5.57	5.79	0.21	0.47	0.02	13.63	0.03	95.62
TW1	22	R	345.45	3.68	4.68	4.94	74.69	5.64	1.24	0.17	0.12	0.05	4.69	0.03	99.93
TW1	23	R	345.95	17.83	22.63	4.48	31.86	3.67	4.42	0.21	0.53	0.01	9.80	0.37	95.81
TW1	24	R	346.45	57.10	31.79	1.23	1.60	0.47	0.62	0.48	3.47	<0.01	0.92	0.06	97.74
TW1	25	KK	346.95	47.73	27.55	1.94	7.29	1.57	1.98	0.32	4.66	<0.01	4.44	0.22	97.70
TW1	26	KK	347.45	27.95	28.85	2.88	18.41	4.74	3.50	0.37	0.69	<0.01	9.02	0.41	96.82
TW1	27	KK	347.95	39.96	25.95	1.98	7.83	1.38	2.45	0.33	11.20	<0.01	5.71	0.26	97.05
TW1	28	KK	348.45	26.73	31.51	2.58	14.01	2.55	4.70	0.17	1.95	<0.01	12.47	0.33	97.01
TW1	29	KK	348.95	9.30	10.76	5.48	52.83	7.64	2.06	0.14	1.51	0.02	7.84	1.29	98.87
TW1	30	KK	349.45	5.01	10.92	6.06	57.72	6.64	2.56	0.22	0.59	0.02	9.49	0.03	99.26
TW1	31	KK	349.95	3.31	25.43	3.78	27.84	4.24	7.07	0.21	1.40	<0.01	20.12	0.05	93.45
TW1	32	KK	350.70	1.75	16.65	4.75	30.41	4.88	5.65	0.21	12.45	0.01	18.47	0.06	95.29
TW1	33	KK	351.45	1.74	20.81	5.08	28.42	3.98	7.74	1.01	1.88	<0.01	23.31	0.02	94.00
TW1	34	KK	351.95	0.79	10.30	6.61	33.83	4.67	8.11	0.38	0.32	0.01	26.52	0.04	91.58
TW1	35	KK	352.45	0.96	0.94	6.77	71.01	10.99	1.00	0.09	0.06	0.03	6.54	0.01	98.40
TW1	36	KK	353.05	0.79	0.68	11.31	42.00	4.77	7.53	0.25	0.22	0.02	25.38	0.03	92.98
TW1	37	KK	353.80	4.27	1.40	12.42	33.86	6.07	7.90	0.44	0.17	0.01	25.49	0.04	92.07
TW1	38	KK	354.45	1.65	2.18	12.13	29.68	4.74	9.11	0.32	0.38	0.01	30.11	0.03	90.34
TW1	39	KK	354.95	2.37	1.86	9.08	31.54	4.46	9.13	0.33	0.29	0.01	31.82	0.03	90.92
TW1	40	KK	355.45	3.35	3.63	17.29	36.82	11.94	3.85	0.15	0.17	0.02	18.49	0.08	95.79
TW1	41	KK	355.95	3.80	2.02	9.05	32.05	5.02	8.49	0.37	0.18	0.01	30.89	0.04	91.92
TW1	42	KK	356.45	3.15	1.98	12.18	46.21	12.94	3.57	0.36	0.13	0.01	16.71	0.03	97.27
TW1	43	KK	356.95	2.54	3.79	10.80	31.45	5.20	8.52	0.35	0.49	0.01	27.01	0.05	90.21
TW1	44	KK	357.45	0.78	6.32	10.89	31.39	6.08	7.48	0.50	0.67	0.01	25.75	0.04	89.91
TW1	45	KK	357.95	7.35	24.14	3.75	22.46	1.88	6.36	0.33	10.70	0.01	15.53	0.08	92.60

Appendix 1: Coal composition data

				XRF										
Well	**Can**	**Seam**	**Mid-point**	**SiO2**	**Al2O3**	**Fe2O3**	**CaO**	**MgO**	**Na2O**	**K2O**	**TiO2**	**Mn3O4**	**SO3**	**P2O5**	**Total**
Ru 1	A3	N	387.65	4.05	4.78	25.42	25.34	4.53	8.97	0.19	0.29	0.27	21.11	0.06	95.01
Ru 1	A2	N	388.09	52.13	7.45	4.88	15.05	2.38	5.54	0.18	0.60	0.02	8.93	0.03	97.19
Ru 1	A6	R	396.75	11.43	18.99	6.88	29.34	3.42	5.79	0.17	1.68	0.02	18.01	0.32	96.05
Ru 1	A5	R	397.29	25.46	17.32	5.92	22.77	3.18	5.68	0.19	0.75	0.01	15.83	0.03	97.14
Ru 1	A4	R	397.81	47.69	31.95	2.48	8.01	1.17	1.82	0.52	3.96	<0.01	1.33	0.18	99.11
Ru 1	A7	R	398.25	64.29	29.18	1.76	0.57	0.54	0.25	0.64	1.82	<0.01	<0.01	0.03	99.08
Ru 1	A8	R	401.18	21.34	26.12	4.17	19.40	2.41	5.20	0.23	0.68	<0.01	11.46	4.41	95.42
Ru 1	A9	R	401.68	33.51	30.32	2.56	12.05	1.33	2.70	0.23	3.01	<0.01	5.61	5.25	96.57
Ru 1	A10	R	402.70	27.58	28.29	3.29	16.19	1.83	3.35	0.19	0.66	<0.01	8.21	6.08	95.67
Ru 1	A11	R	403.20	32.35	32.10	2.88	12.98	1.55	2.66	0.35	1.27	<0.01	5.33	4.90	96.37
Ru 1	A12	R	406.57	59.11	33.04	2.08	0.52	0.72	0.20	1.40	1.97	<0.01	<0.01	0.03	99.07
Ru 1	A16	KK	417.78	23.02	26.13	4.42	18.54	2.12	4.31	0.24	0.85	<0.01	15.29	1.79	96.71
Ru 1	A15	KK	418.20	23.39	22.65	5.10	20.67	2.21	4.60	0.16	3.32	<0.01	14.67	0.06	96.83
Ru 1	A14	KK	418.70	10.02	19.11	6.72	28.47	3.27	5.65	0.20	1.51	0.01	20.64	0.01	95.61
Ru 1	A13	KK	419.20	2.34	2.38	11.82	38.63	3.95	5.95	0.15	0.27	0.01	26.05	0.01	91.56
Ru 1	A17	KK	419.99	3.76	1.56	13.42	36.48	4.07	6.89	0.22	0.27	0.01	24.85	0.02	91.55
Ru 1	A18	KK	420.53	1.74	0.85	13.50	36.72	3.23	6.10	0.16	0.09	0.01	27.83	0.02	90.25
Ru 1	A19	KK	421.08	1.82	0.63	12.80	44.37	3.68	5.99	0.19	0.09	0.01	23.37	0.01	92.96
Ru 1	A20	KK	421.60	2.53	0.86	13.62	35.02	2.83	7.15	0.21	0.10	0.01	28.01	0.02	90.36
Ru 1	A21	KK	422.10	2.35	0.79	12.52	39.43	3.16	6.78	0.22	0.07	0.01	25.41	0.02	90.76
Ru 1	A22	KK	422.70	3.16	1.96	15.22	38.90	2.75	6.26	0.19	0.21	0.03	21.37	0.03	90.08
Ru 1	A23	KK	423.20	1.06	0.68	14.16	40.02	3.15	6.45	0.17	0.06	0.02	24.84	0.02	90.63
Ru 1	A24	KK	423.70	1.87	0.81	26.72	31.72	4.73	5.34	0.16	0.07	0.06	21.12	0.12	92.72
Ru 1	A25	KK	424.20	1.39	4.54	8.80	39.24	2.29	6.08	0.17	0.10	0.03	28.92	0.02	91.58
Ru 1	A26	KK	424.70	0.67	7.37	7.57	36.51	1.96	5.98	0.15	0.08	0.02	31.74	0.01	92.06
Ru 1	A27	KK	430.60	48.27	32.53	2.60	6.97	0.54	1.93	0.76	1.09	<0.01	2.06	0.45	97.20
Ru 2	B1	R	433.66	75.26	7.22	1.97	5.17	0.93	1.99	0.39	0.53	<0.01	3.26	0.02	96.74
Ru 2	B2	R	434.14	71.19	8.49	1.98	6.50	1.07	2.45	0.26	0.25	<0.01	3.96	0.76	96.91
Ru 2	B3	R	434.59	4.09	5.38	9.46	35.00	6.22	10.08	0.22	0.29	0.01	22.82	0.02	93.59
Ru 2	B4	R	435.09	2.70	3.45	10.16	36.06	6.27	10.63	0.27	0.57	0.01	23.00	0.01	93.13
Ru 2	B5	R	435.59	8.22	4.38	8.78	33.50	5.75	9.90	0.37	0.24	0.01	23.47	0.02	94.64
Ru 2	B6	R	436.02	12.90	3.45	9.50	34.31	5.96	9.50	0.30	0.30	0.01	18.19	0.02	94.44
Ru 2	B7	R	436.44	7.55	3.20	10.07	33.69	5.60	9.26	0.50	0.25	0.01	23.45	0.04	93.62
Ru 2	B8	R	436.94	0.96	6.35	8.56	37.66	6.29	10.09	0.30	0.25	0.01	22.61	0.01	93.09
Ru 2	B9	R	437.44	3.59	2.66	10.29	38.22	6.77	9.50	0.21	0.16	0.01	21.48	0.02	92.91
Ru 2	B10	R	437.94	4.25	14.32	8.80	33.05	5.38	9.22	0.21	0.15	0.01	19.09	0.01	94.49
Ru 2	B11	R	438.44	72.60	4.95	2.18	8.33	1.32	2.69	0.18	0.58	<0.01	3.71	0.01	96.55
Ru 2	B12	R	438.94	64.04	9.16	2.40	9.78	1.68	4.16	0.23	0.47	<0.01	5.27	0.19	97.38
Ru 2	B13	R	439.44	40.05	16.37	4.10	16.06	2.42	6.52	0.26	0.53	<0.01	11.10	0.02	97.43
Ru 2	B14	R	439.94	26.53	18.32	4.49	19.89	2.76	8.36	0.31	1.35	<0.01	14.52	0.14	96.67
Ru 2	B15	R	440.34	62.97	27.64	1.90	1.19	0.68	0.61	0.97	1.98	<0.01	0.17	0.03	98.14

Appendix 1: Coal composition data

				XRF											
Well	**Can**	**Seam**	**Mid-point**	**SiO2**	**Al2O3**	**Fe2O3**	**CaO**	**MgO**	**Na2O**	**K2O**	**TiO2**	**Mn3O4**	**SO3**	**P2O5**	**Total**
Ru 2	B16	KK	458.45	46.59	0.74	9.10	21.18	2.34	7.52	0.20	0.05	<0.01	7.76	0.01	95.49
Ru 2	B17	KK	458.95	31.83	1.25	10.44	25.39	2.78	8.42	0.24	0.10	0.01	13.84	0.01	94.31
Ru 2	B18	KK	459.45	35.60	0.89	10.93	24.42	2.57	7.85	0.46	0.07	0.01	11.86	0.01	94.67
Ru 2	B19	KK	459.95	6.38	0.93	15.87	32.43	3.63	10.16	0.26	0.07	0.01	20.97	0.02	90.73
Ru 2	B20	KK	460.45	8.83	1.91	11.97	37.61	3.97	8.91	0.24	0.12	0.01	18.34	0.01	91.92
Ru 2	B21	KK	460.95	4.95	1.07	12.15	38.91	3.86	8.60	0.17	0.11	0.01	21.71	0.01	91.55
Ru 2	B22	KK	461.45	1.59	0.89	15.08	36.03	3.11	8.07	0.23	0.09	0.01	25.67	0.02	90.79
Ru 2	B23	KK	461.98	1.64	1.34	14.78	36.53	2.62	7.57	0.18	0.12	0.01	25.82	0.02	90.63
Ru 2	B24	KK	462.58	4.25	4.27	10.59	40.65	3.03	6.52	0.13	1.34	0.01	20.15	0.01	90.95
Ru 2	B25	KK	463.13	4.03	12.01	8.92	34.64	2.17	8.21	0.28	0.57	0.01	20.24	0.02	91.10
Ru 2	B26	KK	463.73	14.20	31.50	2.50	17.60	0.55	2.51	0.11	6.25	<0.01	4.21	15.30	94.72
Ro 1	C1	N	428.64	94.93	1.23	0.35	1.38	0.20	0.53	0.00	0.33	0.00	0.75	0.10	99.81
Ro 1	C2	R	435.15	30.95	24.19	4.87	18.07	2.89	5.04	1.35	1.08	0.01	9.33	0.05	97.83
Ro 1	C3	R	435.65	7.99	1.78	8.70	37.65	5.45	8.92	0.28	0.12	0.02	22.23	0.01	93.15
Ro 1	C4	R	436.15	37.16	30.33	2.66	12.04	1.49	3.24	0.34	3.76	<0.01	4.99	1.69	97.70
Ro 1	C5	R	436.73	40.94	21.45	2.74	14.07	1.66	3.45	0.22	5.00	<0.01	6.63	1.41	97.57
Ro 1	C6	KK	447.59	38.49	31.34	2.39	11.31	1.37	2.46	0.20	2.62	<0.01	5.62	1.76	97.56
Ro 1	C7	KK	448.14	50.56	7.29	2.99	13.63	1.72	3.28	0.13	12.36	0.01	5.27	0.09	97.33
Ro 1	C8	KK	448.64	14.96	25.26	4.90	26.36	3.47	5.88	0.18	0.87	<0.01	14.70	0.02	96.60
Ro 1	C9	KK	449.09	19.75	25.82	4.56	23.65	2.90	4.74	0.16	2.06	<0.01	12.83	0.28	96.75
Ro 1	C10	KK	449.66	2.44	5.89	14.77	35.30	5.92	7.06	0.19	0.46	0.02	20.86	0.01	92.92
Ro 1	C11	KK	450.21	2.95	10.14	7.87	39.29	4.83	6.45	0.25	1.36	0.01	19.95	0.01	93.11
Ro 1	C12	KK	450.71	21.71	15.36	4.20	22.93	2.39	3.98	0.14	17.57	0.01	8.62	0.10	97.01
Ro 1	C13	KK	451.21	6.37	15.16	5.33	28.32	3.16	5.13	0.18	17.22	0.01	14.82	0.07	95.77
Ro 1	C14	KK	452.65	0.22	0.64	19.20	36.20	5.84	6.33	0.15	0.13	0.02	23.94	0.01	92.68
Ro 1	C15	KK	453.15	0.75	0.82	12.84	44.45	4.71	7.12	0.25	0.16	0.01	22.62	0.01	93.74
Ro 1	C16	KK	453.65	0.38	0.51	12.59	41.17	4.16	7.10	0.29	0.19	0.01	24.06	0.01	90.47
Ro 1	C17	KK	454.15	0.66	0.89	12.18	45.89	4.36	6.92	0.24	0.38	0.01	22.29	0.01	93.83
Ro 1	C18	KK	454.65	0.50	0.63	12.34	47.89	4.35	6.63	0.22	0.09	0.02	21.32	0.01	94.00
Ro 1	C19	KK	455.15	0.76	0.90	11.81	48.43	4.32	6.98	0.25	0.10	0.02	20.87	0.01	94.45
Ro 1	C20	KK	455.65	1.55	0.62	11.63	39.77	3.49	6.53	0.17	0.08	0.01	27.13	0.02	91.00
Ro 1	C21	KK	456.15	0.80	0.66	10.94	47.55	3.84	5.91	0.17	0.10	0.01	24.67	0.01	94.66
Ro 1	C22	KK	456.65	2.15	0.83	15.52	38.95	4.14	6.45	0.20	0.10	0.02	22.36	0.01	90.73
Ro 1	C23	KK	457.15	0.06	1.15	11.29	46.89	3.28	6.13	0.19	0.20	0.02	24.70	0.01	93.92
Ro 1	C24	KK	457.65	0.15	1.64	10.86	46.94	3.22	5.94	0.15	0.19	0.02	24.90	0.01	94.02
Ro 1	C25	KK	458.15	0.33	1.73	9.86	47.54	3.00	5.87	0.14	0.15	0.03	25.55	0.01	94.21
Ro 1	C26	KK	458.70	1.53	22.67	5.38	36.45	1.51	5.42	0.20	0.87	0.03	19.48	0.02	93.56

Appendix 1: Coal composition data

				XRF											
Well	**Can**	**Seam**	**Mid-point**	**SiO2**	**Al2O3**	**Fe2O3**	**CaO**	**MgO**	**Na2O**	**K2O**	**TiO2**	**Mn3O4**	**SO3**	**P2O5**	**Total**
Ma 1	D1	R	482.60	78.01	10.64	0.92	2.76	0.56	0.89	0.49	2.97	<0.01	0.88	0.02	98.14
Ma 1	D2	R	483.10	90.03	1.49	1.07	2.23	0.39	0.50	0.23	0.19	<0.01	0.99	<0.01	97.12
Ma 1	D3	R	483.60	16.37	5.03	7.34	31.25	6.87	9.23	0.23	0.38	0.01	18.34	0.01	95.06
Ma 1	D4	R	484.10	26.69	2.15	7.69	27.65	6.29	8.65	0.24	0.30	0.01	16.08	0.01	95.76
Ma 1	D5	R	484.60	42.57	1.72	6.96	22.49	4.87	6.80	0.33	0.39	<0.01	10.46	<0.01	96.59
Ma 1	D6	R	485.05	16.62	6.61	7.14	29.23	5.78	8.40	0.26	2.72	<0.01	18.41	0.01	95.18
Ma 1	D7	R	485.55	22.60	8.35	6.13	26.36	5.12	8.08	0.33	3.79	<0.01	14.52	0.01	95.29
Ma 1	D8	R	486.05	12.83	10.19	6.35	31.48	6.03	8.03	0.22	1.66	<0.01	17.57	0.01	94.37
Ma 1	D9	R	486.55	7.00	13.39	5.84	28.78	5.43	8.39	0.25	1.95	<0.01	24.30	0.01	95.34
Ma 1	D10	R	487.10	23.64	17.95	4.01	20.66	3.61	5.76	0.28	2.82	<0.01	15.97	1.85	96.55
Ma 1	D11	KK	512.35	18.00	14.56	8.06	23.72	3.04	5.66	0.34	2.84	0.01	18.90	0.08	95.21
Ma 1	D12	KK	512.85	4.47	2.52	10.63	37.81	4.59	7.30	0.27	0.26	0.01	26.19	0.04	94.08
Ma 1	D13	KK	513.35	2.06	1.44	12.46	39.87	4.47	7.00	0.25	0.11	0.03	26.75	0.01	94.45
Ma 1	D14	KK	513.85	1.54	1.28	12.84	36.15	4.34	7.50	0.28	0.09	0.03	27.48	0.01	91.54
Ma 1	D15	KK	514.65	0.91	0.77	13.97	35.61	3.41	7.42	0.25	0.07	0.03	27.89	0.03	90.36
Ma 1	D16	KK	515.15	1.29	1.41	12.33	43.41	3.50	5.53	0.22	0.12	0.05	26.95	0.02	94.83
Ma 1	D17	KK	515.65	1.92	3.24	11.24	37.46	2.99	6.30	0.24	0.17	0.05	27.36	0.01	90.98
Ma 1	D18	KK	516.15	1.78	3.13	11.12	43.46	3.36	6.05	0.22	0.19	0.05	25.35	0.04	94.75
Ma 1	D19	KK	516.68	5.57	27.16	5.00	28.28	1.56	4.53	0.18	4.73	0.04	16.87	1.02	94.94
Ma 1	D20	KK	517.23	39.04	39.81	1.71	5.79	0.35	0.65	0.15	6.20	<0.01	1.69	2.17	97.56
Baco	Ba1	R	428.18	24.41	12.46	8.80	22.81	3.64	7.74	1.20	1.89	0.05	12.93	0.07	96.00
Baco	Ba2	R	428.73	5.47	11.36	11.87	34.88	5.97	10.03	0.87	0.64	0.03	16.27	0.02	97.41
Baco	Ba3	R	429.25	15.91	2.37	18.06	31.43	5.13	8.45	0.81	0.29	0.09	14.27	0.02	96.83
Baco	Ba4	R	429.75	11.89	1.99	11.42	39.72	6.33	9.58	0.85	0.29	0.03	14.90	0.01	97.01
Baco	Ba5	R	430.25	3.71	1.42	11.30	42.19	6.95	11.10	0.99	0.13	0.02	18.99	0.01	96.81
Baco	Ba6	R	430.75	5.63	1.77	11.42	40.80	6.26	9.40	0.68	0.26	0.02	20.48	0.01	96.73
Jasp	J1	R	408.06	78.71	5.90	1.78	7.52	0.54	0.41	0.43	0.61	0.01	0.69	0.10	96.70
Jasp	J2	R	408.56	31.76	7.48	6.57	39.59	2.88	2.99	0.44	0.35	0.06	5.31	0.56	97.99
Jasp	J3	R	409.06	11.75	2.77	10.37	51.32	4.60	5.31	0.29	0.25	0.06	12.71	0.10	99.53
Jasp	J4	R	409.56	21.61	19.11	4.50	28.31	3.22	5.89	0.57	2.13	0.01	10.77	1.71	97.83
Jasp	J5	R	410.18	17.36	13.74	5.13	34.84	4.27	6.23	0.51	0.76	<0.01	14.66	0.38	97.88
Jasp	J6	R	410.60	8.26	5.91	8.85	38.76	6.26	8.92	0.80	0.33	0.01	18.50	0.09	96.69
Jasp	J7	R	411.10	17.94	2.41	8.95	34.96	6.14	7.65	0.43	0.36	<0.01	18.55	0.03	97.42
Jasp	J8	R	411.60	9.32	2.53	10.00	40.78	6.63	7.16	0.35	0.24	<0.01	18.76	0.02	95.79
Jasp	J9	R	412.25	7.49	2.45	9.74	38.62	6.94	8.96	0.47	0.27	<0.01	21.80	0.02	96.76
Jasp	J10	R	412.75	4.61	2.46	10.28	41.53	7.33	8.87	0.50	0.17	0.01	20.01	0.01	95.78
Jasp	J11	R	413.28	18.18	10.46	9.14	34.13	3.77	4.77	0.67	1.71	0.01	12.26	2.27	97.37
Jasp	J12	R	413.79	63.12	26.11	2.10	0.83	0.81	0.40	1.44	1.84	<0.01	0.11	0.04	98.80
Jasp	J13	R	414.21	69.36	22.63	1.76	0.65	0.57	0.29	0.96	1.97	<0.01	0.01	0.04	98.24

Appendix 1: Coal composition data

				XRF											
Well	**Can**	**Seam**	**Mid-point**	**SiO2**	**Al2O3**	**Fe2O3**	**CaO**	**MgO**	**Na2O**	**K2O**	**TiO2**	**Mn3O4**	**SO3**	**P2O5**	**Total**
Mimi	M1	R	407.70	39.40	1.01	8.82	24.00	4.83	8.29	0.54	0.26	0.02	11.82	<0.01	98.99
Mimi	M2	R	408.20	6.78	6.44	12.20	34.34	6.72	12.07	0.36	0.27	0.02	18.27	0.01	97.48
Mimi	M3	R	408.72	21.22	21.38	5.45	23.14	4.14	8.07	0.40	1.56	0.01	9.73	3.05	98.15
Mimi	M4	R	409.31	35.46	20.79	4.27	20.35	2.92	5.72	0.70	0.80	0.01	6.74	1.16	98.92
Mimi	M5	R	409.86	13.35	5.57	7.75	50.52	4.41	5.95	0.20	0.46	0.02	9.21	0.18	97.62
Mimi	M6	R	410.38	9.88	2.44	10.67	50.58	6.19	6.41	0.28	0.25	0.01	12.32	0.05	99.08
Mimi	M7	R	410.88	12.54	2.19	11.71	37.28	7.57	8.83	0.48	0.25	0.01	16.01	0.01	96.88
Mimi	M8	R	411.38	2.87	1.98	12.94	40.63	8.82	10.18	0.60	0.11	0.01	17.51	0.01	95.66
Mimi	M9	R	411.88	5.76	2.55	11.45	38.65	8.06	10.24	0.33	0.24	0.01	18.50	0.01	95.80
Mimi	M10	R	412.51	4.10	1.97	11.33	42.31	7.11	7.89	0.23	0.11	0.01	20.73	0.01	95.80
Mimi	M11	R	413.16	55.97	20.64	2.53	7.89	1.56	2.63	0.49	3.94	<0.01	3.63	0.20	99.48
Mimi	M12	R	413.83	67.19	23.88	1.95	0.69	0.77	0.40	1.49	1.42	<0.01	0.10	0.04	97.93

Ru 1 = Ruawaro 1, Ru 2 = Ruawaro 2, Ro 1 = Rotongaro 1, Ma 1 = Mangapiko 1, Jasp = Jasper 1.
R = Renown seam, KK = Kupakupa seam.

1.3. Forms of Sulphur in the TW1 drill hole

Can	Ash (db)	Sulphur (db)	Sulphate Sulphur (db)	Pyritic Sulphur (db)	Organic Sulphur (db)
	%	%	%	%	%
9	6.2	0.35	<0.01	0.04	0.31
10	4.4	0.34	0.01	0.03	0.31
11	3.2	0.33	0.01	0.03	0.30
13	3.3	0.33	<0.01	0.02	0.31
14	3.4	0.43	0.02	0.03	0.38
15	3.1	0.29	0.01	0.03	0.25
16	2.0	0.26	0.03	0.03	0.20
17	1.9	0.24	0.01	0.01	0.22
18	4.5	0.23	0.02	0.02	0.19
19	1.9	0.24	<0.01	0.01	0.23
20	2.0	0.25	0.02	0.01	0.22
21	3.4	0.25	0.01	0.01	0.23
22	10.3	0.22	<0.01	0.02	0.20
24	36.4	0.23	0.01	0.02	0.20
25	12.0	0.32	0.01	0.01	0.30
26	6.0	0.28	0.01	0.01	0.26
27	7.1	0.29	0.01	0.01	0.27
28	4.0	0.30	0.01	0.01	0.28
29	5.7	0.26	0.01	0.02	0.23
30	4.4	0.26	0.01	0.01	0.24
31	1.9	0.28	0.02	0.01	0.25
32	2.4	0.29	0.01	0.01	0.27
33	1.6	0.31	<0.01	0.01	0.30
35	5.3	0.28	0.01	0.02	0.25
36	1.6	0.26	<0.01	0.02	0.24
37	1.7	0.27	<0.01	0.03	0.24
38	1.2	0.33	0.01	0.02	0.30
39	1.1	0.32	<0.01	0.01	0.31
41	1.3	0.31	<0.01	0.02	0.29
42	2.7	0.28	<0.01	0.04	0.24
43	1.3	0.28	<0.01	0.03	0.25
44	1.1	0.26	0.01	0.02	0.23
45	1.9	0.28	<0.01	0.01	0.27

db = dry basis

1.4. Ultimate analysis data

1.4.1. Ultimate analysis data (db) by canister

Hole	Can	Mid-point	Seam	Ash db	Carbon %	Hydrogen %	Nitrogen %	Sulphur %	Oxygen %
Jasper 1	J1	408.06	Renown	43.88	41.40	2.98	0.61	0.17	10.96
Jasper 1	J2	408.56	Renown	10.12	65.60	4.47	1.13	0.24	18.44
Jasper 1	J3	409.06	Renown	4.72	70.50	4.97	1.14	0.24	18.43
Jasper 1	J4	409.56	Renown	5.65	71.10	4.84	1.15	0.23	17.03
Jasper 1	J5	410.18	Renown	4.19	72.00	4.95	1.17	0.21	17.48
Jasper 1	J6	410.60	Renown	2.96	73.60	5.08	1.19	0.19	16.98
Jasper 1	J7	411.10	Renown	3.05	72.90	5.06	1.13	0.19	17.67
Jasper 1	J8	411.60	Renown	2.93	72.80	4.92	1.17	0.19	17.99
Jasper 1	J9	412.25	Renown	2.60	73.30	5.02	1.15	0.20	17.73
Jasper 1	J10	412.75	Renown	2.72	73.20	4.84	1.25	0.23	17.76
Jasper 1	J11	413.28	Renown	5.88	69.40	4.74	1.03	0.25	18.70
Jasper 1	J12	413.79	Renown	68.58	21.10	2.31	0.25	0.11	7.65
Jasper 1	J13	414.21	Renown	72.01	20.20	1.97	0.23	0.12	5.47
Mimi 1	M1	407.70	Renown	4.12	71.50	5.05	1.13	0.26	17.94
Mimi 1	M2	408.20	Renown	2.59	73.10	5.24	1.15	0.25	17.67
Mimi 1	M3	408.72	Renown	4.93	70.90	4.93	1.15	0.23	17.86
Mimi 1	M4	409.31	Renown	7.24	68.90	4.76	1.10	0.22	17.78
Mimi 1	M5	409.86	Renown	5.41	70.00	4.90	1.13	0.20	18.36
Mimi 1	M6	410.38	Renown	4.00	71.70	5.03	1.14	0.20	17.93
Mimi 1	M7	410.88	Renown	3.09	72.10	4.96	1.14	0.21	18.50
Mimi 1	M8	411.38	Renown	2.74	72.10	4.91	1.17	0.21	18.87
Mimi 1	M9	411.88	Renown	2.63	72.80	4.97	1.16	0.22	18.22
Mimi 1	M10	412.51	Renown	3.01	72.30	4.87	1.17	0.25	18.40
Mimi 1	M11	413.16	Renown	12.29	65.30	4.76	0.97	0.31	16.37
Mimi 1	M12	413.83	Renown	67.40	23.60	2.26	0.27	0.14	6.33
Mimi 1	M2 r	repeat	Renown	2.60	72.40	4.91	1.36	0.25	18.48
Mimi 1	M4 r	repeat	Renown	7.20	68.40	4.54	1.33	0.22	18.31
Mimi 1	M6 r	repeat	Renown	4.00	71.70	4.61	1.29	0.20	18.20
Ruawaro 2	B16	458.45	Kupakupa	2.90	72.20	4.89	1.26	0.24	18.51
Ruawaro 2	B17	458.95	Kupakupa	2.60	73.90	5.17	1.02	0.25	17.10
Ruawaro 2	B18	459.45	Kupakupa	2.60	72.80	4.78	1.26	0.22	18.34
Ruawaro 2	B19	459.95	Kupakupa	2.00	72.30	4.63	1.18	0.19	19.70
Ruawaro 2	B20	460.45	Kupakupa	2.20	74.90	5.36	0.94	0.25	16.40
Ruawaro 2	B21	460.95	Kupakupa	2.00	72.50	4.63	1.30	0.20	19.37
Ruawaro 2	B22	461.45	Kupakupa	1.70	73.90	5.12	1.26	0.23	17.79
Ruawaro 2	B23	461.98	Kupakupa	1.70	74.00	5.37	1.22	0.22	17.49
Ruawaro 2	B24	462.58	Kupakupa	2.30	74.00	5.09	1.04	0.24	17.30
Ruawaro 2	B25	463.13	Kupakupa	2.20	73.10	5.10	1.12	0.21	18.27
Ruawaro 2	B26	463.73	Kupakupa	7.80	68.40	4.89	1.11	0.33	17.47

1.4.2. Ultimate analysis composites

Composites:			**Ultimate % (Dry Basis)**		
Well	**Seam**	**Canisters**	**Carbon**	**Hydrogen**	**Nitrogen**
Ruawaro 1	Renown	A4 - A12	62.11	4.80	1.00
Ruawaro 1	Kupakupa	A13 -A27	74.24	4.98	1.16
Ruawaro 2	Renown	B1 - B15	71.09	4.88	1.15
Ruawaro 2	Kupakupa	B16 - B26	74.44	5.36	1.02
Rotongaro 1	Ngaro	C1	49.48	3.57	0.77
Rotongaro 1	Renown	C2 - C5	68.69	4.90	1.07
Rotongaro 1	Kupakupa	C6 - C26	73.87	5.11	1.00
Mangapiko 1	Renown	D1 - D10	67.84	4.79	1.31
Mangapiko 1	Kupakupa	D11 - D20	72.44	5.29	1.23

1.5. Correlation tables of ash constituents by seam

1.5.1. Correlation tables with all samples included

Renown	Ash db	1/Ash db	SiO2	Al2O3	Fe2O3	CaO	MgO	Na2O	K2O	TiO2	Mn3O4	SO3	P2O5
Ash db	1												
1/Ash db	-0.69	1											
SiO2	0.69	-0.83	1										
Al2O3	0.42	-0.48	0.34	1									
Fe2O3	-0.55	0.72	-0.76	-0.67	1								
CaO	-0.62	0.65	-0.86	-0.61	0.75	1							
MgO	-0.54	0.71	-0.78	-0.63	0.77	0.81	1						
Na2O	-0.69	0.89	-0.80	-0.57	0.82	0.65	0.72	1					
K2O	0.52	-0.29	0.28	0.23	-0.05	-0.32	-0.23	-0.22	1				
TiO2	0.19	-0.35	0.27	0.59	-0.46	-0.46	-0.46	-0.39	0.09	1			
Mn3O4	-0.23	0.14	-0.32	-0.34	0.54	0.48	0.23	0.22	0.11	-0.26	1		
SO3	-0.69	0.93	-0.86	-0.52	0.75	0.68	0.71	0.92	-0.31	-0.31	0.15	1	
P2O5	-0.08	-0.22	0.05	0.46	-0.27	-0.20	-0.27	-0.21	-0.15	0.15	-0.17	-0.21	1

Kupakupa	Ash db	1/Ash db	SiO2	Al2O3	Fe2O3	CaO	MgO	Na2O	K2O	TiO2	Mn3O4	SO3	P2O5
Ash db	1												
1/Ash db	-0.77	1											
SiO2	0.57	-0.63	1										
Al2O3	0.69	-0.70	0.57	1									
Fe2O3	-0.58	0.62	-0.57	-0.81	1								
CaO	-0.52	0.42	-0.78	-0.72	0.52	1							
MgO	-0.30	0.23	-0.42	-0.41	0.36	0.57	1						
Na2O	-0.66	0.78	-0.49	-0.60	0.54	0.25	0.00	1					
K2O	-0.04	0.17	0.13	0.15	-0.15	-0.26	0.02	0.18	1				
TiO2	0.43	-0.47	0.37	0.45	-0.52	-0.46	-0.28	-0.39	-0.08	1			
Mn3O4	-0.29	0.20	-0.47	-0.44	0.51	0.51	0.15	0.07	-0.25	-0.22	1		
SO3	-0.70	0.86	-0.80	-0.67	0.63	0.51	0.16	0.75	0.02	-0.48	0.39	1	
P2O5	0.33	-0.31	0.14	0.36	-0.27	-0.25	-0.22	-0.32	-0.13	0.17	-0.17	-0.34	1

1.5.2. Correlation tables with no high ash yield (>20%) samples included

Renown	Ash db	1/Ash db	SiO2	Al2O3	Fe2O3	CaO	MgO	Na2O	K2O	TiO2	Mn3O4	SO3	P2O5
Ash db	1												
1/Ash db	-0.85	1											
SiO2	0.70	-0.72	1										
Al2O3	0.24	-0.40	0.26	1									
Fe2O3	-0.56	0.59	-0.69	-0.67	1								
CaO	-0.46	0.43	-0.81	-0.56	0.66	1							
MgO	-0.52	0.59	-0.72	-0.62	0.71	0.75	1						
Na2O	-0.69	0.81	-0.70	-0.53	0.76	0.47	0.62	1					
K2O	-0.03	0.01	0.03	-0.06	0.25	-0.06	-0.01	0.14	1				
TiO2	0.33	-0.32	0.29	0.58	-0.47	-0.48	-0.47	-0.41	0.00	1			
Mn3O4	0.37	-0.31	0.07	-0.24	0.36	0.27	-0.12	-0.16	0.23	-0.13	1		
SO3	-0.72	0.89	-0.79	-0.44	0.67	0.52	0.60	0.87	-0.04	-0.30	-0.30	1	
P2O5	0.17	-0.40	0.18	0.58	-0.37	-0.33	-0.37	-0.36	-0.12	0.16	-0.08	-0.36	1

Kupakupa	Ash db	1/Ash db	SiO2	Al2O3	Fe2O3	CaO	MgO	Na2O	K2O	TiO2	Mn3O4	SO3	P2O5
Ash db	1												
1/Ash db	-0.77	1											
SiO2	0.64	-0.66	1										
Al2O3	0.70	-0.70	0.58	1									
Fe2O3	-0.58	0.62	-0.58	-0.81	1								
CaO	-0.54	0.43	-0.79	-0.71	0.52	1							
MgO	-0.28	0.18	-0.42	-0.40	0.35	0.58	1						
Na2O	-0.74	0.82	-0.49	-0.61	0.54	0.25	0.00	1					
K2O	-0.06	0.14	0.15	0.15	-0.15	-0.25	0.00	0.17	1				
TiO2	0.36	-0.45	0.39	0.43	-0.51	-0.45	-0.26	-0.41	-0.10	1			
Mn3O4	0.11	-0.18	-0.23	0.03	0.25	0.21	-0.06	-0.28	-0.26	-0.16	1		
SO3	-0.75	0.88	-0.80	-0.67	0.62	0.51	0.14	0.75	0.00	-0.49	0.08	1	
P2O5	0.37	-0.33	0.14	0.37	-0.27	-0.25	-0.22	-0.31	-0.13	0.18	0.17	-0.34	1

Appendix 2: Coal petrology data

2.1. Vitrinite reflectance histograms

2.1.1. Mangapiko 1 Renown

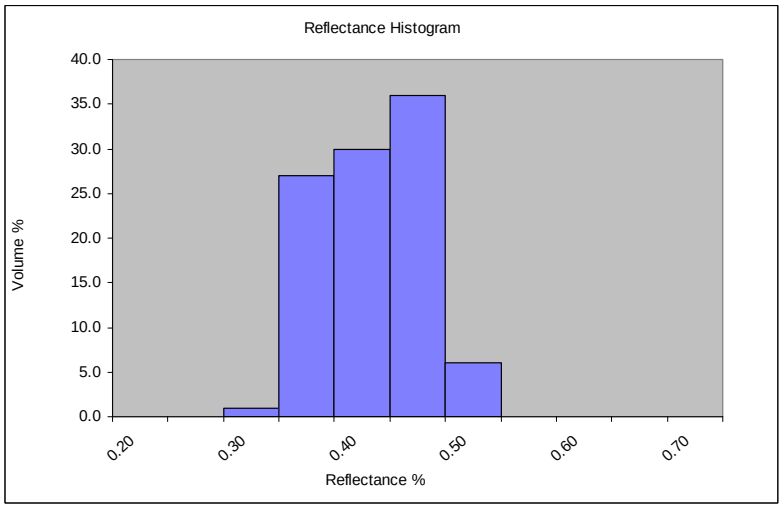

2.1.2. Mangapiko 1 Kupakupa

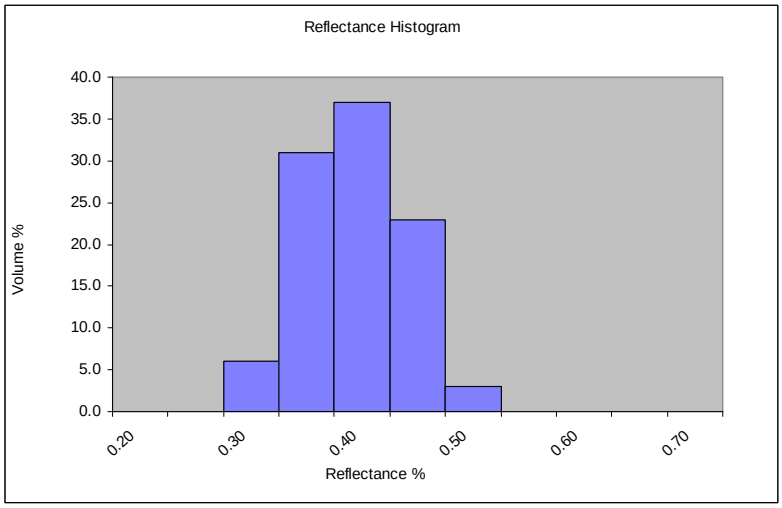

2.1.3. Jasper 1 Renown

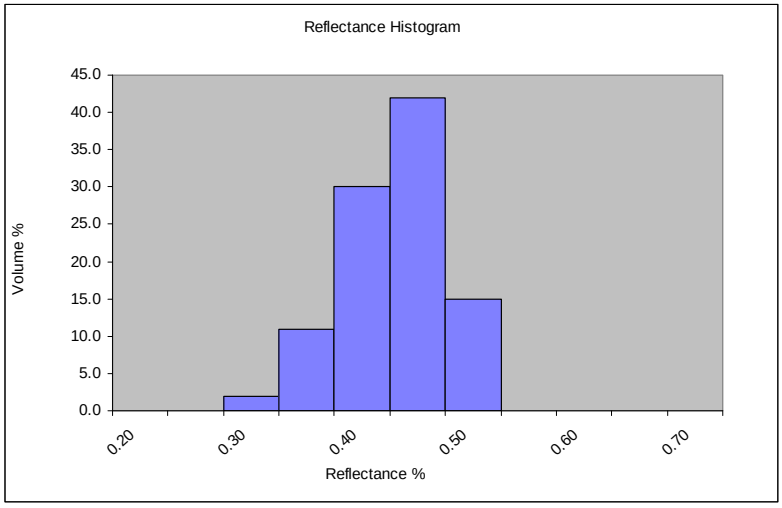

2.1.4. Mimi 1 Renown

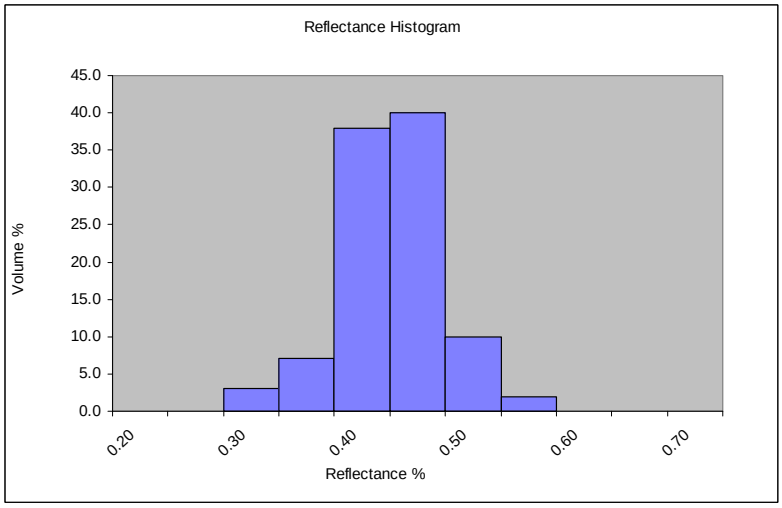

2.2. Suggate plot data

Well	Canister	Mid-point	Seam	Moisture %	Ash %	VM %	FC %	CV (MJ/kg)	Sulphur %	VM % (dmmSf)	CV (dmmSf)
TW1	9	338.95	Renown	11.6	5.5	36.5	46.4	24.98	0.3	43.63	30.41
TW1	10	339.45	Renown	12.9	3.8	35.4	47.9	25.02	0.3	42.21	30.25
TW1	11	339.95	Renown	9.2	2.9	42	45.9	26.9	0.3	47.60	30.78
TW1	12	340.45	Renown					28.18			
TW1	13	340.95	Renown	12.6	2.8	37.8	46.7	25.37	0.28	44.48	30.16
TW1	14	341.45	Renown	11.1	3	41.3	44.5	26.91	0.38	47.89	31.53
TW1	15	341.95	Renown	14	2.7	36.2	47.1	25.03	0.25	43.25	30.21
TW1	16	342.45	Renown	12	1.8	38.3	47.9	26.34	0.23	44.30	30.68
TW1	17	342.95	Renown	12.1	1.7	37.6	48.6	25.74	0.21	43.49	29.97
TW1	18	343.45	Renown	12.3	3.9	35	48.8	24.68	0.2	41.47	29.64
TW1	19	343.95	Renown	12.1	1.6	38.9	47.4	25.94	0.21	44.96	30.16
TW1	20	344.45	Renown	13.9	1.7	35.9	48.5	25.3	0.22	42.40	30.09
TW1	21	344.95	Renown	12.6	3	37.8	46.6	25.48	0.22	44.58	30.35
TW1	22	345.45	Renown	12.6	9	37.1	41.3	21.82	0.19	46.70	28.20
TW1	23	345.95	Renown					25.17			
TW1	24	346.45	Renown	8.4	33.4	29.2	29	16.55	0.21	47.13	30.25
TW1	25	346.95	Kupakupa	10.9	10.7	36	42.4	23.49	0.29		
TW1	26	347.45	Kupakupa	12.7	5.2	35.4	46.7	24.54	0.24	42.73	30.14
TW1	27	347.95	Kupakupa	12.7	6.2	35.4	45.7	24.66	0.25	43.19	30.71
TW1	28	348.45	Kupakupa	15.5	3.4	33.6	47.5	23.99	0.25	41.16	29.77
TW1	29	348.95	Kupakupa	12.8	5	36.1	46.1	24.17	0.23	43.56	29.64
TW1	30	349.45	Kupakupa	13.5	3.8	35.9	46.8	24.13	0.22	43.13	29.37
TW1	31	349.95	Kupakupa	13.8	1.6	36.5	48	25.48	0.24	43.02	30.23
TW1	32	350.70	Kupakupa	12.8	2.1	38.4	46.8	25.97	0.26	44.97	30.66
TW1	33	351.45	Kupakupa	11.2	1.4	39.7	47.7	26.75	0.27	45.32	30.72
TW1	34	351.95	Kupakupa					25.88			
TW1	35	352.45	Kupakupa	11.1	4.7	38.1	46.1	24.68	0.25	44.93	29.54
TW1	36	353.05	Kupakupa	12.3	1.4	36.5	49.7	26	0.23	42.18	30.23
TW1	37	353.80	Kupakupa	11.2	1.5	36.6	50.7	25.99	0.24	41.80	29.88
TW1	38	354.45	Kupakupa	12.1	1	38	48.9	26.81	0.29	43.64	30.96
TW1	39	354.95	Kupakupa	11.4	1	37.9	49.7	26.8	0.28	43.18	30.70
TW1	40	355.45	Kupakupa					26.68			
TW1	41	355.95	Kupakupa	12.3	1.1	36.7	49.7	26.12	0.27	42.28	30.26
TW1	42	356.45	Kupakupa	12.1	2.3	36.6	49	25.49	0.24	42.58	29.92
TW1	43	356.95	Kupakupa	12.2	1.2	37.8	48.9	26.94	0.25	43.55	31.21
TW1	44	357.45	Kupakupa	12.2	1	41.7	45.1	27.91	0.23	47.98	32.25
TW1	45	357.95	Kupakupa	12.5	12.5	37.4	48.5	26.55	0.25	49.01	36.09

Appendix 2: Coal petrology data

Well	Canister	Mid-point	Seam	Moisture %	Ash %	VM %	FC %	CV (MJ/kg)	Sulphur %	VM % (dmmSf)	CV (dmmSf)
Ruawaro 1	A3	387.65	Ngaro	21.6	2.5	32.6	43.3	22.71	0.28	42.74	30.10
Ruawaro 1	A2	388.09	Ngaro	19.8	3.1	36.1	41.0	23.96	0.27	46.60	31.28
Ruawaro 1	A6	396.75	Renown	13.9	2.9	46.0	37.2	27.02	0.39	55.16	32.70
Ruawaro 1	A5	397.29	Renown	17.6	3.5	38.6	40.3	24.45	0.36	48.69	31.23
Ruawaro 1	A4	397.81	Renown	17.5	8.6	34.5	39.4	22.87	0.38	46.04	31.43
Ruawaro 1	A7	398.25	Renown	10.1	66.9	15.3	7.7	4.77	0.08	52.80	29.34
Ruawaro 1	A8	401.18	Renown	20.2	3.1	36.0	40.7	23.68	0.30	46.71	31.08
Ruawaro 1	A9	401.68	Renown	19.0	5.7	36.7	38.6	23.31	0.30	48.34	31.28
Ruawaro 1	A10	402.70	Renown	18.1	4.5	37.6	39.8	23.71	0.31	48.27	30.90
Ruawaro 1	A11	403.20	Renown	18.3	7.4	36.0	38.3	22.84	0.34	47.92	31.15
Ruawaro 1	A12	406.57	Renown	11.2	62.2	17.3	9.3	5.37	0.15	54.40	26.47
Ruawaro 1	A16	417.78	Kupakupa	18.7	2.9	36.5	41.9	24.10	0.46	46.34	30.98
Ruawaro 1	A15	418.20	Kupakupa	19.4	3.2	33.9	43.5	23.57	0.35	43.54	30.68
Ruawaro 1	A14	418.70	Kupakupa	19.1	2.6	35.1	43.2	23.60	0.33	44.62	30.33
Ruawaro 1	A13	419.20	Kupakupa	17.8	1.6	37.4	43.2	24.72	0.26	46.28	30.80
Ruawaro 1	A17	419.99	Kupakupa	19.4	1.5	36.1	43.0	24.15	0.23	45.52	30.65
Ruawaro 1	A18	420.53	Kupakupa	18.0	1.3	37.3	43.4	24.82	0.26	46.12	30.88
Ruawaro 1	A19	421.08	Kupakupa	19.2	1.6	35.0	44.2	24.08	0.25	44.06	30.54
Ruawaro 1	A20	421.60	Kupakupa	17.3	1.2	38.7	42.8	25.26	0.25	47.40	31.11
Ruawaro 1	A21	422.10	Kupakupa	19.3	1.4	35.8	43.5	24.33	0.23	45.03	30.79
Ruawaro 1	A22	422.70	Kupakupa	17.6	1.4	37.6	43.4	25.16	0.21	46.32	31.17
Ruawaro 1	A23	423.20	Kupakupa	19.6	1.5	35.2	43.7	23.82	0.22	44.49	30.30
Ruawaro 1	A24	423.70	Kupakupa	21.0	2.0	33.2	43.8	23.53	0.22	42.95	30.69
Ruawaro 1	A25	424.20	Kupakupa	20.1	1.6	35.7	42.6	23.93	0.29	45.47	30.71
Ruawaro 1	A26	424.70	Kupakupa	19.4	1.7	35.6	43.3	24.30	0.31	44.98	30.95
Ruawaro 1	A27	430.60	Kupakupa	20.5	4.2	29.9	45.4	23.00	0.68	39.27	30.90
Ruawaro 2	B1	433.66	Renown	18.7	3.0	37.5	40.8	23.96	0.25	47.68	30.78
Ruawaro 2	B2	434.14	Renown	18.7	11.1	32.8	37.4	21.33	0.22	45.85	30.94
Ruawaro 2	B3	434.59	Renown	20.2	2.0	33.7	44.1	23.28	0.24	43.15	30.07
Ruawaro 2	B4	435.09	Renown	20.6	1.9	34.0	43.5	23.16	0.22	43.72	30.02
Ruawaro 2	B5	435.59	Renown	20.8	2.1	36.1	41.0	23.24	0.21	46.67	30.28
Ruawaro 2	B6	436.02	Renown	20.8	2.1	35.4	41.7	23.29	0.21	45.76	30.35
Ruawaro 2	B7	436.44	Renown	19.0	2.1	36.2	42.7	23.69	0.22	45.72	30.16
Ruawaro 2	B8	436.94	Renown	18.8	2.0	36.2	43.0	23.90	0.22	45.56	30.31
Ruawaro 2	B9	437.44	Renown	21.1	1.9	34.2	42.8	23.09	0.21	44.26	30.12
Ruawaro 2	B10	437.94	Renown	19.7	2.3	36.4	41.6	23.86	0.21	46.50	30.74
Ruawaro 2	B11	438.44	Renown	18.1	11.3	33.4	37.2	21.46	0.20	46.44	30.96
Ruawaro 2	B12	438.94	Renown	25.8	4.7	31.3	38.2	20.76	0.22	44.64	30.14
Ruawaro 2	B13	439.44	Renown	23.2	3.3	32.9	40.6	22.24	0.27	44.49	30.47
Ruawaro 2	B14	439.94	Renown	21.9	2.8	33.3	42.0	23.08	0.28	43.99	30.84
Ruawaro 2	B15	440.34	Renown	18.0	31.2	25.7	25.1	15.25	0.29	47.34	32.12

Appendix 2: Coal petrology data

Well	Canister	Mid-point	Seam	Moisture %	Ash %	VM %	FC %	CV (MJ/kg)	Sulphur %	VM % (dmmSf)	CV (dmmSf)
Ruawaro 2	B16	458.45	Kupakupa	17.9	2.4	37.3	42.4	24.73	0.24	46.63	31.19
Ruawaro 2	B17	458.95	Kupakupa	18.7	2.0	35.4	43.9	24.25	0.22	44.49	30.72
Ruawaro 2	B18	459.45	Kupakupa	18.4	2.1	36.4	43.1	24.50	0.22	45.63	30.96
Ruawaro 2	B19	459.95	Kupakupa	20.1	1.6	33.8	44.5	23.93	0.19	43.03	30.68
Ruawaro 2	B20	460.45	Kupakupa	20.1	1.6	35.5	42.8	23.59	0.19	45.21	30.24
Ruawaro 2	B21	460.95	Kupakupa	19.0	1.6	35.9	43.5	24.18	0.20	45.09	30.57
Ruawaro 2	B22	461.45	Kupakupa	16.6	1.4	39.8	42.2	25.90	0.23	48.44	31.70
Ruawaro 2	B23	461.98	Kupakupa	16.2	1.4	41.0	41.4	26.24	0.22	49.67	31.96
Ruawaro 2	B24	462.58	Kupakupa	18.1	1.6	37.5	42.8	24.93	0.20	46.58	31.16
Ruawaro 2	B25	463.13	Kupakupa	17.8	1.8	38.7	41.7	25.34	0.21	48.01	31.65
Ruawaro 2	B26	463.73	Kupakupa	19.7	6.3	35.9	38.1	23.04	0.33	48.06	31.50
Rotongaro 1	C1	428.64	Ngaro	21.2	27.5	25.0	26.3	15.57	0.35	45.80	32.23
Rotongaro 1	C2	435.15	Renown	18.9	4.5	36.1	40.5	22.91	0.35	46.80	30.18
Rotongaro 1	C3	435.65	Renown	21.4	2.1	35.6	40.9	22.86	0.23	46.38	30.03
Rotongaro 1	C4	436.15	Renown	19.0	5.2	36.1	39.7	23.06	0.26	47.25	30.70
Rotongaro 1	C5	436.73	Renown	20.3	13.2	33.7	32.8	20.05	0.25	49.68	30.84
Rotongaro 1	C6	447.59	Kupakupa	18.5	9.8	34.3	37.4	21.30	0.28	47.10	30.20
Rotongaro 1	C7	448.14	Kupakupa	21.1	2.4	33.6	42.9	22.80	0.23	43.73	29.96
Rotongaro 1	C8	448.64	Kupakupa	21.1	2.7	33.1	43.1	22.50	0.22	43.22	29.69
Rotongaro 1	C9	449.09	Kupakupa	20.0	2.5	35.8	41.7	23.34	0.20	46.01	30.27
Rotongaro 1	C10	449.66	Kupakupa	20.9	1.7	35.7	41.7	23.28	0.19	46.00	30.20
Rotongaro 1	C11	450.21	Kupakupa	17.6	1.8	40.4	40.2	24.81	0.19	50.01	30.90
Rotongaro 1	C12	450.71	Kupakupa	15.7	4.0	42.8	37.5	25.45	0.22	53.07	31.91
Rotongaro 1	C13	451.21	Kupakupa	18.8	2.7	37.9	40.6	23.84	0.20	48.10	30.53
Rotongaro 1	C14	452.65	Kupakupa	20.1	1.6	35.6	42.7	23.40	0.19	45.34	30.00
Rotongaro 1	C15	453.15	Kupakupa	19.3	1.4	36.5	42.8	23.94	0.21	45.92	30.30
Rotongaro 1	C16	453.65	Kupakupa	18.8	1.3	38.0	41.9	24.35	0.21	47.47	30.58
Rotongaro 1	C17	454.15	Kupakupa	19.4	1.6	35.6	43.4	23.64	0.20	44.94	30.04
Rotongaro 1	C18	454.65	Kupakupa	20.0	1.6	36.0	42.4	23.55	0.17	45.80	30.14
Rotongaro 1	C19	455.15	Kupakupa	19.5	1.7	36.1	42.7	23.66	0.17	45.69	30.13
Rotongaro 1	C20	455.65	Kupakupa	19.6	1.4	36.4	42.6	23.81	0.20	45.97	30.24
Rotongaro 1	C21	456.15	Kupakupa	18.3	1.6	37.4	42.7	24.10	0.20	46.58	30.20
Rotongaro 1	C22	456.65	Kupakupa	20.8	1.4	35.1	42.7	23.53	0.20	45.00	30.35
Rotongaro 1	C23	457.15	Kupakupa	19.0	1.4	37.8	41.8	24.24	0.21	47.39	30.56
Rotongaro 1	C24	457.65	Kupakupa	19.6	1.5	36.4	42.5	23.76	0.21	46.02	30.23
Rotongaro 1	C25	458.15	Kupakupa	19.4	1.4	37.9	41.3	24.15	0.22	47.76	30.60
Rotongaro 1	C26	458.70	Kupakupa	18.7	1.9	37.8	41.6	24.42	0.26	47.47	30.90

Appendix 2: Coal petrology data

Well	Canister	Mid-point	Seam	Moisture %	Ash %	VM %	FC %	CV (MJ/kg)	Sulphur %	VM % (dmmSf)	CV (dmmSf)
Mangapiko 1	D1	482.60	Renown	17.5	24.4	29.1	29.0	17.72	0.29	47.89	31.95
Mangapiko 1	D2	483.10	Renown	15.1	38.9	21.8	24.2	13.57	0.16	42.50	32.31
Mangapiko 1	D3	483.60	Renown	19.9	2.9	35.6	41.6	23.30	0.25	45.90	30.36
Mangapiko 1	D4	484.10	Renown	20.2	2.7	34.4	42.7	23.02	0.25	44.40	30.03
Mangapiko 1	D5	484.60	Renown	19.1	4.4	35.7	40.8	23.29	0.22	46.35	30.68
Mangapiko 1	D6	485.05	Renown	19.0	2.4	37.2	41.4	24.06	0.24	47.16	30.77
Mangapiko 1	D7	485.55	Renown	19.2	2.7	36.9	41.2	24.15	0.25	47.05	31.10
Mangapiko 1	D8	486.05	Renown	18.8	2.2	38.1	40.9	24.16	0.24	48.08	30.74
Mangapiko 1	D9	486.55	Renown	20.6	2.1	35.7	41.6	23.52	0.25	46.02	30.57
Mangapiko 1	D10	487.10	Renown	21.2	3.5	34.8	40.5	22.84	0.29	45.95	30.55
Mangapiko 1	D11	512.35	Kupakupa	20.9	1.5	35.6	42.0	23.64	0.32	45.75	30.61
Mangapiko 1	D12	512.85	Kupakupa	28.4	1.8	32.4	37.4	21.15	0.22	46.27	30.45
Mangapiko 1	D13	513.35	Kupakupa	21.5	1.6	36.1	40.8	23.42	0.23	46.82	30.59
Mangapiko 1	D14	513.85	Kupakupa	21.9	1.6	35.8	40.7	23.33	0.23	46.68	30.63
Mangapiko 1	D15	514.65	Kupakupa	20.2	1.4	38.0	40.4	24.21	0.26	48.37	31.00
Mangapiko 1	D16	515.15	Kupakupa	19.5	1.5	38.1	40.9	24.39	0.24	48.12	31.00
Mangapiko 1	D17	515.65	Kupakupa	18.9	1.6	39.6	39.9	24.80	0.22	49.71	31.32
Mangapiko 1	D18	516.15	Kupakupa	19.9	1.6	38.5	40.0	24.25	0.24	48.94	31.03
Mangapiko 1	D19	516.68	Kupakupa	20.4	3.0	37.7	38.9	24.02	0.30	49.01	31.57
Mangapiko 1	D20	517.23	Kupakupa	18.7	14.0	35.8	31.5	20.65	0.37	52.21	31.47
Baco 1	Ba1	428.18	Renown	17.4	3.3	35.9	43.4	24.30	0.30	45.02	30.85
Baco 1	Ba2	428.73	Renown	16.7	2.4	37.5	43.4	24.86	0.24	46.18	30.88
Baco 1	Ba3	429.25	Renown	15.8	2.9	37.7	43.6	24.80	0.23	46.17	30.67
Baco 1	Ba4	429.75	Renown	15.4	2.5	38.3	43.8	25.11	0.23	46.48	30.74
Baco 1	Ba5	430.25	Renown	16.3	2.2	36.0	45.5	24.60	0.23	44.00	30.32
Baco 1	Ba6	430.75	Renown	15.6	2.2	37.6	44.6	25.01	0.25	45.58	30.57
Jasper 1	J1	408.06	Renown	6.8	40.9	26.5	25.8	15.06	0.17	46.47	31.32
Jasper 1	J2	408.56	Renown	11.1	9.0	37.7	42.2	22.96	0.24	46.57	29.12
Jasper 1	J3	409.06	Renown	11.0	4.2	40.6	44.2	25.53	0.24	47.61	30.32
Jasper 1	J4	409.56	Renown	13.2	4.9	36.9	45.0	24.52	0.23	44.71	30.18
Jasper 1	J5	410.18	Renown	11.7	3.7	39.0	45.6	25.32	0.21	45.85	30.11
Jasper 1	J6	410.60	Renown	12.3	2.6	39.3	45.8	25.65	0.19	46.01	30.28
Jasper 1	J7	411.10	Renown	11.4	2.7	40.7	45.2	26.10	0.19	47.21	30.53
Jasper 1	J8	411.60	Renown	11.3	2.6	39.3	46.8	25.96	0.19	45.47	30.29
Jasper 1	J9	412.25	Renown	11.6	2.3	39.7	46.4	26.10	0.20	45.96	30.44
Jasper 1	J10	412.75	Renown	11.8	2.4	38.1	47.7	25.68	0.23	44.23	30.07
Jasper 1	J11	413.28	Renown	11.6	5.2	37.3	45.9	24.76	0.25	44.47	30.01
Jasper 1	J12	413.79	Renown	6.1	64.4	18.0	11.5	6.65	0.11	50.13	28.93
Jasper 1	J13	414.21	Renown	3.9	69.2	16.2	10.7	5.85	0.12	46.42	29.40

Appendix 2: Coal petrology data

Well	Canister	Mid-point	Seam	Moisture %	Ash %	VM %	FC %	CV (MJ/kg)	Sulphur %	VM % (dmmSf)	CV (dmmSf)
Mimi 1	M1	407.70		15.1	3.5	37.2	44.2	24.64	0.26	45.45	30.47
Mimi 1	M2	408.20		15.1	2.2	39.0	43.7	25.37	0.25	47.01	30.82
Mimi 1	M3	408.72		16.9	4.1	35.2	43.8	23.66	0.23	44.25	30.17
Mimi 1	M4	409.31		15.8	6.1	35.3	42.8	23.29	0.22	44.75	30.11
Mimi 1	M5	409.86		15.0	4.6	37.7	42.7	23.88	0.20	46.58	29.92
Mimi 1	M6	410.38		14.9	3.4	38.3	43.4	24.51	0.20	46.65	30.18
Mimi 1	M7	410.88		12.6	2.7	38.8	45.9	25.49	0.21	45.62	30.24
Mimi 1	M8	411.38		12.3	2.4	38.2	47.1	25.57	0.21	44.61	30.11
Mimi 1	M9	411.88		12.7	2.3	38.5	46.5	25.62	0.22	45.13	30.28
Mimi 1	M10	412.51		13.7	2.6	37.2	46.5	25.10	0.25	44.25	30.14
Mimi 1	M11	413.16		12.1	10.8	36.1	41.0	23.45	0.31	46.05	30.93
Mimi 1	M12	413.83		4.6	64.3	17.8	13.3	7.20	0.14	46.07	29.30

2.3. VIRF analysis figures

2.3.1. Jasper 1 Renown seam

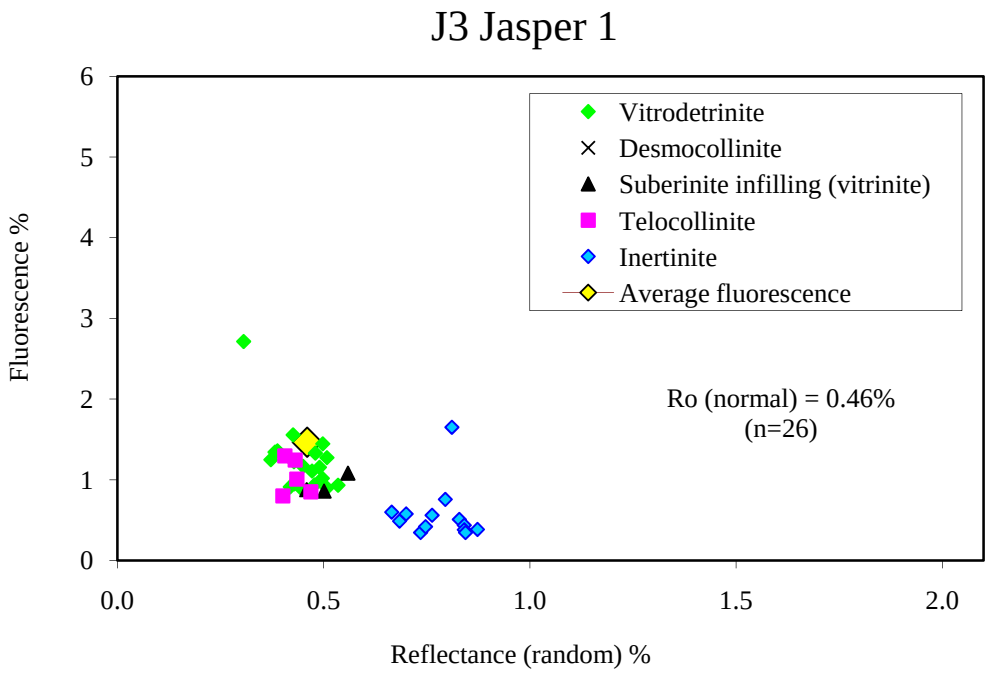

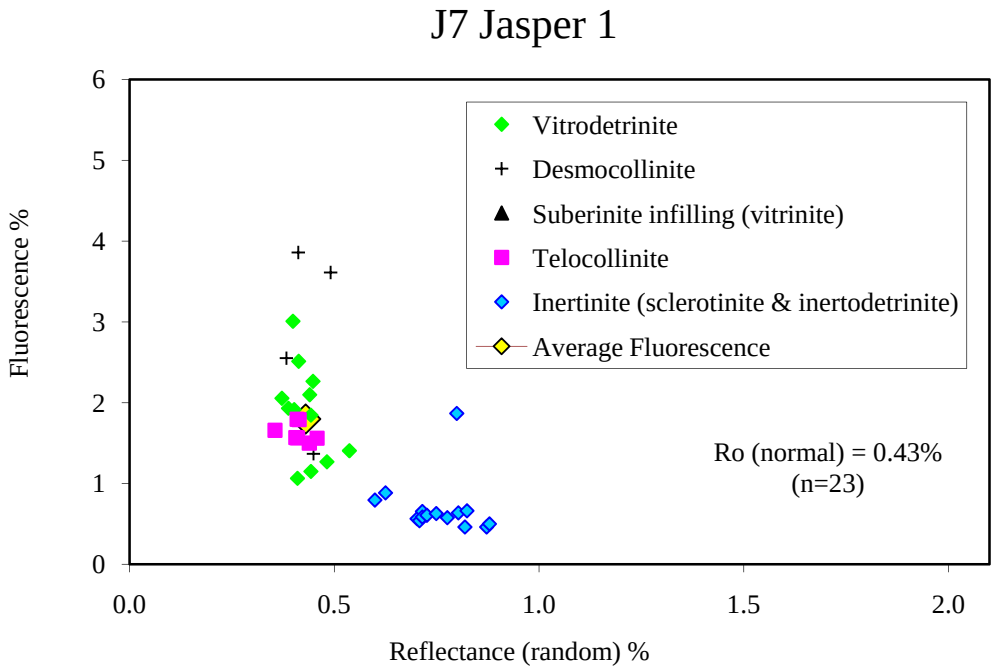

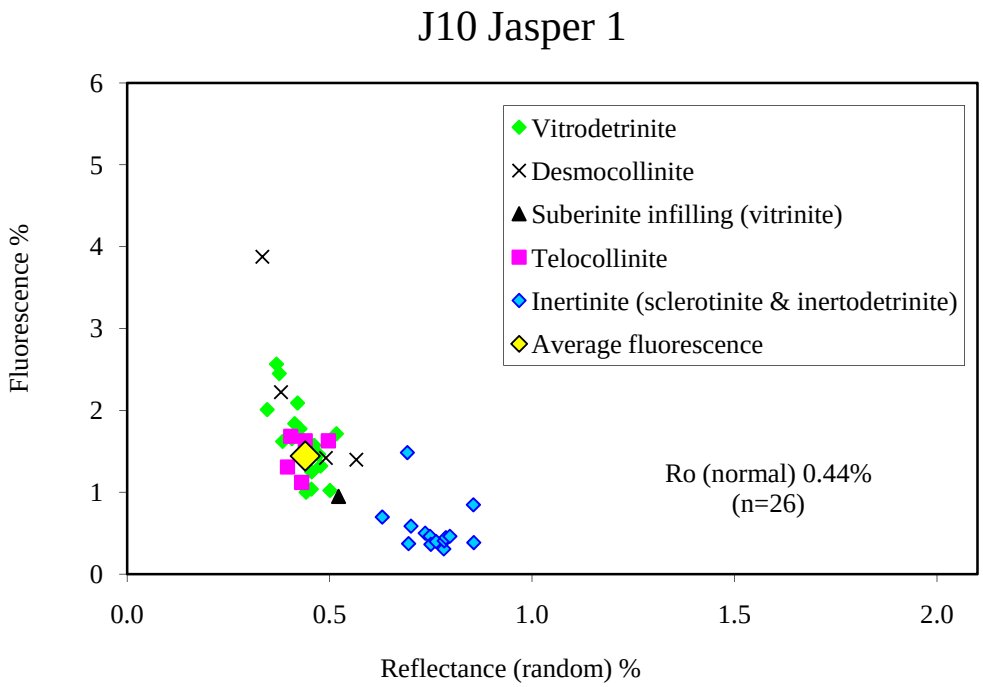

2.3.2. Ruawaro 2 Kupakupa seam

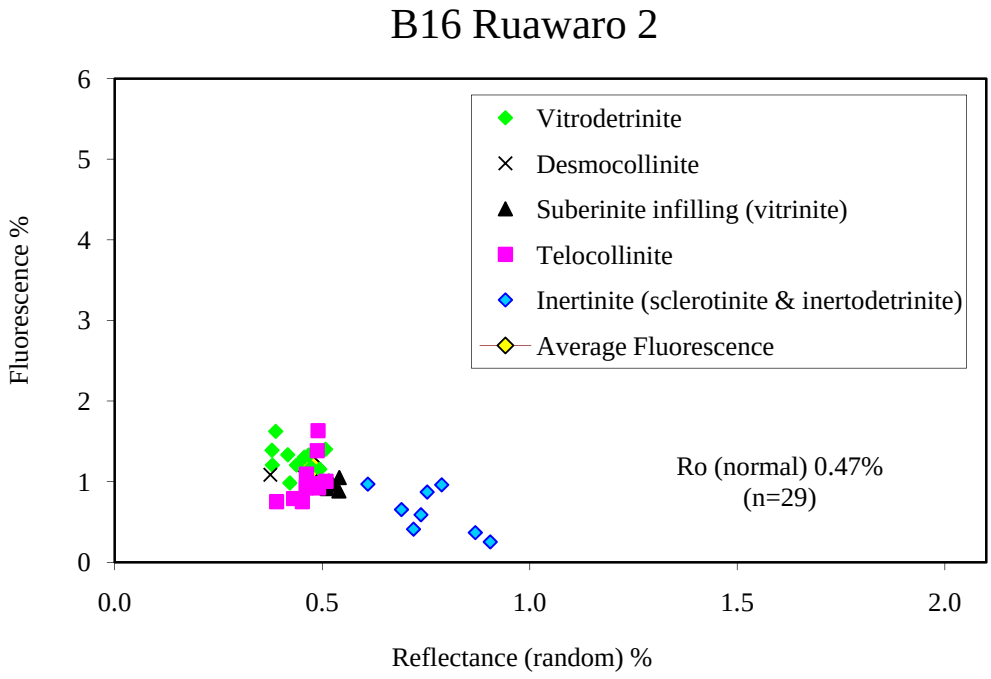

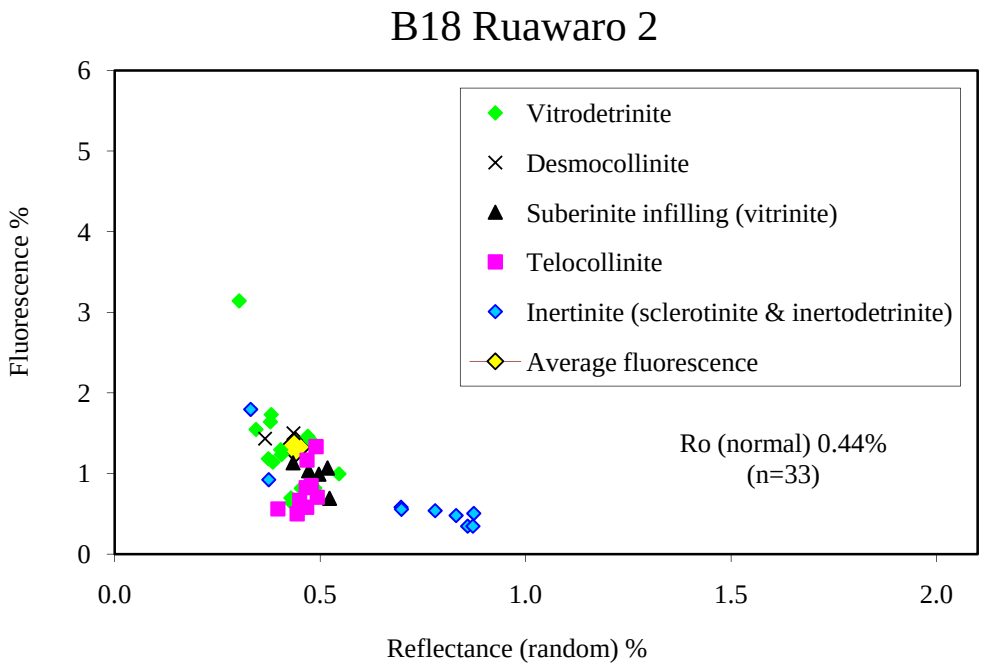
B18 Ruawaro 2
Fluorescence %
Reflectance (random) %
Vitrodetrinite
Desmocollinite
Suberinite infilling (vitrinite)
Telocollinite
Inertinite (sclerotinite & inertodetrinite)
Average fluorescence
Ro (normal) 0.44%
(n=33)
0
1
2
3
4
5
6
0.0
0.5
1.0
1.5
2.0

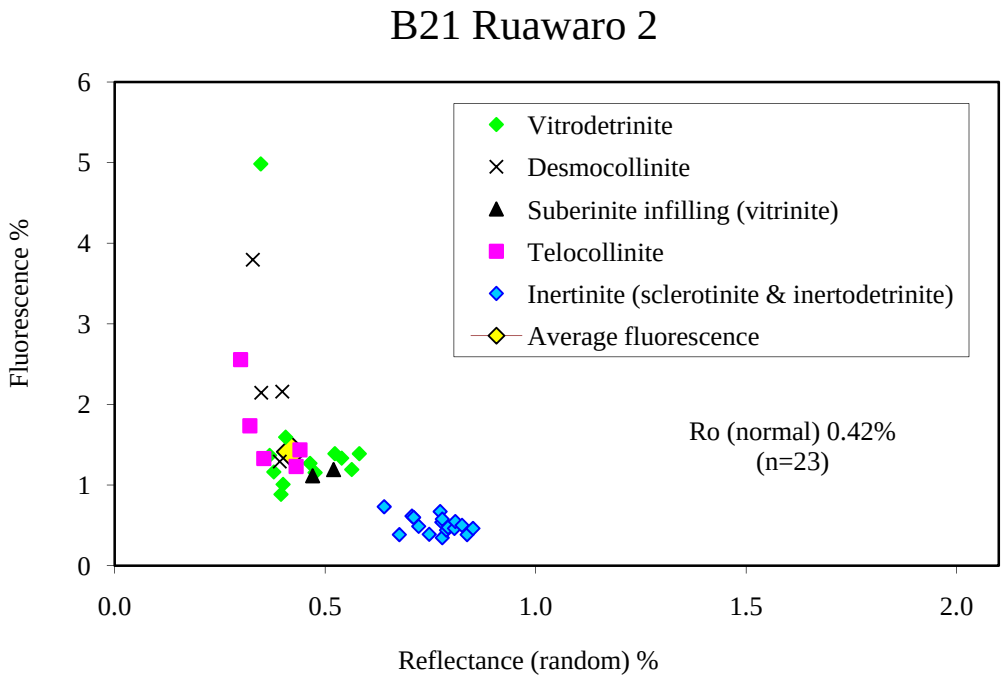
B21 Ruawaro 2
Fluorescence %
Reflectance (random) %
Vitrodetrinite
Desmocollinite
Suberinite infilling (vitrinite)
Telocollinite
Inertinite (sclerotinite & inertodetrinite)
Average fluorescence
Ro (normal) 0.42%
(n=23)
0
1
2
3
4
5
6
0.0
0.5
1.0
1.5
2.0

2.4. Macroscopic logging sheets

2.4.1. TW1

Can	From	To	Counts				Vitrain size (mm)	Coal Type	Comments
			Attrital	Vitrain	Fusain	Total			
9	338.70	339.20	13	6		19	1,1,2,0.5,1,2	BNB	
10	339.20	339.70	17	5	1	23	1,1,1,0.5, 0.5	BNB	
11	339.70	340.20	28	10	1	39	1,1,1,1,1, 0.5,0.5, 1,1,2	BMB	
12	340.20	340.70							desorbing
13	340.70	341.20	18	14		32	0.5, 3, 0.5, 2, 1,1,1,1,0.5, 1,1,1,0.5,30	BMB	
14	341.20	341.70	26	1		27	1	BNB	
15	341.70	341.87						Dirty Coal	
15	341.87	342.20	17	3		20	1,1,1	DNB	Clayey Coal
16	342.20	342.70	23	6		29	1,1,1,1,2,0.5	BNB	
17	342.70	343.20	24	4		28	0.5,1,1,2	BNB	
18	343.20	343.44	9	1		10	2	BNB	
18	343.44	343.55	6	3		9	1,2,3	DMB	Dull appearance, Possibly Fusain
18	343.55	343.70	13	1		14	1	BNB	
19	343.70	344.20	15	5		20	1,1,0.5, 0.5, 1	BMB	
20	344.20	344.70	22	5		27	2,1,1,0.5,25	BNB	0.1 - .16 weird fracture. Fusain?
21	344.70	345.20	11	2		13	0.5,2	BNB	Broken
22	345.20	345.70						BMB	Highly Broken
23	345.70	346.20							desorbing
24	346.20	346.52						BMB	Highly Broken
24	346.52	346.63						Dirty Coal	Highly Broken
24	346.63	346.70						BMB	Highly Broken
25	346.70	347.20						BMB	Highly Broken
26	347.20	347.70						BMB	Highly Broken
27	347.70	348.20	20	5		25	3,2,3,2,3	BMB	@ 0.25 - 1cm brown clay layer
28	348.20	348.70	28	11		39	1,1,0.5,0.5,1,2,1,2,2,2,1	BMB	
29	348.70	349.20	21	9		30	2,3,2,3,5,0.5,2,30,1	BMB	
30	349.20	349.70	18	2		20	1,0.5	BNB	Upper 5cm dull with fusain.
31	349.70	350.20	23	8	2	33	0.5,0.5,6,30,1,4,1,2	BMB	
32	350.20	351.20	17	18		35	0.5,1,2,2,1,1,3,2,0.5,1,5,2,1,3,3,8,2,3	BHB	Some Ca. Cleat.
33	351.20	351.70	24	16		40	0.5,4,0.5,7,0.5,0.5,1,0.5,0.5,0.5,4,5,0 .5,3,1,0.5	BHB	
34	351.70	352.20				0			desorbing
35	352.20	352.70	12	10		22	0.5,1,2,2,1,0.5,1,0.5,0.5,2	BMB	Ca on cleat
36	352.70	353.39	25	15		40	0.5,0.5,1,1,1,1,3,1,4,4,1,3,2,0.5,5	BMB	Ca on cleat.
37	353.39	354.20				0		BMB	Highly broken *
38	354.20	354.70				0		BMB	Highly broken *
39	354.70	355.20				0		BMB	Highly broken *
40	355.20	355.70				0			desorbing
41	355.70	356.20				0		BMB	Highly broken *
42	356.20	356.70				0		BMB	Highly broken *
43	356.70	357.20	21	13		34	0.5,2,0.5,4,1,1,1,2,10,2,3,4,7	BHB	
44	357.20	357.70	7	10		17	1,4,3,3,2,4,7,2,2,1	BHB	Isotherm sample from base
45	357.70	358.20	9	12		21	3,1,1,4,8,1,2,1,2,3,1,3	BHB	

* Bedding plane fracture.

2.4.2. Ruawaro 1

Can	From	To	Counts				Vitrain size (mm)	Coal type	Comments
			Attrital	Fusain	Vitrain	Total			
A3	387.40	387.90	21		9	30	4, 3, 0.5, 0.5, 0.5, 1, 0.5, 0.5, 2	BMB	at 0.36 1cm resin band
A2	387.90	388.16	21		8	29	2, 3, 0.5, 1, 2, 3, 3, 3	BMB	at 0.1 3mm resin band
A2	388.16	388.28						030 dull	
A6	396.48	396.59						312.3	
A6	396.59	397.01	19		8	27	0.5, 1, 0.5, 0.5, 0.5, 6, 2, 0.5	BMB	minor flecks of calcite
A5	397.01	397.56	23		15	38	0.5, 1, 1, 2, 0.5, 2, 1, 3, 1, 0.5, 1, 0.5, 5, 0.5, 0.5	BMB	at 0.15 2mm resin lens, at 0.17 HAC. Calcite flecks throughout
A4	397.56	398.05	22		11	33	2, 1, 2, 1, 4, 0.5, 0.5, 0.5, 2, 4, 2	BMB	at 0.43 calcite
A7	398.05	398.45						310.3	
A8	400.91	401.45	21		5	26	0.5, 2, 0.5, 0.5, 0.5	BNB	at 0.03 HAC (A7); at 0.49 2mm resin lens; last 10cm BMB
A9	401.45	401.90						BMB	too broken, bands visible
A10	402.45	402.95	23		16	39	0.5, 1, 0.5, 0.5, 1, 2, 0.5, 2, 1, 1, 1, 1, 7, 1, 1, 2	BHB	at 0 - 0.03 HAC; at 0.03 - 0.06 resin (?) on cleat; minor resin throughout
A11	402.95	403.45	15		9	24	1, 0.5, 0.5, 0.5, 4, 3, 2, 0.5, 3	BHB	same as A10
A12	406.41	406.73						313.3	
A16	417.61	417.69						373.3	
A16	417.69	417.75						030 dull	
A16	417.75	417.95	20		7	27	0.5, 1, 1, 5, 1, 0.5, 0.5	BNB	minor resin
A15	417.95	418.14	13		5	18	0.5, 5, 1, 5, 2	BMB	minor resin
A15	418.14	418.45	22		4	26	0.5, 0.5, 0.5, 2	BNB	
A14	418.45	418.95	37	1	12	50	0.5, 1, 0.5, 0.5, 0.5, 0.5, 2, 1, 0.5, 0.5, 0.5, 0.5	BNB	calcite 4cm thick + throughout; fusain 2mm
A13	418.95	419.45	24		6	30	4, 0.5, 3, 0.5, 0.5, 0.5	BNB	at 0.40-0.50 resin lenses
CRL	419.45	419.73	8		19	27	1, 1, 3, 1, 1, 2, 0.5, 0.5, 0.5, 0.5, 1, 0.5, 0.5, 0.5, 1, 0.5, 1, 0.5, 0.5	BHB	minor resin, vertical persistent cleat, canister full of water when opened
A17	419.73	420.25	33		11	44	4, 0.5, 0.5, 0.5, 1, 0.5, 5, 1, 1, 1, 8	BMB	
A18	420.25	420.80	14		13	27	1, 0.5, 0.5, 1, 1, 1, 0.5, 0.5, 0.5, 2, 2, 1, 0.5	BHB	resin and calcite throughout
A19	420.80	421.15	10		5	15	2, 2, 0.5, 5, 0.5	BHB	25cm perm sample taken from A19. Coal type change in that interval 12cm added to BMB, 11cm to BNB
A19	421.15	421.35	6		2	8	1, 1,	BNB	
A20	421.35	421.68	23		3	26	3, 3, 8	BNB	resin
A20	421.68	421.85	13		2	15	1, 0.5	BMB	
A21	421.85	422.35	35		11	46	0.5, 1, 1, 20, 6, 0.5, 1, 0.5, 1, 10, 4	BMB	resin and calcite present
A22	422.45	422.95	32		1	33	1	BNB	at 0.45 2mm resin + resin (?) on cleat
A23	422.95	423.45	25		9	34	1, 1, 0.5, 0.5, 3, 0.5, 0.5, 0.5, 0.5	BNB	minor resin
A24	423.45	423.95	34		3	37	6, 2, 1	BNB	
A25	423.95	424.45	23		11	34	4, 1, 2, 0.5, 1, 1, 2, 1, 1, 2, 0.5	BMB	
A26	424.45	424.95	23		20	43	0.5, 0.5, 3, 0.5, 0.5, 3, 3, 4, 1, 3, 1, 0.5, 2, 3, 0.5, 5, 3, 2, 0.5, 3	BHB	resin throughout
A27	430.40	430.55	9		0	9		BNB	mud layers at base
A37	430.55	430.80						310.3	carb. Mst verging on HAC

2.4.3. Ruawaro 2

Can	From	To	Counts				Vitrain size (mm)	Coal type	Comments
			Attrital	Fusain	Vitrain	Total			
B1	433.38	433.93	40		2	42	0.5, 1	BNB	1cm space (parting) between B1 & B2 sandy/muddy
B2	433.94	434.07	7		1	8	1	BNB	
B2	434.07	434.34						CM+HAC	interbedded
B3	434.34	434.48						HAC	
B3	434.48	434.84	15			15		BNB	very uneven rough fracture, may be better to leave counts out
B4	434.84	435.34	25		5	30	0.5, 1, 0.5, 1, 1	BNB	
B5	435.34	435.84	too broken					coal	This is the base 85cm of a core run. No mention of difficulties in logs. Drilling time standard. Probably a real crush zone
B6	435.84	436.19	too broken					coal	
B7	436.19	436.69	11		4	15	1, 0.5, 3, 1	BNB	permeability sample
B8	436.69	437.19	17		3	20	1, 0.5, 2	BNB	resin and perm sample
B9	437.19	437.69	22		3	25	1, 1, 1,	BNB	perm sample
B10	437.69	438.19	20		7	27	0.5, 4, 1, 0.5, 2, 0.5, 1	BNB	some resin
B11	438.19	438.69						323.3	grey and brown layers
B12	438.69	438.95						323.3	grey and brown layers
B12	438.95	439.19	14			14		BNB	
B13	439.19	439.25						BNB	too broken
B13	439.25	439.6						583.3	grades into coal
B13	439.6	439.69						BNB	some resin
B14	439.69	440.19	13		2	15	1, 0.5,	BMB	difficult due to rough fracture, some bands visible
B15	440.19	440.49							too broken with some HAC
B16	458.2	458.7	17		7	24	1, 1, 1, 0.5, 2, 1, 3,	BMB	resin and perm sample
B17	458.7	459.2	25		9	34	1, 11, 1, 9, 3, 0.5, 2, 1, 0.5	BMB	
B18	459.2	459.7	25		10	35	1, 1, 1, 2, 1, 0.5, 0.5, 0.5, 7, 0.5	BMB	resin
B19	459.7	460.2	30		2	32	0.5, 0.5,	BNB	minor resin and sample
B20	460.2	460.7	27		1	28	8,	BNB	
B21	460.7	461.2	31		10	41	2, 3, 0.5, 0.5, 0.5, 2, 15, 0.5, 1,	BNB	
B22	461.2	461.7	24		4	28	2, 2, 4, 4,	BNB	adsorption sample
B23	461.7	462.25	10		12	22	2, 2, 3, 1, 0.5, 1, 2, 0.5, 0.5, 2, 0.5, 1,	BMB	perm sample
B24	462.3	462.4	2		4	6	0.5, 0.5, 0.5, 1,	BHB	some resin
B24	462.4	462.85	19		1	20	1,	BNB	fractures, brittle at base
B25	462.85	463.4	17		8	25	2, 0.5, 2, 0.5, 2, 0.5,	BNB	resin, predominately smashed
B26	463.43	464.03	19		12	31	0.5, 5, 0.5, 0.5, 4, 0.5, 0.5, 0.5, 0.5, 1, 0.5, 4	BHB	resin

2.4.4. Rotongaro 1

Can	From	To	Counts				Vitrain size (mm)	Coal type	Comments
			Attrital	Fusain	Vitrain	Total			
C1	428.39	428.59						coal	too broken
C1	428.59	428.89						310.3	Carbonaceous mudstone with coaly laminae
C2	434.90	435.08	15			15		HAC	
C2	435.08	435.31						BHB	looks like solid vitrinite- wood chunk?
C2	435.31	435.40	7			7		BNB	
C3	435.40	435.60						BNB?	perm sample
C3	435.60	435.90	32			32		BNB	
C4	435.90	436.40	22		1	23	2	BNB	
C5	436.40	437.06						coal	too broken
C6	447.34	447.54	4		9	13	4, 4, 3, 6, 0.5, 3, 1, 1, 3	BHB	minor resin
C6	447.54	447.57						HAC	
C6	447.57	447.84	9		2	11	1, 1	BNB	
C7	447.89	448.02	5			5		BNB	
C7	448.02	448.19						coal	too broken
C7	448.19	448.39	10		4	14	1, 0.5, 3, 1	BMB	
C8	448.39	448.89	19		6	25	6, 1, 1, 1, 0.5, 0.5	BMB	perm sample 448.39-448.53
C9	448.89	449.29	20		8	28	1, 2, 4, 0.5, 0.5, 4, 1, 9	BMB	minor resin
C10	449.36	449.96	23		1	24	1	BNB	very crushed
							C11-C15 were very oily		
C11	449.96	450.03	8		8	8		BMB	minor resin
C11	450.03	450.36	7		3	15	1, 1, 0.5, 5, 0.5, 1, 0.5, 1	BHB	resin and clay?
C11	450.36	450.46	16		14	19	0.5, 0.5, 4	BMB	
C12	450.46	450.96	35		11	49	1, 0.5, 1, 1, 0.5, 0.5, 0.5, 0.5, 0.5, 3, 0.5, 0.5, 1, 0.5	BMB	resin and clay?
C13	450.96	451.46	32		21	43	1, 0.5, 1, 1, 0.5, 1, 2, 0.5, 0.5, 1, 3	BMB	clay?
CRL2	451.46	451.86	22		23	43	1, 0.5, 0.5, 0.5, 1, 0.5, 2, 3, 1, 1, 0.5, 1, 0.5, 0.5, 1, 0.5, 1, 0.5, 0.5, 1, 0.5	BHB	minor resin, canister was dry when opened.(AIR)
CRL1	451.86	452.28	22		10	45	0.5, 0.5, 1, 2, 1, 0.5, 0.5, 1, 0.5, 0.5, 1, 1, 1, 1, 0.5, 05, 0.5, 1, 0.5, 2, 0.5, 1, 0.5	BHB	minor resin, canister filled with water when opened (ARGON)
C14	452.40	452.90	34			44	1, 2, 0.5, 2, 0.5, 1, 0.5, 1, 0.5, 0.5	BMB	red markings- resin? (photo)
C15	452.90	452.97	7		9	7		BNB	
C15	452.97	453.40	20		6	29	1, 1, 0.5, 1, 0.5, 1, 1, 0.5, 0.5,	BMB	minor resin
C16	453.40	453.90	30		3	36	0.5, 0.5, 1, 1, 2, 1	BMB	resin at top
C17	453.90	454.40	15		5	18	0.5, 0.5, 0.5	BNB	top shattered, minor resin, perm sample 454.11-454.30
C18	454.40	454.90	44		6	49	3, 1, 0.5, 0.5, 2	BNB	minor resin
C19	454.90	455.40	45		8	51	0.5, 0.5, 0.5, 3, 0.5, 0.5	BNB	minor resin
C20	455.40	455.65	16		1	24	1, 0.5, 1, 3, 2, 0.5, 0.5, 0.5,	BMB	minor resin
C20	455.65	455.90	16			17	0.5	BNB	minor resin
C21	455.90	455.98						HAC	
C21	455.98	456.20	20		5	20		BNB	
C21	456.20	456.40	9		10	14	1, 0.5, 0.5, 1, 1	BMB	minor resin
C22	456.40	456.90	36		2	46	0.5, 0.5, 2, 1, 0.5, 1, 3, 0.5, 0.5, 1	BMB	minor resin with some resin blobs
C23	456.90	457.40	38			40	3, 0.5	BNB	minor resin
C24	457.40	457.52	12		5	12		BNB	minor resin, perm sample
C24	457.52	457.90	21		1	26	3, 1, 1, 3, 1	BMB	minor resin
C25	457.90	458.04	11		3	12	0.5	BNB	minor resin
C25	458.04	458.19	9		1	12	12, 11, 0.5	BHB	minor resin
C25	458.19	458.40	20		4	21	1	BNB	resin band
C26	458.4	459	36			40	0.5, 1, 1, 1	BNB	

2.4.5. Mangapiko 1

Can	From	To	Counts				Vitrain size (mm)	Coal type	Comments
			Attrital	Fusain	Vitrain	Total			
D1	482.35	482.45	3		1	4	0.5	BMB	minor resin + minor mudstone
D1	482.45	482.72						CM	CM with sandy and coaly lenses + HAC
D1	482.72	482.85	7		5	12	0.5, 1, 0.5, 1, 2	BHB	minor resin + silty lenses
D2	482.85	483.05						coal	perm sample
D2	483.05	483.22						CM	interbedded HAC/CM with sandy/muddy lenses some thick vitrain bands (one solid 14mm chunk)
D2	483.22	483.35	7		3	10	0.5, 0.5, 0.5,	BMB	
D3	483.35	483.65	23		8	31	1, 2, 0.5, 2, 0.5, 3, 1, 0.5	BMB	
D3	483.65	483.75						coal	Adsorption isotherm
D3	483.75	483.85	9		1	10	0.5	BNB	
D4	483.85	484.35	19		8	27	4, 0.5, 3, 1, 1, 1, 0.5, 2	BMB	perm sample
D5	484.35	484.41	1		4	5	2, 4, 5, 2	BHB	
D5	484.41	484.85	24		11	35	1, 2, 1, 0.5, 1, 1, 0.5, 1, 1, 0.5, 1	BMB	some resin, 11-3cm from base some thick brown mud(?) on cleat
D6	484.85	485.02	10		6	16	0.5, 1, 3, 1, 1, 1,	BMB	some resin
D6	485.02	485.25	18		2	20	1, 1	BNB	some resin
D7	485.30	485.46	10			10		BNB	
D7	485.46	485.55	5		3	8	0.5, 3, 0.5	BMB	
D7	485.55	485.80	16			16		BNB	
D8	485.80	486.30	34		16	50	7, 0.5, 1, 10, 0.5, 1, 1, 1, 0.5, 3, 1, 3, 10, 1, 2, 3	BHB	minor resin
D9	486.30	486.80	28		23	51	3, 3, 0.5, 0.5, 6, 1, 1, 1, 0.5, 1, 1, 0.5, 1, 1, 7, 0.5, 1, 1, 9, 5, 6, 1, 1	BHB	resin
D10	486.90	487.01	2		8	10	1, 2, 0.5, 1, 1, 1, 0.5, 0.5	BHB	resin, missing thickness is perm sample
D11	512.10	512.60	23		9	32	1, 0.5, 0.5, 1, 0.5, 1, 0.5, 0.5, 0.5	BMB	crushed at ends, minor resin
D12	512.60	512.75						coal	too broken but can see some bands
D12	512.75	513.00						coal	mushy', biscuit like, crumbles at touch
D12	513.00	513.10						coal	too broken with rough fracture broke up when trying to clean
D13	513.10	513.60	34		8	42	1, 0.5, 1, 0.5, 0.5, 1, 4, 0.5	BMB	minor resin, very brittle
D14	513.60	514.10	20		8	28	1, 1, 0.5, 0.5, 5, 3, 0.5, 0.5	B<20	minor resin, 0.3-0.4 totally crushed
D15	514.40	514.63	7		12	19	1, 1, 1, 0.5, 0.5, 0.5, 0.5, 1, 1, 1, 0.5, 0.5	BHB	
D15	514.63	514.80	17		5	22	0.5, 0.5, 1, 0.5, 0.5	BMB	
D15	514.80	514.90	2		7	9	3, 0.5, 0.5, 0.5, 1, 0.5, 10	BHB	
D16	514.90	515.15	14		9	23	0.5, 0.5, 1, 0.5, 0.5, 0.5, 0.5, 1, 0.5	BMB	some resin
D16	515.15	515.40	12		13	25	7, 0.5, 6, 1, 0.5, 0.5, 3, 1, 4, 3, 0.5, 0.5, 2	BHB	minor resin
D17	515.40	515.90	19		7	26	0.5, 1, 0.5, 2, 2, 1, 2	BMB	24cm perm sample, minor resin, pretty crushed at base
D18	515.90	516.40	22		11	33	0.5, 0.5, 0.5, 1, 1, 1, 2, 0.5, 1, 1, 1	BMB	perm sample, minor resin
D19	516.40	516.95	26		27	53	1, 0.5, 0.5, 0.5, 1, 3, 4, 0.5, 0.5, 1, 0.5, 1, 1, 3, 2, 0.5, 0.5, 0.5, 1, 0.5, 0.5, 1, 3, 1, 1, 0.5, 0.5	BHB	minor resin
D20	516.95	517.45	20		18	38	0.5, 0.5, 1, 2, 0.5, 1, 0.5, 3, 0.5, 2, 0.5, 1, 3, 1, 4, 2, 0.5, 0.5	BHB	minor resin, adsorption isotherm 517.32-517.45m
D20	517.45	517.50						HAC	

2.4.6. Baco 1

Can	From	To	Counts				Vitrain size (mm)	Coal type	Comments
			Attrital	Fusain	Vitrain	Total			
Ba1	427.90	428.45	4		1	5	4	BMB?	Probably BMB, was quite broken but few pieces showed plain matrix with thick ~ 4mm bands. Some whitish material in places- not calcite-clay? Evidence of sub-vert cleat, Base piece showed horizontal, ~15mm spacing. Resin flecks, minor, <1mm diameter
Ba2	428.45	428.85	19		8	27	0.5, 0.5, 0.5, 0.5, 0.5, 1, 0.5, 1	BMB	Thin banding, at 25cm slickenside. Well broken, some minor clay on cleat, sub-vert cleat some ~1cm, ~2cm
Ba2	428.85	429.00	13		0	13		BNB	Had to break - tight
Ba3	429.00	429.50					very disked, some evidence of cleat		minor resin blobs ~1mm diameter
Ba4	429.50	430.00					very disked, some evidence of cleat		some calcite on cleat
Ba5	430.00	430.50					very disked, some evidence of cleat		disking surfaces conchoidal
Ba6	430.50	431.00					very disked, some evidence of cleat		conchoidal disking, some minor calcite on cleat.

2.4.7. Jasper 1

Can	From	To	Counts				Vitrain size	Coal type	Comments
			Attrital	Fusain	Vitrain	Total			
J1	407.81	407.94						HAC/ CM	HAC with mudstone lenses
J1	407.94	407.98						mst	pale mudstone
J1	407.98	408.31						HAC/ CM	HAC with mudstone lenses
J2	408.31	408.81	26		1	27	0.5	BNB?	BNB? hard to tell b/c calcite and break surfaces. Some calcite on cleat from 10cm heavy in bottom 10cm. 23-38cm crushed. persistent cleat throughout, 0.5, 1, 2cm spacing straight, also some wavy cleat breaks at 45deg.
J3	408.81	409.31	26		10	36	1, 3, 1, 0.5, 1, 0.5, 0.5, 0.5, 1, 0.5	BMB	Calcite on cleat top 5cm. Perm sample 409.16-409.31 m. Cleat - top 12cm rough/wavy break, rest straight persistant cleats sub-vert approx 3cm spacing. Minor resin
J4	409.31	409.81	21		8	29	2, 2, 0.5, 1, 1, 0.5, 0.5, 1	BMB	Base 5cm crushed. Calcite on cleat 15-45cm. The top 5cm when cracked with a hammer was DRY inside. Texture difference between top and middle sections. Cleat 0.5, 2, 4 cm throughout some conchoidal. Top 30cm more consolidated- not blocky break. Top 5cm very tight no clear cleat. minor resin
J5	410.00	410.35							Can't log- too broken and solid block is calcite filled. Calcite seen on cleat. Top 15cm all broken into blocks of 1-2cm thickness.
J6	410.35	410.85	31		3	34	2, 1, 1	BNB	minor calcite on cleat ~ 5cm from top. Few bnds in bottom 2cm. Oil sheen when first opened.Cleat ~4cm, fairly solid matrix, few wavy vertical cleats and some sub-vert. Minor resin
J7	410.85	411.10	19		7	26	2, 1, 0.5, 0.5, 0.5, 2, 1	BMB	Solid stick of coal
J7	411.10	411.35	19		0	19		BNB	blocky pulled apart by hand, minor resin
J8	411.35	411.85	25		3	28	0.5, 1, 1	BNB	Generally BNB two 3cm areas of band swarms- ~1 & 40cm. Perm sample 409.16-409.31
J9	412.00	412.50	42		2	44	0.5, 3	BNB	very tight glassy section top 5cm
J10	412.50	412.65				Perm sample			
J10	412.65	412.85	15	1	0	16		BNB	Perm. Slickenside 25cm from top. Minor calcite
J10	412.85	413.00	11		5	16	2, 1, 3, 0.5, 0.5	B<20	
J11	413.00	413.55						Banded	Too broken to log, some calcite on cleat in lower section. Saw some bands
J12	413.55	414.02						CM	carbonaceous mudstone with coaly lenses, some evidence of vertical fracture, some slickenside 15 cm from top
J13	414.02	414.40						CM	carbonaceous mudstone with coaly lenses, some evidence of cleat in the top, some evidence of sub-vertical fracture, some slickenside 10-15 cm from top

2.4.8. Mimi 1

Can	From	To	Counts				Vitrain size	Coal type	Comments
			Attrital	Fusain	Vitrain	Total			
M1	407.45	407.95	21	1	13	35	1, 0.5, 1, 0.5, 1, 0.5, 1, 0.5, 1, 2, 0.5, 1, 0.5	BMB	brown streaks of calcite, also some clay on cleat, faces were rough, some areas more bands than others.
M2	407.95	408.45	22		15	37	2, 1, 0.5, 3, 0.5, 0.5, 1, 1, 0.5, 0.5, 1, 2, 5, 1, 2	BMB	thicker bands
M3	408.45	408.98	26		11	37	2, 3, 1, 1, 1, 2, 1, 3, 1, 9, 2	BMB	very difficult to find faces to log due to calcite throughout almost all cleats regardless of orientation.
M4	409.03	409.58	22		3	25	4, 1, 1	BNB	Calcite throughout. Adsorption sample
M5	409.58	410.13	33		1	34	1	BNB	Perm sample 409.94-410.08. Calcite on cleat in top 8cm, minor throughout rest
M6	410.13	410.33	11		6	17	5, 0.5, 0.5, 1, 1, 1	BMB	Frequent calcite throughout
M6	410.33	410.63	17	1	2	20	1, 1	BNB	
M7	410.63	411.13	38		3	41	0.5, 1, 0.5	BNB	some patches of calcite on main cleat
M8	411.13	411.63	25		3	28	3, 0.5, 0.5	BNB	minor calcite on main cleat
M9	411.63	411.76	8		1	9	1	BNB	
M9	411.76	412.01	9	1	8	18	1, 2, 0.5, 1, 1, 7, 1, 2	BMB	
M9	412.01	412.13	8		1	9	1	BNB	
M10	412.18	412.53	19	1	0	20		BNB	Some slickensides ~17cm, some minor calcite on cleat
M10	412.53	412.83	11		11	22	0.5, 0.5, 1, 0.5, 1, 0.5, 0.5, 1, 1, 1, 1	BMB	
M11	412.83	413.01	16		3	19	2, 0.5, 2	BMB	
M11	413.01	413.15		Perm sample					
M11	413.15	413.48	14		19	33	1, 0.5, 1, 1, 1, 1, 1, 0.5, 0.5, 1, 0.5, 0.5, 1, 2, 0.5, 2, 0.5, 0.5, 1	BHB	Some calcite on cleat near top
M12	413.58	413.83	11		6	17	1, 0.5, 0.5, 1, 0.5, 0.5	D<20	Dirty, dull coal
M12	413.83	414.08						CM	Carb mudstone with plant fossils some slickenside at top and base on mst, oil staining

2.5. Organic petrology counts

2.5.1. Jasper 1 Renown seam

	Telinite	Collotelinite A	Collotelinite B	Collotelinite C	Collotelinite D	Corpo-collinite	Pori-gelinite	Collo-detrinite	Vitro-detrinite
J2	2	22	5	5	14	2	13	133	160
J3	2	17	12	11	19	7	13	173	134
J4	5	16	7	9	95	10	21	119	146
J5	0	9	2	3	103	9	3	121	167
J6	2	7	5	8	46	16	6	122	153
J7	5	5	16	6	40	8	8	140	115
J8	0	13	5	4	31	16	2	114	185
J9	11	15	6	8	39	7	8	141	165
J10	1	11	7	5	27	14	5	110	204
J11	0	9	13	9	110	7	2	103	123

	Cutinite	Suberinite	Sporinite	Resinite	Liptodetrinite	Semifusinite	Funginite	Inertodetrinite	MM
J2	2	2	3	8	48	7	15	24	35
J3	1	5	4	2	61	3	6	20	10
J4	2	0	0	7	31	4	8	17	3
J5	1	3	0	6	34	5	9	21	4
J6	0	9	2	6	50	13	21	32	2
J7	0	7	9	17	74	8	12	27	3
J8	1	3	12	6	47	7	16	37	0
J9	0	3	6	8	34	7	13	29	0
J10	0	3	6	0	55	1	20	30	1
J11	0	5	3	12	51	2	12	33	6

MM = mineral matter

2.5.2. Mimi 1 Renown seam

	Telinite	Collotelinite A	Collotelinite B	Collotelinite C	Collotelinite D	Corpo-collinite	Pori-gelinite	Collo-detrinite	Vitro-detrinite
M1	1	11	10	7	16	10	4	84	221
M2	2	12	28	12	40	16	6	105	176
M3	14	9	15	7	49	12	29	158	127
M4	2	13	11	7	33	15	7	110	173
M5	1	14	4	7	36	17	5	127	161
M6	4	9	8	7	43	15	0	107	156
M7	2	14	9	6	24	9	4	135	164
M8	4	26	8	0	14	16	6	112	200
M9	8	17	16	7	30	14	3	133	160
M10	1	18	15	6	32	21	2	125	190
M11	3	3	21	9	55	7	3	155	96

	Cutinite	Suberinite	Sporinite	Resinite	Liptodetrinite	Semifusinite	Funginite	Inertodetrinite	MM
M1	4	8	9	11	55	5	16	22	6
M2	2	9	2	8	62	0	7	10	3
M3	0	6	3	8	33	2	3	15	10
M4	0	3	3	8	40	6	10	35	24
M5	0	11	9	5	51	8	18	26	0
M6	0	6	10	10	56	2	25	29	13
M7	1	6	10	6	43	7	29	30	1
M8	0	11	4	9	29	5	26	30	0
M9	0	10	2	7	63	0	12	18	0
M10	1	4	5	4	36	1	17	20	2
M11	1	4	5	11	40	3	9	19	56

2.5.3. Ruawaro 1 Kupakupa seam

	Telinite	Collotelinite A	Collotelinite B	Collotelinite C	Collotelinite D	Corpo-collinite	Pori-gelinite	Collo-detrinite	Vitro-detrinite
A16 *	0	3	12	8	25	2	0	46	53
A15	0	4	16	5	41	1	1	171	131
A14	0	7	19	5	44	2	1	142	177
A13	0	25	13	9	46	3	3	99	165
CRL	2	32	17	11	26	9	0	160	158
A17	0	29	5	4	33	8	0	117	217
A18	6	28	16	17	66	13	2	117	124
A19	0	23	7	5	19	6	1	95	250
A20	0	34	21	5	41	5	3	138	175
A21	3	17	6	4	81	6	1	130	164
A22	1	19	3	4	15	5	1	112	222
A23	2	14	4	6	42	2	1	153	195
A24	2	16	5	6	65	3	6	144	184
A25	0	7	6	3	41	1	1	211	134
A26	2	5	11	13	152	7	4	126	89

	Cutinite	Suberinite	Sporinite	Resinite	Liptodetrinite	Semifusinite	Funginite	Inertodetrinite	MM
A16*	5	0	5	3	32	1	3	4	48
A15	0	6	11	2	64	2	9	17	19
A14	1	8	2	5	60	2	7	15	3
A13	0	10	3	13	49	2	15	31	14
CRL	5	9	4	9	50	0	2	4	2
A17	4	9	4	10	43	2	3	9	3
A18	5	11	1	5	50	4	6	13	16
A19	2	5	1	4	57	2	6	17	0
A20	5	1	1	9	45	2	3	12	0
A21	1	7	2	8	35	6	1	16	12
A22	3	12	7	5	54	8	5	24	0
A23	4	3	1	8	37	5	4	19	0
A24	1	1	5	7	40	6	1	7	1
A25	1	2	3	7	33	4	8	38	0
A26	3	4	4	16	31	6	4	15	8

**only 250 counts.*

2.5.4. Ruawaro 2 Kupakupa seam

	Telinite	Collotelinite A	Collotelinite B	Collotelinite C	Collotelinite D	Corpo-collinite	Pori-gelinite	Collo-detrinite	Vitro-detrinite
B16	1	26	15	4	41	22	0	114	191
B17	0	12	7	5	59	10	1	170	160
B18	0	11	15	5	53	14	0	141	165
B19	1	5	4	2	86	5	5	188	129
B20	1	17	1	0	36	4	0	139	216
B21	0	15	8	10	47	8	8	130	176
B22	0	20	19	9	31	9	2	160	159
B23	0	21	11	7	23	9	1	188	179
B24	1	20	16	5	47	12	1	175	154
B25	3	14	12	9	94	14	7	164	104
B26	0	6	15	20	82	15	3	129	89

	Cutinite	Suberinite	Sporinite	Resinite	Liptodetrinite	Semifusinite	Funginite	Inertodetrinite	MM
B16	0	13	0	10	36	0	2	9	16
B17	0	4	0	3	39	1	15	14	0
B18	2	11	1	11	54	0	7	10	0
B19	0	4	3	8	32	0	18	10	0
B20	0	6	1	5	41	1	14	18	0
B21	1	7	2	2	63	1	6	16	0
B22	2	7	1	12	39	0	9	21	0
B23	0	11	3	4	32	0	2	9	0
B24	1	10	1	4	31	2	10	10	0
B25	1	4	4	8	37	0	11	13	1
B26	3	8	6	19	74	0	1	15	15

2.5.5. Other analysed samples

	Telinite	Collotelinite A	Collotelinite B	Collotelinite C	Collotelinite D	Corpo-collinite	Pori-gelinite	Collo-detrinite	Vitro-detrinite
D13	0	28	3	5	19	14	4	169	194
D18	0	18	11	9	37	23	0	181	148
D19	0	6	14	12	174	14	0	199	21
C4	1	20	6	9	31	11	4	174	170
C11	0	17	10	3	49	18	1	163	155

	Cutinite	Suberinite	Sporinite	Resinite	Liptodetrinite	Semifusinite	Funginite	Inertodetrinite	MM
D13	1	13	2	2	24	2	11	9	0
D18	2	13	0	12	32	1	10	2	1
D19	2	5	4	14	25	1	4	2	3
C4	0	4	4	10	25	2	6	17	6
C11	1	11	6	6	36	0	12	12	0

D13, D18 and D19 are from Mangapiko 1 Kupakupa seam.

C4 is from the Renown seam, C11 is from the Kupakupa seam at Rotongaro 1.

2.5.6. Percentage maceral group (mmf) Renown seam

Location	Canister	Vitrinite %	Liptinite %	Inertinite %	Reference
Jasper 1	J2	76.56	13.55	9.89	
Jasper 1	J3	79.18	14.90	5.92	
Jasper 1	J4	86.12	8.05	5.84	
Jasper 1	J5	84.07	8.87	7.06	
Jasper 1	J6	73.29	13.45	13.25	
Jasper 1	J7	69.01	21.53	9.46	
Jasper 1	J8	74.15	13.83	12.02	
Jasper 1	J9	80.00	10.20	9.80	
Jasper 1	J10	76.95	12.83	10.22	
Jasper 1	J11	76.11	14.37	9.51	
Mimi 1	M1	73.68	17.61	8.70	
Mimi 1	M2	79.88	16.70	3.42	
Mimi 1	M3	85.71	10.20	4.08	
Mimi 1	M4	77.94	11.34	10.71	
Mimi 1	M5	74.40	15.20	10.40	
Mimi 1	M6	71.66	16.84	11.50	
Mimi 1	M7	73.55	13.23	13.23	
Mimi 1	M8	77.20	10.60	12.20	
Mimi 1	M9	77.60	16.40	6.00	
Mimi 1	M10	82.33	10.04	7.63	
Mimi 1	M11	79.28	13.74	6.98	
Rotongaro 1	C4	86.23	8.70	5.06	
TW1	10	85.86	8.08	6.06	Butland (2006)
TW1	11	79.80	15.15	5.05	Butland (2006)
TW1	19	79.80	12.12	7.07	Butland (2006)
TW1	21	88.89	6.06	5.05	Butland (2006)
Rangariri West	P8	86.60	6.19	7.22	Edbrooke et al. (1994)
Huntly East	P9	83.51	4.12	12.37	Edbrooke et al. (1994)
Weavers	P10	84.38	4.17	11.46	Edbrooke et al. (1994)
	Minimum	**69.01**	**4.12**	**3.42**	
	Average	**79.44**	**12.00**	**8.52**	
	Maximum	**88.89**	**21.53**	**13.25**	
	SD	**5.17**	**4.19**	**2.91**	

2.5.7. Percentage maceral group (mmf) Kupakupa seam

Location	Canister	Vitrinite %	Liptinite %	Inertinite %	Reference
Ruawaro 1	A15	76.92	17.26	5.82	
Ruawaro 1	A14	79.88	15.29	4.83	
Ruawaro 1	A13	74.69	15.43	9.88	
Ruawaro 1	crl	83.33	15.46	1.20	
Ruawaro 1	A17	83.10	14.08	2.82	
Ruawaro 1	A18	80.37	14.88	4.75	
Ruawaro 1	A19	81.20	13.80	5.00	
Ruawaro 1	A20	84.40	12.20	3.40	
Ruawaro 1	A21	84.43	10.86	4.71	
Ruawaro 1	A22	76.40	16.20	7.40	
Ruawaro 1	A23	83.80	10.60	5.60	
Ruawaro 1	A24	86.37	10.82	2.81	
Ruawaro 1	A25	80.80	9.20	10.00	
Ruawaro 1	A26	83.13	11.79	5.08	
Ruawaro 2	B16	85.54	12.19	2.27	
Ruawaro 2	B17	84.80	9.20	6.00	
Ruawaro 2	B18	80.80	15.80	3.40	
Ruawaro 2	B19	85.00	9.40	5.60	
Ruawaro 2	B20	82.80	10.60	6.60	
Ruawaro 2	B21	80.40	15.00	4.60	
Ruawaro 2	B22	81.80	12.20	6.00	
Ruawaro 2	B23	87.80	10.00	2.20	
Ruawaro 2	B24	86.20	9.40	4.40	
Ruawaro 2	B25	84.37	10.82	4.81	
Ruawaro 2	B26	74.02	22.68	3.30	
Rotongaro 1	C11	83.20	12.00	4.80	
Mangapiko 1	D13	87.20	8.40	4.40	
Mangapiko 1	D18	85.57	11.82	2.61	
Mangapiko 1	D19	88.53	10.06	1.41	
TW1	28	92.93	4.04	2.02	Butland (2006)
TW1	32	87.88	8.08	4.04	Butland (2006)
TW1	37	86.00	8.00	5.00	Butland (2006)
TW1	43	87.00	9.00	4.00	Butland (2006)
Rangariri West	P11	89.69	2.06	8.25	Edbrooke et al. (1994)
Huntly East	P12	90.53	3.16	6.32	Edbrooke et al. (1994)
Weavers	P13	87.63	5.15	7.22	Edbrooke et al. (1994)
	Min	**74.02**	**2.06**	**1.20**	
	Ave	**83.85**	**11.30**	**4.79**	
	Max	**92.93**	**22.68**	**10.00**	
	SD	**4.25**	**4.15**	**2.10**	

2.6. Porosity

2.6.1. Jasper 1 Renown seam

	Pores in tissue (10 per pellet)		% pores open	Total with pores	Number of collotelinite C & D	% Collotelinite C & D with pores
	Resin infilled	Open				
J2	4	4	50.0%	8	19	42.1%
J3	3	0	0.0%	3	30	10.0%
J4	19	1	5.0%	47	104	45.2%
J5	9	11	55.0%	58	106	54.7%
J6	7	13	65.0%	35	54	64.8%
J7	11	1	8.3%	12	46	26.1%
J8	7	7	50.0%	14	35	40.0%
J9	10	10	50.0%	28	47	59.6%
J10	2	8	80.0%	10	32	31.3%
J11	6	14	70.0%	29	119	24.4%

2.6.2. Mimi 1 Renown seam

	Pores in tissue (10 per pellet)		% pores open	Total with pores	Number of collotelinite C & D	% Collotelinite C & D with pores
	Resin infilled	Open				
M1	0	0	0.0%	0	23	0.0%
M2	7	3	30.0%	10	52	19.2%
M3	8	10	55.6%	18	56	32.1%
M4	0	9	100.0%	9	40	22.5%
M5	15	2	11.8%	17	43	39.5%
M6	14	6	30.0%	28	50	56.0%
M7	2	9	81.8%	11	30	36.7%
M8	2	2	50.0%	4	14	28.6%
M9	9	1	10.0%	10	37	27.0%
M10	3	11	78.6%	14	38	36.8%
M11	7	11	61.1%	19	64	29.7%

2.6.3. Ruawaro 1 Kupakupa seam

	Pores in tissue (10 per pellet)		% pores open	Total with pores	Number of collotelinite C & D	% Collotelinite C & D with pores
	Resin infilled	Open				
A15	7	6	46.2%	13	46	28.3%
A14	10	7	41.2%	17	49	34.7%
A13	10	3	23.1%	13	55	23.6%
CRL	4	3	42.9%	7	37	18.9%
A17	6	6	50.0%	12	37	32.4%
A18	13	7	35.0%	34	83	41.0%
A19	2	3	60.0%	5	24	20.8%
A20	6	6	50.0%	12	46	26.1%
A21	11	9	45.0%	70	85	82.4%
A22	5	2	28.6%	7	19	36.8%
A23	7	9	56.3%	20	48	41.7%
A24	5	15	75.0%	39	71	54.9%
A25	2	14	87.5%	14	44	31.8%
A26	7	13	65.0%	80	165	48.5%

2.6.4. Ruawaro 1 Kupakupa seam

	Pores in tissue (10 per pellet)		% pores open	Total with pores	Number of collotelinite C & D	% Collotelinite C & D with pores
	Resin infilled	Open				
B16	4	10	71.4%	14	45	31.1%
B17	7	13	65.0%	25	64	39.1%
B18	3	15	83.3%	25	58	43.1%
B19	11	9	45.0%	69	88	78.4%
B20	6	6	50.0%	12	36	33.3%
B21	6	11	64.7%	17	57	29.8%
B22	4	2	33.3%	6	40	15.0%
B23	4	6	60.0%	10	30	33.3%
B24	7	12	63.2%	21	52	40.4%
B25	4	15	78.9%	30	103	29.1%
B26	8	11	57.9%	19	102	18.6%

2.6.5. Other analysed samples

	Pores in tissue (10 per pellet)		% pores open	Total with pores	Number of collotelinite C & D	% Collotelinite C & D with pores
	Resin infilled	Open				
D13	5	4	44.4%	9	24	37.5%
D18	2	6	75.0%	8	46	17.4%
D19	10	10	50.0%	57	186	30.6%
C4	2	4	66.7%	6	40	15.0%
C11	10	8	44.4%	21	52	40.4%

2.7. Average fluorescence data

Jasper 1 Renown seam	
Canister	**Average fluorescence %**
J2	1.396
J3	1.465
J4	1.247
J5	1.159
J6	1.442
J7	1.798
J8	1.464
J9	1.593
J10	1.442
J11	1.208

Ruawaro 2 Kupakupa seam	
Canister	**Average fluorescence %**
B16	1.175
B17	1.355
B18	1.328
B19	1.080
B20	1.282
B21	1.413
B22	1.456
B23	1.469
B24	1.410
B25	1.331
B26	1.272

Appendix 3: Microstructure data

3.1. Study on the effect of background subtraction

Introduction:

During the data processing stage in the PRINSAS software the user is required to identify the amount of background to be subtracted from the dataset. This is done by moving the background line to where the scattering data flattens out in the high Q-region. Moving the background line results in the high Q-region tending towards a straight line.

Aim:

To examine the effects of under- and overestimating the background subtraction on PRINSAS calculations of pore number density, *f(r)*, specific surface area, SSA, and porosity.

Method:

Different values for background were selected to be roughly symmetric around, both smaller and greater than, the chosen 'actual' background value (Table 1). These different background values were subtracted in the initial PRINSAS data processing stage and then the datasets were processed through to completion as normal.

Table 1. Values chosen for background subtraction.

Background value	Subtraction from actual	Percentage of actual value	Percentage difference
0.2946	-0.2617	53.0%	-47.0%
0.4503	-0.106	80.9%	-19.1%
0.5135	-0.0428	92.3%	-7.7%
0.5563			
0.5855	0.0292	105.2%	5.2%
0.6412	0.0849	115.3%	15.3%
0.7927	0.2364	142.5%	42.5%

Results:

The effect of the different background subtractions on the scattering curve can be seen in Figure 1. Background subtraction only affects the high Q-region, Q > 0.1 $Å^{-1}$ (25 Å) of the scattering curve.

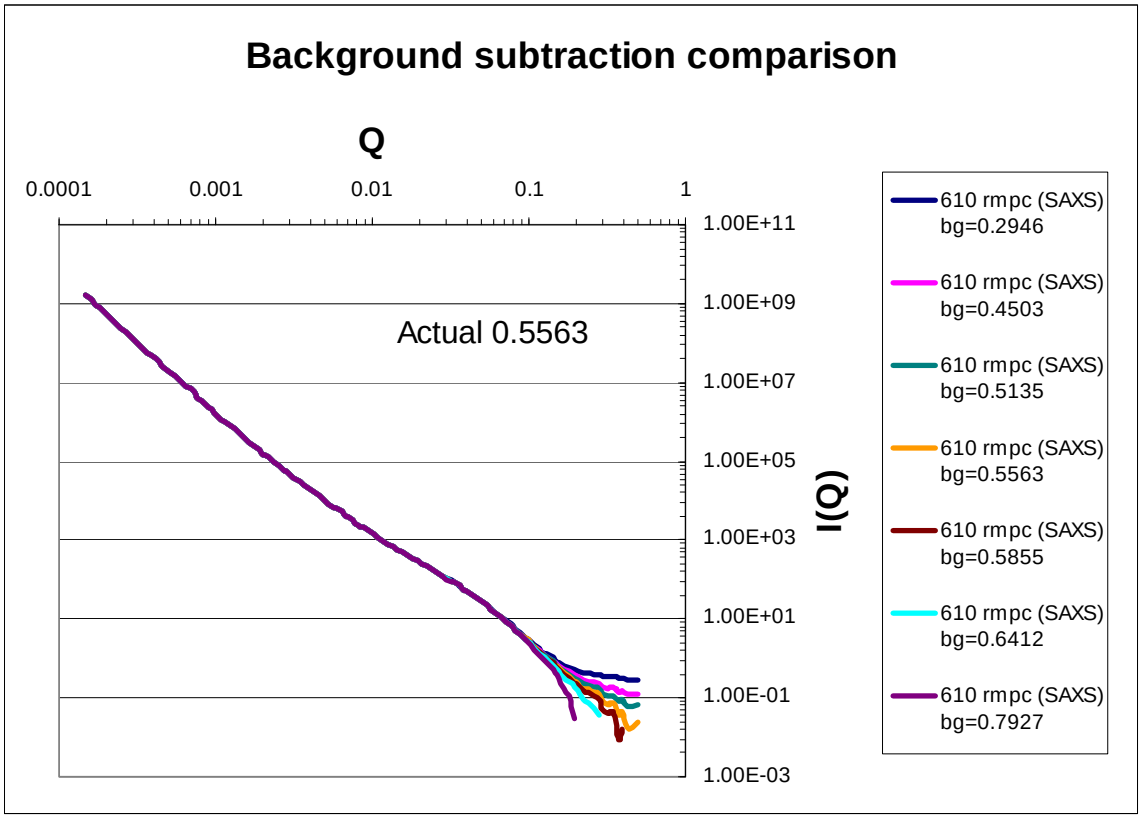

Figure 1. SAXS/USAXS scattering curves corrected for different background values.

Background correction was found to have a significant effect on the calculated histograms for pore size distribution (Figure 2). For pore size of 100 Å, *f(r)* is overestimated by two orders of magnitude if the largest background correction, 0.7927, is used. In contrast, for the smallest background correction, 0.2946, *f(r)* is underestimated by only one order of magnitude. While these values for background correction are extreme they do illustrate that overestimating the value for background has more effect on *f(r)* then underestimating.

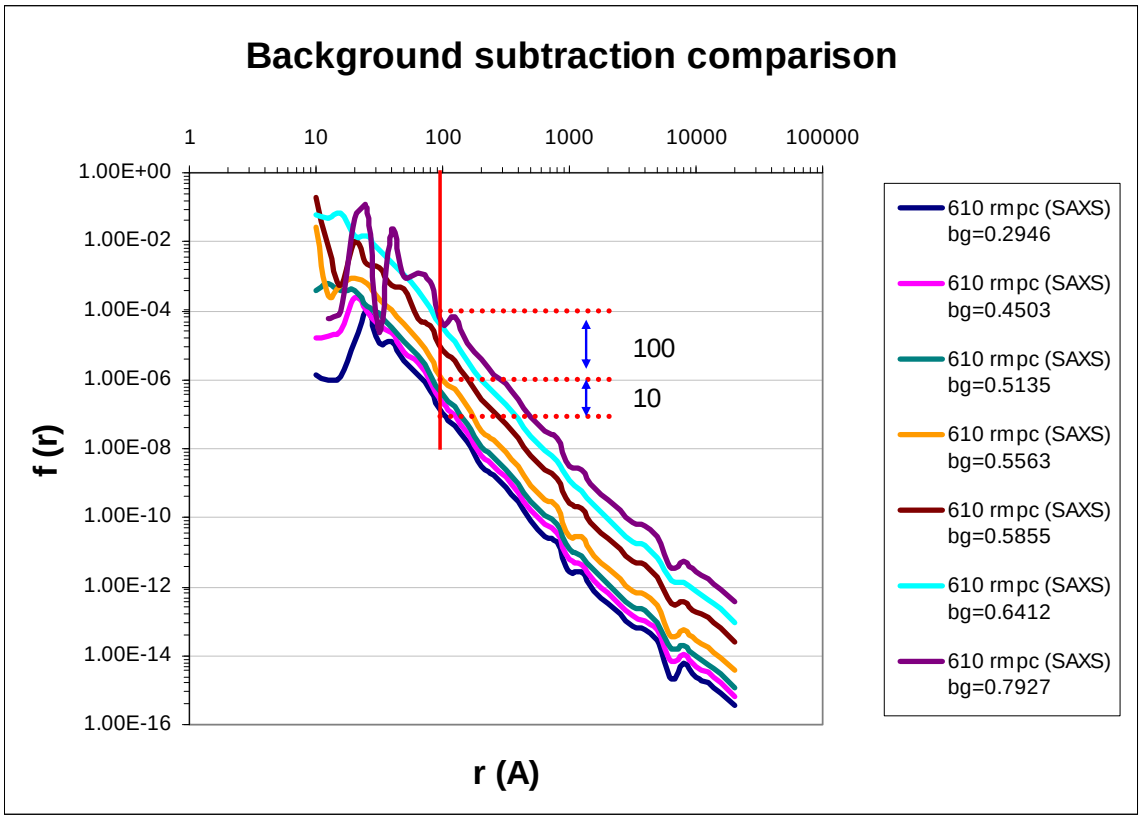

Figure 2. Pore size distribution calculated for the SAXS/USAXS data.

The calculated specific surface area histograms were found to be unaffected by the different values used for background subtraction (Figure 3).

As the calculations for porosity involve *f(r)*, the calculated total porosities have also being affected by the different subtracted values for background. Although variation as a result of the software fits to data is seen throughout the calculations (Figure 4), if only the end members are considered it can be seen that the smallest background subtraction results in an overestimation of porosity while the largest background subtraction results in an underestimation of porosity. In both cases porosity is miscalculated by approximately 10% (Table 2).

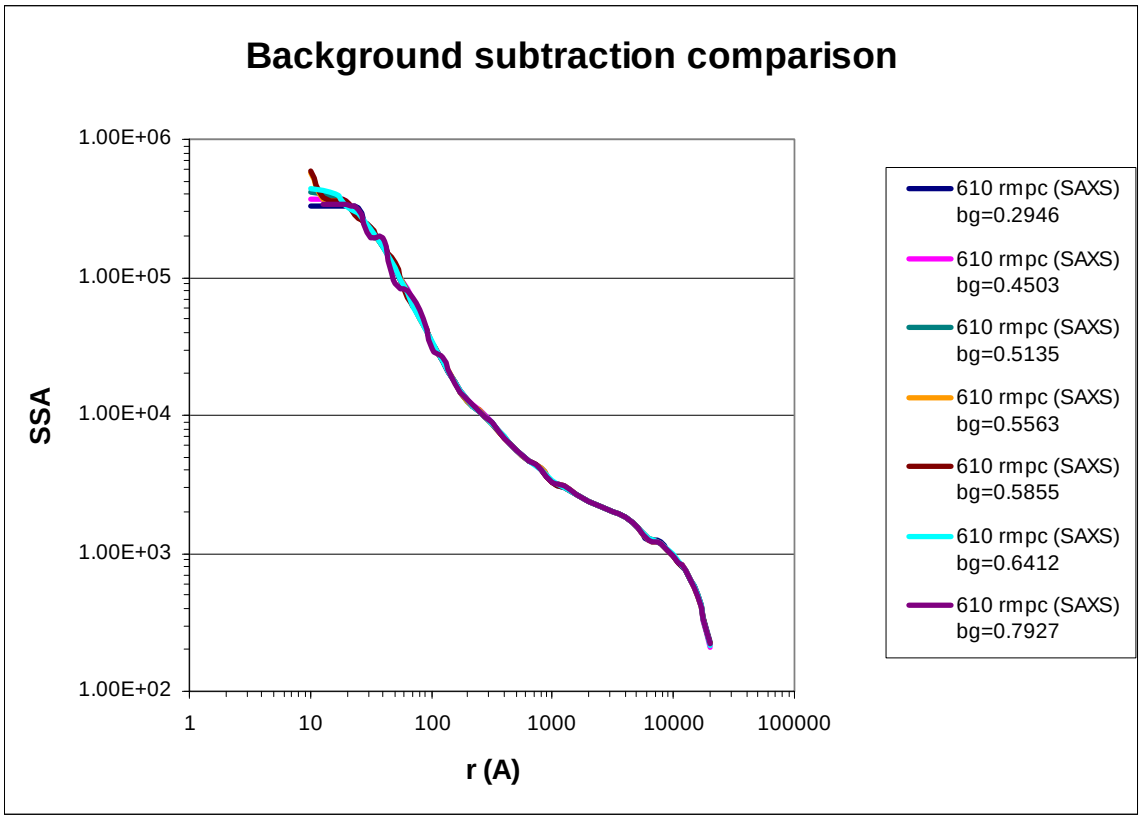

Figure 3. Calculated specific surface area histograms for SAXS/USAXS data.

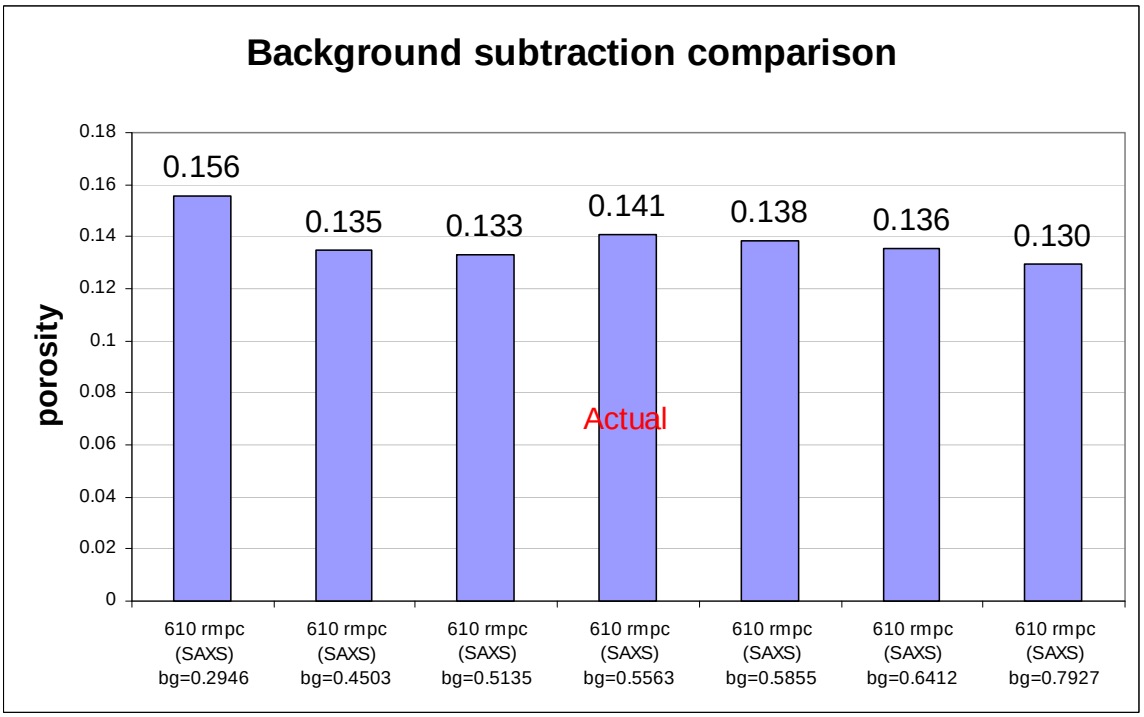

Figure 4. Calculated total porosities for SAXS/USAXS data for 10 Å < *r* < 20,000 Å.

Table 2. Calculated total porosities for different background subtraction.

Background value	Porosity	Subtraction from actual	Percentage of actual value	Percentage difference
0.2946	0.1558	0.0149	110.6%	10.6%
0.4503	0.1348	-0.0061	95.7%	-4.3%
0.5135	0.133	-0.0079	94.4%	-5.6%
0.5563	0.1409			
0.5855	0.1384	-0.0025	98.2%	-1.8%
0.6412	0.1357	-0.0052	96.3%	-3.7%
0.7927	0.1296	-0.0113	92.0%	-8.0%

Conclusions:

Conclusions about the effect of misjudging background subtraction are:

- It only affects the scattering curve in the $Q > 0.1$ $Å^{-1}$ region.
- It significant effects on the calculation of *f(r)*, particularly for overestimates.
- It has no effect on SSA calculations.
- It has effects on calculations of total porosity.

It is therefore important to take the time to estimate the correct background value for subtraction.

3.2. Study on the effect of scattering length density calculations

Introduction:

During the final data processing stage in the PRINSAS software the user is required to enter the already calculated scattering length density (SLD) of the sample. Knowledge of SLD (contrast) is essential for quantitative interpretation of absolutely calibrated small angle scattering (SAS) results. As the SLD is calculated with data from several different analyses (density, ultimate analyses- C, H, O, N, and S) it has a large potential to be affected by various types of error.

An SLD must be calculated for both SANS and SAXS experiments as the physical property responsible for neutron scattering is the coherent scattering amplitude (nuclear potential), while for X-rays it is the electron density (Radlinski, 2006). The formula for SLDs for both SANS and SAXS analyses can be seen in Chapter 2.

Aim:

To examine the effects of under- and overestimating the SLD on PRINSAS calculations of pore number density, *f(r)*, specific surface area, SSA, and porosity.

Method:

Different values for SLD were selected to be symmetric around, both smaller and greater than, the calculated 'actual' SLD value (Table 1). These different SLD values were input into the PRINSAS software when requested during data processing. Only one sample analysed using SAXS techniques has been used to investigate these effects.

Table 1. Values used for SLD.

	SLD (cm^{-2})
minus 10%	7.84E+10
minus 5%	8.28E+10
minus 2.5%	8.49E+10
actual	8.71E+10
plus 2.5%	8.93E+10
plus 5%	9.15E+10
plus 10%	9.58E+10

Results:

The scattering curve is not affected by SLD as the scattering curve is the measured data from the sample and not a calculated function.

The SLD was found to have no effect on the calculation of *f(r)* (Figure 1) but SLD did have an effect on the calculation of SSA. It can be seen in Figure 2 that underestimating SLD results in an overestimation of SSA while overestimating SLD results in an underestimation of SSA.

As the calculations for porosity involve SSA, the calculated total porosities have also being affected by the different SLD calculations. Across the board it can be seen that low SLD results in an overestimation of total porosity while high SLD results in an underestimation of total porosity (Figure 3). For the highest and lowest SLD (+/- 10%) porosity is miscalculated by approximately 20% (Table 2).

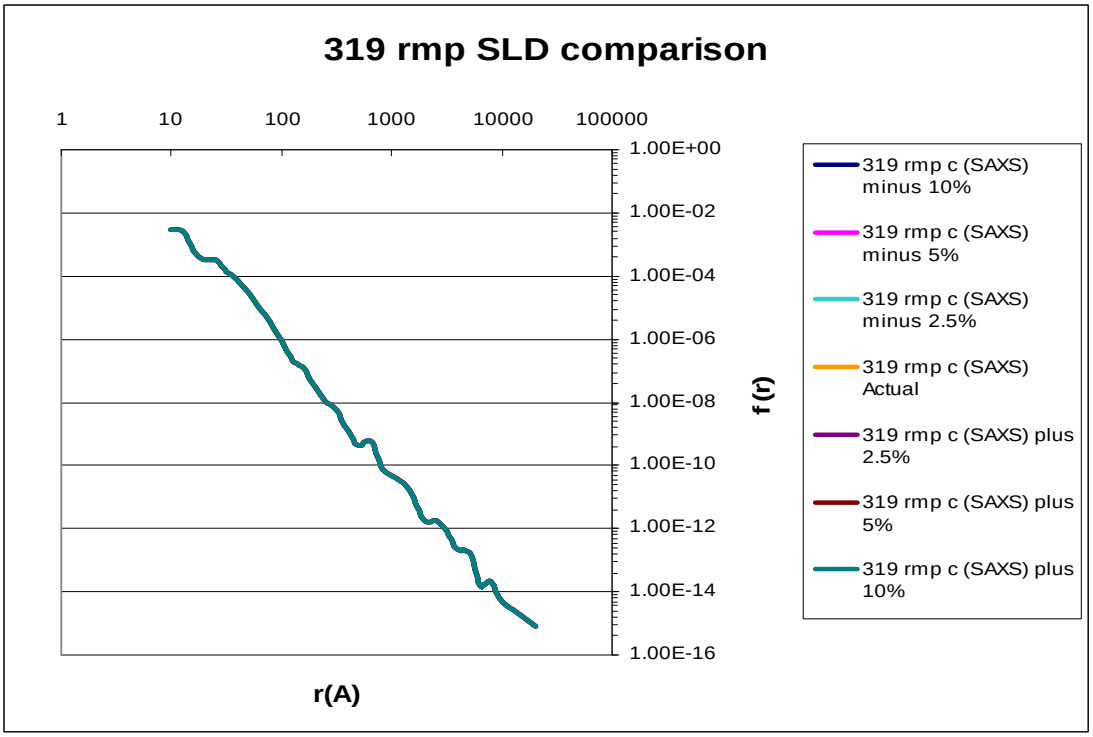

Figure 1. Pore size distribution calculated for the SAXS/USAXS data.

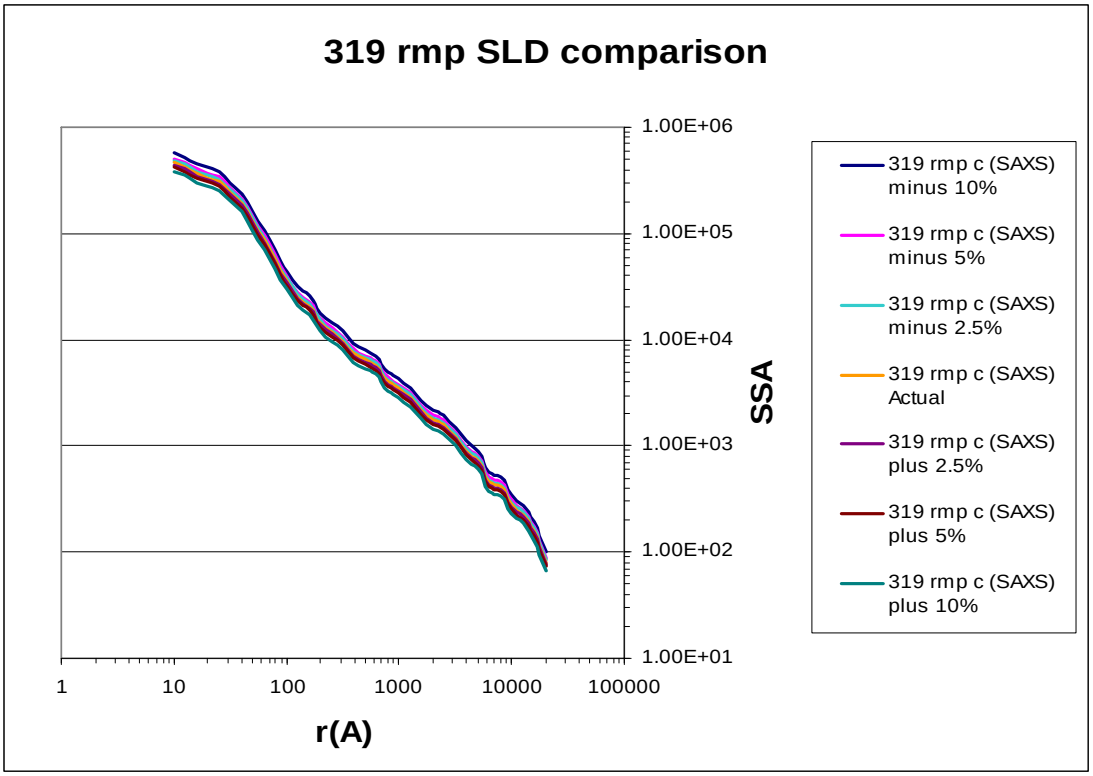

Figure 2. Calculated specific surface area histograms for SAXS/USAXS data.

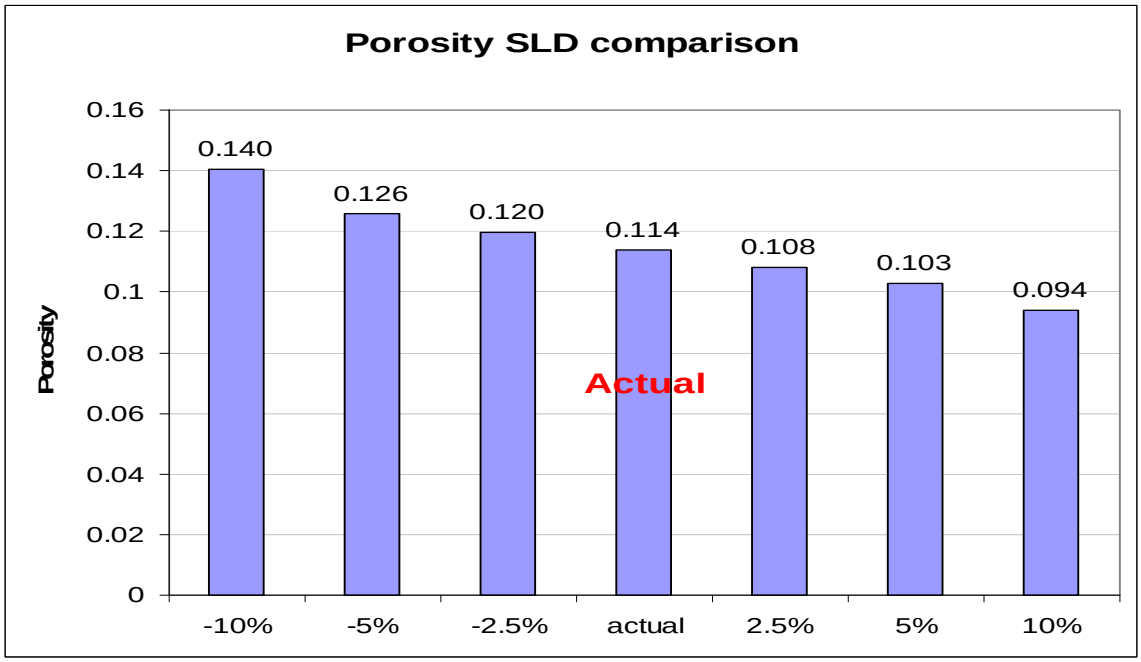

Figure 3. Calculated total porosities for SAXS/USAXS data for 10 Å < *r* < 20,000 Å.

Table 2. Calculated total porosities for different calculated SLD.

	Porosity	Subtraction from actual	Percentage of actual value	Percentage difference
minus 10%	0.1403	0.0266	123.4%	23.4%
minus 5%	0.1258	0.0121	110.6%	10.6%
minus 2.5%	0.1196	0.0059	105.2%	5.2%
actual	0.1137			
plus 2.5%	0.1081	-0.0056	95.1%	-4.9%
plus 5%	0.103	-0.0107	90.6%	-9.4%
plus 10%	0.094	-0.0197	82.7%	-17.3%

Conclusions:

Conclusions about the effect of error in the SLD calculation are:

- It has no effect on the scattering curve.
- It has no effect on the calculation of *f(r)*.
- It effects the SSA calculations with low SLD calculations overestimating SSA and high SLD calculations underestimating SSA.
- It has significant effects on calculations of total porosity.

3.3. Scattering data SAXS/USAXS

3.3.1. Renown seam matrix perpendicular samples (background corrected)

318 rmx ave		319 rmx ave		610 rmx ave		611 rmx ave		612 rmx ave	
Ave Q	Ave I(Q)	Ave Q	Ave I(Q)	Ave Q	Ave I(Q)	Ave Q	Ave I(Q)	Ave Q	Ave I(Q)
0.0001305	334844752	0.000157	293634202	0.0001316	293421898	0.0001381	355798150	0.0001528	215554101
0.000143	271887104	0.0001682	227722141	0.0001422	232116838	0.0001465	282025502	0.0001676	162419395
0.0001591	187594952	0.000177	192704502	0.0001549	173961438	0.0001568	239701755	0.0001824	123865838
0.0002043	97273304	0.0001872	172859458	0.0001725	118908558	0.0001683	200038381	0.0001953	102752011
0.0002197	68858264	0.0001994	140871458	0.0002094	71780063	0.0001854	158456922	0.0002064	87032924
0.0002316	59552880	0.0002167	110480196	0.0002272	52563869	0.0002043	112388475	0.0002225	71126591
0.0002444	56841351	0.0002352	83703794	0.0002469	40257746	0.0002264	83102104	0.0002405	57044787
0.0002627	46809187	0.0002566	65031882	0.0002604	34742679	0.0002569	58567393	0.0002607	44703307
0.0002864	38524530	0.00029	46822370	0.000282	28673260	0.0002775	44733734	0.0002957	31137265
0.0003128	30364949.5	0.0003138	37949812	0.0003028	23573932	0.0002938	39854238	0.0003191	24185014
0.0003542	22119019.5	0.0003321	32628976	0.0003354	19279442	0.0003141	33128016	0.0003461	19217266
0.0003729	19173569.5	0.0003603	25499456	0.0003678	15565673	0.0003427	23547572	0.000374	15300752
0.0004004	14722692.25	0.0003868	20525392	0.0003966	12609216	0.0003767	20105064	0.0004024	12070733
0.0004302	11955756.75	0.000429	15215093	0.0004303	9612489.1	0.0004127	14864723	0.000445	8819540
0.0004741	9019336.75	0.0004674	11466854	0.000464	7549164	0.0004455	11857220	0.0004793	6889600.7
0.0005151	7316842.125	0.0005045	8953705.6	0.0005109	5782842.7	0.0004756	9678800.6	0.0005236	5193615.7
0.0005588	6121460.375	0.0005665	6272923.8	0.0005494	4791894.9	0.0005144	7180754.4	0.0005862	3899720.3
0.0006389	4313380.875	0.0006175	4749214.9	0.0006048	3744254.4	0.000565	5560040.8	0.0006262	3086526.9
0.0006756	3280125.375	0.0006503	3910960.9	0.0006643	2852232	0.0006094	4589055.6	0.0006764	2403824.9
0.000713	2930638.813	0.0007088	2967844.9	0.000707	2269653.8	0.0006659	3370760.1	0.0007347	1954967.1
0.0007881	2253681.813	0.0007794	2218560.5	0.0007791	1667846.6	0.0007349	2375325.7	0.0007743	1590020.7
0.0008263	2065701.313	0.0008333	1775470.3	0.0008317	1394045	0.0007768	2028378.3	0.0008317	1258285.9
0.000895	1535656.156	0.0008927	1433035.7	0.0008977	1199811	0.0008319	1637068.7	0.000896	1004320.6
0.0009552	1334984.719	0.0009669	1150238.6	0.0009601	947480.05	0.0008985	1304514.4	0.0009651	794130.06
0.0010311	1113390.75	0.001057	905114.99	0.0010372	702056.88	0.0009635	1051432.4	0.0010478	619961
0.0011255	842004.375	0.0011441	718557.55	0.0011402	594630.11	0.0010472	843091.81	0.0011436	486915.24
0.0012385	646232.3906	0.0012426	553197.44	0.0012287	470895.67	0.001116	728348.68	0.00123	396645.69
0.0013185	532876.1719	0.0013187	469602.03	0.0013141	381863.48	0.001217	535045.87	0.0013265	308699.09
0.0014061	450227.2656	0.0014163	379036.41	0.0014191	297171.93	0.0013204	390371.38	0.0014157	249429.55
0.0015059	374399.3125	0.0015247	299874.81	0.0015197	252798.51	0.0014084	325542.52	0.0015166	204805.63
0.0016331	292934.6641	0.0016433	244720.89	0.0016469	212788.81	0.0015182	256420.53	0.001643	162057.32
0.0017897	227772.9141	0.0017771	196371.28	0.0017876	173535.51	0.0016292	194737.66	0.0017812	132369.52
0.0019303	181430.5625	0.0019132	158979.23	0.001919	139233.03	0.0017414	170225.82	0.001918	108017.6
0.00206	159138.5625	0.0020526	128157.21	0.0020571	116466.37	0.0018838	131429.24	0.0020539	86144.42
0.002199	123965.3125	0.0022038	103903.45	0.0022151	94580.191	0.0020395	105771.49	0.0022028	70154.876
0.0023694	91531.82031	0.0023709	83802.176	0.0023779	75318.469	0.002186	87164.912	0.0023682	56766.621
0.0025399	72601.71484	0.0025483	66771.066	0.0025429	60480.794	0.0023435	67201.062	0.0025482	44846.122
0.0027213	56834.28125	0.0027425	53787.536	0.0027409	50415.909	0.0025405	49512.596	0.0027343	36866.31
0.0029383	45133.90039	0.0029434	43175.737	0.0029488	42508.5	0.0027141	41690.141	0.0029412	29370.532
0.0031646	35974.23535	0.0031858	34387.249	0.0031641	33533.202	0.0029143	34136.679	0.0031684	23854.714
0.0033945	30350.55078	0.0034098	28011.055	0.0034108	26254.188	0.0031449	26747.785	0.0034228	18789.848
0.0036526	23974.65088	0.00368	22199.29	0.0036631	21531.219	0.0033658	21008.109	0.003666	14790.878
0.0039249	19099.36084	0.0039546	17694.724	0.0039418	18355.434	0.0036267	17081.218	0.0039374	12338.102
0.0042288	14881.86377	0.0042649	14192.594	0.004245	14680.194	0.003903	12866.093	0.0042435	9898.7241
0.0045787	12397.98657	0.0045734	11397.537	0.0045686	11877.08	0.0041937	10555.838	0.0045729	8047.7479
0.0048988	8851.634277	0.0049275	9174.7196	0.0049229	9499.8664	0.0045174	9145.7632	0.0049199	6509.5485
0.0053077	6996.885254	0.0053031	7315.9496	0.005293	7588.8318	0.0048596	7518.5498	0.0053021	5258.8995
0.0056753	6117.297119	0.0057027	5804.8688	0.0056932	6752.6691	0.0052379	5916.0135	0.0057096	4203.6498
0.0060972	4666.798706	0.0061219	4739.9633	0.0061185	5167.6181	0.0056256	4752.3542	0.0061193	3521.5336
0.0065575	3820.888672	0.0065701	3895.3396	0.0065754	4249.9149	0.0060473	3789.4744	0.0065568	2894.8441
0.0070454	3165.699707	0.0070664	3113.504	0.0070846	3552.4478	0.0065035	3088.418	0.0070566	2318.0514

0.0075984	2738.745667	0.0076059	2532.6047	0.007626	2912.9381	0.0069873	2492.5554	0.0076013	1863.6813
0.0081707	2103.889648	0.0081894	2066.4812	0.0081964	2419.8313	0.0075266	2128.5048	0.0081804	1524.2976
0.0087841	1635.824219	0.0088043	1680.0096	0.0088163	1971.3397	0.0081091	1720.6216	0.0087993	1253.353
0.0094374	1317.689392	0.0094717	1371.0764	0.0094771	1562.0842	0.0087114	1308.0393	0.0094549	1013.5908
0.0101463	1101.292816	0.0101806	1128.8379	0.0101846	1379.5394	0.0093563	1081.1637	0.0101691	837.83575
0.0109058	940.8137207	0.0109401	930.09982	0.0109476	1109.656	0.0100545	958.45378	0.0109403	697.15314
0.0117251	712.3686218	0.0117763	764.02827	0.0117708	906.42075	0.0108019	767.50447	0.011748	584.61155
0.0126107	601.4589844	0.0126455	635.0924	0.0126549	779.51902	0.011621	603.07396	0.0126449	476.92261
0.013554	516.4409943	0.0135977	527.59402	0.0135972	635.11508	0.0124924	524.42195	0.0135767	401.47841
0.0145512	402.0792389	0.014598	439.00446	0.0146059	538.39163	0.0134219	435.7369	0.0145829	336.33064
0.0156457	333.6885376	0.0156888	371.79955	0.0157066	447.83533	0.0144261	370.87059	0.0156671	283.76721
0.0168267	318.245842	0.0168578	311.11529	0.0168776	391.06113	0.0155003	308.58734	0.0168479	236.91134
0.0180731	250.3513412	0.0181269	264.72568	0.0181285	335.32161	0.0166519	269.286	0.0181099	194.97738
0.019412	228.4393463	0.0194729	224.39896	0.0194783	282.05935	0.0179085	232.21682	0.0194629	162.24168
0.0208578	205.7018967	0.0209184	191.70628	0.0209301	240.96438	0.019224	193.29207	0.0209004	139.54682
0.0224211	167.897995	0.0224666	165.8272	0.0224854	209.36332	0.0206572	171.07806	0.0224461	119.04928
0.024074	139.5827484	0.0241306	143.57144	0.0241599	173.97908	0.022188	147.1463	0.0241142	100.30871
0.0258781	137.769249	0.0259332	124.42238	0.0259722	151.74984	0.0238503	122.27254	0.0259101	83.307654
0.0278257	120.9891434	0.0278643	108.07218	0.0279031	133.47028	0.0256155	105.31296	0.0278472	70.932327
0.0298662	99.95461273	0.0299378	93.532825	0.0299665	116.04162	0.027527	96.394922	0.0299133	60.446288
0.0320903	88.46973801	0.0321804	81.312856	0.0322065	101.06779	0.0295878	82.142099	0.0321411	52.245739
0.0344945	75.16049576	0.0345855	71.329021	0.0346141	86.896362	0.0317721	66.617103	0.0345582	43.830078
0.0370975	67.61663818	0.0371693	62.016312	0.0372055	75.630948	0.0341378	61.75872	0.0371387	37.067851
0.039857	59.47028732	0.0399334	53.174783	0.0399713	63.559783	0.0366864	50.543777	0.0399026	30.902547
0.0428153	53.07132339	0.042912	45.769325	0.0429641	54.296369	0.0394439	42.963794	0.0428681	25.322317
0.0460462	47.44586754	0.0461125	38.895435	0.0461839	46.77925	0.0423889	38.085747	0.0460726	21.246623
0.049469	39.0237484	0.0495609	33.255838	0.0496167	38.027687	0.0455397	32.585495	0.0495158	17.439983
0.0531553	34.1518631	0.0532666	27.8473	0.0533247	32.026667	0.0489478	27.261927	0.053212	14.167925
0.0571253	28.3554039	0.0572421	23.259504	0.0573044	27.474321	0.0526156	22.408673	0.0571866	11.516354
0.0613858	23.18389225	0.0615202	19.049258	0.0615808	22.462772	0.0565314	18.079606	0.0614557	9.440655
0.0659777	18.97757339	0.0661333	15.628494	0.0661926	18.35731	0.0607557	15.469468	0.0660577	7.5694101
0.0709326	15.28040838	0.0710816	12.763088	0.0711589	14.845326	0.0652961	12.555999	0.0710266	6.0721832
0.0762665	12.29179382	0.0764277	10.157278	0.0765011	11.925931	0.0701858	9.9115539	0.0763435	5.1219352
0.0819807	9.779187202	0.0821757	8.1561138	0.0822626	9.7218044	0.0754657	7.8707588	0.0820832	3.9202504
0.0881839	7.772672415	0.0883586	6.3183687	0.088444	7.6246794	0.0811231	6.0606008	0.088275	3.031455
0.094777	6.097415686	0.0949799	4.9867487	0.0950566	6.0283978	0.0872242	4.8164558	0.0949014	2.3711059
0.1018604	4.793001652	0.1020756	3.8704851	0.1021566	4.5909629	0.0937759	3.8183727	0.1019667	1.8208115
0.1094499	3.678177595	0.1096727	3.0270598	0.1097621	3.6653169	0.1007738	2.9598823	0.1095553	1.4464502
0.1175727	2.797086596	0.1178144	2.3396327	0.1179251	2.7784089	0.1082788	2.3699924	0.1176994	1.1189409
0.1262894	2.138489008	0.1265623	1.7960926	0.1266609	2.1823612	0.1163164	1.8320603	0.1264235	0.8595505
0.1356406	1.611746609	0.135918	1.3932341	0.1360552	1.6802816	0.1249644	1.4194817	0.1357971	0.6816834
0.1456948	1.264167547	0.1459877	1.0668733	0.1461264	1.2867149	0.1342166	1.0751081	0.1458452	0.5422685
0.1564612	0.935303599	0.1567885	0.8349346	0.1569412	0.9665136	0.1441517	0.8242227	0.1566419	0.4140558
0.1680649	0.753359109	0.1684265	0.656208	0.1685906	0.7910443	0.154832	0.6410279	0.1682534	0.34084
0.1805386	0.581523091	0.1809316	0.5084964	0.1811031	0.6001377	0.1662986	0.4936325	0.1807612	0.2570596
0.1939697	0.493081599	0.1943909	0.411178	0.1945803	0.4858903	0.1786365	0.3931182	0.1941905	0.2301883
0.2084324	0.422877103	0.2088371	0.3382036	0.2090431	0.3800686	0.1919186	0.3187049	0.2086284	0.1878202
0.2238859	0.352418572	0.224405	0.276759	0.224606	0.3264397	0.2062118	0.2741236	0.2241608	0.1703538
0.2406611	0.283821225	0.2411174	0.232178	0.2413643	0.2594766	0.221555	0.2175342	0.2408769	0.1385124
0.2585526	0.23470068	0.2591288	0.1912482	0.2593611	0.2069653	0.2380578	0.1770014	0.2588543	0.1180368
0.2779226	0.218640268	0.2784816	0.159636	0.2787624	0.1757086	0.2558474	0.1605304	0.2781899	0.106285
0.2986818	0.168535948	0.2992961	0.1415059	0.2996026	0.1580291	0.2749303	0.126601	0.2989938	0.0900175
0.3210166	0.134346187	0.3216356	0.1261503	0.3219653	0.139263	0.2954754	0.0995246	0.3213202	0.0857582
0.3449194	0.140452385	0.3456915	0.1084988	0.3460289	0.125275	0.3175976	0.0934031	0.345293	0.0729974
0.3707666	0.097415	0.3714895	0.0922597	0.3718988	0.1035478	0.3413104	0.0787605	0.3711157	0.0707637
0.3984385	0.103898495	0.3991465	0.0706118	0.3995485	0.0983959	0.3667281	0.0741758	0.3987896	0.0596779
0.4279407	0.079888731	0.4287962	0.0589694	0.4292055	0.0813751	0.3941167	0.062149	0.428364	0.0478143
0.45965	0.091825336	0.4605951	0.0473811	0.4610832	0.0762292	0.4234433	0.0524675	0.4517042	0.0403709
0.4938024	0.086704344	0.4710006	0.0551541	0.4608867	0.0905593	0.4358908	0.0392734	0.4852416	0.0349953
		0.4937665	0.0476073	0.459667	0.108888	0.4682228	0.0324811	0.4937948	0.0450085
				0.4938194	0.0926898	0.49384	0.0310277		

3.3.2. Renown seam matrix parallel samples (background corrected)

318 rmp ave		319 rmp ave		610 rmp ave		611 rmp ave		612 rmp ave	
Ave Q	**Ave I(Q)**	**Ave Q**	**Ave I(Q)**	**Ave Q**	**Ave I(Q)**	**Ave Q**	**Ave I(Q)**	**Ave Q**	**Ave I(Q)**
0.0001215	790053690	9.941E-05	2.372E+09	0.0001303	636355632	0.0001271	237094723	0.0001267	237551334
0.0001327	601065027	0.0001077	1.776E+09	0.0001526	449573222	0.0001522	136164742	0.0001403	167604461
0.0001452	434208006	0.0001207	1.305E+09	0.0001632	315513562	0.000171	98294482	0.0001644	104544166
0.0001576	320923904	0.0001309	940792371	0.0001729	270747878	0.0001846	76463096	0.0001905	66867139
0.0001759	238495394	0.0001421	699551712	0.0001835	221035866	0.0001986	65370731	0.0002021	57808276
0.0001979	163643113	0.000157	505337926	0.0001975	159967466	0.0002145	51619288	0.0002161	46353914
0.0002253	108057746	0.0001863	288917478	0.0002145	119990911	0.0002314	39880794	0.0002341	38558790
0.0002403	91235872	0.0002088	207286122	0.0002331	89585126	0.0002518	31785722	0.0002516	30884860
0.0002618	73574980	0.0002201	177087278	0.0002595	60577789	0.000273	26220590	0.0002679	26269776
0.0002829	58402566	0.0002329	142071379	0.0002886	45590386	0.0003051	18739517	0.000294	19928454
0.0003012	51982913	0.0002531	110374901	0.0003125	34438524	0.0003379	13037377	0.0003389	12683521
0.0003294	43238889	0.0002713	90471512	0.000334	28298826	0.0003632	10673040	0.0003627	10049016
0.0003746	29926687	0.0002879	74533714	0.0003597	23247918	0.0003997	8087108.6	0.0003919	7537390.5
0.0004029	23283176	0.000329	50822404	0.0003913	17466332	0.0004363	6281059.9	0.0004293	5529028.1
0.0004344	18118317	0.000364	37505723	0.0004292	13455016	0.0004863	4605742.5	0.0004903	3229494.1
0.0004891	12918993	0.0003904	32332346	0.0004713	10046368	0.0005184	3721886.3	0.0005172	2838518.3
0.0005365	9488138.5	0.0004215	26335278	0.000515	7623586.2	0.0005519	3077437.3	0.0005456	2414952.9
0.0005647	8241156.4	0.0004709	18755495	0.0005683	5899828.2	0.0005907	2508980.7	0.0005856	1885861.3
0.0006038	6794531.2	0.0005203	13823051	0.0006191	4615658.7	0.000646	1836830.9	0.0006409	1328307.9
0.0006573	4892288.6	0.0005471	11581151	0.0006607	3725066.7	0.0007015	1382107.3	0.0006894	1056295.7
0.0006965	4193471.7	0.0005829	9681231.4	0.0007107	3028098.9	0.0007579	1083924.7	0.0007456	774407.01
0.0007423	3562722.3	0.0006439	7343477.1	0.0007638	2400297.3	0.0008082	917113.03	0.0007976	587307.17
0.0007984	2852350.5	0.0007067	5290413.3	0.0008142	1967920.9	0.0008713	725610.09	0.0008549	485994.52
0.0008479	2205739	0.0007722	4071088.5	0.0008745	1591137	0.0009498	565963.07	0.0009317	355846.96
0.0009194	1822565.2	0.0008153	3299690.2	0.0009428	1232737.8	0.0010266	439726.54	0.0010205	273207.01
0.0009937	1420192.2	0.0008679	2732591.9	0.0010278	975342.81	0.0011054	353213.73	0.0010938	218987.54
0.0010823	1078800.7	0.0009526	2015864.3	0.0011267	755563.38	0.0011768	290955.31	0.0011706	168387.28
0.0011674	844526.81	0.001051	1537350.7	0.0012178	596564.21	0.0012559	232878.45	0.0012427	129879.84
0.0012484	681823.84	0.0011157	1296607.9	0.0012966	497133.66	0.0013499	188134.58	0.001323	112232.27
0.0013309	544127.72	0.0012086	1010371.4	0.001392	389218.51	0.0014515	153196.81	0.0014279	86836.661
0.0014122	446148.49	0.0012673	830596.79	0.0014928	306649.19	0.0015692	120608.69	0.0015372	66617.173
0.0015177	370043.03	0.0013593	653349.21	0.0016081	254890.61	0.0016846	97442.695	0.0016624	53214.291
0.0016491	278826.12	0.0014571	545741.57	0.0017441	203352.69	0.0018062	79610.02	0.0017732	42725.009
0.001777	223588.22	0.001566	423069.9	0.0018807	158673.38	0.0019182	66762.392	0.0018961	36521.957
0.0019008	181888.18	0.0016987	333779.81	0.0020184	130423.3	0.0020521	54187.548	0.002027	28929.275
0.0020298	150122.49	0.0018218	281837.85	0.002165	106516.68	0.0021995	43121.478	0.0021734	22597.104
0.0021773	118475.86	0.0019435	232394.53	0.0023278	84890.428	0.0023575	34739.713	0.0023282	18525.54
0.0023317	96259.711	0.0020775	179415.93	0.0025076	67202.009	0.0025288	28016.318	0.0024819	14866.816
0.002487	78659.295	0.0022322	139627.63	0.002695	56044.132	0.0027117	22967.126	0.002673	11716.78
0.0026759	63712.941	0.002388	118478.73	0.0028928	45865.518	0.0028995	18799.004	0.0028639	9525.2861
0.0028693	50420.312	0.0025417	99495.817	0.0031213	36290.262	0.0031052	15579.954	0.0030634	7963.4762
0.0030496	42709.661	0.0027576	74827.586	0.0033575	29470.999	0.0033281	12760.429	0.0032877	6704.9449
0.0032791	33558.252	0.0029316	62327.373	0.0036166	23379.23	0.0035784	10191.531	0.003512	5374.7862
0.003522	27422.304	0.0031292	50039.272	0.0038931	18844.631	0.0038228	8433.557	0.0037766	4466.7596
0.0037834	21860.838	0.0033786	39584.546	0.0041926	15199.637	0.0041022	6994.6796	0.0040487	3666.813
0.0040485	17945.096	0.0036018	31909.706	0.0044999	12543.391	0.0043944	5810.9566	0.0043398	3036.5027
0.0043467	14664.104	0.0038915	25452.904	0.0048411	10231.705	0.0047194	4710.0557	0.0046492	2501.2841
0.0046535	12005.146	0.0041515	20112.144	0.005213	8185.6148	0.0050613	3937.9463	0.0049969	2082.1465
0.0049784	10196.277	0.0044655	15831.323	0.0056143	6752.0097	0.0054228	3279.2871	0.0053494	1703.3006
0.0053356	8180.3176	0.0047663	12935.269	0.0060272	5450.6446	0.005797	2719.8043	0.0057195	1391.135
0.0057152	6252.3042	0.0051206	10582.882	0.0064629	4591.1727	0.0062063	2255.5708	0.0061251	1201.9932
0.0061237	5342.4533	0.0054743	8665.9983	0.006948	3699.3242	0.0066408	1908.5998	0.0065577	1002.897
0.0065687	4496.6182	0.005871	7204.2795	0.007481	3056.2158	0.0071096	1571.4966	0.0070134	843.01161
0.0070151	3784.0687	0.0062924	5983.2353	0.0080564	2518.8813	0.0076279	1327.7256	0.0075044	726.53612
0.0074997	3203.383	0.0067345	4841.5129	0.0086705	2039.8226	0.0081632	1143.0649	0.0080459	622.97853
0.0080369	2643.4737	0.0071948	3856.9074	0.0093217	1702.1693	0.0087509	956.15092	0.0086309	524.21617

0.0086175	2236.0037	0.0077065	3307.4497	0.0100183	1419.9541	0.0093782	797.90476	0.009244	451.92878
0.0092391	1897.0404	0.0082629	2823.2195	0.0107736	1184.8104	0.0100495	678.39861	0.0098995	385.05923
0.0099047	1551.3714	0.0088677	2342.0376	0.0115856	976.5973	0.0107409	583.88611	0.0105896	331.3382
0.0106018	1297.0012	0.0094872	1952.2034	0.0124524	821.16873	0.0114948	504.24606	0.0113264	287.39891
0.0113357	1062.9354	0.0101684	1613.8622	0.0133869	680.40637	0.0123124	428.21841	0.0121333	241.20897
0.0121375	915.22123	0.0108685	1360.2506	0.0143725	575.90787	0.0131884	367.26552	0.0129926	208.37135
0.0129967	812.00461	0.0116278	1152.5626	0.0154438	485.67922	0.01411	314.19384	0.0139056	179.65991
0.013911	681.95316	0.0124627	972.47332	0.0166017	409.66074	0.0151022	275.29416	0.0148876	153.28903
0.0148961	584.79307	0.0133422	833.31703	0.0178481	347.57137	0.0161741	232.80392	0.0159482	132.51799
0.0159532	501.0315	0.0142759	692.90151	0.0191778	290.95441	0.0173143	199.8925	0.0170802	115.43933
0.0170929	431.4149	0.0152871	591.39633	0.0206024	248.61453	0.0185198	174.0746	0.0182692	99.566882
0.018258	363.87932	0.0163847	502.13384	0.0221255	210.65423	0.0198094	150.33304	0.0195333	84.478786
0.019531	305.45994	0.017542	433.59918	0.0237664	178.79897	0.0212034	130.34708	0.0209124	71.848895
0.0209259	262.41728	0.0187454	371.88925	0.0255379	149.87148	0.022687	111.35341	0.0223624	63.479832
0.0223735	228.9693	0.0200532	323.065	0.0274438	125.78375	0.0242658	96.144832	0.0239218	54.326467
0.0239336	200.40538	0.0214842	275.07478	0.0294877	107.11413	0.0259606	82.805962	0.0255891	46.305288
0.0255992	173.56874	0.0229449	233.49778	0.0316885	89.331958	0.0277771	70.267606	0.0273847	39.666318
0.0273856	148.58629	0.0245732	203.329	0.0340646	73.540434	0.0297352	59.559277	0.0293129	34.116096
0.0293166	129.65732	0.0262686	169.38366	0.036614	61.669382	0.0318202	50.493661	0.0313705	28.930793
0.0313771	110.77396	0.0281229	142.7783	0.0393378	51.108233	0.034055	42.60765	0.0335679	24.174506
0.0335775	92.69269	0.0300992	122.22432	0.0422669	41.324331	0.0364544	35.166973	0.0359336	20.444163
0.0359379	80.196413	0.0322121	104.44797	0.0454207	33.70107	0.039022	29.348784	0.0384763	16.919921
0.0384589	67.790407	0.0344707	87.996466	0.0488172	27.39799	0.0417539	24.124314	0.0411604	13.903402
0.0411509	57.348721	0.0369057	72.912822	0.0524642	21.675053	0.0446889	19.954359	0.044046	11.650724
0.0440543	47.258698	0.0395109	60.53978	0.0563829	17.072597	0.0478353	16.124891	0.047153	9.7022579
0.0471501	39.023433	0.0422544	49.899337	0.0605923	13.571195	0.0511928	13.059413	0.0504624	7.8531445
0.0504545	31.900694	0.0452435	40.449396	0.0651249	10.74749	0.0547959	10.51143	0.0540162	6.5069324
0.0540062	25.947921	0.048418	33.007198	0.0700106	8.3306761	0.0586488	8.3807916	0.0578185	5.1322804
0.0578154	21.049789	0.051816	26.327276	0.0752733	6.5248082	0.0627704	6.7819757	0.0618679	4.0764284
0.0618755	16.827257	0.0554658	21.177013	0.0809288	5.0946182	0.0671991	5.3171759	0.0662368	3.4007161
0.0662472	13.257817	0.0593706	17.166444	0.0870201	3.8991305	0.0719376	4.2482885	0.0709166	2.6570041
0.0709222	10.639894	0.0635353	13.48975	0.0935538	3.0221264	0.0770151	3.4012104	0.0759086	2.2313483
0.0759226	8.4319832	0.0680385	10.61019	0.1005417	2.3185887	0.0824717	2.6728486	0.0812816	1.8334045
0.0813033	6.6301242	0.0728328	8.3724246	0.1080286	1.7926808	0.0883162	2.1376694	0.0870513	1.3859248
0.0870639	5.2644679	0.0779633	6.5895761	0.1160616	1.3845196	0.0945455	1.695239	0.0932	1.0879462
0.0932108	4.1349406	0.0834983	5.0702154	0.124667	1.0696887	0.1011913	1.3418564	0.0997486	0.901755
0.0997616	3.1959593	0.0894246	3.9818058	0.1338945	0.8271306	0.1082958	1.0774786	0.1067554	0.7012793
0.106768	2.522789	0.095722	3.073462	0.1438138	0.6483232	0.1158725	0.8724038	0.1142281	0.5882272
0.1142389	1.9762308	0.102436	2.4015944	0.1544562	0.5066686	0.1239718	0.6909614	0.1221994	0.46178
0.1222099	1.582742	0.1096352	1.8619028	0.1659109	0.4066321	0.1326063	0.5649309	0.1307414	0.3870886
0.1307271	1.2404322	0.1172897	1.510384	0.1782322	0.3152981	0.141835	0.4482131	0.1398444	0.3132187
0.1398416	0.9847764	0.1254716	1.1736704	0.1914892	0.2679806	0.1517131	0.3824597	0.1495771	0.2572066
0.1495906	0.7857594	0.1342318	0.9155126	0.2057241	0.2194607	0.162304	0.3147831	0.1600184	0.2269774
0.16003	0.6361576	0.1435711	0.7457746	0.2210361	0.1867265	0.1736469	0.2554552	0.1711972	0.1942567
0.1711947	0.51911	0.1535831	0.5906438	0.2375151	0.1523252	0.185799	0.2172711	0.183165	0.1613931
0.1831733	0.4303553	0.1643074	0.481228	0.2552461	0.1278654	0.1988112	0.1840055	0.196002	0.1423578
0.1960159	0.3600299	0.1757843	0.3915444	0.2743069	0.1061065	0.2127388	0.1612513	0.2097305	0.1249166
0.2097431	0.2967254	0.1880849	0.3190094	0.294812	0.0934755	0.227639	0.1391428	0.2244068	0.1093341
0.2244241	0.2568289	0.2012812	0.2770911	0.3168384	0.0868602	0.2436096	0.1110586	0.2401598	0.0980836
0.2401822	0.2257777	0.2153618	0.2293687	0.3405157	0.067411	0.2607325	0.0997735	0.2570249	0.0877458
0.2570509	0.1994829	0.2304394	0.205931	0.3659428	0.0617697	0.2790629	0.0852978	0.2750925	0.0626447
0.2751151	0.1661168	0.2466478	0.1831453	0.3932317	0.0445791	0.2987115	0.0640402	0.2944695	0.0632444
0.2944855	0.1397366	0.2639523	0.1483195	0.4224346	0.0370417	0.3197241	0.0563265	0.3151978	0.0426003
0.3152154	0.1268811	0.2825262	0.1236974	0.4537486	0.0338313	0.3421916	0.0464481	0.3373247	0.0365934
0.3373543	0.1134504	0.3024355	0.1116741	0.4766762	0.0291666	0.3662408	0.0286366	0.3586151	0.0326026
0.3610938	0.0907118	0.323713	0.0985853	0.4937552	0.0404798	0.3919418	0.038329	0.3838311	0.0275124
0.3864691	0.0699012	0.346413	0.0744305			0.4106411	0.027775		
0.4060817	0.0705434	0.3708393	0.0661722			0.4244613	0.0218051		
0.4245202	0.0643582	0.3968429	0.0503878						
		0.4244956	0.0537329						

3.3.3. Kupakupa seam matrix perpendicular samples (background corrected)

320 kmx ave		321 kmx ave		322 kmx ave	
Ave Q	**Ave I(Q)**	**Ave Q**	**Ave I(Q)**	**Ave Q**	**Ave I(Q)**
0.0001398	298604042	0.0001571	420337635	0.0001602	335368080
0.0001632	172448960	0.0001724	310029786	0.0001737	282547624
0.0001755	134564522	0.0001819	248378438	0.0001835	238931648
0.0001853	114308870	0.0001921	208535040	0.0001938	207280874
0.0001975	97881291	0.0002046	176938216	0.0002089	175116602
0.0002119	81257409	0.0002217	142623898	0.0002258	143823944
0.0002297	66761916	0.0002406	112587531	0.0002453	117653788
0.0002528	52990956	0.0002654	87133304	0.0002755	86269046
0.0002786	42272858	0.0002957	65435836	0.0003	69678627
0.0003116	32265030	0.0003274	48774292	0.0003228	59137547
0.0003361	26121936	0.0003487	41733860	0.0003482	48424025
0.0003606	22103436	0.0003761	34343922	0.0003716	42176846
0.0003914	18187545	0.0004106	26491343	0.000411	32904612
0.0004253	14649131	0.0004462	21485215	0.000442	26017807
0.0004665	11598163	0.0004899	15779989	0.0004852	20068507
0.0005112	9064272.1	0.0005341	12335137	0.0005393	15117544
0.0005557	7302824.4	0.0005846	9513952.9	0.0005776	12954856
0.0006147	5647210	0.000644	6982706.5	0.0006327	10364281
0.0006596	4469574.5	0.0006872	5772656.2	0.000686	7756171.5
0.0007036	3755378.1	0.0007329	4645591.3	0.0007333	6399141.4
0.0007624	3080156.5	0.0007938	3519263.3	0.0007999	4908076
0.0008138	2538690.7	0.0008439	2905277.7	0.0008511	3965554.3
0.0008724	2132654.7	0.0009091	2354483.9	0.0009181	3152813.3
0.0009398	1753147.9	0.0009817	1881866.7	0.0009939	2476496.5
0.0010154	1419379.5	0.0010619	1505473.7	0.0010786	1971480.3
0.0011084	1149881.3	0.0011592	1151984.7	0.0011653	1561875.7
0.0011989	937210.01	0.0012579	878557.9	0.0012678	1211858.1
0.0012911	744439.17	0.0013385	715364.04	0.001345	1014118.7
0.0013866	619572.79	0.0014376	562901.16	0.0014492	806792.77
0.001487	510660.82	0.0015491	443555.43	0.0015638	638094.06
0.001598	424412.6	0.0016686	350620.07	0.0016792	508684.55
0.0017217	345812.17	0.0018023	277176.07	0.0018103	405126.3
0.0018607	279764.61	0.0019414	219177.73	0.001952	328082.7
0.0020037	226859.83	0.0020848	175278.91	0.0020983	259236.1
0.0021483	183937.34	0.0022372	141765.63	0.0022523	215104.33
0.0023064	152297.18	0.002404	113249.41	0.0024194	172125.73
0.0024832	124094.46	0.0025854	90799.556	0.0026005	134849.72
0.0026696	99647.115	0.0027847	71997.368	0.0028016	108851.08
0.0028791	80808.694	0.0029943	58310.428	0.0030136	87797.5
0.0030816	64989.055	0.0032208	45670.455	0.0032485	69016.743
0.0033201	52835.029	0.0034614	36244.768	0.0034766	56041.426
0.0035815	42821.505	0.0037319	28554.119	0.003758	43824.917
0.0038559	34155.231	0.0040102	22783.765	0.0040369	35408.024
0.0041389	27563.782	0.0043255	17982.065	0.0043509	28517.089
0.0044625	22394.752	0.004652	14204.361	0.004673	22788.144
0.0048009	18159.826	0.0050108	11606.325	0.0050383	18392.915
0.0051555	14672.167	0.0053818	9272.976	0.0054076	14873.145
0.005548	11858.745	0.0057896	7360.7098	0.0058127	11914.489
0.0059722	9466.8144	0.0062205	6046.8311	0.0062507	9481.9222
0.0064138	7616.5152	0.0066794	4948.5664	0.0067162	7668.1735
0.0068839	6172.85	0.0071777	4050.7505	0.007217	6262.671
0.0074028	4994.6915	0.0077261	3310.8237	0.0077692	5026.3804
0.0079682	4084.4633	0.0083158	2733.3375	0.0083608	4124.547
0.0085781	3262.9619	0.0089441	2215.4638	0.0089869	3303.2841
0.0092264	2692.0299	0.0096229	1853.4078	0.0096783	2717.7513
0.0099147	2205.9599	0.0103398	1519.127	0.010389	2228.9719

0.0106623	1820.9595	0.0111186	1260.8804	0.0111723	1838.1689
0.0114641	1478.2289	0.011958	1028.6846	0.0120223	1484.3841
0.0123217	1214.2427	0.0128445	858.23855	0.0129001	1231.1629
0.0132447	994.99751	0.0138121	712.10126	0.0138788	1013.6698
0.0142359	819.48597	0.0148341	582.34588	0.0149077	825.8262
0.0152876	680.00955	0.0159385	501.68395	0.0160178	694.08025
0.0164289	564.77823	0.0171354	416.28675	0.0172124	580.32951
0.0176567	468.07818	0.0184167	352.0881	0.0185025	483.19792
0.0189748	394.59937	0.0197852	298.91115	0.0198721	404.42194
0.0203927	329.54877	0.0212549	252.04022	0.0213533	341.13751
0.0219007	277.27667	0.0228272	214.24408	0.0229331	287.96273
0.0235221	230.65592	0.0245243	184.02084	0.0246344	245.21027
0.0252685	198.04998	0.0263488	157.9708	0.0264675	208.63705
0.0271469	166.69995	0.0283077	134.08584	0.0284351	178.19463
0.0291836	142.28409	0.0304226	114.25376	0.0305632	151.3486
0.0313577	121.47518	0.0326972	97.77999	0.032849	130.33727
0.0336914	102.95107	0.03514	84.02555	0.0352923	111.48684
0.0362136	87.569089	0.0377686	71.638541	0.0379339	94.850826
0.038923	75.377982	0.0405823	61.102431	0.0407614	81.325484
0.0418182	63.952477	0.0436055	50.943729	0.0438004	69.786771
0.0449304	54.224744	0.0468559	42.569339	0.0470608	58.890055
0.0482873	45.636081	0.0503602	35.787502	0.0505819	50.059894
0.0518944	38.602145	0.0541203	29.919051	0.0543603	42.074672
0.0557727	32.174417	0.0581634	24.574513	0.0584222	35.185262
0.0599501	26.645327	0.0625194	20.072659	0.0628074	28.889169
0.0644238	21.937071	0.0671955	16.276625	0.0674996	23.829937
0.069253	17.850057	0.0722326	13.115386	0.0725468	19.334142
0.0744642	14.458945	0.077671	10.531976	0.0780221	15.590669
0.0800534	11.610242	0.0835056	8.3274997	0.0838841	12.45721
0.0860543	9.2150496	0.0897712	6.6351203	0.0901655	9.8312535
0.0925216	7.265297	0.0964993	5.2102186	0.096919	7.6611164
0.0994466	5.6281307	0.1037011	4.0567151	0.1041639	6.0013009
0.1068513	4.4163193	0.1114095	3.1668322	0.1119092	4.6223779
0.1148037	3.3973853	0.1196931	2.4607125	0.1202186	3.5818322
0.1233208	2.6244049	0.1285705	1.8912463	0.1291403	2.7482427
0.13246	2.0223698	0.1380803	1.4904934	0.1386854	2.1026766
0.1422687	1.5495282	0.148313	1.1404585	0.1489654	1.6070681
0.1528148	1.1951892	0.1592922	0.8869017	0.1600012	1.2328946
0.1641316	0.9239196	0.1711134	0.6965063	0.1718756	0.9388588
0.1763179	0.7188756	0.1838188	0.5355359	0.1846319	0.7293023
0.1894197	0.5663417	0.1974896	0.420573	0.1983667	0.5788599
0.2035189	0.4475423	0.2121891	0.3479283	0.2131341	0.4554339
0.2186545	0.3678446	0.227982	0.2724597	0.2290076	0.36277
0.2349549	0.3167955	0.2449841	0.2204037	0.2460728	0.2898585
0.2524872	0.2622428	0.2632853	0.1942091	0.2644665	0.2481303
0.2713373	0.2128947	0.2829492	0.158646	0.284212	0.2068093
0.2915893	0.1903521	0.3040768	0.1397329	0.30543	0.1618131
0.3133988	0.1630276	0.3268014	0.1158831	0.328252	0.1454688
0.336805	0.1406931	0.3512183	0.1057295	0.3528061	0.1190097
0.3618949	0.1178258	0.3773862	0.0829185	0.3790475	0.105706
0.3888896	0.108989	0.4054926	0.0681918	0.4072616	0.0844965
0.4178537	0.0831869	0.4356305	0.049652	0.4375598	0.0739863
0.4284637	0.0848443	0.4523043	0.0519351	0.4498676	0.0686473
0.4602308	0.0705427	0.4710027	0.0370087	0.4596291	0.080619
0.4823871	0.0684868	0.493768	0.0354836	0.4937702	0.0580933
0.4937705	0.0515283				

3.3.4. Kupakupa seam matrix parallel samples (background corrected)

320 kmp ave		321 kmp ave		322 kmp ave	
Ave Q	**Ave I(Q)**	**Ave Q**	**Ave I(Q)**	**Ave Q**	**Ave I(Q)**
0.000107	2.281E+09	0.0001209	813326515	0.00012	1.138E+09
0.0001258	1.393E+09	0.0001373	474348838	0.000129	825319309
0.0001486	847147648	0.0001637	271346061	0.0001416	629120352
0.0001601	699636621	0.0001847	184235597	0.0001551	506019674
0.0001712	561070317	0.0001962	147482802	0.0001677	382550781
0.0001859	427352262	0.0002078	124273859	0.0001847	287597318
0.0002014	344980762	0.0002218	110174755	0.0002166	193399958
0.000217	278164963	0.0002403	92872667	0.0002363	150676074
0.000232	225430902	0.00026	72859650	0.0002561	123675523
0.0002539	173020862	0.0002897	49697890	0.0002757	103562735
0.0002894	116343950	0.0003233	36941310	0.0002949	87301065
0.0003161	89266064	0.0003538	28169104	0.0003173	72890737
0.0003395	72396107	0.0003794	23941764	0.0003562	53791944
0.0003682	55624162	0.00041	19263626	0.0003873	42089131
0.0004057	42449207	0.0004517	14462717	0.0004238	32084998
0.0004599	29055638	0.0004948	10602612	0.0004631	24901240
0.0004832	25184766	0.0005328	8327697.4	0.0005171	19539762
0.0005113	20868020	0.0005953	6159475.9	0.0005496	16082435
0.0005493	16607172	0.0006466	4793298.9	0.0005898	13092085
0.000601	12358178	0.0006898	4104160.5	0.0006424	9951182.7
0.0006536	9276543.7	0.0007423	3171395.7	0.0006904	7737293.1
0.0007129	7168139.6	0.0007961	2474395.9	0.0007417	5962911.1
0.0007576	5822922.7	0.0008545	1986711.1	0.0008007	4438817.3
0.0008006	4840469.7	0.000922	1567822.5	0.000864	3575025.9
0.0008766	3669045.9	0.0009921	1309210.3	0.0009303	2793926.9
0.0009471	2834428.3	0.0010782	994382.23	0.0010122	2196903.5
0.0010414	2137231.1	0.0011747	751994.71	0.001092	1705450.3
0.0011073	1770208.9	0.001271	586797.18	0.001177	1342624.9
0.001183	1400858.3	0.0013596	464978.03	0.0012552	1084135
0.0012671	1123139.2	0.0014473	398573.63	0.0013422	869759.78
0.0013415	912793.34	0.0015572	327401.39	0.0014355	693152.39
0.0014467	724486.51	0.0016925	242842.56	0.001542	551798.23
0.0015771	554463.23	0.0018368	186257.02	0.0016713	426029.65
0.0017028	437138.07	0.0019706	153114.94	0.0018012	340757.74
0.001801	366963.29	0.0021072	129349.23	0.0019265	278133.07
0.0019154	303076.13	0.0022617	104666.26	0.0020597	234302.98
0.0020493	240987.94	0.0024337	82724.188	0.0022069	186106.93
0.0022089	186312.24	0.0026179	65900.806	0.0023613	146608.97
0.0023754	148372.88	0.0028118	51068.209	0.0025196	121326.73
0.0025334	120868.2	0.0030232	43545.403	0.0027036	97495.345
0.0027102	96680.845	0.0032663	34336.388	0.0028904	80857.086
0.0028976	78100.747	0.0035103	28387.677	0.0030998	63855.733
0.0031082	62830.48	0.0037605	22940.728	0.0033237	51958.413
0.0033552	49560.816	0.0040518	18711.407	0.0035673	40104.833
0.0035615	40309.684	0.0043691	15279.029	0.003822	32875.6
0.003827	32480.285	0.004707	12286.682	0.0040925	26567.673
0.0040947	25673.764	0.0050593	9671.8557	0.0043911	20883.627
0.0043963	20575.575	0.0054636	7456.189	0.0047188	17500.891
0.0047062	16687.237	0.0058581	6232.834	0.0050492	14096.852
0.0050641	13216.115	0.0062774	5192.9271	0.0054079	11804.174
0.0054149	10624.668	0.0067449	4177.2596	0.0057894	9495.8018
0.0057979	8674.3759	0.0072611	3606.4018	0.0062034	7864.6924
0.0061981	7020.47	0.0078204	2924.7744	0.0066343	6448.8558
0.0066363	5692.3854	0.008412	2490.398	0.007109	5127.0455
0.0071366	4546.5587	0.0090454	2080.1784	0.0076004	4333.6798
0.0076171	3794.6187	0.0097186	1681.8247	0.0081431	3548.0196

0.008157	3039.6876	0.0104516	1421.7054	0.0087338	2823.1048
0.0087561	2462.7912	0.0112374	1202.9276	0.0093658	2351.7426
0.0093993	1989.4524	0.0120785	1007.1689	0.0100382	1981.5824
0.0100398	1641.3624	0.0129931	866.32291	0.0107491	1604.4653
0.0107311	1332.3342	0.0139574	733.52494	0.0114983	1338.6853
0.0114946	1083.8241	0.014988	628.19979	0.0123086	1110.8911
0.012326	883.29431	0.016115	527.06494	0.0131814	912.3949
0.0131841	719.52034	0.0173255	430.99691	0.0141103	760.91946
0.0140946	593.13207	0.0186217	377.44323	0.0151046	636.95629
0.0151056	486.50087	0.0200092	318.52141	0.0161785	517.29771
0.016166	398.52227	0.0214862	259.81843	0.017304	430.99693
0.0173025	329.80093	0.023083	229.96943	0.01852	356.08782
0.0184979	268.48355	0.0247969	188.57607	0.0198066	302.82668
0.0197894	222.39276	0.0266472	161.03595	0.0212032	253.57909
0.0211931	182.39962	0.0286394	133.95249	0.0226895	214.52742
0.0226641	150.89976	0.0307562	113.15008	0.0242628	178.01939
0.0242479	124.08234	0.0330547	92.726399	0.0259646	154.17999
0.0259282	102.8159	0.0355432	75.939046	0.0277783	124.16413
0.0277794	83.016389	0.0381985	61.867851	0.029735	103.87391
0.0297184	68.501355	0.0410328	51.664403	0.0318278	88.149149
0.0318049	56.180007	0.0440933	40.510879	0.0340637	71.383552
0.0340352	46.18726	0.0473974	33.510239	0.0364539	59.799043
0.0364439	37.89302	0.0509329	28.157032	0.0390099	49.235851
0.0389958	30.616318	0.0547379	22.261065	0.0417471	40.861252
0.0417334	24.889741	0.0588252	18.056938	0.0446808	33.546629
0.0446775	20.108846	0.0632171	13.642928	0.0478242	27.32742
0.0477997	16.309062	0.0679661	11.092155	0.0511771	21.542314
0.0511455	13.116444	0.0730672	8.559855	0.054784	17.764266
0.054754	10.649089	0.0785461	6.8134906	0.0586446	14.158456
0.0585883	8.432925	0.0844582	5.1756081	0.0627771	11.171132
0.0627084	6.8220184	0.0908266	3.974499	0.067202	8.9611749
0.0671399	5.327354	0.0976123	3.1282448	0.0719465	7.0573973
0.0718749	4.2932541	0.1048824	2.3859517	0.0770237	5.5702691
0.0769428	3.3807798	0.1126849	1.861769	0.0824742	4.4311922
0.0824072	2.7131659	0.1210525	1.4736036	0.0883206	3.4585585
0.0882418	2.1316054	0.1300269	1.1396778	0.0945497	2.6899257
0.0944659	1.6719874	0.1396584	0.8706458	0.1012028	2.1196087
0.1011125	1.3291806	0.1499936	0.6903482	0.1083022	1.6316815
0.1081922	1.0457552	0.161102	0.5660223	0.1158778	1.3042359
0.1157816	0.8340329	0.173051	0.4392591	0.1239604	1.0283389
0.1238559	0.6495656	0.1859106	0.3486997	0.1326024	0.8158633
0.1324891	0.528561	0.1997376	0.3043323	0.1418467	0.6524837
0.1416944	0.4172179	0.2146017	0.2491766	0.1517405	0.5245644
0.1515652	0.3351508	0.2305845	0.2166514	0.1623204	0.4212616
0.1621506	0.2733466	0.2477939	0.1780035	0.1736585	0.3305949
0.1734832	0.2148735	0.2662849	0.1535489	0.1858077	0.2807415
0.1856105	0.1846605	0.2862064	0.1285262	0.1988348	0.2373285
0.1986292	0.1466242	0.3076013	0.1060842	0.2127581	0.1864172
0.2125376	0.1267844	0.3305631	0.0944215	0.2276684	0.1614902
0.2274068	0.107865	0.3552425	0.081042	0.2436449	0.1397838
0.2433839	0.0978805	0.3818151	0.0720078	0.2607662	0.1218952
0.2604799	0.0808929	0.4102155	0.0621216	0.2790974	0.1040917
0.2787947	0.0641494	0.4405942	0.0483479	0.2987453	0.0897276
0.2984417	0.053843	0.4732818	0.0566479	0.3197617	0.076701
0.3194522	0.04571	0.4937724	0.0515566	0.3422401	0.0693031
0.3418405	0.0452542			0.3663029	0.0651358
0.3659131	0.0377563			0.3795436	0.0389375
0.3971301	0.0311041			0.3968886	0.0414696
0.4175365	0.0223486				
0.4244432	0.0292647				

3.3.5. Vitrain perpendicular samples (background corrected)

323 rvx ave		326 kvx ave		327 kvx ave		328 kvx ave	
Ave Q	**Ave I(Q)**	**Ave Q**	**Ave I(Q)**	**Ave Q**	**Ave I(Q)**	**Ave Q**	**Ave I(Q)**
0.0001724	389433084	0.0001584	201734313	0.0001483	304711348	0.0001978	123863940
0.0001903	294086808	0.0001714	149845795	0.0001682	228006952	0.0002122	98708555
0.0002098	212156794	0.0001887	105459038	0.000178	190997174	0.0002269	80652898
0.0002248	156874212	0.0002176	70286726	0.0001879	172495004	0.0002439	71397219
0.0002402	132611478	0.0002334	55573220	0.0001991	145884754	0.0002665	55417364
0.00026	109609470	0.0002493	46028617	0.0002152	120314842	0.000288	43965620
0.000288	81839434	0.0002685	40184705	0.0002335	95157664	0.0003152	34593335
0.0003097	67434845	0.0002933	32476037	0.000254	73703611	0.0003534	25706543
0.0003364	49820313	0.0003163	26118345	0.0002849	56561384	0.0003799	20459839
0.0003621	37788644	0.0003436	20184495	0.0003132	41262775	0.0004128	16125075
0.0003932	28965919	0.0003788	14697948	0.0003308	35032750	0.0004499	12527046
0.0004385	20182496	0.0004069	11903441	0.000357	27893420	0.0004859	9679862.2
0.000469	16293548	0.0004409	9954796.9	0.0003847	22723463	0.0005361	7401692.8
0.0005126	11862884	0.0004737	8401308	0.0004231	17448793	0.0005751	6350169.6
0.0005728	8188501.1	0.0005269	6269272.1	0.0004639	12906330	0.0006265	5006664.5
0.000608	6503576.6	0.0005722	5081398	0.0004999	10150229	0.0006946	3520362.9
0.0006594	4443273.5	0.0006132	4025118.2	0.0005577	7413824.1	0.0007334	2955926.1
0.0007215	3112453.4	0.0006838	2850411.3	0.0006138	5242194.8	0.0007938	2378329.7
0.0007624	2515811.7	0.0007287	2423479.1	0.0006477	4250624.5	0.0008575	1690164.1
0.0008318	1720356	0.0007756	1923274.6	0.000702	3369898	0.0009207	1408223.4
0.0008849	1339266.3	0.0008473	1424143.3	0.0007561	2487397.5	0.0009983	1106396
0.0009612	964100.74	0.0009125	1108640.1	0.0007995	2013737.8	0.0010633	937236.6
0.001032	769401.01	0.000989	880719.94	0.0008609	1561777.6	0.0011549	719434.58
0.0011229	582822.95	0.0010637	754758.17	0.000925	1219775.3	0.0012477	545440.97
0.0012159	424268.39	0.0011584	555595.89	0.0010006	921314.27	0.0013618	416910.6
0.0012969	331448.75	0.0012494	446046.11	0.0011028	673057.2	0.0014646	298438.27
0.0014005	245261.87	0.0013426	367642.92	0.0011958	505857.01	0.0015529	251293.37
0.0015041	193385.56	0.0014454	300323.63	0.0012769	416430.8	0.0016695	200456.55
0.0016253	155203.07	0.0015504	232421.02	0.0013669	318482.74	0.0018073	160298.61
0.0017509	108318.76	0.0016747	194825.63	0.0014619	250381.13	0.0019626	122202.36
0.0018851	82660.86	0.0018108	158137.94	0.0015738	195802.23	0.0021096	91945.84
0.0020276	64131.518	0.001955	124784.96	0.00171	147310.73	0.0022564	74505.925
0.0021804	49877.519	0.0020985	99033.316	0.001848	112880.86	0.0024186	56870.849
0.0023342	38851.264	0.0022475	81400.857	0.0019805	89309.581	0.0026114	44597.538
0.0025104	29587.309	0.0024101	64345.835	0.0021213	70656.479	0.0027968	36499.306
0.0026976	22513.893	0.0025921	53697.537	0.0022801	54863.689	0.0030112	29893.349
0.0029025	17544.758	0.0027824	45343.032	0.0024567	43052.295	0.0032383	24055.394
0.0031278	12884.688	0.002993	36504.704	0.0026394	33739.341	0.0034891	17823.397
0.0033526	10163.285	0.0032206	29819.204	0.0028318	26846.294	0.0037583	13709.68
0.0036119	7795.6121	0.0034627	22909.033	0.0030481	20718.583	0.004034	10985.74
0.003889	6144.3629	0.0037223	19964.933	0.0032927	16607.909	0.0043417	8907.7911
0.0041889	4775.5787	0.0040114	16502.446	0.0035416	13310.398	0.0046723	6956.3623
0.0044927	3756.0166	0.0043155	13520.73	0.0037996	10666.201	0.0050371	5485.7502
0.0048583	2898.5662	0.0046464	11121.786	0.0040938	8442.902	0.0054106	4525.1896
0.0052211	2227.6494	0.0050133	9135.0985	0.0044074	6842.5493	0.0058354	3698.3509
0.0056027	1784.1756	0.0053791	7715.6728	0.0047388	5597.9658	0.0062756	2834.5231
0.0060331	1500.5737	0.0057925	6129.8977	0.0050989	4506.2714	0.006726	2274.5535
0.0064775	1226.1874	0.0062139	5008.1277	0.0055004	3731.3034	0.0072264	1851.7258
0.0069632	940.54485	0.0066812	4401.4738	0.0059081	3084.8762	0.0077743	1512.9766
0.0074834	799.44817	0.0071877	3609.8443	0.0063281	2573.6044	0.0083703	1231.5544
0.0080542	664.66403	0.0077314	3056.6502	0.0067947	2133.2884	0.0090016	962.61027
0.00866	529.17899	0.00832	2673.97	0.0073205	1766.0755	0.0096789	818.55482
0.0093141	454.26009	0.0089434	2172.371	0.0078817	1473.0625	0.0103999	696.19558
0.0100094	384.29581	0.0096143	1824.1568	0.0084836	1222.7132	0.0111804	593.94963
0.0107636	347.72945	0.0103325	1596.3552	0.009121	1020.0049	0.012014	489.58876
0.0115722	303.0375	0.0111103	1386.4035	0.0097994	855.97008	0.012925	405.15762

0.0124408	257.35373	0.0119434	1275.9065	0.0105479	723.60379	0.0138936	349.69219
0.0133689	223.33833	0.0128396	1108.2354	0.0113341	613.92538	0.0149351	308.59326
0.0143671	197.873	0.0138005	924.05173	0.0121866	528.13028	0.0160397	266.71632
0.0154463	184.6994	0.0148311	814.63973	0.0131057	452.20738	0.0172326	234.96778
0.0165896	168.81638	0.0159351	698.26476	0.014067	388.61977	0.018528	210.2261
0.0178409	148.68053	0.0171258	604.77402	0.0151056	338.07315	0.0199027	178.44163
0.0191684	136.2287	0.018411	551.5683	0.0162421	294.66965	0.0214023	163.82207
0.0205961	128.59366	0.0197757	486.35749	0.0174613	255.96495	0.0229845	142.25883
0.0221283	122.75575	0.0212407	424.91941	0.018769	224.1645	0.0246828	128.21511
0.0237696	112.95928	0.0228263	378.1605	0.0201625	197.02382	0.0265241	118.91014
0.0255441	107.49125	0.0245249	326.25646	0.0216462	175.21225	0.028509	105.39457
0.0274354	102.47813	0.0263479	293.99368	0.0232504	157.38477	0.0306344	95.471379
0.0294749	97.108675	0.0283118	261.16371	0.0249786	139.97467	0.0329062	87.073147
0.0316775	92.820879	0.0304235	231.69285	0.026849	125.80805	0.0353555	81.789916
0.0340498	88.512894	0.0326872	205.82558	0.0288494	112.757	0.038009	75.160687
0.0365787	79.21792	0.0351301	185.0265	0.0309889	100.86303	0.0408657	65.977744
0.0393133	76.98241	0.0377548	157.12827	0.033315	91.987783	0.0438999	60.491077
0.0422632	72.859739	0.0405823	135.01335	0.0358171	82.937784	0.0471714	54.569572
0.0454049	69.679308	0.0436042	119.78465	0.0384815	75.054426	0.050706	49.178997
0.048797	63.403863	0.0468574	100.45101	0.0413366	67.35999	0.0544992	43.75031
0.0524447	57.425117	0.050367	85.673378	0.044421	60.286056	0.0585727	38.24518
0.0563526	50.299277	0.054121	72.044185	0.0477426	54.007232	0.0629518	32.696552
0.0605689	43.883813	0.0581633	59.309004	0.0513065	47.709831	0.0676633	27.926718
0.0650995	37.796857	0.0625153	47.438444	0.055141	41.745837	0.0727407	22.804644
0.0699766	32.68107	0.0671906	38.575597	0.0592573	35.983609	0.0781903	18.861813
0.0752211	26.717978	0.0722281	30.705405	0.0636815	30.833883	0.0840454	14.902699
0.0809012	21.515763	0.0776588	24.913649	0.0684661	25.81434	0.0903397	11.779547
0.0869588	17.486633	0.0834968	19.378041	0.0736066	21.284517	0.0971241	9.2270669
0.0934826	13.358938	0.0897589	15.014599	0.0791234	17.367818	0.1043842	6.9878062
0.1004792	10.181661	0.0964928	12.034808	0.0850873	13.768903	0.1121452	5.4634977
0.107966	7.5234237	0.1036882	9.1541259	0.0914992	10.785262	0.1204802	4.1296633
0.1159874	5.7966626	0.1114107	7.1712118	0.0983351	8.3431365	0.1294111	3.1094537
0.1246044	4.225848	0.1196895	5.4743889	0.1056524	6.3625875	0.1390185	2.3104063
0.1338242	3.1670612	0.1285612	4.1263745	0.1135226	4.8211798	0.1493362	1.7225148
0.1437434	2.3758475	0.1380829	3.2363306	0.1219415	3.6698991	0.16039	1.3358469
0.1543817	1.7957128	0.1483128	2.4956275	0.1309745	2.7658081	0.1722812	1.0258916
0.1658205	1.3490033	0.1592933	1.9397481	0.1406766	2.0899524	0.1850711	0.7817985
0.1781277	1.008052	0.1711064	1.5316184	0.1510836	1.5945369	0.1988278	0.5952688
0.1913683	0.7336665	0.1838173	1.1935218	0.1622718	1.2130166	0.2136458	0.4646643
0.2055827	0.5776578	0.1974755	0.9576478	0.1743255	0.9212366	0.2295611	0.3695224
0.2209345	0.437952	0.2121861	0.763794	0.1872886	0.6928201	0.2466636	0.2839848
0.2373553	0.3558324	0.2279916	0.6162358	0.201209	0.5332373	0.2650788	0.2325454
0.2551056	0.2852733	0.2449782	0.5049376	0.2161647	0.4135101	0.2848588	0.1922588
0.2741426	0.201933	0.2632963	0.423313	0.2322789	0.3225728	0.3061683	0.1648952
0.2946295	0.1549757	0.2829457	0.3477047	0.2496126	0.2560032	0.328992	0.1250107
0.31661	0.1036696	0.3040943	0.2878852	0.2682381	0.2169495	0.3535179	0.1231829
0.3403093	0.0993402	0.3268139	0.245862	0.2882891	0.1676176	0.3798534	0.106545
0.3657033	0.0874054	0.3512322	0.1970295	0.3098414	0.1456656	0.3776732	0.0994365
0.392887	0.0643644	0.3773986	0.1973589	0.3329605	0.1254328	0.4058033	0.088713
0.422123	0.0516046	0.4055137	0.1681195	0.3578326	0.1008235	0.4358485	0.0808235
0.4461189	0.0561405	0.4356537	0.1670731	0.3845858	0.0886393	0.4681699	0.0774984
		0.4523315	0.1683224	0.4131676	0.0819185	0.493783	0.0608942
		0.471034	0.1418857	0.4437698	0.0741181		
		0.4937989	0.1496676	0.4766999	0.065911		
				0.4937676	0.0430473		

3.3.6. Vitrain parallel samples (background corrected)

323 rvp ave		327 kvp ave		328 kvp	
Ave Q	**Ave I(Q)**	**Ave Q**	**Ave I(Q)**	**Ave Q**	**Ave I(Q)**
0.0001083	745979328	0.0001176	1.781E+09	0.0001131	435974726
0.0001159	595009280	0.0001278	1.438E+09	0.0001306	249761504
0.0001251	446718440	0.0001361	1.195E+09	0.0001441	166811098
0.0001345	329343552	0.0001439	923213133	0.0001531	128288323
0.000146	233266304	0.0001534	683672934	0.0001641	99813344
0.0001651	181908980	0.0001631	611632422	0.0001782	71955240
0.0001875	126940899	0.0001754	503732378	0.0001941	55187590
0.0002091	84009542	0.0001911	413964803	0.0002082	42590026
0.0002343	57750690	0.0002129	303970320	0.0002224	32491954
0.0002488	45035627	0.0002499	173348227	0.0002514	20944102
0.0002656	38783593	0.0002718	131396634	0.0002838	13992718
0.000284	29811267	0.0002859	108818984	0.0003048	11155155
0.0003133	21337582	0.0003035	97488221	0.000332	8148723
0.0003405	16553025	0.0003278	77476584	0.0003572	6191076.4
0.0003718	12193771	0.0003553	58527495	0.0004058	4129040.4
0.0004011	10343564	0.0003946	39805094	0.0004481	2927934
0.0004351	8077454.8	0.0004229	33777708	0.0004717	2441873
0.0004714	6488966	0.0004504	26815610	0.0004975	2085060
0.0005189	4704198.9	0.0004851	20298560	0.0005412	1617145.6
0.0005651	3620893.7	0.0005252	15385603	0.0006026	1139387.6
0.0006162	2672735.2	0.0005768	11166148	0.0006663	767135.68
0.0006752	2001026.9	0.0006322	8488310.4	0.0007199	576453.76
0.000731	1589297.4	0.0007065	5375726.3	0.0007588	494777.93
0.0008025	1187648.2	0.0007449	4537227.3	0.0008178	393334.83
0.0008729	912663.31	0.0007937	3811288.9	0.0008923	289383.43
0.0009431	689382.17	0.0008625	2719205.5	0.0009675	226446.8
0.0010204	556041.93	0.0009178	2164935.5	0.0010498	175598.78
0.0011068	418913.5	0.000992	1644518.1	0.0011146	147350.84
0.001205	339134.85	0.001059	1262559	0.0012007	112847.16
0.0013074	260943.27	0.0011581	911017.39	0.0012714	93204.18
0.0013918	206821.22	0.0012576	675282.18	0.0013642	72721.913
0.0014972	175742.79	0.0013482	558655.44	0.001475	56627.802
0.0016193	134082.81	0.0014505	425260.85	0.0015966	44034.582
0.0017518	98973.368	0.001552	334604.67	0.0017079	36110.164
0.0018988	80444.632	0.0016533	253867.34	0.0018219	29722.522
0.0020329	68505.417	0.0017952	198664.35	0.0019481	23686.828
0.0021763	57437.77	0.0019432	148421.2	0.0020855	19208.758
0.0023323	46119.815	0.0020853	119029.68	0.0022455	15164.452
0.0025072	35392.397	0.0022366	101179.91	0.0024038	12640.368
0.0026907	29297.409	0.0024282	73045.066	0.002566	10622.904
0.0028902	24372.719	0.0025934	60655.93	0.0027417	8667.6223
0.0031176	20228.087	0.0027796	47593.068	0.0029383	7075.103
0.0033468	17072.984	0.0030046	34832.736	0.0031648	5771.854
0.003599	13726.083	0.0032114	28065.943	0.0033776	4916.9122
0.0038739	11149.957	0.0034584	21098.973	0.003625	3989.941
0.0041642	8759.2393	0.0037283	15872.238	0.0038706	3435.786
0.0044861	7398.9149	0.0039975	12415.913	0.0041608	2900.4168
0.0048323	6253.8641	0.0043102	10156.974	0.0044518	2515.2428
0.0052045	5173.7107	0.0046347	8398.2781	0.0047902	2128.858
0.0055959	4225.8969	0.0050001	6472.7467	0.0051311	1825.5802
0.0060096	3689.5212	0.0053726	5137.4254	0.0054918	1595.5108
0.0064589	3018.038	0.0057712	4045.3743	0.0058861	1379.3512
0.0069456	2617.182	0.0061998	3297.8476	0.0062864	1215.2229
0.0074753	2258.5647	0.0066619	2796.9952	0.0067454	1075.2025
0.0080502	1846.1713	0.007184	2137.201	0.0072282	965.89904
0.0086524	1670.358	0.0077437	1767.007	0.0077355	865.01531

0.0092973	1576.9	0.0083204	1389.407	0.0082841	791.77955
0.0099946	1329.4442	0.0089337	1194.947	0.0088891	714.55474
0.0107409	1130.3694	0.009598	964.90321	0.0095198	668.34745
0.0115466	974.0697	0.0103056	801.99065	0.010184	613.62634
0.0124149	862.24437	0.011096	652.22056	0.0109074	566.62539
0.0133442	779.85146	0.0119319	550.80309	0.0116792	524.4642
0.0143415	651.52922	0.0128223	451.85336	0.0124949	488.81923
0.0154092	581.62906	0.0137702	368.19841	0.0133678	453.55123
0.0165612	501.40388	0.0148027	327.64201	0.0143113	420.47424
0.017801	427.8489	0.0158992	287.66263	0.0153237	390.97083
0.0191195	362.45997	0.0171084	236.36369	0.0164028	364.36503
0.0205418	333.32873	0.0183553	205.90147	0.0175455	334.05905
0.0220679	290.07595	0.0197306	178.22273	0.018786	308.29452
0.0237101	245.23468	0.0211905	159.16457	0.0200894	281.9244
0.0254787	203.58061	0.0227675	133.77299	0.021493	257.12125
0.0273737	186.71754	0.0244588	116.83771	0.023009	232.94464
0.0294176	160.67848	0.0262859	105.21774	0.0246013	210.4822
0.0315934	135.34926	0.0282599	93.375432	0.0263315	187.68108
0.033957	114.43108	0.030331	78.162085	0.0281813	165.8691
0.0364976	95.338228	0.0325853	69.471262	0.0301651	146.2842
0.0392266	81.225018	0.0350245	62.758906	0.0322717	128.19643
0.0421578	65.729635	0.0376599	53.770438	0.0345524	111.03889
0.0452978	54.918255	0.0404702	47.21223	0.0369803	95.150858
0.0486899	45.919819	0.0434762	41.346905	0.0395802	81.13072
0.0523166	37.630155	0.0467282	35.731018	0.0423621	68.34324
0.0562168	31.220132	0.050236	29.663426	0.0453346	57.048409
0.0604123	24.746018	0.0539704	25.545014	0.0485151	47.070878
0.0649291	19.775532	0.0579974	21.3055	0.051927	38.382878
0.0697975	15.55589	0.0623253	18.090561	0.0555693	31.184602
0.0750432	12.140603	0.0669843	14.68768	0.0594752	24.902779
0.080688	9.7224723	0.0720152	11.973643	0.063675	19.774892
0.0867493	7.5280181	0.0774196	9.6793749	0.0681484	15.59625
0.0932621	5.8430222	0.0832512	7.5624352	0.0729657	12.247204
0.1002273	4.5479547	0.0895326	5.8618992	0.0781299	9.4990203
0.1076979	3.5595055	0.0962152	4.6609651	0.0836578	7.4783431
0.1156966	2.7340141	0.103396	3.6491206	0.0895691	5.7528254
0.1242808	2.0897858	0.1110741	2.8434858	0.0958885	4.5151704
0.1334881	1.6232301	0.1193418	2.1648601	0.102637	3.5083341
0.1433645	1.2391291	0.1281838	1.6136039	0.1098244	2.7691742
0.1539836	0.9653891	0.1376708	1.2127337	0.1175063	2.1595927
0.1653857	0.7555706	0.1478619	0.9293742	0.1257079	1.6986645
0.1776642	0.5939759	0.1587935	0.7079583	0.1344515	1.3484279
0.1908767	0.4771439	0.1705574	0.5490137	0.1438214	1.0527119
0.2050678	0.3806837	0.1832489	0.4177071	0.1538401	0.8400154
0.22035	0.3205572	0.1968809	0.3287557	0.164592	0.6639672
0.2367438	0.2721219	0.2115205	0.2604728	0.1761007	0.5362764
0.2544295	0.2292324	0.2272594	0.2105396	0.1884228	0.4424788
0.2734216	0.2023538	0.244231	0.1810629	0.2016108	0.3574976
0.2938738	0.1545043	0.2624377	0.1496783	0.2157491	0.2978342
0.3158351	0.1364979	0.2820696	0.1097895	0.2308656	0.2491642
0.3394435	0.1154294	0.3031853	0.1061633	0.2470546	0.2123537
0.3647777	0.1024061	0.3258281	0.0806698	0.2644316	0.1863557
0.3919934	0.0948716	0.3501302	0.0677346	0.2830431	0.1613305
0.421125	0.0835193	0.3763434	0.0619963	0.3029544	0.140663
0.4523384	0.0817121	0.40437	0.0508712	0.3242478	0.1237745
0.4710461	0.0752124	0.4343047	0.0507966	0.3470625	0.1094632
0.4938173	0.0752485	0.4665176	0.0416785	0.3714124	0.0987013
		0.4938383	0.0392177	0.3906993	0.0903251
				0.4059996	0.0923885
				0.4244197	0.0869182

3.4. Scattering data SANS/USANS

3.4.1. Renown seam matrix samples (background corrected)

318 rmp NU		319 rmx N + 319 rmp U		610 rmp NU		611 rmx N + 611 rmp U		612 rmx N + 612 rmp U	
Q	I(Q)	Q	I(Q)	Q	I(Q)	Q	I(Q)	Q	I(Q)
1.892E-05	6.606E+10	2.508E-05	3.205E+10	1.4E-05	2.647E+11	1.31E-05	3.343E+12	2.141E-05	3.52E+10
2.415E-05	3.477E+10	2.944E-05	2.087E+10	1.922E-05	5.303E+10	1.745E-05	4.199E+11	2.664E-05	1.87E+10
2.938E-05	1.952E+10	3.554E-05	1.404E+10	2.445E-05	2.101E+10	2.268E-05	1.265E+11	3.187E-05	1.129E+10
3.461E-05	1.367E+10	3.99E-05	9.774E+09	2.881E-05	1.168E+10	2.791E-05	4.426E+10	3.71E-05	7.621E+09
3.984E-05	9.239E+09	4.6E-05	6.853E+09	3.404E-05	7.47E+09	3.401E-05	2.787E+10	4.32E-05	5.566E+09
4.507E-05	6.688E+09	5.122E-05	4.96E+09	3.927E-05	5.299E+09	3.837E-05	1.887E+10	4.755E-05	4.216E+09
5.029E-05	5.133E+09	5.558E-05	3.496E+09	4.449E-05	3.844E+09	4.36E-05	1.471E+10	5.278E-05	3.258E+09
5.552E-05	3.681E+09	6.081E-05	2.748E+09	4.972E-05	2.786E+09	4.97E-05	9.548E+09	5.801E-05	2.675E+09
5.988E-05	2.851E+09	6.604E-05	2.255E+09	5.495E-05	2.195E+09	5.405E-05	7.695E+09	6.324E-05	2.119E+09
6.511E-05	2.15E+09	7.127E-05	1.578E+09	6.018E-05	1.689E+09	5.928E-05	6.576E+09	6.847E-05	1.637E+09
7.034E-05	1.546E+09	7.649E-05	1.38E+09	6.541E-05	1.376E+09	6.451E-05	5.427E+09	7.282E-05	1.358E+09
7.644E-05	1.41E+09	8.085E-05	1.132E+09	7.064E-05	1.1E+09	6.887E-05	3.477E+09	7.892E-05	1.193E+09
8.079E-05	1.29E+09	0.0001018	597482088	7.586E-05	953245949	7.409E-05	2.573E+09	9.897E-05	642893018
0.0001017	559001943	0.0003074	30838941	8.022E-05	752812882	7.932E-05	2.844E+09	0.0003046	29892457
0.0003074	12989348	0.0005131	7339418.9	0.0001011	410357522	0.0001011	1.315E+09	0.0005094	6200214.6
0.0005121	4461191.3	0.0020511	107634.59	0.0003068	18780509	0.0003059	70930950	0.0020483	116344.72
0.002051	130974.54	0.00377	21157.789	0.0005124	3918237.2	0.0005107	16308809	0.00377	25855.231
0.00396	14173.877	0.00396	20237.187	0.0020504	77175.747	0.00377	12178.431	0.00396	21264.35
0.00415	10011.116	0.00415	17230.892	0.00436	9690.7589	0.00396	10363.904	0.00415	17014.152
0.00436	11370.562	0.00436	12287.793	0.00458	5266.3817	0.00415	10343.131	0.00436	17370.464
0.00458	8751.0425	0.00458	10181.792	0.00481	6349.4445	0.00436	9539.0296	0.00458	14675.14
0.00481	6355.8851	0.00481	10080.054	0.00505	4604.706	0.00458	7077.4735	0.00481	14561.581
0.00505	5605.5237	0.00505	8688.4805	0.0053	4535.3037	0.00481	6886.2011	0.00505	9488.1563
0.0053	5383.4244	0.0053	6331.2273	0.00557	2955.8917	0.00505	6384.1274	0.0053	7865.249
0.00557	3343.3453	0.00557	4919.5068	0.00584	2921.2232	0.0053	5062.8619	0.00557	6883.0915
0.00584	3035.5263	0.00584	4191.3314	0.00614	2856.8559	0.00557	4959.187	0.00584	4586.6719
0.00614	2795.4332	0.00614	3629.7002	0.00644	2254.5115	0.00584	3674.7593	0.00614	4515.3004
0.00644	2343.0795	0.00644	3185.2608	0.00676	1807.9349	0.00614	2805.6451	0.00644	3826.5186
0.00676	2227.5291	0.00676	2443.44	0.0071	1671.281	0.00644	2488.0919	0.00676	3293.7395
0.0071	1690.4228	0.0071	2121.0429	0.00746	1257.6983	0.00676	2083.2153	0.0071	2739.0974
0.00746	1543.9226	0.00746	1902.9825	0.00783	1273.0132	0.0071	1814.6868	0.00746	2232.6522
0.00783	1257.0565	0.00783	1426.9998	0.00822	1040.8519	0.00746	1363.6981	0.00783	1908.4923
0.00822	1178.9274	0.00822	1326.5782	0.00863	827.17098	0.00783	1292.2089	0.00822	1585.357
0.00863	1006.194	0.00863	1046.5694	0.00907	763.83694	0.00822	1190.4591	0.00863	1355.6609
0.00907	809.15819	0.00907	914.31817	0.00952	647.79957	0.00863	892.38046	0.00907	1198.7907
0.00952	662.93733	0.00952	790.97774	0.00999	578.44784	0.00907	858.81472	0.00952	938.06852
0.00999	631.82914	0.00999	631.52456	0.01049	516.55376	0.00952	715.26184	0.00999	829.26097
0.01049	553.18355	0.01049	558.94757	0.01102	424.9918	0.00999	643.71334	0.01049	674.68402
0.01102	483.45399	0.01102	454.81654	0.01157	384.76177	0.01049	509.4556	0.01102	596.5344
0.01157	425.78551	0.01157	409.33158	0.01215	355.19423	0.01102	442.62829	0.01157	487.8724
0.01215	390.58858	0.01215	362.60393	0.01276	280.46062	0.01157	385.76092	0.01215	444.40139
0.01276	311.21857	0.01276	313.18126	0.01339	265.64362	0.01215	329.95069	0.01276	356.33467
0.01339	292.23761	0.01339	268.70363	0.01406	229.44688	0.01276	302.8159	0.01339	323.75851
0.01406	263.91599	0.01406	230.90226	0.01477	198.78941	0.01339	276.11385	0.01406	278.29024
0.01477	218.06593	0.01477	205.6662	0.0155	183.53335	0.01406	239.26246	0.01477	248.37534
0.0155	195.96968	0.0155	176.66881	0.01628	166.84053	0.01477	204.80489	0.0155	214.83246
0.01628	174.59252	0.01628	154.7493	0.01709	133.35414	0.0155	167.42034	0.01628	182.48399
0.01709	155.45386	0.01709	126.10493	0.01795	122.65823	0.01628	152.64074	0.01709	165.82634
0.01795	141.62964	0.01795	117.94918	0.01885	107.59997	0.01709	133.1641	0.01795	147.82464
0.01885	126.5433	0.01885	107.6517	0.01979	99.068341	0.01795	116.11204	0.01885	122.61569
0.01979	112.59013	0.01979	91.953744	0.02078	94.070212	0.01885	107.55873	0.01979	103.14743
0.02078	103.33366	0.02078	80.486103	0.02182	85.153365	0.01979	95.858443	0.02078	96.159753

0.02182	90.906882	0.02182	68.995103	0.02291	74.032383	0.02078	80.636982	0.02182	78.298243
0.02291	79.238909	0.02291	63.128787	0.02405	61.503133	0.02182	77.515936	0.02291	72.557809
0.02405	70.083614	0.02405	59.162264	0.02526	58.579254	0.02291	65.136241	0.02405	64.934445
0.02526	71.304838	0.02526	51.644214	0.02652	50.290584	0.02405	63.106808	0.02526	57.456658
0.02652	61.992706	0.02652	46.60596	0.02784	47.003376	0.02526	53.499538	0.02652	51.668994
0.02784	55.561329	0.02784	42.688306	0.02924	43.114	0.02652	51.567547	0.02784	45.047026
0.02924	49.40691	0.02924	38.117521	0.0307	37.361627	0.02784	44.003785	0.02924	38.293244
0.0307	46.036757	0.0307	35.926404	0.03223	34.393291	0.02924	38.75298	0.0307	39.016
0.03223	42.256131	0.03223	32.850298	0.03385	33.470694	0.0307	37.082357	0.03223	31.222577
0.03385	38.583192	0.03385	31.200082	0.03554	30.97738	0.03223	32.925068	0.03385	28.755762
0.03554	36.504114	0.03554	26.705388	0.03731	26.28785	0.03385	30.919363	0.03554	27.49591
0.03731	32.365526	0.03731	25.998068	0.03918	24.010032	0.03554	27.68725	0.03731	24.309267
0.03918	31.663986	0.03918	21.652301	0.04114	20.703163	0.03731	26.742177	0.03918	22.573466
0.04114	27.98643	0.04114	20.393546	0.0432	18.89425	0.03918	22.576153	0.04114	19.771917
0.0432	25.400558	0.0432	18.465555	0.04536	17.671398	0.04114	19.486001	0.0432	18.786166
0.04536	21.969724	0.04536	19.08744	0.04762	15.97017	0.0432	19.368003	0.04536	16.954825
0.04762	20.207913	0.04762	18.011071	0.05	15.173812	0.04536	18.056671	0.04762	16.314741
0.05	17.706069	0.05	16.200791	0.05251	14.131973	0.04762	15.767826	0.05	13.981767
0.05251	16.358801	0.05251	15.478485	0.05513	11.937845	0.05	14.400447	0.05251	12.606684
0.05513	14.794308	0.05513	13.701193	0.05789	11.304008	0.05251	13.516845	0.05513	10.879349
0.05789	14.575395	0.05789	12.710259	0.06078	9.5291507	0.05513	12.205316	0.05789	10.507304
0.06078	12.391676	0.06078	11.953898	0.06382	8.4303507	0.05789	11.702535	0.06078	9.9657394
0.06382	11.197833	0.06382	10.741871	0.06701	8.3803503	0.06078	10.520987	0.06382	9.6284355
0.06701	10.925584	0.06701	9.3374017	0.07036	7.5851412	0.06382	9.746942	0.06701	7.951871
0.07036	10.117057	0.07036	9.4142167	0.07388	7.0064864	0.06701	8.7476628	0.07036	7.7218197
0.07388	8.9464305	0.07388	8.756563	0.07757	6.7145061	0.07036	8.6819083	0.07388	7.6474172
0.07757	8.3638881	0.07757	8.2537323	0.08145	6.0375715	0.07388	8.408832	0.07757	7.3981069
0.08145	7.5885474	0.08145	7.715972	0.08553	5.5451574	0.07757	7.701003	0.08145	6.4159576
0.08553	6.9946135	0.08553	6.9118439	0.0898	4.9725722	0.08145	6.9197597	0.08553	6.0320182
0.0898	6.7202059	0.0898	5.8985313	0.09429	4.7709104	0.08553	6.4439351	0.0898	5.4958909
0.09429	6.0150982	0.09429	5.7910152	0.09901	4.6617878	0.0898	6.0540132	0.09429	5.140288
0.09901	5.4525112	0.09901	5.6927982	0.10396	3.8364591	0.09429	5.5555174	0.09901	4.7704839
0.10396	4.8689063	0.10396	5.4734987	0.10915	3.6285435	0.09901	5.5798965	0.10396	4.6176859
0.10915	4.9093162	0.10915	4.9546597	0.11461	3.7552593	0.10396	5.2601618	0.10915	4.0655914
0.11461	4.2818092	0.11461	4.6000683	0.12034	3.5632942	0.10915	5.0523119	0.11461	3.8338491
0.12034	3.9765214	0.12034	4.2824557	0.12636	3.0618782	0.11461	4.5610777	0.12034	3.4823149
0.12636	3.7440241	0.12636	4.3279768	0.13268	2.8700938	0.12034	4.4583548	0.12636	3.883278
0.13268	3.405514	0.13268	4.0719921	0.13931	2.971058	0.12636	4.748015	0.13268	3.4213297
0.13931	3.4843443	0.13931	3.712922	0.14628	2.6951443	0.13268	3.9303712	0.13931	3.2306185
0.14628	3.2792298	0.14628	3.5645603	0.15359	2.6324955	0.13931	3.972169	0.14628	3.1485256
0.15359	2.7845709	0.15359	3.482746	0.16127	2.5410673	0.14628	3.632103	0.15359	2.9041284
0.16127	2.6671123	0.16127	3.4628919	0.16933	2.0812966	0.15359	3.6570704	0.16127	2.6260031
0.16933	2.4643254	0.16933	3.0854528	0.1778	2.1670426	0.16127	3.5565248	0.16933	2.4476467
0.1778	2.3365575	0.1778	2.8809708	0.18669	2.3070421	0.16933	3.2738227	0.1778	2.5028254
0.18669	2.3652743	0.18669	2.4549911	0.19603	2.0147683	0.1778	3.1653926	0.18669	2.0712629
0.19603	2.129669	0.19603	2.606444	0.20583	1.5755219	0.18669	3.2513008	0.19603	2.1991451
0.20583	1.7419158	0.20583	2.5283694	0.21612	1.5663187	0.19603	2.7990339	0.20583	1.9664306
0.21612	1.5677137	0.21612	2.4499244	0.22692	1.5034965	0.20583	2.8783654	0.21612	1.8046266
0.22692	1.3480034	0.22692	2.3186626	0.23827	1.4658521	0.21612	2.7596684	0.22692	1.6580473
0.23827	1.348242	0.23827	2.173475	0.25018	1.3610904	0.22692	2.6317915	0.23827	1.5999814
0.25018	1.0380279	0.25018	2.0339035	0.26269	1.4210923	0.23827	2.3521338	0.25018	1.5733895
0.26269	1.1222487	0.26269	1.8732743	0.27583	1.1993489	0.25018	2.2005134	0.26269	1.2846717
0.27583	0.8953159	0.27583	1.3955888	0.28962	1.4208647	0.26269	2.3272036	0.27583	1.0885812
0.28962	0.8702996	0.28962	1.2669177	0.3041	1.13258	0.27583	2.0122176	0.28962	1.1660523
0.3041	0.8865137	0.3041	1.2408166	0.3193	0.7986531	0.28962	1.9944156	0.3041	0.9184924
0.3193	0.8694587	0.3193	0.9649583	0.33527	0.8462522	0.3041	1.6538012	0.3193	0.8485785
0.33527	0.5370512	0.33527	1.2683762	0.35203	0.678188	0.3193	1.5057244	0.33527	0.9228834
0.35203	0.5733894	0.35203	0.9742765	0.36964	0.8853939	0.33527	1.333112	0.35203	0.7782317
0.36964	0.5644564	0.36964	1.3133162	0.38812	0.8674651	0.35203	1.4437079	0.36964	0.7967428
0.38812	0.4064034	0.38812	0.810945			0.36964	1.433599	0.38812	0.6068017
						0.38812	1.0472477		

3.4.2. Kupakupa seam matrix samples (background corrected)

320 kmp NU		321 kmx N + 321 kmp U		322 kmp NU	
Q	**I(Q)**	**Q**	**I(Q)**	**Q**	**I(Q)**
1.648E-05	1.235E+11	1.32E-05	1.097E+11	1.314E-05	1.894E+11
2.694E-05	1.89E+10	1.843E-05	3.883E+10	1.662E-05	7.694E+10
3.827E-05	8.878E+09	2.453E-05	2.318E+10	2.272E-05	2.417E+10
4.785E-05	4.961E+09	2.888E-05	1.385E+10	2.708E-05	1.271E+10
5.831E-05	2.997E+09	3.411E-05	8.772E+09	3.231E-05	8.262E+09
6.789E-05	2.117E+09	3.934E-05	6.403E+09	3.754E-05	5.732E+09
7.835E-05	1.455E+09	4.457E-05	4.674E+09	4.277E-05	4.3E+09
9.926E-05	693723639	4.98E-05	3.242E+09	4.799E-05	3.234E+09
0.0003049	29621492	5.415E-05	2.717E+09	5.322E-05	2.642E+09
0.0005106	6632411.2	6.025E-05	2.168E+09	5.758E-05	2.103E+09
0.0020485	88910.383	6.461E-05	1.66E+09	6.281E-05	1.697E+09
0.00396	18667.929	6.984E-05	1.393E+09	6.804E-05	1.45E+09
0.00415	13981.168	7.507E-05	1.051E+09	7.326E-05	1.15E+09
0.00436	12203.192	8.117E-05	959623849	7.849E-05	920305148
0.00458	11148.114	0.0001012	517238386	8.372E-05	814142936
0.00481	7757.7677	0.000306	27723491	0.0001046	457335002
0.00505	8654.9553	0.0005116	5121950.7	0.0003094	23133392
0.0053	6307.0456	0.0020496	118705.03	0.0005151	5332318.1
0.00557	6057.4892	0.00415	19793.169	0.0020539	90948.943
0.00584	4576.2942	0.00436	17168.851	0.00396	18708.12
0.00614	3827.688	0.00458	14649.292	0.00415	12995.554
0.00644	3465.0898	0.00481	13100.853	0.00436	14381.002
0.00676	2518.344	0.00505	10897.546	0.00458	11029.191
0.0071	2167.561	0.0053	8235.8878	0.00481	9712.5436
0.00746	2021.2517	0.00557	7745.9898	0.00505	8338.0133
0.00783	1587.0949	0.00584	5586.6206	0.0053	7564.9903
0.00822	1420.3189	0.00614	5069.301	0.00557	5697.0391
0.00863	1160.7257	0.00644	4273.2747	0.00584	5380.8459
0.00907	1037.3704	0.00676	3480.0932	0.00614	4223.1576
0.00952	852.82788	0.0071	3078.5478	0.00644	3621.1971
0.00999	745.07194	0.00746	2484.4199	0.00676	3234.9606
0.01049	647.11616	0.00783	2253.8469	0.0071	2363.0341
0.01102	547.20904	0.00822	1867.0503	0.00746	2135.3536
0.01157	509.86194	0.00863	1561.8682	0.00783	1816.8238
0.01215	415.11753	0.00907	1340.8346	0.00822	1664.1526
0.01276	379.32152	0.00952	1116.1238	0.00863	1391.2707
0.01339	312.79524	0.00999	989.84748	0.00907	1139.8567
0.01406	263.60814	0.01049	829.81234	0.00952	989.77582
0.01477	233.67563	0.01102	760.09639	0.00999	873.64261
0.0155	199.22182	0.01157	664.01172	0.01049	756.17403
0.01628	175.69563	0.01215	602.67952	0.01102	677.50047
0.01709	161.67233	0.01276	493.49627	0.01157	582.56325
0.01795	137.2208	0.01339	427.82249	0.01215	518.12032
0.01885	125.47667	0.01406	359.09357	0.01276	445.60498
0.01979	108.39094	0.01477	309.43423	0.01339	383.96385
0.02078	94.001507	0.0155	272.8871	0.01406	371.94762
0.02182	85.860459	0.01628	241.1202	0.01477	293.33393
0.02291	72.776381	0.01709	209.51807	0.0155	264.16754
0.02405	58.600142	0.01795	208.90064	0.01628	244.00882
0.02526	55.151235	0.01885	166.50839	0.01709	214.42674
0.02652	48.250648	0.01979	146.78453	0.01795	181.47714
0.02784	43.218123	0.02078	132.22068	0.01885	162.26086
0.02924	39.378221	0.02182	122.11475	0.01979	144.30828
0.0307	34.822055	0.02291	103.60817	0.02078	126.20112
0.03223	29.467601	0.02405	92.812851	0.02182	113.4364
0.03385	31.203751	0.02526	86.9243	0.02291	100.09778

0.03554	25.074238	0.02652	72.02207	0.02405	92.019533
0.03731	23.834942	0.02784	70.235907	0.02526	85.413918
0.03918	20.343725	0.02924	60.153406	0.02652	72.498727
0.04114	17.788967	0.0307	54.010691	0.02784	65.488074
0.0432	16.845671	0.03223	48.738018	0.02924	59.781843
0.04536	15.899402	0.03385	44.593893	0.0307	53.660075
0.04762	14.416022	0.03554	41.419885	0.03223	48.83071
0.05	13.401041	0.03731	36.481748	0.03385	42.390245
0.05251	10.752817	0.03918	31.93994	0.03554	40.227053
0.05513	11.188833	0.04114	27.990519	0.03731	36.722851
0.05789	9.6594134	0.0432	26.860169	0.03918	31.828524
0.06078	8.9322322	0.04536	24.021061	0.04114	29.74033
0.06382	8.9505552	0.04762	21.483789	0.0432	26.048445
0.06701	7.6130049	0.05	20.831589	0.04536	25.108713
0.07036	7.2206679	0.05251	18.546935	0.04762	22.250765
0.07388	6.8511245	0.05513	16.924605	0.05	20.26756
0.07757	6.3448337	0.05789	16.628482	0.05251	18.067042
0.08145	5.6420096	0.06078	13.670141	0.05513	16.664802
0.08553	5.3711888	0.06382	12.800566	0.05789	14.66073
0.0898	4.7122512	0.06701	11.927087	0.06078	14.830955
0.09429	4.9508067	0.07036	10.685315	0.06382	12.297363
0.09901	4.0944629	0.07388	9.1948803	0.06701	11.222734
0.10396	3.9988982	0.07757	8.8425646	0.07036	10.736985
0.10915	3.827079	0.08145	8.0791541	0.07388	9.5495918
0.11461	3.7732073	0.08553	7.1927638	0.07757	9.005245
0.12034	3.3566257	0.0898	6.5739161	0.08145	8.5766792
0.12636	3.070003	0.09429	6.2652888	0.08553	7.5860097
0.13268	3.0494227	0.09901	5.6968402	0.0898	6.9771663
0.13931	2.6869607	0.10396	4.8566988	0.09429	6.5771748
0.14628	2.3146915	0.10915	4.3893836	0.09901	6.1798379
0.15359	2.417327	0.11461	4.2941382	0.10396	5.6648705
0.16127	2.1078203	0.12034	3.9355325	0.10915	5.0124023
0.16933	2.0265827	0.12636	3.6379605	0.11461	4.7559009
0.1778	1.8299206	0.13268	3.5683716	0.12034	4.9947767
0.18669	1.6720254	0.13931	3.0709947	0.12636	4.4687498
0.19603	1.7732441	0.14628	2.8608248	0.13268	4.1622054
0.20583	1.6584311	0.15359	2.6929902	0.13931	3.9994766
0.21612	1.5567797	0.16127	2.4504865	0.14628	3.5539538
0.22692	1.1914277	0.16933	2.6366404	0.15359	3.5786066
0.23827	1.3588369	0.1778	2.4917507	0.16127	3.3574588
0.25018	1.0339576	0.18669	1.7466554	0.16933	3.1767598
0.26269	0.8367837	0.19603	1.8115326	0.1778	3.065783
0.27583	0.7875461	0.20583	1.4048701	0.18669	2.8343381
0.28962	0.6699746	0.21612	1.8887798	0.19603	2.4113835
0.3041	0.4692485	0.22692	1.3403424	0.20583	2.5131144
0.3193	0.3464609	0.23827	1.2742308	0.21612	2.3043046
0.33527	0.4927893	0.25018	0.8735463	0.22692	2.0880729
0.35203	0.305064	0.26269	0.9584768	0.23827	2.0790258
0.36964	0.5910909	0.27583	1.101188	0.25018	1.6532468
0.38812	0.1458379	0.28962	0.7838221	0.26269	1.7119112
		0.3041	0.9432259	0.27583	1.5793547
		0.3193	0.7625971	0.28962	1.8480202
		0.33527	0.5460063	0.3041	1.5188225
		0.35203	0.607825	0.3193	0.9677923
		0.36964	0.395889	0.33527	1.0043113
				0.35203	0.7564536
				0.36964	1.0685431
				0.38812	1.0261923

3.4.3. Vitrain samples (background corrected)

323 rvp NU		326 kvx N + 326 kvp U		327 kvp NU	
Q	**I(Q)**	**Q**	**I(Q)**	**Q**	**I(Q)**
1.764E-05	4.939E+10	1.701E-05	3.771E+11	1.755E-05	3.872E+10
2.897E-05	1.301E+10	2.311E-05	1.732E+11	2.801E-05	1.049E+10
3.856E-05	5.692E+09	2.747E-05	6.528E+10	3.846E-05	4.233E+09
4.901E-05	3.018E+09	3.269E-05	4.418E+10	4.892E-05	2.332E+09
5.947E-05	1.97E+09	3.792E-05	2.652E+10	5.938E-05	1.444E+09
6.993E-05	1.169E+09	4.315E-05	2.17E+10	6.983E-05	957454816
7.951E-05	762880197	4.838E-05	1.376E+10	7.942E-05	671724276
0.0001004	355561382	5.361E-05	1.07E+10	0.0001003	340498280
0.0003052	9286509.9	5.796E-05	7.662E+09	0.000306	14989365
0.0005117	2212668.2	6.406E-05	7.076E+09	0.0005108	2655697.4
0.0020497	58300.17	6.842E-05	4.526E+09	0.0020496	54507.242
0.00415	6839.2068	7.365E-05	3.38E+09	0.00396	9963.6211
0.00436	4974.2528	7.888E-05	3.023E+09	0.00415	9047.0662
0.00458	4018.2072	9.979E-05	1.366E+09	0.00436	5327.472
0.00481	4249.6342	0.0003046	27968815	0.00458	6283.6639
0.00505	2867.8657	0.0005102	6626346.2	0.00481	6159.5731
0.0053	2969.7627	0.00415	8536.3963	0.00505	4308.1759
0.00557	1996.7175	0.00436	5665.3103	0.0053	3941.3209
0.00584	1972.2384	0.00458	4660.6761	0.00557	3091.8122
0.00614	1635.1452	0.00481	5317.6083	0.00584	2916.6228
0.00644	1496.0452	0.00505	4596.6711	0.00614	2612.1497
0.00676	1197.9949	0.0053	3521.9849	0.00644	1935.2633
0.0071	1041.1849	0.00557	2856.3777	0.00676	1816.8085
0.00746	843.20139	0.00584	2517.7996	0.0071	1625.3108
0.00783	763.47902	0.00614	2405.1174	0.00746	1219.0867
0.00822	668.64985	0.00644	2147.1943	0.00783	1009.8254
0.00863	636.6232	0.00676	1827.7117	0.00822	941.96912
0.00907	585.84111	0.0071	1649.4691	0.00863	759.2617
0.00952	442.50994	0.00746	1379.6458	0.00907	767.61073
0.00999	434.10762	0.00783	1147.4748	0.00952	619.46
0.01049	387.65729	0.00822	1059.6575	0.00999	551.81697
0.01102	386.01379	0.00863	933.55246	0.01049	518.83877
0.01157	341.98313	0.00907	824.53753	0.01102	398.09132
0.01215	287.50723	0.00952	725.95606	0.01157	377.35154
0.01276	253.88076	0.00999	616.64357	0.01215	327.4877
0.01339	223.70696	0.01049	541.70472	0.01276	287.17812
0.01406	215.95642	0.01102	519.18461	0.01339	262.6437
0.01477	187.82593	0.01157	442.037	0.01406	223.18642
0.0155	168.717	0.01215	410.35016	0.01477	211.57325
0.01628	162.31898	0.01276	348.51826	0.0155	177.77651
0.01709	142.3349	0.01339	333.01052	0.01628	170.37925
0.01795	132.19198	0.01406	289.37698	0.01709	152.46696
0.01885	125.49607	0.01477	275.86003	0.01795	139.17357
0.01979	111.26067	0.0155	238.8441	0.01885	118.90856
0.02078	100.84243	0.01628	233.03478	0.01979	111.15243
0.02182	95.376419	0.01709	206.62049	0.02078	94.794104
0.02291	91.719425	0.01795	191.55632	0.02182	84.783238
0.02405	81.85805	0.01885	175.45531	0.02291	82.651291
0.02526	73.650747	0.01979	159.33176	0.02405	67.84402
0.02652	71.679513	0.02078	155.22966	0.02526	65.395215
0.02784	68.855746	0.02182	136.98017	0.02652	56.13754
0.02924	60.729903	0.02291	130.88598	0.02784	58.802802
0.0307	57.560209	0.02405	117.59598	0.02924	50.089498
0.03223	51.674628	0.02526	106.15253	0.0307	42.021715
0.03385	46.503891	0.02652	99.902358	0.03223	42.897276
0.03554	44.604912	0.02784	99.798899	0.03385	38.274497

0.03731	38.693908	0.02924	87.6477	0.03554	35.621307
0.03918	37.236521	0.0307	79.486318	0.03731	32.16759
0.04114	33.858543	0.03223	78.356422	0.03918	29.209626
0.0432	30.991436	0.03385	72.988782	0.04114	26.748615
0.04536	27.720765	0.03554	70.26729	0.0432	26.050173
0.04762	26.001656	0.03731	65.100332	0.04536	23.469714
0.05	24.117092	0.03918	58.074124	0.04762	20.234517
0.05251	21.03783	0.04114	53.166755	0.05	20.355543
0.05513	18.43044	0.0432	51.985731	0.05251	18.648264
0.05789	17.484447	0.04536	46.108944	0.05513	17.473923
0.06078	15.938953	0.04762	40.965752	0.05789	15.685198
0.06382	14.881577	0.05	39.370266	0.06078	14.33958
0.06701	12.932936	0.05251	35.24015	0.06382	13.203785
0.07036	11.758691	0.05513	32.561203	0.06701	11.632286
0.07388	11.263231	0.05789	30.20316	0.07036	10.880991
0.07757	10.431269	0.06078	25.876926	0.07388	10.116195
0.08145	9.0019913	0.06382	24.730392	0.07757	9.3944594
0.08553	8.4011919	0.06701	22.286428	0.08145	8.4445687
0.0898	7.7181317	0.07036	20.091126	0.08553	8.2704435
0.09429	6.9489634	0.07388	17.641717	0.0898	7.202922
0.09901	6.2970679	0.07757	15.8023	0.09429	6.5394771
0.10396	6.0479875	0.08145	13.349179	0.09901	6.2027912
0.10915	5.4296462	0.08553	13.038619	0.10396	5.664515
0.11461	5.0214671	0.0898	11.506401	0.10915	5.0612692
0.12034	4.7720404	0.09429	9.7563905	0.11461	5.0944764
0.12636	4.5797134	0.09901	9.3053184	0.12034	4.8816201
0.13268	3.9870454	0.10396	8.4409988	0.12636	4.0917525
0.13931	3.5756995	0.10915	7.3984369	0.13268	3.8939816
0.14628	3.7625016	0.11461	6.5985454	0.13931	3.7654248
0.15359	3.0855309	0.12034	6.5710849	0.14628	3.4327173
0.16127	3.1169862	0.12636	5.7568666	0.15359	3.3814806
0.16933	3.1414103	0.13268	5.2075746	0.16127	3.195559
0.1778	3.1153043	0.13931	4.8615022	0.16933	2.9003073
0.18669	2.7179003	0.14628	4.4582451	0.1778	2.9870705
0.19603	2.7408372	0.15359	4.0885377	0.18669	2.603517
0.20583	2.1451045	0.16127	3.6915107	0.19603	2.2248578
0.21612	1.9476126	0.16933	3.4518457	0.20583	2.2947883
0.22692	2.02486	0.1778	3.1961063	0.21612	2.0161305
0.23827	2.1427417	0.18669	2.8905105	0.22692	1.5889873
0.25018	1.5939071	0.19603	2.6529436	0.23827	1.7966328
0.26269	1.6639036	0.20583	2.4081391	0.25018	1.590712
0.27583	1.4943268	0.21612	2.2811381	0.26269	1.7353033
0.28962	1.2432418	0.22692	2.2857156	0.27583	1.7075186
0.3041	1.267183	0.23827	2.0703672	0.28962	1.0661967
0.3193	1.1961738	0.25018	1.8447772	0.3041	1.3398252
0.33527	1.5112728	0.26269	1.7806391	0.3193	0.719536
0.35203	1.2549286	0.27583	1.3298787	0.33527	1.0549641
0.36964	1.1208981	0.28962	1.7361899	0.35203	0.8971727
0.38812	0.8561882	0.3041	1.3266345	0.36964	0.7230613
		0.3193	1.3286263	0.38812	0.9044246
		0.33527	1.0863409		
		0.35203	1.1365321		
		0.36964	1.0714717		
		0.38812	0.7090667		

N = SANS, U = USANS analysed sample.

3.5. Pore size distribution SAXS/USAXS

3.5.1. Renown seam matrix samples perpendicular

318 rmx ave		319 rmx ave		610 rmx ave		611 rmx ave		612 rmx ave	
Ave r(Å)	Ave f(r)	Ave r(Å)	Ave f(r)	Ave r(Å)	Ave f(r)	Ave r(Å)	Ave f(r)	Ave r(Å)	Ave f(r)
5.0118722	0.849298	5.0118722	0.7900302	5.0118722	0.8407185	5.0118722	0.7574371	5.0118722	0.7008196
6.3095736	0.0010607	6.3095736	0.0375889	6.3095736	0.0064786	6.3095736	0.0642701	6.3095736	0.1031815
7.943283	9.379E-05	7.943283	0.0050376	7.943283	0.0011544	7.943283	0.0009628	7.943283	0.0146816
10	9.289E-05	10	0.0020117	10	0.0002268	10	0.0042711	10	0.000802
12.589255	0.0027993	12.589255	0.0018064	12.589255	0.0016093	12.589255	0.0014851	12.589255	0.0003518
15.848934	0.0003838	15.848934	0.0012269	15.848934	0.0011315	15.848934	0.0019925	15.848934	0.0010854
19.952626	0.0005238	19.952626	0.0007732	19.952626	0.0006453	19.952626	0.0003245	19.952626	0.0003894
25.11887	0.00041	25.11887	0.0003967	25.11887	0.0003421	25.11887	0.0006201	25.11887	0.0003872
31.622785	0.00011	31.622785	0.0001638	31.622785	0.0001437	31.622785	0.0001403	31.622785	8.152E-05
39.81073	4.788E-05	39.81073	6.136E-05	39.81073	5.243E-05	39.81073	6.641E-05	39.81073	6.079E-05
50.118743	1.518E-05	50.118743	1.852E-05	50.118743	1.553E-05	50.118743	2.866E-05	50.118743	1.193E-05
63.095762	2.067E-06	63.095762	4.104E-06	63.095762	3.931E-06	63.095762	4.647E-06	63.095762	5.214E-06
79.432863	4.325E-07	79.432863	1.062E-06	79.432863	1.2E-06	79.432863	1.27E-06	79.432863	1.872E-06
100.00005	2.511E-07	100.00005	3.092E-07	100.00005	3.581E-07	100.00005	4.013E-07	100.00005	3.671E-07
125.89258	7.055E-08	125.89258	1.172E-07	125.89258	9.331E-08	125.89258	1.576E-07	125.89258	1.568E-07
158.48934	1.473E-08	158.48934	4.62E-08	158.48934	3.783E-08	158.48934	6.135E-08	158.48934	6.786E-08
199.52621	1.026E-08	199.52621	1.668E-08	199.52621	2.015E-08	199.52621	1.083E-08	199.52621	2.16E-08
251.18856	4.282E-09	251.18856	6.745E-09	251.18856	6.108E-09	251.18856	5.746E-09	251.18856	8.087E-09
316.22759	2.09E-09	316.22759	2.569E-09	316.22759	1.844E-09	316.22759	3.961E-09	316.22759	3.111E-09
398.10686	4.892E-10	398.10686	1.022E-09	398.10686	9.165E-10	398.10686	8.376E-10	398.10686	1.27E-09
501.18674	2.35E-10	501.18674	4.201E-10	501.18674	4.244E-10	501.18674	4.587E-10	501.18674	5.219E-10
630.95658	1.154E-10	630.95658	1.789E-10	630.95658	9.127E-11	630.95658	1.489E-10	630.95658	1.931E-10
794.3271	6.86E-11	794.3271	7.549E-11	794.3271	5.407E-11	794.3271	6.418E-11	794.3271	6.624E-11
999.99835	1.073E-11	999.99835	2.635E-11	999.99835	2.562E-11	999.99835	2.244E-11	999.99835	3.624E-11
1258.9231	1.169E-11	1258.9231	1.135E-11	1258.9231	6.056E-12	1258.9231	1.81E-11	1258.9231	1.167E-11
1584.8899	5.234E-12	1584.8899	4.244E-12	1584.8899	2.566E-12	1584.8899	3.442E-12	1584.8899	5.196E-12
1995.2577	4.85E-13	1995.2577	1.423E-12	1995.2577	1.07E-12	1995.2577	2.23E-12	1995.2577	1.535E-12
2511.8801	5.644E-13	2511.8801	6.096E-13	2511.8801	3.387E-13	2511.8801	1.044E-12	2511.8801	7.393E-13
3162.269	2.103E-13	3162.269	2.571E-13	3162.269	1.683E-13	3162.269	3.451E-13	3162.269	3.855E-13
3981.0599	5.529E-14	3981.0599	1.1E-13	3981.0599	6.558E-14	3981.0599	1.356E-13	3981.0599	9.354E-14
5011.8564	2.901E-14	5011.8564	7.672E-14	5011.8564	2.697E-14	5011.8564	7.61E-14	5011.8564	8.591E-14
6309.552	1.092E-14	6309.552	2.108E-14	6309.552	1.1E-14	6309.552	2.176E-14	6309.552	1.831E-14
7943.2536	3.341E-15	7943.2536	9.072E-15	7943.2536	2.252E-15	7943.2536	1.187E-14	7943.2536	1.373E-14
9999.9616	2.137E-15	9999.9616	3.392E-15	9999.9616	9.179E-16	9999.9616	4.079E-15	9999.9616	5.7E-15
12589.21	1.545E-16	12589.21	1.409E-15	12589.21	9.178E-16	12589.21	2.42E-15	12589.21	1.654E-15
15848.873	3.84E-16	15848.873	7.222E-16	15848.873	2.838E-16	15848.873	6.677E-16	15848.873	1.2E-15

3.5.2. Renown seam matrix samples parallel

318 rmp ave		319 rmp ave		610 rmp ave		611 rmp ave		612 rmp ave	
Ave r(Å)	**Ave f(r)**	**Ave r(Å)**	**Ave f(r)**	**Ave r(Å)**	**Ave f(r)**	**Ave r(Å)**	**Ave f(r)**	**Ave r(Å)**	**Ave f(r)**
5.0118722	0.6835003	5.0118722	0.6915077	5.0118722	0.791151	5.0118722	0.6307985	5.2714125	0.1625829
6.3095736	0.103295	6.3095736	0.0939757	6.3095736	0.0246193	6.3095736	0.0854502	6.6363155	0.0691986
7.943283	0.0192793	7.943283	0.0217843	7.943283	0.0071547	7.943283	0.0277366	8.3546264	0.2944236
10	0.0041614	10	0.004399	10	0.0104752	10	0.0307148	10.517851	0.0471556
12.589255	0.0012425	12.589255	0.0013989	12.589255	0.0009952	12.589255	0.0045852	13.241191	0.0004697
15.848934	0.0008902	15.848934	0.0005221	15.848934	0.0004173	15.848934	0.0002577	16.669672	0.0016516
19.952626	0.0006255	19.952626	0.0006041	19.952626	0.00068	19.952626	0.001016	20.985875	0.0005728
25.11887	0.0003325	25.11887	0.0003582	25.11887	0.0003225	25.11887	0.0003479	26.419653	0.0011987
31.622785	0.0001677	31.622785	0.0001367	31.622785	0.0001611	31.622785	0.0002245	33.260374	0.0002859
39.81073	7.264E-05	39.81073	8.945E-05	39.81073	6.972E-05	39.81073	9.878E-05	41.872333	0.0001485
50.118743	2.993E-05	50.118743	3.21E-05	50.118743	3.033E-05	50.118743	3.384E-05	52.714147	5.538E-05
63.095762	1.035E-05	63.095762	1.181E-05	63.095762	1.059E-05	63.095762	1.828E-05	66.363182	1.879E-05
79.432863	2.547E-06	79.432863	3.866E-06	79.432863	3.425E-06	79.432863	4.232E-06	83.546301	7.2E-06
100.00005	6.144E-07	100.00005	9.285E-07	100.00005	8.232E-07	100.00005	1.397E-06	105.17856	1.786E-06
125.89258	2.17E-07	125.89258	2.889E-07	125.89258	3.404E-07	125.89258	3.907E-07	132.41193	5.629E-07
158.48934	9.294E-08	158.48934	1.08E-07	158.48934	1.03E-07	158.48934	1.25E-07	166.69671	1.532E-07
199.52621	3.312E-08	199.52621	3.493E-08	199.52621	3.269E-08	199.52621	4.226E-08	209.85868	6.878E-08
251.18856	9.327E-09	251.18856	1.42E-08	251.18856	1.491E-08	251.18856	1.733E-08	264.19637	2.272E-08
316.22759	3.648E-09	316.22759	4.645E-09	316.22759	5.153E-09	316.22759	4.852E-09	332.60345	6.422E-09
398.10686	1.481E-09	398.10686	1.742E-09	398.10686	1.945E-09	398.10686	2.356E-09	418.72284	1.71E-09
501.18674	5.011E-10	501.18674	7.779E-10	501.18674	7.209E-10	501.18674	7.899E-10	527.14071	1.204E-09
630.95658	2.557E-10	630.95658	3.513E-10	630.95658	2.943E-10	630.95658	3.377E-10	663.63069	3.358E-10
794.3271	8.685E-11	794.3271	1.442E-10	794.3271	1.301E-10	794.3271	1.164E-10	835.46135	1.326E-10
999.99835	3.552E-11	999.99835	6.838E-11	999.99835	3.64E-11	999.99835	5.656E-11	1051.7833	4.022E-11
1258.9231	1.756E-11	1258.9231	2.21E-11	1258.9231	1.985E-11	1258.9231	2.256E-11	1324.1164	2.319E-11
1584.8899	5.848E-12	1584.8899	1.07E-11	1584.8899	6.758E-12	1584.8899	8.265E-12	1666.9635	1.035E-11
1995.2577	3.427E-12	1995.2577	3.9E-12	1995.2577	2.836E-12	1995.2577	3.465E-12	2098.5822	3.11E-12
2511.8801	1.15E-12	2511.8801	1.776E-12	2511.8801	1.167E-12	2511.8801	1.332E-12	2641.9579	1.551E-12
3162.269	6.541E-13	3162.269	8.65E-13	3162.269	5.245E-13	3162.269	7.306E-13	3326.0272	1.121E-12
3981.0599	2.276E-13	3981.0599	2.227E-13	3981.0599	2.054E-13	3981.0599	1.5E-13	4187.2192	4.391E-13
5011.8564	1.006E-13	5011.8564	1.692E-13	5011.8564	1.074E-13	5011.8564	1.265E-13	5271.3955	2.675E-13
6309.552	5.661E-14	6309.552	4.145E-14	6309.552	1.71E-14	6309.552	4.606E-14	6636.2923	1.084E-13
7943.2536	1.487E-14	7943.2536	1.724E-14	7943.2536	1.853E-14	7943.2536	9.918E-15	8354.5952	5.225E-14
9999.9616	2.912E-15	9999.9616	5.788E-15	9999.9616	6.841E-15	9999.9616	1.05E-14	10517.811	2.252E-14
12589.21	1.308E-15	12589.21	4.098E-15	12589.21	4.813E-15	12589.21	3.166E-15	13241.142	4.787E-15
15848.873	1.199E-15	15848.873	1.91E-15	15848.873	2.457E-15	15848.873	1.708E-15	16669.607	2.203E-15
19952.544	5.62E-16	19952.544	8.124E-16	19952.544	9.248E-16	19952.544	5.303E-16	20985.787	1.913E-15
25118.76	2.534E-16	25118.76	3.466E-16						

3.5.3. Kupakupa seam matrix samples perpendicular

320 kmx ave		321 kmx ave		322 kmx ave	
Ave r(Å)	**Ave f(r)**	**Ave r(Å)**	**Ave f(r)**	**Ave r(Å)**	**Ave f(r)**
5.0118722	0.7999358	5.0118722	0.7439467	5.0118722	0.7655401
6.3095736	0.0343933	6.3095736	0.0632211	6.3095736	0.0489933
7.943283	0.0027113	7.943283	0.0103158	7.943283	0.0062406
10	0.0010206	10	0.0030209	10	0.0015775
12.589255	0.0019864	12.589255	0.0019666	12.589255	0.0032101
15.848934	0.0008619	15.848934	0.0015383	15.848934	0.0017913
19.952626	0.0009194	19.952626	0.0011535	19.952626	0.0013058
25.11887	0.0003734	25.11887	0.0004079	25.11887	0.000556
31.622785	0.0001724	31.622785	0.0002079	31.622785	0.0002573
39.81073	5.964E-05	39.81073	7.271E-05	39.81073	8.411E-05
50.118743	1.483E-05	50.118743	2.371E-05	50.118743	2.308E-05
63.095762	4.442E-06	63.095762	6.937E-06	63.095762	5.794E-06
79.432863	1.374E-06	79.432863	1.888E-06	79.432863	1.903E-06
100.00005	4.527E-07	100.00005	5.794E-07	100.00005	6.619E-07
125.89258	1.778E-07	125.89258	2.019E-07	125.89258	2.308E-07
158.48934	6.484E-08	158.48934	7.79E-08	158.48934	8.63E-08
199.52621	2.344E-08	199.52621	2.786E-08	199.52621	3.495E-08
251.18856	1.017E-08	251.18856	1.015E-08	251.18856	1.351E-08
316.22759	3.852E-09	316.22759	3.78E-09	316.22759	5.374E-09
398.10686	1.356E-09	398.10686	1.252E-09	398.10686	1.892E-09
501.18674	6.88E-10	501.18674	5.504E-10	501.18674	1.015E-09
630.95658	2.492E-10	630.95658	2.574E-10	630.95658	3.273E-10
794.3271	9.106E-11	794.3271	1.203E-10	794.3271	1.381E-10
999.99835	4.03E-11	999.99835	4.48E-11	999.99835	6.664E-11
1258.9231	1.496E-11	1258.9231	1.607E-11	1258.9231	2.742E-11
1584.8899	5.235E-12	1584.8899	7.629E-12	1584.8899	1.023E-11
1995.2577	1.923E-12	1995.2577	3.176E-12	1995.2577	5.327E-12
2511.8801	6.799E-13	2511.8801	1.491E-12	2511.8801	2.124E-12
3162.269	2.152E-13	3162.269	4.981E-13	3162.269	1.068E-12
3981.0599	1.138E-13	3981.0599	2.123E-13	3981.0599	3.498E-13
5011.8564	4.275E-14	5011.8564	1.264E-13	5011.8564	1.278E-13
6309.552	1.017E-14	6309.552	2.719E-14	6309.552	4.313E-14
7943.2536	4.316E-15	7943.2536	1.471E-14	7943.2536	1.868E-14
9999.9616	1.95E-15	9999.9616	5.224E-15	9999.9616	5.564E-15
12589.21	1.052E-15	12589.21	2.396E-15	12589.21	1.813E-15
15848.873	2.746E-16	15848.873	9.288E-16		
19952.544	3.948E-17	19952.544	6.066E-16		

3.5.4. Kupakupa seam matrix samples parallel

320 kmp ave		321 kmp ave		322 kmp ave	
Ave r(Å)	**Ave f(r)**	**Ave r(Å)**	**Ave f(r)**	**Ave r(Å)**	**Ave f(r)**
5.0118722	0.5626057	5.0118722	0.8320709	5.2714125	0.6839084
6.3095736	0.1618184	6.3095736	0.0120571	6.6363155	0.0825604
7.943283	0.0417866	7.943283	0.0017996	8.3546264	0.0141263
10	0.0074985	10	0.0010637	10.517851	0.0030001
12.589255	0.0017258	12.589255	0.0027071	13.241191	0.0012313
15.848934	0.0017097	15.848934	0.0004047	16.669672	0.0010461
19.952626	0.0005453	19.952626	0.0003509	20.985875	0.000695
25.11887	0.000556	25.11887	0.0003017	26.419653	0.0003192
31.622785	0.0001633	31.622785	9.783E-05	33.260374	0.0001419
39.81073	8.678E-05	39.81073	5.511E-05	41.872333	8.108E-05
50.118743	3.549E-05	50.118743	2.103E-05	52.714147	2.944E-05
63.095762	1.434E-05	63.095762	6.226E-06	66.363182	1.026E-05
79.432863	5.089E-06	79.432863	2.182E-06	83.546301	3.856E-06
100.00005	1.923E-06	100.00005	9.63E-07	105.17856	1.159E-06
125.89258	7.047E-07	125.89258	2.263E-07	132.41193	3.82E-07
158.48934	2.766E-07	158.48934	6.487E-08	166.69671	1.469E-07
199.52621	1.024E-07	199.52621	2.704E-08	209.85868	6.277E-08
251.18856	4.322E-08	251.18856	8.383E-09	264.19637	2.643E-08
316.22759	1.69E-08	316.22759	3.334E-09	332.60345	7.594E-09
398.10686	6.445E-09	398.10686	1.113E-09	418.72284	3.229E-09
501.18674	2.604E-09	501.18674	4.092E-10	527.14071	1.503E-09
630.95658	1.269E-09	630.95658	2.646E-10	663.63069	4.798E-10
794.3271	4.874E-10	794.3271	8.323E-11	835.46135	2.346E-10
999.99835	2.147E-10	999.99835	1.657E-11	1051.7833	1.02E-10
1258.9231	8.297E-11	1258.9231	1.581E-11	1324.1164	3.528E-11
1584.8899	4.107E-11	1584.8899	5.264E-12	1666.9635	1.298E-11
1995.2577	1.439E-11	1995.2577	1.443E-12	2098.5822	7.652E-12
2511.8801	6.683E-12	2511.8801	1.137E-12	2641.9579	2.937E-12
3162.269	3.233E-12	3162.269	2.84E-13	3326.0272	1.682E-12
3981.0599	9.759E-13	3981.0599	1.701E-13	4187.2192	5.825E-13
5011.8564	6.683E-13	5011.8564	5.7E-14	5271.3955	3.196E-13
6309.552	2.108E-13	6309.552	1.948E-14	6636.2923	6.224E-14
7943.2536	7.906E-14	7943.2536	1.165E-14	8354.5952	2.89E-14
9999.9616	3.632E-14	9999.9616	2.721E-15	10517.811	1.162E-14
12589.21	1.67E-14	12589.21	1.461E-15	13241.142	2.832E-15
15848.873	6.856E-15	15848.873	5.922E-16	16669.607	1.876E-15
19952.544	2.948E-15	19952.544	3.291E-16	20985.787	1.014E-15
25118.76	1.095E-15	25118.76	2.406E-16	25118.76	4.676E-16

3.5.5. Vitrain samples perpendicular

323 rvx ave		326 kvx ave		327 kvx ave		328 kvx ave	
Ave r(Å)	**Ave f(r)**	**Ave r(Å)**	**Ave f(r)**	**Ave r(Å)**	**Ave f(r)**	**Ave r(Å)**	**Ave f(r)**
5.0118722	0.5887388	5.0118722	0.8452238	5.0118722	0.8218935	5.0118722	0.8146065
6.3095736	0.037734	6.3095736	0.0017546	6.3095736	0.0094507	6.3095736	0.0187049
7.943283	0.0049076	7.943283	0.0001585	7.943283	0.0007907	7.943283	0.002161
10	0.0020402	10	0.0001252	10	0.0004464	10	0.0004848
12.589255	0.0481477	12.589255	0.0027335	12.589255	0.0036592	12.589255	0.0014235
15.848934	0.0038519	15.848934	0.0011128	15.848934	0.0020791	15.848934	0.002469
19.952626	0.007558	19.952626	0.0005967	19.952626	0.0015377	19.952626	0.0010378
25.11887	0.0063879	25.11887	0.0004054	25.11887	0.0007439	25.11887	0.0007221
31.622785	0.0022034	31.622785	0.0001768	31.622785	0.0003284	31.622785	0.0003085
39.81073	0.0008864	39.81073	5.975E-05	39.81073	0.0001034	39.81073	0.0001025
50.118743	2.971E-05	50.118743	2.15E-05	50.118743	1.259E-05	50.118743	1.375E-05
63.095762	3.351E-06	63.095762	5.408E-06	63.095762	2.345E-06	63.095762	1.841E-06
79.432863	4.746E-07	79.432863	7.98E-07	79.432863	6.632E-07	79.432863	5.88E-07
100.00005	1.506E-07	100.00005	2.222E-07	100.00005	2.526E-07	100.00005	2.43E-07
125.89258	9.593E-08	125.89258	7.328E-08	125.89258	9.999E-08	125.89258	8.301E-08
158.48934	1.068E-07	158.48934	3.648E-08	158.48934	3.225E-08	158.48934	2.478E-08
199.52621	3.988E-08	199.52621	1.14E-08	199.52621	9.638E-09	199.52621	1.022E-08
251.18856	4.702E-09	251.18856	2.331E-09	251.18856	3.407E-09	251.18856	4.884E-09
316.22759	1.982E-09	316.22759	7.843E-10	316.22759	1.286E-09	316.22759	1.204E-09
398.10686	2.531E-09	398.10686	4.585E-10	398.10686	4.985E-10	398.10686	5.333E-10
501.18674	5.289E-10	501.18674	2.092E-10	501.18674	1.464E-10	501.18674	4.043E-10
630.95658	1.181E-10	630.95658	3.509E-11	630.95658	4.923E-11	630.95658	1.442E-10
794.3271	1.397E-10	794.3271	2.094E-11	794.3271	2.683E-11	794.3271	2.51E-11
999.99835	6.074E-11	999.99835	8.341E-12	999.99835	1.191E-11	999.99835	3.351E-11
1258.9231	2.075E-11	1258.9231	4.276E-12	1258.9231	5.02E-12	1258.9231	1.094E-11
1584.8899	1.403E-11	1584.8899	1.458E-12	1584.8899	2.81E-12	1584.8899	4.427E-12
1995.2577	3.589E-12	1995.2577	5.344E-13	1995.2577	1.081E-12	1995.2577	2.875E-12
2511.8801	2.783E-12	2511.8801	1.444E-13	2511.8801	5.816E-13	2511.8801	7.473E-13
3162.269	1.125E-12	3162.269	1.101E-13	3162.269	2.826E-13	3162.269	6.306E-13
3981.0599	1.121E-12	3981.0599	5.72E-14	3981.0599	1.226E-13	3981.0599	8.406E-14
5011.8564	5.796E-13	5011.8564	1.882E-14	5011.8564	7.992E-14	5011.8564	1.099E-13
6309.552	1.129E-13	6309.552	3.834E-15	6309.552	1.933E-14	6309.552	1.872E-14
7943.2536	6.994E-14	7943.2536	2.317E-15	7943.2536	1.056E-14	7943.2536	7.592E-15
9999.9616	2.923E-14	9999.9616	5.846E-16	9999.9616	3.094E-15	9999.9616	6.247E-15
12589.21	8.714E-15	12589.21	6.163E-16	12589.21	1.904E-15	12589.21	8.643E-16
15848.873	4.868E-15	15848.873	4.279E-17	15848.873	3.938E-16	15848.873	8.122E-16

3.5.6. Vitrain samples parallel

323 rvp ave		327 kvp ave		328 kvp ave	
Ave r(Å)	**Ave f(r)**	**Ave r(Å)**	**Ave f(r)**	**Ave r(Å)**	**Ave f(r)**
5.0118722	0.8508845	5.0118722	0.8126686	5.0118722	0.8225985
6.3095736	0.0021401	6.3095736	0.0087944	6.3095736	0.0218055
7.943283	0.0001834	7.943283	0.0011107	7.943283	0.0024753
10	0.0001149	10	0.00612	10	0.0007808
12.589255	0.0018753	12.589255	0.0044783	12.589255	0.0005987
15.848934	0.0002565	15.848934	0.0009454	15.848934	0.0007723
19.952626	0.0005863	19.952626	0.0016054	19.952626	0.0005829
25.11887	0.0002642	25.11887	0.0006685	25.11887	0.0001982
31.622785	0.0001032	31.622785	0.0002711	31.622785	0.0001346
39.81073	4.985E-05	39.81073	0.0001045	39.81073	6.744E-05
50.118743	1.832E-05	50.118743	2.886E-05	50.118743	2.921E-05
63.095762	5.456E-06	63.095762	4.981E-06	63.095762	8.36E-06
79.432863	1.735E-06	79.432863	1.387E-06	79.432863	2.188E-06
100.00005	4.775E-07	100.00005	3.88E-07	100.00005	4.717E-07
125.89258	1.177E-07	125.89258	1.75E-07	125.89258	8.534E-08
158.48934	4.508E-08	158.48934	4.346E-08	158.48934	1.558E-08
199.52621	1.383E-08	199.52621	1.405E-08	199.52621	3.491E-09
251.18856	3.3E-09	251.18856	6.937E-09	251.18856	1.015E-09
316.22759	1.273E-09	316.22759	2.893E-09	316.22759	3.605E-10
398.10686	2.126E-10	398.10686	7.223E-10	398.10686	1.419E-10
501.18674	1.595E-10	501.18674	3.805E-10	501.18674	5.789E-11
630.95658	7.334E-11	630.95658	1.501E-10	630.95658	2.071E-11
794.3271	2.203E-11	794.3271	8.773E-11	794.3271	6.134E-12
999.99835	7.177E-12	999.99835	3.542E-11	999.99835	2.753E-12
1258.9231	2.352E-12	1258.9231	1.83E-11	1258.9231	1.415E-12
1584.8899	1.565E-12	1584.8899	2.454E-12	1584.8899	4.582E-13
1995.2577	4.305E-13	1995.2577	2.97E-12	1995.2577	2.111E-13
2511.8801	3.021E-13	2511.8801	1.66E-12	2511.8801	1.018E-13
3162.269	3.96E-14	3162.269	6.312E-13	3162.269	4.084E-14
3981.0599	5.421E-14	3981.0599	4.573E-13	3981.0599	1.088E-14
5011.8564	1.327E-14	5011.8564	1.148E-13	5011.8564	1.001E-14
6309.552	6.642E-15	6309.552	9.724E-14	6309.552	3.303E-15
7943.2536	2.754E-15	7943.2536	3.301E-14	7943.2536	1.289E-15
9999.9616	8.243E-16	9999.9616	1.206E-14	9999.9616	9.052E-16
12589.21	7.525E-16	12589.21	4.843E-15	12589.21	4.191E-16
15848.873	2.251E-16	15848.873	2.591E-15	15848.873	3.146E-16
		19952.544	8.595E-16	19952.544	1.053E-16
		25118.76	6.716E-16	25118.76	5.385E-17

3.6. Pore size distribution SANS/USANS

3.6.1. Renown seam matrix samples

318 rmp N + U		319 rmx N + 319 rmp U		610 rmp NU		611 rmx N + 611 rmp U		612 rmx N + 612 rmp U	
r(Å)	f(r)	r(Å)	f(r)	r(Å)	f(r)	r(Å)	f(r)	r(Å)	f(r)
6.3095736	0.6269069	6.3095736	0.6686898	6.3095736	0.6626792	6.3095736	0.6683365	6.3095736	0.6802745
7.943283	0.0318849	7.943283	0.0095583	7.943283	0.0151309	7.943283	0.0125298	7.943283	5.359E-06
10	0.005789	10	0.0014952	10	0.0017264	10	0.001138	10	1.173E-05
12.589255	0.002778	12.589255	0.0010324	12.589255	0.0005068	12.589255	0.0002348	12.589255	0.0025484
15.848934	0.00167	15.848934	0.0004893	15.848934	0.0002679	15.848934	7.369E-05	15.848934	0.0003118
19.952626	0.0001455	19.952626	6.163E-05	19.952626	0.0001218	19.952626	2.918E-05	19.952626	0.0001279
25.11887	3.733E-05	25.11887	3.273E-05	25.11887	3.714E-05	25.11887	1.527E-05	25.11887	3.214E-05
31.622785	2.837E-05	31.622785	9.196E-06	31.622785	1.354E-05	31.622785	7.732E-06	31.622785	1.076E-05
39.81073	8.054E-06	39.81073	4.708E-06	39.81073	3.962E-06	39.81073	3.685E-06	39.81073	3.991E-06
50.118743	2.135E-06	50.118743	8.01E-07	50.118743	1.298E-06	50.118743	9.019E-07	50.118743	9.751E-07
63.095762	9.322E-07	63.095762	1.64E-07	63.095762	5.026E-07	63.095762	9.072E-08	63.095762	2.65E-07
79.432863	2.046E-07	79.432863	5.362E-08	79.432863	1.197E-07	79.432863	4.893E-08	79.432863	1.009E-07
100.00005	3.748E-08	100.00005	2.569E-08	100.00005	3.977E-08	100.00005	1.74E-08	100.00005	3.717E-08
125.89258	1.844E-08	125.89258	7.081E-09	125.89258	1.344E-08	125.89258	1.146E-08	125.89258	1.578E-08
158.48934	9.264E-09	158.48934	3.314E-09	158.48934	5.263E-09	158.48934	2.833E-09	158.48934	4.889E-09
199.52621	2.394E-09	199.52621	1.442E-09	199.52621	1.509E-09	199.52621	3.095E-10	199.52621	1.878E-09
251.18856	8.32E-10	251.18856	4.706E-10	251.18856	7.791E-10	251.18856	4.466E-11	251.18856	6.818E-10
316.22759	3.184E-10	316.22759	2.612E-10	316.22759	2.301E-10	316.22759	8.624E-12	316.22759	4.099E-10
398.10686	1.532E-10	398.10686	2.04E-10	398.10686	1.35E-10	398.10686	2.681E-12	398.10686	2.494E-10
501.18674	9.653E-11	501.18674	9.673E-11	501.18674	6.527E-11	501.18674	1.151E-12	501.18674	1.345E-10
630.95658	4.424E-11	630.95658	5.565E-11	630.95658	2.563E-11	630.95658	1.197E-12	630.95658	7.359E-11
794.3271	3.313E-11	794.3271	1.907E-11	794.3271	1.68E-11	794.3271	2.233E-12	794.3271	2.302E-11
999.99835	5.754E-12	999.99835	3.048E-12	999.99835	4.694E-12	999.99835	1.96E-11	999.99835	6.868E-12
1258.9231	8.463E-12	1258.9231	1.688E-12	1258.9231	6.871E-13	1258.9231	7.612E-12	1258.9231	2.248E-12
1584.8899	9.693E-13	1584.8899	4.073E-13	1584.8899	6.38E-13	1584.8899	3.19E-13	1584.8899	6.901E-13
1995.2577	1.284E-12	1995.2577	9.651E-14	1995.2577	1.03E-12	1995.2577	1.204E-12	1995.2577	3.162E-12
2511.8801	2.836E-13	2511.8801	5.612E-14	2511.8801	1.314E-13	2511.8801	1.874E-13	2511.8801	1.755E-13
3162.269	7.147E-14	3162.269	3.099E-14	3162.269	2.246E-14	3162.269	7.007E-14	3162.269	1.806E-14
3981.0599	1.495E-14	3981.0599	1.286E-14	3981.0599	7.549E-15	3981.0599	4.278E-14	3981.0599	3.044E-15
5011.8564	3.312E-15	5011.8564	1.982E-14	5011.8564	2.392E-15	5011.8564	9.809E-15	5011.8564	6.741E-16
6309.552	8.275E-16	6309.552	3.815E-15	6309.552	1.354E-15	6309.552	4.231E-15	6309.552	4.127E-16
7943.2536	2.56E-16	7943.2536	3.205E-16	7943.2536	1.392E-15	7943.2536	2.263E-15	7943.2536	1.901E-15
9999.9616	1.493E-16	9999.9616	9.109E-17	9999.9616	4.525E-16	9999.9616	6.68E-16	9999.9616	1.362E-15
12589.21	2.317E-16	12589.21	1.989E-17	12589.21	1.517E-16	12589.21	2.678E-16	12589.21	1.872E-16
15848.873	1.045E-16	15848.873	1.264E-17	15848.873	5.26E-17	15848.873	8.485E-17	15848.873	6.876E-17
19952.544	2.213E-17	19952.544	4.201E-17	19952.544	1.629E-17	19952.544	2.366E-17	19952.544	3.053E-17
25118.76	2.029E-17	25118.76	1.446E-17	25118.76	5.007E-18	25118.76	8.964E-18	25118.76	6.17E-18
31622.638	6.706E-18	31622.638	1.871E-18	31622.638	2.186E-18	31622.638	3.876E-18	31622.638	3.034E-18
39810.533	2.25E-18	39810.533	3.71E-19	39810.533	9.975E-19	39810.533	1.422E-18	39810.533	1.444E-18
50118.481	7.406E-19	50118.481	8.132E-19	50118.481	2.379E-19	50118.481	1.481E-19	50118.481	4.826E-19
63095.416	6.418E-19	63095.416	6.311E-19	63095.416	4.961E-20	63095.416	1.535E-20	63095.416	1.69E-19
79432.405	6.411E-20	79432.405	1.982E-21	79432.405	1.725E-20	79432.405	4.267E-21	79432.405	5.074E-20
99999.451	3.78E-20	99999.451	1.263E-22	99999.451	9.46E-21	99999.451	5.676E-21	99999.451	2.76E-20
125891.82	2.595E-20			125891.82	1.504E-20	125891.82	3.485E-20	125891.82	1.552E-20
158488.38	8.185E-21			158488.38	1.195E-20	158488.38	5.52E-20		
				199525	7.037E-21	199525	2.94E-20		

3.6.2. Kupakupa seam matrix samples

320 kmp NU		321 kmx N + 321 kmp U		322 kmp NU	
r(Å)	**f(r)**	**r(Å)**	**f(r)**	**r(Å)**	**f(r)**
6.3095736	0.4163054	6.3095736	0.5757947	6.3095736	0.650066
7.943283	0.1592167	7.943283	0.070213	7.943283	0.0225235
10	0.034535	10	0.0086669	10	0.0030734
12.589255	0.0059785	12.589255	0.0021254	12.589255	0.0009607
15.848934	0.0008386	15.848934	0.0012412	15.848934	0.0003721
19.952626	0.0001659	19.952626	0.0003026	19.952626	0.000119
25.11887	0.0001302	25.11887	6.62E-05	25.11887	3.706E-05
31.622785	2.765E-05	31.622785	3.553E-05	31.622785	1.458E-05
39.81073	8.609E-06	39.81073	1.19E-05	39.81073	4.92E-06
50.118743	2.822E-06	50.118743	2.731E-06	50.118743	1.501E-06
63.095762	8.975E-07	63.095762	7.896E-07	63.095762	4.878E-07
79.432863	3.483E-07	79.432863	2.919E-07	79.432863	1.418E-07
100.00005	1.114E-07	100.00005	1.154E-07	100.00005	4.575E-08
125.89258	4.837E-08	125.89258	2.876E-08	125.89258	1.623E-08
158.48934	1.988E-08	158.48934	1.14E-08	158.48934	6.211E-09
199.52621	5.019E-09	199.52621	4.777E-09	199.52621	2.461E-09
251.18856	2.808E-09	251.18856	2.419E-09	251.18856	8.126E-10
316.22759	1.496E-09	316.22759	9.722E-10	316.22759	3.732E-10
398.10686	5.564E-10	398.10686	4.46E-10	398.10686	2.251E-10
501.18674	4.622E-10	501.18674	3.643E-10	501.18674	1.234E-10
630.95658	1.554E-10	630.95658	1.338E-10	630.95658	4.32E-11
794.3271	3.052E-11	794.3271	3.58E-11	794.3271	8.108E-12
999.99835	8.614E-12	999.99835	6.591E-12	999.99835	3.056E-12
1258.9231	2.222E-12	1258.9231	3.014E-12	1258.9231	9.37E-13
1584.8899	2.129E-12	1584.8899	1.337E-12	1584.8899	5.87E-13
1995.2577	2.564E-12	1995.2577	1.385E-12	1995.2577	9.157E-13
2511.8801	5.877E-13	2511.8801	2.588E-13	2511.8801	1.57E-13
3162.269	1.458E-13	3162.269	5.85E-14	3162.269	3.177E-14
3981.0599	5.744E-14	3981.0599	1.863E-14	3981.0599	1.056E-14
5011.8564	1.916E-14	5011.8564	6.655E-15	5011.8564	3.471E-15
6309.552	8.249E-15	6309.552	3.827E-15	6309.552	1.686E-15
7943.2536	4.751E-15	7943.2536	3.623E-15	7943.2536	1.172E-15
9999.9616	1.68E-15	9999.9616	1.07E-15	9999.9616	4.222E-16
12589.21	6.566E-16	12589.21	3.086E-16	12589.21	1.607E-16
15848.873	2.312E-16	15848.873	1.1E-16	15848.873	5.385E-17
19952.544	7.379E-17	19952.544	3.389E-17	19952.544	1.659E-17
25118.76	2.764E-17	25118.76	1.074E-17	25118.76	5.431E-18
31622.638	1.328E-17	31622.638	4.38E-18	31622.638	2.218E-18
39810.533	5.882E-18	39810.533	2.046E-18	39810.533	9.43E-19
50118.481	1.261E-18	50118.481	8.065E-19	50118.481	2.453E-19
63095.416	3.332E-19	63095.416	2.606E-19	63095.416	5.064E-20
79432.405	1.392E-19	79432.405	8.747E-20	79432.405	1.705E-20
99999.451	5.76E-20	99999.451	3.772E-20	99999.451	1.057E-20
125891.82	5.857E-20	125891.82	1.061E-20	125891.82	1.013E-20
158488.38	4.41E-20	158488.38	3.672E-21	158488.38	6.228E-21
		199525	3.491E-21	199525	2.549E-21

3.6.3. Vitrain samples

323 rvp NU		326 kvx N + 326 kvp U		327 kvp NU	
r(Å)	**f(r)**	**r(Å)**	**f(r)**	**r(Å)**	**f(r)**
6.3095736	0.66949	6.3095736	0.604953	6.3095736	0.6425739
7.943283	0.0103096	7.943283	0.058872	7.943283	0.026625
10	0.0011096	10	0.0022228	10	0.0038248
12.589255	0.0003966	12.589255	0.000417	12.589255	0.001199
15.848934	0.0003904	15.848934	0.0005153	15.848934	0.000539
19.952626	0.0001251	19.952626	0.0004185	19.952626	0.0001645
25.11887	6.036E-05	25.11887	0.0001167	25.11887	5.293E-05
31.622785	2.094E-05	31.622785	2.969E-05	31.622785	2.102E-05
39.81073	4.59E-06	39.81073	1.57E-05	39.81073	5.829E-06
50.118743	1.83E-06	50.118743	3.525E-06	50.118743	1.515E-06
63.095762	5.863E-07	63.095762	7.691E-07	63.095762	3.692E-07
79.432863	1.381E-07	79.432863	1.22E-07	79.432863	1.099E-07
100.00005	2.607E-08	100.00005	3.315E-08	100.00005	4.139E-08
125.89258	6.778E-09	125.89258	1.325E-08	125.89258	1.392E-08
158.48934	2.423E-09	158.48934	4.677E-09	158.48934	4.973E-09
199.52621	1.204E-09	199.52621	1.439E-09	199.52621	1.486E-09
251.18856	3.351E-10	251.18856	5.196E-10	251.18856	5.37E-10
316.22759	7.814E-11	316.22759	9.546E-11	316.22759	3.346E-10
398.10686	2.766E-11	398.10686	1.386E-11	398.10686	1.251E-10
501.18674	4.934E-11	501.18674	4.594E-12	501.18674	8.056E-11
630.95658	1.406E-11	630.95658	4.621E-12	630.95658	2.336E-11
794.3271	8.284E-12	794.3271	1.643E-11	794.3271	6.322E-12
999.99835	2.836E-12	999.99835	1.567E-11	999.99835	2.658E-12
1258.9231	8.916E-13	1258.9231	5.51E-12	1258.9231	7.803E-13
1584.8899	4.696E-13	1584.8899	6.119E-13	1584.8899	4.451E-13
1995.2577	1.664E-13	1995.2577	2.573E-13	1995.2577	2.851E-13
2511.8801	5.116E-14	2511.8801	2.586E-13	2511.8801	7.735E-14
3162.269	1.486E-14	3162.269	4.888E-14	3162.269	1.737E-14
3981.0599	4.315E-15	3981.0599	1.241E-14	3981.0599	5.587E-15
5011.8564	1.432E-15	5011.8564	3.366E-15	5011.8564	2.21E-15
6309.552	5.809E-16	6309.552	1.28E-15	6309.552	1.287E-15
7943.2536	2.656E-16	7943.2536	6.925E-16	7943.2536	1.154E-15
9999.9616	1.111E-16	9999.9616	3.207E-16	9999.9616	3.285E-16
12589.21	5.572E-17	12589.21	2.621E-16	12589.21	9.004E-17
15848.873	2.745E-17	15848.873	1.638E-16	15848.873	3.608E-17
19952.544	1.023E-17	19952.544	3.875E-17	19952.544	1.297E-17
25118.76	4.315E-18	25118.76	1.696E-17	25118.76	4.607E-18
31622.638	2.242E-18	31622.638	7.315E-18	31622.638	2.157E-18
39810.533	1.59E-18	39810.533	3.905E-18	39810.533	8.607E-19
50118.481	1.406E-19	50118.481	2.004E-18	50118.481	2.241E-19
63095.416	4.941E-20	63095.416	4.117E-19	63095.416	7.23E-20
79432.405	2.053E-20	79432.405	1.331E-19	79432.405	3.727E-20
99999.451	3.397E-20	99999.451	1.291E-19	99999.451	2.087E-20
125891.82	1.103E-20	125891.82	8.909E-20	125891.82	8.667E-21
158488.38	6.939E-22	158488.38	2.555E-20	158488.38	1.996E-21

3.7. Specific surface area SAXS/USAXS

3.7.1. Renown seam matrix samples perpendicular

318 rmx ave		319 rmx ave		610 rmx ave		611 rmx ave		612 rmx ave	
Ave r(Å)	**Ave SSA**	**Ave r(Å)**	**Ave SSA**	**Ave r(Å)**	**Ave SSA**	**Ave r(Å)**	**Ave SSA**	**Ave r(Å)**	**Ave SSA**
5.0118722	3465225.9	5.0118722	2664655.7	5.0118722	3423381.4	5.0118722	1961001.2	5.0118722	1821261.4
6.3095736	723363.44	6.3095736	852804.15	6.3095736	777406.86	6.3095736	660751.48	6.3095736	518438.79
7.943283	716533.22	7.943283	696999.29	7.943283	744249.25	7.943283	484464.9	7.943283	337177.51
10	715328.25	10	655394.06	10	733072.29	10	479378.76	10	288603.02
12.589255	712947.31	12.589255	620877.8	12.589255	728577.91	12.589255	436580.76	12.589255	279936.11
15.848934	569729.52	15.848934	556852.11	15.848934	664954.76	15.848934	405085.03	15.848934	271498.96
19.952626	530549.98	19.952626	471026.23	19.952626	547184.64	19.952626	319606.24	19.952626	232046.62
25.11887	423845.33	25.11887	362577.04	25.11887	427774.5	25.11887	290191.23	25.11887	191524.84
31.622785	257179.02	31.622785	251640.44	31.622785	297869.37	31.622785	178777.53	31.622785	130491.35
39.81073	167945.01	39.81073	160510.76	39.81073	189286.95	39.81073	131946.04	39.81073	99034.673
50.118743	90454.367	50.118743	92417.486	50.118743	111187.25	50.118743	80418.216	50.118743	60098.463
63.095762	41445.565	63.095762	51820.697	63.095762	67524.53	63.095762	41650.032	63.095762	43276.871
79.432863	28135.589	79.432863	33633.449	79.432863	43011.188	79.432863	28237.167	79.432863	28683.382
100.00005	22578.036	100.00005	24221.264	100.00005	28580.065	100.00005	20002.732	100.00005	18463.284
125.89258	16139.415	125.89258	18792.556	125.89258	20897.248	125.89258	14549.086	125.89258	14365.344
158.48934	12529.971	158.48934	14681.104	158.48934	16508.141	158.48934	10896.247	158.48934	11182.722
199.52621	11026.517	199.52621	11441.899	199.52621	12895.91	199.52621	7987.0872	199.52621	8282.1878
251.18856	8937.77	251.18856	9135.0817	251.18856	9231.658	251.18856	6834.8015	251.18856	6369.3051
316.22759	7196.9038	316.22759	7253.5359	316.22759	7026.831	316.22759	5578.6169	316.22759	5004.5063
398.10686	5503.0829	398.10686	5823.9098	398.10686	5600.3946	398.10686	4172.4489	398.10686	4087.5487
501.18674	4711.8719	501.18674	4705.4352	501.18674	4312.6476	501.18674	3555.0047	501.18674	3156.4385
630.95658	3952.8665	630.95658	3768.7536	630.95658	3056.036	630.95658	2776.3948	630.95658	2433.6441
794.3271	3209.851	794.3271	2969.2149	794.3271	2549.9845	794.3271	2298.2177	794.3271	1990.2868
999.99835	2328.218	999.99835	2305.1061	999.99835	1975.8667	999.99835	1932.3588	999.99835	1615.8254
1258.9231	2053.2092	1258.9231	1838.2897	1258.9231	1345.5807	1258.9231	1676.3491	1258.9231	1216.5962
1584.8899	1455.3715	1584.8899	1438.098	1584.8899	1065.9226	1584.8899	1280.4545	1584.8899	978.84452
1995.2577	921.21216	1995.2577	1136.9766	1995.2577	831.03063	1995.2577	1071.1286	1995.2577	767.86591
2511.8801	822.40903	2511.8801	937.30858	2511.8801	634.64376	2511.8801	885.37166	2511.8801	644.39911
3162.269	593.08258	3162.269	764.83243	3162.269	523.54825	3162.269	671.78687	3162.269	520.80783
3981.0599	422.68288	3981.0599	624.30181	3981.0599	383.04494	3981.0599	545.50525	3981.0599	402.16331
5011.8564	333.21838	5011.8564	506.07054	5011.8564	284.81273	5011.8564	425.09927	5011.8564	336.47333
6309.552	239.56943	6309.552	343.26906	6309.552	205.09023	6309.552	291.0647	6309.552	232.73853
7943.2536	169.28442	7943.2536	255.44459	7943.2536	137.34842	7943.2536	242.84646	7943.2536	193.41876
9999.9616	126.35564	9999.9616	177.65718	9999.9616	111.6776	9999.9616	160.57258	9999.9616	126.03964
12589.21	71.579477	12589.21	120.54174	12589.21	90.223285	12589.21	120.38326	12589.21	75.503603
15848.873	63.675549	15848.873	74.775365	15848.873	48.9093	15848.873	50.538124	15848.873	44.539881

3.7.2. Renown seam matrix samples parallel

318 rmp ave		319 rmp ave		610 rmp ave		611 rmp ave		612 rmp ave	
Ave r(Å)	**Ave SSA**	**Ave r(Å)**	**Ave SSA**	**Ave r(Å)**	**Ave SSA**	**Ave r(Å)**	**Ave SSA**	**Ave r(Å)**	**Ave SSA**
5.0118722	2333499.8	5.0118722	1911207	5.0118722	1662063.2	5.0118722	1037361.8	5.2714125	574367.53
6.3095736	937564.33	6.3095736	791631.26	6.3095736	526915.79	6.3095736	449629.33	6.6363155	456567.13
7.943283	632311.83	7.943283	554242.19	7.943283	469805.93	7.943283	351054.49	8.3546264	383321.78
10	524061.12	10	458197.01	10	439079	10	304792.57	10.517851	167974.19
12.589255	472575.85	12.589255	415550.04	12.589255	354516.36	12.589255	225226.45	13.241191	106440.86
15.848934	440843.93	15.848934	381771.02	15.848934	330895.54	15.848934	172952.61	16.669672	102091.71
19.952626	395482.86	19.952626	358067.36	19.952626	313892.71	19.952626	164803.67	20.985875	94444.359
25.11887	331270.44	25.11887	308274.38	25.11887	259014.03	25.11887	141846.36	26.419653	86059.293
31.622785	260399.57	31.622785	246478.52	31.622785	209417.71	31.622785	112374.2	33.260374	60609.863
39.81073	193403.66	39.81073	199342.72	39.81073	158015.57	39.81073	87787.488	41.872333	46019.756
50.118743	131577.01	50.118743	137280.37	50.118743	113489.78	50.118743	62405.111	52.714147	32121.974
63.095762	83804.659	63.095762	93911.117	63.095762	76020.813	63.095762	43482.166	66.363182	21619.009
79.432863	49762.586	79.432863	60338.301	79.432863	48809.658	79.432863	25774.763	83.546301	14024.687
100.00005	32503.698	100.00005	38296.669	100.00005	31542.256	100.00005	16299.373	105.17856	8370.4359
125.89258	23960.979	125.89258	27525.268	125.89258	23426.233	125.89258	10562.902	132.41193	5616.1593
158.48934	17799.811	158.48934	20444.505	158.48934	16796.176	158.48934	7455.0986	166.69671	3890.7225
199.52621	13149.821	199.52621	15520.28	199.52621	12526.607	199.52621	5521.0819	209.85868	2898.0501
251.18856	9851.4606	251.18856	12581.033	251.18856	9821.5229	251.18856	4104.9361	264.19637	2049.1804
316.22759	7864.6321	316.22759	9753.5292	316.22759	7498.188	316.22759	3065.5571	332.60345	1490.332
398.10686	6305.8656	398.10686	7972.7279	398.10686	5874.2814	398.10686	2426.9761	418.72284	1181.2396
501.18674	5057.7253	501.18674	6796.6075	501.18674	4616.8349	501.18674	1893.6719	527.14071	999.08932
630.95658	4229.7124	630.95658	5725.149	630.95658	3675.8444	630.95658	1526.9312	663.63069	790.89214
794.3271	3400.2186	794.3271	4649.0033	794.3271	2941.3153	794.3271	1195.365	835.46135	650.98224
999.99835	2805.4519	999.99835	3842.1852	999.99835	2296.9137	999.99835	998.68875	1051.7833	560.13725
1258.9231	2335.6003	1258.9231	2980.5061	1258.9231	1894.9415	1258.9231	792.96803	1324.1164	497.08948
1584.8899	1872.8912	1584.8899	2500.0705	1584.8899	1498.2909	1584.8899	641.7767	1666.9635	424.98168
1995.2577	1568.1852	1995.2577	2015.9298	1995.2577	1235.956	1995.2577	509.3791	2098.5822	364.37131
2511.8801	1254.2091	2511.8801	1661.3225	2511.8801	997.68466	2511.8801	410.74528	2641.9579	327.11659
3162.269	1019.0176	3162.269	1324.9145	3162.269	817.78619	3162.269	336.23939	3326.0272	290.35506
3981.0599	755.51271	3981.0599	992.23295	3981.0599	648.38701	3981.0599	253.43245	4187.2192	239.90599
5011.8564	596.07881	5011.8564	824.89784	5011.8564	530.14128	5011.8564	212.41163	5271.3955	206.76898
6309.552	447.38014	6309.552	585.18599	6309.552	409.48219	6309.552	155.89279	6636.2923	159.80552
7943.2536	292.52824	7943.2536	474.84716	7943.2536	365.42185	7943.2536	113.5742	8354.5952	123.32947
9999.9616	207.73947	9999.9616	371.57377	9999.9616	285.14507	9999.9616	95.179872	10517.811	84.945937
12589.21	171.46953	12589.21	309.23458	12589.21	228.79837	12589.21	60.671178	13241.142	51.415041
15848.873	138.24894	15848.873	208.25724	15848.873	150.73587	15848.873	39.411266	16669.607	37.677954
19952.544	79.919268	19952.544	127.24047	19952.544	66.435891	19952.544	19.215156	20985.787	21.874451
25118.76	39.481633	25118.76	70.812178						

3.7.3. Kupakupa seam matrix samples perpendicular

320 kmx ave		321 kmx ave		322 kmx ave	
Ave r(Å)	**Ave SSA**	**Ave r(Å)**	**Ave SSA**	**Ave r(Å)**	**Ave SSA**
5.0118722	3592392.5	5.0118722	2549726.3	5.0118722	3388619.7
6.3095736	1081934.1	6.3095736	1063029.1	6.3095736	1294430.4
7.943283	876953.68	7.943283	822346.93	7.943283	1099085.5
10	844499.7	10	745201.9	10	1059300.5
12.589255	822178.54	12.589255	700147	12.589255	1038366.6
15.848934	739826.24	15.848934	638146.86	15.848934	901147.13
19.952626	656944.81	19.952626	540252.94	19.952626	779242.89
25.11887	484305.74	25.11887	401650.22	25.11887	574634.73
31.622785	345571.57	31.622785	298389	31.622785	409549.06
39.81073	218639.13	39.81073	196290.51	39.81073	255419.3
50.118743	131136.63	50.118743	124783.36	50.118743	154894.09
63.095762	87978.313	63.095762	77972.078	63.095762	97909.381
79.432863	61935.12	79.432863	50626.53	79.432863	70260.38
100.00005	45928.497	100.00005	35835.998	100.00005	52437.298
125.89258	35410.724	125.89258	26802.831	125.89258	40252.674
158.48934	27134.272	158.48934	20534.022	158.48934	31589.215
199.52621	21100.17	199.52621	15649.375	199.52621	25060.114
251.18856	16731.638	251.18856	12153.717	251.18856	19855.312
316.22759	12908.52	316.22759	9670.9844	316.22759	15955.337
398.10686	10071.37	398.10686	7838.118	398.10686	12849.898
501.18674	8074.2438	501.18674	6616.3	501.18674	10759.236
630.95658	6023.7003	630.95658	5537.1533	630.95658	8395.957
794.3271	4534.8436	794.3271	4530.9932	794.3271	6886.1099
999.99835	3489.0142	999.99835	3587.8138	999.99835	5622.5614
1258.9231	2526.2743	1258.9231	2891.0736	1258.9231	4453.0861
1584.8899	1811.1624	1584.8899	2397.3328	1584.8899	3502.7466
1995.2577	1313.4371	1995.2577	1923.7479	1995.2577	2826.471
2511.8801	949.40419	2511.8801	1530.7842	2511.8801	2154.6155
3162.269	697.5512	3162.269	1164.6345	3162.269	1591.4961
3981.0599	539.97958	3981.0599	924.89517	3981.0599	1109.0688
5011.8564	354.86791	5011.8564	719.01422	5011.8564	781.89709
6309.552	237.92078	6309.552	471.37313	6309.552	489.35487
7943.2536	178.21804	7943.2536	368.33588	7943.2536	338.21881
9999.9616	118.79207	9999.9616	254.38967	9999.9616	209.15458
12589.21	77.222382	12589.21	174.64881	12589.21	110.39021
15848.873	34.5622	15848.873	98.869566		
19952.544	14.904176	19952.544	70.610958		

3.7.4. Kupakupa seam matrix samples parallel

320 kmp ave		321 kmp ave		322 kmp ave	
Ave r(Å)	**Ave SSA**	**Ave r(Å)**	**Ave SSA**	**Ave r(Å)**	**Ave SSA**
5.0118722	894148.2	5.0118722	2515367.9	5.2714125	1469594.9
6.3095736	467760.69	6.3095736	572824.53	6.6363155	611792.38
7.943283	307589.51	7.943283	523882.49	8.3546264	430769.9
10	238794.52	10	509896.21	10.517851	373726.11
12.589255	218709.77	12.589255	493795.42	13.241191	349821.45
15.848934	203986.36	15.848934	406302.87	16.669672	328509.59
19.952626	172546.33	19.952626	378645.72	20.985875	288626.17
25.11887	157530.33	25.11887	326423.53	26.419653	242888.33
31.622785	121182.06	31.622785	247813.45	33.260374	198081.86
39.81073	101578.15	39.81073	193756	41.872333	156701.28
50.118743	78153.905	50.118743	134027.33	52.714147	114633.37
63.095762	60641.686	63.095762	89057.217	66.363182	81319.362
79.432863	46361.044	79.432863	62122.085	83.546301	58892.96
100.00005	35879.323	100.00005	43108.708	105.17856	42368.775
125.89258	28254.219	125.89258	26477.657	132.41193	32225.163
158.48934	22628.793	158.48934	18804.855	166.69671	25390.897
199.52621	18228.738	199.52621	14357.417	209.85868	20116.32
251.18856	15012.696	251.18856	10620.791	264.19637	15750.056
316.22759	12312.194	316.22759	8390.8396	332.60345	12326.382
398.10686	10163.463	398.10686	6551.4205	418.72284	10070.742
501.18674	8520.392	501.18674	5330.2536	527.14071	8391.1541
630.95658	7229.0955	630.95658	4448.9334	663.63069	6752.1185
794.3271	5962.1358	794.3271	3294.815	835.46135	5709.3665
999.99835	4966.5823	999.99835	2584.1242	1051.7833	4636.0886
1258.9231	4133.6944	1258.9231	2305.1336	1324.1164	3764.2991
1584.8899	3451.3092	1584.8899	1746.0093	1666.9635	3136.1379
1995.2577	2807.5092	1995.2577	1395.37	2098.5822	2682.427
2511.8801	2351.3051	2511.8801	1193.2407	2641.9579	2148.0658
3162.269	1926.7897	3162.269	884.6578	3326.0272	1758.7989
3981.0599	1497.0738	3981.0599	726.12521	4187.2192	1298.2032
5011.8564	1253.7837	5011.8564	542.18242	5271.3955	958.59055
6309.552	917.24967	6309.552	420.06805	6636.2923	600.47571
7943.2536	703.54012	7943.2536	333.74625	8354.5952	458.70411
9999.9616	544.28875	9999.9616	233.02894	10517.811	331.42036
12589.21	403.95174	12589.21	185.86446	13241.142	224.28828
15848.873	271.33145	15848.873	135.75666	16669.607	180.96797
19952.544	168.72083	19952.544	93.571732	20985.787	116.80968
25118.76	77.902514	25118.76	58.286481	25118.76	61.029338

3.7.5. Vitrain samples perpendicular

323 rvx ave		326 kvx ave		327 kvx ave		328 kvx ave	
Ave r(Å)	**Ave SSA**	**Ave r(Å)**	**Ave SSA**	**Ave r(Å)**	**Ave SSA**	**Ave r(Å)**	**Ave SSA**
5.0118722	2953145.8	5.0118722	6708058.2	5.0118722	3444507.4	5.0118722	3482710.6
6.3095736	1611526.7	6.3095736	1658504.8	6.3095736	1264326.5	6.3095736	1144304.3
7.943283	1505916.9	7.943283	1639443.1	7.943283	1219024.7	7.943283	1091999.4
10	1480309.1	10	1636147.4	10	1211669.8	10	1080554.7
12.589255	1467382.3	12.589255	1631054.6	12.589255	1203470.1	12.589255	1075007.4
15.848934	1247680.9	15.848934	1393424.3	15.848934	1067583.7	15.848934	1016400.3
19.952626	1079988.2	19.952626	1180542.6	19.952626	891526.91	19.952626	809148.56
25.11887	864284.7	25.11887	966177.75	25.11887	648403.75	25.11887	636950.68
31.622785	509466.73	31.622785	671314.3	31.622785	410980.95	31.622785	397898.73
39.81073	237390.21	39.81073	416698.53	39.81073	200008.25	39.81073	190903.65
50.118743	45479.367	50.118743	240904.07	50.118743	69216.803	50.118743	53863.27
63.095762	18859.695	63.095762	117238.04	63.095762	37003.291	63.095762	25953.277
79.432863	12450.448	79.432863	53917.26	79.432863	25248.721	79.432863	19128.246
100.00005	9873.6206	100.00005	35742.842	100.00005	18585.413	100.00005	14832.399
125.89258	8081.4463	125.89258	25557.162	125.89258	13500.619	125.89258	11111.981
158.48934	6364.7	158.48934	19028.57	158.48934	9488.5061	158.48934	8151.6077
199.52621	4800.6117	199.52621	12360.682	199.52621	6888.2729	199.52621	6514.7059
251.18856	3651.4248	251.18856	8057.7866	251.18856	5340.3792	251.18856	5392.5132
316.22759	3069.9887	316.22759	6394.5911	316.22759	4261.5776	316.22759	4364.2932
398.10686	2685.5323	398.10686	5310.3363	398.10686	3440.2219	398.10686	3835.8177
501.18674	2380.2872	501.18674	3987.2664	501.18674	2800.4525	501.18674	3389.1618
630.95658	2225.2318	630.95658	2813.6705	630.95658	2429.8904	630.95658	2729.9385
794.3271	2003.8894	794.3271	2417.4977	794.3271	2183.2711	794.3271	2287.8442
999.99835	1790.915	999.99835	1928.4488	999.99835	1910.7085	999.99835	2106.4398
1258.9231	1647.6836	1258.9231	1545.1125	1258.9231	1670.1023	1258.9231	1713.834
1584.8899	1493.7259	1584.8899	1176.9651	1584.8899	1467.6725	1584.8899	1418.6209
1995.2577	1349.008	1995.2577	915.25705	1995.2577	1245.5697	1995.2577	1194.1356
2511.8801	1224.1414	2511.8801	729.77693	2511.8801	1074.0474	2511.8801	908.69401
3162.269	1100.9494	3162.269	628.80903	3162.269	890.02278	3162.269	743.89713
3981.0599	970.33269	3981.0599	464.74235	3981.0599	711.23307	3981.0599	495.68071
5011.8564	758.19531	5011.8564	307.51676	5011.8564	561.08337	5011.8564	426.23351
6309.552	550.25291	6309.552	197.53098	6309.552	366.86596	6309.552	245.79902
7943.2536	386.46802	7943.2536	156.98913	7943.2536	274.83769	7943.2536	182.96252
9999.9616	267.07074	9999.9616	107.99875	9999.9616	173.45692	9999.9616	129.77546
12589.21	142.48632	12589.21	77.198079	12589.21	112.44509	12589.21	52.800949
15848.873	68.803597	15848.873	29.515073	15848.873	40.134111	15848.873	38.61554

3.7.6. Vitrain samples parallel

323 rvp ave		327 kvp ave		328 kvp ave	
Ave r(Å)	**Ave SSA**	**Ave r(Å)**	**Ave SSA**	**Ave r(Å)**	**Ave SSA**
5.0118722	4098536.6	5.0118722	2135631.1	5.0118722	2954983.3
6.3095736	737696.11	6.3095736	720517.3	6.3095736	751511.66
7.943283	723102.35	7.943283	693667.69	7.943283	633260.06
10	720657.43	10	687896.9	10	607411.58
12.589255	717754.21	12.589255	643070.04	12.589255	591920.79
15.848934	629756.4	15.848934	563072.07	15.848934	568188.94
19.952626	602795.73	19.952626	498155.06	19.952626	502656.32
25.11887	459711.93	25.11887	371155.73	25.11887	406247.38
31.622785	347317.09	31.622785	243114.9	31.622785	338963.77
39.81073	251075.75	39.81073	152141.33	39.81073	250435.46
50.118743	162813.47	50.118743	79293.027	50.118743	160748.54
63.095762	97235.333	63.095762	41122.515	63.095762	83696.773
79.432863	57719.49	79.432863	27313.863	79.432863	39730.536
100.00005	34459.634	100.00005	19035.445	100.00005	16749.068
125.89258	20583.201	125.89258	14621.509	125.89258	6901.2742
158.48934	13362.381	158.48934	11026.376	158.48934	3370.5685
199.52621	8712.4403	199.52621	8880.1461	199.52621	2084.5936
251.18856	5863.0276	251.18856	7464.0272	251.18856	1505.7498
316.22759	4048.1223	316.22759	6287.1796	316.22759	1166.6757
398.10686	2871.3631	398.10686	5172.3259	398.10686	924.18448
501.18674	2491.9689	501.18674	4643.752	501.18674	734.51511
630.95658	1904.3033	630.95658	4133.7815	630.95658	583.35323
794.3271	1349.5877	794.3271	3686.0879	794.3271	477.04067
999.99835	1069.782	999.99835	3285.5686	999.99835	413.11116
1258.9231	891.0324	1258.9231	2852.6599	1258.9231	355.84598
1584.8899	777.20309	1584.8899	2425.4327	1584.8899	297.51243
1995.2577	599.28817	1995.2577	2324.6183	1995.2577	259.96189
2511.8801	509.39667	2511.8801	2034.0961	2511.8801	224.9571
3162.269	383.96709	3162.269	1723.8966	3162.269	191.83334
3981.0599	351.18048	3981.0599	1506.593	3981.0599	165.18595
5011.8564	262.29986	5011.8564	1166.9168	5011.8564	151.05305
6309.552	218.61989	6309.552	991.0811	6309.552	125.46938
7943.2536	176.98912	7943.2536	737.38879	7943.2536	108.54574
9999.9616	139.8733	9999.9616	554.26267	9999.9616	95.535245
12589.21	118.58049	12589.21	417.89554	12589.21	77.148116
15848.873	79.860901	15848.873	283.68446	15848.873	59.988586
		19952.544	185.31679	19952.544	35.722135
		25118.76	128.12132	25118.76	17.94676

3.8. Specific surface area SANS/USANS

3.8.1. Renown seam matrix samples

318 rmp N + U		319 rmx N + 319 rmp U		610 rmp NU		611 rmx N + 611 rmp U		612 rmx N + 612 rmp U	
r(Å)	SSA	r(Å)	SSA	r(Å)	SSA	r(Å)	SSA	r(Å)	SSA
6.30957	9872525	6.30957	17096538	6.30957	13120831	6.30957	21304652	6.30957	13371204
7.94328	1917977.625	7.94328	1158002.75	7.94328	1027670.563	7.94328	1130524.125	7.94328	664348.125
10.00000	1110747.125	10.00000	703428.4375	10.00000	476733.625	10.00000	375879.2188	10.00000	664148.3125
12.58925	818321.75	12.58925	561543.375	12.58925	351309.375	12.58925	239120.375	12.58925	663276.25
15.849	538325.563	15.849	366086.000	15.849	277843.906	15.849	182821.984	15.849	285170.406
19.953	202488.984	19.953	181240.484	19.953	200369.984	19.953	147568.234	19.953	192872.563
25.119	144117.516	25.119	134785.125	25.119	130063.797	25.119	119713.938	25.119	117298.430
31.623	114233.234	31.623	85563.289	31.623	87299.039	31.623	90629.344	31.623	79415.852
39.811	68909.352	39.811	57968.148	39.811	56182.320	39.811	61246.414	39.811	54124.242
50.119	43238.281	50.119	29782.117	50.119	38022.414	50.119	33305.125	50.119	35398.113
63.096	29658.340	63.096	20213.355	63.096	26146.775	63.096	19661.303	63.096	26269.064
79.433	17830.143	79.433	16305.347	79.433	16974.115	79.433	16922.736	79.433	21318.197
100.000	12649.185	100.000	13755.396	100.000	12614.797	100.000	13975.649	100.000	17558.955
125.893	10755.832	125.893	11317.359	125.893	9725.546	125.893	11884.531	125.893	14795.105
158.489	8896.896	158.489	9976.615	158.489	7776.702	158.489	9136.388	158.489	12453.580
199.526	7033.910	199.526	8724.657	199.526	6254.650	199.526	7781.002	199.526	11006.213
251.189	6073.221	251.189	7637.889	251.189	5383.803	251.189	7485.562	251.189	9896.718
316.228	5407.143	316.228	6930.107	316.228	4486.777	316.228	7400.501	316.228	9093.133
398.107	4898.567	398.107	6146.342	398.107	3958.088	398.107	7367.729	398.107	8129.184
501.187	4410.315	501.187	4924.979	501.187	3339.479	501.187	7347.401	501.187	6959.151
630.957	3796.425	630.957	3769.389	630.957	2742.554	630.957	7329.982	630.957	5699.767
794.327	3235.128	794.327	2442.943	794.327	2274.887	794.327	7293.845	794.327	4325.142
999.998	2396.357	999.998	1536.111	999.998	1663.277	999.998	7159.339	999.998	3467.271
1258.923	2105.721	1258.923	1246.912	1258.923	1322.276	1258.923	4803.947	1258.923	2956.524
1584.890	1252.784	1584.890	927.257	1584.890	1222.675	1584.890	2978.826	1584.890	2622.932
1995.258	1057.849	1995.258	773.388	1995.258	1038.146	1995.258	2826.203	1995.258	2418.622
2511.880	542.489	2511.880	700.648	2511.880	443.640	2511.880	1676.719	2511.880	551.019
3162.269	315.413	3162.269	616.243	3162.269	292.396	3162.269	1319.712	3162.269	344.136
3981.060	201.247	3981.060	523.260	3981.060	240.798	3981.060	1053.452	3981.060	301.671
5011.856	153.596	5011.856	446.252	5011.856	206.193	5011.856	729.108	5011.856	287.389
6309.552	132.533	6309.552	209.468	6309.552	184.316	6309.552	580.707	6309.552	281.078
7943.254	122.034	7943.254	118.538	7943.254	159.604	7943.254	452.986	7943.254	273.370
9999.962	115.554	9999.962	103.297	9999.962	108.927	9999.962	316.693	9999.962	202.520
12589.210	108.014	12589.210	94.654	12589.210	76.050	12589.210	236.423	12589.210	101.269
15848.873	84.662	15848.873	90.888	15848.873	54.064	15848.873	172.224	15848.873	73.491
19952.544	63.655	19952.544	86.112	19952.544	38.850	19952.544	131.633	19952.544	53.136
25118.760	54.773	25118.760	54.450	25118.760	29.453	25118.760	109.048	25118.760	35.100
31622.638	38.530	31622.638	32.698	31622.638	23.687	31622.638	91.976	31622.638	27.829
39810.533	27.818	39810.533	27.083	39810.533	18.665	39810.533	77.248	39810.533	20.695
50118.481	20.647	50118.481	24.862	50118.481	14.093	50118.481	66.467	50118.481	13.921
63095.416	15.938	63095.416	15.148	63095.416	11.917	63095.416	64.227	63095.416	9.403
79432.405	7.794	79432.405	0.106	79432.405	11.012	79432.405	63.763	79432.405	6.247
99999.451	6.171	99999.451	0.012	99999.451	10.384	99999.451	63.506	99999.451	4.356
125891.822	4.261			125891.822	9.696	125891.822	62.824	125891.822	2.303
158488.380	1.646			158488.380	7.516	158488.380	54.468		
				199525.005	4.061	199525.005	28.060		

3.8.2. Kupakupa seam matrix samples

320 kmp NU		321 kmx N + 321 kmp U		322 kmp NU	
r(Å)	**SSA**	**r(Å)**	**SSA**	**r(Å)**	**SSA**
6.309573618	6082433.5	6.309573618	9370453	6.309573618	17141068
7.943283001	3436247.75	7.943283001	2732824.75	7.943283001	1925220
10	1416966.125	10	1117858.875	10	873320.125
12.58925481	543055.6875	12.58925481	720108.125	12.58925481	586926
15.84893366	241200.6719	15.84893366	525492.3125	15.84893366	408303.9688
19.95262644	156717.0156	19.95262644	298724.8438	19.95262644	270253.4688
25.11886983	123365.2109	25.11886983	188421.4219	25.11886983	182151.4531
31.62278528	71153.46094	31.62278528	140272.5	31.62278528	127426.2344
39.81073017	49028.86719	39.81073017	88714.875	39.81073017	84458.64844
50.11874262	35283.875	50.11874262	54244.08203	50.11874262	55531.92969
63.09576216	26293.33789	63.09576216	38467.12109	63.09576216	37918.41016
79.43286272	20588.53906	79.43286272	29364.51758	79.43286272	26500.67773
100.0000549	16170.5791	100.0000549	22650.62109	100.0000549	19876.60156
125.8925826	13351.72363	125.8925826	17355.73438	125.8925826	15613.04004
158.4893366	10909.61426	158.4893366	14722.03027	158.4893366	12596.38184
199.5262096	8906.693359	199.5262096	12638.51367	199.5262096	10292.34863
251.1885604	7897.775879	251.1885604	10897.00781	251.1885604	8470.972656
316.2275924	6771.772461	316.2275924	9137.859375	316.2275924	7270.915527
398.1068646	5574.789551	398.1068646	7726.899414	398.1068646	6171.124023
501.1867384	4686.412598	501.1867384	6435.452148	501.1867384	4847.935547
630.9565824	3214.014893	630.9565824	4330.863281	630.9565824	3400.198486
794.3271009	2226.439941	794.3271009	2788.33252	794.3271009	2389.104492
999.9983531	1839.395142	999.9983531	1964.998047	999.9983531	2010.443115
1258.923062	1621.412598	1258.923062	1662.5177	1258.923062	1725.707642
1584.889886	1509.248047	1584.889886	1386.515747	1584.889886	1551.505615
1995.257714	1294.74646	1995.257714	1142.253784	1995.257714	1333.7323
2511.880088	779.4398193	2511.880088	637.2148438	2511.880088	655.9840698
3162.26898	543.7205811	3162.26898	448.9854736	3162.26898	424.1188354
3981.059904	427.0880737	3981.059904	364.0816345	3981.059904	330.4938965
5011.856378	335.3830566	5011.856378	310.1378174	5011.856378	268.4333801
6309.551969	274.3293152	6309.551969	271.6879272	6309.551969	227.7163544
7943.253567	221.8942719	7943.253567	227.5687714	7943.253567	188.2479248
9999.961572	161.6420135	9999.961572	144.2458344	9999.961572	133.5010071
12589.20989	119.1320496	12589.20989	95.1269455	12589.20989	94.15855408
15848.87276	85.98152161	15848.87276	66.8659668	15848.87276	64.28012085
19952.54428	62.69428635	19952.54428	46.76506042	19952.54428	44.30482864
25118.75951	47.86217117	25118.75951	34.4119072	25118.75951	32.02451706
31622.63772	36.77614975	31622.63772	26.60118103	31622.63772	24.00349045
39810.53347	26.14905548	39810.53347	20.24517441	39810.53347	17.46849442
50118.48124	16.75697517	50118.48124	14.32170105	50118.48124	11.92411995
63095.41578	12.74121857	63095.41578	9.662268639	63095.41578	9.046251297
79432.40485	10.62307739	79432.40485	6.658148289	79432.40485	7.86087513
99999.45102	8.858017921	99999.45102	4.646250248	99999.45102	7.064673901
125891.8224	7.400355339	125891.8224	2.915066242	125891.8224	6.080001354
158488.3796	4.442989349	158488.3796	1.943376064	158488.3796	4.197169781
		199525.0047	1.272562385	199525.0047	1.886697769

3.8.3. Vitrain samples

323 rvp NU		326 kvx N + 326 kvp U		327 kvp NU	
r(Å)	**SSA**	**r(Å)**	**SSA**	**r(Å)**	**SSA**
6.309573618	17764450	6.309573618	14672050	6.309573618	15165008
7.943283001	1189059.5	7.943283001	3210683	7.943283001	2060773
10	679775.4375	10	985202.1875	10	977399.8125
12.58925481	570404.8125	12.58925481	817544.3125	12.58925481	666876
15.84893366	492409.875	15.84893366	754790.375	15.84893366	472645.125
19.95262644	339232.1563	19.95262644	600053.3125	19.95262644	298438.5313
25.11886983	241297.3281	25.11886983	349310.4688	25.11886983	192376.1094
31.62278528	147009.7813	31.62278528	209767.0313	31.62278528	124272.5859
39.81073017	81733.42188	39.81073017	138955.9219	39.81073017	70299.9375
50.11874262	53187.42969	50.11874262	64250.10547	50.11874262	40441.10938
63.09576216	30482.94922	63.09576216	30783.04883	63.09576216	24955.1582
79.43286272	15966.26367	79.43286272	16211.6709	79.43286272	17425.33008
100.0000549	9146.302734	100.0000549	11598.89355	100.0000549	12953.38965
125.8925826	6576.76123	125.8925826	9098.705078	125.8925826	9593.067383
158.4893366	5243.817383	158.4893366	7104.921387	158.4893366	7337.958008
199.5262096	4293.140625	199.5262096	5700.558594	199.5262096	5730.687012
251.1885604	3350.676025	251.1885604	4838.191895	251.1885604	4772.688965
316.2275924	2827.140381	316.2275924	4217.030273	316.2275924	4081.716064
398.1068646	2583.589111	398.1068646	3989.340332	398.1068646	3222.617188
501.1867384	2411.544189	501.1867384	3923.397705	501.1867384	2581.700439
630.9565824	1799.306152	630.9565824	3879.774902	630.9565824	1758.315918
794.3271009	1451.091064	794.3271009	3792.226074	794.3271009	1281.838379
999.9983531	1041.851685	999.9983531	3171.11499	999.9983531	1024.603394
1258.923062	762.2816162	1258.923062	1989.204956	1258.923062	808.8406372
1584.889886	586.9458008	1584.889886	1160.064575	1584.889886	682.4384155
1995.257714	402.6853333	1995.257714	976.3295288	1995.257714	538.5620728
2511.880088	272.4199829	2511.880088	822.1628418	2511.880088	354.7206726
3162.26898	192.506134	3162.26898	513.0484619	3162.26898	255.1943359
3981.059904	146.1830902	3981.059904	396.4638977	3981.059904	210.5998077
5011.856378	119.3500061	5011.856378	337.4039612	5011.856378	181.9823914
6309.551969	101.5780945	6309.551969	305.4465027	6309.551969	159.3960724
7943.253567	87.19665527	7943.253567	281.1916504	7943.253567	133.1476288
9999.961572	74.07440186	9999.961572	255.0145264	9999.961572	86.18462372
12589.20989	63.12860107	12589.20989	230.8289185	12589.20989	59.51143265
15848.87276	52.17036057	15848.87276	191.3880615	15848.87276	44.92543411
19952.54428	41.39900208	19952.54428	142.207077	19952.54428	33.26446152
25118.75951	33.38938904	25118.75951	118.9886932	25118.75951	24.89916992
31622.63772	26.64898109	31622.63772	98.71111298	31622.63772	18.97164345
39810.53347	19.66179276	39810.53347	81.26395416	39810.53347	13.43316364
50118.48124	9.771762848	50118.48124	62.6817131	50118.48124	9.024213791
63095.41578	8.027688026	63095.41578	43.64945602	63095.41578	6.734089851
79432.40485	6.804325104	79432.40485	35.84961319	79432.40485	5.259597301
99999.45102	5.790071964	99999.45102	30.81665802	99999.45102	3.743202448
125891.8224	2.442094803	125891.8224	21.07959557	125891.8224	2.049093008
158488.3796	0.272286713	158488.3796	7.673008919	158488.3796	0.645124078

3.9. Calculated porosity SANS/USANS

		Micropores 10-20A	Mesopores 20-500A	Macropores 500-100,000A	Total Porosity 10-100,000A
Renown seam	318	9.22	5.44	3.22	17.88
	319	11.70	4.26	5.30	21.26
	610	8.58	4.97	2.19	15.74
	611	14.23	5.02	5.58	24.83
	612	10.10	5.06	3.66	18.82
Kupakupa seam	320	8.57	4.00	3.04	15.61
	321	12.28	3.22	3.31	18.81
	322	14.02	5.72	2.92	22.66
Vitrain	323	12.43	6.89	1.87	21.19
	326	10.56	7.17	6.03	23.76
	327	11.55	6.57	2.00	20.12

3.10. Calculated volume fractions for average scattering curves of vitrain samples

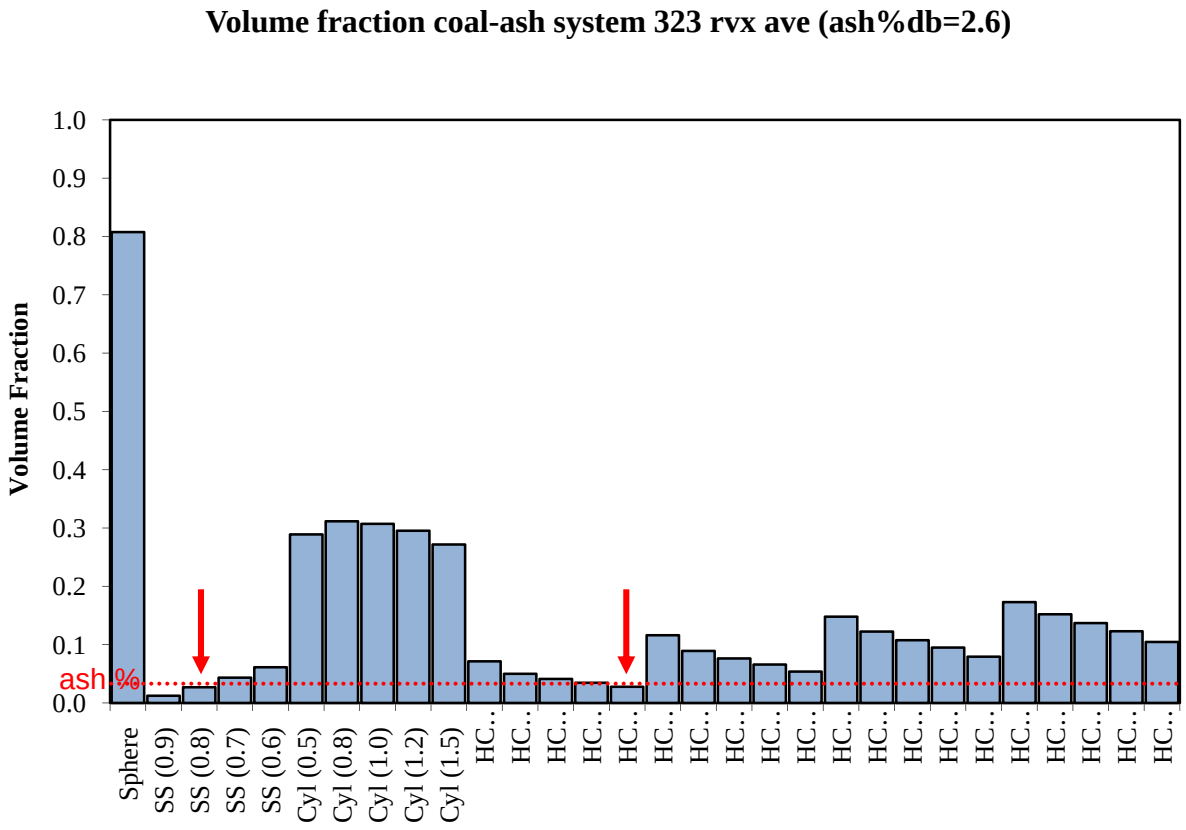

Volume fraction coal-ash system 326 kvx ave (ash%db=2.6)

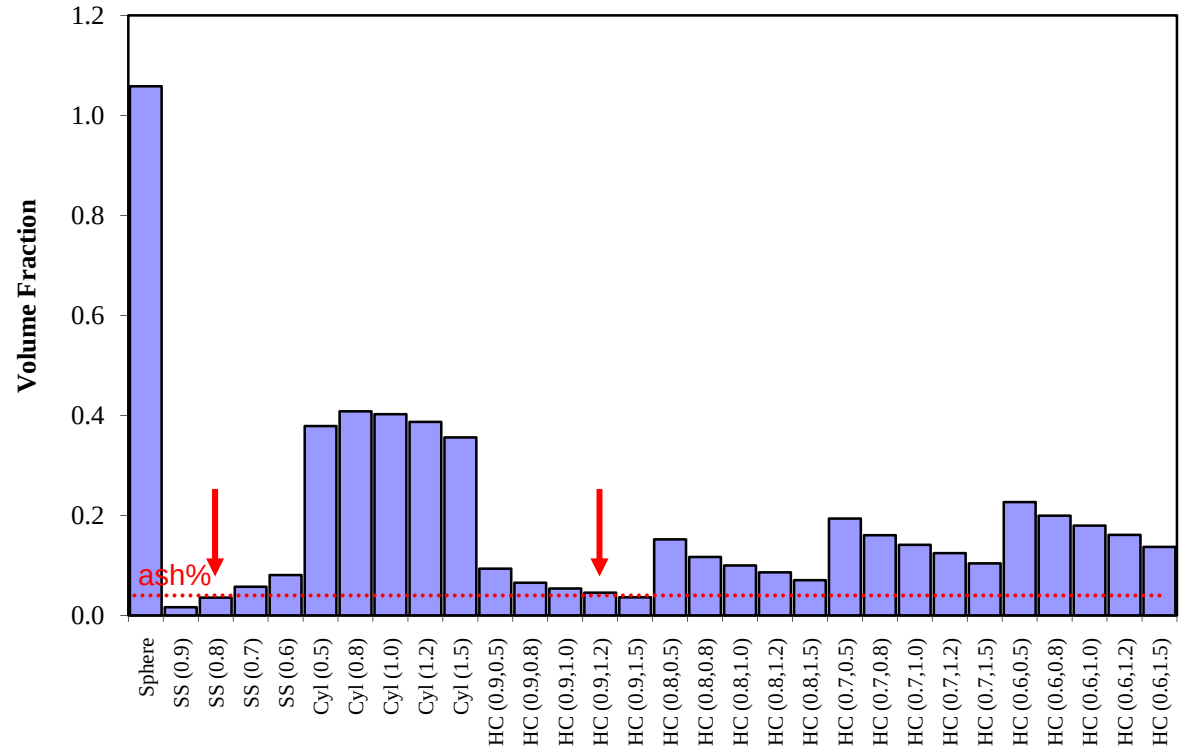

Volume fraction coal-ash system 327 kvx ave (ash%db=2.2)

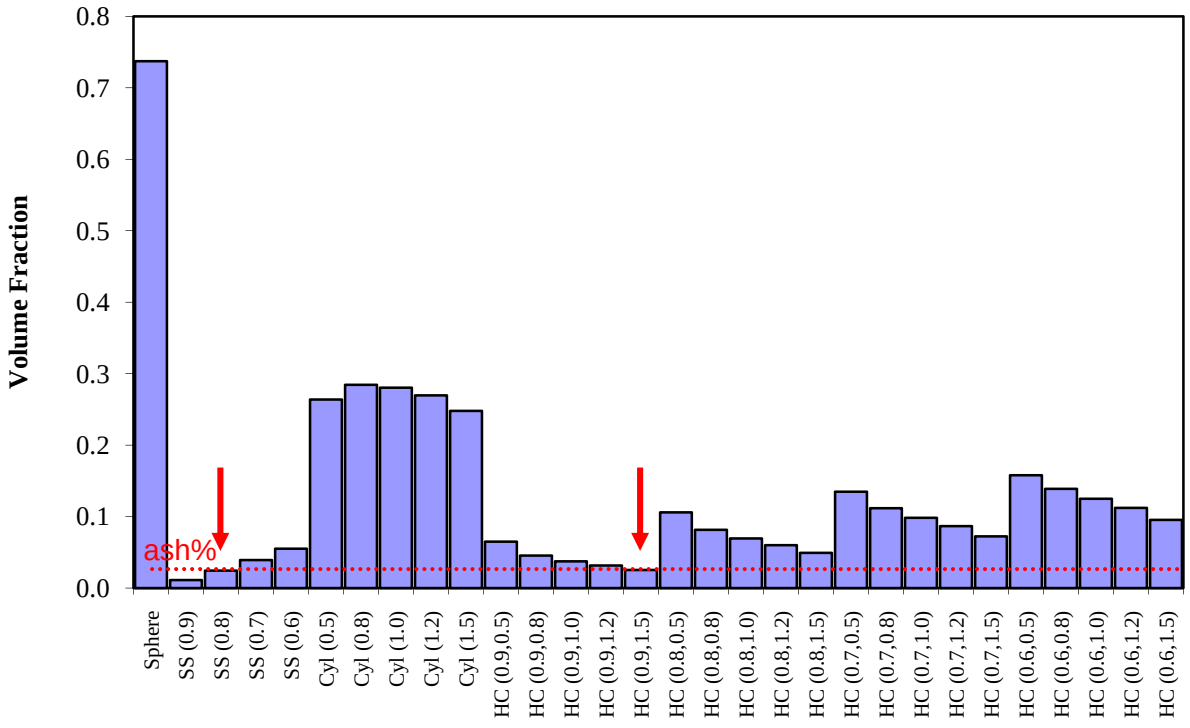

Volume fraction coal-ash system 328 kvx ave (ash%db=2.6)

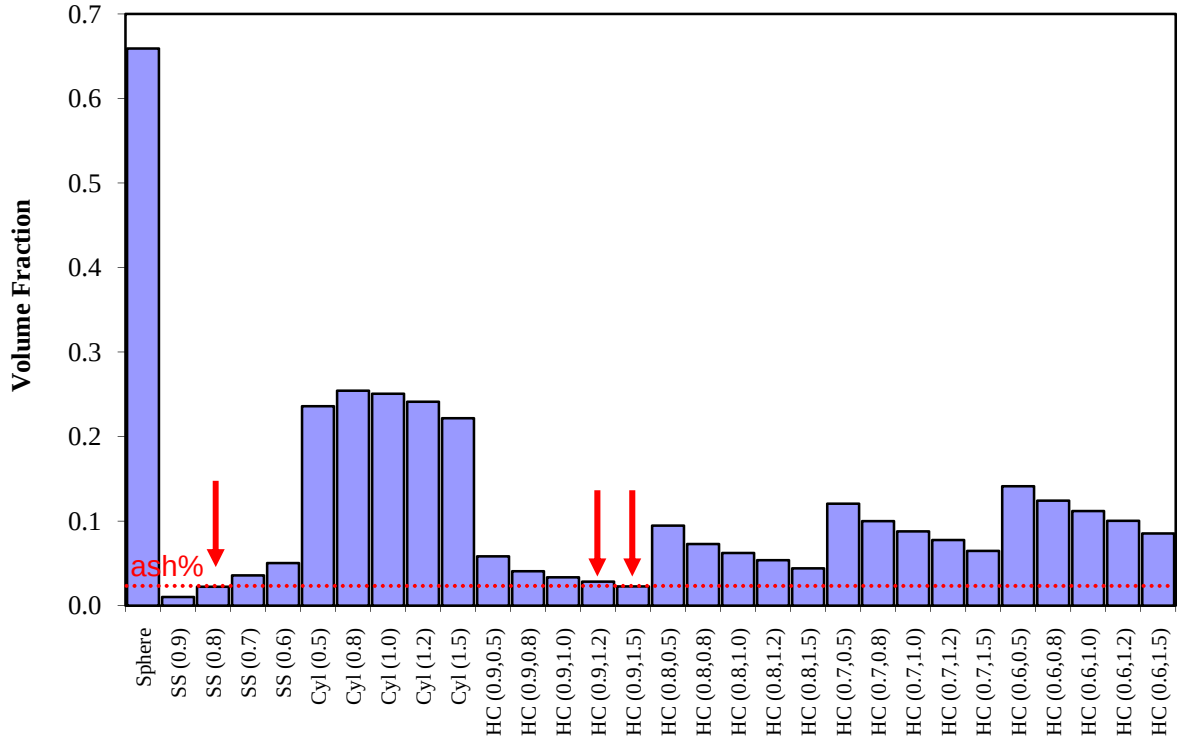

Volume fraction coal-ash system 328 kvp ave (ash%db=2.6)

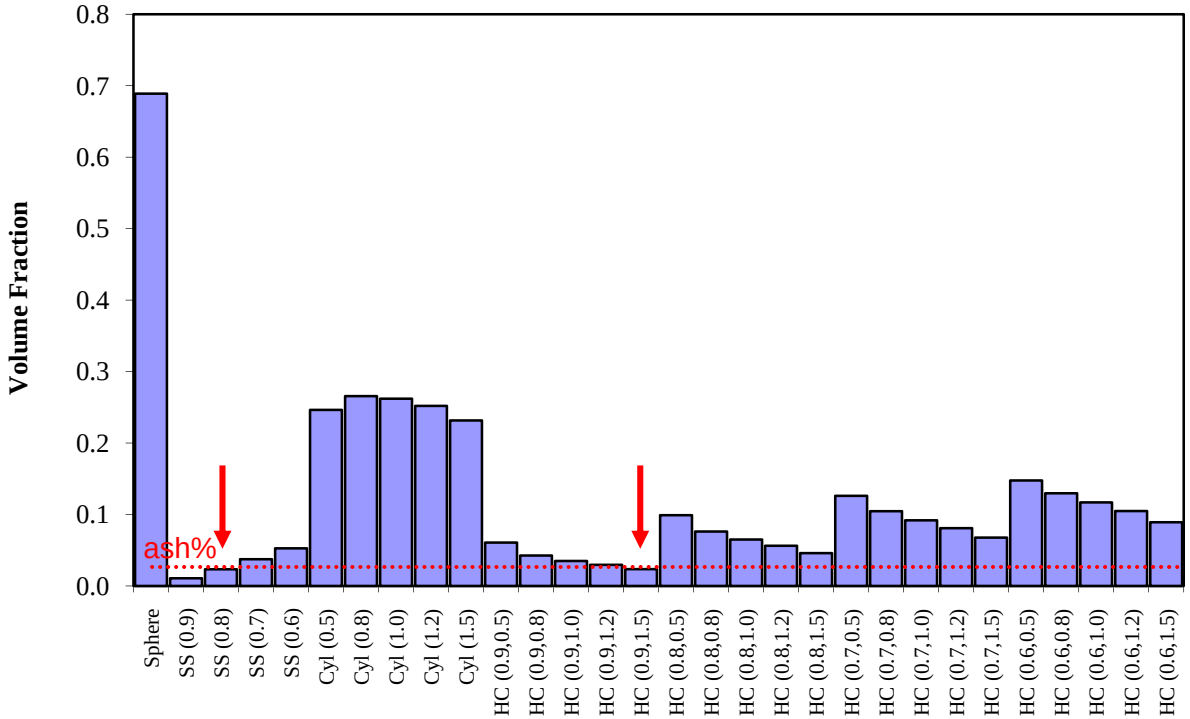

Appendix 4: Gas data

4.1. Adsorption isotherm data

4.1.1. Methane adsorption capacity

Well	Sample	Collect	Depth From	Depth To	Seam	Ash % (eqm moist)	Eqm Moist	Helium density	Test temp	P_L aa	V_L aa	P_L daf	V_L daf
Ma 1		Field	486.80	486.90	Renown	1.70	20.70	1.33	35.10	3.84	4.94	3.84	6.37
Jasp		Field	411.85	412.01	Renown	2.30	20.50	1.30	31.50	5.90	7.11	5.90	9.22
Mimi		Field	407.19	407.48	Renown	2.10	21.90	1.32	31.50	3.25	5.75	3.25	7.57
Ru 1	A	Field	422.35	422.45	Kupakupa	1.00	18.90	1.34	32.60	4.30	4.37	4.30	5.46
Ru 2	A	Field	458.04	458.20	Kupakupa	10.90	18.00	1.39	33.60	3.92	5.28	3.92	7.42
Ro 1		Field	449.29	449.39	Kupakupa	1.40	20.10	1.34	33.10	3.26	5.05	3.26	6.43
Ro 1		Field	452.28	452.40	Kupakupa	0.80	19.00	1.32	33.10	3.99	4.24	3.99	5.28
Ma 1		Field	511.98	512.10	Kupakupa	1.20	19.50	1.28	35.10	7.41	7.90	7.41	9.96
Ru 2	B10	post	438.09	438.19	Renown	1.80	20.50	1.30	33.60	4.41	7.62	4.41	9.80
Ro 1	C4	post	436.02	436.15	Renown	2.30	20.90	1.31	33.30	4.65	7.67	4.65	9.99
Ma 1	D3	post	483.64	483.75	Renown	3.00	19.10	1.32	35.10	3.40	7.41	3.40	9.52
Jasp	J1	post	407.81	408.31	Renown	37.90	17.00	1.57	32.00	4.57	5.82	4.57	12.89
Jasp	J2	post	408.31	408.81	Renown	4.70	22.30	1.30	32.00	8.35	9.57	8.35	13.11
Jasp	J3	post	408.81	409.31	Renown	1.20	23.50	1.29	32.00	6.89	8.09	6.89	10.75
Jasp	J4	post	409.31	409.81	Renown	2.90	23.60	1.29	32.00	6.79	6.99	6.79	9.51
Jasp	J5	post	410.00	410.35	Renown	3.40	21.10	1.29	32.00	9.66	10.28	9.66	13.62
Jasp	J6	post	410.35	410.85	Renown	1.90	21.40	1.31	32.00	3.94	4.18	3.94	5.45
Jasp	J7	post	410.85	411.35	Renown	2.20	19.80	1.30	32.00	5.39	7.60	5.39	9.74
Jasp	J8	post	411.35	411.85	Renown	1.90	20.80	1.32	32.00	2.43	5.67	2.43	7.34
Jasp	J9	post	412.00	412.50	Renown	1.40	24.50	1.28	32.00	4.61	6.67	4.61	9.00
Jasp	J10	post	412.50	413.00	Renown	1.50	22.80	1.28	32.00	5.77	7.70	5.77	10.17
Jasp	J11	post	413.00	413.55	Renown	3.90	23.60	1.31	32.00	2.76	4.81	2.76	6.64
Jasp	J12	post	413.55	414.02	Renown	64.60	13.70	1.92	32.00	2.10	1.54	2.10	7.07
Jasp	J13	post	414.02	414.40	Renown	69.00	12.20	1.93	32.00	7.31	1.91	7.31	10.15
Mimi	M4	post	409.03	409.58	Renown	4.40	21.20	1.33	32.00	6.32	6.34	6.32	8.53
Ru2	B22	post	461.49	461.58	Kupakupa	1.20	20.10	1.29	33.60	6.23	7.69	6.23	9.77
Ro 1	C11	post	450.05	450.16	Kupakupa	1.00	19.10	1.30	33.30	5.43	6.94	5.43	8.68
Ma 1	D20	post	517.32	517.45	Kupakupa	31.70	15.70	1.52	35.10	7.34	6.03	7.34	11.46

Ru 1 = Ruawaro 1, Ru 2 = Ruawaro 2, Ro 1 = Rotongaro 1, Ma 1 = Mangapiko 1, Jasp = Jasper 1.
Eqm = Equilibrium, P_L = Langmuir pressure, V_L = Langmuir volume, aa = as analysed, daf = dry ash-free.

4.1.2. Carbon dioxide adsorption capacity

Well	Sample	Collect	Depth From	Depth To	Seam	Ash % (eqm moist)	Eqm Moist	Helium density	Test temp	PL aa	VL aa	PL daf	VL daf
Ma 1		Field	486.80	486.90	Renown	1.70	20.70	1.33	35.10	4.66	36.98	4.66	47.63
Jasp		Field	411.85	412.01	Renown	2.30	20.50	1.30	31.50	3.60	33.41	3.60	42.92
Mimi		Field	407.19	407.48	Renown	2.10	21.90	1.32	31.50	3.88	35.34	3.88	46.73
Ru 1	A	Field	422.35	422.45	Kupakupa	1.00	18.90	1.34	32.60	3.83	35.37	3.83	44.15
Ru 2	A	Field	458.04	458.20	Kupakupa	10.90	18.00	1.39	33.60	4.25	34.55	4.25	48.60
Ma 1		Field	511.98	512.10	Kupakupa	1.20	19.50	1.28	35.10	5.21	42.93	5.21	54.12

Ru 1 = Ruawaro 1, Ru 2 = Ruawaro 2, Ro 1 = Rotongaro 1, Ma 1 = Mangapiko 1, Jasp = Jasper 1.
Eqm = Equilibrium, P_L = Langmuir pressure, V_L = Langmuir volume, aa = as analysed, daf = dry ash-free.

4.2. Gas content data

Well	Can	Seam	Mid-point	Ash % aa	Gas Content (m3/t) aa				TG
					Lost	Measured	Residual	Total	daf
TW1	9	Renown	338.95	5.5	0.04	1.10	0.27	1.41	1.70
TW1	10	Renown	339.45	3.8	0.05	1.10	0.21	1.36	1.63
TW1	11	Renown	339.95	2.9	0.05	1.00	0.22	1.27	1.44
TW1	12	Renown	340.45		0.05	1.30	0.54	1.89	
TW1	13	Renown	340.95	2.8	0.06	1.10	0.25	1.41	1.67
TW1	14	Renown	341.45	3.0	0.06	1.10	0.20	1.36	1.58
TW1	15	Renown	341.95	2.7	0.04	0.90	0.22	1.16	1.39
TW1	16	Renown	342.45	1.8	0.03	0.70	0.74	1.47	1.71
TW1	17	Renown	342.95	1.7	0.02	0.60	0.96	1.58	1.83
TW1	18	Renown	343.45	3.9	0.04	0.80	0.81	1.65	1.97
TW1	19	Renown	343.95	1.6	0.02	0.60	0.86	1.48	1.71
TW1	20	Renown	344.45	1.7	0.03	0.80	0.78	1.61	1.91
TW1	21	Renown	344.95	3.0	0.03	0.90	0.37	1.30	1.54
TW1	22	Renown	345.45	9.0	0.06	1.10	0.36	1.52	1.94
TW1	23	Renown	345.95		0.08	1.60	0.20	1.88	
TW1	24	Renown	346.45	33.4	0.05	0.70	0.13	0.88	1.51
TW1	25	Kupakupa	346.95	10.7	0.06	1.00	0.45	1.51	1.93
TW1	26	Kupakupa	347.45	5.2	0.11	1.20	0.34	1.65	2.01
TW1	27	Kupakupa	347.95	6.2	0.02	0.60	0.97	1.59	1.96
TW1	28	Kupakupa	348.45	3.4	0.03	1.00	0.37	1.40	1.73
TW1	29	Kupakupa	348.95	5.0	0.02	0.90	0.88	1.80	2.19
TW1	30	Kupakupa	349.45	3.8	0.04	1.10	0.50	1.64	1.98
TW1	31	Kupakupa	349.95	1.6	0.03	0.90	0.83	1.76	2.08
TW1	32	Kupakupa	350.70	2.1	0.03	1.00	0.63	1.66	1.95
TW1	33	Kupakupa	351.45	1.4	0.02	0.70	0.84	1.56	1.78
TW1	34	Kupakupa	351.95		0.02	1.20	0.66	1.88	
TW1	35	Kupakupa	352.45	4.7	0.02	0.60	1.07	1.69	2.01
TW1	36	Kupakupa	353.05	1.4	0.02	0.60	1.06	1.68	1.95
TW1	37	Kupakupa	353.80	1.5	0.05	1.20	0.61	1.86	2.13
TW1	38	Kupakupa	354.45	1.0	0.05	1.30	0.54	1.89	2.17
TW1	39	Kupakupa	354.95	1.0	0.06	1.40	0.28	1.74	1.99
TW1	40	Kupakupa	355.45		0.06	1.60	0.26	1.92	
TW1	41	Kupakupa	355.95	1.1	0.05	1.20	0.35	1.60	1.85
TW1	42	Kupakupa	356.45	2.3	0.08	1.20	0.77	2.05	2.39
TW1	43	Kupakupa	356.95	1.2	0.02	0.50	1.13	1.65	1.91
TW1	44	Kupakupa	357.45	1.0	0.03	0.90	0.94	1.87	2.15
TW1	45	Kupakupa	357.95	12.5	0.03	0.80	0.83	1.66	2.21

Appendix 4: Gas data

Well	Can	Seam	Mid-point	Ash % aa	Gas Content (m3/t) aa				TG
					Lost	Measured	Residual	Total	daf
Ruawaro 1	A3	Ngaro	387.65	2.5	0.12	0.58	0.33	1.03	1.36
Ruawaro 1	A2	Ngaro	388.09	3.1	0.19	0.59	0.24	1.02	1.32
Ruawaro 1	A6	Renown	396.75	2.9	0.09	0.75	0.38	1.22	1.47
Ruawaro 1	A5	Renown	397.29	3.5	0.09	0.78	0.34	1.21	1.53
Ruawaro 1	A4	Renown	397.81	8.6	0.12	0.40	0.33	0.85	1.15
Ruawaro 1	A7	Renown	398.25	66.9	0.27	0.17	0.07	0.51	2.22
Ruawaro 1	A8	Renown	401.18	3.1	0.10	0.80	0.28	1.18	1.54
Ruawaro 1	A9	Renown	401.68	5.7	0.13	0.84	0.28	1.26	1.67
Ruawaro 1	A10	Renown	402.70	4.5	0.12	1.00	0.14	1.26	1.63
Ruawaro 1	A11	Renown	403.20	7.4	0.09	0.39	0.22	0.70	0.94
Ruawaro 1	A12	Renown	406.57	62.2	0.29	0.30	0.07	0.66	2.48
Ruawaro 1	A16	Kupakupa	417.78	2.9	0.29	0.45	0.32	1.06	1.35
Ruawaro 1	A15	Kupakupa	418.20	3.2	0.17	0.87	0.27	1.31	1.69
Ruawaro 1	A14	Kupakupa	418.70	2.6	0.16	0.85	0.25	1.26	1.61
Ruawaro 1	A13	Kupakupa	419.20	1.6	0.01	0.75	0.45	1.37	1.70
Ruawaro 1	A17	Kupakupa	419.99	1.5	0.06	0.77	0.36	1.19	1.50
Ruawaro 1	A18	Kupakupa	420.53	1.3	0.09	0.76	0.39	1.24	1.54
Ruawaro 1	A19	Kupakupa	421.08	1.6	0.07	0.70	0.37	1.14	1.44
Ruawaro 1	A20	Kupakupa	421.60	1.2	0.07	0.62	0.49	1.18	1.45
Ruawaro 1	A21	Kupakupa	422.10	1.4	0.07	0.77	0.33	1.17	1.48
Ruawaro 1	A22	Kupakupa	422.70	1.4	0.07	0.77	0.50	1.34	1.65
Ruawaro 1	A23	Kupakupa	423.20	1.5	0.06	0.90	0.27	1.23	1.56
Ruawaro 1	A24	Kupakupa	423.70	2	0.08	0.94	0.13	1.15	1.49
Ruawaro 1	A25	Kupakupa	424.20	1.6	0.09	0.83	0.30	1.22	1.56
Ruawaro 1	A26	Kupakupa	424.70	1.7	0.08	0.89	0.37	1.34	1.70
Ruawaro 1	A27	Kupakupa	430.60	4.2	0.14	0.47	0.33	0.94	1.25
Ruawaro 2	B1	Renown	433.66	3	0.12	2.01	1.05	3.19	4.07
Ruawaro 2	B2	Renown	434.14	11.1	0.12	1.31	0.50	1.93	2.75
Ruawaro 2	B3	Renown	434.59	2	0.04	1.96	0.50	2.50	3.21
Ruawaro 2	B4	Renown	435.09	1.9	0.15	1.61	0.35	2.11	2.72
Ruawaro 2	B5	Renown	435.59	2.1	0.34	2.11	0.14	2.59	3.36
Ruawaro 2	B6	Renown	436.02	2.1	0.57	2.18	0.24	2.99	3.88
Ruawaro 2	B7	Renown	436.44	2.1	0.21	1.97	0.67	2.85	3.61
Ruawaro 2	B8	Renown	436.94	2	0.21	2.12	0.89	3.22	4.07
Ruawaro 2	B9	Renown	437.44	1.9	0.05	1.88	0.31	2.24	2.91
Ruawaro 2	B10	Renown	437.94	2.3	0.21	2.17	0.33	2.71	3.47
Ruawaro 2	B11	Renown	438.44	11.3	0.09	1.03	0.41	1.53	2.17
Ruawaro 2	B12	Renown	438.94	4.7	0.13	0.85	0.13	1.11	1.60
Ruawaro 2	B13	Renown	439.44	3.3	0.19	1.02	0.13	1.34	1.82
Ruawaro 2	B14	Renown	439.94	2.8	0.25	2.25	0.16	2.66	3.53
Ruawaro 2	B15	Renown	440.34	31.2	0.44	1.33	0.11	1.88	3.70

Appendix 4: Gas data

Well	Can	Seam	Mid-point	Ash % aa	Gas Content (m3/t) aa				TG
					Lost	Measured	Residual	Total	daf
Ruawaro 2	B16	Kupakupa	458.45	2.4	0.09	1.02	1.00	2.11	2.65
Ruawaro 2	B17	Kupakupa	458.95	2	0.12	1.28	0.76	2.16	2.72
Ruawaro 2	B18	Kupakupa	459.45	2.1	0.12	1.35	0.80	2.27	2.86
Ruawaro 2	B19	Kupakupa	459.95	1.6	0.20	1.57	0.70	2.47	3.15
Ruawaro 2	B20	Kupakupa	460.45	1.6	0.22	1.75	0.37	2.34	2.99
Ruawaro 2	B21	Kupakupa	460.95	1.6	0.09	1.46	0.83	2.38	3.00
Ruawaro 2	B22	Kupakupa	461.45	1.4	0.14	1.54	0.78	2.46	3.00
Ruawaro 2	B23	Kupakupa	461.98	1.4	0.15	1.43	0.81	2.39	2.90
Ruawaro 2	B24	Kupakupa	462.55	1.6	0.19	1.57	0.79	2.55	3.18
Ruawaro 2	B25	Kupakupa	463.13	1.8	0.13	1.45	0.72	2.30	2.86
Ruawaro 2	B26	Kupakupa	463.73	6.3	0.10	1.48	0.27	1.85	2.50
Rotongaro 1	C1	Ngaro	428.64	27.5	0.20	1.03	0.09	1.32	2.57
Rotongaro 1	C2	Renown	435.15	4.5	0.08	0.34	0.24	0.66	0.86
Rotongaro 1	C3	Renown	435.65	2.1	0.06	0.37	0.20	0.63	0.82
Rotongaro 1	C4	Renown	436.15	5.2	0.04	0.42	0.21	0.67	0.88
Rotongaro 1	C5	Renown	436.73	13.2	0.09	0.48	0.12	0.69	1.04
Rotongaro 1	C6	Kupakupa	447.59	9.8	0.14	0.29	0.18	0.61	0.85
Rotongaro 1	C7	Kupakupa	448.14	2.4	0.17	0.26	0.24	0.67	0.88
Rotongaro 1	C8	Kupakupa	448.64	2.7	0.10	0.25	0.27	0.62	0.81
Rotongaro 1	C9	Kupakupa	449.09	2.5	0.19	0.26	0.19	0.64	0.83
Rotongaro 1	C10	Kupakupa	449.66	1.7	0.10	0.40	0.21	0.71	0.92
Rotongaro 1	C11	Kupakupa	450.21	1.8	0.11	0.21	0.31	0.63	0.78
Rotongaro 1	C12	Kupakupa	450.71	4	0.10	0.23	0.30	0.63	0.78
Rotongaro 1	C13	Kupakupa	451.21	2.7	0.10	0.23	0.24	0.57	0.73
Rotongaro 1	C14	Kupakupa	452.65	1.6	0.09	0.19	0.27	0.55	0.70
Rotongaro 1	C15	Kupakupa	453.15	1.4	0.01	0.10	0.32	0.43	0.54
Rotongaro 1	C16	Kupakupa	453.65	1.3	0.10	0.18	0.31	0.59	0.74
Rotongaro 1	C17	Kupakupa	454.15	1.6	0.12	0.17	0.25	0.54	0.68
Rotongaro 1	C18	Kupakupa	454.65	1.6	0.12	0.29	0.22	0.63	0.80
Rotongaro 1	C19	Kupakupa	455.15	1.7	0.09	0.23	0.20	0.52	0.66
Rotongaro 1	C30	Kupakupa	455.65	1.4	0.07	0.16	0.29	0.52	0.66
Rotongaro 1	C21	Kupakupa	456.15	1.6	0.06	0.19	0.21	0.46	0.57
Rotongaro 1	C22	Kupakupa	456.65	1.4	0.06	0.13	0.20	0.39	0.50
Rotongaro 1	C23	Kupakupa	457.15	1.4	0.03	0.15	0.30	0.48	0.60
Rotongaro 1	C24	Kupakupa	457.65	1.5	0.05	0.14	0.25	0.44	0.56
Rotongaro 1	C25	Kupakupa	458.15	1.4	0.09	0.22	0.28	0.59	0.74
Rotongaro 1	C26	Kupakupa	458.70	1.9	0.04	0.17	0.26	0.47	0.59

Appendix 4: Gas data

Well	Can	Seam	Mid-point	Ash % aa	Gas Content (m3/t) aa				TG
					Lost	Measured	Residual	Total	daf
Mangapiko 1	D1	Renown	482.60	24.4	0.06	0.51	0.12	0.69	1.19
Mangapiko 1	D2	Renown	483.10	38.9	0.08	0.54	0.17	0.79	1.72
Mangapiko 1	D3	Renown	483.60	2.9	0.04	0.58	0.37	0.99	1.28
Mangapiko 1	D4	Renown	484.10	2.7	0.04	0.52	0.38	0.94	1.22
Mangapiko 1	D5	Renown	484.60	4.4	0.06	0.62	0.33	1.01	1.32
Mangapiko 1	D6	Renown	485.05	2.4	0.08	0.61	0.35	1.04	1.32
Mangapiko 1	D7	Renown	485.55	2.7	0.04	0.69	0.39	1.12	1.43
Mangapiko 1	D8	Renown	486.05	2.2	0.03	0.52	0.48	1.03	1.30
Mangapiko 1	D9	Renown	486.55	2.1	0.04	0.66	0.36	1.06	1.37
Mangapiko 1	D10	Renown	487.10	3.5	0.03	0.57	0.17	0.77	1.02
Mangapiko 1	D11	Kupakupa	512.35	1.5	0.03	0.30	0.16	0.49	0.63
Mangapiko 1	D12	Kupakupa	512.85	1.8	0.09	0.40	0.06	0.55	0.79
Mangapiko 1	D13	Kupakupa	513.35	1.6	0.03	0.32	0.14	0.49	0.64
Mangapiko 1	D14	Kupakupa	513.85	1.6	0.04	0.34	0.16	0.54	0.71
Mangapiko 1	D15	Kupakupa	514.65	1.4	0.02	0.18	0.27	0.47	0.60
Mangapiko 1	D16	Kupakupa	515.15	1.5	0.03	0.26	0.19	0.48	0.61
Mangapiko 1	D17	Kupakupa	515.65	1.6	0.03	0.30	0.16	0.49	0.62
Mangapiko 1	D18	Kupakupa	516.15	1.6	0.02	0.23	0.18	0.43	0.55
Mangapiko 1	D19	Kupakupa	516.68	3	0.04	0.29	0.15	0.48	0.63
Mangapiko 1	D20	Kupakupa	517.23	14	0.03	0.21	0.12	0.36	0.53
Baco 1	B1	Renown	428.18	3.3	0.64	1.83	0.14	2.62	3.30
Baco 1	B2	Renown	428.73	2.4	0.64	1.93	0.43	3.00	3.71
Baco 1	B3	Renown	429.25	2.9	0.25	1.89	0.10	2.23	2.74
Baco 1	B4	Renown	429.75	2.5	0.37	2.05	0.14	2.56	3.11
Baco 1	B5	Renown	430.25	2.2	0.30	1.93	0.09	2.33	2.85
Baco 1	B6	Renown	430.75	2.2	0.33	2.02	0.10	2.44	2.97
Jasper 1	J1	Renown	408.06	40.9	0.18	1.27	0.23	1.68	3.21
Jasper 1	J2	Renown	408.56	9	0.25	1.68	0.43	2.36	2.96
Jasper 1	J3	Renown	409.06	4.2	0.19	2.05	0.68	2.91	3.43
Jasper 1	J4	Renown	409.56	4.9	0.21	1.96	0.22	2.39	2.92
Jasper 1	J5	Renown	410.18	3.7	0.26	1.76	0.32	2.34	2.76
Jasper 1	J6	Renown	410.60	2.6	0.14	1.84	0.61	2.59	3.05
Jasper 1	J7	Renown	411.10	2.7	0.13	1.87	0.57	2.57	2.99
Jasper 1	J8	Renown	411.60	2.6	0.13	1.85	0.41	2.39	2.78
Jasper 1	J9	Renown	412.25	2.3	0.16	1.98	0.67	2.81	3.26
Jasper 1	J10	Renown	412.75	2.4	0.14	1.87	0.63	2.64	3.07
Jasper 1	J11	Renown	413.28	5.2	0.15	1.86	0.25	2.27	2.73
Jasper 1	J12	CM	413.79	64.4	0.11	0.55	0.20	0.86	2.92
Jasper 1	J13	CM	414.21	69.2	0.13	0.50	0.08	0.71	2.64

Appendix 4: Gas data

Well	Can	Seam	Mid-point	Ash % aa	Gas Content (m3/t) aa				TG
					Lost	Measured	Residual	Total	daf
Mimi 1	M1	Renown	407.70	3.5	0.26	2.36	0.25	2.87	3.52
Mimi 1	M2	Renown	408.20	2.2	0.27	2.63	0.26	3.16	3.82
Mimi 1	M3	Renown	408.72	4.1	0.28	2.43	0.15	2.87	3.63
Mimi 1	M4	Renown	409.31	6.1	0.37	2.30	0.15	2.82	3.60
Mimi 1	M5	Renown	409.86	4.6	0.26	2.38	0.41	3.05	3.80
Mimi 1	M6	Renown	410.38	3.4	0.22	2.39	0.17	2.78	3.40
Mimi 1	M7	Renown	410.88	2.7	0.20	2.31	0.27	2.78	3.28
Mimi 1	M8	Renown	411.38	2.4	0.24	2.36	0.35	2.95	3.46
Mimi 1	M9	Renown	411.88	2.3	0.25	2.43	0.22	2.90	3.41
Mimi 1	M10	Renown	412.51	2.6	0.26	2.38	0.16	2.80	3.34
Mimi 1	M11	Renown	413.16	10.8	0.22	2.45	0.18	2.85	3.69
Mimi 1	M12	CM	413.83	64.3	0.14	0.58	0.15	0.87	2.79

CM = Coal measures, aa = as analysed, TG = total gas content, daf = dry ash-free.

Appendix 5: Publications

The following eight papers were published using work produced during the course of this study. The papers are included at the back of this thesis. Where possible, the papers are reprinted with their original pagination.

Mares, T.E. and Moore, T.A., 2007. Does size matter?: Compositional influences on gas content in an Eocene CBM play in New Zealand. 2007 Joint Meeting of the Canadian Society for Coal Science and Organic Petrology, The Society for Organic Petrology and the International Committee for Coal and Organic Petrology, Victoria, Canada, 39-40.

Mares, T.E. and Moore, T.A., 2008a. Assessing Coalbed Methane prospects: How reliable are your numbers? New Zealand Petroleum Conference, Auckland, 10th-12th March, Ministry of Economic Development, Wellington, New Zealand, unpaginated.

Mares, T.E. and Moore, T.A., 2008b. The influence of macroscopic texture on biogenically-derived coalbed methane, Huntly coalfield, New Zealand. International Journal of Coal Geology, 76(1-2): 175-185.

Mares, T.E., Moore, T.A. and Moore, C.R., 2009. Uncertainty of gas saturation estimates in a subbituminous coal seam. International Journal of Coal Geology, 77(3-4): 320-327.

Mares, T.E., Radlinski, A.P. and Moore, T.A., Cookson, D., Thiyagarajan, P., Ilavsky, J. and Klepp, J., 2009. Assessing the potential for CO_2 adsorption in a subbituminous coal, Huntly Coalfield, New Zealand, using Small Angle Scattering techniques. International Journal of Coal Geology, 77(1-2): 54-68.

Crosdale, P.J., Moore, T.A. and **Mares, T.E.,** 2008. Influence of moisture content and temperature on methane adsorption isotherm analysis for coals from a low rank, biogenically-sourced gas reservoir. International Journal of Coal Geology, 76(1-2): 166-174.

Moore, T.A., **Mares, T.E.** and Butland C.I., 2008. Gas saturation: controls and uncertainty in biogenically-derived coalbed methane, examples from New Zealand coal fields. 33rd International Geological Congress, 5th-14th August, Oslo, Norway.

Moore, T.A., **Mares, T.E.** and Moore, C.R., 2009. Assessing uncertainty of coalbed methane resources. IPA09-G-056, Thirty-Third Annual Convention & Exhibition, Indonesian Petroleum Association, Indonesia, 11 pp.

The candidate's contribution to the papers that she was first author on included:

- Conducting almost all field work
- Conducting all laboratory work except where otherwise noted
- Interpretation of the data
- Writing of the manuscripts for submission
- Modifying and editing as required by the journal editor

Contributions of co-authors were as follows:

- Assisting with field work and machine (small angle scattering) use
- Guidance on data processing
- General supervision, discussion and advice on data interpretation and manuscript preparation.
- The statistical analysis and some text in Mares, Moore and Moore (2009) were contributed by Dr. Catherine Moore and Dr. Tim Moore. This paper is based on the Petroleum Conference paper Mares and Moore (2008a).

For the Crosdale, Moore and Mares (2008) paper, the candidate contributed the work in section 6.2.1 with the text and the rest of the research conducted by Dr. Peter Crosdale and Dr. Tim Moore.

The two second author papers were written by Dr. Tim Moore and included work produced during this thesis.

Does size matter?: Compositional influences on gas content in an Eocene CBM play in New Zealand

Tennille E. Mares[1] and Tim A. Moore[1,2]

[1]*Department of Geological Sciences, University of Canterbury, Private Bag 4800, Christchurch, New Zealand*
[2]*Solid Energy NZ Ltd., P.O. Box 1303, Christchurch, New Zealand*

Total gas content appears to be related to compositional characteristics in Eocene age subbituminous coals of the Huntly coalfield, New Zealand. However, the relationships are opposite between the two major coal seams in the basin, despite their stratigraphic proximity (less than 25m).

In this study 163 coal desorption canisters were collected from eight drill holes. The retrieved coal was characterized by gas adsorption capacity, gas desorption and proximate analyses as well as being macroscopically logged for coal type and vitrain banding characteristics. Vitrain bands were quantitatively point counted and the longest dimension of the shortest axis measured. Three coal types were recognized: bright non-banded, bright with <20% banding and bright with >20% banding. Band thickness, converted to the phi ($-\log_2$) scale, was found to increase across the coal types with the thickest bands being associated with the most banded coal type. Overall, when normalized by seam and location, the dataset reveals a relationship between coal type and gas content with the non-banded coal type having the highest gas contents and the most banded the lowest.

However, when the seams are considered separately, it can be seen that in the upper Renown seam, gas has an *indirect* association with increasing band thickness while the lower Kupakupa seam has a *direct* relationship. Interestingly the Renown seam which has a greater percentage of non-banded material generally has a greater adsorption capacity in association with a greater gas content. It is unclear why the two seams should be so different in their gas contents and adsorption characteristics as related to composition. It is possible that the differences in the proportions of the coal types between the two seams has a fundamental control on micropore and fracture systems ultimately controlling the available surface area for gas adsorption.

Assessing Coalbed Methane prospects: How reliable are your numbers?

Mares, T.E.[1] and Moore, T.A.[1,2*]

1 *Department of Geological Sciences, University of Canterbury, Private Bag 4800, Christchurch, New Zealand. tem36@student.canterbury.ac.nz*

2 *Solid Energy NZ Ltd., P.O. Box 1303, Christchurch, New Zealand.*

**Present address : Arrow Energy, Level 13, 10 Eagle Street, Brisbane, Qld. 4000, Australia. tmoore@arrowenergy.com.au*

Abstract

To assess the commercial viability of a coalbed methane prospect two of the key geological parameters measured are gas content (desorbed gas) and gas holding capacity (adsorption capacity). These two measures, together with reservoir pressure, give an estimate of the saturation of a reservoir. Typically saturation has been assessed by collecting one adsorption isotherm sample and assuming it is representative of the whole seam reservoir conditions. This study addresses that assumption.

To understand the level of variation, and thus the inherent uncertainty in saturation, one core from the Huntly coalfield in New Zealand was analysed in detail. Ten canisters of coal (representing the whole seam) were desorbed for ten days and then analysed for adsorption capacity. Desorption analyses for measured gas (average in-situ basis) ranged from 2.69 to 3.35 m^3/t (standard deviation (sd) = 0.25 m^3/t) and gas adsorptive capacity at 4 MPa (average in-situ basis) from 2.50 to 4.19 m^3/t (sd = 0.46 m^3/t) resulting in saturations ranging from 68% to 123% (sd = 15).

Allowing for a ±7 % error in adsorption capacity, saturation was calculated for each sample using total gas contents with ±5, 10, and 15 % error estimates. This resulted in a ±12, ±17 and ±23 % difference in saturation values respectively, ranging from 54 % to 152 %. To assess how many samples are required to make a realistic assessment of reservoir properties, random samples were averaged in lots of 2, 3, 4 etc and compared to the overall mean for the 10 samples. It was found at least three samples are required to bring the average within to one standard deviation of the overall mean for total measured gas content, adsorption capacity and saturation.

Keywords: *coal bed methane; gas adsorption capacity; desorption; saturation; subbituminous; uncertainty*

Introduction

Studies of gas contents from biogenic coal seam reservoirs have shown that although they tend to be high in methane (>90% composition), the gas volume and gas storage capacity can be quite variable both within a seam and between stratigraphically different coal seams in the same location (Flores et al., 2001; Moore et al., 2001; Stricker et al., 2006; Butland and Moore, 2008; Mares and Moore, 2008). As saturation is calculated using results from adsorption and desorption analyses, unsurprisingly saturation has also been reported with significant variation. Stricker and Flores (2002) found saturation to vary from 23 % to 66 % while Butland and Moore (2008) found downhole variation in saturation values of greater than 40 %. Knowledge of the saturation in a reservoir is important for economic

assessment of gas deposits. The level of saturation dictates the reservoir gas pressure which ultimately determines the gas recoverability (see also Bustin and Bustin, 2008).

The level of saturation is determined through comparing the measured gas (i.e. the desorption isotherm) with that of the adsorption isotherm, for the correct pressure/depth of the reservoir. However sample retrieval in the field usually results in the collection of numerous desorption samples and very few adsorption samples. Reported ratios of adsorption: desorption sample numbers include 47: 615 (Stricker and Flores, 2002), 75: 615 (Stricker et al., 2006), 4: 90 (Butland and Moore, 2008), 8: 163 (Mares and Moore, 2008), and 14: 76 (Warwick et al., 2008). The question being raised in this study is: are the relatively low proportions of adsorption to desorption samples sufficient to characterize a core or a seam?

To address this question a complete seam profile from the Renown seam was collected in 2006 from the Jasper-1 well as part of an appraisal pilot program to assess CBM potential in the Huntly coalfield. Sequential desorption canisters were collected and analysed followed by adsorption and proximate analyses conducted on sub-splits from each of the canisters. The study was designed so that all results could be considered on a canister by canister basis with the aim of assessing the uncertainty and variability present in standard reservoir assessment parameters and ultimately to determine the number of samples required to estimate reservoir saturation. It is recognized that this study represents only one core, from one seam of subbituminous rank in a single coalfield in New Zealand. However, this study may form the basis for the same question being asked and evaluated in other coals in other basins.

Location

The Waikato Coal Measures occur throughout the Huntly coalfield and are comprised of a number of coal seams, with the Renown and Kupakupa seams being the main targets for mining and CBM. The coals are Eocene in age, subbituminous C to A in rank (Edbrooke et al., 1994; Newman et al., 1997) and vitrinite reflectance (%Ro) ranging from 0.34 to 0.53% (Edbrooke et al., 1994; Twombly et al., 2004). Previous studies have found that the carbon isotope values and the high methane contents (averaging >90%) indicate that the gas is primarily of secondary biogenic origin, generated by the reduction of CO_2 (Moore and Butland, 2005; Moore and Twombly, 2006; Butland and Moore, 2008; Mares and Moore, 2008). In the study area the water table resides approximately 20 m below surface level.

Methods

The Jasper-1 well intersected the Renown coal seam at 408 m depth and 4.90 m of continuous core was retrieved using a wire-line coring system. Once at the surface, the coal core was immediately taken from the core barrel, quickly logged to identify any inorganic partings and sealed within PVC gas desorption canisters (for canister design see Moore et al., 2004).

Gas desorption

Ten canisters each containing approximately 0.5 m lengths of coal were collected from the Jasper-1 well. Once sealed the canisters were maintained at reservoir temperature (approximately 32° C; Zarrouk and Moore, 2007) during desorption analyses using a water bath, and later a temperature controlled room, with gas volume readings being taken initially every 15 minutes. The time interval between readings was increased as the desorbed volume of gas decreased (see Barker et al., 2002; Moore et al., 2004; Moore and Butland, 2005 for these commonly used procedures). The canisters were desorbed over a 10 day period. Residual gas was determined using methods outlined in Moore et al (2004) and Moore and Butland (2005), while the lost gas correction and total measured gas volume were calculated using a modified version of the U.S. Geological Survey CBM spreadsheet (Barker et al, 2002). It is important to note that this method does not take free gas into consideration (Bodden and Ehrlich, 1998).

Gas adsorption

After gas desorption a representative coal split from each of the canisters was collected for methane adsorption analyses, procedures outlined by Moore and Crosdale (2006) and Crosdale et al. (2008) at a reservoir temperature of approximately 32°C (Moore and Crosdale, 2006; Zarrouk and Moore, 2007). All gas adsorption analyses were conducted at the same laboratory (Energy Resources Consulting, Australia) under the same temperature and equilibrium moisture conditions. Methane adsorption curves were produced using the Langmuir equation assuming a mono-layer gas adsorption mechanism (Gregg and Sing, 1982). Moore and Crosdale (2006) and Crosdale et al. (2008) recognized, for methane adsorption isotherm samples collected from this field, that samples analyzed post-desorption yielded consistently higher gas holding capacities than samples collected and analysed immediately (that is, with no desorption). As such it needs to be stated that the gas holding capacities reported here are likely to be greater than the actual gas holding capacities but as this paper is a study of in seam variability it is the relative differences that are important. For more accurate adsorption capacities of the Huntly coalfield see Mares and Moore (2008).

Coal properties

Coal properties were determined on coal from each canister (CRL Energy Ltd). Analysis methods used were ISO 5068-2 for moisture (ISO, 2007), ISO 1171 for ash (ISO, 1997), ISO 562 for volatile matter (ISO, 1998), whilst fixed carbon was calculated by difference. Relative density was obtained using AS 1038.21.1.1 (Standards Australia International, 2002) and a representative seam composite was analysed for vitrinite reflectance (Newman Energy Research) using method ISO 7404-5 (ISO, 1994)

Saturation

As gas adsorption and desorption data was collected for each canister, saturation was also calculated for each interval and reported on an in-situ basis using the formula:

$$\text{Saturation} = 1-[(\text{adsorption} - \text{desorption})/\text{adsorption}] \quad (1)$$

In-situ basis or data corrected to seam average moisture and ash contents has been used as it is thought to be the best representative of reservoir conditions.

Data Manipulation

In this study, the total variance of gas is considered to be the sum of experimental error and the natural variation because of physical differences in the coal between samples. Both types of variance are considered, first how experimental error affects the uncertainty around saturation estimates and second how the number of samples taken affects how certain an average is in estimating gas properties of the whole seam.

Estimating experimental error in either adsorption or desorption analyses is not a straight forward exercise. Firstly, there have not been many studies which quantify repeatability in adsorption tests because of concerns of the effect that repeated tests may have on the same sample. This study, however, uses an experimental error of ± 7 % which is based on an Australian inter laboratory study (Crosdale et al, 2005). For a full discussion of potential sources of error see Mavor (2004).

Selecting experimental error for measured gas (desorption) is more difficult as once a canister has been desorbed, it can not be desorbed again, thus precluding any type of quantification. It is recognized that desorption values can be the greatest source of error in saturation calculations because of lost gas and oxidation, particularly in low rank coals (Mavor and Nelson, 1997; Hayton, 2003). Thus, generous experimental errors have been selected at ±5, 10, and 15 %.

The gas data in this study has also been manipulated in a second way. Coalbed methane plays draw gas from the whole seam and not just selected parts of the seam. Therefore, in the exploration stage,

accurately assessing the behavior of the whole seam intersection is necessary. However, neither adsorption nor desorption analyses can take a single sample that representatively reflects the average property of the whole seam. Thus, either the whole seam is sampled numerous times (as is often the case for desorption analyses) or only a limited number of samples are taken across the whole seam (as seen for most adsorption tests). The first method may 'over sample' (i.e. needlessly take more samples than needed to estimate a seam's average value) and the latter method may give an abnormally high or abnormally low value that is not representative for the whole seam.

In this study, the mean of the ten samples for adsorption and desorption were taken as representative for the seam. The goal of this part of the study was to see what would have been the minimum number of samples needed from the 10 canisters in order to approximate the mean within 'acceptable' limits of uncertainty (see below for further discussion of this). Thus each adsorption or desorption value for a canister was assigned a random number. Then these numbers were selected randomly and averaged accordingly. Thus, the first two in the sequence was averaged. Then the first three were averaged, then the first four and so on till all 10 were averaged and thus representing the 'true' mean. This procedure (i.e. randomly selecting the sample order) was repeated ten times, giving ten lines.

Results and Discussion

Coal properties

Coal properties by canister can be seen in Table 1. Variability of proximate analyses within the seam is relatively low although no attempt to suggest controls on gas content or gas holding capacity is made in this study. Values for average seam moisture content, 11.70 %, and average seam ash yield, 3.96 %, were used to correct gas data to in-situ basis. A vitrinite reflectance (Ro max) of 0.45% was determined for the Jasper-1 well.

Total measured gas content

Total gas content (lost + measured + residual gas on an in-situ basis) was found to vary from 2.69 m^3/t to 3.45 m^3/t (a 22 % difference), with an average of 3.00 m^3/t and a standard deviation of 0.25 m^3/t (see Fig. 1 and Table 1). A total variation of 0.76 m^3/t or about 25 % of the average total measured gas content is significant over the seam interval.

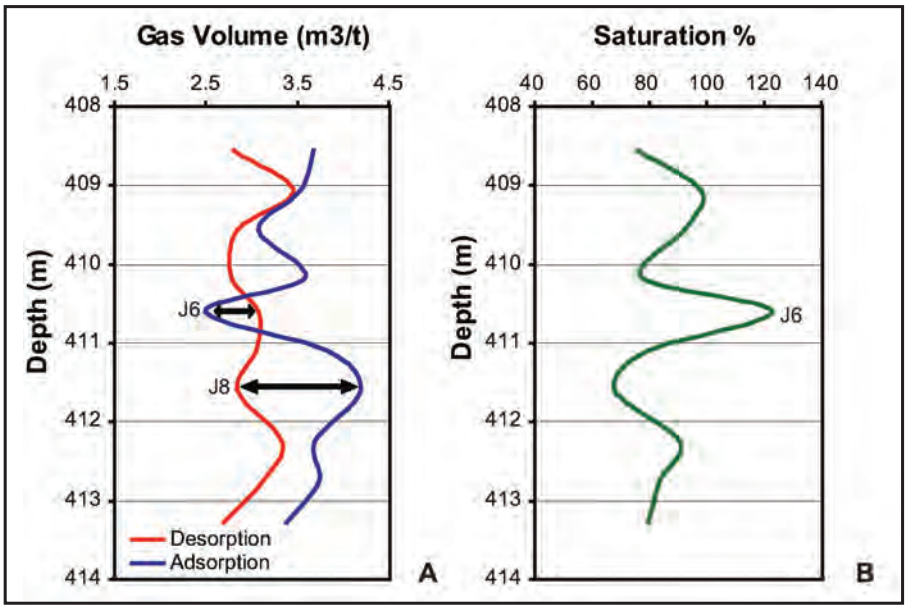

Figure 1. Gas properties of the Renown seam in the Jasper-1 well on an average in situ basis. (A) Vertical profiles of total gas content and gas adsorption cappacity (at 4 MPa) showing no relationship between the two. Samples J6 and J8 have been labelled identifying the risk of collecting only one sample. (B) Vertical profile of percentage gas saturation. Note the oversaturated sample J6.

Table 1. Coal properties, gas content, gas adsorption capacity and calculated saturation (equation 1) by canister. Gas properties are reported on an average in situ basis.

Canister	Mid-point m	Moisture adb %	Ash adb %	Volatile matter adb %	Fixed carbon adb %	Relative density (g/cc)	Total gas content (m3/t)	Adsorption capacity at 4 Mpa (m3/t)	Saturation (%)
J2	408.56	11.10	9.00	37.70	42.20	1.43	2.80	3.68	76.19
J3	409.06	11.00	4.20	40.60	44.20	1.37	3.45	3.52	97.93
J4	409.56	13.20	4.90	36.90	45.00	1.37	2.84	3.08	92.29
J5	410.18	11.70	3.70	39.00	45.60	1.36	2.77	3.57	77.63
J6	410.60	12.30	2.60	39.30	45.80	1.35	3.07	2.50	122.92
J7	411.10	11.40	2.70	40.70	45.20	1.36	3.04	3.84	79.23
J8	411.60	11.30	2.60	39.30	46.80	1.35	2.84	4.19	67.73
J9	412.25	11.60	2.30	39.70	46.40	1.36	3.33	3.69	90.43
J10	412.75	11.80	2.40	38.10	47.70	1.36	3.13	3.74	83.56
J11	413.28	11.60	5.20	37.30	45.90	1.41	2.69	3.38	79.70
Minimum		11.00	2.30	36.90	42.20	1.35	2.69	2.50	67.73
Average		11.70	3.96	38.86	45.48	1.37	3.00	3.52	86.76
Maximum		13.20	9.00	40.70	47.70	1.43	3.45	4.19	122.92
SD		0.64	2.07	1.32	1.51	0.03	0.25	0.46	15.46

adb= air dried basis; SD = standard deviation;

Gas adsorption capacity

Methane gas adsorption capacity was found to vary substantially from 2.50 m^3/t to 4.19 m^3/t (a 40 % difference), when using a pressure of 4 Mpa, with an average of 3.52 m^3/t and a standard deviation of 0.46 m^3/t (Table 1). The vertical profile plotted in Figure 1 shows that there is no relationship between gas content and gas holding capacity. This is not surprising as adsorption capacity is a physical property of the coal whilst the gas has been generated by biogenic processes not necessarily related to the coal structure (Mares and Moore, 2008).The risks involved by taking only one sample to estimate reservoir capacity can clearly be seen by considering samples J6 and J8.

As the adsorption capacity for J6 is actually 0.57 m^3/t smaller than the next smallest capacity, and greater than 1 m^3/t smaller than the samples either side, there was some concern about its validity. The experimental procedures for the adsorption analysis for J6 was thoroughly reviewed and showed no abnormalities. Other than the macroscopic log noting that the interval had a “fairly solid looking matrix” (Mares, 2006, unpublished data) no other unusual properties have been identified. If J6 is excluded, the gas adsorption capacity varies from 3.08 m^3/t to 4.19 m^3/t (27 % difference) at 4 Mpa, with an average of 3.63 m^3/t and a standard deviation of 0.31 m^3/t. Whether J6’s adsorption value is real or erroneous, it does illustrate the danger of using just one sample to estimate a whole seam.

Saturation

Saturation was found to vary from 67.73 % to 122.92 % (45 % difference), with an average of 86.76 % and a standard deviation of 15.46 (Table 1). The vertical profile displayed in Fig. 1 shows that if only one sample was collected for adsorption and desorption analyses from either the J6 or J8 regions, in spite of only a metre separation, very different estimates on reservoir saturation (68 % versus 123 %), potential gas retrieval and commercial viability would be obtained. As such a large oversaturation is unlikely; it was decided to remove J6 from future variation calculations. With J6 excluded, saturation still shows considerable variation with a range from 67.73 % to 97.93 % (31 % difference) and an average of 82.76 % (standard deviation of 9.34).

Effect of experimental error on saturation calculation

The effect of cumulative experimental error of adsorption and desorption analyses have been considered. For example, recalculating saturation with adsorption ± 7 % and total gas content ±5 % error results in around ± 12% difference in saturation values (Table 2). When desorption experimental error is increased to ± 10 % this results in an uncertainty of ± 17 % for saturation values; finally, a ± 15 % experimental error for desorption gives a ± 23 % uncertainty. These types of uncertainties illustrate that interpretations or exploration/development decisions made based on levels of gas saturation should be carefully considered.

Table 2. Results of experimental error assessment on saturation both including and excluding J6

		Measured % saturation for Jasper-1	Adsorption Desorption	Experimental Error -7% 5%	7% -5%	-7% 10%	7% -10%	-7% 15%	7% -15%
Including J6	Minimum	67.7%	Influence on values of experimental error	76.5%	60.1%	80.1%	57.0%	83.8%	53.8%
	Average	86.8%		98.0%	77.0%	102.6%	73.0%	107.3%	68.9%
	Maximum	122.9%		138.8%	109.1%	145.4%	103.4%	152.0%	97.6%
Excluding J6	Minimum	67.7%		76.5%	60.1%	80.1%	57.0%	83.8%	53.8%
	Average	82.7%		93.4%	73.5%	97.9%	69.6%	102.3%	65.7%
	Maximum	97.9%		110.6%	86.9%	115.8%	82.4%	121.1%	77.8%
		Difference from mean		11.4%	-12.6%	15.5%	-18.9%	19.1%	-25.9%

Assessment of within seam variation

Within seam variation in the Jasper-1 well is considerable (Fig. 1). Over and above any experimental error (as just previously described) natural variations in the seam require more than one sample be collected in order to approximate mean values for reservoir gas properties.

Fig. 2 shows the overall mean value for total gas content with one standard deviation (± 8.4 %) uncertainty. For the Jasper-1 well, 8 out of 10 of the averaging runs were within one standard deviation of the mean when averaging only two randomly selected samples. Thus for whole seam estimates if one standard deviation is an acceptable level of uncertainty, only three or more canisters for desorption would have been required. For gas adsorption capacity, excluding J6, the average of three samples were required to be within one standard deviation (± 8.5 %) of the mean (Fig. 3) while for percent saturation, again at least three saturation calculations were required to be within one standard deviation (± 11.3 %) of the mean (Fig. 4). So in all analyses at least three samples would have been required to be within ± 10 % of the mean. An additional benefit of collecting at least three samples is that anomalous or unusual results can be more easily identified and treated with caution.

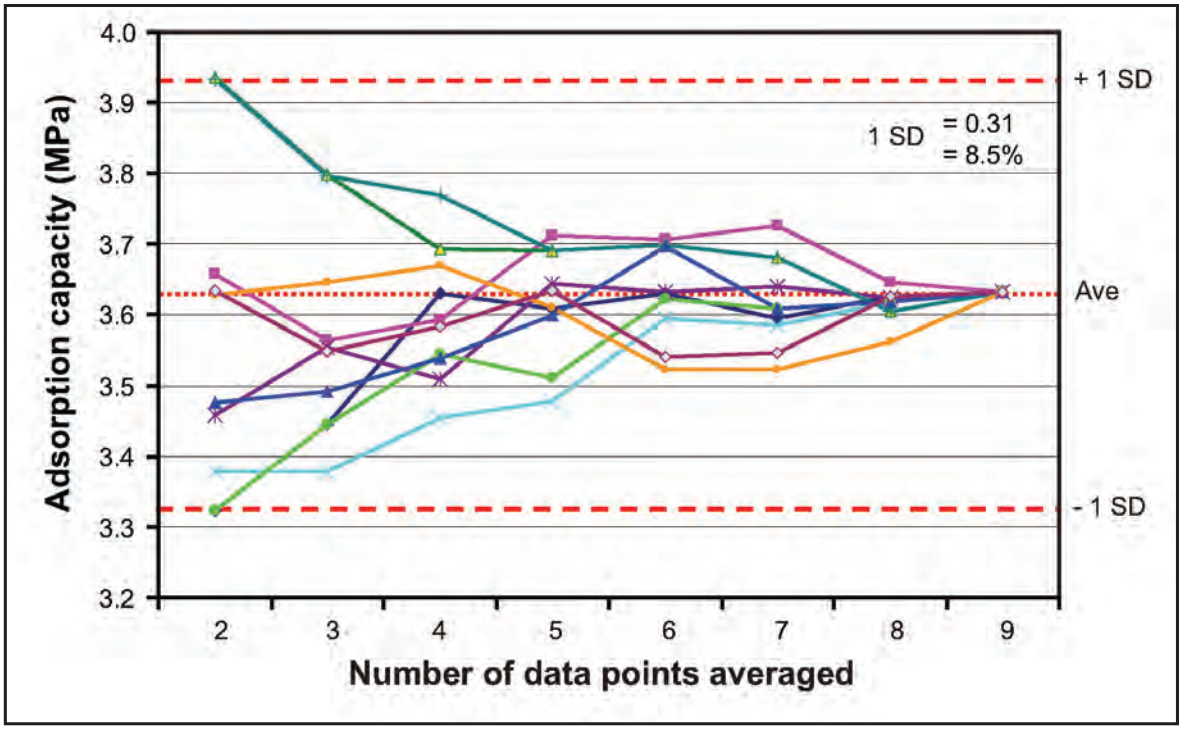

Figure 2. Results of assessment of how many total gas samples are required to be within one standard deviation of the overall mean. It can be seen that at least three samples are required.

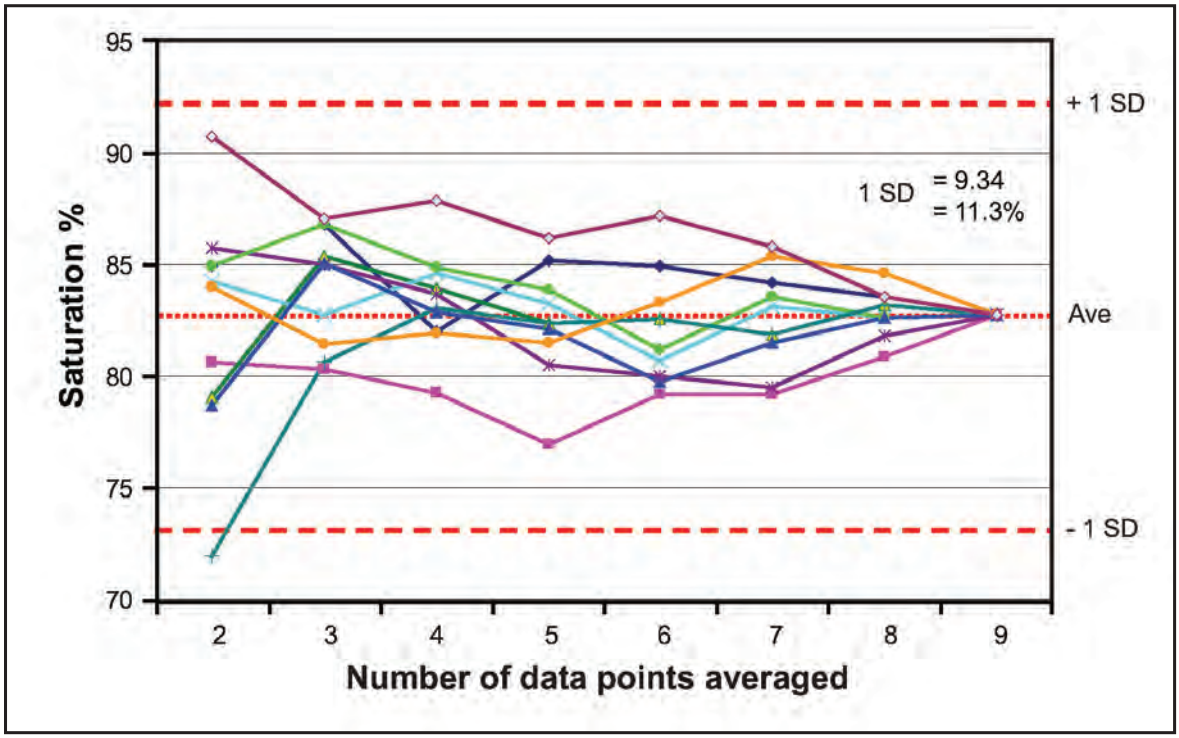

Figure 3. Results of assessment of how many gas adsorption isotherm samples are required to be within one standard deviation of the overall mean. It can be seen that at least three samples are required.

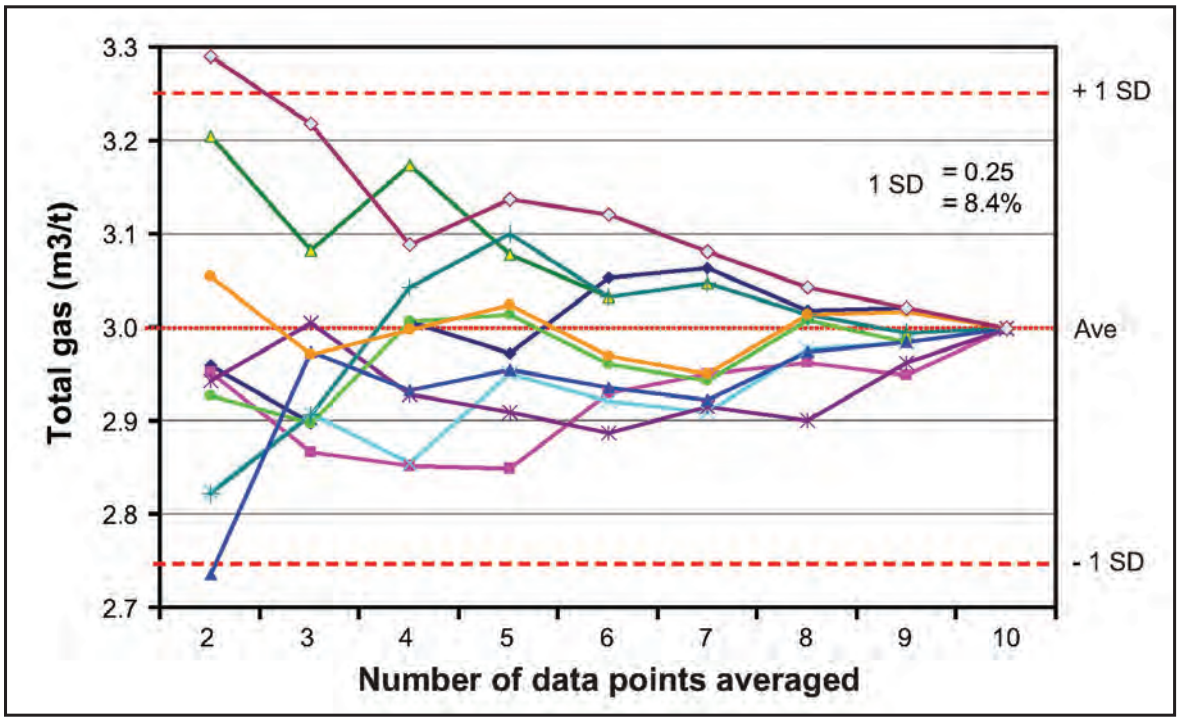

Figure 4. Results of assessment of how many saturation calculations are required to be within one standard deviation of the overall mean. It can be seen that at least three samples are required.

Conclusions

The results of this study show that considerable down hole variability can exist in adsorption, desorption and thus saturation within a single seam. The level of saturation in a coalbed methane reservoir is thought crucial to assessing its economic viability. Yet, adsorption isotherms, which are one of the two essential tests needed to determine percent saturation (the other being gas desorption), are chronically under-sampled. In a best case scenario, recalculating saturation with estimated experimental errors for adsorption (± 7 %) and desorption analyses (± 5 %), there is a 22 % uncertainty in saturation (that is ± 11 % around any saturation value). As such, if a saturation value was 75%, it could actually be anywhere from 64 to 89 %. If natural variation in coal type is taken into account, and its affect on desorption, adsorption and thus saturation values, at least three samples (of each type of analyses, desorption and adsorption) would have been required for the Jasper-1 well in order to be within one standard deviation of the mean, with one standard deviation varying from 8.4 to 13.1 % (for desorption and adsorption analyses). It is important to note that the uncertainty values used here are just what this study has chosen to be 'acceptable limits of uncertainty', others may have higher or lower tolerances.

What are 'acceptable' limits of uncertainty? This depends on the level of accuracy that is required by the individual, the bank, the investor or the available budget. There is no right answer for this. In a preliminary study, explorers may be comfortable with an uncertainty of ± 20 %. With more investment however, banks or investors may demand lower levels of uncertainty (and thus less risk).

It is recognized that this study only looked at one coal core, from one seam, in one basin within New Zealand and may not be applicable to other coal seams. However it does raise questions as to what is the variability of in saturation in other coal seams and the minimum number of samples needed in order to obtain an acceptable level of uncertainty.

Acknowledgements

This research is part of a broader study on controls on gas properties, the funding for which has come from a number of sources. Firstly, we thank the support both financial and in the field provided by Solid Energy NZ Ltd., Resource Development Technology LLC, and Coal Bed Methane Ltd. The New Zealand Foundation for Research, Science and Technology through its Technology New Zealand funding has provided the stipend for the senior author. We would also like to thank the input and assistance of Steve Weaver, Grant Gillard, Sadiq Zarrouk, Greg Twombly, Steve Stepanek, Jaco Fourie, Tom Bowman, Jane Newman and Peter Crosdale. Thanks to Cath Moore who has helped both authors in their understanding of the importance of quantifying uncertainty. This research could not have been conducted without the understanding and support of Rob, Jan and Chris Beverland who allowed unfretted assess to their farm during the drilling and evaluation phase of this research.

References

Barker, C.E., Dallegge, T.A. and Clark, A.C., 2002. USGS coal desorption equipment and a spreadsheet for analysis of lost and total gas from canister desorption measurements. U.S. Geological Survey Open File Report 02-496. 13 pp. http://pubs.usgs.gov/of/2002/ofr-02-496/.

Bodden, W.R. and Ehrlich, R., 1998. Permeability of coals and characteristics of desorption tests: Implications for coalbed methane production. International Journal of Coal Geology, 35(1-4): 333-347.

Bustin, A.M.M., and Bustin, R.M., 2008, Coal reservoir saturation: Impact of temperature and pressure: AAPG Bulletin, v. 92, p. 77-86.

Butland, C.I. and Moore, T.A., 2008. Biogenic coal seam reservoirs in New Zealand: A preliminary assessment. In Flores, R.M. (Ed.), Microbes, Methanogenesis, and Microbial Gas in Coal. International Journal of Coal Geology Special Issue (in press).

Crosdale, P.J., Saghafi, A., Williams, R., and Yurakov, E., 2005, Inter-laboratory comparative CH4 isotherm measurement on Australian coals, *in* Beeston, J.W., ed., Bowen Basin Symposium 2005- The future for coal- Fuel for thought.: Yeppoon, Geological Society of Australia Inc. Coal Geology Group and the Bowen Basin Geologists Group, p. 273-277.

Crosdale, P.J., Moore, T.A. and Mares, T.E., 2008. Influence of moisture content and temperature on methane adsorption isotherm analysis for coals from a low rank, biogenically-sourced gas reservoir. In Flores, R.M. (Ed.), Microbes, Methanogenesis, and Microbial Gas in Coal. International Journal of Coal Geology Special Issue (in press).

Edbrooke, S.W., Sykes, R. and Pocknall, D.T., 1994. Geology of the Waikato Coal Measures, Waikato Coal Region, New Zealand, Monograph 6. Institute of Geological and Nuclear Sciences Limited, Lower Hutt, New Zealand. 236 pp.

Flores, R.M., Moore, T.A., Stanton, R.W. and Stricker, G.D., 2001. Textural controls on coalbed methane content in the subbituminous coal of the Powder River Basin, GSA Annual Meeting, Boston.

Gregg, S.J. and Sing, K.S., 1982. Adsorption, surface area and porosity. Academic Press, London, 303 pp.

Hayton, S., 2003, Technical Note: Oxidation of coal in desorption canisters, Petroleum Report Series, PR 2948, Crown Minerals, p. 4.

International Organization for Standardization, 2007. ISO 5068-2 Brown coals and lignites - Determination of moisture content - Part 2: Indirect gravimetric method for moisture in the analysis sample. 5 pp.

International Organization for Standardization, 1997. ISO 1171 Solid Mineral Fuels - Determination of ash. 4 pp.

International Organization for Standardization, 1998. ISO 562 Hard coal and coke - Determination of volatile matter. 7 pp.

International Organization for Standardization, 1994. ISO 7404-5 (1994) Methods for the petrographic analysis of bituminous coal and anthracite -- Part 5: Method of determining microscopically the reflectance of vitrinite. International Organisation for Standardisation, Geneva, Switzerland, 11pp.

Mares, T.E. and Moore, T.A., 2008. The influence of macroscopic texture on biogenically-derived coalbed methane, Huntly coalfield, New Zealand. In Flores, R.M. (Ed.), Microbes, Methanogenesis, and Microbial Gas in Coal. International Journal of Coal Geology Special Issue (in press).

Mavor, M., 2004. Uncertainty in Sorption Isotherm Measurements, International Coalbed Methane Symposium: Tuscaloosa, Alabama.

Mavor, M., and Nelson, C., 1997. Coalbed reservoir Gas-In-Place analysis. GRI-97/0263, Gas Research Institute, Chicago, Illinois, U.S.A.

Moore, T.A. and Butland, C.I., 2005. Coal seam gas in New Zealand as a model for Indonesia. In: S. Prihatmoko, S. Digdowirogo, C. Nas, T. van Leewen and H. Widjajanto (Editors), IAGI Special Issues 2005: Indonesian Mineral and Coal Discoveries. Indonesian Association of Geologists, Indonesia, pp. 192-200.

Moore, T.A. and Crosdale, P.J., 2006. The effect of moisture and temperature on adsorption isotherms of a low-rank coal: Implications for reservoir modelling, 2006 International Coalbed Methane Symposium, Tuscaloosa, Alabama.

Moore, T.A., Flores, R.M., Stanton, R.W. and Stricker, G.D., 2001. The role of macroscopic texture in determining coal bed methane variability in the Anderson-Wyodak coal seam, Powder River Basin, Wyoming. In: C.R. Robinson (Editor), Eighteenth Annual Meeting of The Society for Organic Petrology, Houston, Texas, pp. 85-88.

Moore, T.A., Gillard, G.R., Boyd, R., Flores, R.M., Stricker, G.D. and Galceran, C.M., 2004. A mighty wind: determining the methane content of New Zealand coal seams. The Society for Organic Petrology, 21st Annual Meeting, Sydney, Australia, p. 114-116.

Moore, T.A. and Twombly, G., 2006. Cracking the CSG code with the three Rs: Reasoned, rigorous and responsive development. Proc. 2006 New Zealand Petroleum Conference. Ministry of Economic Development, Auckland, New Zealand, unpagnated 6 pp.

Nelson, C.R., Hill, D.G., and Pratt, T.J., 2000. Properties of Paleocene Fort Union Formation Canyon Seam Coal at the Triton Federal coalbed methane well, Campbell County, Wyoming, SPE/CERI Gas Technology Symposium: Calgary, Alberta Canada, 3-5 April 2000.

Newman, N.A., Moore, T.A. and Esterle, J.S., 1997. Geochemistry and petrography of the Taupiri and Kupakupa coal seams, Waikato Coal Measures (Eocene), New Zealand. International Journal of Coal Geology, 33(2): 103-133.

Standards Australia International, 2002. AS 1038.21.1.1-2002: Coal and coke - Analysis and testing - Higher rank coal and coke - Relative density - Analysis sample/density bottle method. Standards Australia International Ltd. 5pp.

Stricker, G.D., and Flores, R.M., 2002. Coalbed methane content in the Powder River Basin, Wyoming: Saturation by coal rank and depth, 2002 Pittsburgh Coal Conference.

Stricker, G.D., Flores, R.M., McGarry, D.E., Stillwell, D.P., Hoppe, D.J., Stillwell, C.R., Ochs, A.L., Ellis, M.S., Osvald, K.S., Taylor. S.L., Thorvaldson, M.C., Trippi, M.H., Grose, S.D., Crockett, F.J. and Shariff, A.J., 2006. Gas desorption and adsorption isotherm studies of coals in the Powder River Basin, Wyoming and adjacent basins in Wyoming and North Dakota. U.S. Geological Survey Open-File Report 2006-1174, 21pp.

Twombly, G., Stepanek, S.H. and Moore, T.A., 2004. Coalbed methane potential in the Waikato Coalfield of New Zealand: A comparison with developed basins in the United States, 2004 New Zealand Petroleum Conference Proceedings.

Warwick, P.D., 2008. Biogenic origin of coalbed gas in the northern Gulf of Mexico Coastal Plain, USA. In Flores, R.M. (Ed.), Microbes, Methanogenesis, and Microbial Gas in Coal. International Journal of Coal Geology Special Issue (in press).

Zarrouk, S. J. and Moore, T. A., 2007. Preliminary assessment of the geothermal signature and ECBM potential of the Huntly coalbed methane field, New Zealand. Proceedings of the 29th New Zealand Geothermal Workshop, Auckland, 19-21 November, 2007.

Speaker

TENNILLE MARES graduated from the University of New South Wales with first class honours in geology in 2003. After studying as a postgraduate at the University of Queensland for 18 months she accepted a NZ Technology in Industry Funding [TIF] Scholarship for a PhD at the University of Canterbury and Solid Energy NZ Ltd.

Tennille has been awarded a Royal Society of New Zealand Travel Grant, The Society for Organic Petrology Spackman Award, a New Zealand Postgraduate Study Abroad Award and a grant from the Mason Trust to conduct research in France and the US as well as to present at conferences in Canada and Australia. Her work has also included 3 months in the field as part of the CBM exploration and appraisal well drilling programs conducted by Solid Energy NZ Ltd. Tennille currently has 3 papers in review.

doi:10.1016/j.coal.2008.05.013

The influence of macroscopic texture on biogenically-derived coalbed methane, Huntly coalfield, New Zealand

Tennille E. Mares[a], **and Tim A. Moore**[a, b, 1],

[a]Department of Geological Sciences, University of Canterbury, Private Bag 4800, Christchurch, New Zealand

[b]Solid Energy NZ Ltd., P.O. Box 1303, Christchurch, New Zealand

Received 7 August 2007;
revised 15 May 2008;
accepted 27 May 2008.
Available online 3 June 2008.

Abstract

Secondary biogenic gas content can be related to textural characteristics in Eocene age subbituminous coals from the Huntly coalfield, New Zealand. However, the relationships between the two major coal seams in the basin are considerably different despite their close stratigraphic proximity (less than 25 m).

In this study, 163 coal samples were collected and desorbed from eight drill holes. Gas adsorption capacity and proximate analyses were conducted as well as macroscopic logging for coal type and vitrain banding characteristics. Vitrain bands were quantitatively point counted and the longest dimension of the shortest axis measured. Three coal types were recognized: bright luster non-banded, bright moderately banded and bright highly banded. Vitrain band thickness, converted to the phi ($-\log_2$) scale, was found to increase across the coal types with the thickest bands being associated with the most banded coal type. Overall, when normalized by seam and location, the dataset reveals a relationship between coal type

and gas content with the non-banded coal type having the highest gas contents and conversely, the coal types with the most vitrain bands having the lowest gas contents.

However, when the seams are considered separately, it can be seen that in the stratigraphically higher Renown coal seam, gas has an *indirect* association with increasing band thickness, in agreement with the overall trend, while the stratigraphically lower Kupakupa coal seam appears to have a *direct* relationship. Interestingly the Renown seam, which has a greater percentage of non-banded material, generally has a greater methane adsorption capacity as well as a greater gas content compared to the Kupakupa seam. It is believed these differences are related to macroscopic texture and that the differing proportions of the coal types between the two seams has a fundamental effect on microporosity, ultimately controlling the available surface area for gas adsorption.

doi:10.1016/j.coal.2008.07.002

Uncertainty of gas saturation estimates in a subbituminous coal seam

Tennille E. Mares[a], **Tim A. Moore**[a, b, 1], **and Catherine R. Moore**[c]

[a]Department of Geological Sciences, University of Canterbury, Private Bag 4800, Christchurch, New Zealand

[b]Solid Energy NZ Ltd., P.O. Box 1303, Christchurch, New Zealand

[c]Lincoln Ventures Ltd., Lincoln University, P.O. Box 133, Lincoln, Christchurch, New Zealand

Received 25 January 2008;
revised 3 July 2008;
accepted 11 July 2008.
Available online 19 July 2008.

Abstract

To assess the commercial viability of a coalbed methane prospect two of the key geological parameters measured are gas content (desorbed gas) and gas holding capacity (adsorption capacity). These two measures, together with reservoir pressure, give an estimate of the gas saturation of the reservoir. Typically gas saturation has been assessed by collecting one adsorption isotherm sample and assuming it is representative of the whole seam reservoir conditions. This study addresses that assumption.

To understand the level of variation, and thus the inherent uncertainty in saturation, one core (Jasper-1) from the Huntly coalfield in New Zealand was analysed in detail. Ten samples (representing the whole coal seam) were placed into gas desorption canisters and desorbed for ten days and then analysed for adsorption capacity. Desorption analyses for total

measured gas content (average in-situ basis) ranged from 2.32 to 2.89 m^3/t (standard deviation (sd) = 0.18) and gas adsorptive capacity at 4 MPa (average in-situ basis) from 2.11 to 3.51 m^3/t (sd = 0.38) resulting in saturations ranging from 66% to 120% (sd = 15).

Determination of how many samples are required to make a realistic assessment of average reservoir properties requires a consideration of: (i) the level of accuracy desired, (ii) the limit of accuracy possible, which is governed by the magnitude of experimental error, and (iii) the innate variability of the seam. It was found that a minimum of five samples each for adsorption and desorption were required in order to significantly decrease the uncertainty in gas saturation estimates for a subbituminous coal.

doi:10.1016/j.coal.2008.04.004

Influence of moisture content and temperature on methane adsorption isotherm analysis for coals from a low-rank, biogenically-sourced gas reservoir

Peter J. Crosdale[a], **Tim A. Moore**[b, c, d] and **Tennille E. Mares**[c]

[a]Energy Resources Consulting Pty Ltd., PO Box 54, Coorparoo, Qld 4151, Australia

[b]Solid Energy NZ Ltd., P.O. Box 1303, Christchurch, New Zealand

[c]Department of Geological Sciences, University of Canterbury, Private Bag 4800, Christchurch, New Zealand

[d]Arrow Energy NL, GPO Box 5262, Brisbane, Qld 4000, Australia

Received 5 June 2007;
revised 9 April 2008;
accepted 9 April 2008.
Available online 16 April 2008.

Abstract

Samples of subbituminous coal from the Huntly Coalfield, New Zealand, were analyzed for methane adsorption at a variety of moisture contents and temperatures. Density and moisture determinations as part of the procedure were used to experimentally confirm that the packing density of water adsorbed to the coal's surface is equivalent to that of normal liquid water. Moisture content was found to be critical in evaluating the storage capacity of these coals. Low moisture was associated with elevated adsorption isotherms. The relationship between moisture content and gas adsorption is non-linear. Temperature over the range we tested was found to play only a small role in storage capacity for this coal. A series of algorithms were developed to correct for moisture and temperature variations between samples. Testing of the

algorithms by using an additional sample indicated that they are close to predicting experimental data but that the constants still require further refinement. These algorithms only apply to this coalfield and are not intended to be widely applied. In addition, it was found that methane adsorption isotherms determined on samples collected after desorption were elevated in comparison to those determined on samples which were collected immediately after drilling.

doi:10.1016/j.coal.2008.07.007

Assessing the potential for CO_2 adsorption in a subbituminous coal, Huntly Coalfield, New Zealand, using small angle scattering techniques

Tennille E. Mares[a], Andrzej P. Radliński[b, c, d], Tim A. Moore[a, e, 1], David Cookson[f, g], P. Thiyagarajan[h], Jan Ilavsky[i] and Jürgen Klepp[j, k]

[a]Department of Geological Sciences, University of Canterbury, Private Bag 4800, Christchurch, New Zealand

[b]Geoscience Australia, Canberra, Australian Capital Territory 2609, Australia

[c]Cooperative Research Centre for Greenhouse Gas Technologies, Canberra, Australian Capital Territory2601, Australia

[d]Nanoscale Science and Technology Centre, Griffith university, Brisbane, Queensland 4111, Australia

[e]Solid Energy NZ Ltd., P.O. Box 1303, Christchurch, New Zealand

[f]Australian Synchrotron, 800 Blackburn Road, Clayton, VIC 3168, Australia

[g]School of Physics, University of Melbourne, VIC 3010, Australia

[h]Intense Pulsed Neutron Source, Argonne National Laboratory, Argonne, IL 60439, USA

[i]X-ray Operations Division, Advanced Photon Source, Argonne National Laboratory, Argonne, IL, USA

[j]Institut Laue Langevin, Boîte Postale 156, F-38042 Grenoble Cedex 9, France

Received 23 May 2008;
revised 16 July 2008;

accepted 22 July 2008.
Available online 25 July 2008.

Abstract

Small angle scattering techniques (SAXS and SANS) have been used to investigate the microstructural properties of the subbituminous coals (R_{max} 0.42–0.45%) from the Huntly Coalfield, New Zealand. Samples were collected from the two thick (> 5 m) coal seams in the coalfield and have been analysed for methane and carbon dioxide sorption capacity, petrography, pore size distribution, specific surface area and porosity.

Specific surface area (SSA) available for carbon dioxide adsorption, extrapolated to a probe size of 4 Å, ranged from 1.25×10^6 cm^{-1} to 4.26×10^6 cm^{-1} with total porosity varying from 16% to 25%. Porosity was found to be predominantly composed of microporosity, which contributed the majority of the available SSA. Although considerable variation was seen between samples, the results fit well with published rank trends.

Gas holding capacity at the reservoir pressure (approximately 4 MPa) ranged from 2.63 to 4.18 m^3/t for methane on a dry, ash-free basis (daf) and from 22.00 to 23.72 m^3/t daf for carbon dioxide. The resulting ratio of CO_2:CH_4 ranged from 5.7 to 8.6, with an average of 6.7:1.

Holding capacities for both methane and carbon dioxide on a dry ash free basis (daf) were found to be correlated with sample microporosity. However, holding capacities for the two gases on an as analysed (aa) basis (that is including mineral matter and moisture), showed no such correlation. Carbon dioxide (aa) does show a negative correlation with both specific surface area and microporosity. As the coals have low inorganic matter content, the reversal is thought to be related to moisture which is likely concentrated in the pore size range 12.5–125 Å. Methane holding capacity, both daf and aa, correlates with macroporosity, thus suggesting that the holding capacity of micropores is diminished by the presence of moisture in the pores.

Gas saturation: controls and uncertainty in biogenically-derived coalbed methane, examples from New Zealand coal fields

Tim A. Moore[1,2,] Tennille E. Mares[2] and Carol I. Butland[1]

[1]*Arrow Global CBM Pty Ltd., 10 Eagle Street, Brisbane, Australia*
[2]*Department of Geological Sciences, University of Canterbury, Private Bag 4800, Christchurch, New Zealand*

Gas saturation is probably second only to permeability in determining whether a coalbed methane reservoir will yield gas at rates deemed commercial. Yet, the controls on gas saturation which are biogenically-derived in coal beds are not well understood. In New Zealand, the Greymouth, Ohai and Huntly coalfields were investigated and all found to be biogenic to mixed biogenic/thermogenic in origin. There was also a wide variance in the degree of gas saturation within and between deposits. The Ohai coalfield has the highest $\delta^{13}C$ isotopes values but is intermediate in rank between the Greymouth and Huntly coals. It is postulated that it's relatively high gas saturations (>75%) are the result of gas migration up-dip from more thermally mature coal beds. It should be noted, however, that potentially large uncertainties can exist around gas saturation values. To assess this, one coal core from the Huntly coalfield was sampled from top to bottom (10 samples) for desorption and adsorption gas properties. Desorption analyses for measured gas (average in-situ basis) ranged from 2.69 to 3.35 m^3/t (standard deviation (sd) = 0.25) and gas adsorptive capacity at 4MPa (average in-situ basis) from 2.50 to 4.19 m^3/t (sd = 0.46) resulting in saturations ranging from 68% to 123% (sd = 15). Allowing for a ±7 % error in adsorption capacity, saturation was calculated for each sample using measured gas contents with ±5, 10, and 15 % error estimates. This resulted in a ±11, ±16 and ±21 % difference in saturation values respectively, ranging from 54 % to 152 %. To assess how many samples are required to make a realistic assessment of reservoir properties, random samples were averaged in lots of 2, 3, 4 etc and compared to the overall mean for the 10 samples. It was found at least three adsorption and desorption samples would have been required in the Huntly core to bring the average within to one standard deviation of the overall mean for measured gas content, adsorption capacity and saturation.

PROCEEDINGS, INDONESIAN PETROLEUM ASSOCIATION

Thirty-third Annual Convention & Exhibition, May 2009

Assessing uncertainty of coalbed methane resources

Tim A. Moore[1,2], Tennille E. Mares[2] and Catherine R. Moore[3]

[1]PT Arrow Energy Indonesia, Jl. Taman Kemang No. 32B, Jakarta, Indonesia (tmoore@arrowenergy.com.au)

[2]University of Canterbury, Department of Geological Sciences, University of Canterbury, Christchurch, New Zealand (tem36@student.canterbury.ac.nz)

[3]Butler Partners Pty Ltd., P.O. Box 2267, Fortitude Valley BC, Qld., Australia (cmoore@butlerpartners.com.au)

ABSTRACT

While estimating reserves for coal, oil and natural [conventional] gas is relatively routine and standarised, resource calculations for gas in coal is neither. Because gas in coal is held in such a fundamentally different way than in conventional gas reservoirs, these variables should be derived commensurate with coal-gas properties. Thus, a methodology has been developed to determine resource size and to assign uncertainty around those estimates.

The underlying tenet for assessing a resource should be to understand the uncertainty around the key components of the estimation process. For coalbed methane those components are rock

volume and gas content. Rock volume needs to take into account the area, coal bed thickness and density of the organic material, while gas volume needs to assess the adsorption properties of the coal and likely saturation levels. A refined assessment also considers the level (%) of gas types such as CH_4, CO_2, C_2H_6 etc. By defining the uncertainty of each of these parameter estimates (most simply in terms of worst, base and best case, or more completely as parameter distributions), and potentially any correlation between these parameters, it is possible to undertake probabilistic analyses to quantify the uncertainty of the gas resources. Acceptable limits of uncertainty will be a reflection of individual investor's appetite for risk. Defining uncertainty allows a fairly objective means of distilling geological data into levels of probability.

INTRODUCTION

Coal is generally a black, brittle, highly carbonaceous rock. Like limestone, it forms and is transformed in a fundamentally different way than the clastic sedimentary rocks which usually surround it. It is well recognised that the carbon which comprises greater than 90% of coal gives it unique properties among rocks, certainly in terms of its interaction with gaseous components. Yet, assessing gas potential in coal often uses methodologies not suited to its inherently carbon-based composition. Using the wrong method for calculating gas content in coal can result in significant potential error of gas in-place estimates. Additionally a significant source of resource estimate uncertainty relates to the difficulty in characterising the heterogeneity of the coal resource.

Despite the likelihood of some degree of uncertainty accompanying any resource estimate, it is common procedure to report a single coalbed methane (CBM) resource estimate. . For example, in Indonesia, a single resource estimate value has been given for the country and for regions such

as South Sumatra and Kalimantan (e.g. Stevens et al., 2001; Hadiyanto and Stevens, 2005). This reporting of a single estimate incorrectly conveys a degree of certainty when in fact the range of coal bed methane resource estimates consistent with prior knowledge and data is usually reasonably large(Moore and Butland, 2005; Mares et al., 2009b).

The purpose of this paper is to set out, firstly, what parameters should be considered in estimating the gas resources of a coal seam, basin or region. Secondly, the methodology of estimating uncertainty in gas in-place estimates will be explained and examples given. In addition, some background on how methane is held in coal and the differences between a *reserve* and a *resource* will be briefly discussed below.

Methane in Coal

It is essential to understand how methane is held in coal because it is so fundamentally different from how gas is held in conventional reservoirs. In clastic sediments, it is the volume of pores that determine the potential gas charge; the methane is held, more or less, as 'free' gas.

In contrast, methane in coal forms a physio-chemical bond *along the pore walls,* where the gas is adsorbed onto the coal. Thus, rather than pore volume determining the maximum holding capacity for methane, it is the sum of the surface area of all the pores which dictate how much gas can be held. Total pore volume can remain the same, but if there are more pores, rather than less, this will result in greater surface area and therefore greater gas holding capacity. On average, just one cubic centimetre of coal – a very small amount! - has about three square metres – that's a lot! - of surface area (Radlinski et al., 2004; Mares et al., 2009a).

Therefore, while grain size and the degree of secondary mineralisation will determine pore volume in clastic sediments, coal composition and type may also ultimately determine pore-size distribution (and thus surface area) in coal (Mares et al., 2009a).

In all probability 'free' gas also exists in a coal reservoir. But, it is generally accepted that the majority of methane in coal will be held as adsorbed gas onto the surfaces within pores. Thus it is essential that gas character in coal is assessed with this property in mind.

Reserve versus Resource

An additional distinction is required before proceeding with the uncertainty analysis that is the focus of this paper, and relates to the difference between resource and reserve estimates. This paper is concerned only with estimating *resources*, not reserves (Fig. 1). Resource estimates, are preliminary estimates of the possible gas content in a coal resource, and are based upon an assumed character of the reservoir, and supported to varying extents by data from widely spaced exploration wells. In contrast, gas reserve estimates relate to how much of that gas content can be extracted (and when), and can only be made once data from existing flowing wells is available.. Reserves are divided into 1P, 2P and 3P which are respectively 'proven', 'proven plus probable' and 'proven plus probable plus possible' gas reserves.

For coalbed methane reservoirs, resources are usually estimated based upon the results from exploration drill holes. An advantage of coalbed methane exploration is that these wells are generally inexpensive compared to their oil and gas equivalents. The primary purpose of coalbed

methane exploration wells are to gain quantitative data on maximum holding capacity of the target coal seam (measured through adsorption isotherms), the gas charge (measured through desorption isotherms), gas quality (i.e. $\%CH_4$) and then the calculated gas saturation. The variability of each of these measurements, allows a description of the level of uncertainty for the gas resource to be obtained.

In some cases, especially in preliminary assessments, there is no reservoir data available. Estimates can still be made, if the rank, coal bed thickness and distribution of the reservoir are known to some degree. Through comparison with other coal beds with similar character, gas properties can be inferred, however a wide range of possible gas properties needs to be represented in this case, commensurate with the high level of uncertainty associated with this extrapolation of data. .

CONCEPT OF UNCERTAINTY

Parameters used to represent real world properties in models of fluid flow in geologic media are inevitably accompanied by uncertainty. Sources of this parameter uncertainty relate to:

(i) various types of measurement error;

(ii) necessary model simplifications of real world geological complexity;

(iii) the insufficiency of data to discern more than a fraction of the detail of this complexity; and in some cases

(iv) uncertainty regarding the general assumptions in the conceptual model itself.

Inaccuracies may occur for example in the definition of strata boundaries and depths, fault locations, isotherm relationships, hydraulic recharge areas and flow rates. The interplay of these factors determines the magnitude of this error, e.g. a handful of measurements may be sufficient to discern a realistic parameterisation for very homogeneous geological strata, whereas a lot of data would be required to obtain realistic parameter representations of heterogeneous geological strata (see also Mares et al., 2009b). Clearly, any prediction made on the basis of these estimated parameters will also be uncertain, and the correct approach to this inherent uncertainty is to strive to provide a description of the potential error of any predictions made on the basis of these uncertain parameters.

One way that the uncertainty of each parameter can be expressed is through assignment of a 'best', 'base' and 'worst' value. Where data is plentiful or heterogeneity is known to be low, the range of a variable from 'best' to 'worst' may be small; and conversely, where little is known about a variable the range between 'best' and 'worst' scenarios can be large, to reflect the greater parameter uncertainty. This approach of assessing 'worst','base' and 'best' parameter values is adopted in this paper, allowing a conceptually simple uncertainty analysis for resource estimates. Furthermore, this approach allows an exploration of the relative contribution that various components of resource estimation make to the uncertainty of those estimates.

ROCK/RESERVOIR VOLUME

The first component of coal bed methane resource estimation relates to assessing the size of a coalbed methane resource, which is expressed in terms of the volume or tonnage of the coal resource. For coalbed methane, reservoir volume is defined by the area, the thickness of the coal

and coal density. These variables are used to calculate the tonnage of the coal which is present in any given area. Tonnage is calculated because gas resources are usually reported as cubic metres of gas per ton of coal (m^3/t). Because a reservoir is inherently geological in nature, each of these variables can be expected to vary throughout the reservoir. Incorporating some description of this variability in the resource estimation process provides the basis of the uncertainty analysis described herein.

Area/Domain

In almost all cases, the area of a prospect is known exactly. However the size of the area that the coal actually occupies within that prospect is difficult to define precisely. Coal seams may thin and be absent in some areas as a result of depositional thinning, 'washouts', and faulting, while other areas may be inaccessible for assessment because of existing surface infrastructure (e.g. towns, factories, roads). The extent to which this variability is known will depend on the density of data within the permit area.

In general the 'best' case scenario would assume that the coal resource occupies the full permit area (unless there is data to show otherwise). The percentage of the whole permit or assessment area used for the 'base' or 'worst' case scenarios would be dependant on available data and/or as inferred from extrapolating the experience with similar projects

Where it is available, geological and/or gas information can be used to divide the permit area into smaller blocks or domains (see Esterle et al., 2006). Division of these blocks can be based upon

geological properties such as faults, depth, coal thickness, gas data, or even just data density (Fig. 2). Other factors, such as depth of the reservoir, can also be used to subdivide the area as this has a strong impact on maximum holding capacity. The important outcome of subdivision of the permit into smaller areas is that it reduces the range of any particular variable, effectively reducing the uncertainty of resource estimates pertaining to that subarea.

Coal Seam Thickness

The thickness of a coal seam can change abruptly, thus making this variable an especially hard one to estimate accurately over any given spatial distance. Within a permit, there may be areas where coal seam thickness is more uniform and predictable, but also areas where thickness can change rapidly. Additionally, within a permit area, the data density will be greater in some parts than others. In other words, one source of uncertainty of thickness estimates is related to data control (i.e. some areas have more drill hole data than others) and the degree to which this creates uncertain thickness estimates is related to another source of uncertainty,*viz*. the rate of change of the thickness over a given area (i.e., two areas may have equal data density, but one is more heterogeneous than the other, and so would result in more uncertain estimates of uncertainty).

As noted in the previous discussion on area, variation in coal seam thickness can be used to subdivide the permit area into smaller blocks. Again, this can be done based on uniformity of thickness (thus meaning there is little uncertainty in thickness) or defining areas where rapid thickness changes occurs (i.e. areas of high uncertainty) or areas of different data density (thus, less and more uncertainty, respectively).

Density

In order to calculate volume and tonnage of the reservoir, the density of the coal is estimated. However while density is straightforward to estimate, the coal components that influence density have significant implications for coal adsorption properties which needs to be considered.

The greatest influence on the density of a unit of coal is its ash yield; that is, the amount of inorganic material present in the coal seam. In general, the density of organic components of any coal ranges from about 1.25 – 1.35 g/cm^3 dependant on the rank of the coal. Coals with high inertinite content can have density values as great as 1.45 g/cm^3 because of the inherently higher density of the mostly carbon-composed inertinite macerals. In contrast, the inorganic material in coal is usually greater than 2.60 g/cm^3 (kaolinite is 2.60 g/cm^3; quartz is 2.65 g/cm^3). However, methane does not adsorb on to the inorganic fraction in coal (see Laxminarayana and Crosdale, 1999, 2002; higher ash yield coal having less absorbed gas is well documented; see Butland and Moore, 2008; Mares and Moore, 2008; Warwick et al., 2008; Wang, 2007). So, if a coal has relatively high inorganic constituents (say >10%), then the total tonnage of the reservoir will be increased and superficially would appear to have a greater gas in-place. But, the gas holding capacity will decrease with this high inorganic component; a fact which if not recognised and considered could cause considerable overestimation of gas in-place.

This negative correlation between high ash content (high density) and low methane adsorption could be addressed via the delineation of high and low ash coal intervals and assigning them different gas holding capacities.

Calculating Volume/Tonnage

Table 1 summarises an example calculation for 4 hypothetical domains of a coal reservoir, calculating (coal) volume and tonnage (using a density of 1.30 g/cm^3), where volume is simply the product of area and thickness, and tonnage is the product of volume and coal density. Note that, as already discussed, there are 'best', 'base' and 'worst' case scenarios around each of the two main variables (area and coal seam thickness), but density has been fixed with a single value in this calculation.

The calculation leads to 'best', 'base' and 'worst' case scenarios for coal volume and tonnage. The uncertainty of any particular domain can be expressed through the range from best to worst cases. For example, in coal thickness, domain 3 has less uncertainty than domain 4 even though the base case coal thickness is the same for both zones.

GAS VOLUME

Estimating gas volume in a coalbed methane reservoir is the second component of coal bed resources estimation (after reservoir size estimation). This component is based on two measurements: (1) the maximum gas holding capacity of the target seam, and (2) the total gas in the seam. The first measurement is a laboratory measurement and represents the hypothetical amount of gas that can be held by that sample at any given pressure and temperature. The second measurement is from fresh core and represents the actual amount of gas in the coal. A way of thinking of these two measurements is, the first test tells you how big your cup is, and the second measurement tells you how full it is. These two measurements are used to calculate the

gas saturation of the reservoir (expressed as a percentage), which is a key parameter in determining whether the reservoir could be commercial or not.

Maximum Gas Holding Potential

The test to determine maximum holding capacity in a coal is commonly referred to as an adsorption isotherm, or more often just 'isotherm'. The 'isotherm' refers to the test procedure that a coal sample is tested for its maximum methane holding capacity at different pressures but at the same temperature.

The maximum gas holding capacity of any given coal is influenced by a number of parameters, not the least of which are coal rank, type (i.e. composition) and quality (see discussion in the section on density). As well as these parameters, the holding capacity is determined by both the pressure and temperature of the reservoir.

The pressure of the reservoir, in almost all cases, is determined by the depth below surface. The pressure is a simple hydrostatic head function. Thus when reading an adsorption isotherm, the pressure translates into different depths (rule of thumb is that about 4 MPa is about 400 m hydrostatic head). It is crucial that the depth of a sample is known, otherwise, calculation of %gas saturation will not be possible (see below).

When collecting samples for adsorption testing, it has been demonstrated that these samples must be fresh, otherwise an overestimation of the storage capacity will ensue (Crosdale et al., 2008) which can also result in an erroneously low % gas saturation determination. Additionally, it has

been shown that more than one adsorption sample per seam needs to be taken. Mares et al. (2009b) reports that even in a fairly homogenous coal seam, a minimum of 5 adsorption samples would be needed to have a reasonable constraint on the uncertainty. The fitting of the isotherm to the data is another source of potential estimation error.

Gas Desorption ("Measured" Gas)

The second crucial measurement in estimating gas volume is gas desorption. This analysis determines the amount of gas actually desorbed (released) off of the coal (from a core sample). This is a direct measure of the gas and must be taken off of fresh core, immediately upon arrival at the surface. The procedure for measuring gas from coal has been discussed elsewhere (Barker et al., 2002; Moore and Butland, 2005; among others).

Measured gas can have significant in-seam variation (Butland and Moore, 2008; Mares and Moore, 2008) and thus, a minimum number of gas canisters need to be taken in order to capture that variability and determine the uncertainty. The minimum number of canisters will vary depending on the inherent heterogeneity of the seam (Mares et al., 2009b). At the beginning of an exploration project, it thus could be wise to take more, rather than less, samples for desorption.

Gas Saturation

Gas saturation of a reservoir is simply derived from the ratio between actual (measured) and potential (adsorption isotherm) gas in a coal seam at any given pressure or temperature. The percentage gas saturation is usually expressed as, for example "70% saturated", meaning the

'glass is 70% full'. Sometimes gas saturation is expressed as a percentage of its level of under-saturation, for example "30% under-saturated, or 'the glass is 30% empty'.

Note that in some cases, no data for either, or both, adsorption or desorption will exist for a new prospect area. What can be done however is to use isotherm and gas saturation data from coals of similar rank and composition from another location. Of course, there are errors associated with the extrapolation of data from one site to another, which need to be reflected in the larger range of values for each of the variables explored (and thus, the commensurate increase in the range of uncertainty for saturation estimates).

The percentage of gas saturation for a reservoir is also an important parameter when undertaking gas reserved estimates, and is probably only second to permeability in influencing how difficult it will be to develop a gas play commercially.

Calculating Gas Volume

Table 2 shows an hypothetical variation in maximum holding capacity and % gas saturation for four domains (derived from the ratio between desorption and adsorption data). Again, note that some domains in the permit area have the same base case values, but because of higher unknowns or natural variability, the ranges between the 'worst' and 'best' case values are larger, reflecting a greater uncertainty associated wth variables in these domains

The product of the tonnage and saturation estimates are then used to calculate the total gas in-place for each domain, expressed as BCF (billion cubic feet) of gas. For the example given here,

the uncertainty is fairly large, with gas in place values ranging from 13 (worst case) to 91 (best case) BCF of gas in-place with a base case of 36 BCF.

CALCULATING UNCERTAINTY

The purpose of assigning ranges to geological parameters in coalbed methane prospects is to define the uncertainty of gas in-place in probabilistic terms. In order to accomplish this we use a Monte Carlo estimate undertaken with @risksoftware (Palisade, 2007). The variables that are assessed are the primary ones: area, seam thickness, gas holding capacity and saturation. The reader is referred to the published @risk module summary, but the type of distributions assigned to each of the major variables is important. To reflect a typical scarcity of data we adopted simple distributions; using a uniform distribution for area, and a triangular distribution for all other parameters which reflect our general knowledge of the distributions expected for these parameter types

Using the hypothetical test data summarized in Tables 1 and 2, a probabilistic gas in-place distribution has been derived and is shown in Figure 3. A total of 100,000 runs were completed for the distribution and as can be seen in the probability distribution results in a median, or P50 value, of 39.6 BCF with P10 and P90 being 32.5 and 46.9, respectively. That means there is an 80% chance that the predicted gas in-place is between 32.5 and 46.9 BCF.This is a pretty 'tight' distribution, when compared with that defined by the worst and best case scenarios, and reflects the fact that it is very unlikely that all of the worst case variables occur together within a single domain . Of course, the probability estimate is only as good as the input distribution data.

SUMMARY

The procedure of estimating and quantifying the level of uncertainty through probabilistic analysis presented in this paper, is just one of many possible approaches that could be adopted. We have used this approach as it is a relatively fast and conceptually simple procedure, and is also straightforward to audit. While not perfect, the procedure robustly portrays the inherent uncertainty associated with estimates of coalbed methane resources. Furthermore, it also conveys that in some areas parameters are more well known than in others.. Additionally, as a prospect is moved forward and more data is collected or becomes available, the values used in the probability analysis can be easily revised and estimates updated.

Where data is particularly scarce, extrapolation from reservoir data of other, similar, coals can be used, but larger ranges of parameter uncertainty are necessary to reflect this extrapolation. Analysis of existing literature, to better quantify this extrapolation error, would be a beneficial extension to this work.

Finally, as stated at the beginning of this paper, the method presented is for application to resource estimation not reserve estimation. As most reservoir engineers know, gas in-place estimates may indicate a potentially large gas play, but flowing that gas to surface requires a whole different set of reservoir parameters which must be delineated and used in the design of production wells that can flow commercial rates of gas. The associated range of uncertainty of reserve estimates is much narrower than for resources estimates, however more complicated uncertainty analysis methods are required for its assessment; which must honour the collected flow data and measurements of the system response to that flow.

REFERENCES

Barker, C.E., Dallegge, T.A. and Clark, A.C., 2002. USGS coal desorption equipment and a spreadsheet for analysis of lost and total gas from canister desorption measurements, U.S. Geological Survey Open-File Report 02-496, Reston, Va., USA, 13 pp.

Butland, C.I. and Moore, T.A., 2008. Biogenic coal seam gas reservoirs in New Zealand: A preliminary assessment. International Journal of Coal Geology 76, 151-165.

Crosdale, P.J., Moore, T.A., Mares, T.E., 2008. Influence of moisture content and temperature on methane adsorption isotherm analysis for coals from a low-rank, biogenically-sourced gas reservoir. International Journal of Coal Geology, 76, 166-174.

Esterle, J.S., William,s R., Sliwa, R. and Malone, M., 2006. Variability in coal seam gas parameters that impact on fugitive gas emissions estimations for Australian black coals. 36th Sydney Basin Symposium 2006: Advances in the Study of the Sydney Basin. 26-28 November, University of Wollongong, Wollongong, Australia, 10p.

Hadiyanto and Stevens, S., 2005: Coalbed methane prospects in lower rank coals of Indonesia. In: S. Prihatmoko, S. Digdowirogo, C. Nas, T.v. Leeuwen and H.Widjajanto (Editors), Indonesian Mineral and Coal Discoveries. Indonesian Association of Geologisits, Bogor, Indonesia, pp 152-162.

Laxminarayana, C. and Crosdale, P.J., 1999. Role of coal type and rank on methane sorption character of Bowen Basin, Australia, coals. International Journal of Coal Geology, 40, 309-325.

Laxminarayana, C. and Crosdale, P.J., 1999. Controls on methane sorption capacity of Indian coals. American Association of Petroleum Geologists Bulletin, 86, 201-212.

Mares, T.E. and Moore, T.A., 2008. The influence of macroscopic texture on biogenically-derived

coalbed methane, Huntly coalfield, New Zealand. International Journal of Coal Geology 76, 175-185

Mares, T.E., Radlinski, A.P., Moore, T.A., Cookson, D. Thiyagarajan, P., Ilavsky, J., Klepp, J., 2009a. Pore size distribution and specific surface area available for CO_2 adsorption in a subbituminous coal, Huntly Coalfield, New Zealand. International Journal of Coal Geology, 77, 54-68.

Mares, T.E., Moore, T.A. and Moore, C.R., 2009b. Uncertainty in gas saturation in a subbituminous coal seam, International Journal of Coal Geology 77, 320-327

Moore, T.A. and Butland, C.I., 2005. Coal seam gas in New Zealand as a model for Indonesia. In: S. Prihatmoko, S. Digdowirogo, C. Nas, T.v. Leeuwen and H.Widjajanto (Editors), Indonesian Mineral and Coal Discoveries. Indonesian Association of Geologisits, Bogor, Indonesia, pp. 192-200.

Palisade, 2007. @Risk – risk analysis and simulation add-in for Microsoft Excel. Version 5.0. Decemeber 2007. Palisade Corporation, 798 Cascadilla St., Ithaca, NY, USA 14850; http://www.palisade.com

Radlinski, A.P., Mastalerz, M., Hinde, A.L., Hainbuchner, M., Rauch, H., Baron, M., Lin, J.S., Fan, L., Thiyagarajan, P., 2004. Application of SAX and SANS in evaluation of porosity, pore size distribution and surface area of coal. International Journal of Coal Geology, 59, 245-271.

Stevens, S.H., Sani, K. and Hardjosuwiryo, S., 2001. Indonesia's 337 TCF CBM resource: a low-cost alternative to gas, LNG. Oil & Gas Journal, October 22nd: 40 – 45.

Warwick, P.D., Breland, C., Hackley, P.C.., 2008. Biogenic origin of coalbed gas in the northern Gulf of Mexico Coastal Plain, U.S.A.. International Journal of Coal Geology 76, 119-137.

Wang, X., 2007. Influence of coal quality factors on seam permeability associated with coalbed methane production. PhD Thesis, University of New South Wales, Sydney, Australia, 338 pp.

Table 1: Estimates of tonnage of coal in different geological 'domains' within a hypothetical prospect.

	AREA (m^2)			net THICK (m)			VOLUME (m^3)			TONNAGE (t) (1.30 g/cm^3)		
Domain/Area	**Worst**	**Base**	**Best**	**Worst**	**Base**	**Best**	**Worst**	**Base**	**Best**	**Worst**	**Base**	**Best**
1	7,074,324	7,467,342	7,860,360	10	15	25	70,743,240	112,010,130	196,509,000	91,966,212	145,613,169	255,461,700
2	1,320,605	1,393,972	1,467,339	1	3	8	1,320,605	4,181,916	11,738,712	1,716,787	5,436,491	15,260,326
3	9,312,899	9,830,283	10,347,666	5	10	15	46,564,497	98,302,827	155,214,990	60,533,846	127,793,675	201,779,487
4	3,110,192	3,282,981	3,455,769	5	10	25	15,550,961	32,829,806	86,394,225	20,216,249	42,678,747	112,312,493
GRAND TOTALS	**20,818,021**	**21,974,577**	**23,131,134**				**134,179,303**	**247,324,679**	**449,856,927**	**174,433,093**	**321,522,082**	**584,814,005**

Table 2: Estimates of gas in-place in different geological 'domains' within a hypothetical prospect.

	Adsorption Gas Content (SCF/t)			Saturation (%)			Gas in-Place BCF		
Domain/Area	**Worst**	**Base Case**	**Best**	**Worst**	**Base Case**	**Best Case**	**Worst**	**Base Case**	**Best Case**
1	100	124	155	60%	70%	80%	5.52	12.60	31.68
2	205	220	250	60%	65%	70%	0.21	0.78	2.67
3	150	175	200	70%	75%	85%	6.36	16.77	34.30
4	100	175	225	60%	75%	90%	1.21	5.60	22.74
GRAND TOTAL							**13**	**36**	**91**

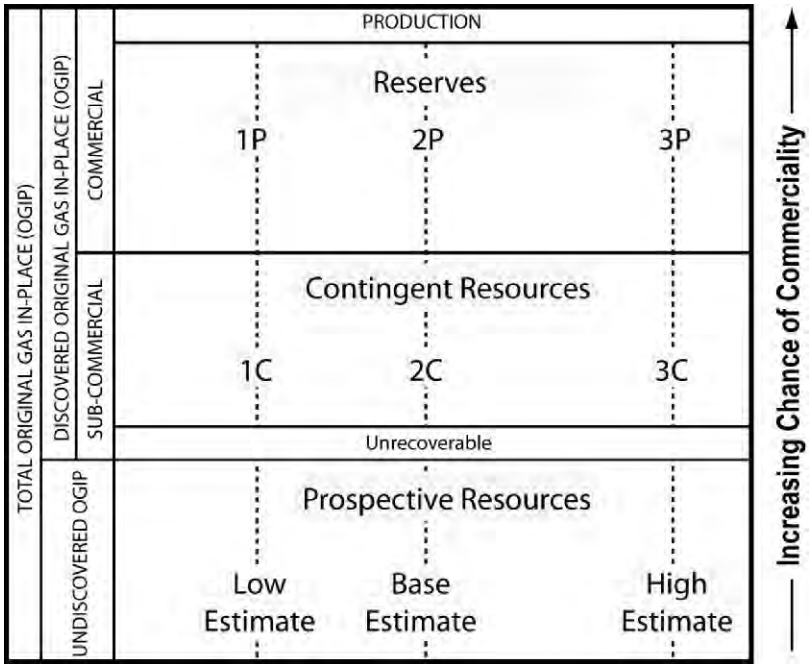

Figure 1: Resource and reserve classification (from SPE).

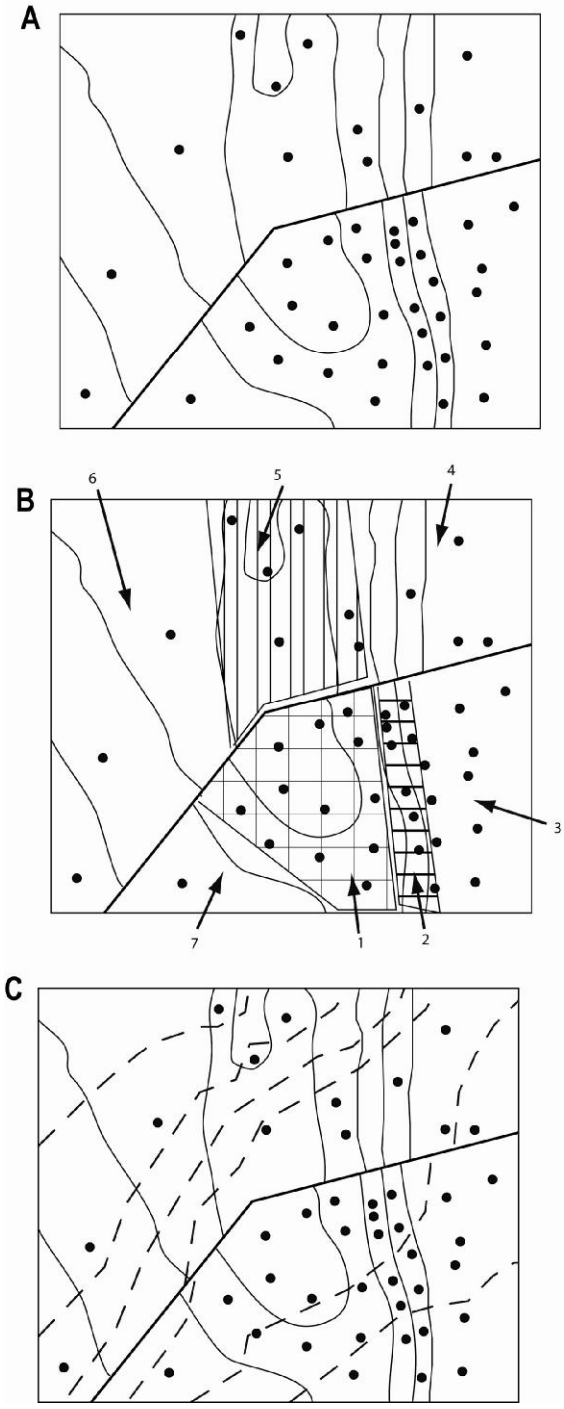

Figure 2: (A) Schematic of coal thickness, thin solid lines, faults (thick lines) and data (black dots). (B) sample map divided into 'domains', 1 through 7. (C) Dotted lines are structure contours.

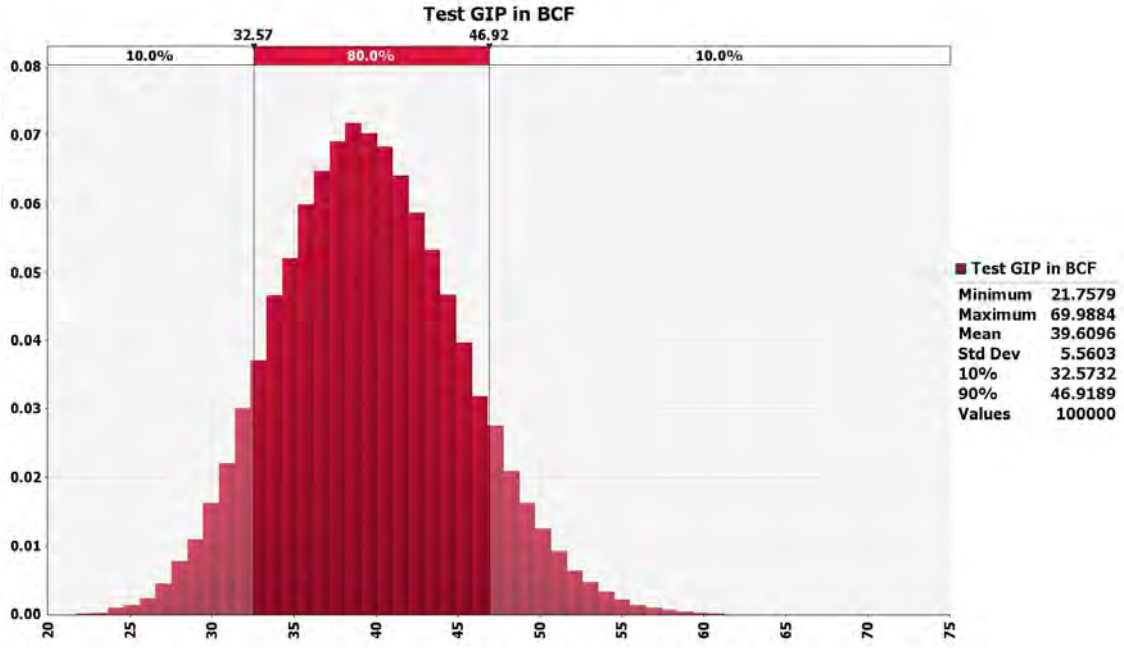

Figure 3: Probabilistic distribution of gas in-place for data used in Tables 1 – 2.